RQR8

A universal safety switch for cellular therapies

BRIAN PHILIP

Department of Haematology

UCL Cancer Institute

University College London

A thesis submitted for the degree of Doctor of Philosophy

2015

Declaration

I, Brian Philip confirm that the work presented in this thesis is my own. Where information has been derived from other sources, I confirm that this has been indicated in the thesis.

Abstract

Cancer immunotherapy represents a rapidly developing field with potential to address shortcomings from current therapies. A compact marker-suicide gene reliant upon off-the-shelf reagents would offer considerable utility for these adoptive cellular therapies.

Marker genes enable measurement of transduction efficiency and allow purification of transduced cells while suicide genes facilitate deletion of T-cells in case of toxicity. Previous marker genes include Neomycin resistance, truncated nerve growth factor receptor and CD34. However limitations of current marker genes include immunogenicity, unexpected biological activity and long coding regions respectively. Similarly, several suicide genes have been described with Herpes Simplex Virus Thymidine Kinase and inducible Caspase 9 in clinical use. Here, limitations include either immunogenicity or limited availability of the inducing drug. We sought to generate a compact marker-suicide gene that enables clinical grade sorting and effective deletion using CD34 cliniMACS and rituximab respectively. By using minimal epitopes required for binding, we hoped to reduce the size of the construct. We first sought to locate the epitope from CD34 which binds QBEnd10, the monoclonal antibody used in Miltenyi cliniMACS CD34 selection system. By epitope mapping, we identified a 16 amino acid linear fragment of CD34, which demonstrates approximately equivalent binding of QBEnd10 as the native antigen. Next, we sought to incorporate rituximab binding epitopes to engender rituximab mediated deletion. Following optimisation we established a 136 amino acid construct, designated RQR8, composed of two rituximab binding epitopes flanking the QBEnd10 epitope on a CD8 stalk which enables selection with the cliniMACS CD34 system and deletion through both CDC and ADCC with rituximab.

Further, we demonstrate functional co-expression of RQR8 alongside chimeric antigen receptors and transgenic T-cell receptors. Finally, we validate functional efficacy of RQR8 deletion *in vivo* through a murine haploidentical transfer model.

We predict that RQR8 will make T-cell gene therapy both safer and cheaper.

Acknowledgments

I would like to thank my supervisor Dr Martin Pulé whose guidance, insight, support and friendship have proven invaluable to the success of this project. Moreover, his vision and efforts for translational application have ensured that the impact from this research will extend far beyond these pages.

Mention must also be made of the multitudes, named and unnamed, whose assistance, enthusiasm, support, guidance and camaraderie have proven crucial toward successful completion of this research. Arnie, whose ability to revive the aged Cyan ensured successful completion of CDC and ADCC assays against all odds. Barry, whose expert training and guidance for a 'quick final' experiment has led to many years of further highly successful modelling experiments! Also the many conscripted into assistance with the endless series of *in vivo* experiments which proved more marathon than race, but most especially Eva, Leila, Fred and Gordon. And to the many whose assistance, guidance and training all proved instrumental in successful completion of this journey including Simon, Amit, Alicja, Karin, Ben G. and Ben D., Claire R. and Clare S, Emily, Dimitra, David, Sergio, Karl, Ronjon, Kerry, Gaurav, Berend and Teresa.

Mention must be made of Simon Cheesman for his generous assistance in supplying the therapeutic antibodies which enabled this research. Also the multitudes of PBMC donors from Haematology whose anonymous generosity was essential in enabling this research to be completed.

To my parents and family for support and enthusiasm and for having inspired my academic curiosity; and to those lost along the journey who will never be forgotten: Dad, Andy, Jim and Jack.

Lastly but most crucially, for the indefatigable support of my loving wife Susan, whose tolerance for the years of long days, short nights and absent weekends, which have proven necessary to complete this project, has been immeasurable.

Table of Contents:

Index of Figures

Index of Tables

Abbreviations

a.a.	Amino acid
AAV	Adeno-associated virus
ACT	Adoptive cellular therapy
ACK	Ammonium chloride potassium (lysis buffer)
ADCC	Antibody dependent cellular cytotoxicity
APC	Allophycocyanin
AZT	Azidothymidine
ADA-SCID	Adenosine deaminase severe combined immunodeficiency
AKT	Protein kinase B
Apaf-1	Apoptotic protease activating factor 1
BCR	B-cell receptor
BCR-Abl	Breakpoint cluster region – Abelson murine leukaemia viral oncogene homolog 1 (aka Philadelphia chromosome)
BME	β-mercaptoethanol
BSA	Bovine serum albumin
CAR	Chimeric antigen receptor
CD	Cluster of differentiation marker
CDC	Complement dependent cellular cytotoxicity
cDNA	Complementary deoxyribonucleic acid
CDR	Complementarity determining region
CML	Chronic myeloid leukaemia
CLL	Chronic lymphocytic leukaemia
CMV	Cytomegalovirus
ConA	Conconavalin A
CO_2	Carbon dioxide
CTL	Cytotoxic T-lymphocyte
ΔEGFR	Truncated epidermal growth factor receptor
ΔlNGFR	Truncated low affinity nerve growth factor receptor
DLI	Donor lymphocyte infusion
DNA	Deoxyribonucleic acid
DMSO	Dimethyl sulfoxide
DTT	Dithiothreitol
ELISA	Enzyme linked immunosorbant assay
eBFP2	Enhanced blue fluorescent protein
eGFP	Enhanced green fluorescent protein
EBV	Epstein Barr virus
EDTA	Ethylenediaminetetraacetic acid
FACS	Fluorescence activated cell sorting
Fab	antigen binding Fragment
Fc	constant Fragment
FCS/FBS	Foetal calf/bovine serum
FDA	(US) Food and Drug Administration
FITC	Fluorescein isothiocyanate
GAPDH	Glyceraldehyde 3-phosphate dehydrogenase
GM	Genetically modified
GM-CSF	Granulocyte macrophage colony stimulating factor
GPI	Glycophosphatidylinositol anchor
GvHD	Graft versus host disease
GvL	Graft versus leukaemia
Gy	Gray

HACA	Human anti-chimeric antibody
HBSS	Hanks buffered saline solution
H&E	Haematoxylin and eosin staining
HIV-1	Human immunodeficiency virus type I
HLA	Human leukocyte antigen
HPLC	High performance liquid chromatography
HSC	Haematopoietic stem cell
HSCT	Haematopoietic stem cell transplant
HSVtk	Herpes simplex virus thymidine kinase
iFas	Inducible Fas
iCaspase9	Inducible Caspase 9
IFN	Interferon
Ig	Immunoglobulin
IHC	Immunohistochemistry
IL	Interleukin
IM	Insertional mutagenesis
IMDM	Iscove's modified Dulbecco's medium
IMPDH	Inosine 5' monophosphate dehydrogenase
i.p.	Intraperitoneal
iPS	Inducible pluripotent stem cell
IRES	Internal ribosomal entry site
i.v.	Intravenous
LB	Luria Bertani broth
LTR	Long terminal repeat
LV	Lentiviral
mAb	Monoclonal antibody
MACS	Magnetic activated cell sorting
MAPK	Mitogen activated protein kinase
MFI	Mean fluorescence intensity
MHC	Major histocompatibility complex
MLV	Murine leukaemia virus
MWCO	Molecular weight cut off
NFκB	Nuclear factor kappa B
NHL	Non-Hodgkins lymphoma
NK	Natural killer cell
NT	non-transduced/transfected
ORF	Open reading frame
OTNA	Off-target nuclease activity
OTOT	On-target, off tumour toxicity
PBMC	Peripheral blood mononuclear cell
PBS	Phosphate buffered saline
PCR	Polymerase chain reaction
PE	Phycoerythrin
PFA	Paraformaldehyde
PHA	Phytohaemagglutinin
PI	Propidium iodide
PIC	Pre-integration complex
PNH	Paroxysmal nocturnal hemoglobinuria
PPT	Polypurine tract
Q	QBEnd10 binding epitope
R	Rituximab binding epitope
RCF	Relative centrifugal force
RCL	Replication competent lentivirus

RIC	Reduced intensity conditioning regimen
RIPA	Radio immunoprecipitation assay (buffer)
RNA	Ribonucleic acid
RPM	Revolutions per minute
RPMI	Roswell Park memorial institute
RV	Retrovirus
scFv	Single chain variable fragment
SCID	Severe combined immunodeficiency disorder
SDS-PAGE	Sodium dodecyl sulphate-polyacrylamide gel electrophoresis
SIN	Self inactivating
S/MAR	Scaffold/Matrix attachment region
SOE-PCR	Splicing by overlap extension PCR
TAA	Tumour associated antigen
Taq	Thermus aquaticus DNA polymerase
TaV 2A	*Thosea asigna* virus 2A sequence
TBI	Total body irradiation
TCR	T-cell receptor
TGE	Transient gene expression
TIL	Tumour infiltrating lymphocyte
TNF	Tumour necrosis factor
Treg	Regulatory T-lymphocyte
VSVg	Vesicular stomatitis virus glycoprotein
WT1	Wilms tumour antigen-1
X-gal	5-bromo-4-chloro-3-indolyl-β-D-galactopyranoside
wt	Wild-type
ZFN	Zinc finger nuclease

Chapter One

Due to rapid advances in genetic engineering and molecular biology, cancer immunotherapy has evolved into a broad term broadly encompassing any therapeutic strategy that modulates the native immune response. These include therapeutic monoclonal antibodies, cancer vaccines, adoptive cell transfer technologies and recombinant proteins[1]. In light of the aim of this project, subsequent discussion will focus upon cancer immunotherapy mediated by adoptive cell therapy.

1.1. Therapy with genetically engineered cells

Adoptive immunotherapy represents an established and evolving therapeutic strategy for the treatment of malignant and infectious diseases. The graft-versus leukaemia (GvL) effect in haematopoietic stem cell transplantation (HSCT) can result in sustained remissions of certain haematological malignancies. More directed approaches, such as administration of *ex vivo* expanded tumour infiltrating lymphocytes (TILs) shown to achieve dramatic remissions of metastatic melanoma, are also possible[2]. Further, adoptive cellular therapy (ACT) with virus specific T-cells has been shown to reconstitute antiviral immunity against Epstein Barr virus (EBV)[3] and Cytomegalovirus (CMV)[4] resulting from concomitant immunosuppression following HSCT. However, apart from these examples, it is typically difficult or impossible to generate therapeutic T-cell product with traditional methods of selection and expansion. Advances in gene-therapy afford us alternative strategies: namely transgenic re-targeting of T-cells to tumour-antigens. One such strategy is the use of chimeric antigen receptors (CAR's) which allow specific targeting without the imposition of MHC-restriction. In a recent neuroblastoma clinical trial, cytotoxic-T-lymphocytes (CTL's) specific for Epstein-Barr virus (EBV) were modified with an anti-GD2 CAR achieving clinical response in half of the subjects treated[5]. An alternative strategy involves transgenic expression of native alpha-beta T-cell receptor (TCR) chains specific for a cancer antigen. In a small clinical trial, two of seventeen melanoma patients responded to this therapy and this strategy is currently being evaluated in a larger clinical trial[6].

However, although cellular therapy offers great promise, identification of the potential risks which may result remain less defined. In contrast to a therapeutic protein or small molecule drug whose adverse events usually abate with the half-life of the therapeutic, T-cells engraft and replicate, potentially resulting in escalating and fulminant toxicity. With advanced engineering designed to establish non-immunogenic therapeutic product, there remains a need to identify a uniform strategy to enable simple discontinuation of cellular therapies in case of undesirable toxicities.

As ACT remains a rapidly developing field, this introduction commences with a brief overview of immunotherapy and adoptive cell therapy. A brief synopsis of the evolution of ACT pre- and post-genetic engineering is followed by a discussion of the various genetic engineering strategies employed in T-cell cancer immunotherapy. As marker genes and suicide gene strategies have both evolved concurrently with advances in adoptive cellular therapy, and due to their primary role within this project, these will be examined independently. Finally, in consideration of the aim to be compatible with current therapeutic antibodies, the final section of the introduction briefly introduces monoclonal antibody technology.

In this thesis, I describe the creation of a novel modular gene cassette which offers potential for application as a universal safety mechanism for adoptive cellular therapy.

1.1.1. Immunotherapy

Coincident advances in immunology and molecular biology have enabled the rapid evolution of the developing field of immunotherapy, which can be defined as: the clinical modulation of the immune response to facilitate suppression of immune-mediated pathology or to enhance an immune response against infectious or malignant disease. Immunotherapeutic strategies include nonspecific stimulation of endogenous immunity, active immunisation mediated through cancer vaccines, monoclonal antibody modulation of immune responses and adoptive cellular immunotherapy[7]. As the focus of this research was to establish a marker/suicide gene for cellular therapy, the following will offer a general introduction to immunotherapy approaches, with the primary focus directed toward adoptive cellular immunotherapy.

The first reproducible successful application of anti-cancer immunotherapy was achieved through stimulation of endogenous immunity mediated by cytokine therapy, clearly reviewed by Rosenberg[8]. However, although clinical benefit was observed, cytokine therapy also imposes significant toxicity, thus subsequent research sought less toxic strategies. Observations of tumour infiltrating lymphocytes isolated from tumour resections suggested potential for the presence of endogenous immunity against malignant disease. Although observations of TIL's proved variable and typically limited, this observation suggested there might exist endogenous immunity which could theoretically be enhanced through vaccination. However, although vaccination programmes against infectious disease represent a triumph of modern medicine, similar attempts to apply vaccination against malignant disease have proven largely disappointing. Although further discussion of vaccination for cancer immunotherapy remains beyond the scope of this thesis, the current state of cancer vaccination as an immunotherapeutic approach is reviewed by Lichty *et al*[9]. Finally, monoclonal antibody technology offers great potential for modulating the immune response. Antibodies can be directed against cellular antigens to block signalling pathways modifying immune responses, succinctly reviewed by Blank *et al*[10].

1.1.2. Adoptive cell immunotherapy

Adoptive cell transfer represents a complex and rapidly developing field within immunotherapy with reports citing clinical efficacy against autoimmunity, malignant and infectious diseases. *Ex vivo* expansion of regulatory T-cells (Tregs) has demonstrated promise in therapy against Crohn's disease[11] and is currently being investigated as a therapy against type 1 diabetes[12]. Immune suppression, commonly coincident with ACT modalities, may impair infectious immunity which would otherwise control environmental and endogenous pathogens. Attempts to address these co-morbidities using ACT has demonstrated efficacy in restoring or mediating antiviral immunity against Epstein-Barr virus[3] and Cytomegalovirus[4] as well as antifungal immunity against *Aspergillus fumigatus*[13]. Further, advances in molecular biology and genetic engineering vastly extend the potential for therapeutic application of cellular therapies such as T-cell re-targeting through expression of engineered T-cell receptors or chimeric antigen receptors. Reflecting the

proposed application for our marker-suicide gene, subsequent discussion regarding immunotherapy will be restricted to cellular cancer immunotherapy.

Advances in HSCT and applications for DLI as therapeutic strategies established the groundwork to enable further adoptive cell therapies. Genetic engineering enables the ability to correct genetic deficits and endow cells with novel functional capabilities. The following will briefly introduce the premise for adoptive cell therapy.

1.1.3. Risks and challenges

Observations of clinical efficacy frequently highlight further barriers, similarly necessary to be overcome, to achieve therapeutic success. Thus, progressive evolution of cancer immunotherapy continues to increase the range of transgenes required to overcome obstacles presented by tumour targets. Cellular retargeting of T-cells can be achieved through inclusion of a transgenic T-cell receptor (TCR) or chimeric antigen receptor (CAR) directed against tumour associated antigens (TAA), which are otherwise invisible due to immune tolerance mechanisms. Where cellular retargeting has proven insufficient to mediate remission in itself, efficacy can be enhanced through modifications to T-cell trafficking capacity and enhanced functionality achieved by later generations CAR's (*vide infra*). Inclusion of drug resistance genes or selective engineering of virus specific cytotoxic T-lymphocytes (CTL) can facilitate a selective advantage for enhanced *in vivo* persistence. Modifications designed to enhance T-cell survival and proliferation can improve efficacy in the face of oppressive tumour microenvironments, whilst inclusion of marker and suicide genes offer assessment of T-cell survival and persistence, or can facilitate cellular deletion in the face of toxicity respectively[14]. Figure 1 illustrates strategies currently employed in T-cell engineering, further addressed in 1.2.2, p36 and 6.2, p180.

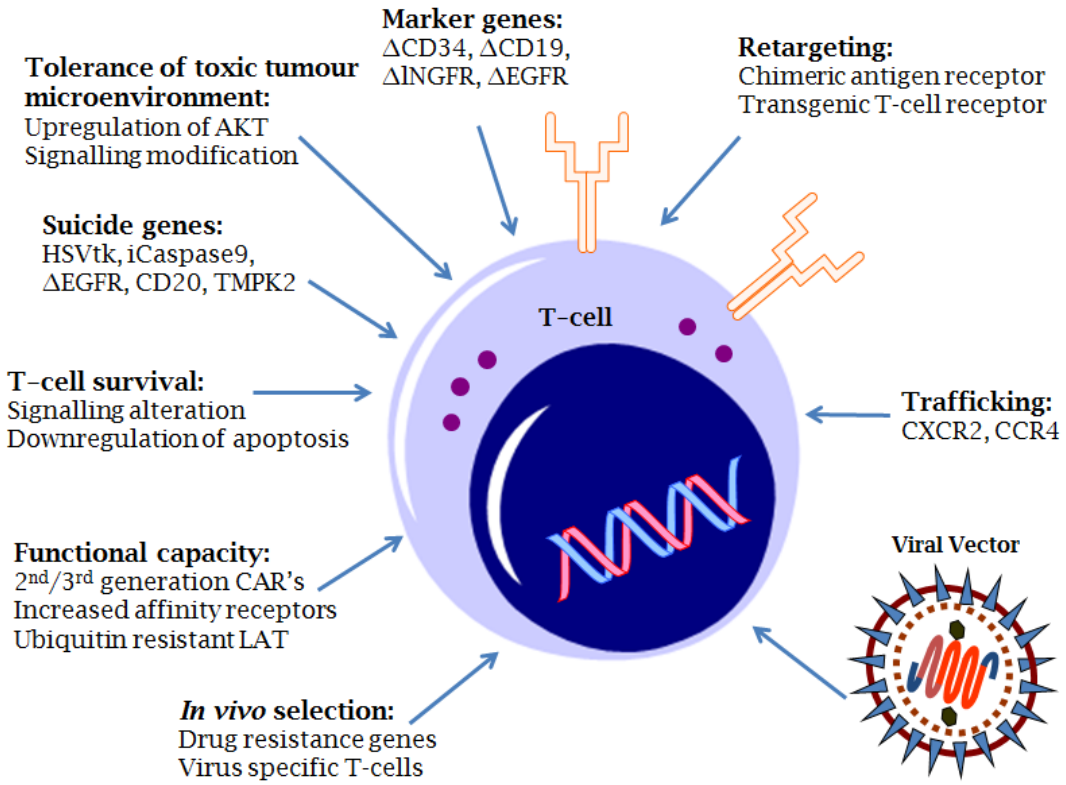

Figure 1 Genetic engineering strategies for T-cells
Adapted from Kershaw *et al*[14]. Coincident advances in molecular biology and immunology enable an ever increasing array of potential modifications to T-cell biology such as facilitating redirected targeting or trafficking, with many further engineering modifications already described. To ensure sustained gene expression by modified T-cells despite cellular proliferation, genetic modification strategies commonly employ integrating retro- or lentiviral vector cassettes to mediate gene delivery.

A report citing sustained engraftment of CD4ζ CAR T-cells more than a decade following adoptive transfer[15] provides evidence for the promise of long-term persistence and highlights the coincident potential for chronic toxicities yet to be identified. Similarly adverse events such as graft versus host disease and cytokine storms represent acute toxicities resulting from cellular immunotherapy.

The range of risks associated with adoptive cellular therapies is multifaceted and dependent upon the desired therapeutic effect, concomitant therapies and the adoptive cellular strategy employed. Toxicity can result from engineering strategies, source of donor cells and potential re-targeting toxicity. Engineering strategies which require transgenic integration or deletion impose risks of insertional mutagenesis (IM)[15, 16] and toxicity resulting from off-target nuclease toxicity (OTNA)[16, 17]. Use of allogeneic derived donor cells imposes risk of graft versus host disease (GvHD)[18, 19]. Re-targeting strategies impose risks of on-

target, off-tumour toxicity (OTOT)[20]. Furthermore, therapeutic administration protocols and even disease burden can result in toxicities such as tumour lysis syndrome[21], macrophage activation syndrome[22] and cytokine storms[20]. Currently identified potential toxicities associated with adoptive cellular therapies are summarised by Table 1.

Table 1 Potential applications for suicide gene in cellular therapies
Adapted from Sadelain, 2011[23]

Donor cell type	Therapeutic intent	Toxicity
Donor T cells	Graft versus tumour	GvHD[18]
Engineered T cells	Tumour deletion	OTOT, cytokine storm[20], tumour lysis syndrome[21], macrophage activation syndrome[22], GvHD[19]
Haematopoietic stem cells	Correction of monogenic disorders	Genotoxicity from IM or OTNA[16]
Pluripotent stem cell progeny (embryonic or iPS derived)	Regenerative medicine for genetic or degenerative disorders	Genotoxicity from IM or OTNA[16, 17], residual teratoma forming cells[17]

However, despite these concerns, adverse events following ACT have largely been restricted to isolated cases. From a 10 year review of adoptive T-cell therapy involving 381 T-cell products, no grade 3-4 infusion reactions were observed; of the twenty four mild reactions which were observed most resulted from the cryoprotectant. The conclusion from this review was that infusion of T cell products is safe in the outpatient setting[24]. Most importantly, no adverse events related to insertional mutagenesis (IM) of T cells have yet been reported to date despite over twenty years of adoptive T-cell therapy[25]. This is in marked contrast with the experience involving retroviral transduction of haematopoietic stem cells. However, although therapeutic benefit was observed from GT trials for both adenosine deaminase - severe combined immunodeficiency (ADA-SCID) and common γ-chain X-SCID, IM mediated clonal proliferation was only observed from the X–SCID trial. Observations have been made noting the relationship between the clonal proliferation and the potential biologic consequences mediated by the therapeutic transgene. In X-SCID, the common γ-chain provides a proliferation signal which may pose an untenable risk when this is associated with an oncogenic insertional mutagenic event[26]. Similarly, from a gene therapy trial to resolve Wiskott Aldrich syndrome, although all patients demonstrate positive clinical outcomes to cell mediated therapy, 6 out of the 10 patients treated

developed T-cell acute lymphoblastic leukaemia. This reflects the predilection of retroviral vectors to target proto-oncogenes such as the LMO2 or MSD1 gene loci when used to transduce haematopoietic stem cells[27].

In light of the intended application of putative marker-suicide gene for application in neuroblastoma solid tumour cancer immunotherapy following from previous clinical trial results[5], research was performed using the MLV-based splicing gammaretroviral vector SFG[28].

All genetic modification strategies will impose a degree of risk which can only be predicted. However, a defining divergence between adoptive cellular therapies and conventional chemotherapy lies in the resolution of adverse events and therapeutic toxicities. In contrast to the resolution of undesirable side effects resulting from chemotherapy which can most frequently be resolved by passive discontinuation of therapy, the potential permanence of the therapeutic benefit from ACT represents both the primary reward and the greatest risk of these therapies. The greatest challenge of cancer therapy is to establish suitable targets that enable specific discrimination of the desired target for elimination. Adverse events following ACT represent a parallel with this scenario where specific elimination of the problematic adoptive cell population also poses a specificity challenge. Genetic modification with an entirely novel target imposes a risk for immunogenic deletion by the recipient, whilst a non-immunogenic host-derived target extends specificity of deletion beyond the adoptively transferred population. The challenge is to establish a suitable safety switch which enables effective deletion only when deletion is the desired outcome.

1.2. Historical overview of adoptive cellular therapy

1.2.1. Pre–genetic engineering ACT

The evolution of adoptive cellular therapies owes much to parallel pioneering research; HSCT/DLI therapy for haematological malignancies, TIL's for metastatic melanoma and EBV-CTL's for latent EBV reactivation each represent independent research tangents, all of which demonstrate the vast potential of adoptive cellular immunotherapy to resolve conditions which otherwise exceed the capacity for endogenous or compromised immunity alone.

1.2.1.1. HSCT

The rationale behind allogeneic haematopoietic stem cell transplantation (HSCT) was two-fold: as a rescue strategy, HSCT enables application of high-dose myeloablative radiation and/or chemotherapy, designed to improve anti-tumour therapeutic efficacy, but without supplementary haematopoietic rescue would prove lethal. Additionally, it was hoped that destruction of the bone marrow resulting from myeloablative conditioning followed by stem cell transfer would achieve replacement of the diseased haematopoietic system with one derived from the healthy donor[29]. Despite promise from animal modelling, initial attempts at HSCT proved largely unsuccessful; although the earliest cited attempt at a bone marrow transplant dates to 1939[30], it wasn't until 1959 that the first successful transplant was achieved[31]. Following from this success, it was a further six years before the first demonstration of sustained engraftment of donor marrow[32]. Finally by 1968, the first successful marrow transplants were achieved in patients with severe combined immunodeficiency and Wiskott-Aldrich syndrome. During the ensuing decades, successes from continuous advances to improve efficacy and reduce toxicity have converted HSCT from a treatment of last resort into a common, and in some instances, a first line therapeutic strategy against a wide array of haematological diseases[33]. In addition to malignant disease, HSCT is also considered for many non-malignant conditions including benign haematological disorders, immune deficiencies, autoimmune disorders, and even as a strategy to establish tolerance induction in preparation for solid organ transplant[29].

Early animal modelling experiments identified many of the key mechanisms underlying allogeneic HSCT, including: demonstration of bone marrow infusion as a successful rescue strategy against lethal irradiation, identification of the separate graft versus leukaemia effect in addition to the therapeutic benefit mediated by high dose therapy, and identification of graft versus host disease as highlighted by Figure 2[29].

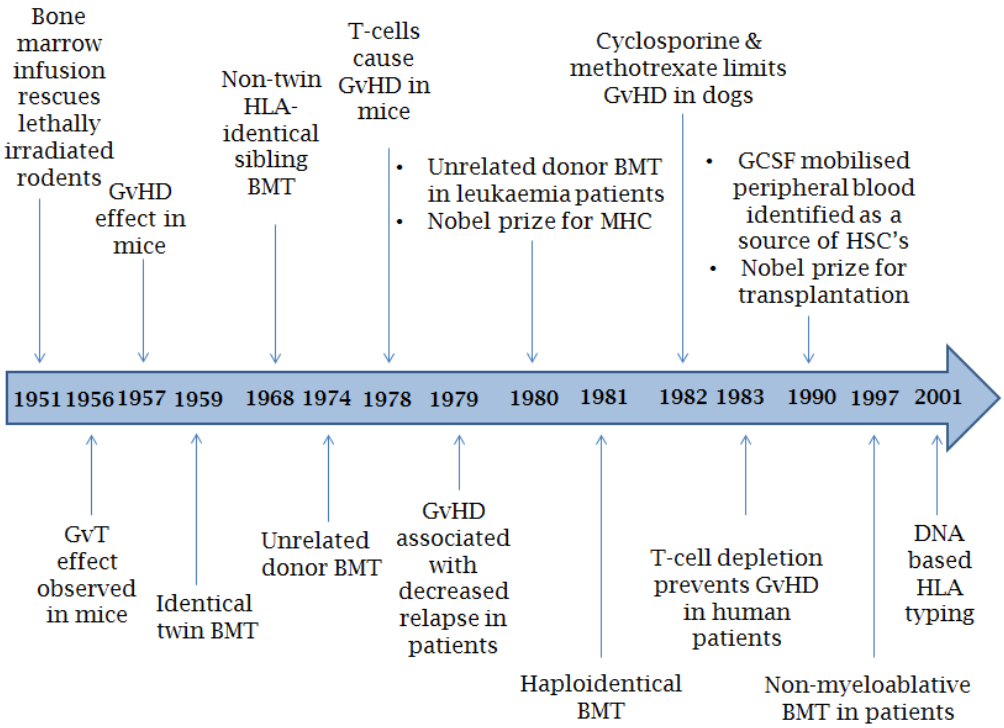

Figure 2 Milestones in haematopoietic stem cell transplantation (HSCT)
Adapted from Jenq *et al.*[29] Ongoing advances in the fields of transplantation therapy and molecular biology have enabled development of adoptive cell transplants to progress from a treatment of last choice into a first line therapy in many instances. This timeline highlights some of the key advances in HSCT.

However, further understanding of the underlying mechanisms involved in the GvL and GvHD effects required identification of the major histocompatibility complex (MHC). The MHC was initially identified as the genetic region encoding tissue antigens which elicit graft rejection when recognised as variant from 'self'[34]. Discovery of the human leukocyte antigen (HLA) system led to development of histocompatibility tissue typing methods; initially achieved through serological techniques, recent advances in molecular typing have reduced donor-recipient mis-matching thereby reducing toxicity but thus imposing a concurrent reduction in the potential donor pool. Following identification of the role of T-cells as mediators of the GvHD effect, T-cell depletion from allografts was premised as a strategy to reduce toxicity. However, although this successfully resolves GvHD, it also increases the risk of relapse highlighting the relationship between the GvL and GvHD effects[33]. These observations helped to establish the immunological capacity for effector cells from the donor inoculum against malignancy, thus establishing HSCT as the earliest form of individualised adoptive cellular cancer immune therapy[29].

A biological definition for haematopoietic stem cells is: the population of cells which are capable of rescuing lethally irradiated animals[33]. Although demonstration of the bone marrow as a source of stem cells had been established through recovery of rodents following lethal irradiation[35], a breakthrough in the identification of human stem cells was the identification and association of the CD34 cell surface protein as an identifying marker on haematopoietic progenitors followed by the subsequent demonstration of haematopoietic reconstitution in lethally irradiated baboons using this subpopulation[36]. Subsequent discovery for the potential of granulocyte macrophage colony stimulating factor (GM-CSF) to mobilise CD34 stem cells into the peripheral blood enabled blood to be exploited as a source of stem cells expanding the potential scope for HSCT therapy[37].

Following from identification of the major histocompatibility complex (MHC), preparative regimens perform two key functions: to eradicate underlying disease, and to provide sufficient immunosuppression to enable administration of the graft without subsequent rejection. However, much of the expense associated with HSCT results from risks and complications occurring both during and following treatment requiring hospitalisation and/or further therapy. In addition to GvHD, mucositis, veno-occlusive disease and pulmonary complications pose the most common therapy related complications whilst fungal and viral re-activation resulting from immunosuppression pose frequent infection related complications. Finally, long-term survivors remain at increased risk for secondary malignancies and patients whose preparatory regimen included total body irradiation are at greater risk for developing cataracts. Thus, strategies designed to reduce toxicity and complications not only reduce morbidity and mortality related to HSCT, they also reduce therapeutic expense.

1.2.1.2. DLI

As the effectors of cell mediated immunity, T-lymphocytes offer great potential for therapeutic resolution of both malignant and infectious disease. Consideration of the therapeutic potential for T-cell mediated immunity facilitated through donor lymphocyte infusion (DLI) therapy resulted in parallel research tangents, three of which are discussed further below.

1.2.1.2.1. DLI following HSCT

Prior to the advent of donor lymphocyte infusion (DLI), therapeutic options for patients who developed graft failure or disease relapse were limited to HSCT. However, the identification of T-cells as the mediators of the GvL effect coupled with observations that T-cells reactive to minor histocompatibility antigens could inhibit leukaemia, (as observed through *in vitro* and *in vivo* modelling experiments) led to the development of DLI, proving to become the next major advance for adoptive cellular therapy[38]. The initial test of DLI was as a salvage therapy for relapsed haematological malignancy following allo HSCT[39]. In this trial, three chronic myeloid leukaemia (CML) patients who had relapsed post HSCT were given supplementary DLI in the absence of additional chemo- or radiotherapy. Following DLI therapy, all patients demonstrated effective haematologic and cytogenetic remission, thus supporting the capability of subsequent adoptive immunotherapy to achieve therapeutic efficacy. Subsequently, DLI therapy post-transplant relapse was extended to further haematological malignancies including multiple myeloma, lymphomas and acute leukaemias, although therapeutic efficacy appears disease dependent with response rates optimal against CML followed by lymphoma, multiple myeloma and acute leukaemias respectively[38].

Building upon initial promise, DLI offered the potential for cellular infusion following reduced intensity conditioning (RIC) regimens, promising to achieve the beneficial allogeneic GvL effect but with a reduced transplant related toxicity associated with autologous stem cell transplants. In this scenario, RIC provides haematological space to enable donor cells to engraft whilst imposing sufficient immunosuppression to prevent rejection. The lower toxicities associated with RIC regimens enable application for patients who are older or who present with significant co-morbidities[38].

However, as with HSCT, GvHD remains a common therapeutic complication following DLI, typically occurring in 50-60% of recipients but with the benefit of indicating an anti-tumour response typically associated with longer disease-free survival. Further, there is a lower mortality resulting from DLI-associated GvHD thought to result from the absence of preconditioning regimens. Post-DLI aplasia represents the other primary therapy-associated complication occurring at a frequency up to 40%[38].

Further, in contrast with HSCT, DLI offers greater potential to resolve GvHD through genetic modification of the adoptive cellular population. Concurrent advances in cellular engineering presented a novel solution to the problem posed by GvHD through inclusion of dlNGFR and HSVtk as marker and suicide genes respectively[40]. Thus, DLI represented a bridging technological advance; coupled with the potential for genetic modification of the DLI, all that remained outstanding was the development of strategies to mediate cellular retargeting.

1.2.1.2.2. Tumour infiltrating lymphocyte infusion therapy

Early pioneering research by Rosenberg *et al*[41] demonstrated the potential to exploit endogenous anti-tumour immunity as a novel therapeutic modality. It was observed that tumour infiltrating lymphocytes (TIL's) could be isolated from tumour resections, expanded *ex vivo* and returned to the patient demonstrating therapeutic benefit. The TCR receptors of these TIL's recognised tumour associated antigens (TAA's) present in the metastatic melanoma resections. However, identification and isolation of effective TIL's from tumours is variable dependent on the immunogenicity of the TAA's present in the tumour.

1.2.1.2.3. EBV–CTL infusion therapy

One further demonstration of successful DLI therapy follows from resolution of Epstein-Barr virus (EBV) associated post-transplant lymphoproliferative disorder (PTLD) facilitated through EBV-specific cytotoxic T-lymphocyte (CTL) DLI. Although more than 95% of the global adult population are infected with EBV, disease is typically self-limiting controlled by the T-cell mediated cellular response. However profound immunosuppression applied alongside HSCT or solid organ transplant can induce viral reactivation resulting in unchecked EBV-driven B-cell lymphoproliferation. Peak incidence occurring 6-12 months post-transplant suggests a role of impaired T-cell function in this pathology[42]. One solution to this problem, first demonstrated by Papadopoulos *et al*[43], involves adoptive transfer of virus-specific CTL's. Additionally, EBV-CTL's represent an attractive source for therapeutic product for two reasons: Firstly, the selection of EBV-CTLs as the source for allogeneic cellular product presents a considerably reduced risk for potential GvHD due to the defined specificity of the T-cell receptor[44], and secondly, exploitation of anti-viral immunity concurrent with T-cell re-engineering strategies offers potential for

enhanced persistence and anti-tumour efficacy of CAR-modified T-cell product[5].

1.2.2. Post–genetic engineering ACT

Advances in molecular biology have increased the opportunities for genetic engineering and allow for ever-increasing modifications to optimise the capacity of GM T-cells to achieve a safe and effective anti-tumour immune response and even novel functional capabilities, such as: molecular re-targeting mediated through inclusion of a TCR or a CAR moiety; drug resistance capability such as calcineurin or mycophenolate resistance; modifications to trafficking behaviour to home toward tumours; ability to secrete cytokines to enhance a desired immune response; enhanced proliferative capacity and/or survival; and, inclusion of a marker gene for assessing persistence and a suicide gene for resolution of therapeutic toxicity as illustrated by Figure 1.

1.2.2.1. Transgenic T–cell receptors

However, despite initial success demonstrated by application of TILs against metastatic melanoma, this process remains costly, time consuming and limited by the inherent immunogenicity posed by novel tumour antigens. Hence, concurrent with advances in molecular biology, research shifted towards identification of alternative TAA-specific TCR's. Using integrating retroviral transduction, T-cells can be transduced with TCR α and β chains demonstrating a desired specificity to redirect T-cells against tumours expressing the appropriate TAA's. However, despite the promise which this strategy offers, it is not without limitation or risk. As TCR-mediated cytotoxicity is MHC restricted, down-regulation of MHC-I presentation represents a common immune escape mechanism available to cancer[45]. Also, due to MHC-restriction, transgenic TCR genes identified from tumour resections remain restricted to application within a subset of potential patients limiting the breadth of application. Further, this strategy imposes the risk for TCR mispairing whereby hybrid TCR's could result from cross pairing of the endogenous and transgenic TCR's within the cell, resulting in novel receptor specificities which could lead to pathological autoimmunity as demonstrated through mouse modelling experiments[46]. One strategy employed to circumvent this potential involves engineering of a hybrid TCR composed of murine and human regions to prevent mispairing. However this strategy may

restrict potential for clinical application due to induction of neutralising antibodies against the murine epitopes[14]. Despite these limitations, therapeutic application of TIL's has proven highly effective against metastatic melanoma highlighting the potential for TCR-mediated gene transfer as a strategy to mediate physiological anti-tumour adoptive T-cell therapy.

1.2.2.2. Chimeric antigen receptors

Advances in the understanding of both the similarity and variation between T- and B- cell receptor-mediated antigen recognition led to consideration of the potential for ectopic expression of antibody defined specificity on T-lymphocytes to enable targeted re-definition of the cell mediated immune response in an MHC independent manner. Development of this research tangent resulted in the evolution of T-bodies, clearly reviewed by Eshhar[47], which represent the precursor of chimeric antigen receptors (CAR's).

However, initial CAR trials employing first generation CAR-retargeted T-cells against solid tumour targets typically proved disappointing; although cellular infusions were well tolerated, reports of therapeutic success were rare. In contrast, later trials involving later generation CAR-mediated therapy against haematological malignancies remain a developing clinical success story[21, 48].

MHC-independence also presents a challenge to CAR T-cell function due to alterations of endogenous T-cell signalling mechanisms. Optimal T-cell stimulation requires 3 signals: signal 1, Antigen recognition mediated via the TCR; signal 2, target validation mediated through co-stimulation (e.g. CD28); and signal 3, a cytokine support signal (e.g. IL2). Therefore, although inclusion of the CD3ζ stimulation domain alone enables some anti-tumour capacity by a CAR, achieving effective engraftment and sustained anti-tumour activity has required generation of second and third generation CARs containing additional co-stimulation domains.

CARs, as illustrated by Figure 3, offers a ready solution to limitations imposed by TCR-retargeting strategies. CARs exploit the humoral equivalent to the TCR, notably antibodies, which compose the soluble form of the B-cell receptor, to enable HLA-independent, target specific re-direction of T-cell immunity. Genetic retargeting of T-cells using CARs has a number of distinct advantages over the TAA-specific TCR strategy: MHC I restriction independence, a shorter and simpler production protocol required to generate therapeutic T-cell

product, and enhanced proliferation and survival profile according to variation of the signalling endodomain component of the receptor. First generation CAR's were bipartite constructs composed of an antibody-derived binding moiety for target recognition fused to a lymphocyte activating signalling chain. Observations of limited *in vivo* persistence from first generation CARs resulted in the generation of second and third generation CARs including addition of second and third signalling components within the endodomain respectively.

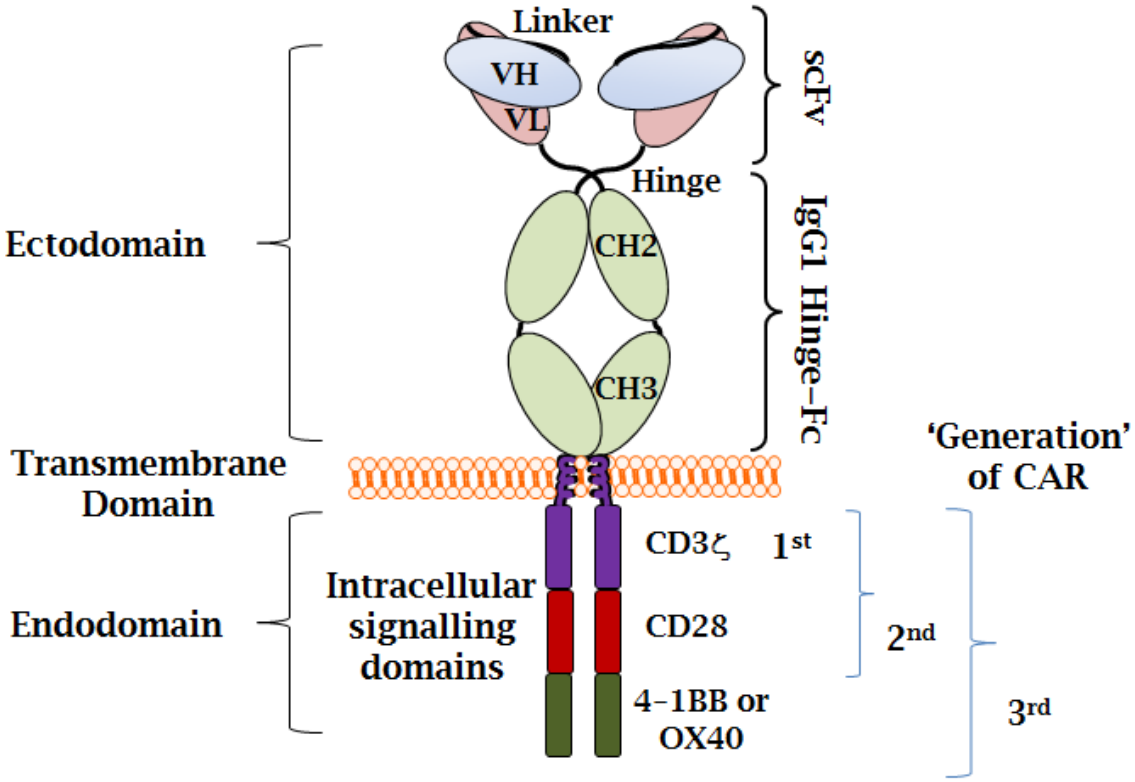

Figure 3 Cartoon illustration of a chimeric antigen receptor
Chimeric antigen receptors offer the potential for molecular retargeting of T-cells. They are composed of the variable regions derived from a monoclonal antibody joined by a serine-glycine peptide linker sequence. A molecular spacer or hinge domain facilitates projection of the binding domain away from the cellular surface whilst intracellular co-stimulation signalling domains mediate signalling to compensate for the lack of TCR and MHC co-stimulation. scFv - single chain, VH/VL Variable chain heavy and light chain respectively, CH2-CH3, antibody IgG1 constant heavy domains (2 and 3 respectively).

However, despite the promise, clinical trial results from ACT employing T-cells re-directed with first generation CAR's proved somewhat disappointing as the therapeutic T-cell product demonstrated limited *in vivo* survival and anti-tumour activity[49, 50]. Evolution on this theme led to co-stimulation strategies to enhance transduced T-cell persistence. Transduction of EBV-CTL's with a GD2-CAR for neuroblastoma therapy exploited the endogenous stimulation

afforded by EBV-positive patients and demonstrated prolonged persistence compared with a polyclonal transgenic T-cell population, demonstrating tumour regression in half of the subjects treated[5]. Alternative strategies involve inclusion of additional co-stimulation domains to enhance T-cell persistence and anti-tumour activity.

1.2.3. Summary

The field of ACT has evolved substantially from initial successes. Ever increasing potential for cellular engineering offers vast potential for cancer immunotherapy. However, as clinical experience from application of engineered cells remains limited, there are likely many lessons left to learn.

Novel hazards arise coincident with technological and therapeutic advances. Clear benefit demonstrated by gene therapy for primary immunodeficiencies[51] was swiftly overshadowed by the risk posed by insertional mutagenesis[52]; gene therapy for cancer has shown great promise, yet challenges with target specificity, dosage, toxicity and the potential of unchecked lymphoproliferation of therapeutic product remain. Inducible pluripotent stem cell (iPS) technologies offer great promise, however teratoma formation, inherent to the nature of iPS cells, also represents the greatest risk posed by this new technology. Future applications such as universal donor T-cells and advanced genetic engineering strategies involving zinc finger nucleases (ZFNs), TALENS, and genomic integration strategies each present further potential concerns.

Owing to limitations in the predictive value of animal modelling and safety profiling, the ever increasing applications of cell based technologies highlight the pressing need for a universal safety mechanism which offers simplicity, efficacy and compatibility to complement present and future cellular therapeutic modalities. This said, as animal modelling offers the only mechanism by which to model the complexity imposed by cellular therapies, it remains a necessary process in the pre-clinical work-up to validate these novel therapies prior to clinical application.

Reflecting research presented in this thesis, the following will briefly summarise the common allogeneic transfer toxicity: graft versus host disease.

1.3. GvHD

Graft versus host disease is an immunological therapeutic toxicity which has been identified following the advent of grafting. GvHD is a multi-organ disorder with damage most obvious to the skin, gastrointestinal tract and liver and remains a potentially lethal toxicity despite advances in chemotherapeutic resolution.

1.3.1. GvHD background

GvHD is a severe inflammatory reaction representing the most serious complication following HSCT. Without post-transplant immunosuppression, most patients will develop GvHD. Observations regarding presentation of GvHD led Billingham to propose the following three preconditions as necessary to establish GvHD[53]: immunologically competent mediators (mature T-cells) must be present within the graft to produce the response; the recipient must be immunocompromised to prevent allograft rejection, and finally, the recipient must express tissue antigens variant from donor antigens to act as an antigenic target to trigger the response. Although corticosteroids remain the first line therapy, successful resolution is only achieved in approximately one-half of cases[54]. Therapeutic strategies for steroid-refractory GvHD vary but may include immunosuppressive cocktails, anti-thymocyte globulin or antibody therapy[55], however even these strategies only achieve therapeutic resolution in approximately 75% of cases whilst imposing increased risk for infection resulting from immunosuppression[56]. Thus, despite advances in prevention of GvHD, progression to grade IV acute GvHD remains a fatal outcome in most cases[54].

1.3.2. GvHD immunology

GvHD results from T-cell allorecognition, which is defined as the ability of T-cells to recognise non-self MHC molecules derived from the same species. Such GvHD reflects the ability of T-cells to respond against cellular antigens which differ in their expression pattern between the donor and the host. With human leukocyte antigen (HLA) mismatched transplants, alloreactive T-cell responses occur against both epitopes on HLA molecules as well as peptide HLA complexes. However, GvHD responses can also result from a matched donor transplant induced by polymorphic genes known as minor histocompatibility antigens[57]. As proposed by Janeway[58], the adaptive immune system evolved to

enable organisms to discriminate the infectious non-self from the non-infectious self. A central feature of the adaptive immune response is the T-cell recognition principle, in that thymic development restricts T-cell recognition of peptide to that presented in the context of self-MHC. Strongly self-reactive T-cells are negatively selected, whilst T-cells with moderate self-recognition are positively selected. However T-cells have also been shown to mount immune responses against allogeneic peptide-MHC complexes, contrary to the tenet of MHC restricted presentation. Evidence for this observation suggests that T-cell allorecognition requires both peptide and MHC interactions akin to the cognate TCR-antigen recognition. The prevailing arguments for these observations are the 'mistaken identity' and the *'déjà vu'* hypotheses. Briefly, the 'mistaken identity' premise holds that it is possible for the conformational structure generated by alternative antigenic epitopes to demonstrate sufficient similarity as to enable an alternative binding solution for a TCR-peptide-MHC interaction, whereas the *'déjà vu'* hypothesis suggests that a slight variation in the architecture of an alternative TCR-peptide-MHC interaction could prove sufficiently similar to a previous activation signal as to be considered effectively identical[59]. Regardless of the mechanism involved, the allorecognition response has a precursor frequency 100 to 1000 times greater than any equivalent foreign peptide-MHC complex specificity[60]. Thus, in the absence of autologous or syngeneic donor cells, potential alloreactivity will always pose a risk.

As therapeutic resolution of GvHD remains problematic, many experimental strategies remain under consideration designed to prevent development of, or progression to GvHD, including: selective depletion to exclude alloreactive T-cells[61], co-infusion of mesenchymal stem cells alongside haematopoietic stem cells[54], low dose interleukin-2 (IL2) supplementation to enhance regulatory T-cell (Treg) activity[62], and infusion of Treg's prior to HSCT infusion[63]. Cell processing strategies for therapeutic cell product to prevent the risk for alloreactivity of adoptive cells include: photodynamic or pharmacologic elimination of allospecific T-cells, regulatory T-cell enrichment of the infusion product and *ex vivo* anergisation of patient responsive T-cells[64]. However, as adoptive cell therapies already pose a high economic burden, the desire to reduce GvHD must be balanced against the potential effect additional handling would impose on the efficacy of the therapeutic product.

Therefore, allogeneic adoptive cell therapies face the challenge of opposing evolutionary adaptation of T-cell recognition of non-self MHC molecules. Hence, there remains a therapeutic need to enable strategic resolution of GvHD by selective deletion of the pathology-inducing population for adoptive cell therapies.

1.4. T–cell engineering

As adoptive cellular therapies represent a broad and rapidly growing field, this discussion will focus on T-cell engineering as a strategy for cancer immunotherapy. Genetic modification of T-cells allows us opportunity to enhance, re-direct and engender T-cells with functionalities which can greatly enhance therapeutic potential beyond natural limitations. However, therapeutic benefit is accompanied by theoretical risk; thus gene transfer strategy, therapeutic protocol and transgenic cassette all present potential variables to be considered when generating cellular product.

1.4.1. Gene transfer strategies

Implicit to T-cell effector function following target recognition is cellular proliferation. Correspondingly, consideration regarding T-cell genetic modification strategies must rely on integrating vectors to ensure effective sustained transgene expression by cellular progeny. Although a range of genetic modification strategies exist, discussion will focus on the three integrating vector strategies in current clinical application: retroviral vectors, lentiviral vectors and transposons. In the interest of brevity, discussion will focus on key variations between these strategies; namely transduction requirements and integration bias.

1.4.1.1. Retroviral vectors

The desired role of a retroviral vector is to achieve stable integration of a replication deficient provirus into chromosomal DNA. Due to the simple genomic architecture of gammaretroviruses combined with powerful constitutive promoters, vectors derived from the Moloney murine leukaemia virus (MLV) remain the most frequently employed strategy to achieve transgene integration for T-cell gene transfer[65, 66]. Three key stages must occur to achieve successful transduction: viral entry, reverse-transcription and proviral integration. Viral entry is mediated through either receptor mediated

endocytosis or viral envelope/plasma membrane fusion. Following entry, the retroviral plus-stranded RNA genome must then be modified and transported to the nucleus. Reverse transcriptase, supplied by the vector, converts the ssRNA genome into dsDNA. This is followed by formation of the pre-integration complex (PIC) which combines the dsDNA genome along with viral and host proteins to mediate transport to the nucleus. However, as the PIC of gammaretroviruses such as MLV are relatively unstable, these are unable to cross the intact nuclear membrane of non-dividing cells[33, 67]. Therefore, a key limitation to retroviral transduction relates to the obligatory requirement for stimulation which has been shown to negatively impact antiviral immunity and alloreactivity and skew cellular phenotype[68, 69]. Further examination of stimulation imposed limitations necessary for retroviral transduction protocols suggest that increasing cellular dosage or depletion of Tregs prior to stimulation can enable retention of the desired cellular effector capacity[70].

1.4.1.2. Lentiviral vectors

In contrast to retroviral vectors, the PIC of lentiviruses such as HIV-1, is relatively stable allowing for transport across an intact nuclear membrane[33]. Hence, the capability to transduce quiescent cells attracted keen interest into application of lentiviral vectors as an alternative to retroviral mediated strategies. Discussion will focus on HIV-1 derived lentiviral vectors which compose the majority of lentiviral vectors in current application.

A key advantage of LV transduction is the preservation of a less differentiated T-cell phenotype. Although stimulation is required to achieve effective retroviral transduction, mitogenic stimulation of T-cells via the T-cell receptor is associated with a loss of naïve T-cell subsets resulting in reductions in immune functionality, inversion of the CD4/8 ratio, and alterations to the TCR repertoire[71]. Although activation of T-cells from G_0 to G_{1b} appears necessary to enable LV-mediated gene delivery, effective LV transduction efficiency has been demonstrated using IL7 cytokine stimulation ensuring retention of the phenotype, antiviral and allogeneic responsiveness[69, 72].

As the HIV-1 lentiviral genome is considerably more complex than gammaretroviral genomes, there has been progressive evolution of lentiviral vectors in the attempt to ensure biosafety from these gene transfer vehicles, with second or third generation LV composing the bulk of vectors in current

application with third generation LV offering the best safety profile. Third generation LV production only requires 3 of the original 9 HIV genes, whilst significant deletions to the viral LTR domains establish self-inactivating (SIN) vectors which demonstrate LTR independence from viral factors. Furthermore, separation of plasmids required for viral production ensure that three separate recombination events would be required to generate replication competent lentivirus (RCL). However, enhanced biosafety is achieved at the cost of reduction in viral titre, although the capacity for the VSVg envelope to withstand ultracentrifugation, and thereby enable concentration of viral particles, partially compensates for this limitation[73].

Perhaps an additional concern regarding the risk of application of LV as a vector is the increasing prevalence of HIV within the population. Presence of competent virus pre- or post-therapy offers the potential risk for RCL resulting from use of an integrating virus which may impose further limitations on the use of these vectors in gene transfer applications.

1.4.1.3. DNA–transposon mediated gene delivery

The final integration strategy to be discussed involves use of transposons to introduce defined DNA sequences into genomic DNA. There are currently two transposon/transposase systems offering potential for T-cell gene transfer application: sleeping beauty[74] and *piggyBac* [75].

DNA transposons are class II transposable elements offering a simple genomic organisation optimal for potential application for gene transfer. Excision and integration of the transposon element is mediated by the transposase enzyme, with the transposon element/cassette defined by internal terminal repeats containing the binding sites required to enable transposition. Safety of this system is achieved through simple separation of the transposase enzyme from the transposable DNA resulting in generation of a non-autonomous transposable element[76]. Hence, a key benefit of transposon delivery in contrast to viral vectors is the abrogation of risk from potential replication competent virus which imposes a significant financial burden into gene transfer protocols[77].

1.4.1.4. Vector integration bias

The second key variation between integration strategies involves integration bias demonstrated by the various vector strategies.

MLV derived vectors, such as SFG[28], demonstrate non-random integration patterns within T-cells, showing clear site-specific preference for promoters and regulatory regions of genes which are transcriptionally active at the time of transduction. MLV site specific integration preference suggests a possible association between components of the RNA polymerase II transcriptional machinery and the MLV PIC, which further indicates that the risk from MLV-mediated IM could vary dependent upon both the transcriptional activation status and target cell being transduced. Analysis of MLV T-cell integration sites, pre- and post-infusion, from patients enrolled in HSVtk/ΔlNGFR clinical trials demonstrate clustering patterns for MLV integration events with genes targeted by MLV clusters showing association in functional networks involved in T-cell function. However, post infusion analysis of integration clusters showed little or no preference towards genes involved in signal transduction, cell proliferation or proto-oncogenes. Thus, in contrast to the perceived risk, this variation between pre- and post-infusion integration profile suggests a negative selective pressure on T-cells where integration events affect T-cell specific functions[78]. However, as the transgenes involved in this analysis confer no proliferative advantage, this promising absence of genotoxic risk may not be generally applicable to all MLV vector transgenes.

Similarly, a retrospective analysis of HIV-1-based LV lentiviral vector integration in CD4 T-cells identified preferential integration within active transcription units. HIV-1 LV appears to favor integration into weakly conserved primary sequence, preferentially targeting gene rich chromosomes. Although there appeared to be no bias towards integration proximal to proto-oncogenes, it was noted that integrations near 5' ends of proto-oncogenes remained higher than anticipated occurring by chance alone[79]. Perhaps the best support for safety of LV integration is the single report citing HIV-mediated transformation into lymphoma despite extensive global HIV infection rates[80]. However, enhanced survival mediated by anti-retroviral therapy may increase observation of similar events.

Evidence from sleeping beauty transposon integration patterns indicates no preference for integration within transcription units or proximal to transcription start sites[81]. Although T-cell integration analysis for the *piggyBac* transposon indicated a non-random integration profile with a preference for transcriptional units, *piggyBac* integration within transcription start sites for

proto-oncogenes remained lower than frequencies identified for either RV or LV integration[82]. Following extensive examination of viral integration events, evidence suggests that despite observed frequencies for viral integration proximal to proto-oncogenes, oncogenic transformation remains restricted within a small subset of these integration events suggesting a requirement for subsequent 'hits' to incur uncontrolled cell proliferation[77].

Finally, the sleeping beauty transposon system offers a superior safety profile with respect to alternative integrating vector strategies although transgenic cargo capacity remains the key limitation. In this respect, a minimal sort-suicide gene may offer the greatest potential for this application enabling maximum function alongside the safest integration strategy.

1.4.1.5. Gene transfer strategy summary

Despite the improved safety profile, analysis of viral integration in haematopoietic progenitors highlights the possibility of SIN LV integration into genomic regions which can result in proto-oncogene upregulation and therefore the risk for insertional mutagenesis mediated toxicity remains[83]. Overall risk may vary dependent upon many factors which may prove additive in combination, including: target cell for modification, transgene and presence of co-stimulation, or integration risk combined with associated therapeutic genotoxicity, thereby excluding broad general extrapolations. Limited extended follow-up involving second and third generation CAR trials may have overestimated safety of CAR co-stimulation. Perhaps CD19-CAR clinical trials will offer defining insight into optimal gene transfer strategies for T-cells as all three integration strategies discussed are in current application in clinical trials[84]. Therefore, integration strategy selection may ultimately depend upon a range of factors including cellular target, transgenic cassette and therapeutic aim with no single strategy proving optimal for all scenarios.

As a final note, research into alternative strategies remains ongoing; hence, mRNA electroporation[85] has been proposed as an alternative approach for gene transfer to address toxicity and risk posed by integrating vectors. Although this strategy achieves rapid gene expression, detectable as early as thirty minutes post transfection, gene expression remains transient only lasting up to seven days.

1.4.2. Risks associated with genetic engineering

However, coincident with desired anti-tumour efficacy, manipulation of the immune response may result in unforeseen and undesirable toxicities. Four primary safety concerns regarding T-cell therapy have been identified: insertional mutagenesis: toxicity resulting from the introduction of genetic material; on-target, off-tumour toxicity (OTOT): aberrant deletion of non-tumorous tissue; immunological toxicity following therapeutic infusion such as GvHD resulting from an allogeneic response or autonomous proliferation independent of antigen/target binding, and finally, therapeutic toxicities resulting from concomitant therapy parallel to ACT, such as toxicity resulting from the preconditioning regimen, or sustained immunosuppression[84].

1.4.2.1. Insertional mutagenesis (IM)

As any alteration to the genome is mutagenic, risks resulting from genetic modification can only ever be predicted. Furthermore, integrating vectors may impose mutagenic toxicity through a range of mechanisms. As the retroviral LTR can function as an efficient promoter/enhancer sequence, the primary risk from LTR-mediated gene expression is the potential impact upon cellular gene expression. Interaction between cellular transcription factors and the integrated viral LTR can result in activation of adjacent cellular proto-oncogenes. Although this is most readily apparent through aberrant growth associated with oncogenesis, impacts such as transcriptional read-through may impair cellular functions without obvious phenotypic effect. As observed from the SCID trial[52], this risk may reflect an additive impact resulting from both the transgenic cassette and the integration site. Alternatively, direct vector insertion within coding sequences may cause deletion or abnormal truncation of cellular transcripts[86]. Further, vector enhancer sequences have been demonstrated to mediate dysregulation of endogenous gene expression of genes located hundreds of kilobases from the viral integration site[87]. Additionally, vector insertion may cause genomic disruption through impacts upon genetic regulatory domains resulting in altered splicing or polyadenylation[88] or by alterations to microRNA cistrons, thereby impairing the internal cellular regulatory machinery[89]. Finally, even application of SIN-lentiviral vectors doesn't preclude potential for phenotoxicity resulting from non-physiological activation of adjacent loci to vector insertion sites, such as *HMGA2* activation as observed in the β-thallassaemia trial[90].

Recent reports of leukaemic risk from insertional mutagenesis from the X-SCID clinical trials demonstrated a clear risk from gene marking, thus terminating further gene marking studies due to the absence of clinical benefit[91]. However substantial research suggests that the degree of risk appears dependent upon multiple factors including the cellular target for genetic modification and the transgene involved. Perhaps to put the risk from retroviral modification into perspective, it has been proposed that between 4-10% of the vertebrate genome is composed of retroviral remnants[92]. Moreover, this fraction is greater than that corresponding to gene encoding sequences. Viewed in this light, perhaps the nature of the transgenic cassette coding sequence presents a far greater risk than the genetic modification strategy. To date, despite over a decade of T-cell engineering clinical trials, there remains to be a single incidence of clonal proliferation resulting from T-cell modification[25]. This may reflect a reduced sensitivity for transformation present in T-cells compared with haematopoietic stem cells[93].

1.4.2.2. On target, off–tumour toxicity (OTOT)

Immunotherapy requires the presence of an antigenic target to enable identification of the cancer cell. These tumour associated antigens (TAAs) can be segregated into five categories[94]: i) tumour specific antigens, such as characteristic mutated antigens which remain truly tumour specific such as the BCR-Abl 'Philadelphia chromosome'[95], ii) overexpressed antigens where expression of a normal cellular protein may be significantly upregulated by a tumour, such as tyrosinase in malignant melanoma[96], iii) oncofoetal antigens; antigens expressed during foetal development but are rarely expressed in adult tissue, such as alpha fetoprotein[97] and carcinoembryonic antigen (CEA)[98], iv) differentiation or lineage antigens such as CD19 in B-cell leukaemia and lymphomas, and finally v) testis antigens shared by spermatocytes and tumour cells, such as MAGE antigens[99]. Thus, apart from rare cases such as viral proteins or characteristic mutations, expression of most tumour antigens is not exclusive to the tumour target.

As a result, targeted immunotherapy may also result in OTOT. In some cases, collateral damage resulting from therapeutic deletion of 'expendable' tissue may be readily resolved such as with CD19, where depletion of the B-cell compartment can be compensated with gamma globulin replacement therapy. Although CAR's are based on antibody technology which can enable binding

affinities extending beyond the affinity which can be achieved through T-cell isolation, OTOT can result from either CAR or TCR redirected T-cells. Furthermore, although pre-clinical animal modelling experiments may offer insight into the capacity for T-cell targeting efficacy, these models can never fully reflect the scenario within a human patient. Therefore, despite much promise, there have been a number of adverse events resulting from T-cell cancer immunotherapy as summarised by Table 2. Examples include: when T-cells were directed against minor-histocompatibility antigens to treat leukaemic relapse, severe toxicity resulted from target antigen expression on lung tissue[100]; during a recent clinical trial involving transgenic T-cells specific for ERBB2, low level expression of the target antigen on lung epithelium resulted in a lethal cytokine storm[20]; therapeutic application of modified T-cells against MART-1 in melanoma therapy was associated with toxicity to melanin-expressing cells in the inner ear and the retina[101]. In a trial against metastatic colorectal cancer involving TCR retargeted autologous cells against the CEA antigen, a dose limiting toxicity of severe transient inflammatory colitis was observed[102]. CAR re-targeted T-cells against the renal carcinoma target, carbonic anhydrase IX (CAIX), resulted in liver toxicity due to target antigen expression on bile duct epithelium[103]; and finally, TCR retargeted T-cells against the MAGE-A3 antigen resulted in neural toxicity with two patients eventually succumbing from the neural insult[104].

Further, the risk of potential TCR mis-pairing raises the spectre for generation of novel specificities of unknown toxicity generated by the inadvertent cross-pairing of transgenic and endogenous TCRs. Experiments in rodent models have demonstrated that this raises the risk for autoimmunity and GvHD[46]. Therefore TCR-mediated re-targeting strategies commonly employ a hybrid TCR domain including murine regions to exclude risk for cross-pairing. Although application of this strategy improves safety, it may also limit efficacy due to potential immunogenicity of the transgenic TCR[14].

Table 2 Therapeutic toxicities resulting from re–targeted T–cells
(Adapted from Shi *et al*[105].)

Retargeting modification	Antigen	Toxicity
CAR	CAIX	Liver toxicity[103]
CAR	ERBB2	Lung toxicity, cytokine storm[20]
CAR	CD19/CD20	B-cell aplasia, tumour lysis syndrome, cytokine release syndrome, macrophage activation syndrome[106]
Ex–vivo expanded T-cells	Minor histocompatibility antigens	Pulmonary toxicity[100]
TCR	MAGE-A3	Neurological toxicity[104] Cardiac toxicity[107]
TCR	CEA	CEA expressed in normal colonic mucosa[102]
TCR	MART-1	Melanocytes in skin, eye and ear[101]
TCR mis-pairing	Self-antigens	GvHD / autoimmunity Proposed toxicity identified from *in vivo* modelling experiments[46]

1.4.2.3. Immunological toxicities

A further risk associated with genetically engineered T-cell include immunological toxicities such as GvHD resulting from TCR cross-pairing or alloreactivity as previously addressed, *vide supra*.

Also, supraphysiological stimulation and/or signal leakage from later generation CAR's can theoretically result in cellular proliferation in the absence of cognate antigen recognition. Further, combination of possible insertional mutagenesis coupled with potential selective advantage mediated by co-stimulation domains could pose an untenable risk of lymphoproliferation in the absence of a regulatory control mechanism such as a suicide gene. However it should be noted that in the event of an acute immunological toxicity such as a cytokine storm, it is unlikely that by the time toxicity has been identified, that the physiological impact could be resolved by any suicide-gene strategy alone.

1.4.2.4. Concomitant therapeutic toxicities

Therapeutic toxicities resulting from lymphodepleting regimens such as post-transplant lymphoproliferative disease[108] may also arise, however as these require alternative strategies for resolution separate to application of suicide gene machinery, these will not be discussed further.

1.4.2.5. Risks associated with genetic engineering summary

Despite significant clinical success, T-cell cancer immunotherapy remains in its infancy with many lessons yet to be learned. Research into further alternative T-cell modification strategies remain under development; retargeting achieved by transient gene expression following electroporation with mRNA offers transient gene expression thereby avoiding risk for insertional mutagenesis. Alternatively, selective modification of γδ T-cells may offer a strategy to reduce the risk from supraphysiological stimulation from later generation CAR's as therapeutic administration of aminobiphosphonate can mediate selective proliferation of this population post infusion potentially reviving potential for first generation CAR therapy[84]. With a view towards stream-lining gene therapy for improved accessibility, various groups are investigating strategies designed to achieve 'universal T-cells'[109] such as through deletions of the endogenous TCR through genomic editing strategies which may offer therapeutic transfer across MHC barriers, by selective modification and differentiation of HSC's or otherwise[84].

As research into better targets remains ongoing, perhaps improved specificity can be achieved in the future through further engineering; however, the risk of OTOT will likely remain to be established for every individual TAA. Therefore, inclusion of a suicide gene to offer a degree of protection from some of the risks posed by T-cell cancer immunotherapy remains a pressing need.

1.5. Marker genes and gene marking

A marker gene encodes for a protein absent from unmodified cells, which can enable selective identification and selection of genetically modified cells.

1.5.1. Historical overview

Excellent reviews by Barese[110] and Tey[91] explore the historical progression of gene marking within cell and gene therapy. As it was the outcome of early pioneering efforts which established the foundations for subsequent gene

transfer applications and protocols, some of the key advances which have resulted from gene marking studies will be summarised as follows.

At the advent of gene therapy research, genetic transfer efficiency was insufficient to enable therapeutic application, thus the first approved gene transfer protocols involved gene marking studies with an informative aim rather than therapeutic intent[111-113]. Gene marking demonstrated that bone marrow transfer could contribute to long term haematological reconstitution, that residual tumour present in autologous bone marrow transplants could contribute to subsequent relapse, that *ex vivo* manipulation of cells could impair their subsequent *in vivo* efficacy whilst lymphodepletion could enhance *in vivo* expansion of adoptive cells. Thus, gene marking research was critical to understanding and defining subsequent gene transfer protocols. Gene marking also demonstrated evidence supporting the role for gene modified cells in targeted adoptive cell therapies by illustrating the contribution of adoptively transferred tumour infiltrating lymphocytes to the anti-tumour effect through evidence of functional immune surveillance of adoptive cells in the absence of observable disease, and enabling tumour specific trafficking of adoptive cells.

Finally, gene marking studies have highlighted risks and challenges associated with these new technologies. Gene marking identified the first evidence for an immune response against immunogenic proteins present within a vector cassette[114]. Also, despite the impressive safety profile from gene marking studies spanning years of research, including both modified bone marrow and T-cells, no observed clonal proliferation has been observed[91]. This is in sharp contrast to observations of insertional mutagenesis resulting from severe combined immunodeficiency (SCID) trials where leukaemogenesis was observed in five patients resulting from insertional mutagenesis out of a combined total of twenty patients from separate gene therapy trials[115]. Two arguments were cited to explain the variation between the scenarios. First, the observation that due to poor transduction efficiency from early gene marking studies, a smaller number of transduced cells were present which contained fewer integration events. Secondly, and notably, a growth promoting capacity was absent from these gene marking studies[91]; an observation which may prove important in consideration of ongoing cancer gene therapy strategies, *vide infra*.

1.5.2. Potential applications

The inclusion of a marker gene which could facilitate clinical-grade sorting of transduced cells would enable cellular purification and ensure consistency in the therapeutic product. Furthermore, marker genes also enable verification of transduction success, essential for expression of intracellular proteins such as calcineurin[116] resistance or the p47phox protein employed in chronic granulomatous disease gene therapy[117], as well as membrane bound proteins which may prove difficult to identify by antibody staining such as CD8-stalk bound CARs[21]. Finally, *in vivo*, marker genes offer potential for assessing cellular engraftment.

1.5.3. Alternative marker genes and their limitations

Integral to assessing gene transfer efficiency, marker genes have evolved parallel with gene transfer technology, with three primary tangential strategies having developed. Visual reporters along with metabolic and cell surface selection markers each offer an alternative mechanism for measurement of gene transfer. Visual reporter genes, such as luciferases and fluorescent proteins, are probably the most frequently employed enabling ready detection of gene transfer through bioluminescence imaging, fluorescence microscopy or flow cytometry analysis. Although convenience and clarity make these obvious choices for *in vitro* research and *in vivo* modelling, the xenogeneic origins of these proteins preclude clinical application owing to inherent immunogenicity and toxicity. Thus, metabolic selection and cell surface selection markers define the primary competing strategies for clinical marker genes.

1.5.3.1. Metabolic selection markers

Like GFP, early metabolic selection markers were derived from non-human enzymes enabling antibiotic selection such as neomycin, puromycin and hygromycin resistance genes. Although these proteins offer effective exclusion of non-transduced cells, immunogenicity resulting from their xenogeneic origin limits their application to highly immunosuppressed contexts. Furthermore, off-target functional activity from these enzymes may impose unpredictable impact upon cellular behaviour, such as impaired growth of HL60 cells observed to result from expression of the neomycin resistance marker[118]. However, significant illumination into the impact of tumour relapse and cellular tracking has been achieved following gene marking studies using

neomycin. An additional observation of interest from neomycin application was that prolonged *ex vivo* culture required to enable effective selection resulted in impaired T-cell function. Furthermore, expression of proteins of microbial origin could impose metabolic alteration upon genetically modified cells even in the absence of a prodrug[68]. Furthermore, G418 also imposes a degree of toxicity to primary cells imposing further impact on cellular function. The evolutionary product following *in vitro* selection marker genes were the *in vivo* selectable marker genes designed to increase engraftment mediated by therapeutic administration of drugs which are toxic to unmodified cells within the graft. Such marker genes include: multi-drug resistance (MDR-1), dihydrofolate reductase (DHFR) and O6-methylguanine-DNA methyltransferase (MGMT)[110]. However, although these strategies also suffer from limited efficiency and/or drug toxicity, they paved the way for later modular drug resistance cassettes conferring selective advantage concurrent with therapeutic administration, such as calcineurin or Inosine 5' monophosphate dehydrogenase (IMPDH) mutants offering tacrolimus and cyclosporin or mycophenolate resistance, respectively. Thus Ouaselect[119], an ouabain resistance gene, was developed to address the short-comings highlighted by earlier metabolic marker genes. Ouaselect is based on a mutation in the ubiquitously expressed Na/K/ATPase. Two point mutations in this protein; Q118R and N129D, mediate a 2-log increase in the ouabain resistance. Furthermore, a long history of cardiac glycosides in clinical application supports a safe history for clinical application of the prodrug, which induces a rapid induction of cell death resulting in 99% purity of modified cells within 48 hours. However, a critical application of marker genes is co-expression with a suicide gene to enable cellular deletion in case of toxicity. As Ouaselect only offers the marker gene moiety for this role, at 1023aa in length, this imposes a considerable transcriptional burden. Furthermore, as an intracellular protein, identification of marked cells is limited to intracellular flow cytometry or selection culture limiting the capability for functional assessment to *in vitro* application.

1.5.3.2. Cell surface marker proteins

Cell surface marker proteins represent the alternative strategy; cell surface expression enables facile detection through the use of antibodies thereby allowing for swift detection of genetically modified samples by flow cytometry.

A similar evolution of cell surface proteins has occurred with a range of proteins having been considered as putative marker genes. Initial studies using murine CD24[120] and a truncated form of murine CD4ζ[121] were supplanted by the human derived CD4[122] and Thy-1[123] proteins. These, in turn were subsequently excluded due to expression on alternative haematopoietic lineages. A recent proposal for ΔEGFR, a truncated form of the human epidermal growth factor receptor (EGFR)[124], as a putative marker gene, covers two functions, enabling both selection and cetuximab-mediated deletion. However, despite deletion of both the epidermal growth factor binding domains from the ectodomain and truncation of the signalling endodomain, proposed to ablate biological function, this marker-suicide gene remains a considerable 624 amino acids in length. Magnetic bead selection is achieved through a two-step process involving initial binding mediated by user-generated biotin-conjugated cetuximab, followed by anti-biotin selection. Further, as cetuximab is a chimeric antibody, this strategy imposes the potential for a possible human anti-chimeric antibody (HACA) priming response from therapeutic infusion of cetuximab-selected cells due to residual cetuximab bound to cells following selection[124]. Most recently, ΔCD19[125], ΔlNGFR[126] and ΔCD34[127] have all shown promise as effective cell surface marker genes with all three in current clinical application. Although all three have demonstrated functional efficacy, long coding domains impose significant transcriptional burden. ΔlNGFR is the shortest of the three at 277aa in length, followed by ΔCD19 and ΔCD34 at 332 and 323aa residues, respectively. ΔCD19 allows for clear identification, although expression profiles of CD19 impose a requirement for additional co-staining to allow for exclusion of the B-cell population from clinical samples. ΔlNGFR is a 277aa marker gene which has the longest history of clinical application. An early report[128], suggesting leukaemic risk resulting from ectopic expression and residual signalling capacity from ΔlNGFR gene marking, appears to have been tempered by subsequent research[129, 130] indicating insertional mutagenesis as the cause of leukaemogenesis. However, the risk of unknown metabolic perturbations resulting from residual signalling capacity remains. Hence, of the marker genes in current clinical application, the 323aa ΔCD34 appears to represent the superior cell surface marker gene as CD34 expression is excluded from haematopoietic lineages apart from stem cells, and thus far no evidence has been presented suggesting metabolic perturbation resulting from

ΔCD34 expression. Furthermore, *in vitro* assays using modified and selected T-cells including the ΔCD34 marker gene, the enriched T-cells demonstrated a 5-6x increase in anti-tumour activity suggesting that the selection process also enhances the functional capacity of the therapeutic population[131]. Finally, similar to ΔlNGFR, despite early concerns regarding aberrant homing of CD34 marked cells[132], ΔCD34 appears to offer promise as an effective marker gene; however, a comprehensive interpretation of potential risk can only be achieved through long term follow-up study.

Table 3 Summary of current marker genes

Marker gene	Advantages	Disadvantages
Visual reporters		
Luciferases[133]	Good signal to noise ratio Transgenic animals available	Xenogeneic & immunogenic
Fluorescent proteins[134, 135]	Simple to detect Enables FACS selection Transgenic animals available	Xenogeneic & immunogenic High expression can be toxic
***In vitro* metabolic markers**		
Blasticidin/ Hygromycin/ Neomycin/ Puromycin/ Zeocin resistance genes[136]	Most data suggest no impact on cell function	Selection is time consuming Prolonged culture can impair cellular function Xenogeneic & immunogenic
Ouaselect[119]	Rapid selection (48hr)	Long transcript size Intracellular localisation limits cell detection
***In vivo* metabolic markers**		
MDR-1 / DHFR / MGMT[110]	*In vivo* selection resolves impact imposed by prolonged *in vitro* selection	Intracellular localisation limits cell detection Limited by toxicity & efficacy
Calcineurin[116] / IMPDH mutants	Offers selective advantage concurrent with therapy	Intracellular localisation limits cell detection
Cell surface markers		
mCD24[120], mCD4[121]	Cell surface expression enables simple detection by flow cytometry analysis	Xenogeneic & immunogenic
hCD4[122], hThy-1[123] (CD90)	Enables simple detection by flow cytometry analysis	Discrimination confounded by presence of marker on other haematopoietic lineages
ΔEGFR[124]	Offers both marker & suicide gene capabilities	Selection reagents require in-house generation Limited experience
ΔCD19[125]	Enables clinical grade selection & flow cytometry detection	Discrimination confounded by presence of marker on other haematopoietic lineages
ΔlNGFR[126]	Enables clinical grade selection & flow cytometry detection	Concern for residual signalling capacity[128]
tCD34[127]	Enables clinical grade selection & flow cytometry detection	Concerns regarding homing & differentiation of transduced cells[132]

The premise of gene marking is to imprint a readily identifiable marker during genetic modification that enables facile discrimination between modified and unmodified cells. Although the exact criteria desired may vary dependent upon application, characteristics which define an ideal marker gene include: human derivation to avoid immune rejection; stable cell surface expression limited to engineered cells; acute sensitivity to allow for clear detection by flow cytometry analysis; compatible with current technology to enable clinical grade selection; composed from a compact coding sequence whilst remaining biologically inert. Western blot analysis and immunohistochemistry represent further characteristics which may also be desired.

1.5.4. QBEnd10 as a putative marker gene

For this purpose, we have generated a minimal marker gene based upon the CD34 epitope which is bound by the monoclonal antibody QBEnd10 clone utilised by the Miltenyi CliniMACS systems.

1.6. Suicide genes

A suicide gene encodes for a protein, absent from unmodified cells that enables selective destruction of transgenic cells following exposure to a therapeutic agent such as an antibody or small molecule drug.

1.6.1. Introduction

A suicide gene encodes for a protein which can enable selective destruction of administered cells in the face of unacceptable toxicity. Thus, inclusion of a suicide gene engenders a safety strategy to enable targeted deletion of engineered cells in case of GvHD, IM, OTOT or other adverse therapeutic events. Further, the efficacy of this strategy has been demonstrated by resolution of GvHD in a number of clinical trials involving engineered T-cells which include a suicide gene[137-143].

The ideal suicide gene would: impose no basal toxicity, be non-immunogenic, be inducible with a readily available pharmaceutical and would enable complete cellular deletion.

Inclusion of a suicide gene during donor lymphocyte infusion to control alloreactivity following allogeneic HSCT represents one of the widest applications for T-cell based gene transfer. The underlying principle behind

this strategy follows from the observation that the clinical efficacy mediated by HSCT against malignancy is dependent upon the GvL effect, which is concurrent with the risk for GvHD. Resolution of GvHD can prove to be challenging, requiring non-specific immunosuppressive drugs such as steroids thereby imposing additional risk of infection to the patient. Thus, inclusion of a suicide gene allows for specific deletion of the pathology inducing population with minimal impact on overall immune constitution. Thus, in the case of post allogeneic HSCT GvHD, application of the inducing drug should selectively eliminate the genetically modified lymphocytes thereby resolving the GvHD pathology without interfering with the natural process of immune reconstitution that follows HSCT.

Also, as the high costs associated with HSCT often reflect the requirement for additional treatment to resolve subsequent complications such as GvHD, infections and disease relapse, application of a suicide gene in DLI protocols can offer resolution of GvHD without impairing immune reconstitution. Thus the cost of inclusion of the suicide gene may prove favourable to the cost of therapy for post-transplant complications[144].

Early putative suicide genes including: D-amino acid oxidase, purine nucleotide phosphorylase, cytosine deaminase and herpes simplex thymidine kinase (HSVtk) were all derived from microbial components. Whilst offering specificity due to novel molecular circuitry, the immunogenic nature of these proteins has restricted application of all but HSVtk to direct targeted cancer gene therapy[145]. Therefore these early proteins will not be discussed further and the remaining discussion will focus on suicide genes which offer potential for therapeutic application.

As with marker genes, suicide genes have evolved substantially from the initial concept, and similarly can be loosely segregated into categories dependent upon the induction strategy, which I will define as metabolic or indirect. However, in all cases it should be noted that induction of the suicide gene machinery is achieved through application of an exogenous therapeutic agent.

Metabolic strategies can be further subdivided into non-toxic pro-drug and small molecule strategies. In metabolic strategies, the functional effect resulting from application of the inducing drug is mediated by intrinsic cellular pathways. As quiescence or mutation represent potential escape

mechanisms for these strategies, induction of suicide gene machinery imposes a selection advantage for cells able to escape deletion through functional escape from suicide gene mediated machinery. In contrast, indirect induction strategies rely on extrinsic cellular machinery to mediate deletion thereby reducing the potential for cellular escape. In all cases, low, or down-regulated gene expression may offer potential for target cells to escape selection through sub-threshold gene expression. If absolute deletion is essential, combination of suicide gene strategies may prove appropriate.

Finally, although marker genes offer independent utility, implicit to the strategy of a suicide gene is the requirement for co-expression with a compatible marker gene. Thus, the impact of inclusion of a suicide gene regulatory component must consider the combined impact for both the marker and suicide moieties, in addition to any additional transgenes which may be desired.

1.6.2. HSVtk application and suicide gene evolution

There is a long history of HSVtk in clinical trials which has demonstrated a clear efficacy in resolving GvHD when required supporting the initial premise behind the strategy, *vide supra*.

HSVtk was the first transgene expressed by retroviral technology[146] and remains in clinical application. Many advances in GT protocols have followed from HSVtk research including; optimisation of transduction protocols, revision of vector strategies, marker gene evolution and suicide gene re-engineering. Some key advances as reviewed by Bonini *et al.*[144], are briefly detailed below.

1.6.2.1. Optimisation of transduction protocols:

Initial genetic modification protocols employed a CD3 monoclonal antibody to mediate the required T-cell stimulation to enable retroviral gene transfer. However, subsequent observations identified that T-cell stimulation in the absence of co-stimulation preferentially activates mature lymphocytes resulting in the production of a predominantly effector phenotype population with low alloreactive potential, thus impairing the GvL effect. Further, this transduction protocol, along with culture and selection strategies, was demonstrated to preferentially exclude T-cell precursors with EBV-specificity[68,

[147] impairing EBV immune reconstitution. Revision of T-cell transduction protocols to include two-signal stimulation was subsequently demonstrated to ensure both retention of alloreactive potential and transduction of a broad T-cell repertoire with no evidence of clonal selection nine years post infusion[144].

1.6.2.2. Revision of vector strategies:

Due to observations regarding vector mediated toxicity resulting from integration site analysis, lentiviral vectors were considered to offer a safer alternative strategy in light of observations regarding variation in the preferred integration sites between Moloney based retroviral vectors and lentiviral vectors, with third generation lentiviral vectors demonstrating an optimal safety profile for both viral production and T-cell transduction protocols. Furthermore, lentiviral vectors can transduce non-dividing cells through active transport of the pre-integration complex into the nucleus. Although LV cannot transduce quiescent cells in G_o, low dose gamma chain cytokine incubation has been demonstrated to promote cell cycle progression from G_o to G_1b which is sufficient to enable LV transduction[144].

1.6.2.3. Marker gene evolution:

Due to the imperative requirement for co-expression of a marker gene alongside a suicide gene, there has been a parallel evolution in clinical marker genes. Neomycin resistance was the first marker gene used in conjunction with a suicide gene; however, evolution to cell surface markers intended to resolve culture and G418-selection mediated impairment of EBV immunity resulted in ΔlNGFR becoming the first cell surface marker gene to be used in a clinical trial. Subsequently, ΔCD34 evolved to become the second cell surface marker gene to enter clinical application[148], with ΔCD19[125] and ΔEGFR[124] representing the most recent additions to clinical marker genes.

1.6.2.4. Suicide gene re–engineering:

Finally, therapeutic application of HSVtk has also suffered from a number of critical failures. Identification of an alternative splice variant generated from the wild-type (wt) HSVtk gene was shown to result in production of an inactive form of the enzyme. Retention of cryptic donor and acceptor splice sites from the wt HSVtk gene resulted with inclusion of an inactive form of the enzyme present in approximately 10% of retroviral particles and, correspondingly, approximately 10% of genetically modified cells[149]. Resolution of alternative

splicing was achieved through a conservative point mutation which was subsequently demonstrated to preclude production of undesired splice variants. However, despite the genetic correction, a subsequent report highlighted further ganciclovir resistant forms of HSVtk resulting from partial transgene deletions and post-translational proteolytic events resulting from a ΔCD34/HSVtk fusion protein[150]. TK.007 represents the current evolution of therapeutic HSVtk, a codon-optimised construct containing a point mutation conferring enhanced GCV sensitivity and reduced nonspecific toxicity[151]. However, despite these limitations and failings, HSVtk has clearly demonstrated a proof of principle in that suicide gene therapy can offer resolution of GvHD.

1.6.3. Alternative suicide genes

Existing suicide genes include Herpes simplex virus thymidine kinase (HSVtk)[142], inducible caspase9[125, 152], inducible FAS (iFas)[153], CD20[154], Δc-myc[155], ΔEGFR[124] and human thymidylate kinase (TMPK2)[156, 157] with the former two currently in clinical use.

Table 4 Summary of current suicide genes

Suicide gene / *prodrug*	**Advantages**	**Disadvantages**
Metabolic strategies		
HSVtk[142] *Ganciclovir*	Clear history of clinical efficacy	Limited to application under profound immunosuppression. e.g. Haploidentical transfer Potential for escape through cellular quiescence
TMPK2 (TmpkF105Y)[156, 157] *AZT*	Human derivation	Limited efficiency, delay in deletion, AZT toxicity Potential for escape through cellular quiescence
iCaspase9[125, 152] *AP1903*	Human derivation Clear resolution of GvHD demonstrated from initial clinical trial	Restrictive access to inducing drug Limited experience for potential small molecule toxicity Residual population may possess reduced sensitivity
Tamoxifen inducible caspase[158] *4–Hydroxytamoxifen*	Human derivation	Limited experience; current application limited to developmental biology research
iFas[153] *AP1903*	Human derivation	Target upstream of apoptosis inhibitors presents risk for escape
Indirect strategies		
CD20[154, 159] *Rituximab*	Human derivation	Possible residual signalling capacity Long coding sequence Requires co-expression with a separate marker gene
Δc-myc[155] *c–myc antibody*	Human derivation Small size Potential to function as both marker & suicide gene	Lack of clinical c-myc antibody Experience limited to TCR GT
ΔEGFR[124] *Cetuximab*	Human derivation Potential to function as both marker & suicide gene	Limited lytic capacity of cetuximab

1.6.3.1. HSVtk

The HSVtk system involves selective phosphorylation of the non-toxic prodrug ganciclovir by the HSV-TK enzyme generating GCV-triphosphate. Incorporation of this metabolite into DNA results in chain termination and single strand breaks in dividing cells[160]. However, due to the viral origin, a key limitation to clinical application of HSVtk is the inherent immunogenicity of the protein.

Observations from clinical application demonstrate that the immunogenicity of the HSVtk protein depends upon the level immune constitution of the patient at time of infusion. Immunosuppressed patients do not generate a response against HSVtk unless they receive a subsequent infusion at a time point where they have achieved a degree of immune reconstitution. This suggests that the HSVtk protein remains largely ignored by the immune system[144]. However, this immunogenic limitation effectively restricts application of HSVtk to scenarios involving profound immunosuppression such as haploidentical transplant therapy. Furthermore, cytomegalovirus (CMV) reactivation following transplant related immunosuppression is a potential complication following cell therapy and ganciclovir therapy required to resolve CMV reactivation would also delete the HSV-TK transgenic cells. Finally, HSVtk represents a metabolic strategy with deletion efficacy dependent on enzymatic function. Thus deletion is non-immediate, whilst cellular quiescence offers protection from ganciclovir-mediated deletion.

1.6.3.2. Inducible caspase9

The iCaspase9 system remains the primary alternative to HSVtk, utilising a synthetic fusion gene construct derived from the human caspase9 activation domain fused to a synthetic FKBP12 binding domain[152]. Induction of suicide-gene machinery is mediated through therapeutic administration of AP1903, a lipid-permeable, non-toxic analogue of the FDA-approved dimerising drug FK506. In a recent clinical trial[125], a single dose of AP1903 achieved effective resolution of GvHD symptoms in all patients treated, with 90% of transgenic cells deleted within 30 minutes following therapeutic administration. Where subsequent therapeutic administration was employed to resolve resurgence from the residual adoptive cellular population, approximately 85% deletion was achieved. Furthermore, following transduction and selection in the clinical trial, cellular purity ranged between 90-93%, indicating that as much as 10% of the infusion sample excluded the suicide-gene machinery. It remains unclear whether this decrease in efficacy of deletion indicates a growing presence of a sub-threshold population, or possibly indicates the potential resurgence of unmodified cells. As secondary therapeutic administration has already been employed to resolve adoptive cell resurgence, concerns regarding potential resistance and/or presence of unmodified cells present within the cellular infusion remain, however initial results appear promising.

As with HSVtk, iCaspase9 offers only the suicide-inducing capacity and thereby requires additional co-expression of a suitable marker gene. At 402aa in length, this suicide-gene moiety alone imposes a significant payload for a transgenic cassette. Furthermore, iCaspase9 represents a metabolic suicide gene strategy. Cellular deletion is dependent upon apoptosis mediated via cellular machinery including apoptotic protease activating factor 1 (Apaf-1). Association of a splice variant of Apaf-1 in prostate cancer suggests a possible escape mechanism for this suicide-gene strategy[161]. The therapeutic drug represents a further concern regarding this strategy as increasing observation of HLA-linked hypersensitivities involving small-molecule drugs, such as abacavir hypersensitivity syndrome and Stevens-Johnson syndrome, raise concern regarding therapeutic safety of small-molecule drugs with limited clinical experience[162]. Finally, accessibility of the inducing drug is limited by exclusive licensing by the US pharmaceutical company necessitating further regulatory research to broaden potential clinical application.

1.6.3.3. Tamoxifen inducible apoptosis

A variation from the iCaspase9 strategy involves tamoxifen inducible caspase constructs with dimerization achieved via synthetic fusion of a mutant estrogen receptor ligand binding domain to caspase8 or caspase9 domains.[158]. In theory tamoxifen offers potential for clinical application, hence inclusion within this list, although to date application of this strategy appears limited to developmental biology research.

1.6.3.4. Inducible Fas

Effectively a precursor to iCaspase9, inducible-Fas (iFas) is a fusion construct composed of the FKBP12 binding domain fused to Fas-associated death domain containing protein (FADD)[153]. Although killing efficacy proved promising, selection of a target upstream of apoptosis inhibitors may result in variation of killing efficacy dependent upon cell type. Furthermore, limitations in the observed killing efficiency were thought to pose an untenable risk for cellular escape[160]. As a result, this strategy was supplanted by iCaspase9 as a putative suicide-gene strategy.

1.6.3.5. CD20

CD20 initially appeared to offer the perfect choice as a putative marker-suicide gene, offering both clinical grade selection using Miltenyi magnetic sorting

beads and depletion mediated by rituximab, a well characterised therapeutic monoclonal antibody[154, 159].

Despite initial promise, evolution of this strategy has resulted in the generation of a bicistronic construct containing ΔCD34 as the marker gene, suggesting limitations for the application of CD20 as a marker gene for transgenic T-cells. This corresponds with our own observations of toxicity resulting from CD20 based bead-selection of transgenic T-cells (data not shown). As the biological role for CD20 in B-cells remains unclear, it is difficult to demonstrate the lack of a biological role of ectopic CD20 expression in T-cells although bead selection based toxicity does suggest that residual signalling capacity remains, and raises further concern as to what impact this may pose in genetically modified cells. Furthermore, although codon optimisation appears to have resolved earlier limitations in transgene expression, the large size of the construct remains disappointing as transgene length is known to negatively impact upon viral titre and transduction efficiency[119, 163]. Finally, consideration for application of CD20 as a putative suicide gene for CD19 targeted CAR T-cell based therapies precludes application of rituximab/ofatumumab in the preconditioning regimen due to the prolonged half-life of these therapeutic antibodies.

1.6.3.6. Δc–myc

Consideration of Δc-myc[155] as a putative suicide-gene follows from previous strategies designed to combine marker-suicide gene capacity within a single construct. Selection of a 10a.a. tag derived from the human c-myc protein offers both minimal size and human derivation for this construct. However, to achieve effective expression enabling the desired functional capacity, a double-myc tag construct localised to the amino-terminus of the variable region of the TCR alpha chain was required. In addition to limiting this strategy to TCR-based gene therapy, inherent variation of TCR variable regions questions the generalisability for this strategy even within TCR-based gene therapy, likely imposing additional functional testing to ensure effective marker, suicide and TCR functionality in all cases. Furthermore, localisation of the c-myc binding to the TCR amino-terminus suggests the possibility of potential signalling resulting from antibody binding raising the risk for inducing a cytokine storm during therapeutic depletion. Finally, the lack of a current c-myc therapeutic

effectively restricts this strategy to research application for the foreseeable future.

1.6.3.7. ΔEGFR

Further to potential as a proposed marker gene, a 336 residue ΔEGFR construct has also been proposed as a putative suicide gene with deletion mediated through cetuximab therapy[124]. Cetuximab is a chimeric monoclonal antibody which recognises a conformational epitope in the third domain of EGFR. Antitumour activity of cetuximab is indicated as resulting from inhibition of tyrosine kinase signalling and EGFR signalling blockade leading to induction of pro-apoptotic pathways[164].

Suicide-gene strategies based on transgenic expression of a binding target for a therapeutic antibody have been proposed[124, 155, 165, 166] with the cetuximab based system[124] being the closest to the strategy which we are proposing. Here, ΔEGFR is expressed on a T-cell with depletion effected by the anti-EGFR therapeutic mAb cetuximab. Although the human derivation offers a low risk for immunogenicity, the choice of cetuximab as the therapeutic agent imposes some limitations. Cetuximab therapy is accompanied by acneiform follicular skin exanthema in more than 80 % of patients. Severe exanthema (grade III/IV) develops in about 9-19 % of patients with the necessity of cetuximab dose reduction or cessation[167], which certainly poses some concern for a putative suicide gene strategy. In contrast, rituximab monotherapy is well tolerated by the majority of patients with little increase in opportunistic infection[168, 169], no maximally tolerated dose[165] and a solid reputation as a lymphodepleting agent in human subjects[170, 171].

1.6.3.8. TMPK2

TMPK2 is a mutant thymidylate kinase of human derivation which employs a similar strategy to HSVtk involving selective enzymatic conversion of a non-toxic prodrug azidothymidine (AZT) into a toxic metabolite. Limited efficacy from an earlier enzyme[156] has resulted in the directed evolution of TmpkF105Y[157], a modified TMPK enzyme with increased catalytic capacity for AZT. Cellular deletion mediated by this enzyme is proposed to progress by two alternative mechanisms; incorporation of phosphorylated AZT into DNA during replication results in premature chain termination, whilst activated AZT

can damage mitochondrial membrane potentials resulting in caspase-3 mediated apoptosis.

However, as with HSVtk, primary concerns regarding metabolic suicide gene strategies remain. Notably, as cellular deletion is dependent upon the activity of the target enzyme, adoptive cells can escape deletion through quiescence. Furthermore, the therapeutic window required to achieve deletion may prove too prolonged to achieve effective resolution dependent on the nature of the ACT-based toxicity causing concern. Finally, reports of genomic toxicity and promotion of genomic instability mediated by AZT raise concerns for general application of this strategy as a suicide gene for ACT, particularly for cancer therapies where the potential of promoting genomic instability seems especially risky[172].

1.6.3.9. Alternative suicide gene summary

Despite the array of alternative suicide genes which have been considered, only HSVtk and iCaspase9 have been validated through clinical application with trial results pending for ΔEGFR. From an *in vitro* comparison of HSVtk, iCaspase9, CD20 and TMPK2, equivalent deletion was observed for iCaspase9, CD20 and HSVtk although HSVtk requiring four days to achieve equivalent depletion as observed for iCaspase9 and CD20. Although the profile of TMPK2-mediated deletion proved similar to that observed for HSVtk, a maximum efficacy of approximately 70% would likely preclude clinical application[173]. Metabolic and antibody-mediated suicide gene strategies each possess both advantages and limitations and the ultimate decision to consider a single, multiple or no suicide gene strategy should be balanced with the threat associated with the therapeutic application.

1.6.4. Rituximab binding motif as a putative suicide gene

Following upon the premise of using CD20 as a suicide gene, we have generated a suicide gene based upon the R3-C mimotope described by Perosa *et al*[174] which is bound by the common therapeutic monoclonal antibody rituximab. Due to the minimal size of this antibody-binding epitope domain, it is optimal for co-expression alongside our QBEnd10 binding marker gene.

1.7. Monoclonal antibody technology

1.7.1. Introduction to monoclonal antibodies

Antibodies compose the humoral arm of the adaptive immune response. In the membrane bound form, these act as the B-cell receptor mediating target recognition analogous to the T-cell receptor. In the soluble form, they mediate the effector functions of the humoral response. There are five classes of antibodies defined by heavy chain constant regions: IgM, IgG, IgA, IgE and IgD. As most therapeutic antibodies are based on the IgG isotype, these will form the basis for further discussion.

The initial concept for a therapeutic application for antibodies was proposed by Paul Erlich late in the nineteenth century[175], however it wasn't until the advent of hybridoma technology in 1975[176] that monoclonal antibody technology became a reality. Monoclonal antibody therapy is a natural evolution from immunoglobulin replacement therapy dating from the 1970s with early monoclonal antibodies derived from antibodies raised in mice. However, the immunogenic capacity of murine-derived antibodies identified one of the first challenges in applying monoclonal antibody technology to clinical application. In addition to being immunogenic, early murine-derived antibodies also suffered from poor efficacy due to limited recruitment of immunological effector functions. Thus began progressive evolution of antibody engineering. To address the immunogenic potential, antibodies were re-engineered to be first chimeric, then humanised and finally fully humanised in an attempt to exclude the immunogenic impact of non-self-origin.

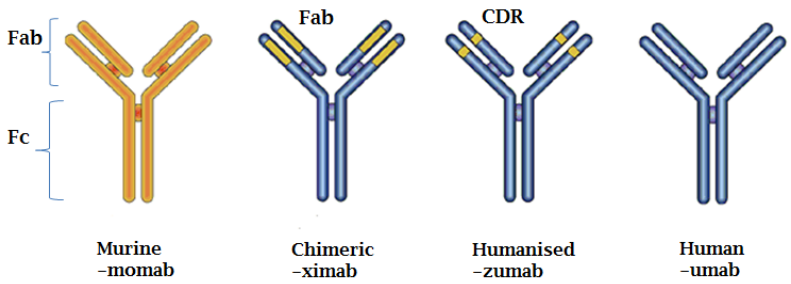

Figure 4 Progressive evolution of monoclonal antibodies
(Adapted from Brekke *et al.* 2003[177]) Initial antibody technology employed murine antibodies obtained directly from hybridomas but which subsequently were established to be immunogenic. This elicited three major advances in antibody engineering to achieve fully humanised antibodies. By 1984 molecular biology enabled formation of chimeric antibodies by fusing human Fc to a murine Fab domain. Chimeric antibodies remain 1/3 murine and 2/3 human in derivation. By 1986, further reductions from the parental murine sequence enabled exclusive transfer of only the CDR domains required to confer antigen specificity. A final

evolution using CDR grafting or veneering techniques developed in 1989 enabled generation of fully human antibodies which retain the desired antigen binding capacity[178].
Abbreviations: Fab –antibody binding fragment, Fc –constant fragment, CDR – complementary determining region

Therapeutic antibodies mediate biological activity through one of three primary mechanisms: indirectly via effector-mediated lysis, following complement activation and/or effector cell recruitment (e.g. rituximab/alemtuzumab); cytotoxicity mediated through a toxic/radio-labelled conjugate moiety (e.g. mylotarg/epratuzumab); and through neutralising behaviours, (e.g.infliximab/basiliximab/ipilimumab)[179]. Further, the capacity for biological activity can be modulated where desired. The anti-CD20 therapeutic antibody ofatumumab was selected for enhanced complement-mediated lytic capacity premised to result from an alternative binding location against CD20[180]. In contrast, antibody-engineering of the anti-GD2 ch14.18 antibody involved inclusion of a point mutation in the Fc domain, designed to reduce complement fixation, with a view to attenuate therapy-related allodynia observed during therapy against neuroblastoma[181].

Antibodies can be subdivided into distinct functional units: the antigen binding (Fab) fragment, and the constant (Fc) fragment. The Fab is the variable region of the antibody, with variability primarily restricted to three complementary determining regions (CDR's) which define the antigen recognition specificity of the antibody. The constant Fc domain defines the isotype of the antibody as indicated above, and mediates the effector functions of the immune response (CDC/ADCC) as well as facilitating antibody stability, further mediated by FcRn receptors. A further role for the Fc domain is physiological stability; the prolonged serum half-life of antibodies results from interaction of IgG with the neonatal Fc receptor (FcRn). FcRn receptors present on vascular endothelium can reversibly bind serum IgG allowing for return to the circulation and preventing lysosomal catabolism en route to the lymphatics[179].

Humans and mice differ in their ability to recruit effector mechanisms based on antibody isotype, therefore definition of equivalent counterparts are based on similarity in functional behaviour with mouse IgG2a and IgG2b demonstrating similar complement-mediated functional capacity as human IgG1 and IgG3, respectively[182]. From animal models using CD20 depleting

antibodies, B-cell depletion efficacy was observed to perform relative to antibody subclass as follows: IgG2a>IgG1>IgG2b>IgG3[183]. In humans, complement mediated sensitivity shows a similar antibody subclass defined pattern: IgG1>IgG3>IgG2>IgG4[184].

1.7.2. Rituximab

Rituximab is a clinical success story; originating as a CD20 targeted chimeric antibody developed by IDEC pharmaceuticals under the name IDEC-C2B8, in 1997 rituximab became the first FDA approved antibody drug for the treatment of malignancy. Initially approved for use against chemotherapy refractory non-Hodgkins lymphoma, rituximab has subsequently been approved for clinical application in chronic lymphocytic leukaemia, rheumatoid arthritis, Wegener's granulomatosis and microscopic polyangiitis with further off-label applications, including myasthenia gravis, systemic lupus erythematosus (SLE), immune thromocytopenic purpura, type I diabetes and multiple sclerosis, currently under investigation[185]. Despite the clear efficacy demonstrated by rituximab, definitive attributions for the various mechanisms involved in the therapeutic effect remains in dispute. Although, direct signaling, sensitization to chemotherapeutic drugs, CDC and ADCC all appear to be involved in the therapeutic effect[186, 187]; from both *in vitro* and *in vivo* data, it has been suggested that the relative importance of different mechanisms may vary dependent on the therapeutic and physiological scenario involved.

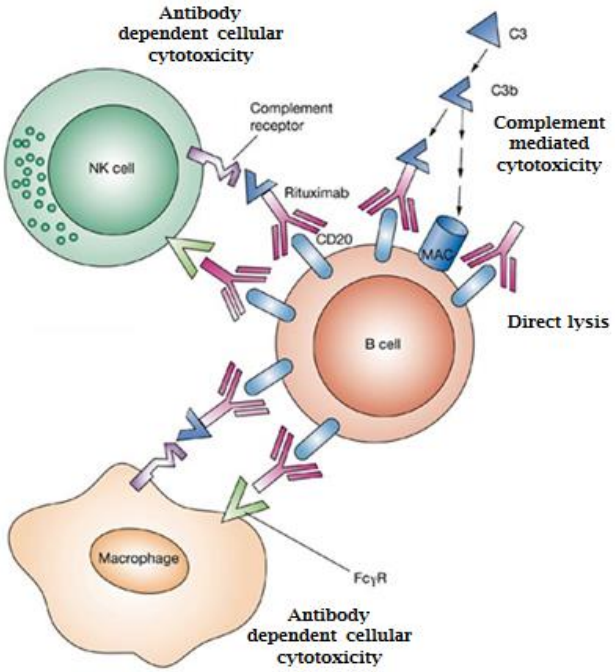

Figure 5 Proposed mechanisms of rituximab mediated cellular deletion
Adapted from Taylor *et al*[88]. Rituximab mediated deletion has been proposed to result from 3 separate mechanisms: direct toxicity imposed by signalling resulting from antibody-mediated cross-linking of CD20, complement dependent cellular cytotoxicity (CDC) resulting from activation of the complement system and antibody dependent cellular cytotoxicity (ADCC) mediated by cellular effectors.

Evidence for the role of direct signaling mediated toxicity are primarily derived from *in vitro* assays involving cross-linking of rituximab with secondary antibodies. As the secondary antibodies usually possess a greater affinity for rituximab than rituximab has for the Fc receptors, these results may reflect artificial amplification of the signal thus raising doubt for the potential clinical relevance of direct signaling as a cytotoxic mechanism. Despite these limitations, this evidence suggests that rituximab-mediated restructuring of cellular CD20 molecules into lipid rafts mediates inhibitory cellular signaling through p38 MAPK, NFκB, ERK 1/2 and AKT survival pathways.

Evidence for CDC-mediated toxicity of rituximab reflects both *in vitro* assays and *in vivo* observations. *In vitro* assays have demonstrated expression of complement inhibitory molecules CD55 and CD59 on targets which correlates with the CDC-mediated efficacy of rituximab. While CDC has been shown to be a primary mechanism for rituximab-mediated deletion in some animal models, what remains contentious is the clinical relevance of CDC-mediated deletion, and to what degree this might occur outside of the intravascular compartment. A clinical observation suggestive for the role of CDC in patients relates to

residual chronic lymphocytic leukaemia (CLL) cells present following rituximab therapy, having been shown to express elevated levels of CD59 when compared against pre-therapy samples[187]. Further clinical evidence for the role of CDC in rituximab efficacy is indicated by enhanced therapeutic efficacy against CLL following plasma infusion to replenish plasma complement levels[189]. Finally, the role of CDC-mediated deletion in rituximab efficacy has been considered sufficiently crucial as to merit future CD20 antibody engineering to enhance the complement fixation effect. Ofatumumab, a new therapeutic CD20 mAb which binds to the small membrane-proximal extracellular loop of CD20 was selected based upon enhanced ability to mediate CDC-mediated lysis[180].

ADCC represents the third proposed primary mechanism for rituximab-mediated efficacy. Most research exploring rituximab-mediated ADCC has examined the role of natural killer (NK) cell FcγRIIIa (CD16) in ADCC mediated lysis. However this strategy may distort the physiological setting as NK cells are unique as effectors of ADCC in that expression of the inhibitory FcγRIIb (CD32) is absent, therefore FcR cross-linking mediated activation proceeds uninhibited. ADCC can be mediated by a range of effector cells including granulocytes, macrophages and NK-cells, and apart from NK cells, the resulting activation decision reflects the combination of activating and inhibitory signals received by the cell. However, as high affinity CD64 FcγRIa (CD64) expression can be upregulated on granulocytes by IFNγ, and as NK cells are a source of IFNγ, it could be postulated that NK-cell CD16 may play a primary activating role in the process of ADCC-mediated deletion. The role of NK cells in ADCC is discussed further in Chapter five.

As only CDC and ADCC mechanisms are relevant in the mechanism for deletion of our construct, we have used CDC assays using baby rabbit complement, and ADCC assays using donor derived, *ex vivo* expanded NK cells as effectors.

1.8. Project aim

To generate a minimal epitope-based, selection and suicide gene cassette, engineered for solid tumour chimeric antigen receptor immunotherapy.

1.8.1. Project milestones

- To epitope map the QBEnd10 binding epitope from the CD34 antigen
- To establish a minimal marker gene expression construct using the QBEnd10 epitope which enables Miltenyi MACS selection of transgenic cells
- To identify and establish a minimal rituximab binding epitope construct
- To establish an effective co-expression construct for both minimal epitope binding domains
- To establish flow-cytometry based *in vitro* CDC deletion assays sufficient to enable effective comparative assessment of complement mediated deletion between similar epitope expression constructs
- To establish flow-cytometry based *in vitro* ADCC deletion assays sufficient to enable effective comparative assessment of effector mediated depletion between similar epitope expression constructs
- To demonstrate a modular capacity of the marker suicide gene construct in conjunction with standard T-cell engineering components
- To demonstrate functional efficacy of the marker-suicide gene construct through *in vivo* adoptive transfer modelling using a murine model

We have engineered RQR8 as a putative suicide gene for adoptive cell therapy. Although design and validation of RQR8 function has been with a view for application for cancer immunotherapy, it seems reasonable to premise that the functional capacity RQR8 could extend to general ACT application.

T-cell gene therapy remains a young and rapidly developing field. Whilst many lessons have learned through clinical trials, therapeutic triumphs have been accompanied by tragedy. However, so long as risk of therapeutic toxicities exist, inclusion of effective safety mechanisms remains as crucial to ensuring general acceptance for ACT as therapeutic success.

Chapter two

2. Materials and Methods

2.1. Materials

2.1.1. Reagents

2.1.1.1. General reagents and chemicals:

Acetic acid (glacial)	BDH	10001CU
Agarose	Bioline	BIO-41025
Agarose (Cell culture)	Lonza Seaprep agarose	50302
Bovine Serum Albumin	Sigma-Aldrich	A7906
Boric acid	VWR International	20185.360
Bromophenol blue	Sigma-Aldrich	B3269
CaCl 2-hydrate	BDH Chemicals	437053L
Carbenicillin	VWR International	69101-3
Cellstor pot (10% NBF)	Cellpath	BAF-6000-08A
^{51}Chromium radionuclide	Perkin Elmer	NEZ030001MC
Citric acid monohydrate	Sigma-Aldrich	27491
Coomassie R-250 dye	Thermo Scientific	20278
ECL prime	GE Healthcare Life sciences	RPN2232
EDTA Disodium salt	VWR International	20302.260
Ethidium bromide	BDH Chemicals	443922U
Glycerol	Sigma-Aldrich	G5516
Laemmli sample buffer	Sigma-Aldrich	S3401
Luria-Bertani (LB) Medium	MP Biomedicals LLC	3002-031
LB-Agar Medium	MP Biomedicals LLC	3002-231
Marvel skim milk powder		
Neutral buffered formalin	Genta Medical	BFN010
PBS tablets	Oxoid	BR0014G
PFA 4% in PBS	Insight Biotechnology Ltd	sc-281692
pH indicator strips	VWR International	1.09542.0001
Propidium iodide	Sigma-Aldrich	P4170
Sodium Chloride	BDH Chemicals	27810-364
Sodium phosphate heptahydrate	Sigma-Aldrich	S9390
Sodium phosphate monobasic	Sigma-Aldrich	S0751
Sodium citrate	Sigma-Aldrich	S4641
Terrific broth (TB)	Merck Chemicals Ltd	1.01629.0500
Trisodium citrate	Sigma-Aldrich	C8532
Tris base	Fisher Scientific UK	BPE152-5
Trypan Blue solution	Sigma-Aldrich	T8154
X-gal	Sigma-Aldrich	B4252
X-ray film (18x24)	Amersham	28906844

2.1.1.2. Molecular cloning enzymes and reagents:

Restriction enzymes	New England Biolabs UK Ltd	Various
Hyperladder DNA ladder	Bioline Limited	BIO-33026
Phusion DNA polymerase	New England Biolabs UK Ltd	M0530L

Platinum PCR SuperMix	Invitrogen	12532-016
TOPO TA cloning kit	Invitrogen	45-0641
Murine GAPDH primer	Qiagen	QT01658692
M-MLV reverse transcriptase	Ambion	AM2044
Oligo primers	IDT DNA	

2.1.1.3. Bacteria:

NEB 5-α Competent *E. coli* (Subcloning Efficiency) C2988		
	New England Biolabs UK Ltd	C2988J
NEB 5-α Competent *E. coli* (High Efficiency) C2987		
	New England Biolabs UK Ltd	C2987H

2.1.1.4. Tissue culture plasticware:

Cryogenic vial internal thread	Corning	430488
Flask Ez Nunclon 175Cm	Thermo Electron	159910
Flask Ez Nunclon 75Cm	Thermo Electron	156499
Flask Ez Nunclon 25Cm	Thermo Electron	156367
100mm TC dishes	Corning	430167
6 Well plate TC treated	Corning	3506
12 Well plate TC treated	Corning	3513
24 Well plate TC treated	Corning	3524
24 Well plate non-TC treated	BD Biosciences	351147
48 Well plate TC treated	Corning	3548
96 Well plate flat bottom	Corning	3596
96 Well plate V-bottom	Greiner Bio-One	650-180
96 Well plate round-bottom	Corning	3799
15ml Centrifuge tubes	Corning	430791
50ml Centrifuge tubes	Corning	430829
250ml centrifuge tubes	Corning	430776
0.2μM pore syringe filter	Sartorius	16532K
0.45μM pore syringe filter	Sartorius	16537K

2.1.1.5. Tissue culture media and supplements:

2-Mercaptoethanol	Sigma-Aldrich	M7522
ACK Lysing buffer	Lonza Sales AG	10-548E
Baby rabbit complement	AbD Serotec	C12CA
CD34 microbeads (human)	Miltenyi Biotec	130-046-702
CD56 microbeads (human)	Miltenyi Biotec	130-050-401
Cell dissociation medium	Sigma-Aldrich	C5914
CellTRACE violet	Invitrogen Life Technologies	C34557
Concanavalin A	Sigma-Aldrich	C5275
Counting beads	Beckman Coulter	6605359
Cryopreservation Medium	Lonza Bio Science Ltd	US12-132A
DMSO	Sigma-Aldrich	D2650
DPBS solution	Invitrogen Life Technologies	14190169
EDTA solution (0.5M)	Sigma-Aldrich	E7889
FBS, Ultra-Low IgG	Invitrogen Life Technologies	16250-086
FBS, IgG stripped	Biosera	S1811
FCS	Biosera	S1900/500
Ficoll-Paque	GE Healthcare Life sciences	17-1440-03
Genejuice	Merck Chemicals Ltd	70967-3

GlutaMAX	Invitrogen Life Technologies	35050087
HBSS 10x	Sigma	H1641
Heparin sodium	Leo Laboratories Ltd	PL 0043/0149
HEPES solution (1M)	Sigma-Aldrich	H0887
Horse serum	Life technologies	16050130
IL-2 Recombinant human	Genscript	Z00368
IL-2 Recombinant mouse	Invitrogen Life Technologies	PMC0021
IL7 Recombinant mouse	PeproTech EC Ltd	217-17
IMDM	Lonza Bio Science Ltd	BE12-726F
IMDM L-Glut^{+}, Phenol Red^{-}	Invitrogen Life Technologies	21056-023
Normocin	InvivoGen	ant-nr-1
PHA	Sigma-Aldrich	L9017
Polybrene	Millipore	TR-1003-G
Retronectin	Lonza Bio Science Ltd	T100B
RPMI	Lonza Bio Science Ltd	BE12-167F
Sfm4Transfx-293	Fisher Scientific UK	HYC-014-020V
Trypsin-EDTA solution	Sigma-Aldrich	T4049

2.1.1.6. Tools:

Dissecting Scissors 115mm	SLS	INS4800
Forceps 115mm, fine tip curved	Onecall	D00834
Forceps straight with blunt tips	Fisher Scientific UK	DKC-510-G
Haemocytometer	Hirschmann Laborgeraete GmbH	8100103
Histosette cassettes	Simport scientific Inc	M490-2
LS Columns	Miltenyi Biotec	130-042-401
MS Columns	Miltenyi Biotec	130-042-201
Nalgene® Mr. Frosty®	Thermo Scientific	5100-0001
Parafilm	VWR International	291-1212
Pellicon XL Biomax 50 TFF	Millipore	PXB050A50
Portable Pipet-Aid XP	Drummond Scientific	4-000-101
Vacuum filter unit	Corning	431097

2.1.1.7. Kits:

Qiagen Gel extraction kit	Qiagen	28706
Qiagen Miniprep kit	Qiagen	27106
Quick Ligation kit	New England Biolabs UK Ltd	M2200L
Nucleospin Miniprep kit	Thermo Scientific Abgene	NZ740588250
Nucleobond Midiprep kit	Thermo Scientific Abgene	NZ74041050
BD Mouse IgG2a ELISA set	BD Biosciences	552576
BD OptEIA Reagent Set B	BD Biosciences	550534

2.1.2. Buffers and solutions

Unless otherwise indicated, buffers and solutions were prepared in deionised reverse osmosis filtered laboratory grade water and either autoclave sterilised at 121°C for 15 minutes, or sterile filtered by vacuum filtration through a 0.22μM filter.

Composition of buffer solutions is detailed as follows:

Buffer	Ingredients / composition
Annexin V buffer [150mM NaCl, 10mM HEPES, 10mM CaCl]	8.71g of sodium chloride, 10ml 1M Hepes solution (Sigma) and 1.47g of Calcium chloride diluted into 1L of deionised water.
Propidium iodide (PI) stock solution	25mg PI (sigma) was suspended into 10ml of deionised laboratory grade water to establish a 2.5mg/ml stock solution
20mM sodium phosphate (pH7)	3.27g sodium phosphate heptahydrate and 0.94g sodium phosphate monobasic diluted into 1L of deionised water pH balanced to pH7.0 with concentrated HCl solution
0.1M citric acid	21.01 g of citric acid monohydrate dissolved into 1L of deionised water
0.1M trisodium citrate	29.41g trisodium citrate dehydrate dissolved into 1L of deionised water
0.1M sodium citrate (pH3.6)	Composite solution composed of 68.5ml of 0.1M citric acid and 31.5ml of 0.1M trisodium citrate as indicated by Sigma. [http://www.sigmaaldrich.com/life-science/core-bioreagents/biological-buffers/learning-center/buffer-reference-center.html]
Tris-HCl buffer (pH9)	1M solution (121.14g diluted into 1L deionised water), pH adjusted with concentrated HCl solution.
MACS/FACS buffer	1% FCS in PBS
0.25% Coomassie stain [50% methanol, 10% acetic acid, 40% water]	2.5g Coomassie R-250 dissolved in 500ml methanol, 100ml Glacial acetic acid and 400ml deionised water
Coomassie de-stain [25% methanol, 7% acetic acid, 68% water]	250ml methanol, 70ml Glacial acetic acid and 680ml deionised water
RIPA buffer Radio immunoprecipitation assay buffer	150mM NaCl, 10mM Tris, pH 7.2, 0.1% SDS, 1.0% Triton-X-100, 1% Deoxycholate, 5mM EDTA

TBE (Tris, Boric Acid, EDTA)	108g Tris, 55g Boric acid, 108g Tris base, diluted into 1L of de-ionised laboratory grade water to establish a 10x solution, subsequently further diluted with an additional 9L of de-ionised laboratory grade water.

2.1.3. Antibodies and staining reagents

OneComp eBeads	eBioscience	01-1111-42

Note: regarding antibody staining: for flow cytometry typically 1-2µl of antibody was used to stain $1x10^6$ cells for both preconjugated and secondary antibodies. Therapeutic antibodies were diluted to 1mg/ml in PBS, with 1µl of antibody used as the primary antibody per $1x10^6$ cells. For Western blotting, antibodies were diluted according to manufacturer's instructions.

2.1.3.1. General antibodies

Annexin V-APC	BD Biosciences	550474
Streptavidin-APC	AbD Serotec	STAR119
Streptavidin-PerCP	BD Biosciences	554064
Anti-Flag M2	Sigma	F3165
Anti-nuclear matrix protein p84	AbCam	ab487
Anti myc-tag biotin	AbD Serotec	MCA2200B
Anti PI3Kinase p85	Merck Millipore	06-497
Anti HA tag biotin	AbCam	ab26228
Anti OLLAS tag	Novus Biologicals	NBP1-06713
Anti V5 tag biotin	Bioss	bs2109R
Anti V5 tag APC	AbCam	ab72560
Anti T7 tag biotin	Bioss	bs2107R

2.1.3.2. Anti–human antibodies

CD3-PE	Beckman Coulter	PN IM1282
CD16-PE	BD Pharmingen	555516
CD20-PE	Dako UK	R7013
CD34-(581)-APC	BD Biosciences	555824
CD34-(QBEnd10)-Biotin	AbD Serotec	MCA547B
CD34-(QBEnd10)-PC5	Beckman Coulter	IM2650U
CD34-(QBEnd10)-AF700	Exbio	A7-566-T100
CD34-(QBEnd10)	Dako UK	M7165
CD56-FITC	BD Biosciences	345811
Anti-human IL15	Sigma-Aldrich	WH0003600M1
Anti-human 4-1BB Ligand	Biolegend	311502
Goat-anti-human-Fc Cy5	Jackson ImmunoResearch	109-175-098
Goat-anti-hFc DyLight488	Jackson ImmunoResearch	109-485-098
Goat-anti-hFc DyLight649	Jackson ImmunoResearch	109-496-127
WT1-TCR Dextramer-PE	Pro-Immune (NLVPMVATV) dextramer	
Rituximab	MAbThera (UCL pharmacy)	

Ofatumumab	(UCL pharmacy)

2.1.3.3. Anti–mouse antibodies

CD4 PE	eBioscience	
CD4 PE-Cy7	eBioscience	25-0041-82
CD4 FITC	eBioscience	11-0042-85
CD8a eFluor 450	eBioscience	48-0081-82
CD90.1 (Thy1.1)	eBioscience	25-0900-82
MHC Class I (H-2Kb) FITC	eBioscience	11-5958-82
MHC Class I (H-2Kd) PE	eBioscience	12-5957-82
Goat anti-mouse Fc-DL649	Jackson ImmunoResearch	115-495-071
Goat anti-mouse Fc-APC	BD Biosciences	550826

2.1.4. Cell lines

HEK293T	Human embryonic kidney cell line
K562	Human chronic myeloid leukaemia
Jurkat	Human acute lymphoblastic leukaemia
Raji	Human Burkitt's lymphoma
SupT1	Human acute lymphoblastic leukaemia
LinXE	Ecotropic envelope packaging cell line
IDEC2B8 Hybridoma	Murine Rituximab Hybridoma HB-11388
2.4G2 hybridoma	Murine 2.4G2 Hybridoma HB-197

2.1.5. Media

Table 5 Supplementary additives to culture media

Medium	Supplements
Complete RPMI (Lonza)	10% FCS (Biosera), 1% GlutaMAX (Invitrogen)
Complete IMDM (Lonza)	10% FCS (Biosera), 1% GlutaMAX (Invitrogen)
mRtx-IgG2a IMDM Phenol red negative (Invitrogen)	2.5% IgG stripped FCS (Biosera/Invitrogen), 1% GlutaMAX (Invitrogen)
Splenocyte media	Complete RPMI + 1% 1M HEPES solution (Sigma) + β mercaptoethanol (BME) at a final concentration of 0.1mM
PBMC assay medium	Complete RPMI as above supplemented with 50i.u. of recombinant human IL2
2.4G2 hybridoma medium	IMDM (Lonza) supplemented with 5% horse serum (Life technologies), 5% FCS (Biosera), 1% GlutaMAX (Invitrogen)
Cryopreservation medium (Lonza)	18ml of FCS was added to Lonza cryopreservation medium to generate a solution containing 15% FCS and 13% DMSO

β mercaptoethanol working stock	50µl of 14.3M BME (Sigma) was added to 7.05ml of molecular biology grade water to generate a 1000x working stock at 0.1M concentration. This was stored at 4°C for up to one month. BME supplementation was performed immediately prior to experimental application.

2.1.6. Equipment

Geneflow Limited	NGene transilluminator
Clare Chemical research	Dark reader DR89X transilluminator
Olympus IX70	Inverted fluorescence microscope
Beckman Coulter	CyAn ADP flow cytometer
BD Biosciences	LSR Fortessa cell analyser
Nanodrop®	ND-1000 Spectrophotometer
AGO HS MP–1	X–ray irradiator
GE Healthcare life sciences	ÄKTAprime plus
Millipore Labscale	Tangential flow filtration (TFF) system
Invitrogen Surelock™	XCell blot module
LKB Wallac	1282 Compugamma Gamma Counter
Vacuum filter dryer	SG200 Savant integrated gel dryer

Heidolph polymax horizontal wave shaker 1040

2.1.7. Monoclonal antibody protein purification:

HiTrap rProtein A FF	GE Healthcare Life sciences	17-5080-01
Vacuum filter unit	Nalgene Labware	450-0020
SnakeSkin Dialysis Tubing, 10,000 MWCO	Thermo Fisher Scientific Inc.	68100
Pellicon XL 50 Ultrafiltration Cassettes	Millipore	PXB050A50

2.1.8. Software

Summit	Beckman Coulter Inc
Flowjo	Treestar data Inc
Clone manager	Sci-Ed software

2.2. Methods

2.2.1. Molecular biology

2.2.1.1. Nucleic acid manipulation and purification

2.2.1.1.1. Splicing by overlapping extension PCR based cloning:

Expression plasmid transgene cassettes were generated using splicing by overlap extension PCR (SOE-PCR). Putative epitope binding fragments were generated in two fragments; with the N-terminal fragment containing NcoI site and the signal sequence and the C-terminal fragment containing the CD8 stalk,

anchor and MluI restriction site. The target site under interrogation was defined by the overlapping internal oligonucleotide primers complimentary to both the flanking sequences and the desired modification. The primary PCR fragments were generated by PCR: (35) cycles of amplification were performed using the following conditions: Melting temperature: 98°C for 120s, Annealing temperature 65°C for 42s and extension temperature 72°C using Phusion polymerase (Extension duration defined by amplicon length; approximately 70 seconds per 1000 base pairs of sequence to be amplified). Following PCR amplification, products were separated by gel electrophoresis and purified using Qiaquick PCR clean-up columns. Primary PCR products were combined using a secondary fusion PCR reaction using the same conditions as above. Following verification of successful amplification, the PCR product was then cleaned up, again using Qiaquick PCR clean-up columns digested using NcoI and MluI restriction enzymes and subcloned into a suitably digested SFG.I2.eGFP destination vector. Sequence integrity of epitope expression mutants were confirmed by capillary sequencing performed in-house by Scientific Support Services. Further details regarding cloning strategies are addressed in Appendix 1.

2.2.1.1.2. Small scale DNA preparation:

Cloning screening scale DNA preparation (miniprep) DNA was prepared as follows: Following bacterial transformation, single colonies were picked from an agar plate and grown overnight in 4ml LB supplemented with 100µg/ml carbenicillin. Following overnight culture, the Qiagen miniprep kit was used to isolate plasmid DNA according to manufacturer's instructions. Constructs were verified by restriction digest and/or DNA sequencing.

2.2.1.1.3. Large scale DNA preparation:

Generation of DNA for *in vitro* and/or *in vivo* modelling (midiprep) DNA was prepared as follows: 50ml of TB were inoculated with 250-500µl of bacterial culture and cultured for 16-18 hours in a bacterial shaking incubator; 220 RPM at 37°C. The Macherey Nagel midiprep kit was used to isolate plasmid DNA as per manufacturer's instructions. Midiprep DNA was verified by separate restriction digests cutting in the vector backbone, retroviral LTR and transgene insert respectively.

2.2.1.1.4. Measurement of DNA concentration:

DNA concentration reflects the property of DNA absorbance of light at wavelength 260nm, while the ratio of absorbance at 260nm:280nm can be used to establish purity. An A260nm:A280nm ratio of 1.8 indicates a high degree of DNA purity with little RNA or protein contamination. Purity and concentration of plasmid DNA was assessed using a nanodrop ND-1000 spectrophotometer.

2.2.1.1.5. Restriction endonuclease digestion

Restriction digests were performed according to manufacturer's instructions (NEB) to establish cloning fragments of DNA with 'sticky' ends to facilitate DNA ligation. For inserts derived by PCR, the entire sample was digested. To generate vector backbone, or vector derived insert fragments, 5µg of plasmid vector DNA was used. In either occasion, the reaction volume was adjusted with molecular grade water such that the final reaction volume was 100µl. Buffer selection and addition of BSA was defined by the manufacturer, with a final enzyme concentration of 5% v/v of the final reaction volume. Where buffers were incompatible, double digestions were performed serially with the digestion sample prepared between the reactions using the Qiagen QIAquick clean-up kit.

2.2.1.1.6. Gel electrophoresis

DNA fragment size verification of restriction digests for molecular cloning plasmids and PCR product DNA was accomplished by DNA separation using agarose gel electrophoresis. 1% Agarose gels were prepared in 1x TBE buffer with agarose solubilisation achieved by microwave heating of the solution. Once solubilisation had been achieved, the agarose was then cooled and infused with 0.5-1µg/ml of ethidium bromide to enable UV visualisation of the DNA. Samples were mixed with loading buffer at a ratio 10:1 prior to loading into the gel to enable visualisation of the sample progression within the gel. Agarose gels were electrophoresed at 110V in 1xTBE buffer until appropriate separation was achieved. DNA visualisation was then achieved using an Ngene transilluminator (dark reader blue light box).

2.2.1.1.7. Gel extraction:

Following separation of DNA fragments by agarose gel electrophoresis, bands were visualised using a dark reader blue light box to prevent UV-mediated

mutagenesis and excised from the gel with a clean scalpel. Gel extraction of DNA was then accomplished using Qiagen QIAquick or Macherey Nagel gel extraction kits, according to manufacturer's instructions.

2.2.1.1.8. PCR clean–up

Following fusion PCR reactions and where it was necessary to perform serial restriction digests due to buffer incompatibility, the Qiagen QIAquick kit was used according to manufacturer's instructions to remove contaminants from the sample prior to downstream processing.

2.2.1.1.9. DNA Ligation

Following gel extraction of the digested vector and insert fragments, DNA ligations were performed using Quick Ligase (NEB) according to the manufacturer's instructions with a vector:insert molar ratio between 1:3-1:6. Following 5 minute incubation at room temperature, 2µl of the resulting ligation mix was used for bacterial transformation of high efficiency C2987 (NEB) chemically competent *E. coli* bacteria.

2.2.1.1.10. Plasmids

The gammaretroviral vector SFG[28] was used for all constructs examined during this course of research. SFG is based on the Moloney MLV, with the transgene start codon located at the start site of the deleted viral envelope gene. Bicistronic transgene expression was achieved by one of two strategies: in constructs indicated with 'I2', the primary transgene was followed by inclusion of the encephalomyocarditis internal ribosomal entry site (IRES) allowing expression of the downstream reporter gene eGFP. In constructs including '2A' within the name, the dual construct was translated as a single peptide, with separation of the separate components achieved by the self-cleaving activity mediated by the TaV (*Thosea asigna* virus) 2A sequence resulting in equimolar expression of both transgenes. Constructs denoted SFGmR also include a scaffold attachment region to enhance transgene expression.

Please see Appendix 1 for further details regarding vector design and modular cloning.

2.2.1.1.11. Codon optimisation / gene synthesis

Codon optimisation/gene synthesis of novel DNA was designed using pMol software written by Dr Martin Pulé. This software is designed to raise the GC

content to 70%, eliminate local sequence repeats, hairpins, cryptic splice sites and to code for preferential codons to enhance gene expression. Overlapping oligonucleotides were designed such that short sections of DNA sequence would be defined by the sequence overlap as illustrated by Figure 6. Using the overlapping oligos as template, two rounds of DNA amplification were performed; the first reaction resulted in short sections of synthetic DNA, with amplification of the desired sequence achieved during the second reaction as defined by the two terminal primers.

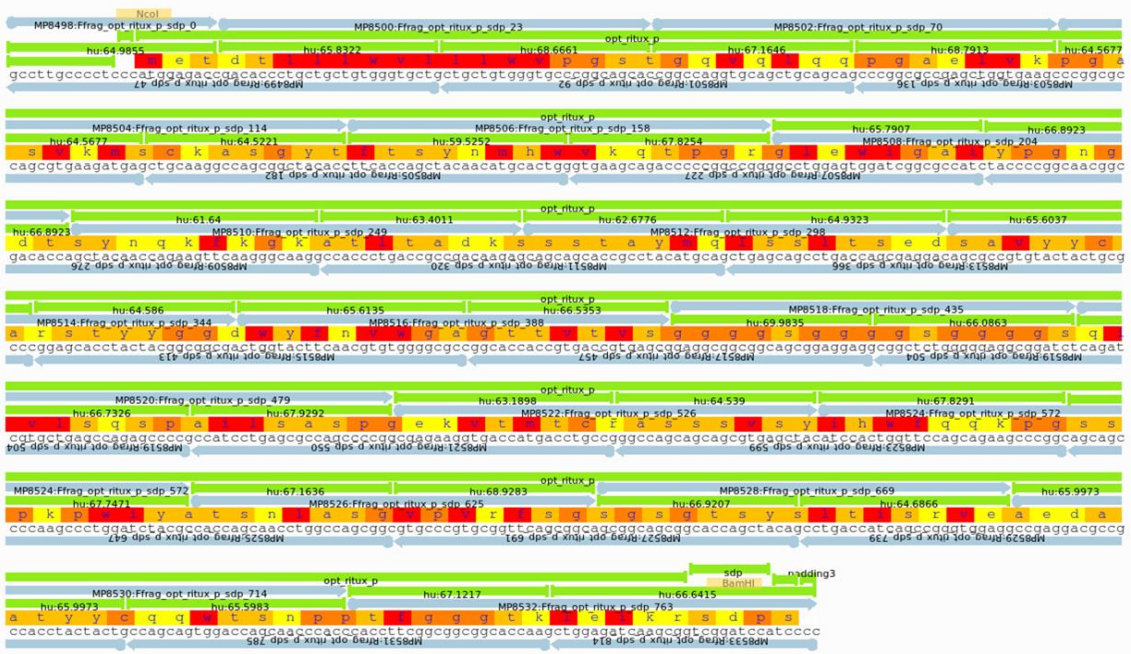

Figure 6 Gene synthesis of the rituximab binding domain in an single-chain variable fragment format
Gene synthesis is achieved through application of overlapping oligonucleotides employed to establish a template DNA sequence following a primary PCR reaction. This template sequence is then amplified through a secondary PCR reaction facilitated by primers binding to terminal sequences which contain engineered restriction sites to facilitate facile restriction-digest mediated cloning. Further detail regarding this cloning is illustrated by Figure 61, p207.

2.2.1.1.12. Trizol®-based RNA isolation

5x10^6 peripheral primary human blood monocytes isolated by ficoll extraction were resuspended in 1 ml of Trizol® reagent, with pipette agitation to achieve generation of single cell suspension to ensure effective cellular lysis. Cells were incubated in Trizol® for 5 minutes at room temperature. Trizol®-cell suspension was then transferred to a sterile eppendorf tube. 200µl of chloroform was added to the Trizol lysate. This suspension was then vigorously vortexed for 15 seconds, incubated at room temperature for 3

minutes then centrifuged at 11500G for 15 minutes. The upper/clear aqueous phase was carefully aspirated and transferred to a fresh sterile eppendorf tube. 500µl of isopropanol was added to this sample which was then inverted twice and incubated at room temperature for 10 minutes. This sample was centrifuged at 11,000G for 10 minutes at 4°C. The supernatant was aspirated by pipette, and the pellet was then washed twice with 1ml of 75% ethanol, each time the sample was re-pelleted by centrifugation at 7000G for 5 minutes at 4°C. Following the second wash, the ethanol supernatant was aspirated by pipette and the eppendorf tube was dried in a sterile hood for 20 minutes. The RNA sample was then resuspended in 40µl of molecular biology grade water and the RNA concentration was assessed by spectrophotometric measurement by nanodrop prior to cDNA generation.

2.2.1.1.13. Generation of cDNA

cDNA was generated from RNA through a two-step process: In the first step, a 20µl reaction mixture composed of 1µg of RNA, 2µl of Random Decamers, 4µl of 2mM dNTP's, with molecular biology grade water composing the remainder of the sample, was heated at 70°C for 3 minutes then transferred to ice for 1 minute. 2µl of 10x reverse transcriptase buffer was then added to the above reaction mixture followed by 1µl of RNasin and 1µl of reverse transcriptase. This second reaction mixture was then incubated for 1 hour at 42°C, followed by 5 minute incubation at 95°C to deactivate the polymerase enzyme. Confirmation of successful cDNA generation was achieved by amplification of the GAPDH housekeeping gene. Forward and reverse primers for the human GAPDH sequence (GCCGAGCCACATCGCTCAGA, GAGGCATTGCTGATGATCTTG respectively) were kindly supplied by Prof. Rosemary Gale. Primers for murine GAPDH amplification (Qiagen) were generously supplied by Dr. Jenny McIntosh.

2.2.1.1.14. Isolation of heavy & light chains from Hybridoma

Hybridoma RNA extraction and successful cDNA generation were confirmed by amplification of the murine GAPDH housekeeping gene using primers supplied by Qiagen. Primers for heavy and light chain amplification were obtained from IDT according to the protocol by Dübel *et al*[190] and amplified using the platinum PCR SuperMix high fidelity kit (Invitrogen) which employs *Taq* polymerase for amplification, selected to facilitate subsequent TOPO-TA

cloning. Successful amplicons were TOPO-TA cloned as per manufacturer's instructions (Invitrogen).

2.2.1.1.15. TOPO–TA cloning

To facilitate facile screening of putative hybridoma cDNA amplicons, we employed a TOPO-TA (Invitrogen) cloning strategy to identify successful isolates. Briefly, the supplied TOPO plasmid vector is supplied in a linearized format possessing a single 3'-thymidine (T) overhang with the Topoisomerase I enzyme covalently linked to the vector. As the *Taq* polymerase demonstrates a non-template-dependent terminal transferase activity, *Taq*-enzyme PCR amplicons possess a 3'-terminal deoxyadenosine (A) overhang. The presence of the corresponding T-A overhangs and the Topoisomerase I enzyme facilitates efficient ligation of *Taq*-amplified PCR products into the linearized vector as illustrated by Figure 7. Following ligation, high-efficiency *E. coli* (NEB) were transformed with the TOPO vector and plated onto Carbenicillin infused agar plates pre-coated with X-gal. Further discrimination of successful vector integrants is achieved through the chromogenic identification facilitated by deletion of galactosidase enzyme activity. X-gal is a lactose analogue which will form an indigo pigmented substrate due to dimerization of 5-bromo-4-chloro-3-hydroxyindole following galactosidase-mediated cleavage. Where the galactosidase enzyme sequence of the TOPO vector is interrupted by PCR ligation, enzymatic activity is ablated and resultant colonies will appear white on the agar plate. Following overnight culture, white colonies located proximal to indigo colonies were isolated for further analysis.

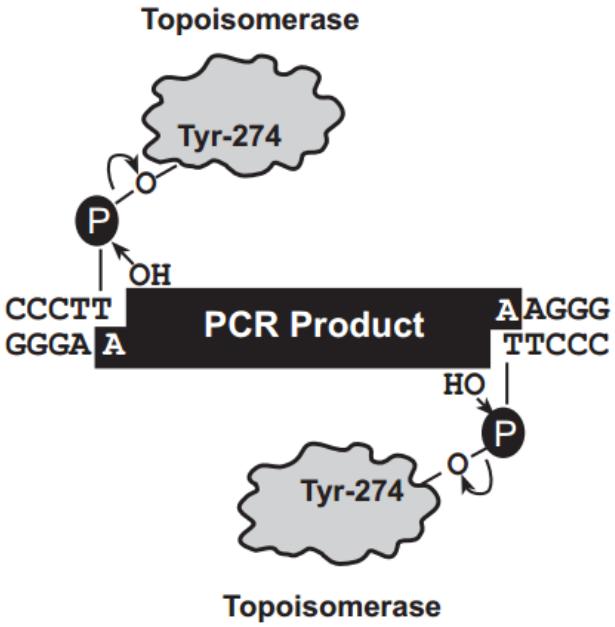

Figure 7 TOPO–TA cloning strategy
Illustration from TOPO-TA cloning manual (Invitrogen).

2.2.1.2. Bacterial manipulation

2.2.1.2.1. Growth and maintenance of *E. coli*

DH5α *E. coli* bacteria were grown in liquid Luria-Bertani (LB) or terrific broth (TB) media (for mini-prep or midi-prep culture respectively) supplemented with 100µg/ml carbenicillin and cultured at 37°C with agitation at 220rpm or on LB-agar infused with 100µg/ml carbenicillin in a static or shaking 37°C incubator as required.

2.2.1.2.2. Bacterial transformation

Chemically competent DH5α *E. coli* bacteria were transformed by a heat shock protocol detailed as follows: 25µl of bacteria were thawed on wet ice. 2µl of ligation mix (for PCR based cloning into C2987 *E. coli*), or 1µl of mini-prep DNA (for retransformation into C2988 *E. coli*) was added to the bacteria and incubated on ice for 30-45 minutes. Bacteria were transiently heat-shocked by incubation in a 42°C water bath for 35 seconds, followed by incubation on ice for 5 minutes. Bacteria were transferred to 250µl of SOC media and allowed to recover for 30 minutes on a shaking incubator (37°C, 220 RPM). Following recovery, bacteria were streaked onto an LB-agar plate infused with Carbenicillin (100µg/ml) and incubated at 37°C overnight in an inverted orientation.

2.2.2. Tissue culture

2.2.2.1. Propagation of cell lines

2.2.2.1.1. Propagation of adherent cell lines

The adherent cell lines HEK293T and LinXE were cultured in complete IMDM in 175cm^2 tissue culture coated flasks at 37^{o}C with a 5% CO_2 atmosphere. Cellular passage was performed, biweekly, once 80-90% confluency was reached. Cells were washed with 1x PBS, incubated for 5 minutes at 37^{o}C with 5ml trypsin/EDTA. Cells were harvested by washing the flask with 20ml of complete IMDM. During maintenance culture, LinXE cells were cultured under hygromycin selection (50µg/ml), but LinXE cells were passaged once in the absence of hygromycin prior to supernatant production.

2.2.2.1.2. Propagation of non–adherent cell lines

The non-adherent cell lines; Jurkat and SupT1 cells were cultured in complete RPMI while K562 cells, were cultured in IMDM, in 80cm^2 tissue culture coated flasks placed in vertical orientation at 37^{o}C with a 5% CO_2 atmosphere. Cell culture densities were maintained approximately between 0.2 and 1x10^6/ml, by 1:8-1:20 dilution with fresh medium as determined by discolouration of phenol red indicator dye contained within the medium.

2.2.2.1.3. Single cell cloning by limiting dilution

For applications where a highly stable cell line was required, single cell cloning was performed to identify a stable isolate. Single cell isolation was achieved by limiting dilution. From a sample of cells previously verified for successful transgene expression and FACS sorted for purity, we performed multiple cell counts using a Haemocytometer to ensure the count was accurate. Cells were diluted appropriately to ensure that on average, 1 cell would be isolated into every third well of a flat bottom 96 well plate. Cellular isolates were cultured until a clear population had been established, which were subsequently screened for transgene expression and culture stability.

2.2.2.1.4. Cryopreservation and recovery of cell lines

As required, transgenic cell lines were cryopreserved for long term storage as follows: Cells to be cryopreserved were harvested whilst in optimal growth conditions. Following centrifugation, cells were resuspended at 5x10^6 cells/ml in chilled cryopreservation medium (Lonza) and aliquoted into 1ml aliquots into cryovials (Corning). Cryovials were placed into a ‘freezy’ tub which was

then transferred to a -80°C freezer. The isopropanol bath of the freezy tub ensures a controlled cooling rate of 1°C/minute. The following day, frozen cells were then transferred to a liquid nitrogen storage dewar for long term storage.

2.2.2.1.5. Cellular recovery from cryopreservation

As the DMSO cryoprotectant is toxic to actively metabolising cells at the concentration present in cryopreservation medium, it is imperative to minimise DMSO exposure during cellular recovery. Vials of cryopreserved cells were thawed by suspension in a 37°C water bath. Once thawed, cells were immediately washed in 25ml of the respective pre-warmed complete media, followed by resuspension in appropriate media and transfer to a 37°C incubator.

2.2.2.2. Primary cell culture

2.2.2.2.1. Isolation of PBMC's

PBMCs were sourced from a departmental donor pool of consenting individuals who had signed an institutional consent form. Whole blood was obtained by venesection into 50 ml syringes prepared with appropriate 0.5M EDTA solution to achieve a final concentration of 5mM EDTA to serve as an anti-coagulant. Whole blood was diluted 1:1 with unsupplemented RPMI with each 25ml of blood solution layered onto 10ml Ficoll-Paque in 50ml centrifuge tubes. Tubes were centrifuged at 750 RCF for 40 minutes at room temperature applying minimum acceleration and without brake. Following centrifugation, the buffy coat layer, localised to the Ficoll:plasma interface, was removed by pastette aspiration. PBMC's were washed twice: once with unsupplemented RPMI and once with complete RPMI prior to final resuspension into a volume of complete RPMI matching the volume of the initial blood donation.

2.2.2.2.2. PBMC stimulation and culture

PBMCs were cultured in 24-well, TC-treated plates at a density of 2×10^6 cells/well. PBMCs were stimulated with PHA on the day of isolation. 24 hours later, PBMC's were stimulated with 100u of IL2 with transductions performed 24 hours following IL2 stimulation.

2.2.2.2.3. Monocyte cell culture

PBMC's isolated by ficoll extraction as detailed in 2.2.2.2.1, were cultured in a T175cm^2 flask overnight in horizontal orientation without stimulation. The following day, the suspension cells were aspirated and the adherent cell fraction was detached by incubation with 5ml of cell dissociation solution for 10 minutes at room temperature. Cells were harvested by washing the flask with 10 of chilled sterile PBS into a 50ml centrifuge tube. Cells were enumerated and pelleted by centrifugation (400 RCF x 5 minutes) pending RNA extraction.

2.2.2.2.4. NK cell expansion for *in vitro* ADCC assays

K562.A5 cells (established as detailed by 2.2.2.1.3 and 0) cultured in complete IMDM were harvested and resuspended in complete RPMI at 1x10^6 cells/ml. 1ml of this cell suspension was placed into each well of a tissue-culture treated 24-well plate. This plate was then irradiated with 120 gray of X-ray irradiation using an AGO HS MP-1 X-ray irradiator. Following irradiation, cells were returned to a 37^{o}C incubator during preparation of PBMC's. Sufficient PBMC's (isolation as described 2.2.2.2.1) were isolated to provide for both the required NK-cell proliferation co-culture and for transduction of cellular targets. PBMC's for NK-cell proliferation co-culture were re-suspended in complete RPMI supplemented with 80u IL2/ml, with 1ml of this cellular suspension added to each well of the irradiated K562 cells detailed above, thereby diluting the Il2 supplementation to a final concentration of 40u/ml. Partial media changes were performed as required dependent on media discolouration as indicated by the phenol-red indicator dye. Cellular co-cultures were mixed as required by pipette agitation to maintain cellular interactions. Additional media supplied during partial media changes was supplement with 40u IL2. Following one week of cellular co-culture and one day prior to commencement of each ADCC assay, the entire PBMC-K562 co-culture was harvested by pipette aspiration and harvested by centrifugation (400 RCF x 5 minutes). Cells were washed once with chilled PBS prior to Miltenyi bead separation using CD56 MACS beads. Following MACS separation, purified NK cells were resuspended in complete RPMI supplemented with IL2 (40u/ml) at 1-1.5x10^6 cells/ml in 24 well tissue culture treated plates. MACS sorted NK cells were used for *in vitro* assays within 24 hours of MACS selection. Validation of the purity and cellular phenotype of bead selected NK

cells was achieved by flow cytometry following antibody staining of the sample against CD56 and CD16.

2.2.2.2.5. Splenocyte extraction

2.2.2.2.5.1. Dissection

Following sacrifice of the donor animal by terminal CO_2 narcosis, confirmed by cervical dislocation, the fur and implements were liberally sprayed with 70% IMS to prevent contamination. Using forceps, the abdominal wall was tented and cut with scissors to enable access to the abdominal cavity. Gentle pressure was applied to the spleen by tweezers located below the organ to identify the vascular pedicle points which were then cut with scissors to release the organ. This was then transferred to a bijou tube pre-filled with sterile PBS and placed on ice until splenocyte extraction could be performed in a sterile tissue culture hood.

2.2.2.2.5.2. Splenocyte extraction

A cell strainer was placed into a 10cm tissue culture dish. Using sterile surgical implements, the spleen was then cut in half. 1ml of ACK lysing buffer was then pipetted over the spleen which was then mashed through the strainer using the blunt end of a 1ml sterile syringe. Once tissue chunks could no longer be reduced by maceration, the cellular suspension was incubated with ACK lysing buffer (Lonza) for 3-5 minutes. Next, the cell strainer was transferred to a 50ml centrifuge tube and 2ml of splenocyte medium was added to the sample to terminate lysis prior to transfer of the cell suspension through the 0.4µm strainer into the centrifuge tube. The tissue culture dish was then washed with an additional 5ml of splenocyte media [RPMI + 10% FCS + 1% Glutamax + [BME]]. Cells were then pelleted by centrifugation (400 RCF for 5 minutes) prior to resuspension at 1-1.5 x 10^6 cells/ml stimulated with Concanavalin A (2µg/ml) and murine IL7 (1ng/ml), plated in 24 well tissue culture plates.

2.2.3. Retroviral work

2.2.3.1. Retronectin coating preparation of TC plates

Non-tissue culture treated 24-well plates were prepared by pre-coating plates with 500µl of PBS supplemented with 8µl of retronectin/ml at least 24 hours prior to suspension cell transduction, with plates wrapped in parafilm and

stored at 4°C until required. Retronectin supplemented PBS was reused twice by direct transfer to fresh plates and stored as above until required.

2.2.3.2. Transient transfection for expression testing

Transient transfections were performed in multiwell TC-treated dishes or plates as defined by experimental requirements with volumes of media, genejuice and DNA as indicated by Table 6

Table 6 Transfection calculation matrix

Plate / dish	Genejuice	Plain media	DNA
100mm dish	30µl	470µl	12.5µg
6-well plate	5µl	95µl	2µg
12-well plate	2.5µl	47.5µl	1µl
24-well plate	1.25µl	23.75µl	0.5µg

2×10^6 HEK293T cells were plated into 6-well plates, 2ml cell culture/well, 24 hours prior to transfection. Cellular confluence was assessed by microscopic examination to ensure optimal density prior to transfection. For transient transfection experiments, cellular confluence between 50-70% proved suitable to achieve consistent clear results.

A bulk transfection mixture was prepared where 5µl of genejuice (Merck) was added to 95µl of plain RPMI for each transfection condition to be tested. Genejuice is a lipid-based transfection reagent that complexes with DNA to mediate transport of DNA into cells during transfection. Following a 5 minute incubation to allow formation of genejuice-micelles, 100µl of the transfection mixture was transferred to a separate well of a round-bottomed 96-well plate. 2µg of plasmid DNA was used for each separate condition to be tested. Following a 15 minute incubation of DNA, transfection was performed by dropwise addition of the transfection mixture over the HEK293T culture.

2.2.3.3. Generation of viral supernatant by transient transfection

Variations in retroviral supernatant production protocols were necessary due to variation in cellular targets and experimental scale required for transduction; alternative protocols are indicated below.

2.2.3.4. General protocol for retroviral supernatant production

2.25 x 10^6 HEK293T cells were plated into 10cm tissue culture treated dishes 24 hours prior to transfection. Cellular confluence was assessed by microscopic examination to ensure an optimal density of 50-60% confluence prior to transfection.

A transfection mastermix was prepared as indicated by Table 6. Following five minute incubation at room temperature, a total volume of 12.5µg of DNA was added for each plate to be transfected. For triple transfections, the following ratios were used to establish the respective volume of plasmid DNA required: 3/8 Gagpol, 2/8 Envelope and 3/8 retroviral vector plasmid. Following addition of plasmid DNA, the mixture was incubated for a further fifteen minutes at room temperature prior to dropwise addition to the HEK293T cell culture. Plates were gently agitated following transfection. Supernatant harvested at 48 hours was stored at 4°C, and then combined with the 72 hour harvest prior to aliquoting and storage at -80°C.

2.2.3.5. LinXE transfections

The LinXE cell line is an ecotropic envelope retroviral producer line selected for constitutive expression of gagpol and ecotropic envelope proteins. This enables the entire 12.5µg capacity of genejuice to be exploited for transfection of the retroviral expression plasmid of interest.

2.2.3.6. Retroviral transduction of cell lines and primary cells

2.2.3.7. General transduction protocol for suspension cells

Retronectin coated wells were aspirated and pre-coated with 250µl of retroviral supernatant and maintained at 4°C during the cellular harvest process.

2.2.3.8. Retroviral transduction of suspension cell lines

Cells were harvested, counted and resuspended at a concentration of 6x10^5 cells/ml. 500µl of this cell suspension was transferred to each well of the retronectin coated plate 1.5ml of retroviral supernatant was added to each well, with cells spin transduced at 1000 RCF for 40 minutes prior to return to the incubator for 2 days.

2.2.3.9. Retroviral transduction of human PBMC's

Retronectin was aspirated from the precoated non-tissue culture plates and wells were incubated with 250µl of retroviral supernatant whilst PBMC's were prepared. Primary human PBMCs, isolated and stimulated as described by 2.2.2.2.1 and 2.2.2.2.2 respectively, were harvested, counted and resuspended at a concentration of $6x10^5$ cells/ml. The PBMC suspension was supplemented with 400i.u./ml of IL2 pending dilution with viral supernatant, resulting in a final transduction IL2 concentration of 100u/ml. Following removal of the retroviral supernatant, 500µl of the PBMC suspension was transferred to each well to be transduced. 1.5ml of retroviral supernatant was added to each well, with cells spin transduced by spinoculation at 1000 RCF for 40 minutes at 37°c prior to return to a 37°C/5%CO_2 incubator for 2 days.

2.2.3.10. Retroviral transduction of murine splenocytes

Stimulated splenocytes were harvested by pastette aspiration into a 50ml centrifuge tube followed by centrifugation (400 RCF for 5 minutes). Cells were resuspended in complete splenocyte media to enable enumeration. Splenocytes were then repelleted, and resuspended in neat supernatant at 1-1.5 x 10^6/ml supplemented with BME but without additional stimulation, and plated onto pre-treated retronectin coated 24 well plates – 1ml/well. Splenocytes were then transferred to a centrifuge and centrifuged at 1000 RCF, at ambient temperature for 90 minutes without application of the centrifugal brake. At completion of the centrifugation, the splenocytes were transferred to an incubator overnight. 24 hours following transduction, splenocytes were then aspirated from the retronectin plate, washed with complete splenocyte RPMI then resuspended in complete RPMI supplemented with IL2 and plated at 1-1.5 x 10^6 cells/ml into 24 well tissue culture plates.24 hours following IL2 stimulation, splenocyte transduction efficiency was measured by flow cytometry analysis prior to progression with downstream experimentation.

2.2.3.11. Retroviral transduction of adherent cell lines

HEK293T cells were transduced as follows: Cells were plated at 1 x 10^6 cells/6-well plate, with 2ml of medium plated per well. The following day, plates were observed for confluence with the well selected for transduction based on confluence, growth and attachment profiles. Transduction was achieved by aspiration of cellular media which was replaced with 2ml of retroviral supernatant supplemented with 20µg of polybrene. Following media exchange,

cells were returned to the 37°C incubator overnight. The above transduction process was repeated daily until the HEK293T cells achieved confluence, when they were subcultured into a 175cm^2 flask.

2.2.4. Flow cytometry

Transduction efficiencies were assessed by flow cytometry based on marker gene expression as indicated by fluorescent protein expression and/or antibody staining. Where antibody staining was performed, the general protocol was performed with modifications performed as indicated. Flow cytometry was performed using Beckman Coulter CyAn ADP or BD LSR Fortessa instruments.

2.2.4.1. General antibody staining protocol

24 hours post transduction recovery; transgenic cells were assessed for transduction efficiency. 3x10^5 cells were washed with PBS, stained with antibody, then washed and resuspended in FACS buffer and placed on ice pending analysis. Where multiple staining steps were required, samples were washed with PBS between individual staining steps. Isotype and/or non-transduced controls were included as required to establish an appropriate benchmark for comparison. All staining steps were performed at room temperature in subdued lighting with 30 minute incubations per stain unless indicated otherwise.

Antibody staining protocol modifications:

2.2.4.1.1. Rituximab staining protocol

Samples were washed with 1% BSA-PBS prior to antibody staining. Samples were stained separately by 0.5µl/sample of Mabthera Rituximab followed by 0.5µl/sample anti-human IgG as a secondary antibody with a PBS wash between stainings.

2.2.4.1.2. Splenocyte staining protocol

Samples were blocked with 300µl of 2.4G2 hybridoma supernatant for 15-30 minutes at room temperature prior to any antibody staining steps. Where anti-human IgG was used for staining, this was applied as the primary stain, followed by QBEnd10 staining, with all remaining antibodies added collectively in the final staining step.

2.2.4.1.3. Annexin V / PI staining protocol

As calcium ions have been proposed to be involved in cellular attachment processes[191], these ions are typically excluded from PBS buffers to reduce cellular aggregation. However as calcium is a required co-factor to achieve Annexin-V binding as indicated by the supplier (BD), preparation of a suitable calcium supplemented buffer is necessary when performing Annexin V staining as described, *vide supra*.

Samples were washed with Annexin V buffer instead of PBS prior to staining. Annexin V staining was performed at room temperature for 15 minutes. PI staining was achieved by resuspending cells into Annexin V buffer supplemented with 5µl of PI stock per ml of buffer sample. Samples were retained on ice pending analysis.

2.2.4.1.4. PFA fixation protocol

Where sample analysis was delayed overnight, following the final wash after antibody staining, samples were fixed by final resuspension into 0.4% PFA-PBS solution and stored at 4°C pending flow cytometry acquisition.

2.2.4.1.5. CellTRACE™ staining protocol

Miltenyi CD56 bead purified NK cells were labelled with CellTRACE™ violet (Invitrogen) according to the manufacturer's protocol immediately prior to inclusion into ADCC assay co-cultures.

2.2.4.1.6. Preparation of counting beads

Where it was necessary to enable cellular enumeration within a sample, or to enable effective comparison between samples, samples were supplemented with a pre-determined quantity of fluorescent 'counting beads' as an internal control. Beckman Coulter Flow-Check™ fluorospheres are supplied at $1x10^6$ beads/ml in an aqueous solution containing preservative surfactant. To prevent toxicity to cellular samples, beads were washed once with PBS prior to addition to samples. Following centrifugation (400 RCF x 5 minutes), beads were resuspended in an equal volume of FACS buffer with 10µl of beads (10,000) added to each sample.

2.2.5. *In vitro* assays:

2.2.5.1. Serial dilution assay to assess QBEnd10 binding sensitivity

One of the proposed applications for RQR8 is to function as a marker gene to enable periodic engraftment assessment from clinical samples. To model this capacity, we premised that it would be necessary to mimic the clinical scenario as accurately as possible. Peripheral human blood PBMCs were transduced and MACS selected for purity. Following confirmation of purity by flow cytometry, transgenic and freshly isolated PBMCs solutions were prepared at 1 x 10^6 cells/ml. MACS sorted PBMCs were mixed with autologous PBMCs freshly isolated from the same donor used to generate the transgenic cell product which were then combined in a 50:50 ratio generating the top dilution sample. Subsequent dilutions were achieved by serial dilutions of this sample into equal volumes of fresh PBMCs at 1 x 10^6 cells/ml. Efficacy of cellular marking was examined by flow cytometry assessing the ratio of QBEnd10$^+$/CD3$^+$ against QBEnd10$^-$/CD3$^+$ fractions.

2.2.5.2. *In vitro* magnetic selection protocols

Miltenyi MACS reagents were used to facilitate both positive and negative selection of cells as required. Protocol was adapted from manufacturer's instructions as indicated. In all cases, following cell harvest, cells were washed once in chilled MACS buffer prior to resuspension in 300µl of MACS buffer and incubation of MACS beads (volume of beads used as indicated). Incubation with magnetic beads was performed on ice for 25-30 minutes followed by a single wash with MACS buffer prior to column separation.

2.2.5.3. CD34 magnetic bead positive selection

Magnetic bead selections were performed for cell lines as well as both primary human T-cells and murine splenocytes. For cell lines, 20µl of beads were used to select <1.0x10^7 cells, separated using an MS column. For both human and murine primary T-cells, 100µl of beads were used to select <1.0x10^8 cells, separated using LS columns. Finally, to achieve effective separation of murine splenocytes, it was necessary to block Fcγ-receptors present in the cellular population to reduce background binding. This was achieved by incubation of each cellular sample in 1ml of 2.4G2 hybridoma supernatant for 15 minutes at room temperature. 1ml of conditioned medium was then added to the cells to ensure viability retention with cells incubated with 2.4G2 supernatant for an

additional 15 minutes at room temperature prior to a single wash with MACS buffer followed by magnetic bead incubation and separation as above. Where required, multiple separations were performed in tandem.

2.2.5.4. CD56 magnetic bead positive selection

Primary human NK cells were isolated from K562.A5:PBMC co-culture by CD56 magnetic bead positive selection. As above, 100µl of beads were used to select $<1.0x10^8$ cells, separated using LS columns. Where required, multiple separations were performed in tandem.

2.2.5.5. CD56 magnetic bead negative selection

To exclude residual NK cells and potential lymphokine activated killer cells prior to chromium release assays, samples were depleted of CD56 expressing effector cells. For negative depletions, 20µl of beads were used to select $<1.0x10^7$ cells, separated using LD columns. Where required, multiple separations were performed in tandem.

2.2.5.6. CDC assays

2.2.5.6.1. General CDC assay protocol

Cells were harvested, counted and resuspended at $1x10^6$ cells/ml in RPMI supplemented with 50u of IL2/ml. 300µl of cellular suspension was transferred into each of 4 wells of a 48-well TC plate. 100µl of complete media was added to the first well. 96µl of complete media and 4µl of Mabthera Rituximab was added to the second well. 100µl of freshly prepared baby rabbit complement was added to the third well and 96µl of baby rabbit complement and 4µl of Mabthera Rituximab was added to the fourth well. Plates were returned to the 37°C incubator for 2 hours. The assay was terminated by addition of 1ml of chilled Annexin V buffer and transfer of the sample into a pre-prepared FACS tube containing 3ml of Annexin V buffer. Samples were harvested by centrifugation, the supernatant was discarded and residual buffer was blotted on paper towelling. Samples were then stained with 1µl of Annexin V-APC, vortexed, and incubated in subdued lighting for 15 minutes. Samples were then washed with Annexin V buffer and resuspended in Annexin V buffer supplemented with 5µl of propidium iodide/ml buffer and placed on ice pending flow cytometry analysis performed immediately following final suspension. Procedural variations to the general protocol are indicated below.

2.2.5.6.2. Sensitivity CDC assay protocol

Transgenic PBMCs were verified by antibody staining to establish approximately equivalent transduction efficiency prior to progression with the *in vitro* CDC assay.

2.2.5.6.3. Specificity CDC assay protocol

Primary human PBMCs were transduced with SFG.Q8.I2.eBFP2 as an internal negative control compared against epitope constructs as indicated, but always and SFG.RQR8.I2.eGFP. Following transduction, transgenic PBMC's were positive sorted with CD34 Miltenyi magnetic beads and recovered for 1-2 days prior to CDC assay. Cells were counted and then mixed together such that an approximate 50:50 mix of the two populations was achieved. Sample mixture was confirmed by flow cytometry analysis prior to progression to CDC assay where the target population was exposed to rituximab (100µg/ml) in the presence (CDC), or absence (control) of baby rabbit complement for 4 hours. Following 4 hour incubation, cells were Annexin V / PI stained and analysed by flow cytometry to assess the deletion of the eGFP expressing target population.

2.2.5.6.4. Time–course / Dose–titration CDC assay protocol

Sample preparation protocol was as described by 2.2.5.6.3 above, with analyses extended to additional assay durations of: 1, 5, 10, 30, 60 and 120 minutes and alternative rituximab concentrations of 12.5, 25, 50 and 100µg/ml.

2.2.5.7. ADCC assays

2.2.5.7.1. General ADCC Assay protocol

Effector cells were harvested and resuspended at $6.4x10^6$ cells/ml in assay media. Appropriate effector target ratios were achieved by serial dilution of the effector stock solution resulting in the final effector:target ratios: 16:1, 8:1, 4:1 and 2:1. Target cells were harvested and resuspended at $1x10^6$ cells/ml in assay media. Wells of a 48 well plate were prepopulated with 400µl of assay media. 100µl of target cell suspension was added to each well to be tested. 10µl of rituximab stock sample was then added to each well. Finally, 500µl of the effector cell suspension was added to the respective wells. A control well to identify background killing was established by combining effectors and targets in the absence of rituximab. Assay duration was defined by the window

between additions of the effector population to the harvest of the assay suspension into chilled Annexin V buffer. Procedural variations to the general protocol are indicated below.

2.2.5.7.2. ADCC assay optimisation

To optimise ADCC assay conditions, the efficacy of alternative effector populations was compared. Effector cells considered were NK cells purified by Miltenyi CD56 positive selection (2.2.5.4), or freshly ficolled PBMCs. In either condition, the effector cell population was derived from the same donor as the transgenic cellular targets.

2.2.5.7.3. Sensitivity ADCC assay

NK cell effectors were stained with CellTRACE™ reagent (Invitrogen) immediately prior to preparation for the assay (2.2.4.1.5).

2.2.5.7.4. Specificity ADCC assay

All targets and effectors were Miltenyi MACS sorted 24 hours prior to assay.

Target population was composed of an approximate 50:50 mix of Q8.I2.eBFP2 transgenic PBMC's mixed with an equal ratio of the desired target in question. Sample composition was assessed by flow cytometry to ensure optimal profile was achieved.

Cellular killing was assessed by comparison of the 'initial ratio' (IR) against the 'final ratio' (FR) based on the fluorescently labelled target populations according to the following equation: Killing %=100*[eGFP:eBFP2 (IR) – eGFP:eBFP2 (FR)]. The IR was defined by the ratio between fluorescently labelled eGFP targets compared to the eBFP2 labelled controls from the effector:target condition cultured in the absence of rituximab.

2.2.5.8. ^{51}Cr release assays

Chromium release assays remain the gold standard for assessing cellular cytotoxicity. Briefly: target cells are 'loaded' with radiolabelled sodium chromate, which becomes retained within target cells due to binding of chromium to cellular proteins. In co-culture assays, cellular lysis resulting from cytotoxicity can be assessed by release of radiolabelled ^{51}Cr into the cellular supernatant. As chromium loading varies between cell types and there can be spontaneous release of chromium from the target cells, it is necessary

to include minimum (background release) and maximum release (achieved through Triton-X-100 mediated target lysis) controls to establish the parameters for the assay.

Functional demonstration of the modular capability of RQR8, and the abrogation of functional activity was measured by chromium release assays performed against SupT1 target cells transgenic for GD2.

Chromium release was calculated as follows:
Chromium release = [(Experimental release – background release)*100] / (Maximum release – background release)

2.2.5.8.1. ^{51}Cr loading of SupT1 target cells

Approximately 1x10^{6} target cells were isolated for each target to be assessed. Cells were harvested by centrifugation, the supernatant was discarded and the residual cell pellet was gently flick re-suspended. 3.7 MBq of ^{51}Cr as sodium-chromate was added to each tube of targets. Target cells were gently agitated every 15 minutes during the one-hour ^{51}Cr loading step. Following chromium loading, residual chromium was removed by 5 complete media washes, prior to resuspension of the target cells for enumeration.

2.2.5.8.2. Effector cell preparation

Donor PBMC's were transduced with the RQR8.2A.GD2-CARpvaa construct. Following transduction, cells were purified by CD34 Miltenyi bead positive selection. Purified cells were then combined with non-transduced PBMC's from the same donor such that the resulting population was approximately equal in distribution for transduced and non-transduced cells. This cellular mixture was then divided in half and subjected to a complement lysis assay in which only one sample was exposed to Rituximab although both samples were incubated with complement. Following 2-hour incubation, cellular samples were recovered and cultured for 2-3 days prior to inclusion into the ^{51}Cr release assay. Cytotoxic capacity of the cellular populations was compared against a non-transduced control effector assay against the same cellular targets.

2.2.5.9. Wax embedding of cell pellets for Immunohistochemistry

In an attempt to enable immunohistochemistry (IHC) using cells expanded through *in vitro* culture, we performed the following protocol to embed a cell

pellet within agarose. Briefly, cell pellets were composed of approximately $10x10^6$ cells with the following compositions: (a) NT PBMC:Raji pellet - $1.85x10^6$ non-transduced PBMCs and $7x10^6$ wt Raji cells, (b) NT/RQR8 PBMC:Raji pellet $3.6x10^6$ non-transduced PBMCs, $1.85x10^6$ RQR8 transduced and MACS sorted PBMCs and $4.5x10^6$ wt Raji cells. Once the cell compositions had been generated, cells were pelleted by centrifugation and resuspended in 3ml of neutral buffered formalin and fixed overnight at room temperature. The following day, a 2% agarose gel was generated using cell culture grade agarose prepared in deionised laboratory grade water. This was then cooled to 60 °C using a water bath. 500µl of the 2% agarose was transferred to a 1.5ml eppendorf tube and allowed to set. The fixed cell compositions were then pelleted by centrifugation and the NBF supernatant was discarded. Cells were briefly warmed in the 60°C water bath, then resuspended using 750µl of the 2% agarose and transferred to the eppendorf containing the set agarose base then briefly centrifuged at 7000 RCF for 15 seconds to establish a cellular layer within the agarose matrix. Following agarose solidification, the pellet was extruded from the eppendorf tube in preparation for sectioning and IHC. Sectioning and IHC was performed by Jennifer Patterson and Teresa Marafioti.

2.2.5.10. Protein work

Sodium dodecyl sulphate polyacrylamide gel electrophoresis (SDS-PAGE) is a common technique used to separate proteins based upon molecular weight. SDS is an amphipathic detergent comprising an anionic headgroup and a lipophilic tail. SDS binds non-covalently to proteins conferring a negative charge thereby masking the intrinsic charge of the native protein resulting in proteins within a sample to possess similar mass-charge ratios. Thus PAGE of SDS-labelled proteins results in 2-dimensional protein separation essentially based upon molecular weight. Following protein transfer to a nitrocellulose membrane, separated proteins can be visualised by protein staining dyes such as Coomassie R-250 or through enhanced chemiluminescence (ECL) involving chemical reactions between hydrogen peroxide, horseradish-peroxidase and a luminol substrate. Protein binding by Coomassie R dyes is thought to be analogous to SDS binding as both molecules are amphipathic containing both a negative charge and hydrophobic moieties[192].

2.2.5.10.1. Western blotting (Protein immunoblotting)

2.2.5.10.1.1. Western blot sample preparation

Carboxy-terminal flag-tagged derivative constructs of the CD8 stalk-bound constructs: Q8 and RQR8, were compared against a similar CD8 stalk construct lacking an epitope Jurkat cell populations transduced with the respective constructs were harvested by centrifugation. Supernatant was discarded and the pellet was freeze fractured through three cycles of freeze-thaw cycling using a dry ice ethanol bath to freeze cells and a 37°C water bath for rapid thawing. Finally, the sample was thawed by addition of 1ml of radio immunoprecipitation assay (RIPA) buffer supplemented with 40µl of protease inhibitor cocktail. Samples were then placed onto a pre-chilled shaking incubator at 4°C for 1 hour to degrade the membrane fraction. Following cellular lysis, the protein sample was then centrifuged to pellet the cellular debris; protein supernatant was gently aspirated by pipette, aliquoted into Eppendorf tubes and stored at -80°C until required for Western blotting.

2.2.5.10.1.2. Western blotting

Western blotting was performed by Clare Shepherd with staining details as indicated in figures.

2.2.5.10.2. Coomassie staining

2.2.5.10.2.1. Coomassie sample preparation

Protein samples were diluted with water as required with the final sample diluted by1/2 with Laemmli sample buffer prior to separation.

2.2.5.10.2.2. Coomassie staining

Protein samples were separated using a 7.5% acrylamide gel. Post-separation, the gel was transferred to a staining tray, covered with 0.25% Coomassie R-250 stain solution and stained for 30 minutes assisted with gentle agitation supplied by a rotating plate shaker. Staining solution was decanted and the gel was destained with a Coomassie destain solution, again with gentle agitation with paper towelling added to the tray to mop up the Coomassie stain. Further destain solution was added as required until the protein bands became clearly visible. Finally, the protein gel was transferred onto a matching size piece of Whatman filter paper, covered with cling film and dried with a vacuum filter dryer for 30 minutes.

2.2.5.11. Protein production / Murine rituximab purification

2.2.5.11.1. Production

Murine rituximab (mRtx-IgG2a) production was achieved by batch culture of the K562.A7 producer line. For each production run, a fresh sample of the cryopreserved producer line bank was thawed and recovered for one passage, cultured in standard IMDM medium, prior to generation of the seed culture for a batch production run. Once sufficient producer cells had been generated, cells were harvested and washed once with PBS prior to transfer to the antibody production media. A seed sample of 5-10 x 10^6 producer cells was transferred to 100ml of culture medium in T175cm culture flasks placed in horizontal orientation. Flasks were gently agitated once daily to ensure sample mixing. K562.A7 culture was allowed to progress for approximately 7 days or until a toxic density had been reached indicated by reduction in cellular viability. Batch culture was harvested into 250ml centrifuge tubes with cells pelleted by centrifugation (10 minutes at 400 RCF). The cellular supernatant was transferred to Duran bottles with a sample isolated for a test titration against transgenic targets to confirm presence of protein prior to downstream processing.

2.2.5.11.2. Concentration

Protein supernatant samples were vacuum filtered through a 0.22µm filter prior to concentration using a Millipore Labscale tangential flow filtration (TFF) system. A ten-fold concentration was achieved with each litre of cellular supernatant concentrated to a final volume of 100ml. Samples were taken at intervals for subsequent analysis to ensure sample concentration had been successful prior to antibody harvest.

2.2.5.11.3. Dialysis mediated buffer exchange

Following concentration, the concentrated protein sample was transferred into snakeskin tubing and dialysed overnight into the column loading buffer: 20mM Sodium phosphate pH 7.0, at 4°C with gentle agitation mediated by magnetic stirrer to ensure effective buffer transfer.

2.2.5.11.4. Purification

Antibody harvest was achieved by Protein A purification using an ÄKTAprime plus system with each 100ml of concentrated sample purified separately.

The protein A column was prepared as per manufacturer instructions prior to sample loading. Sample was loaded at 1ml/min with 5 volumes of loading buffer washed through the column following sample loading, or until the loading profile reflected an absence of sample. Target eppendorf tubes pre-filled with 100µl of pH 9.0 Tris-HCl buffer were prepared for the elution fractions and antibody was eluted with pH 3.5 sodium citrate elution buffer into 1ml fractions. Dilute elution fractions were combined and concentrated using Microcon columns, then pooled with peak elution fractions. The pH of the concentrated antibody product was assessed using pH indicator strips and balanced to pH7 with pH9 Tris-HCl.

2.2.5.11.5. Murine Rituximab product validation

Antibody product was then syringe filtered with a 0.22µm syringe filter for sterility with protein concentration assessed by A280 spectrophotometry and confirmed by ELISA. Functional activity of the product was verified by *in vitro* CDC and indirect staining assays.

2.2.6. *In vivo* modelling of RQR8 depletion

Following *in vitro* development of the RQR8 marker-suicide gene, functional efficacy of cellular deletion afforded by this putative suicide gene was examined *in vivo* with respect of intended clinical application. The use of animal models in research is generally considered acceptable when *in vitro* investigation cannot adequately mimic the wider biological environment and where suitable animal models exist. As the complex interplay between effector mechanisms mediating deletion in the face of antigenic challenge cannot be fully investigated *in vitro*, we believe it is justified to use animal models to examine efficacy of RQR8-mediated deletion. *In vivo* modelling was performed under a UK home-office approved project license and in accordance with institutional policies. Experiments employed female Balb/c, C57BL/6 or CB6F1 mice aged between 6-10 weeks, as indicated in experimental designs. Mice were housed in individually ventilated cages.

2.2.6.1. Preparation of cells for injection

Transgenic splenocytes prepared by the five-day protocol (0) were maintained in optimum culture conditions until immediately prior to transfer when they were washed once with PBS, then resuspended into a minimal volume of

chilled plain RPMI supplemented with 1% HEPES such that each 200µl would contain the desired dosage.

2.2.6.2. Preparation of therapeutic reagents for injection

Therapeutic doses of mRtx-IgG2a were prepared by dilution of the stock sample with PBS such that each 200µl of injection sample contained 150µg of mRtx-IgG2a. Control recipients were infused with an equal volume of sterile PBS.

2.2.6.3. I.V. & I.P. injection (preparation)

Experimental animals were transferred to a warming chamber set at 39-42°C to facilitate peripheral vasodilation prior to I.V. injections.

2.2.6.4. Bone marrow harvest

Following animal euthanasia by CO_2 narcosis and confirmed by cervical dislocation, the right femur was removed and transferred to PBS pending cellular harvest. The ends of the bone were removed by scissors with the contents of the bone PBS flushed using a 25G needle into a 50ml centrifuge tube. Cells were pelleted by centrifugation. Bone marrow samples were then resuspended into 1ml of ACK lysis buffer, vortexed, then incubated for 5 minutes to lyse residual RBCs; termination of lysis was achieved through 10x dilution with PBS followed by filtration through a 70µm filter, centrifugation and final resuspension into PBS followed by transfer to a 96-well U-bottom plate for antibody staining.

2.2.6.5. Tail vein venepuncture and peripheral blood preparation

Animals were heated in a warming box to 39°C prior to blood collection to assist tail vein identification. 1ml syringes with 27G needles were prepared with 10µl of Heparin sulphate solution (1000IU/ml)/100µl of blood to be collected. Following collection, blood was transferred to a 1.5ml eppendorf tube and placed on ice pending further handling. Red blood cell lysis was achieved by osmotic shock as follows: 4.5ml of deionised distilled water was transferred into a 15ml centrifuge tube. 1ml of water was aspirated by pastette and used to wash the peripheral blood sample from the eppendorf tube. The blood was then mixed 3x in the water sample before being osmotically stabilised by addition of 500ml of 10x HBSS buffer solution. Samples were then harvested by centrifugation prior to subsequent staining.

2.2.6.6. Organ preparation for histology

At the conclusion of GvHD modelling experiments, samples of tissue were obtained for immunohistochemistry (IHC) analysis in addition to those obtained for flow cytometry analysis. To enable effectively isolation of all tissues required, samples were obtained in the order detailed below:

Following CO_2 sacrifice confirmed by cervical dislocation, mice were placed on tissue paper and liberally sprayed with ethanol. The skin from the nape of the neck was tented up by tweezers and excised by scissors and placed in a flattened orientation in the IHC chamber. Next, the lymph nodes then spleen were extracted and transferred to PBS. Then a section of liver tissue was taken for IHC analysis. The diaphragm was then perforated to enable access to the lungs with a section of lung tissue also taken for IHC analysis. Next the intestines were moved to once side to enable identification of the large bowel working back from the anus. A 1-2cm section of bowel was excised and perfused with sterile PBS by syringe to extrude faecal matter. Then the bowel was cut by scissors and opened outward to form a sheet and transferred to the IHC chamber. Finally, the right hind limb was removed and the femur and tibia were extracted and transferred to PBS to enable bone marrow analysis.

Tissue samples for IHC were placed into plastic histosette cassettes prepared with PBS moistened paper towelling to prevent desiccation during sample preparation. Following isolation, chambers were secured and transferred to PFA pots pending wax embedding and sectioning. Samples for flow cytometry were placed into bijou tubes prepared with PBS and maintained on ice pending further handling.

Chapter three

3. QBEnd10 and Rituximab epitope mapping

An epitope represents the minimal antigenic determinant required to mediate specific identification by an antibody. Reduction of the requirement for expression of an entire cell surface antigen to the minimal epitope sufficient to enable antibody-mediated identification could significantly reduce the molecular footprint required to achieve transgene expression for gene marking or an antibody-mediated suicide gene strategy.

3.1. Aims

- To identify and epitope map the QBEnd10 binding domain from the CD34 antigen
- To establish an optimal expression mechanism to test putative epitope expression
- To demonstrate effective MACS sorting of QBEnd10 binding epitope construct in transgenic PBMC's
- To identify a minimal rituximab binding epitope
- To establish a dual expression construct demonstrating good binding capacity for both target monoclonal antibodies

3.2. Introduction

3.2.1. The CD34 antigen

Features of an ideal marker gene include: cell surface expression limited to engineered cells without significant leakage of antigen, of human derivation so as to be non-immunogenic, should not interfere with cellular metabolism and should enable clinical grade selection compatible with current technology[127]. As the CD34 antigen meets all the criteria for a suitable marker gene, it is unsurprising that it was identified as a putative marker gene by Fehse *et al*[127]. However, recognising that only the QBEnd10 epitope is required to enable this functional capacity, we propose an elegant refinement to previous work to achieve this effect without imposing the full transcriptional burden into an expression cassette.

The CD34 antigen is a 115 kDa, 385 amino acid heavily glycosylated type I transmembrane sialomucin. The large molecular mass of this antigen is

primarily attributed to extensive O and N-linked glycosylation, with the predicted mass of the native protein sequence alone approximated to be only 40 kDa. Research into the CD34 antigen largely followed from the identification of CD34 as a stem cell antigen, with isolated $CD34^+$ cells proving capable of reconstituting all haematopoietic lineages. In addition to haematopoietic stem cells, CD34 is also expressed on a range of other tissues, including small vessel endothelial cells, fibroblasts and some leukaemias[193, 194].

Despite significant research into the CD34 antigen, a definitive biological role remains to be established. Although no ligands have been identified for the stem cell isoform of the CD34 antigen, when expressed on high endothelial venules variant glycosylation of the CD34 antigen enables tethering and transmigration of leukocytes mediated by L-selectin-CD34 interactions[195, 196]. Early reports suggesting a potential role for CD34 as an adhesion molecule conflict with more recent evidence implying a role for CD34 and similar family members as anti-adhesion molecules. However, as indicated in the early literature, the absence of a defined ligand for CD34 might indicate an indirect role in adhesion by which CD34-mediated activation could result in upregulation of alternative adhesion molecules thus potentially explaining this observation[197, 198].

A naturally occurring 323 amino acid splice variant of CD34 also exists resulting from introduction of a translational stop codon[193]. Some evidence suggesting variant regulation in cellular differentiation patterns resulting from expression of the full-length versus truncated isoform may suggest a role for the CD34 antigen[199]. This alteration in signalling behaviour might reflect the lack of protein kinase C interaction domains from the endodomain in the truncation variant.

CD34 antibodies have been separated into three classes based upon epitope properties; type I antibody epitope are sensitive to both neuraminidase and O-sialoglycoprotein endopeptidase (OSGE) treatment, type II antibody epitopes such as QBEnd10 are neuraminidase resistant but remain sensitive to OSGE, whilst class III antibody epitopes are resistant to treatment with both enzymes[193, 194]. The QBEnd10 is the monoclonal antibody utilised by Miltenyi in their CD34 CliniMACS reagents.

3.2.2. The CD20 antigen

The CD20 antigen, (Bp35), is a 33-37 kDa, 297 amino acid, non-glycosylated phosphoprotein with expression restricted to the B-lymphocyte lineage. CD20 expression is further restricted within specific B-cell development stages between the pre-B cell stages through to mature B-cells whilst remaining mostly absent from pro-B-cells and plasma cells as illustrated by Figure 8.

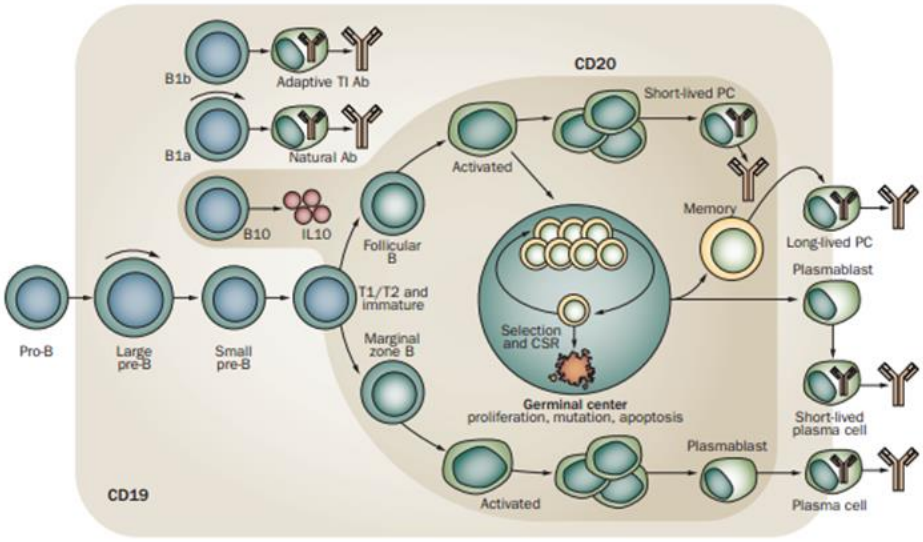

Figure 8 CD20 expression during B cell development
Tedder, 2009[200]. As illustrated by this cartoon, CD20 expression remains primarily restricted to mature B-cells excluding early B-cell precursors and plasma cells. As a result, although rituximab-mediated depletion of the B-cell compartment may impose B-cell aplasia, humoral immunity remains largely intact due to immunoglobulin stability and retention of the plasma cell compartment.

Thus, transient therapeutic ablation of the B-cell compartment does not significantly impair immunoglobulin production, nor does it harm the development of new B-cells. Furthermore, B-cells represent a disposable tissue in that antibodies, the B-cell product of adaptive immunity, can be readily supplemented through immunoglobulin infusion therapy as required. The tetraspan structure of the CD20 antigen results in the formation of two extracellular loops; one minor, and one major loop with the rituximab epitope localised to the major loop[201]. Despite significant research, no natural ligand for CD20 has yet been identified and as CD20 knockout mice retain a near normal phenotype, current understanding of the function of CD20 has been inferred from antibody-ligation signalling experiments[186, 201]. CD20 appears to be involved in regulating cellular calcium levels following B-cell receptor (BCR) ligation by acting as a store operated calcium channel. Further, following BCR

ligation this CD20-BCR association is lost with CD20 subsequently associating with calmodulin-binding and phosphoproteins implying a role in signal transduction. Overall, evidence suggests a role for CD20 in amplifying the signal mediated by the BCR in immature and mature B-cells[202]. Treatment of CD20 bearing target cells by some anti-CD20 antibodies results in the segregation of CD20 molecules into lipid rafts and this behaviour appears to correlate with the ability of the antibody to mediate complement mediated cytotoxicity[201].

CD20 was identified as an attractive target for monoclonal antibody therapy for multiple reasons; it is neither shed into the circulation nor internalised following antibody binding, it is not present in soluble form in the circulation, it possesses a favourable expression profile demonstrating a relatively high level of expression and the extracellular epitopes are located proximal to the cell surface allowing localisation of bound antibody close to the target cell thereby enabling effective engagement of Fc-dependent effector mechanisms[186, 202]. The characteristics, which make CD20 an ideal target for non-Hodgkins lymphoma (NHL) remain equally valid for the argument to establish CD20, as a putative suicide gene.

Due to cell surface localisation of CD20 and the existence of both therapeutic and CliniMACS reagents, in theory CD20 could offer dual functionality posing as both sort and suicide gene moieties. Moreover, rare instances of CD20 positive lymphomas and leukaemias suggest potential for CD20 expression on T-cells[203]. However, reports of toxicity resulting from CD20-mediated selection have necessitated the co-expression of a marker gene to enable cellular selection for CD20 suicide gene constructs[154]. Whatever the mechanism imposing this toxicity, this observation suggests potential retention of signalling capacity which poses concern given the limited understanding of the biological function of CD20. Given this concern, it seems logical to consider truncation of the CD20 endodomain to delete the functional capacity of the antigen. However in our hands deletion of the signalling endodomain further impairs CD20 expression. Further, despite multiple groups attempting to establish CD20 as a suicide gene, the lack of truncated forms of CD20 cited in the literature suggest other researchers may have noted similar observations.

Lastly, mimotopes are short peptide sequences, identified by phage display, which mimic the epitope recognised by a therapeutic antibody. Having a smaller size than the native antigen, mimotopes can be readily synthesized and manipulated for applications such as antibody research or vaccination to induce immune responses against the native antigen[204]. For our purposes, theoretically they offer pre-mapped epitope binding alternatives.

3.3. Results: Generation of Retroviral library from CD34

Experimental aim: to epitope map the QBEnd10 epitope from the CD34 antigen to establish an effective cell surface presentation strategy for this epitope.

The CD34 cell-surface antigen is a highly glycosylated sialomucin widely used for identification of haematopoietic stem cells. Previous work with the CD34 protein suggested that the QBEnd10 binding epitope of the CD34 antigen is localised to the amino terminus of the molecule[193]. To minimize the QBEnd10 epitope from the CD34 antigen, a retroviral library of overlapping PCR fragments was generated from a collection of overlapping primers amplifying a portion of the amino terminus as illustrated by Figure 9.

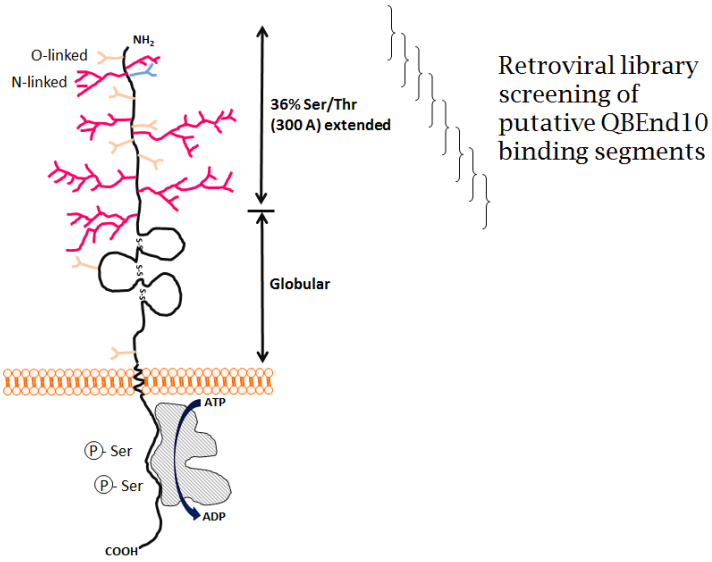

Figure 9 Library generation of putative QBEnd10 binding fragments
Figure adapted from Sutherland *et al*[205]. The cell surface antigen CD34 is heavily glycosylated containing multiple O- and N-linked glycosylation sites, which in addition to the globular domains, are proposed to mediate projection of this antigen away from the cellular surface. As the QBEnd10 epitope has been proposed as a linear epitope localised to the amino terminus of the CD34 antigen, a library of overlapping sequences was established by PCR amplification with the aim to identify only the critical residues which are required to facilitate QBEnd10 binding. This work was performed by Dr. Martin Pulé.

PCR products were then cloned into a retroviral expression vector and subcloned into NcoI/MluI sites of the retroviral vector SFG.I2.eGFP upstream of the internal ribosomal entry site (IRES) to enable co-expression of eGFP as a reporter gene. As the native conformation of the QBEnd10 epitope is localised to the extreme amino terminus of a large heavily glycosylated protein, we postulated that physical access to this epitope when localised proximal to the cell surface might limit antibody binding. To address this potential impediment, we considered use of a molecular spacer which could project the epitope away from the cell surface. As the biological role of the 49 amino-acid residue heavily glycosylated stalk is to project the apical domain of CD8 the required 2.6 Å to reach down to the constant region of MHC I on the opposite cell[206], we selected the CD8α stalk, a commonly used molecular spacer, to perform this role. Finally, as antigen-antibody binding occasionally requires a particular orientation, we also considered a construct where the putative QBEnd10 epitope was separated from the CD8 stalk by a flexible serine-glycine (S-G-G-G-S) linker sequence. From this work, we isolated the QBEnd10 binding fragment from the extreme amino terminus of CD34. Binding of QBEnd10 to this epitope when cloned directly proximal to a transmembrane domain was considerably less efficient than to full length CD34, whereas approximately equivalent binding affinity compared to the native antigen appeared to be mediated by both CD8α stalk-bound constructs, with or without inclusion of an S-G-G-G-S linker sequence, as illustrated by Figure 10. [These steps were performed by Dr. Martin Pulé]. As the flexible linker sequence appeared superfluous to facilitating antibody binding, further minimisation constructs for the QBEnd10 epitope were presented on the CD8α stalk without a linker sequence. Molecular detail of the CD8 stalk presentation format from the final construct illustrated by Figure 29, p138, with sequence cited in supplementary data of Appendix 2, p319.

Note regarding plasmids and vectors used within this project: plasmids used are listed in Appendix 1, p305, with sequences for key plasmids listed in supplementary data of the corresponding publication in Appendix 2, p319.

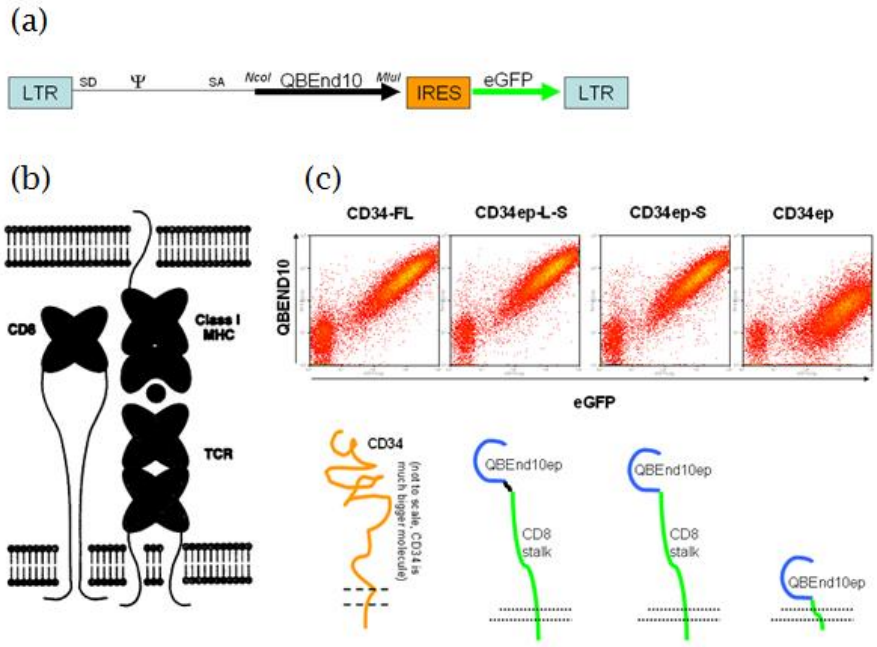

Figure 10 Optimisation of epitope expression strategy
(a) Cartoon illustration of the bicistronic SFG retroviral vector expression cassette. Gene expression is facilitated by the Moloney retroviral promoter/enhancer sequences located in the LTR domain. Bicistronic expression of a putative QBEnd10 binding domain alongside the eGFP marker gene is mediated through inclusion of an internal ribosomal entry site located upstream of eGFP, with engineered NcoI and MluI sites flanking the transgene of interest allowing facile generation of alternative epitope presentation iterations. (b) Artistic model of the T-cell receptor CD8 interaction with the MHC-antigen complex illustrating the proposed molecular spacer capacity of the CD8 stalk as adapted from Leahy[207] (c) Optimisation of epitope expression was achieved through presentation of putative QBEnd10 binding domains presented in three alternative formats: at the terminus of a truncated portion of the CD8 antigen, with or without an additional serine-glycine linker sequence to facilitate flexibility, contrasting with a shorter cell surface localised construct. As illustrated, presentation on the CD8 stalk enhanced QBEnd10 binding efficacy compared with the cell-surface localised iteration, with no clear benefit demonstrated by inclusion of the flexible linker sequence. This work was performed by Dr. Martin Pulé.

3.4. Fine mapping and functional validation of QBEnd10 epitope

Experimental aim: to achieve fine epitope mapping of the QBEnd10 epitope.

Having approximately identified the region of CD34 to which QBEnd10 binds, further minimisation of the epitope was achieved using a sequential bi-directional deletion strategy using PCR primers which progressively minimised the parental QBEnd10 epitope. Once both the carboxy and amino termini minimisation limits had been established, the amino terminal deletion series was combined with the minimal carboxy terminal construct to establish B2A0 as the final minimal epitope domain composed of 16 residues as confirmed by flow cytometry analysis; illustrated by Figure 11. This domain is subsequently

referred to as 'Q'. Details of deletion series sequences for the various epitope constructs examined are illustrated in Figure 110.

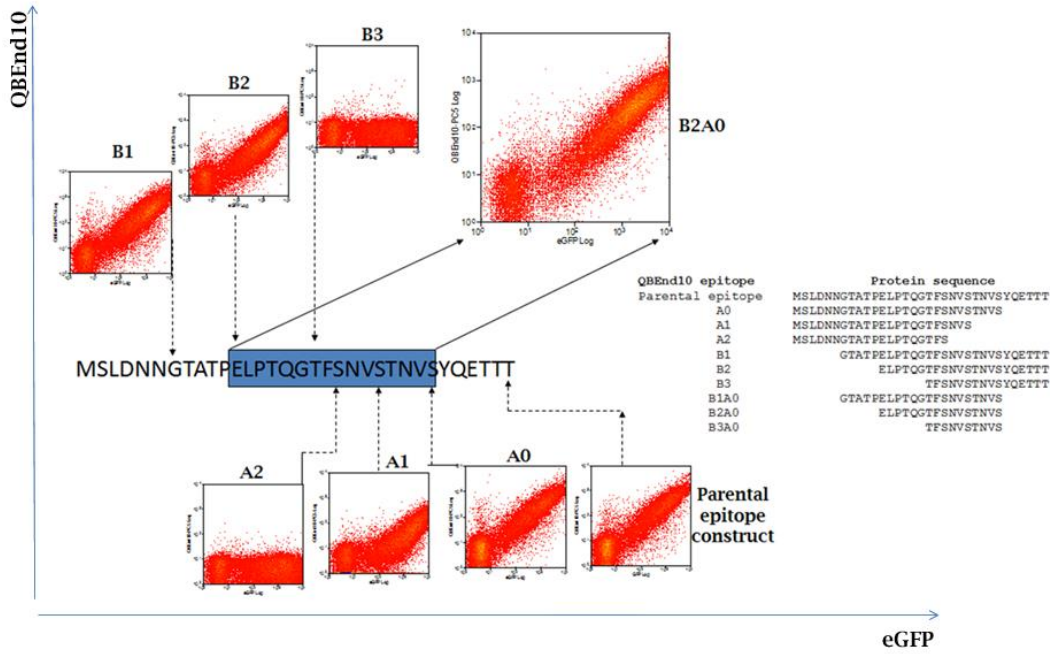

Figure 11 Fine mapping of QBEnd10 epitope
Following optimisation of the QBEnd10 epitope presentation as illustrated by Figure 10, p115, further discrimination of the critical residues was achieved through a bi-directional deletion strategy. Commencing from the parental QBEnd10 binding fragment, further deletion iterations were screened by flow cytometry analysis of transfected HEK293T cells to identify the carboxy and amino terminal limits of the QBEnd10 epitope. Finally, these limits were combined to identify the minimal 16 residue QBEnd10 binding domain as demonstrated by the B2A0 construct.

3.5. Epitope mapping rituximab binding epitope

Experimental aim: to identify a minimal rituximab binding epitope.

Previous research into the rituximab binding epitope of CD20 had localised the binding domain to the disulphide bond constrained large extracellular loop as illustrated by Figure 12[208].

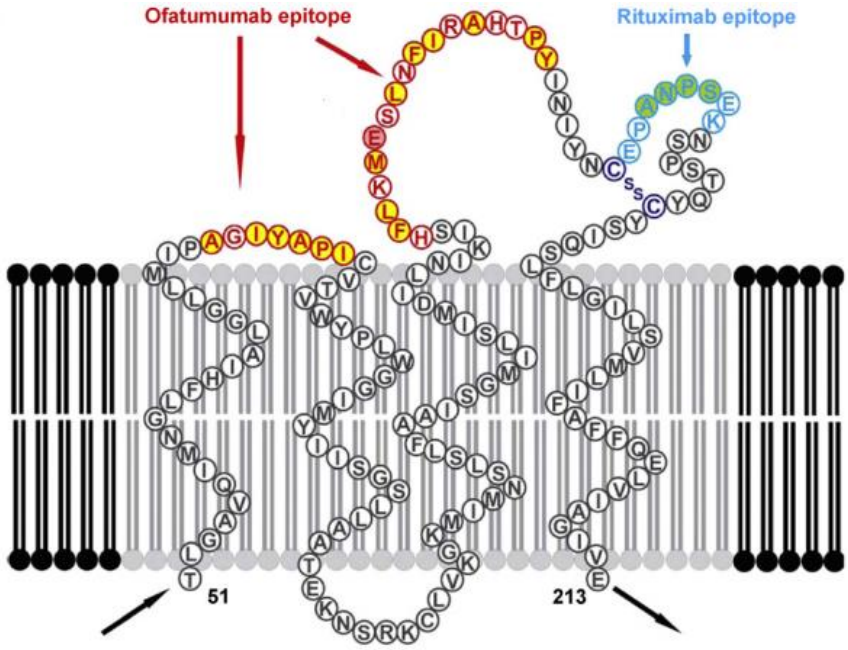

Figure 12 Cartoon illustration of CD20 antigen
Figure adapted from Du *et al*[209]. As illustrated by this cartoon, crystallographic binding data[201] has identified the rituximab binding epitope is localised to the cysteine-constrained large extracellular loop and is discrete and independent to the epitope identified by the alternative CD20 therapeutic antibody ofatumumab.

Similar to the QBEnd10 epitope mapping procedure employed previously, next we sought to express putative rituximab binding epitopes projected from the cell surface on a CD8 stalk. To this end, we designed two variant presentations of the disulphide bond constrained loop: a primary construct including five flanking residues extending beyond the cysteine residues delineating the extracellular loop and an alternative iteration expressing a tightly bounded loop constrained by the cysteine residues. However we were disappointed to observe that neither construct demonstrated binding affinity equivalent to that observed for the full length CD20 control with no rituximab binding observed against the more conservative alternative construct. In light of the likely conformational nature of the rituximab binding epitope, next we considered whether application of mimotopes might prove a more suitable strategy to achieve our desired aim. Mimotopes are antibody binding mimics derived from phage display libraries. Thus, next we selected linear (R5-L) and circular (R3-C) mimotopes from a report[174] describing rituximab-binding mimotopes as an alternative epitope identification strategy which we compared against our initial CD20 antigen derived constructs. As illustrated by Figure 13, contrasting with the limited or absence of rituximab binding by

constructs derived directly from the CD20 antigen, the circular mimotope offered rituximab binding efficacy matching that demonstrated by full-length CD20 while the linear mimotope produced a curiously biphasic binding pattern. Therefore the circular R3-C mimotope was selected for further investigation. This initial design work was performed by Dr. Martin Pulé.

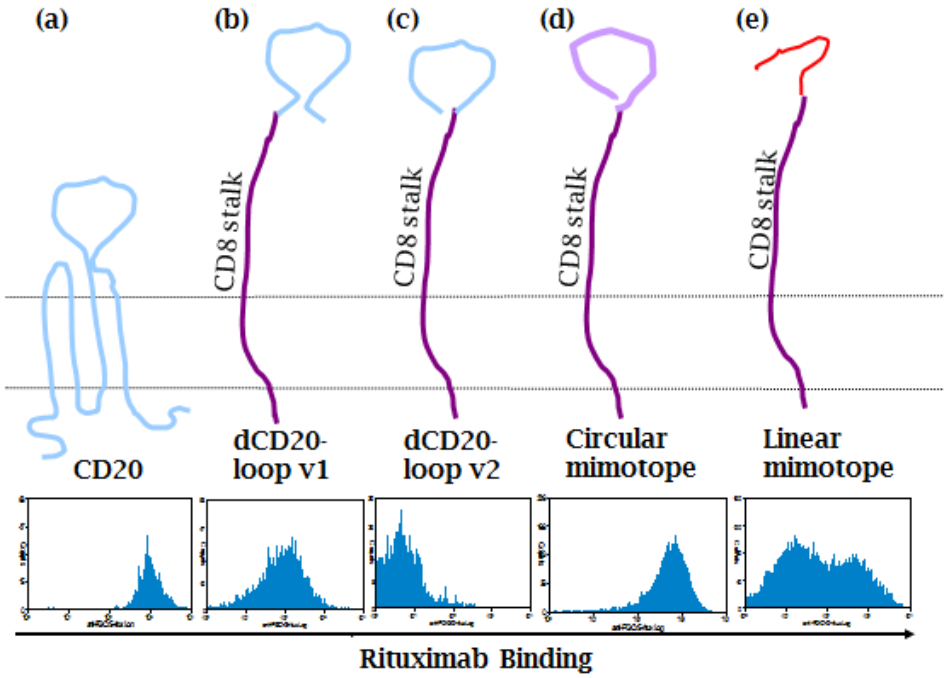

Figure 13 Screening of putative rituximab binding epitope constructs
Flow cytometry analysis of transfected HEK293T cells was performed to assess the comparative efficacy of putative rituximab epitope expression constructs. (a) Rituximab binding by the native CD20 antigen (b) Rituximab binding by the large extracellular loop of CD20 including flanking residues (c) Rituximab binding by the large extracellular loop of CD20 with protein sequence tightly constrained to the cysteine bounded loop (d) rituximab binding by R3-C circular mimotope construct (e) rituximab binding by R5-L linear mimotope construct. Circular and linear mimotopes as described by Perosa *et al*[174]. This work was performed by Dr. Martin Pulé.

3.6. Functional co–expression of QBEnd10 and Rituximab epitopes

Experimental aim: to engineer a molecular co-expression cassette for cell-surface expression of both the minimal QBEnd10 and rituximab binding epitopes.

Having successfully identified antibody binding epitopes for both target antibodies, the next challenge we faced was to establish a combination construct presenting both the QBEnd10 and rituximab epitopes whilst retaining similar functional binding capacity as observed for each of the individual epitope expression constructs. Double epitope constructs

comprising both the QBEnd10 (designated subsequently as 'Q'), and rituximab (designated 'R') binding epitopes were established in both orientations attached to the CD8 stalk (designated '8') to establish which orientation would enable the optimal rituximab binding. As illustrated by Figure 14, both RQ8 and QR8 iterations facilitate clear binding to both target antibodies; however superior rituximab binding demonstrated by the RQ8 construct compared to that observed for QR8 from flow cytometry assays led to selection of the RQ8 construct for initial optimisation of *in vitro* CDC assays.

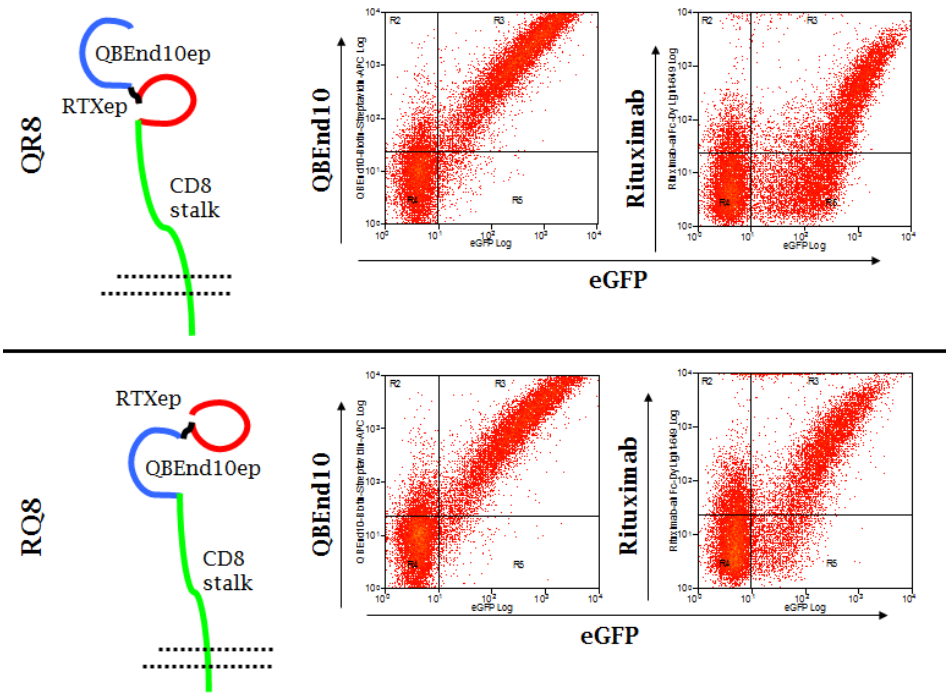

Figure 14 Epitope binding assay with double epitope constructs
Putative dual QBEnd10 and rituximab binding epitope constructs were generated by PCR with epitopes presented in either order as indicated by cartoon illustrations at left-hand side. QBEnd10 and rituximab antibody binding of dual epitope constructs was confirmed by flow cytometry analysis of transduced primary human PBMCs (compared against native CD20 and CD34 antigen expression; (data not shown). Human PBMC transduction according to protocol 2.2.3.6, p94, using retroviral supernatant generated according to protocol 2.2.3.3, p93.

Lastly we sought to demonstrate the capacity for our QBEnd10 binding epitope marker gene constructs to enable CD34 magnetic bead selection using Miltenyi selection reagents as illustrated by Figure 15.

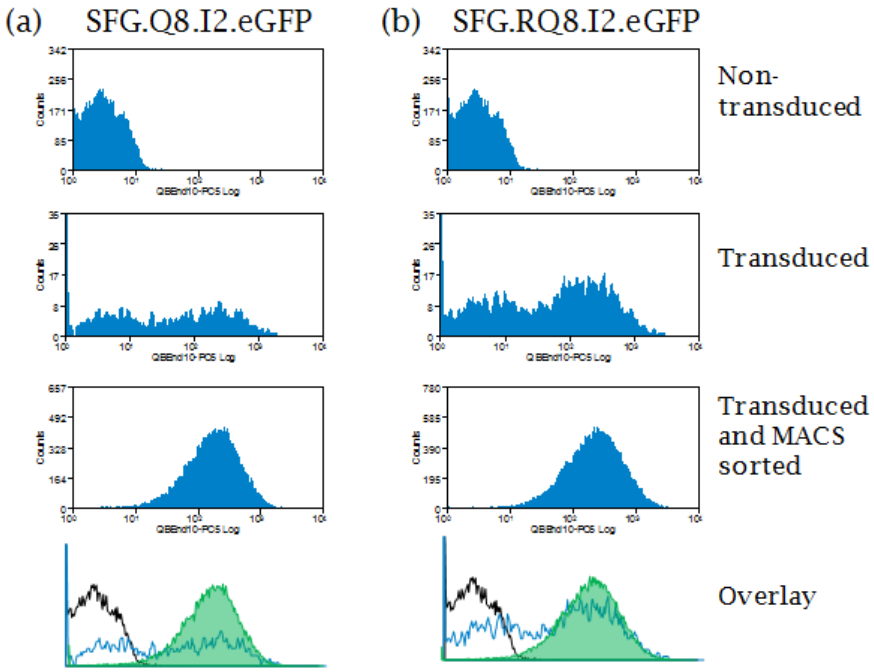

Figure 15 Demonstration of magnetic bead selection in PBMCs
Primary human PBMCs were transduced with the Q8 (B2A0) QBEnd10 construct as identified by Figure 11, p116 and the RQ8 binding construct as illustrated by Figure 14, p119. Results illustrate the typical cellular purification result achieved following CD34 magnetic bead selection (Miltenyi) of primary human T-cells transduced with (a) SFG.Q8.I2.eGFP and (b) SFG.RQ8.I2.eGFP. Data reflects a typical result from more than 10 replicates.

3.7. Conclusions

From our epitope mapping work of the QBEnd10 epitope from the CD34 antigen, we have confirmed that this is a linear epitope localised to the amino terminus of CD34. Further, we have established that presentation of the 16a.a. QBEnd10 epitope on the CD8 stalk offers sufficient access for antibody binding without requirement of a flexible linker sequence as to enable approximately equivalent antibody binding as demonstrated by the full-length antigen. This may reflect that the extensive glycosylation of the CD8 stalk results in a similar projection of the QBEnd10 epitope as occurs in the conformation of the native antigen projected at the terminus of the highly glycosylated CD34 antigen.

In contrast, the conformational nature of the rituximab epitope proved incompatible to our simplistic reduction strategy requiring utilisation of the R3-C mimotope to achieve effective binding from a minimal a.a. sequence.

Although previously proposed as a discontinuous epitope comprised of the ^{170}ANPS^{173} and ^{182}YCYSI^{186} residues from the large extracellular loop of CD20

when brought into proximity by a disulphide bond formed between cysteine residues 167 and 183[208] (Figure 12), recent crystallographic data has established that the complementarity determining region (CDR) loops of rituximab appear to interact primarily with the ANPS motif[201]. Further, observations suggesting that biochemical disruption of the disulphide bond ablates rituximab binding and cytotoxicity supports evidence indicating that the rituximab binding epitope is conformational rather than linear[208, 210]. Combined, this may suggest that previous observations regarding a role for the YCYSI domain as a secondary component of a discontinuous epitope may in fact reflect a role for this domain to establish and stabilize the conformation of the critical ANPS epitope to enable effective rituximab-mediated recognition. Further, from the crystallographic binding data, it was noted that the ANPS motif remains deeply buried within the binding pocket formed by the CDR loops such that the binding cavity remains too deep to accommodate alternative residues other than serine in exchange for [170]alanine[201]. Notably, the R3-C mimotope retains the critical NPS motif and contains a serine residue in place of the aforementioned alanine[174].

We have succeeded in establishing dual minimal epitope expression constructs that demonstrate clear binding affinity for both monoclonal antibodies QBEnd10 and rituximab when presented in either orientation. The linear QBEnd10 binding epitope comprised of 16 residues compares favourably to the 385 present in the native antigen. Similarly, the 11 residue R3-C mimotope compares favourably against the 297 residue CD20 parent antigen. Further, presentation of the QBEnd10 epitope in this manner retains the functional capacity to enable Miltenyi CD34 magnetic bead selection of transgene expressing PBMC's.

3.8. General conclusions

- We have identified a 16 amino acid residue QBEnd10 binding epitope from the native sequence of the CD34 antigen which, when presented on a CD8α stalk, demonstrates approximately equivalent binding affinity for the QBEnd10 monoclonal antibody as the native CD34 antigen as assessed by flow cytometry assays
- We have established a CD8α stalk-bound rituximab binding construct containing the 11 residue R3-C mimotope, which demonstrates

approximately equivalent binding affinity for rituximab as the native CD20 antigen as assessed by flow cytometry assays

- Combination QBEnd10 and rituximab epitope binding constructs facilitate orientation independent antibody binding for both target monoclonal antibodies
- Both Q8 and RQ8 transgenic PBMCs retain the functional capacity to facilitate QBEnd10-mediated Miltenyi CD34 magnetic bead selection

Chapter four

4. *In vitro* CDC assays

As illustrated by Figure 5, rituximab is proposed to mediate cellular deletion through three mechanisms: CDC, ADCC and direct toxicity via apoptosis[211]. Due to the epitope binding capacity of our construct, *in vitro* CDC and ADCC assays were considered to model the efficacy of rituximab-mediated deletion of our constructs. This chapter describes our work in establishing protocols to enable sensitive *in vitro* flow cytometry based CDC assays sufficient to enable discrimination between similar epitope expression constructs.

4.1. Aims

- To establish and optimise an effective flow cytometry based CDC assay
- To demonstrate CDC-mediated deletion of transgenic PBMCs
- To assess the efficacy of CDC-mediated deletion of epitope constructs through comparative sensitivity, specificity and titration assays
- To identify and establish a sort-suicide gene construct which demonstrates equivalent sensitivity to CDC-mediated lysis as current technology

4.2. Introduction

The complement cascade of innate immunity was first discovered over a century ago, identified as a first line mechanism of anti-microbial immunity. Since then, it has become clear that the range and breadth of complement mediated immune regulation extends far beyond this capacity. In addition to the defensive role, complement also performs immune surveillance behaviour discriminating between healthy tissue, cellular debris and apoptotic cells. Further less obvious roles for complement include involvement in angiogenesis, mobilisation of stem cell progenitors, tissue regeneration and lipid metabolism. With such a broad spectrum of activity, tight regulation of complement activation is critical to maintain homeostasis. Correspondingly, dysregulation of complement activation has been associated in the pathogenesis of infectious conditions such as sepsis and anaphylaxis; also in a wide array of pathogenic inflammatory processes and diseases including

paroxysmal nocturnal hemoglobinuria (PNH), myocardial infarction, myasthenia gravis, systemic lupus erthematosus, and multiple sclerosis[212, 213].

The complement activation cascade can be initiated through three separate mechanisms; the classical pathway, following antibody binding, as well as the alternative and lectin pathways. All stages of the complement cascade are strictly controlled by multiple regulators and inhibitors, and regardless of initiating trigger, converge into a uniform pathway through assembly of the C3 convertase. In humans, only IgM and IgG are effective at mediating complement activation, with two molecules of the monomeric IgG required to induce activation as illustrated by Figure 18. Host cells are protected from aberrant complement-mediated deletion through expression of membrane-bound complement regulator proteins including CD21, CD46, CD55, CD59 and CRIg. Notably, both CD55 and CD59 are glycophosphatidylinositol (GPI) anchor linked membrane receptors. Mutations in the *PIG–A* gene resulting in non-functional GPI anchor synthesis preventing expression of these inhibitors results in the pathology PNH, illustrate how small perturbations in complement regulation can result in pathology[214, 215].

In consideration of intended application in T-cell engineering, we premised it would be necessary to use transduced PBMC's as target cells in our *in vitro* assays to best assess the functional sensitivity to CDC-mediated deletion as conferred by our rituximab binding constructs.

4.3. Results: Initial CDC assay modelling

Experimental aim: to establish an *in vitro* assay capable of assessing variation in sensitivity to complement mediated cytoxicity (CDC) for transgenic human PBMCs in the presence of rituximab.

Having previously demonstrated effective rituximab binding by dual-epitope binding constructs, we proceeded to test the functional rituximab-mediated deletion of RQ8 through *in vitro* CDC assays. Referring to CDC assay conditions reported from the literature[159, 216], we performed an initial CDC assay incubating target populations with 100μg/ml rituximab and 25% baby rabbit complement (BRC) for two, four and twenty-four hour durations to establish whether we could identify any indication of CDC-mediated deletion. As illustrated by Figure 16, although CDC-mediated deletion was observed at all

time-points, there was suggestion of non-specific complement-mediated toxicity from the twenty-four hour timepoint condition. Further, as the four-hour incubation results appeared to offer superior consistency, this incubation duration was chosen for subsequent assays.

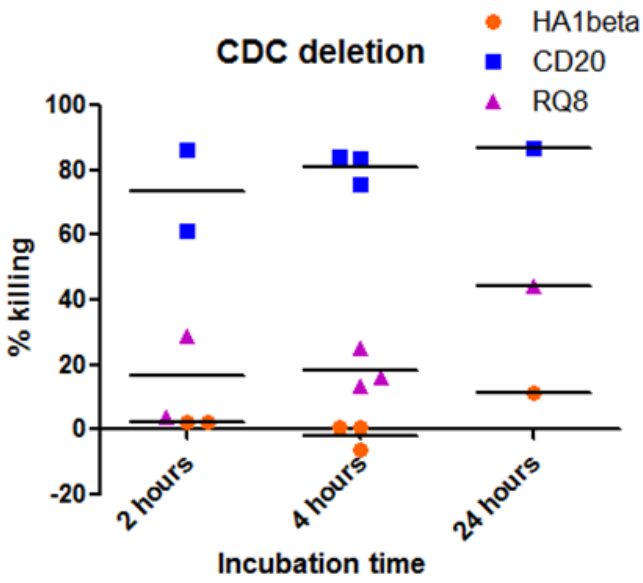

Figure 16 Comparison of CDC mediated deletion versus time
Peripheral human PBMCs were transduced with constructs as indicated. Following FACS verification of successful transduction (data not shown), samples were assessed for sensitivity to CDC-mediated deletion according to the protocol as described (2.2.5.6.2, p100) variant dependent on incubation time. Data for the 2, 4 and 24 hours illustrate results from two, three and single donors respectively. Black lines indicate the mean values.

From these assays we were disappointed to find that CDC-mediated deletion of RQ8 was considerably less effective than what was observed for the CD20 positive control. Moreover, as illustrated by Figure 17, deletion appeared to be limited to the high expressing population, suggesting a density-dependent limitation to CDC-mediated deletion. As CD20 expression has been observed to become localised to lipid rafts following antibody binding[204] this might in part explain the enhanced sensitivity of the CD20 positive control despite suggestions of similar binding efficacy between CD20 and the RQ8 construct.

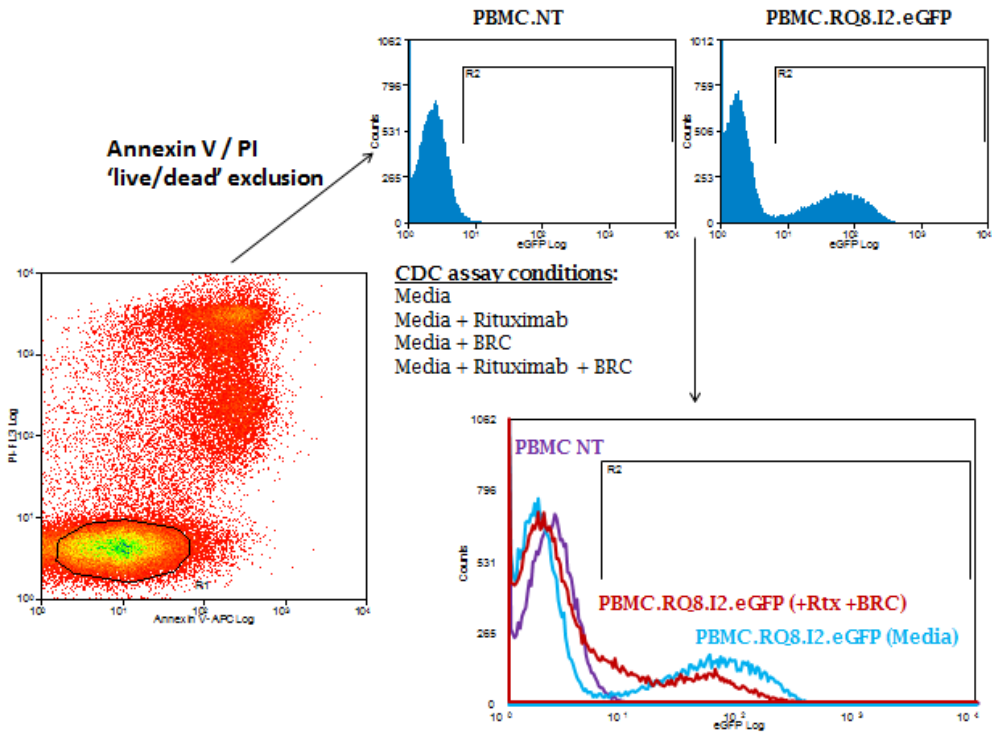

Figure 17 Expression limited CDC sensitivity
Transduced peripheral human PBMCs were subjected to a CDC assay as described (2.2.5.6.2, p100). Efficacy of cellular deletion was assessed by flow cytometry with the residual live population identified as the Annexin V and PI negative fraction, subsequently gated onto an eGFP histogram to identify the residual transgenic fraction. As illustrated for the RQ8 target, although some killing was observed, sensitivity to CDC-mediated deletion appeared to be primarily restricted to the high-expressing population. Due to assessment of deletion by flow cytometry, indirect assessment of killing by identification of the live population was necessary to exclude confounding 'noise' imposed by autofluorescence from cellular proteins.

4.4. Epitope re–engineering

Experimental aim: To engineer alternative molecular iterations of our epitope expression constructs to establish whether sensitivity to rituximab mediated deletion may be affected by the epitope expression format.

From the classical pathway of complement activation, reduction of off-target toxicity is achieved through the requirement for C1q cross-linking of two molecules of IgG immunoglobulin prior to activation of the complement cascade as illustrated by Figure 18.

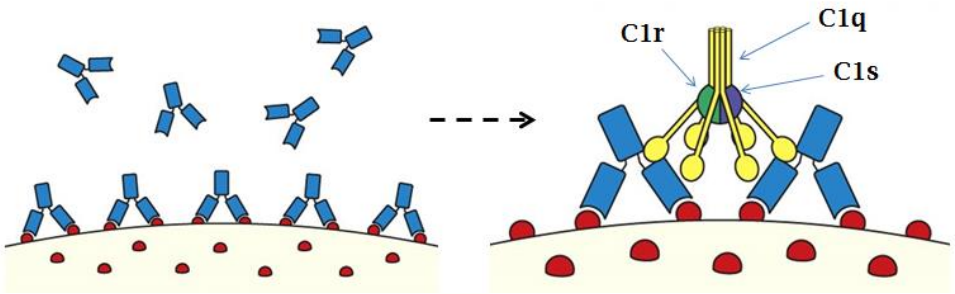

Figure 18 C1q cross-linking triggering complement activation
Adapted from figure 10.29 Murphy *et al*[17].
Complement-mediated toxicity is prevented by the requirement of the complement protein C1q to bind two separate bound antibodies to induce activation of the complement cascade. Following antibody binding of cognate antigen (a), two separate arms of C1q are required to engage bound antibody prior to initiation of the complement cascade (b). Thus, the natural process of complement activation is inherently density dependent, supporting the observation of density-dependent deletion as illustrated by Figure 17, p126.

As both CDC and ADCC-mediated killing are constrained by the degree of cross-linking by the respective receptors, we premised that a strategy that could increase the epitope valency of the constructs might therefore increase the sensitivity of low expressers. Following from this logical reasoning and in an attempt to improve killing, we generated a series of alternative constructs to further examine the functional roles that the presentation motif and/or binding moiety might play in defining the sensitivity to CDC-mediated deletion illustrated by Figure 19. These modifications included a membrane-proximal construct to consider whether membrane localisation might enhance complement mediated toxicity (R') , bivalent constructs (RRQ8, RQR8) with a view to increase valency, and a monomeric construct (RQR4) to compare against dimeric RQ8 and R-HCH2CH3 constructs. Alternative stalk-based constructs included: a minimal flush construct (R') with the rituximab epitope localised proximal to the cell membrane without any stalk-based projection, an alternative presentation strategy whereby the rituximab epitope was localised to the apical terminus of the human IgG1 antibody constant domain on a rigid homodimeric stalk (R-HCH2CH3) and finally, a monomeric CD4 stalk-bound construct (RQR4) to establish whether projection from the cell surface was required and what role alternative binding orientations might present regarding rituximab-mediated CDC sensitivity. We also considered increased valency constructs where CD8-stalk bound versions of the rituximab binding epitopes were presented either in series preceding (RRQ8), or flanking the QBEnd10 binding epitope (RQR8) compared against both of the original dual

epitope variants (RQ8, QR8). The QBEnd10 binding epitope on the CD8 stalk was included as a negative control and a full-length expression construct for CD20 in conjunction with truncated CD34 was included as a positive control. To prevent homologous recombination of the multi-valent constructs: RRQ8, RQR8 and RQR4 during retroviral synthesis, the DNA sequence for the rituximab-binding domain was 'wobbled' by the use of alternative codons as illustrated by Figure 29.

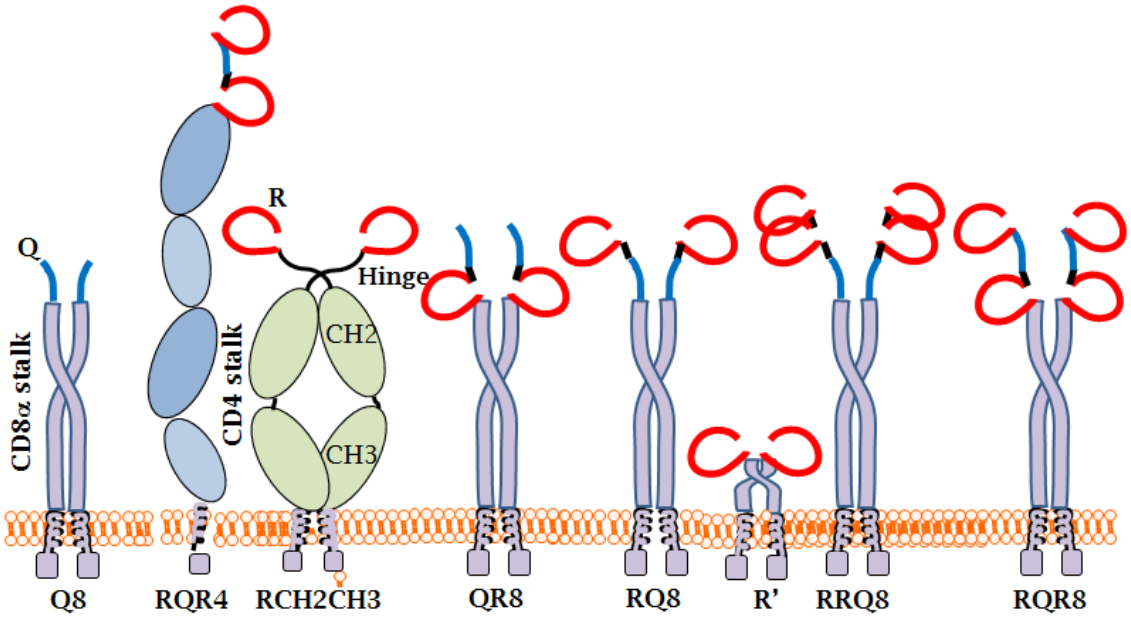

Figure 19 Cartoon illustration of alternative epitope constructs
In an attempt resolve the density dependent limitation to rituximab-mediated deletion, further epitope constructs were engineered to address potential hypothesised limitations: R', R-HCH2CH3 and RQR4 were designed to assess the potential role of projection from the cell-surface with respect to complement activation with RQR4, RRQ8 and RQR8 all engineered to increase epitope valency. In construct nomenclature: Q indicates the QBEnd10 binding epitope, R indicates the rituximab binding epitope, 8 indicates the CD8α stalk domain, 4 denotes the CD4 stalk domain whilst CH2CH3 indicate the respective constant domains from the human IgG1 antibody.

Following from our initial CDC assay strategy and epitope construct engineering; we proceeded to examine the efficacy of deletion through a range of CDC assays as illustrated by Figure 20.

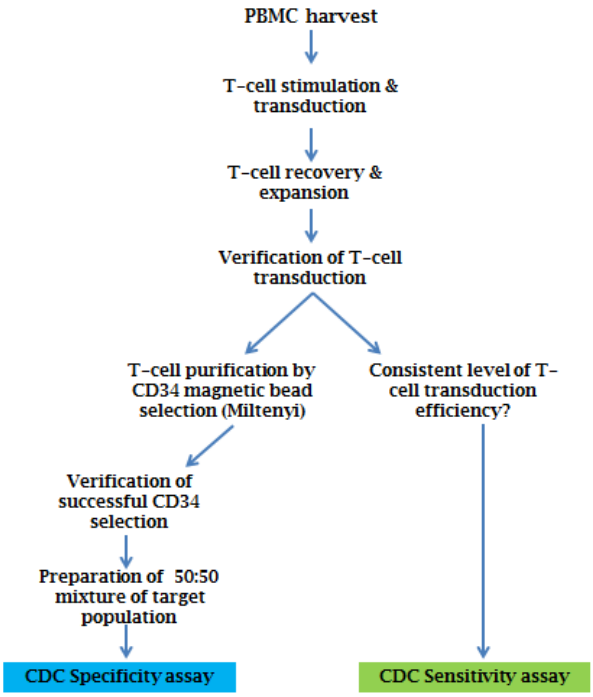

Figure 20 CDC assay flowchart
All CDC assays were performed using transduced primary human PBMC targets. Sensitivity assays as described (2.2.5.6.2, p100) were performed using transduced but unsorted PBMC targets which were assessed by flow cytometry to confirm equivalent transduction efficiencies prior to assay progression. Specificity assays as described (2.2.5.6.3, p100): PBMCs were transduced with SFG.RQR8.IRES.eGFP and SFG.Q8.IRES.eBFP2, purified by CD34 magnetic bead selection and combined at equal concentration to establish the target population.

4.5. *In vitro* CDC assays

In total, three separate CDC assays were considered: 1) Sensitivity assays which employed unsorted target cells to assess the comparative sensitivity of several similar epitope expression constructs to complement mediated lysis, 2) Specificity assays designed to demonstrate the stringent efficacy of complement mediated lysis of our optimal construct when compared against a nearly identical target population, and 3) Time-course / dose titration CDC assays, which formed a derivative of the specificity CDC assay, designed to further investigate the reaction kinetics of complement-mediated sensitivity.

4.5.1. Sensitivity CDC assays

Experimental aim: To assess the variation in sensitivity to rituximab mediated CDC for our panel of alternative epitope expression constructs.

From CDC assays using transduced but unsorted PBMC's from three separate donors, the flush and CD4 stalk-bound constructs showed sensitivity barely above that of the negative control. The IgG1 homodimeric stalk-bound

construct performed similarly to the monovalent parental constructs, whilst the multivalent constructs demonstrated the greatest sensitivity with the RQR8 construct clearly demonstrating acute sensitivity to CDC-mediated killing equivalent to that demonstrated by the CD20 expressing positive control construct as illustrated by Figure 21.

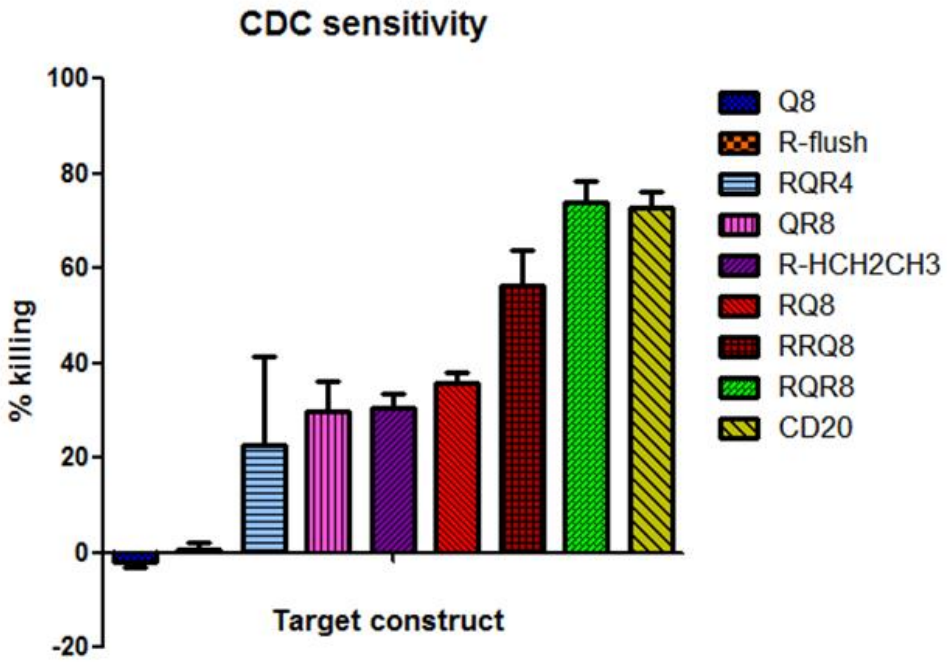

Figure 21 CDC sensitivity assay comparison
Human PBMCs were transduced with alternative epitope construct iterations and assessed in parallel for their comparative sensitivity to CDC mediated deletion through *in vitro* assays as previously described (2.2.5.6.2, p100). Results as illustrated reflect the level of deletion observed following independent assays from three separate donors. Error bars reflect SEM.

4.5.2. Specificity CDC assays

Experimental aim: To demonstrate sensitivity to rituximab mediated deletion remains restricted to rituximab-binding epitope expression constructs.

As our initial demonstration of the retention for magnetic bead selection function was assessed with Q8 and RQ8 (illustrated by Figure 15), it was necessary to confirm that RQR8 retains this capacity to enable specificity CDC assays as demonstrated by Figure 22.

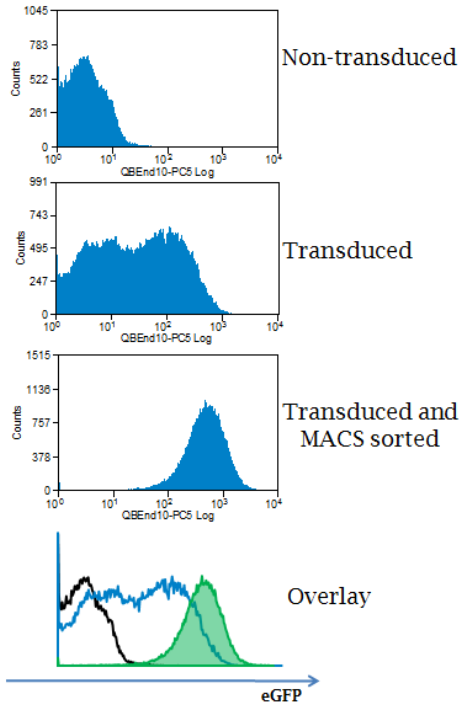

Figure 22 Demonstration of MACS selection with RQR8 transgenic PBMCs
Peripheral human PBMCs were transduced with RQR8.I2.eGFP, resulting in the heterogeneous population as illustrated in the 'transduced' histogram. From this mixed population, a pure population of RQR8 positive cells, typically of greater than 95% purity, can be readily attained following a single CD34 magnetic-bead selection (Miltenyi). Successful selection was confirmed by flow cytometry 24 hours following MACS selection. Plots represent a typical result from more than a dozen independent replicates.

Next we sought to demonstrate the specificity of CDC-mediated deletion against RQR8 expressing targets. The minimal size of RQR8 is designed to enable functional modular capacity alongside other T-cell engineering components such as re-targeting moieties. In this capacity, the marker gene would enable clinical grade purification using Miltenyi cliniMACS reagents prior to ACT to ensure consistency of the therapeutic cell product. Furthermore, inclusion of a suicide gene is designed for a pure product to ensure ablation of the adoptive population in the event of toxicity. Thus sensitivity assays were designed to assess the *in vitro* rituximab-mediated sensitivity of RQR8 which would best match that anticipated for potential therapeutic cellular product. To demonstrate the acute sensitivity of RQR8, we generated the Q8.I2.eBFP2 construct to act as an internal control. Briefly, this construct is identical to Q8.I2.eGFP, variant only by the co-expressed fluorescent protein. Cloning of this construct was achieved by ‘cut and paste’ cloning as described by (13.1.2, p306) in Appendix 1. Inclusion of the QBEnd10 epitope in this construct enables cliniMACS selection while the eBFP2

fluorescent marker protein allows for separate identification in flow cytometry based CDC assays. Finally, as these cells would have been subjected to the identical handling as the RQR8-transgenic cellular targets they most accurately reflect the acute specificity afforded by RQR8 for deletion. Inclusion of the Q8 internal control in a 1:1 ratio with RQR8 targets allows for clear demonstration of the specificity and efficacy of RQR8 mediated deletion against a virtually identical control population. Similar to the sensitivity assays, successful progression through multiple steps were required prior to progression with the specificity assays as illustrated by Figure 20 and Figure 23.

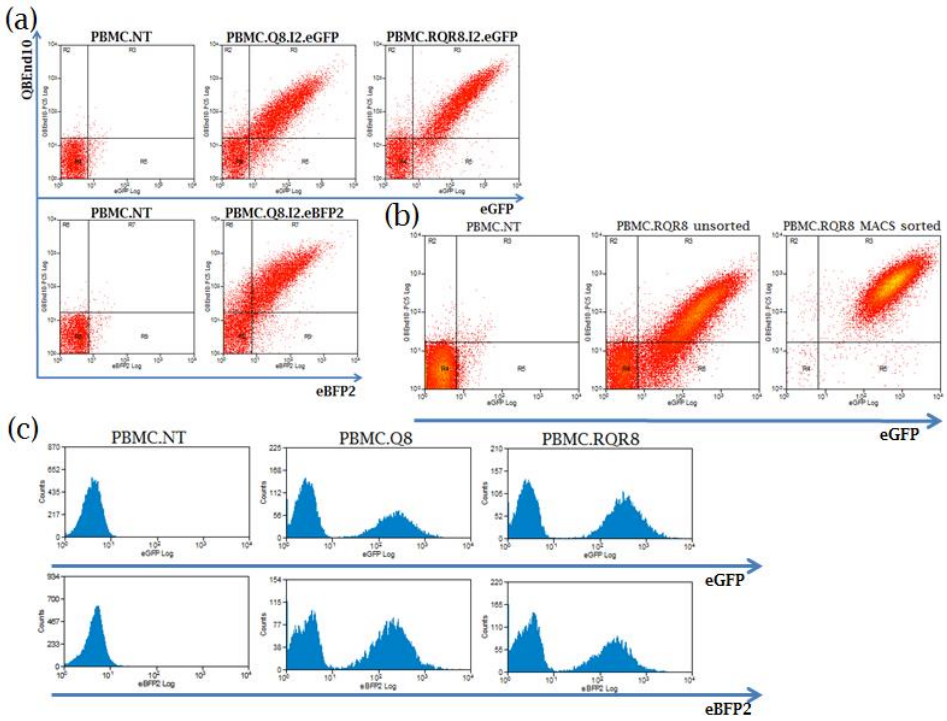

Figure 23 CDC specificity assay preparation
Successful cell preparation for CDC specificity assays was achieved through a progressive series of handling steps requiring multiple critical checkpoints to be met prior to assay progression. (a) Transduction: Human PBMCs were transduced with RQR8.I2.eGFP, Q8.I2.eGFP, or Q8.I2.eBFP2. Confirmation of successful transduction was achieved by flow cytometry. (b) Selection: Transduced cell populations were purified by CD34 magnetic bead selection (Miltenyi) with successful selection confirmed by flow cytometry. Note: selection result only illustrated for the RQR8.I2.eGFP target population. (c) Target preparation and validation: Purified RQR8.I2.eGFP or Q8.I2.eGFP target populations were mixed with an equal proportion of Q8.I2.eBFP2 transduced and purified cells to act as an internal control. Sample mixtures were confirmed by flow cytometry prior to progression with specificity CDC assays, full protocol as detailed by 2.2.5.6.3, p100.

From specificity assays performed from multiple donors, it is clear that despite the target population being reduced to background noise, the control population remains seemingly untouched. Figure 24 illustrates a typical result

from a CDC specificity assay. Further illustrations of specificity CDC assay efficacy are illustrated by Figure 28, Figure 42, Figure 49, Figure 53 and Figure 69.

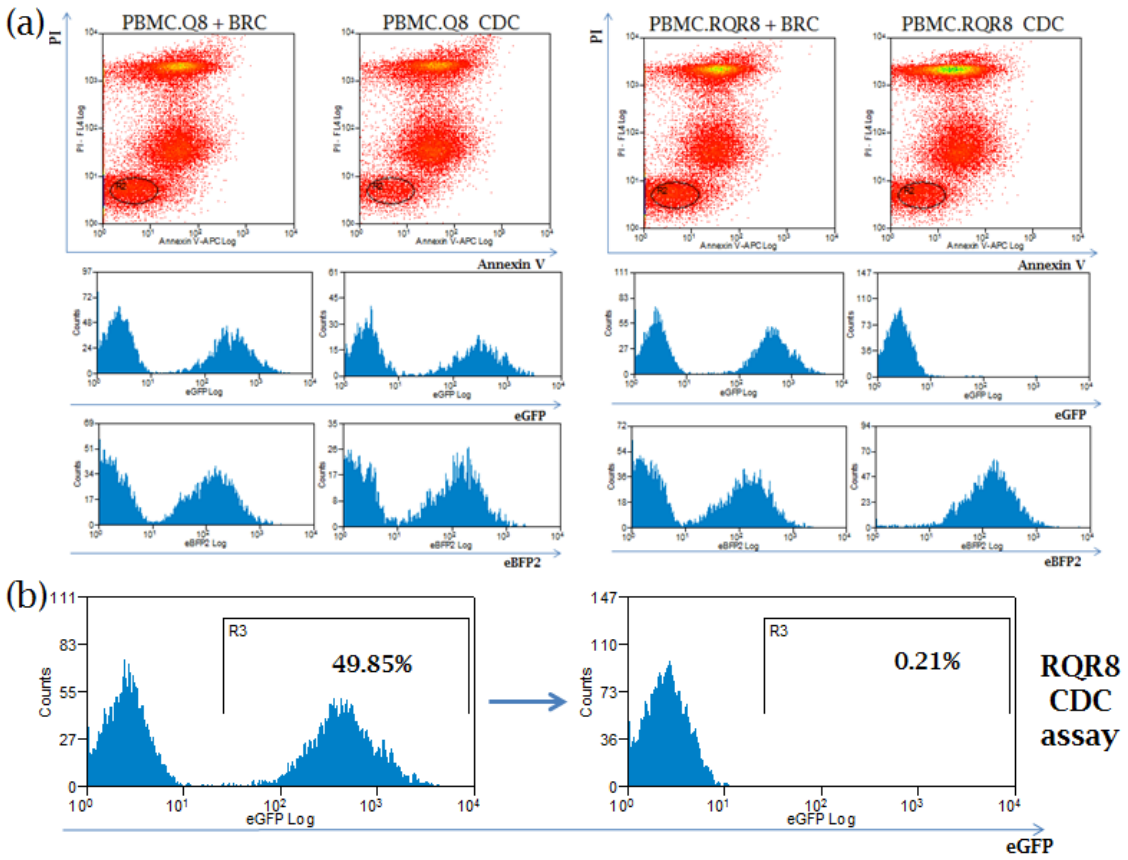

Figure 24 Typical result from a CDC specificity assay
Human PBMCs were separately transduced with target constructs: RQR8.I2.eGFP or Q8.I2.eGFP as well as Q8.I2.eBFP2 included as an internal control. Following transduction, all samples were purified by MACS-selection. To demonstrate specificity of CDC-mediated deletion, RQR8.I2.eGFP or Q8.I2.eGFP targets were combined in equal concentration with Q8.I2.eBFP2 internal control targets and subjected to a CDC assay as described (2.2.5.6.3, p100). At lower left, the histograms illustrate how the control target condition retains the original sample following CDC assay illustrating both target (eGFP) and control (eBFP2) populations whilst at right the RQR8 expressing targets are deleted leaving only the internal control population remaining. Illustration reflects a typical result from 6 separate assays taken from separate donors.

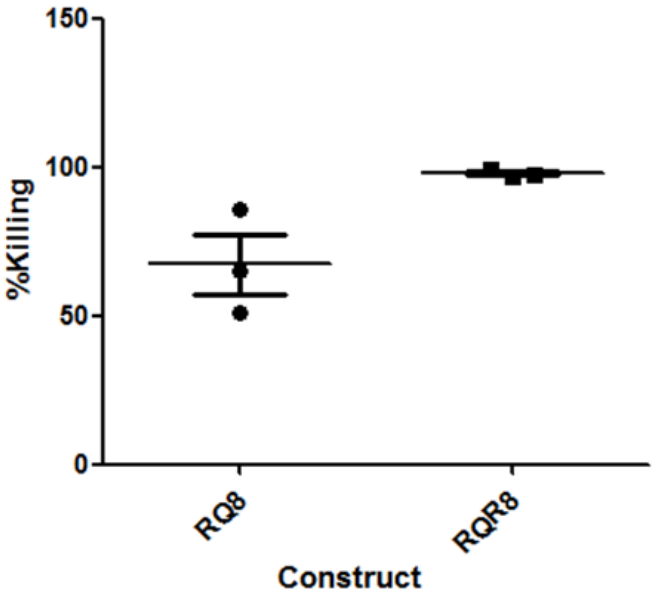

Figure 25 Specificity CDC assay comparison between RQ8 and RQR8
Specificity CDC assays examining rituximab-mediated deletion of peripheral human PBMCs was performed according to protocol as described 2.2.5.6.3, p100. Despite MACS selection, efficacy of deletion of RQ8 transgenic PBMCs remained inconsistent, albeit considerably higher than what was observed from sensitivity assays, whereas the degree of RQR8 deletion was consistently in excess of 96%. Results as illustrated reflect the level of deletion observed following independent assays from three separate donors. Error bars reflect the standard error of the mean.

4.5.3. Time–course / Dose titration CDC assays

Experimental aim: To review the *in vitro* CDC assay conditions to more accurately assess the sensitivity of RQR8 to rituximab mediated CDC.

As our initial CDC assay protocol had been established with a view to facilitate CDC-mediated deletion of our epitope constructs, we next examined whether it would be possible to titrate the observed sensitivity through variation of the primary assay parameters as assessed through a time-course and dose titration assay, as illustrated by Figure 26. Although maximum CDC-mediated deletion was observed at the 100µg/ml concentration, similar efficacy of deletion was observed even from the 12.5µg/ml concentration illustrating the acute sensitivity of RQR8 to rituximab-mediated CDC which appears to occur with approximately equivalent efficacy at all concentrations of rituximab observed. Based on maximum serum measurements of rituximab taken during administration at the 375mg/m^2 dosage as indicated for NHL which range between 118.9µg/ml to 663.9µg/ml[171], it seems clear from these assays performed in two donors that the rituximab mediated sensitivity is readily

achieved at levels well below the physiological levels associated with therapeutic administration.

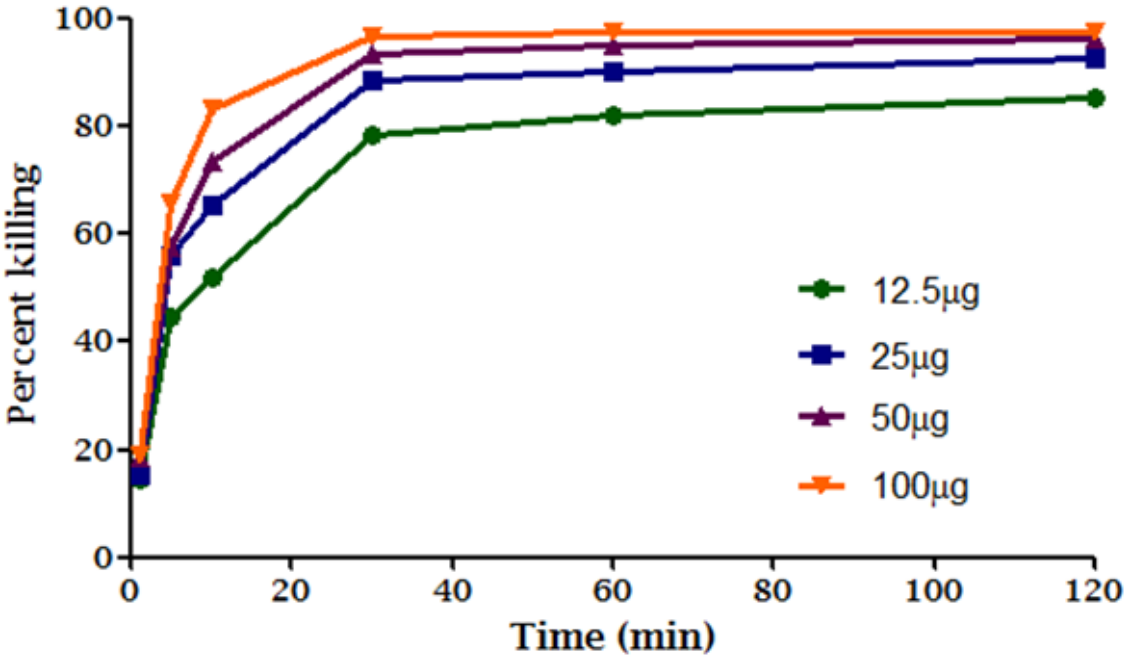

Figure 26 Time–course / dose–titration CDC assays
Having demonstrated effective deletion of RQR8 targets, assay conditions were reviewed through a time-course/dose-titration assay to consider whether similar levels of deletion could be achieved using lower doses of rituximab and/or shorter durations of incubation. Human PBMCs were separately transduced with the target construct RQR8.I2.eGFP and the internal control Q8.I2.eBFP2, purified by MACS-selection following transduction, then combined in equal proportions prior to inclusion into a CDC assay as described (2.2.5.6.3, p100). As illustrated, similar levels of deletion were achieved at significantly lower doses and durations of incubation. Results illustrated reflect average depletion from two separate assays from two separate donors.

4.5.4. Rituximab versus ofatumumab CDC assays

Experimental aim: To demonstrate absence of RQR8 sensitivity to ofatumumab demonstrating the capacity for coincident therapeutic administration.

The acute sensitivity of RQR8 to rituximab-mediated depletion even at dilute concentration contrasting with the prolonged serum residence of rituximab ranging between 25-30 days[218], clearly precludes rituximab chemotherapy prior to RQR8 ACT. However, ofatumumab offers an alternative anti-CD20 therapeutic antibody which could theoretically be employed in conjunction with RQR8. To consider the potential for concurrent chemotherapeutic and cellular therapy regimes, a panel of alternative CD20 antibodies were assessed for their capacity to bind to RQR8 as illustrated by Human PBMCs were separately transduced with target constructs: RQR8.I2.eGFP, Q8.I2.eGFP or CD20opt.I2.eGFP as well as Q8.I2.eBFP2 functioning as an internal control. Following transduction verification, assay target populations were supplemented with Q8.I2.eBFP2-transduced PBMCs such that all cellular target populations contained an equal proportion of epitope-targets and Q8.I2.eBFP2

expressing controls. Cellular populations were subjected to an *in vitro* CDC assay as described (2.2.5.6.3, p100). Results illustrate efficacy of deletion observed from a single experiment.

Table 7 (Binding assay kindly performed by Prof. Mark Cragg). Lack of binding to RQR8 by ofatumumab, and by extension theoretical resistance to ofatumumab-mediated CDC deletion, could demonstrate that ACT with RQR8 could function in conjunction with ofatumumab therapy. To verify the lack of ofatumumab binding, we performed binding assays comparing QBEnd10, rituximab and ofatumumab against a 50:50 mixed population of non-transduced and transduced Jurkat T-cells modified with Q8.I2.eGFP, RQR8.I2.eGFP and CD20opt.I2.eGFP respectively as illustrated in Figure 27.

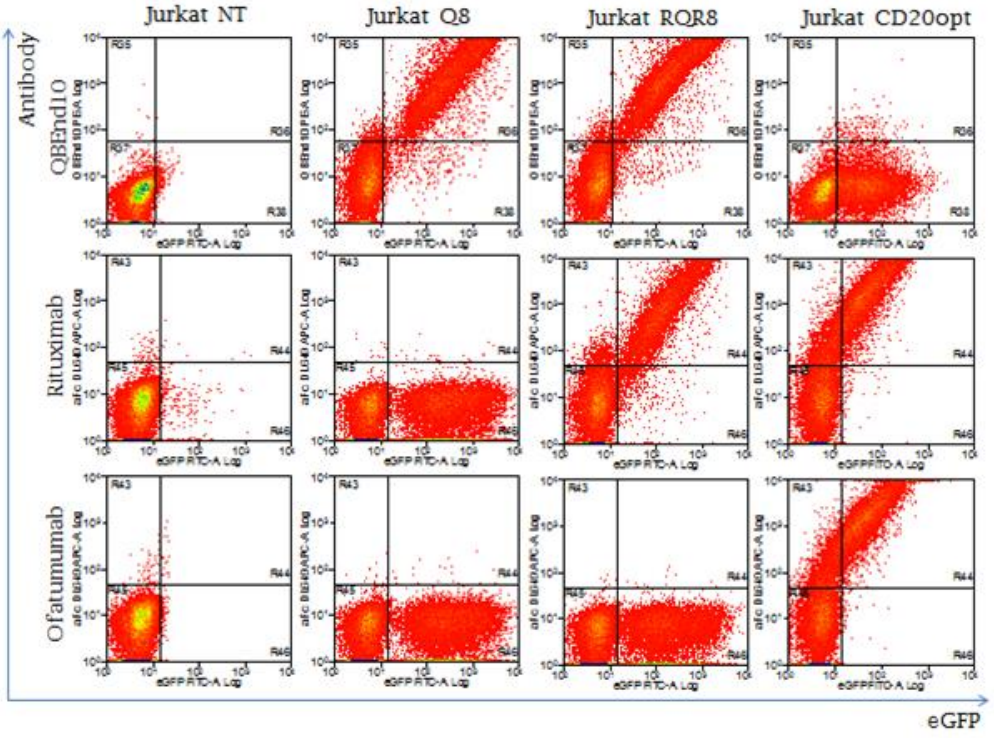

Figure 27 Ofatumumab binding assay in Jurkat T-cells
Binding assay to demonstrate absence of ofatumumab binding against RQR8-expressing targets: separately purified populations of SFG.Q8.I2.eGFP, SFG.RQR8.I2.eGFP and SFG.CD20opt.I2.eGFP transduced Jurkat T-cells were mixed with equal quantities of non-transduced Jurkat T-cells as an internal control then stained with QBEnd10, rituximab or ofatumumab to enable assessment of comparative binding efficacy by flow cytometry. Therapeutic antibody binding was assessed indirectly through secondary anti-human Fc staining; QBEnd10-biotin binding was assessed using APC-conjugated streptavidin as the secondary stain. Clear binding of QBEnd10 was observed against both Q8 and RQR8; clear binding of rituximab was demonstrated by both RQR8 and CD20opt, however only CD20opt demonstrated any appreciable binding of ofatumumab.

Having demonstrated no appreciable binding of ofatumumab by RQR8, we proceeded to demonstrate the lack of functional activity of ofatumumab

through a specificity CDC assay against similar mixtures of transduced PBMC's as illustrated by Figure 28.

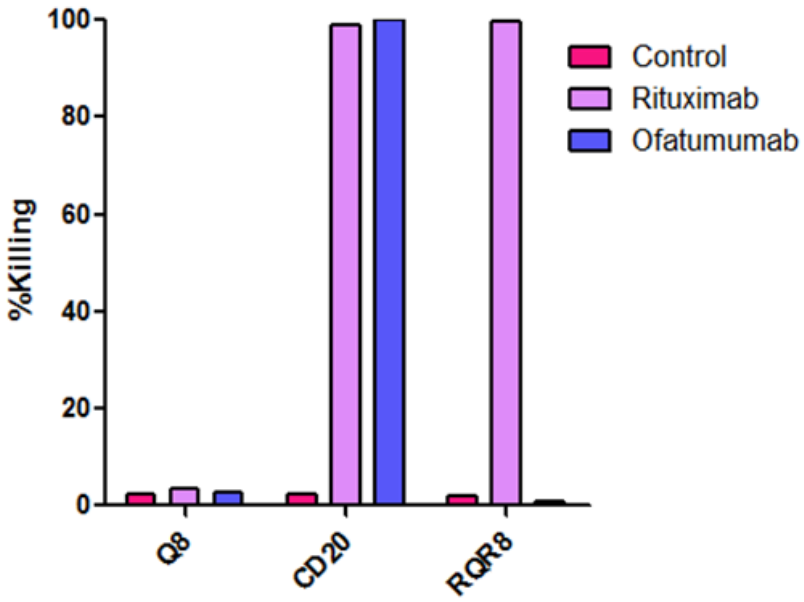

Figure 28 Ofatumumab vs. Rituximab CDC assay in PBMCs
Human PBMCs were separately transduced with target constructs: RQR8.I2.eGFP, Q8.I2.eGFP or CD20opt.I2.eGFP as well as Q8.I2.eBFP2 functioning as an internal control. Following transduction verification, assay target populations were supplemented with Q8.I2.eBFP2-transduced PBMCs such that all cellular target populations contained an equal proportion of epitope-targets and Q8.I2.eBFP2 expressing controls. Cellular populations were subjected to an *in vitro* CDC assay as described (2.2.5.6.3, p100). Results illustrate efficacy of deletion observed from a single experiment.

Table 7 RQR8 binding by alternative CD20 monoclonal antibodies
Jurkat T-cells transgenic for RQR8 were assessed for binding of alternative CD20 monoclonal antibodies; alternative CD20 antibody staining kindly performed by Prof. Mark Cragg.

Antibody	Antibody binding affinity
Rituximab	++
Ofatumumab	-
GA101	-
1F5	++
NKI-B20	++
B9E9	+
AT20	+

4.6. Molecular characterisation of RQR8

4.6.1. Molecular features of RQR8

As illustrated by Figure 29, Q8 and RQR8 are highly similar in structure whereby the CD8α stalk presentation strategy is achieved through the generation of fusion constructs comprising our epitope domains located

within the architecture of the CD8α protein. The extensive glycosylation and rigid stability afforded by the dimeric CD8alpha stalk appears to mimic the native presentation format of the QBEnd10 epitope in the CD34 antigen. As the presence of repetitive sequences was required to facilitate duplicate expression of the rituximab binding domain, 'codon wobbling' was employed to preclude homologous recombination. This was achieved through use of alternative codons to encode for the identical protein sequence afforded by the degeneracy of the genetic code.

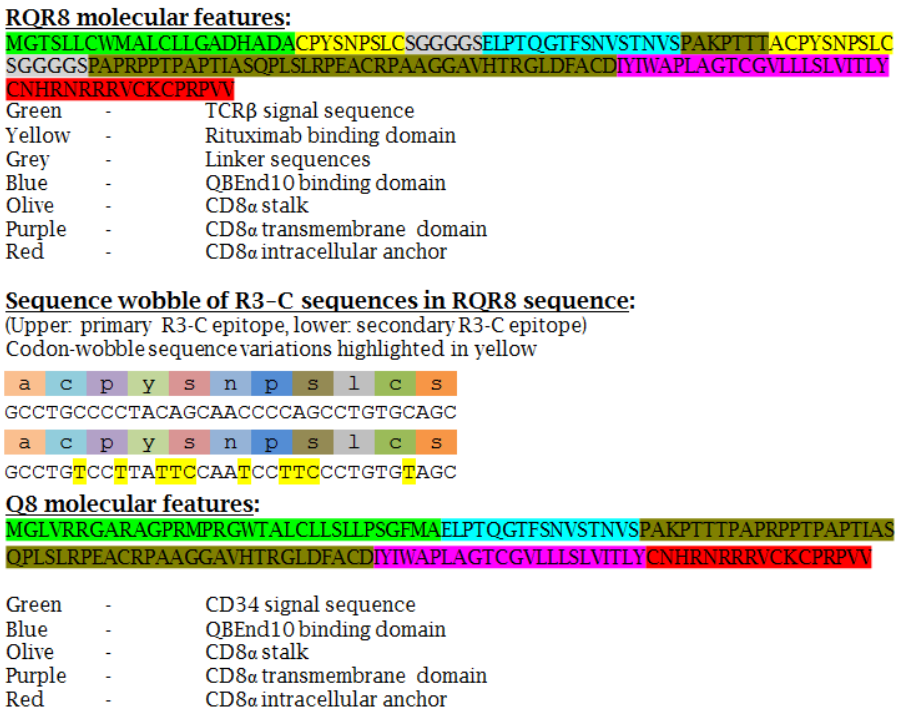

Figure 29 Illustration of the molecular features of Q8 and RQR8
Epitope expression constructs are composed of modular components as indicated: a signal sequence to facilitate cell surface expression, an epitope domain and a portion of the CD8α stalk functioning as a molecular spacer, including the extracellular, transmembrane and intracellular anchor domains. To prevent potential homologous recombination resulting from sequence duplication of the rituximab binding domain in the bivalent RQR8 construct, codon-wobbling was employed through the use of alternative codons thereby imposing sequence variation despite the identical protein sequence.

4.6.2. Marking sensitivity of RQR8

Experimental aim: To model the functional capacity of RQR8 to serve as a marker gene for clinical application.

In light of the desired functional capacity to function as a marker gene to enable cellular tracking *in vivo*, we sought to assess the sensitivity of cellular marking using a representative sample composition. As illustrated by Figure

30, this assay demonstrates the sensitive marking potential afforded by RQR8 to enable detection of transgenic cells from primary samples even when present at low levels. The consistent indication of cellular detection exceeding numbers of transgenic cells which were anticipated to be present in this assay may reflect a counting error during assay set-up.

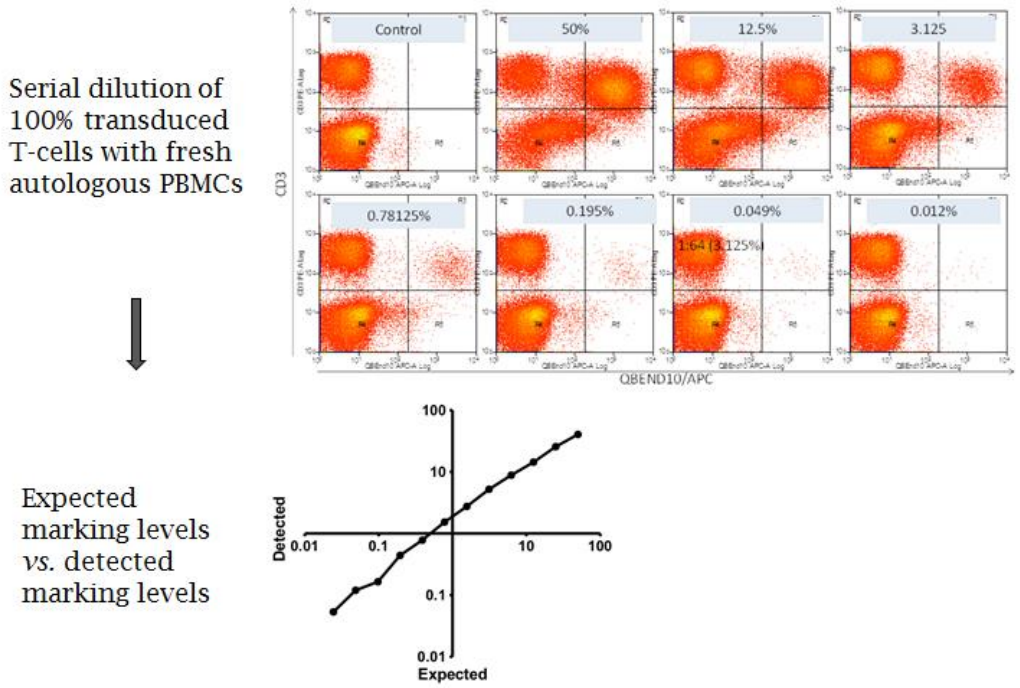

Figure 30 Sensitivity of RQR8 gene marking by serial dilution
To model the proposed sensitivity of RQR8 gene marking as might be observed when assessing primary patient samples, the following assay was performed. Peripheral human blood PBMCs were transduced with RQR8.I2.eGFP then purified by MACS selection. Following confirmation of purity by flow cytometry, sorted PBMCs were mixed with freshly isolated PBMCs derived from the same donor in a 50:50 ratio. Subsequently, this parental sample was serially diluted into pure populations of freshly isolated PBMCs establishing dilutions as indicated. Efficacy of cellular marking was assessed by flow cytometry to compare the level of marking observed against what was anticipated. Data presented reflects a result from a single donor; assay performed by Eva Kokalaki.

4.6.3. QBEnd10 / Rituximab co–staining

Experimental aim: To demonstrate QBEnd10 marker gene capacity is retained even in the presence of saturating rituximab antibody as would be present during clinical application.

Demonstration of co-staining of RQR8 with both QBEnd10 and rituximab: following from successful demonstration of the sensitivity afforded by RQR8 gene marking, we next sought to confirm the proposed ability to detect the presence of residual cells through QBEnd10 gene marking in the presence of

saturating levels of rituximab. Due to the minimal size of the RQR8 protein, we postulated that steric hindrance due to the presence of bound rituximab might preclude effective QBEnd10 staining which could result in overestimation in the efficacy of cellular clearance following therapeutic administration. To investigate this line of reasoning, we assessed the ability to identify target cells by QBEnd10 staining in the presence or absence of rituximab antibody. As illustrated by Figure 31, the RQR8 transgenic population can be clearly identified through QBEnd10 staining despite pre-staining with 200µg of rituximab; however there does appear to be an approximately ½ log attenuation of the signal suggestive of some steric hindrance of the QBEnd10 antibody binding.

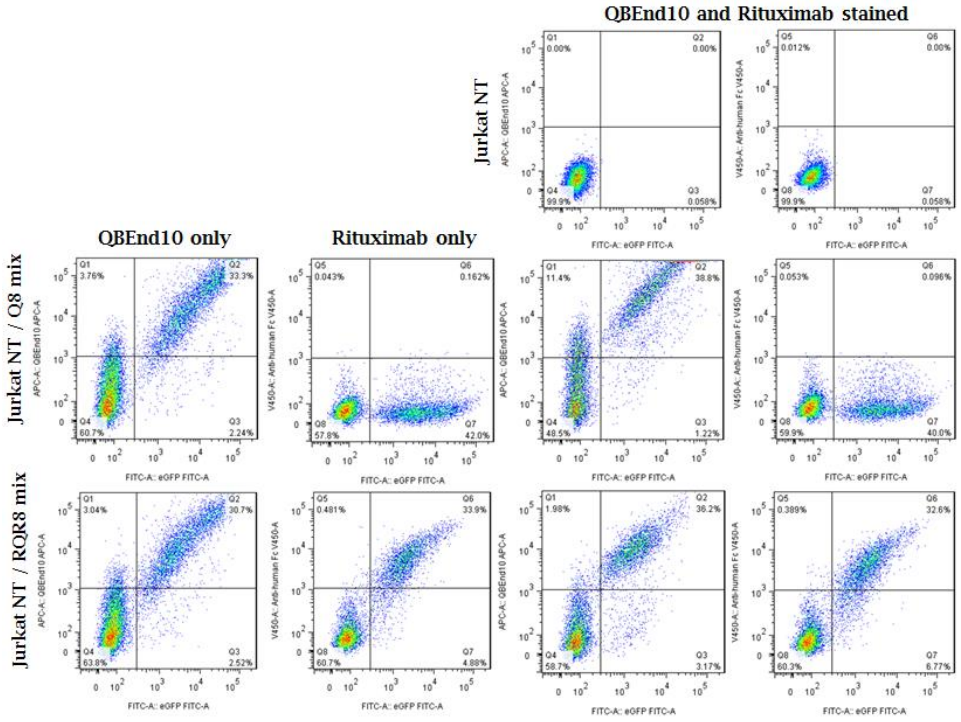

Figure 31 QBEnd10/rituximab RQR8 co-staining assay
To establish whether marker gene capacity would be retained in the presence of saturating antibody, purified Jurkat T-cell populations transgenic for Q8 or RQR8 were combined with non-transduced Jurkat T-cells in an equal ratio. Samples were indirectly stained with 200µg of rituximab, with anti-human Fc Dylight 450 employed as the secondary antibody prior to QBEnd10 staining. Results illustrated are from a single experiment.

4.6.4. Immunogenicity of RQR8

Experimental aim: To assess the potential immunogenicity of RQR8 *in silico* to predict the potential for immunological rejection by therapeutic recipients.

As with all non-native genes used for T-cell engineering, immunogenicity presents a potential limitation of RQR8. E.g. Chimeric antigen receptors, commonly derived from murine antibodies, often retaining the parental murine derived Fab domain, are typically presented in a format which may leave junctional and linker sequences exposed; both factors risk presentation of potentially novel immunogenic epitopes. Similarly, RQR8 has novel and junctional sequences which may prove to be immunogenic. A bioinformatics analysis of B- and T-cell immunogenicity of RQR8 is presented in Figure 32, identifying 6 T-cell and 24 B-cell epitopes as assessed using the LBtope[219] linear B-cell epitope prediction server and the NetCTL 1.2[220] servers respectively. However, in light of the proposed application of RQR8 in conjunction with re-targeted T-cell therapies, it should be noted that current CAR and TCR adoptive immunotherapy protocols typically employ profoundly lymphodepleting preparatory regimens resulting in profound immunosuppression at the time of T-cell administration. This may reduce the occurrence of, and may prevent development of an immune response. Notably, with respect to T-cell epitopes, RQR8 immunogenicity is only predicted for four MHC supertypes, conspicuously excluding the MHC supertype A2, which represents the most common serotype for almost all ethnic groups[221]. Ultimately, only clinical studies can determine the practical consequences of immunogenicity of any particular T-cell engineering component. Further discussion regarding immunogenicity of RQR8 is considered in 12.3.

Putative T-cell epitopes of RQR8:

MHC supertype	# of novel CTL epitopes identified	CTL epitopes identified
A1	0	
A2	0	
A3	1	VSTNVSPAK
A24	0	
A26	0	
B7	3	CPYSNPSLC SPAKPTTTA KPTTTACPY
B8	0	
B27	0	
B39	0	
B44	1	SELPTQGTF
B58	0	
B62	1	ADHADACPY

Proposed potential B-cell epitopes
LGADHADACPYSNPS
CPYSNPSLCSGGGGS
PYSNPSLCSGGGGSE
YSNPSLCSGGGGSEL
SELPTQGTFSNVSTN
PTQGTFSNVSTNVSP
TQGTFSNVSTNVSPA
QGTFSNVSTNVSPAK
GTFSNVSTNVSPAKP
TFSNVSTNVSPAKPT
FSNVSTNVSPAKPTT
PAKPTTTACPYSNPS
CPYSNPSLCSGGGGS
PYSNPSLCSGGGGSP
YSNPSLCSGGGGSPA
SNPSLCSGGGGSPAP
NPSLCSGGGGSPAPR
PSLCSGGGGSPAPRP
SLCSGGGGSPAPRPP
LCSGGGGSPAPRPPT
CSGGGGSPAPRPPTP
SGGGGSPAPRPPTPA
GGGGSPAPRPPTPAP
GGGSPAPRPPTPAPT

Figure 32 Bioinformatics assessment of RQR8 immunogenicity
Bioinformatics analysis of B- and T-cell immunogenicity of RQR8 as assessed using the LBtope[219] linear B-cell epitope prediction server and the NetCTL 1.2[220] servers respectively.

4.6.5. Western blot analysis of RQR8

Experimental aim: To confirm the approximate molecular mass of the RQR8 protein corresponds with that predicted by *in silico* algorithms and to establish whether cell-surface localised RQR8 is present in monomeric or dimeric format.

Assessment of protein size was achieved through Western blotting. Initial attempts at Western blotting using the QBEnd10 antibody resulted with an indistinct smear pattern suggestive of extensive glycosylation (data not shown). However, this result was not unexpected as both the CD8 stalk[207] and the CD34 antigen[193] are known to be heavily glycosylated and a bioinformatics analysis of putative glycosylation of epitope constructs using the NetOGlyc[222] and NetNGlyc[223] servers respectively, identified both N- and O-glycosylation sites as indicated by Figure 33. Due to the minimal fragment of the CD34 antigen present within the QBEnd10 binding domain, the majority of proposed glycosylation sites appear to be localised to the CD8 stalk region. In order to confirm that glycosylation predominantly results from sites localised to the CD8 stalk domain and to enable approximate assessment of the predicted molecular mass of Q8 and RQR8 as indicated by Table 8, we generated

carboxy-terminal FLAG-tagged versions of both the Q8 and RQR8 constructs, compared against a 'headless' iteration presenting the CD8 stalk domain lacking an amino terminal epitope domain as illustrated by Figure 33. Subsequently, Western blotting analysis of FLAG-tagged epitope proteins were performed with or without inclusion of the reducing agent dithiothreitol (DTT), from transgenic Jurkat T-cell samples. Additionally, the RQR8-FLAG protein was assessed from Jurkat T-cell samples, cultured in the presence or absence of an O-glycosylation inhibitor, and one condition where protein samples derived from cells grown in the presence of an O-glycosylation inhibitor were also treated with PNGase to remove N-glycosylation. Western blotting results are indicated by Figure 34.

Table 8 Bioinformatics prediction of protein epitope masses
Bioinformatics prediction of protein mass[224]. Values in brackets indicate proposed mass of the dimeric structure.

Protein	Mass kDa (Dimeric mass)
Headless-FLAG	11.96 (23.92)
Q8-FLAG	14.23 (28.46)
RQR8-FLAG	17.04 (34.08)

Comparison of protein samples separated under reducing or non-reducing conditions illustrated by Figure 34a, suggests that the CD8 stalk is likely present as a dimer which becomes separated into monomers under reducing conditions resulting in protein bands approximately ½ the mass under reducing conditions as the non-reducing counterparts. Notably, the presence of multiple bands may reflect protein shearing resulting either, from sample preparation or protein degradation. Following initial failure to obtain protein samples for Western blotting from lysis buffer incubation alone, a freeze-fracturing strategy was employed to damage the membrane before incubation in the lysis buffer. Although this strategy proved successful for generating protein supernatants, the generation of multiple fragments may reflect the presence of natural breaking points within the proteins under examination. Figure 34b illustrates the comparison between RQR8 samples separated under reducing and non-reducing conditions, as well as when samples were grown in the presence of an O-glycosylation inhibitor and subsequently treated to remove N-glycosylation. Although no difference was observed when comparing the samples grown in the presence or absence of the O-glycosylation inhibitor

which may reflect loss of function of the inhibitor during the extended culture duration required, a reduction in the observed protein mass of larger fragments following PNGase treatment to remove N-glycosylation supports the predicted presence of N-glycosylation at amino-terminal residues. Further, the consistent presence of approximately 12-14 kDa protein fragments between epitope samples remains unclear, but again, may reflect protein shearing resulting from the severe conditions required to achieve effective separation of protein from the plasma membrane. Notably, as indicated by the monomeric mass of the headless FLAG-tagged iteration, these consistent bands might identify CD8 stalk monomers which have been stripped of the epitope domains during processing possibly highlighting structural stability of the CD8 stalk with the epitope junction posing as a natural ‘break-point’ when the protein is subjected to profound shearing forces, such as were required to extract protein from cellular samples.

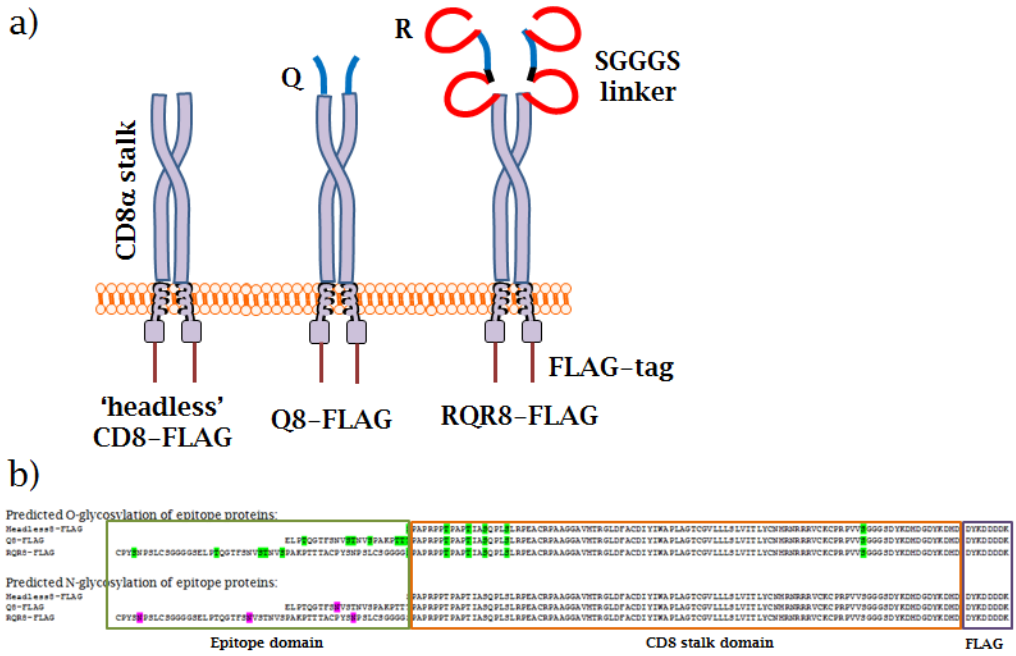

Figure 33 Cartoon of FLAG–tagged constructs and putative glycosylation
(a) To enable demonstration that glycosylation evidenced from initial Western blots resulted from the CD8 stalk (data not shown), it was necessary to establish FLAG-tag marked CD8 stalk-bound constructs. Three constructs were generated as indicated: a control construct expressing no epitope, denoted as 'headless', Q8 and RQR8 respectively. (b) Putative glycosylated residues for each protein sequence are identified as indicated. As highlighted by the top row which details the 'headless' CD8 stalk, residues which might possess O-glycosylation appear localised to both the epitope and CD8 stalk domains whilst the lower sequences illustrate that proposed residues containing N-glycosylation are exclusively associated with the epitope domains.[222, 223]

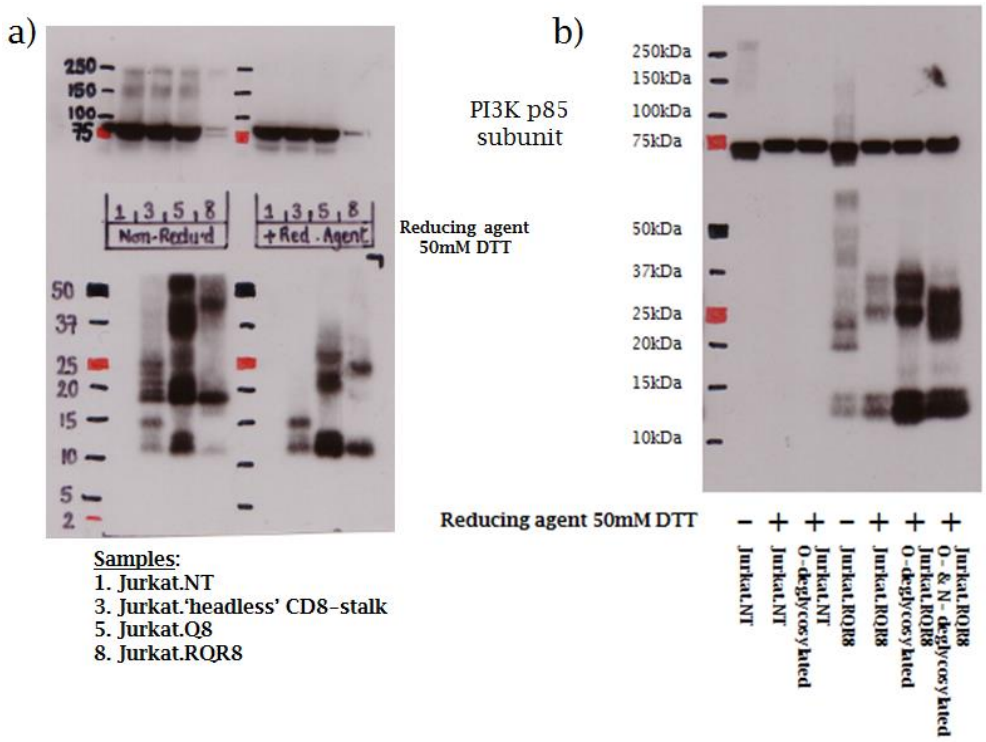

Figure 34 Western blot analyses of Q8 and RQR8
Jurkat T-cells were transduced with FLAG-tagged derivatives of Q8, RQR8 as well as a 'headless' iteration presenting the CD8 stalk without an additional epitope domain (Cartoon illustration of epitope constructs presented by figure 33). Transduced cell populations were FACS sorted based on equivalent eGFP expression in an attempt to establish roughly comparable transduction efficiencies. (a) 'Headless', Q8 and RQR8 protein samples were separated by Western blotting in the presence or absence of 50mM DTT reducing agent. As indicated by protein samples exposed to DTT, the reduction of the 20kDa band into a 10kDa band suggests that the CD8 stalk is likely present as a dimer on the cell-surface. (b) RQR8 protein samples were prepared with or without protocols to exclude O- or N-glycosylation as described (2.2.5.10.1.1, p104). The presence of reduced bands present in the sample modified to exclude N-glycosylation suggests that some residues within RQR8 contain this modification. Absence of reduction in protein sizes despite culture in the presence of an O-glycosylation inhibitor may be inconclusive due to loss of function of the inhibitor due to extended cell culture duration which was required to generate sufficient cell product to enable protein sample generation.

4.7. Conclusions

Although rituximab binding by the R3-C mimotope facilitates clear binding of rituximab, sensitivity to complement mediated deletion appears to occur in a density dependent manner. Thus, further engineering was required to fully achieve a level of efficacy matching that of the positive control. Following further examination considering a range of alternative iterations, RQR8, a 136aa construct composed of 2 rituximab binding mimotopes flanking the QBEnd10 binding sequence was identified which appears to offer at least

equivalent sensitivity to CDC-mediated deletion as afforded by the full length CD20 control construct. Furthermore, in addition to demonstrating acute sensitivity to CDC-mediated deletion, the sensitivity afforded by RQR8 appears to be highly specific with no killing observed against Q8 expressing control targets and only limited killing demonstrated against the highly similar RQ8 expressing target as illustrated by Figure 25. Finally, as verified by timecourse and dose-titration assays, CDC-mediated deletion occurs both rapidly and well within therapeutic dosages.

Following the clear demonstration of acute sensitivity to CDC-mediated deletion, further examination was considered to identify the potential mechanism involved. As indicated by Figure 18, C1q cross-linking is required to initiate complement activation. Premising that the increased sensitivity might result from bi-valent binding of rituximab by the RQR8 construct, this would result in any surface expression of RQR8 offering potential for cross-linking of C1q provided rituximab was present at sufficient concentration. To interrogate this possibility, *in silico* assessment of the molecular span separating the rituximab-CD20 interactions was assessed by Rasmol, measuring the binding pockets from the protein data bank reference 2OSL, derived from crystallographic binding data as identified by Du *et al*[201]. Having selected the threonine residue located in the centre of the cluster of residues involved in the rituximab-CD20 interaction as a reference point, we predicted a molecular distance of 76.57Å separating the threonine 58 residue in antibody chain A from the equivalent threnonine residue within antibody chain H, as measured using the Swiss protein data viewer (SPDV). Next we sought to approximate the molecular distance separating the alpha carbon atoms from adjacent amino acid residues from a linear peptide sequence. Again using SPDV, we approximated this distance to be 14.19Å, or 2.84Å per amino acid residue. As we predict that the 30 residues separating the rituximab binding domains within RQR8 compose a linear sequence derived from the QBEnd10 binding domain, the SGGGS linker sequence and a fragment of the CD8 stalk, this suggests a molecular separation between the rituximab binding motifs of >85Å which exceeds the 76.57Å span separating the rituximab binding domains predicted by *in silico* modelling as illustrated by Figure 35. Further examination of this interaction would require crystallographic binding analysis which exceeds the bounds of this project; however this approximation

suggests that RQR8 possesses the capacity for bi-valent binding of rituximab which might explain the enhanced sensitivity to CDC-mediated deletion as observed through *in vitro* CDC assays.

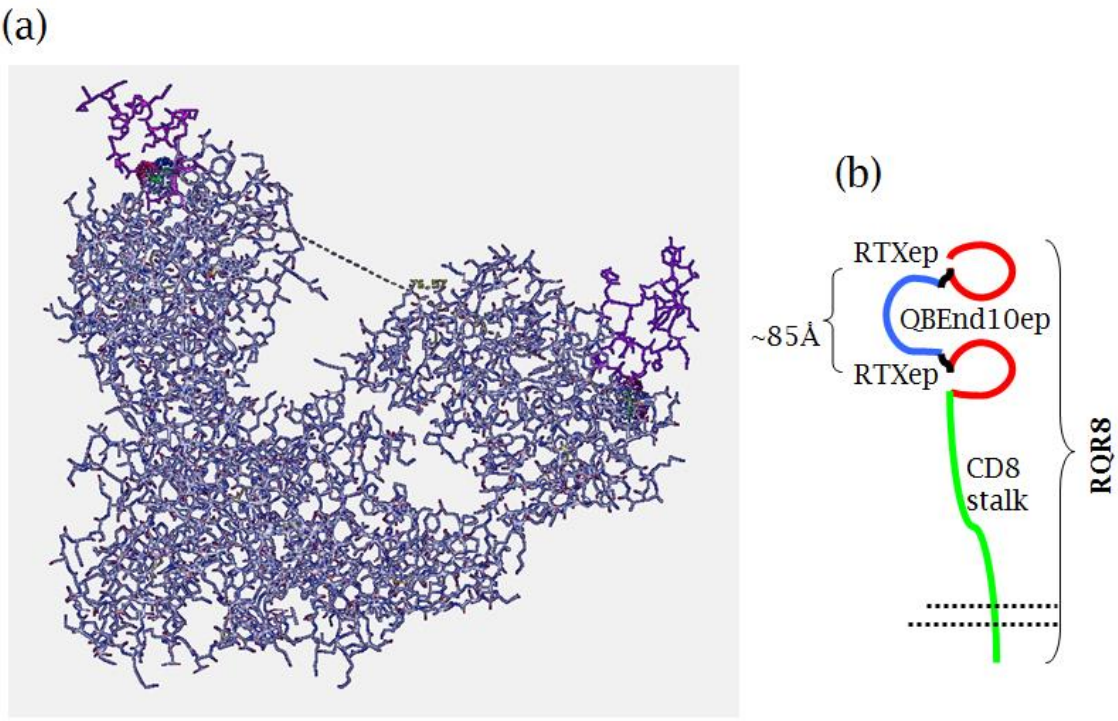

Figure 35 *In silico* modelling of rituximab–CD20 interaction
In silico modelling was considered in an attempt to identify whether RQR8 might truly offer a bivalent epitope expression format. (a) The distance separating the threonine residues identified in the centre of the rituximab-CD20 interaction were measured as 76.57Å using the Swiss protein data viewer (SPDV). (b) From a known linear peptide sequence, the distance separating alpha-carbon residues within protein sequences was approximated to be 2.84(Angstrom units) as assessed using SPDV. (Data not shown). Therefore, considering the approximately 30 amino acids, present in what we premise as a linear sequence, separating the two rituximab-binding domains; the molecular distance between rituximab binding epitopes within RQR8 was approximated to exceed 85Å which is greater than the span of rituximab. Generation of *in silico* modelling illustration and analysis was achieved with the kind assistance of Dr. Amit Jathoul.

4.8. General conclusions

- CDC-mediated deletion can be clearly achieved following incubation of transduced PBMCs with 25% BRC and 100μg/ml rituximab without any apparent impact upon control target viability
- Inclusion of eGFP & eBFP2 marker genes alongside Annexin V – APC and PI staining enable flow cytometry assessment of cellular deletion resulting from *in vitro* CDC assays

- Although the R3-C mimotope facilitates clear binding of rituximab, CDC-mediated deletion appears to occur in a density dependent manner from monovalent constructs
- Following re-engineering, a bivalent construct: RQR8, was identified which demonstrated equivalent CDC-mediated sensitivity as the full-length CD20 positive control
- CDC-mediated deletion facilitated by RQR8 appears to be sensitive, specific, rapid and occurs well within physiological levels following therapeutic rituximab administration

Chapter five

5. *In vitro* ADCC assays

5.1. Aims

- To establish a more reflective CD20 positive control through codon optimisation
- To generate an IL15/4-1BBL K562 cell line clone as per Imai *et al*[225].
- To achieve effective *in vitro* NK cell amplification sufficient to enable ADCC modelling
- To demonstrate *ex vivo* expanded NK cells represent a suitable effector population
- To demonstrate *in vitro* mediated ADCC deletion resulting from a primary effector cell population
- To establish and optimise a flow cytometry based ADCC assay
- To assess the comparative sensitivity and specificity of rituximab-mediated target deletion through *in vitro* ADCC assays

5.2. Introduction

As mentioned previously, rituximab mediated deletion occurs through a number of mechanisms including antibody dependent cellular cytotoxicity (ADCC)[186, 187]. Thus following from successful demonstration of CDC-mediated deletion of RQR8, we next sought to assess the potential role and efficacy of ADCC-mediated deletion of our epitope constructs. However prior to progression with ADCC assays, we identified a number of factors which required further consideration in preparation for this research tangent including: review of the capacity of our positive control to accurately reflect cellular deletion, the choice of effector population to be used within our ADCC assays and how to establish a consistent effector population to ensure experimental consistency.

5.2.1. Codon optimisation

Owing to degeneracy of the genetic code, individual species demonstrate codon bias suggesting species selective advantages to individual codon selection. Whilst many levels of control mechanisms are involved in the

regulation of gene expression, codon optimisation has been shown to improve levels of gene expression of genes in human cells[226].

Although the inclusion of a CD20 positive control construct is clearly required to establish the comparative efficacy of rituximab mediated deletion between RQR8 and the native CD20 antigen, we were concerned regarding potential limitations of our experimental strategy which might overestimate the efficacy of deletion of the positive control unfavourably skewing assay results. In our experimental design, we employed the eGFP and eBFP2 fluorescent proteins as marker genes to identify the target populations with the view that these would represent a consistent control. However, we had noted a trend for attenuated fluorescent marking from constructs possessing a longer primary transgene which corresponds with a report citing lower gene expression following an IRES[227]. Although we could consistently observe clear separation between eGFP expression levels with epitope expressing targets compared against non-transduced PBMCs, this separation remained less distinct for the CD20 positive control as illustrated by Figure 36. Furthermore, from observations suggesting poor T-cell viability when transgenic for CD20, we premised that codon optimisation of CD20 might boost transgene expression similar with previous observations from work with other transgenes by Dr. Simon Thomas, and correspondingly might result in enhanced IRES mediated eGFP expression. Results for codon optimisation of CD20 are described in section 5.3, p158.

5.2.2. ADCC

Antibody dependent cellular cytotoxicity (ADCC) reflects the capacity of an effector population to selectively destroy a cellular target through non-phagocytic processes. ADCC can be mediated directly through release of cytotoxic granules or reactive oxygen intermediates, or indirectly through induction of cellular apoptotic machinery via expression of cell-death inducing molecules. Efficacy of ADCC depends upon multiple variables including antigen density on the target cell surface, antibody affinity for the target antigen and the Fc-receptor (FcR) affinity for the respective antibody subclass[228]. ADCC effector populations are derived from both myeloid and lymphocyte lineages and include NK cells, macrophages, monocytes, neutrophils, dendritic cells and γδ-T-cells[228, 229].

The lack of non-specific activation of effector cells despite high levels of monomeric antibody molecules present in serum was initially premised to result primarily from the low affinity of most FcγR proteins for immunoglobulin Fc domains. However, similar to CDC, NK cell effector activation is contingent upon molecular cross-linking of FcγR's. The molecular explanation for requirement of FcγR cross-linking was established following elucidation of the crystal structure of FcγR-Fc interactions. This interaction results in formation of an asymmetrical contact between the FcγR and the immunoglobulin Fc domain which sterically precludes binding of a subsequent FcγR to the same Fc fragment. Thus innate effector cell activation depends upon binding of multiple antibody-Fc fragments which is only achieved at sufficient density as occurring within immune complexes. A secondary level of regulation results from the requirement of adapter molecules, as with the exception of FcγRIIa and FcγRIIc, activating FcγRs are unable to transmit activation signals without association with a signal transducing adapter molecule containing a cytoplasmic ITAM domain. Furthermore, variation of adapter molecules between effectors represents an additional layer of regulation within the ADCC-mediated response. Finally, pro-inflammatory mediators such as TNFα, IFNγ and LPS have been shown to mediate upregulation of FcγR expression. Upregulation of FcR expression mediated by the late components of the complement pathway, such as C5a, also highlight potential synergism between humoral mediated immunological pathways. However, despite variation between mechanisms involved in generation of an activating signal, resultant signalling pathways remain similar for all FcγRs[230].

Furthermore, the presence of multiple subclasses of Fcγ-receptors (FcγR's) containing activating or inhibitory endodomains (possessing either an ITAM or ITIM motif respectively), offer an additional layer of complexity to ADCC efficacy whereby the decision to impose a cytotoxic or inhibitory response against the target cell depends upon the composite signalling input from all of the respective FcγR's by the effector cell. Correspondingly, alterations in FcγR functionality due to aberrant expression or allelic variation have been associated with pathologies such as arthritis and systemic lupus erythematosus[231].

5.2.3. NK cells as an ADCC effector population

Note: due to variation between human and murine NK-cell biology, this discussion is restricted to human NK cells.

Natural killer (NK) cells, first described in 1975[232, 233], are relatively short-lived granular lymphocytes, distinct from both B and T-cells. NK cells represent a minority lymphoid subset, typically composing between 2-18% of the peripheral blood lymphocyte population[234]. NK cells perform three primary functions: cytotoxicity, cytokine and chemokine secretion and lastly contact dependent cell co-stimulation facilitating a bridge between innate and adaptive immunity[235].

5.2.3.1. Cytotoxicity

As most research into the ADCC-mediated efficacy of rituximab has been derived from NK cell interactions, further discussion regarding ADCC will focus on the role of NK-cells[187]. NK cells can be broadly sub-divided into two subsets which demonstrate variation in homing and functional capacity[234]: $CD56^{bright}$ NK cells appear to function in a primarily immunoregulatory capacity producing IFNγ >16 hours following activation and tend to localise to the tonsils and lymph nodes, whereas the $CD56^{dim}/CD16^{+}$ NK-cell subset, primarily responsible for NK cell mediated cytotoxicity, release IFNγ rapidly following activation and account for 90% of the NK cells located in the spleen and peripheral blood[235, 236]. NK cells are capable of killing target cells without prior activation, sensitisation or MHC restriction; however the kill/spare decision remains dependent upon the balance between activating and inhibitory signals which the cell receives[235]. Due to the extensive repertoire of potential activating and inhibitory signalling receptors which may be present[237], deconvolution of NK cell signalling can prove quite complicated, however a minimalistic view can separate the decision for NK cell killing primarily to the presence of an activating signal, such as bound antibody on a target cell, or the absence of an inhibitory signal, such as MHC-I typically present on the surface of virtually all cells, with ‘missing self’, ‘altered self’ and ‘stress-induced self’ describing three models by which NK-cell mediated killing results from the lack of an inhibitory signal.

Once the decision for a cytotoxic response has been established, NK cell killing can be mediated through a number of mechanisms[235]:

i. Release of cytotoxic granules (Perforin/granzymes)
   Cytotoxic granule release results in target cell apoptosis through both caspase-dependent and independent mechanisms.
ii. Death receptor mediated apoptosis
   Induced expression of FasL or TNF-related apoptosis inducing ligand (TRAIL) on the NK-cell surface interact with the cognate ligands, Fas or TRAILR respectively, on the target cell to induce apoptosis

   Activated NK cells can also secrete TNFα inducing target cell apoptosis following binding to TNFR1/2
iii. Secretion of effector molecules
   a. Activated NK cells secrete IFNγ which may exert cytotoxicity through a range of mechanisms including stimulation of adaptive immunity
   b. Cytokine activation of NK cells may also result in cytotoxicity mediated by reactive oxygen and/or nitrogen intermediates

While the presence of preformed perforin/granzyme granules facilitate the characteristic rapid cytotoxicity of the NK cell response, other mechanisms such as induced expression of death receptors require a longer kinetic to achieve maximal efficacy.

5.2.3.2. Cytokine/Chemokine secretion

Cytokine and chemokine secretion by NK cells, including IL3, GM-CSF, TNFα and IFNγ, facilitates the capacity to recruit and moderate responses from both the innate and adaptive immune compartments in addition to mediating cytotoxicity[235].

Furthermore, recent research suggests kinetic variation in the capacity of NK-cell subset cytokine secretion relevant to proposed immunological roles. Rapid IFNγ secretion by the $CD56^{dim}/CD16^{+}$ NK-cell subset, as rapidly as 2 hours following activation, but terminating before 16 hours post activation was proposed to correlate with the primary role of NK cells to mediate a rapid innate immunological response. In contrast, the IFNγ secretion mediated by

the $CD56^{bright}$ subset demonstrates a delayed response typically commencing 16 hours following an activating stimulus. This was proposed to be consistent with an immunoregulatory role[236]. Although obviously the net result following IFNγ secretion remains the same, the variation in the kinetics of the reactions reflects the capacity of NK cells to mediate both short and sustained immunological responses.

5.2.3.3. Contact dependent cell co–stimulation

Finally, NK cells can mediate contact dependent cell costimulation. As NK cells express T and B cell co-stimulatory ligands such as CD40L and OX40L, they can act as a bridge between the innate and adaptive immune responses. NK cells express a range of surface receptors known as inhibitors and activators. Current models for NK cell activation predict that the particular response of an NK cell is dependent on the composite balance between the activating and inhibitory signals which the cell receives. E.g. Self MHC class I molecules deliver an inhibitory signal to prevent unchecked autoimmunity. However, down-regulation of self MHC-I results in unopposed activation signals delivered to the NK cell due to 'missing self-recognition'[238].

5.2.3.4. NK 'missing self' and licensing hypotheses

The binding ratio between IgG subtypes against the inhibitory FcγRIIb and the various activating FcγR's define the ADCC activation threshold of effector cells. However, as indicated by Table 9, due to the lack of expression of the inhibitory FcγRIIb, NK cells possess significant potential to impose unchecked toxicity if alternative protective mechanisms remained absent. Hence evolution has provided the related NK-cell licensing and MHC-I mediated inhibition 'missing-self' mechanisms as alternative protective strategies.

Table 9 FcγR expression and indicative binding affinities
Indicative FcγR binding affinities adapted from Beutler *et al* and Smith *et al*[3, 231].
Effector populations: NK – Natural killer cells, MO – Monocytes, MA – Macrophages, N – Neutrophils, DC - Dendritic cells, M – Mast cells, E – Eosinophils, B – Basophils, P – Platelets

FcγR\Effector	Activating or Inhibitory	NK	MO	MA	N	DC	M	E	B	B–cell / Plasma cell	P
FcγRI (CD64)	Activating	–	+	+	+	+	–	+	–	–	–
FcγRIIa (CD32)	Activating	–	+	+	+	+	–	–	–	–	+
FcγRIIb (CD32)	Inhibitory	–	+	+	+	+	+	–	+	+	–
FcγRIIc (CD32)	Activating	+	–	–	–	–	–	–	–	–	–
FcγRIIIa (CD16)	Activating	+	+	+	–	+	–	–	–	–	–
FcγRIIIb (CD16)	Activating	–	–	–	+	–	+	+	–	–	–

5.2.3.4.1. Missing self

The missing-self hypothesis[239] describes a mechanism of self-protection against autoaggression mediated by inhibitory interactions between killer cell immunoglobulin like receptor (KIR) interactions with MHC-I. Since virtually all normal cells express MHC-I, reduced or absence of expression of MHC-I attenuates the inhibitory signal of NK-cell KIR's, thereby reducing or removing the block preventing cytotoxicity[240]. Correspondingly, due to the crucial role of KIR's, a secondary mechanism of control is necessary to ensure the NK-cell compartment is capable of identifying self-MHC prior to enabling the capacity for cytotoxicity; this is achieved through a process known as NK-cell licensing.

5.2.3.4.2. NK–cell licensing

The KIR genes comprise of a multigene family containing both activating and inhibitory receptors demonstrating significant inter-individual variation such that individuals may express between 7-14 separate KIR genes. The potential for NK-cells to express a KIR lacking a cognate HLA ligand, arises from the fact that the KIR locus and the corresponding HLA genes are encoded by separate chromosomes. Furthermore, there can be significant intra-individual NK-cell clonal variation resulting from differential patterns of KIR expression[238, 241]. Hence, the process of NK cell licensing, which can be viewed as an analogous system to tolerance induction processes occurring during T and B cell ontogeny is required.

As the 'missing-self' hypothesis describes the importance for the role of inhibitory KIRs in preventing autoaggression in the lack of an activating signal,

'NK-cell licensing' ensures that capacity for NK-cell cytotoxicity is restricted to those cells which have demonstrated the ability to identify self-MHC. As a result of the NK-cell licensing process, two populations of self-tolerant NK cells result: one population which possess self-tolerance mediated by the self-MHC molecule by which it became licenced, and a second population which remains tolerant due to cellular anergy resulting from a failure to become licenced[240].

5.2.3.5. NK cell summary

NK-cells remain under constitutive inhibition as defined by the 'missing-self' hypothesis, which requires a sufficient activation signal to be overcome[238]. As NK-cells lack expression of the inhibitory FcγRIIb, an additional layer of NK-cell regulation is achieved through restriction of FcγR expression to the low affinity FcγRIIIa (CD16) and FcγRIIc (CD32) subclasses, which unable to bind monomeric IgG, are limited to binding IgG when associated in an immune complex[231]. Finally, NK-cell licensing imposes tolerance toward self-HLA limiting NK-cell mediated autoimmunity[240].

Having selected NK-cells as our effector population for ADCC assays, it was necessary to establish a strategy to ensure consistent production of an effector population which could enable effective assessment of ADCC-mediated cytotoxicity detailed further in section 5.6. As ADCC-mediated deletion comprises both rapid and sustained components, *in vitro* assay design should consider both phases to ensure a fully reflective result is obtained.

Rituximab is a chimeric antibody composed of the murine derived antibody-binding Fab domain and the human IgG1 Fc constant domain. Although we selected NK-cells as the effector population for ADCC modelling experiments, as illustrated by Table 9 and Table 10, as all FcγR's can demonstrate binding to the IgG1 subclass, ADCC is not restricted to NK cells. Thus *in vitro* NK-cell ADCC assays confirm or preclude whether ADCC is involved in depletion of epitope expressing targets, but due to the exclusion of effector populations expressing the high affinity FcγR's, these assays do not fully model the potential depletion which could be achieved.

Table 10 Indicative FcγR–IgG binding affinities
Indicative immunoglobulin binding affinities adapted from Beutler *et al* and Smith *et al*[83, 231].

Functional capacity/ Antibody subclass	IgG1	IgG2	IgG3	IgG4
Complement fixation	++	+/–	+++	–
ADCC	+	–	+	–
FcγRI (CD64)	+++	+	++++	++
FcγRIIa (CD32) [Variant H131]	+++	++	++++	+
FcγRIIb (CD32)	++	–	+++	++
FcγRIIc (CD32)	++	–	+++	++
FcγRIIIa (CD16) [Variant V158]	++	+/–	+++	+/–
FcγRIIIb (CD16) [GPI anchored]	+	–	+++	–

5.3. Results: Codon optimisation of CD20

Experimental aim: To improve functional expression of full-length CD20 through codon optimisation of the coding sequence.

During *in vitro* CDC assay experiments, we observed a trend of typically poor expression of the CD20 antigen on T-cells when coded by the native cDNA sequence. Moreover, expression of the downstream eGFP marker gene presented a limiting factor for discrimination of cellular deletion as assessed by flow cytometry analysis with co-culture assays where the signal to noise ratio is impaired by a high effector to target ratio. This results in skewing the deletion as assessed by *in vitro* assays in favour of the positive control. Premising that codon optimisation might result in enhanced expression levels, we designed a codon optimised version of CD20 for this purpose. Codon optimisation of the CD20 sequence was achieved using pMol software using an algorithm written by Dr. Martin Pulé. This algorithm is designed to preferentially select codons based on the most common tRNAs present in human cells. In addition, hairpins, literal repeats, and cryptic splice sites were removed, whilst the GC content was raised to 70%. This coding sequence was then generated by gene synthesis using overlapping oligos and subcloned as an NcoI-MluI fragment into SFG.I2.eGFP. Correct clones were identified by restriction digest followed by DNA sequencing. Comparison of the original CD20 wild-type construct compared with the codon-optimised CD20opt

construct was assessed by flow cytometry staining of retrovirally transduced PBMC's as illustrated by Figure 36.

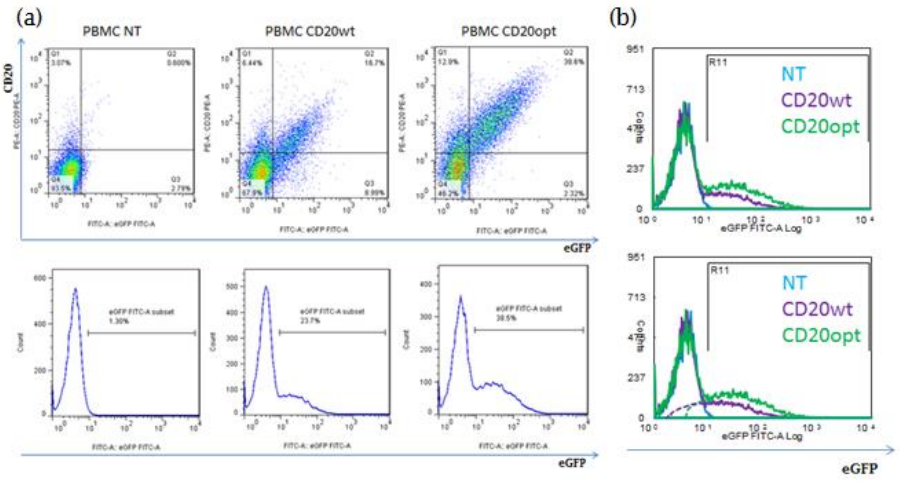

Figure 36 Comparison of wild-type vs. codon-optimised CD20 expression
(a) Primary human PBMCs were transduced with SFG.CD20.I2.eGFP and SFG.CD20opt.I2.eGFP. CD20 expression was assessed by flow cytometry shown by the top row, whilst the bottom row illustrates enhanced co-expression of the eGFP marker gene employed to measure cytotoxicity through in vitro assays. (b) An exaggerated extrapolation of the fluorescence bleed by the eGFP marker into the non-transduced fraction is indicated in the lower panel to highlight potential for over-interpretation of the sensitivity to CDC-mediated deletion of the CD20 positive control construct. This limitation is notable given the clarity of the eGFP marker expression afforded by epitope constructs under interrogation which are illustrated by Figure 45, comparative analysis of transduction efficiency, page]. Flow cytometry data illustrates a representative sample from more than five donors.

Although the effect of codon-optimisation was modest regarding improving eGFP expression by the bicistronic vector, Figure 36 clearly illustrates enhanced CD20 expression between samples with comparable eGFP expression. However we did observe a consistent improvement in the level of transduction which was achieved by the codon-optimised construct typically achieving 35-50% transduction efficiencies compared with 20-35% which had been achieved from the CD20wt construct. Figure 36a illustrates typical histogram profiles from transduced PBMC's, with Figure 36b modified to suggest potential improvement in the capacity of CD20opt.I2.eGFP construct to accurately reflect cellular deletion from ADCC assays. We proceeded with ADCC modelling using the CD20opt.I2.eGFP construct recognising that limited efficacy of the CD20 positive control to fully represent ADCC mediated deletion might result in under-representation of the efficacy of our epitope constructs.

5.4. Cloning of IL15 / 4–1BBL constructs

Experimental aim: To generate a functional molecular cassette to mediate cell surface expression of IL15 and 4-1BBL.

Following from our decision to employ NK cells as the effector population for *in vitro* ADCC assays, we faced the challenge of how to consistently establish a sufficient population to enable effective modelling. Each assay as described in 2.2.5.7.3, required almost $3x10^7$ NK cells; as this would require between 140ml-1.4L of peripheral blood per donor based on typical NK-cell composition within peripheral blood, it was essential to identify an alternative strategy to establish the effector cell population. Ideally, we desired a strategy which would enable consistent generation of a functional NK cell effector population which could be established concurrent with transduction, and selection where required, of the target population, all derived from the same donor to preclude NK-cell 'missing-self' activation and preferably from a single peripheral blood draw of reasonable volume.

Previous work by Imai *et al*[225] has demonstrated the ability to amplify NK cells *in vitro* through co-culture with the MHC-I negative K562 cell line[242], modified to express cell-surface localised IL15 and the 4-1BB ligand. Using this strategy, this group demonstrated NK cell proliferation through ectopic expression of IL15 and the 4-1BB ligand on modified K562 cells resulting in a 1000-fold amplification of NK cells following 3-week co-culture of PBMC's with modified K562 cells[225]. Briefly, it was known that the K562 myeloid leukaemia line[243] demonstrates acute sensitivity to lymphocyte mediated cytotoxicity[244] and co-culture of NK cells with irradiated K562 cells can substitute for ionomycin as a mitogenic signal although it was premised that optimal NK cell proliferation would require additional co-stimulation[245]. Relative to our research, IL15 has been identified as a potent activator of NK cell effector function promoting both NK-cell development and NK cell survival[225, 234], IL2 promotes NK-cell proliferation and cytotoxicity[234] and the 4-1BBL was observed to enhance NK-cell activation and production of IFNγ and GM-CSF cytokines[225].

As we were unable to obtain this modified K562 cell line, we recapitulated this research to generate our own NK-cell amplifying K562 clone. As an expression plasmid encoding the 4-1BBL had already been generated by Dr. Martin Pulé, only the coding sequence for the IL15 cytokine was required. The coding

sequence for IL15 was sourced from monocyte cDNA, achieved by Trizol-based RNA extraction from monocytes as described (2.2.1.1.12), followed by cDNA generation using an Ambion reverse transcriptase kit. Successful generation of cDNA was confirmed by PCR amplification of the GAPDH housekeeping gene from the cDNA sample prior to progression with IL-15 amplification using monocyte derived cDNA as template.

Premising that IL15 presentation format might affect NK cell expansion, we generated two alternative IL15 / 4-1BBL expression constructs variant for the size of the CD8 molecular spacer presenting the IL15 cytokine. Both constructs present the IL15 cytokine upstream of a TaV 2A sequence followed by the 4-1BBL transgene were sub-cloned into a similarly digested SFG.I2.eBFP2 vector as AgeI-MluI to generate the expression constructs. As indicated by Figure 37, MP6930 utilises the same CD8 stalk as the QBEnd10 epitope presentation strategy whereas the membrane-proximal construct MP6891 contains only the transmembrane and anchor domains derived from the CD8 stalk. Successful cloning was verified by restriction digest followed by DNA sequencing. Finally, functional verification of IL15 and 4-1BBL expression by the alternative constructs was confirmed by indirect flow cytometry (data not shown).

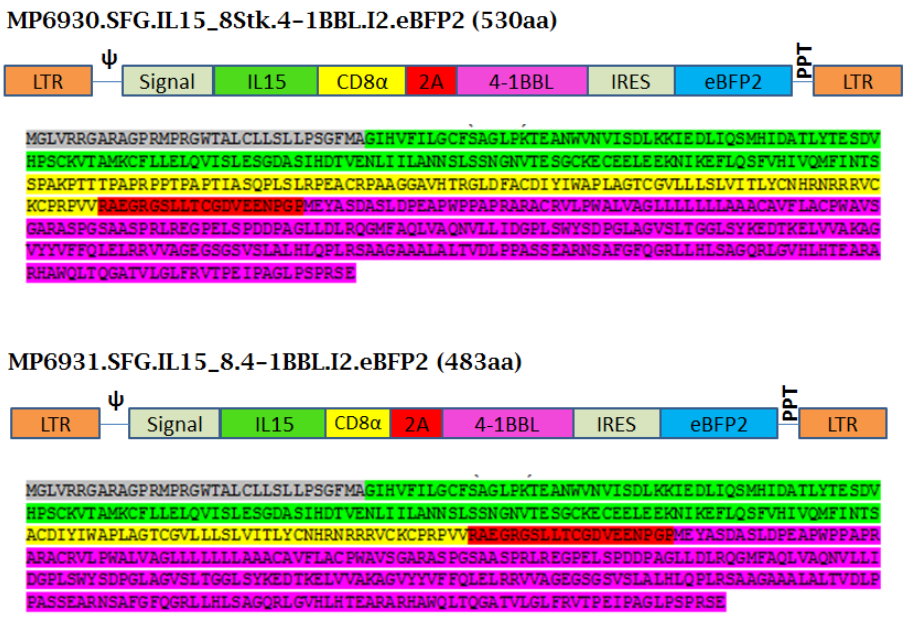

Figure 37 Molecular design of IL15 / 4-1BBL expression constructs
To facilitate ectopic cell-surface localised IL15 cytokine presentation, it was necessary to engineer a signal sequence, molecular spacer and anchoring domain into the expression cassette. Equimolar bi-cistronic expression of 4-1BBL was achieved through deletion of the 5' transgenic STOP codon and inclusion of the self-cleaving TaV 2A peptide sequence localised

between the separate transgenes. Modular design of the engineered protein through inclusion of the separate protein domains as indicated. The IL15 / 4-1BBL cassette was sub-cloned into the SFG.I2.eBFP2 vector as an AgeI-MluI fragment.

5.5. Generation of K562 clone

Experimental aim: To generate a stable K562 clone expressing high level cell-surface localised IL15 and 4-1BBL, as a platform to mediate *in vitro* NK-cell expansion.

To ensure consistent NK cell proliferation, we premised that it would be necessary to establish a single cell clone expressing the IL15/4-1BBL construct. To this end, we generated RD114 pseudotyped retroviral supernatant for both constructs. Following a single round of retroviral transduction, transduction efficiencies over 90% were achieved for both constructs. Successful surface expression of both IL15 and 4-1BBL was confirmed by flow cytometry through indirect staining illustrated by Figure 38.

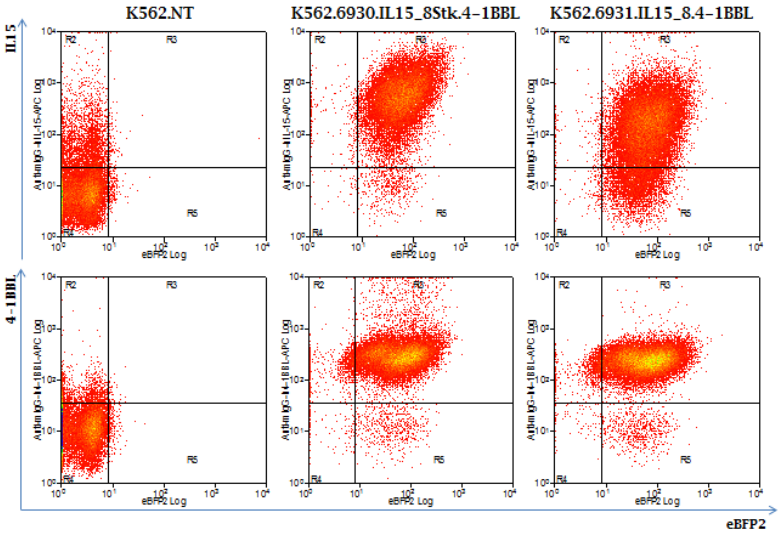

Figure 38 Verification of IL15 and 4–1BBL expression in K562 cells
K562 cells were separately transduced with both iterations of the IL15 / 4-1BBL expression cassette. The eBFP2 fluorescent protein marker identified transgenic cells thereby enabling confirmation of successful expression of the desired surface antigens achieved through indirect antibody staining. Successful binding by the murine anti-IL15 or anti-4-1BBL primary antibodies was achieved by secondary staining using an anti-mouse APC secondary antibody with binding efficacy assessed by flow cytometry. Although both constructs demonstrated similar levels of 4-1BBL expression, the CD8-stalk bound presentation format appeared to offer superior presentation for the IL15 cytokine as illustrated by the MP6930 construct.

Next we isolated high expressing K562 populations for each construct by flow cytometry using a Beckman Coulter MoFlo cell sorter based on the eBFP2 fluorescent protein marker; cell sorting performed by Arnold Pizzey. Finally

single cell clones isolated by limiting dilution (2.2.2.1.3), were screened based on expression levels of the respective protein targets compared against the internal eBFP2 fluorescent marker as illustrated by Figure 39. For the MP6930 construct, the A5 clone demonstrated the highest level of transgene expression combined with an optimal growth profile. For the MP6931 construct, both the E1 and E5 clones were selected as they demonstrated equivalent expression profiles. Cell banks for the identified clones were cryopreserved with fresh aliquots thawed and transiently passaged as required.

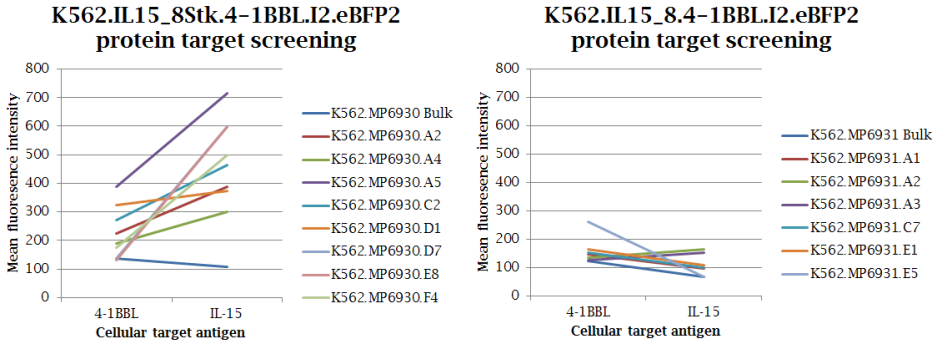

Figure 39 K562 single cell clone screening of IL15 / 4-1BBL expression
To reduce potential experimental variation between in vitro NK-cell expansions, transgenic K562 populations were single cell cloned to enable consistent IL15/4-1BBL expression and therefore theoretically equivalent IL15/4-1BBL stimulation. Single cell isolates were stratified based upon the mean fluorescence intensity of antibody binding against both the IL15 and the 4-1BBL protein targets as compared against eBFP2 fluorescent protein marker gene expression. As illustrated, for the MP6930 series the A5 clone demonstrated clearly superior expression for both targets. In contrast, the MP6931 clones demonstrated a consistent and reduced expression than what was observed for the MP6930 series, and both the E1 and E5 clones were retained for subsequent consideration.

5.6. NK cell production

Experimental aim: To demonstrate consistent and sufficient *in vitro* NK-cell expansion as to enable downstream ADCC assays using NK-cells as the effector population.

Having established stable modified K562 cells, we next sought to confirm efficacy of NK-cell proliferation following PBMC:K562 co-culture. From a series of co-culture expansions with separate donors, we observed clear evidence of NK-cell expansion in all instances (more than 6 donors, data not shown). As successful amplification was consistently achieved in all donors following co-culture with the K562.A5 clone, contrasting with typically more modest expansion resulting from the K562.E1 co-culture, the K562.A5 clone was

selected for expansion of NK-cell effectors for all subsequent ADCC assay experiments (data not shown). In our hands, following a 7 day co-culture with the K562.A5 clone typically, 0.5-1.0 x 10^6 NK cells can be isolated for each 1.0 x 10^6 PBMC's supplied in the initial PBMC:K562 co-culture. NK-cells were isolated by CD56 positive selection following seven days of co-culture. NK-cell phenotype was confirmed by flow cytometry analysis following overnight recovery post-MACS selection, with ADCC assays initiated within 24 hours of NK cell selection. An example of NK-cell profile following MACS selection is illustrated by Figure 40.

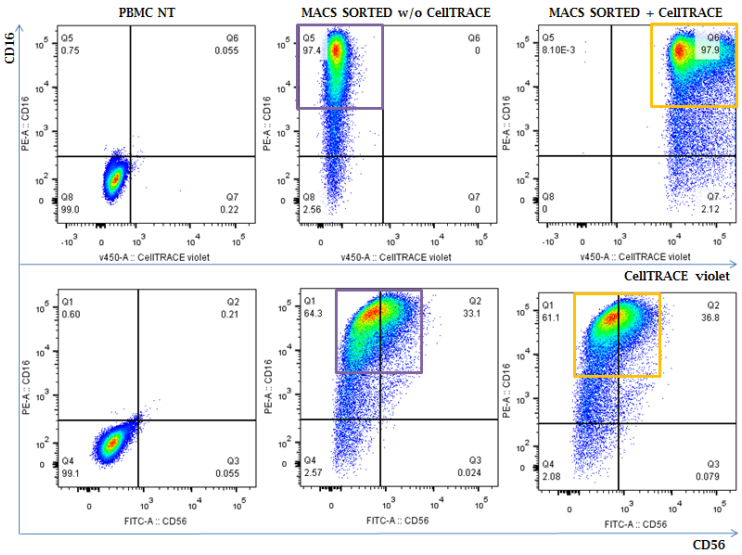

Figure 40 Purified NK–cell effector profile
Primary human PBMC's were expanded *in vitro* for 7 days as described (2.2.2.2.4, p91). Following a 7-day *in vitro* expansion, NK-cells were positively selected by CD56 magnetic bead selection, recovered overnight then assessed by flow cytometry for confirmation of purity and phenotype confirmation prior to inclusion into ADCC assays. As illustrated at far right, NK-cell effectors for the sensitivity assay were identified (and excluded) based upon CellTRACE violet staining. For both assays, as indicated by the middle samples, NK-cell effectors were confirmed as possessing a $CD56^{dim}/CD16^{+}$ phenotype prior to assay progression.

Successful NK cell proliferation can be predicted based on alterations to the co-culture profile by microscopic analysis over time as illustrated by Figure 41. At the start of cellular co-culture, the larger K562 cells clearly dominate the culture sample; following extended co-culture, K562 cells are progressively cleared by the developing NK cell populations ultimately becoming the clearly dominant population.

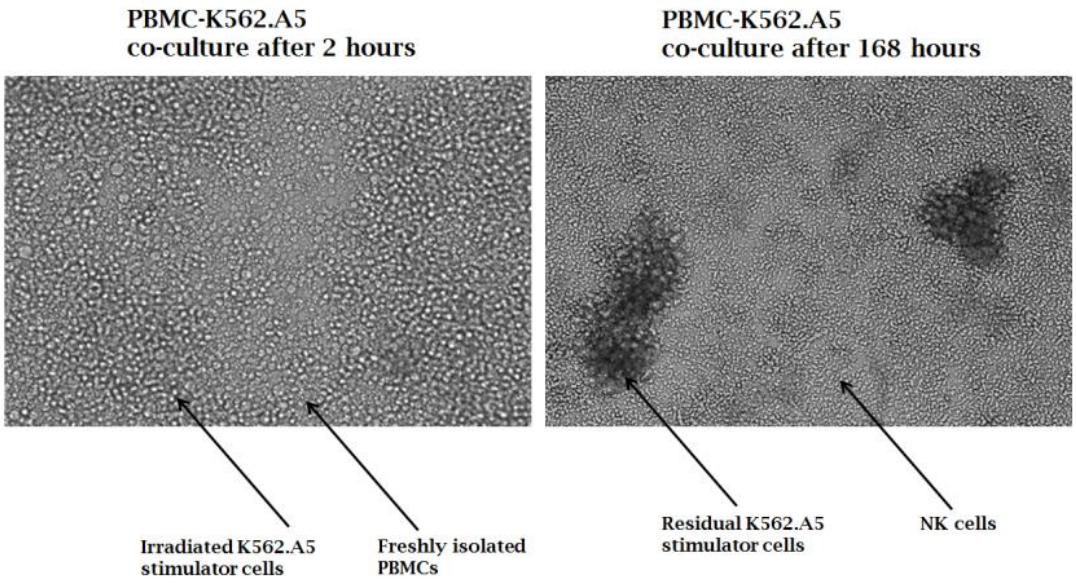

Figure 41 Microscopic illustration of PBMC:K562.A5 co–culture progression
Primary human PBMCs were co-cultured with irradiated K562.A5 cells according to protocol as described 2.2.2.2.4, p91 to mediate *ex vivo* NK cell expansion. Successful amplification of NK cells could be predicted by visualisation of progressive deletion of the larger K562 cells concurrent with expansion of the smaller lymphocyte population as indicated. Image at 40x magnification.

5.7. ADCC assay optimisation

Experimental aim: To establish a flow-cytometry based *in vitro* ADCC assay capable of discriminating sensitivity to ADCC-mediated deletion between closely related molecular targets.

Having successfully established a strategy to generate our chosen effector population, we next sought to demonstrate ADCC-mediated deletion through a flow cytometry based assay to correspond with our previous CDC deletion assays. Failings identified from an initial series of ADCC assays directed modifications required to optimise flow-cytometry assay protocols allowing assessment of both sensitivity and specificity of ADCC-mediated target depletion. Modifications included: functional confirmation of ADCC by the NK-cell effector population, optimisation of staining strategies to enable cellular discrimination within the assays, and altering of the duration of effector:target incubation to enhance assay sensitivities.

5.7.1. Confirmation of functional effector capacity

In our preliminary ADCC assays, we reprised the strategy employed for Specificity CDC assays, utilising Q8.I2.eBFP2 as an internal control,

RQR8.I2.eGFP as the specific target, using Annexin V-APC/PI staining for viability discrimination. From this initial series of assays, we observed modest ADCC mediated deletion of RQR8 expressing targets. Although technical problems precluded full and complete assessment of the efficacy of deletion as illustrated by Figure 42, the level of ADCC mediated deletion appeared clearly inferior to what had been observed from CDC mediated deletion. This in part likely reflects an exaggerated indication of the efficacy of CDC-mediated deletion due our choice of baby rabbit complement for CDC assays. As early monoclonal antibodies demonstrated a poor ability to activate complement, historically rabbit serum was chosen as an alternative to human complement to enhance CDC efficacy due to the inability of cell surface complement inhibitors, such as CD35, CD46, CD55 and CD59, to inactivate the heterologous complement cascade[246]. From these initial ADCC assays, we observed an average level of ADCC-mediated deletion of approximately ten percent.

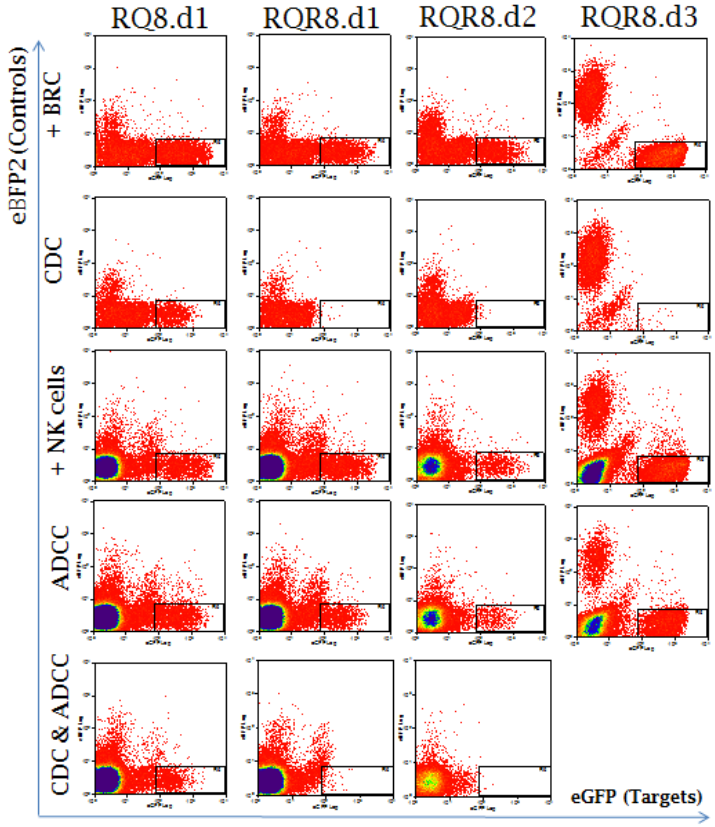

Figure 42 Preliminary ADCC assays
Primary human PBMCs were transduced with RQ8.I2.eGFP, RQR8.I2.eGFP or Q8.I2.eBFP2, with each sample separately purified by CD34 magnetic bead selection (Miltenyi). Subsequently, the RQ8.I2.eGFP and RQR8.I2.eGFP populations were independently combined with the Q8.I2.eBFP2 population to establish a 50:50 assay target suspensions. These target

populations were then incubated for 4 hours with NK-cell effectors derived from the same donor at an effector:target ratio of 8:1 with or without rituximab at 100µg/ml. RQ8 assay reflect the result from a single donor; RQR8 assay illustrations reflect results from three separate donors. Note: For donors 1 and 2, the Q8.I2.eBFP2 population appears absent due to problems with the violet laser on the Cyan cytometer precluding effective detection.

During consideration regarding how best to proceed with subsequent assays, we premised that it remained plausible the modest level of ADCC-mediated killing observed might reflect an accurate illustration of the level of deletion which could be expected. However, we remained concerned that, the degree of depletion observed might alternatively reflect an impaired capacity of NK-cells resulting from *ex vivo* manipulation and/or impaired functional capacity resulting from the CD56 positive selection purification strategy (personal communication with Anthony Allen, Miltenyi Biotec). Additionally, the limited four-hour assay duration might under-represent effector mediated cytotoxicity through exclusion of the more prolonged mechanisms. Lastly, in consideration of a report describing impaired NK-cell mediated ADCC in combination assays including complement due to steric hindrance resulting from proximity of the C3b and the FcγRIIIa (CD16) receptor epitope on IgG1[247], we elected to assess CDC and ADCC efficacy independently in subsequent assays.

5.7.2. Review of assay duration and effector population

Although ^{51}Cr release assays remain the gold standard for cytotoxicity assays, spontaneous release can restrict the maximum duration for these assays thereby excluding some of the slower effector mechanisms of ADCC[248]. Further, a recent report by Veeramani *et al.*[249], attempting to shed insight on the contentious issue regarding the role of FcγR polymorphisms in rituximab mediated deletion as identified by Cartron *et al.*[250], suggests that the variation in efficacy of ADCC -mediated deletion due to FcγR polymorphisms might result from an experimental artefact whereby FcγR polymorphisms impose a delay in the rate of the ADCC mediated response rather than an impaired capacity to mediated a response, thus implying that extended incubation durations may improve reflective accuracy.

Further, to address the possibility that *ex vivo* manipulation of NK cells may impair functional capacity, we considered an alternative ADCC assay whereby freshly ficolled PBMC's were employed as the source for our effector population again responding against MACS sorted target populations.

Furthermore, in consideration of the absence of *ex vivo* stimulation of the PBMC effectors, we also considered whether a prolonged assay duration might enhance sensitivity, we measured ADCC-mediated efficacy following 2, 4, 8 and 24 hours of co-culture incubation as illustrated by Figure 43a. Results from a single donor at the 2, 4 and 8 hour timepoints appeared to match the 10% level of depletion observed from our preliminary 4 hour ADCC assays, whereas the degree of depletion indicated at the 24 hour timepoint appeared to be in excess of 20%. Buoyed by this result but concerned regarding potential for significant variation resulting from application of freshly ficolled PBMC's as effectors, we performed a final optimisation experiment comparing efficacy of PBMC effectors against *ex vivo* expanded NK cells, assessing ADCC-mediated depletion following 24, 48 and 72 hours of incubation as illustrated by Figure 43b. From this assay, NK-effectors appeared to consistently offer superior depletion compared with PBMC effectors, demonstrating the greatest degree of depletion following 48 hour co-culture. As our ultimate intention was to assess comparative sensitivity for a range of similar constructs, we premised that the optimum assay conditions would be required to ensure effective discrimination between highly similar targets. Therefore, we selected the 48 hour assay duration, employing NK cell effectors to ensure consistency, to assess the comparative sensitivity of ADCC-mediated deletion of our epitope constructs.

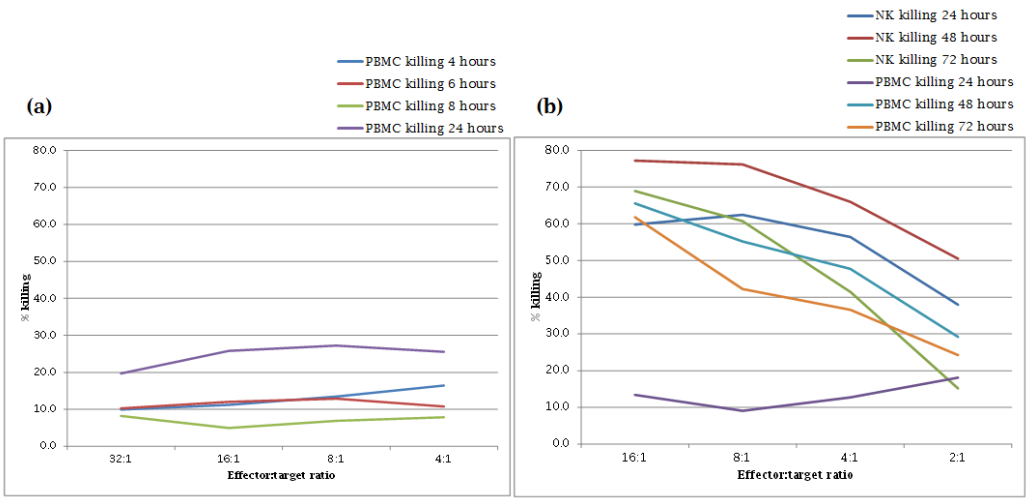

Figure 43 Optimisation of effector population and ADCC assay duration
Primary human PBMCs were transduced with RQR8.I2.eGFP or Q8.I2.eBFP2, with each sample separately purified by CD34 magnetic bead selection (Miltenyi). Subsequently, the RQR8.I2.eGFP and Q8.I2.eBFP2 populations were combined to establish an equal 50:50 assay target suspension. Target populations were then incubated with effector populations at effector:target ratios as indicated, in the presence (query) or absence (control) of rituximab at 100ug/ml. (a) Freshly isolated PBMC's from the same donor as the RQR8.I2.eGFP expressing targets were assessed for their capacity to mediate ADCC at timepoints as indicated. (b) Freshly isolated PBMC's from the same donor as the RQR8.I2.eGFP expressing targets were compared for their capacity to mediate ADCC assessed against *ex vivo* expanded NK cells as an alternative effector population. As illustrated, optimal clarity of ADCC-mediated killing was observed following 48 hours of effector:target co-culture when NK-cells were employed as the effector population.

5.7.3. Effector discrimination

Optimisation assays also identified the further challenge of achieving effective cellular discrimination by flow cytometry, due to autofluorescence noise imposed by the high cellular volume involved. Following unsuccessful attempts to identify the NK-cell effector population and thereby enable gating exclusion through anti-CD56 antibody staining, we next considered a strategy whereby we marked the effector population using a membrane staining dye. For this purpose, we employed the CellTRACE violet dye to mark the NK-cell effector population. Even following 48 hour co-culture, the intensity of the CellTRACE stain remained sufficient to clearly identify and exclude the NK cell effectors, without any notably observation of fluorescent-bleed between cellular populations, thereby facilitating clear exclusion of the majority effector fraction to facilitate clear focus on the target population of interest.

5.7.4. ADCC optimisation summary

Following ADCC assay optimisation, we successfully established a protocol whereby we could generate sufficient populations of both NK-cell effectors and transgenic targets from a single peripheral blood draw of 60ml, enabling assay initiation 8 days following PBMC isolation and allowing for both flow-cytometry based sensitivity and specificity assessments consistent with previous CDC assays. Both ADCC assays required confirmation of successful progression at multiple checkpoints prior to assay initiation; these are reflected by Figure 44 which illustrates an assay flowchart to highlight commonality and procedural divergence between the assays.

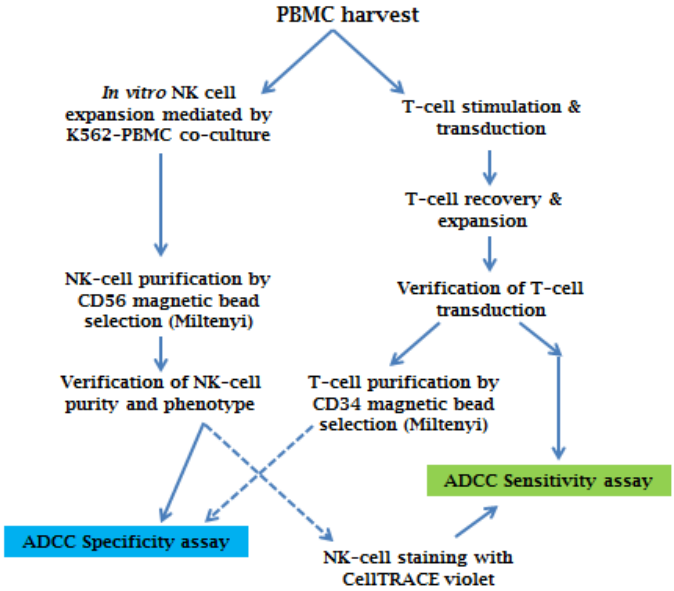

Figure 44 ADCC assay protocol flowchart
CDC and ADCC represent the two primary mechanisms of effector mediated deletion available for the RQR8 construct. As with CDC-mediated deletion previously, separate protocols were established to assess both sensitivity (2.2.5.7.3, p101) and specificity (2.2.5.7.4, p101) of ADCC mediated deletion. Briefly: human PBMCs were separated into two populations and expanded *ex vivo* to establish both target and effector populations. Successful NK cell expansion and T-cell transduction of all constructs under interrogation were defined as essential criteria prior to assay progression. For all ADCC assays, NK cells were CD56 magnetic bead selected the day prior to ADCC assay set-up with selection confirmed by flow cytometry. To enable exclusion of the NK-cell effector population in sensitivity assays, NK-cells were labelled with CellTRACE violet according to manufacturer's instructions (Invitrogen). For specificity assays, a heterogenous target population was employed including an eBFP2 marked control leaving NK cells remaining unstained.

5.8. Sensitivity ADCC assays

Experimental aim: To stratify the sensitivity of alternative rituximab-epitope expression constructs to *in vitro* ADCC-mediated deletion.

Note regarding experimental variation: Following a parallel research tangent considering the generalizability for cell-surface epitope expression discussed further in Chapter eleven, we had concurrently generated a GPI-anchored RQR-motif expression construct at the point when we had completed ADCC assay optimisation. As we had previously established that the QR8 target was inferior to RQ8, and faced with a limited population of NK-cell effectors, we elected to replace the QR8 target with RQR-GPI in ADCC assays.

As illustrated by Figure 44, the ADCC sensitivity protocol required identification of effective progression at several checkpoints prior to assay initiation, including: validation of sufficient NK-cell expansion, successful CD56 selection, confirmation of effector phenotype and effective CellTRACE labelling concurrent with successful transduction of all target populations; all derived from the same donor to exclude 'missing-self' activation. Transduction verification of target populations was assessed by antibody staining to ensure approximately equivalent transduction efficiencies were achieved and to enable comparative binding efficacy for the various targets for the respective antibodies, as illustrated by Figure 45. Similarly, NK cell effector populations were verified by antibody staining to ensure the effector profile remained consistent between donors.

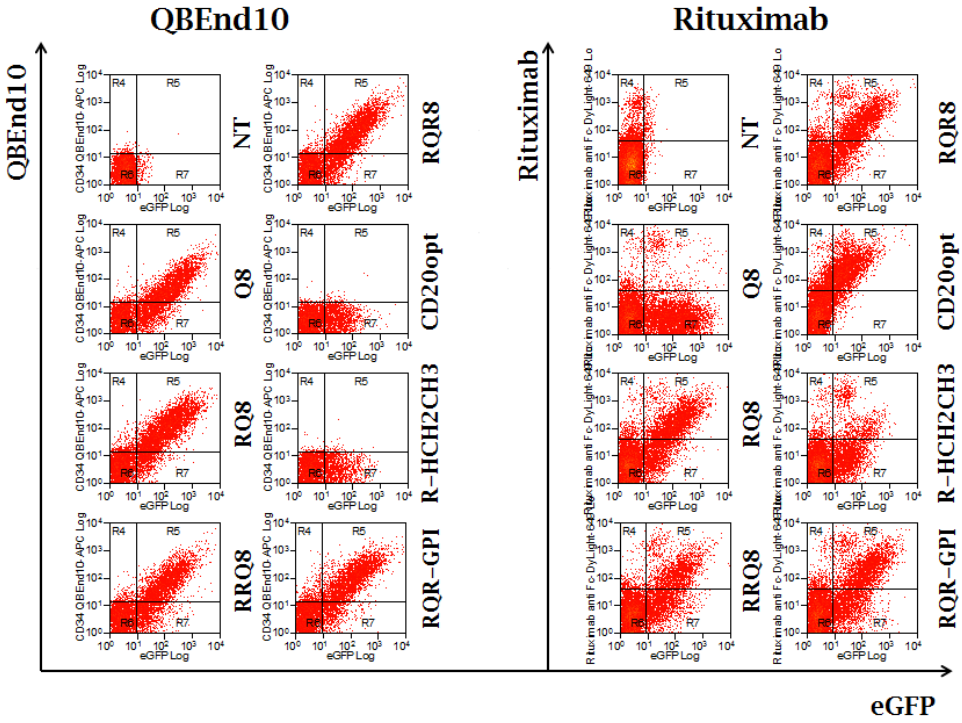

Figure 45 Comparative analysis of transduction efficiency
Primary human PBMCs were transduced with epitope constructs under consideration. Prior to progression with ADCC assay modelling, transduction verification was assessed by flow cytometry of QBEnd10 or rituximab antibody stained transgenic samples to confirm successful transduction and to ensure approximately equivalent levels of transduction were achieved for all constructs. Staining as illustrated reflects a typical transduction result from three separate experiments derived from separate donors.

Transduced, but unsorted target populations were assessed for their sensitivity to ADCC mediated deletion through a range of effector:target ratios (16:1, 8:1, 4:1 and 2:1) with killing efficacy compared against a control sample containing 8:1 ratio of NK cell effectors in the absence of rituximab. ADCC sensitivity assay results displaying the 8:1 effector:target ratio from three separate donors are illustrated by Figure 47. From sensitivity ADCC assays, RQR8 demonstrated superior sensitivity to ADCC-mediated deletion proving even more sensitive than the codon optimised CD20 positive control. Notably, as indicated by the comparative antibody binding efficacy inset within Figure 47, excluding the CD20 positive control, rituximab binding capacity for the various constructs appears to correspond with the level of ADCC mediated depletion achieved. Typical histogram profiles illustrating ADCC-mediated depletion are illustrated by Figure 46.

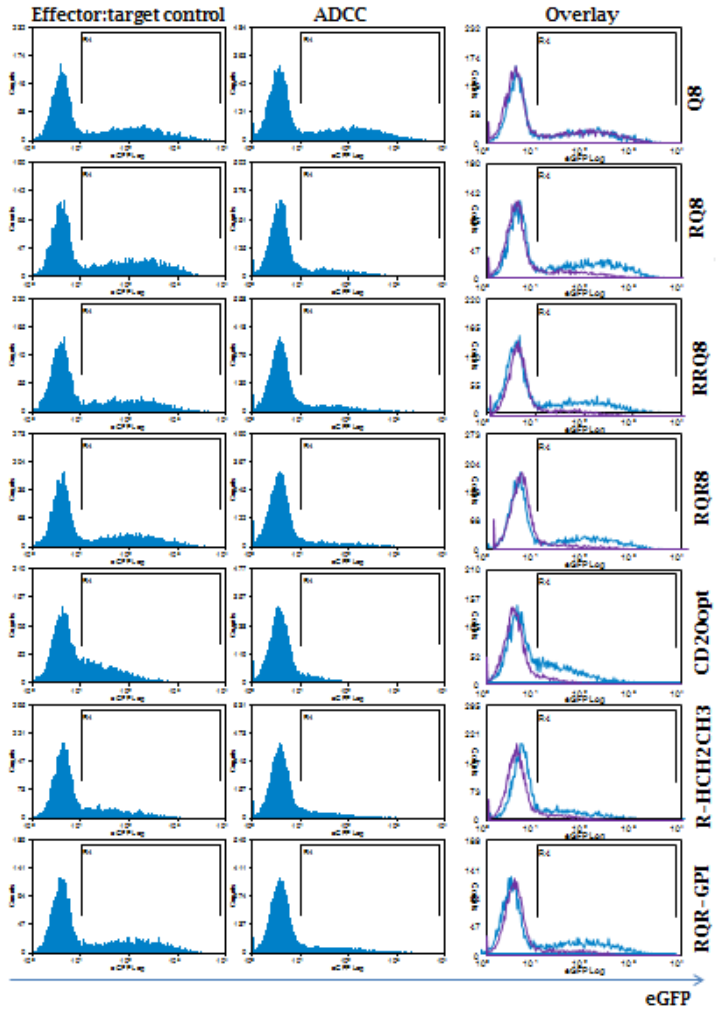

Figure 46 Typical ADCC sensitivity assay depletion
Primary human PBMCs were transduced with epitope constructs under consideration and assessed for sensitivity to ADCC-mediated deletion mediated by NK cells through *in vitro* assays. Assessment of depletion achieved was identified through the residual eGFP-expressing population. Results from a typical donor are illustrated with results from 3 separate donors summarised in Figure 47.

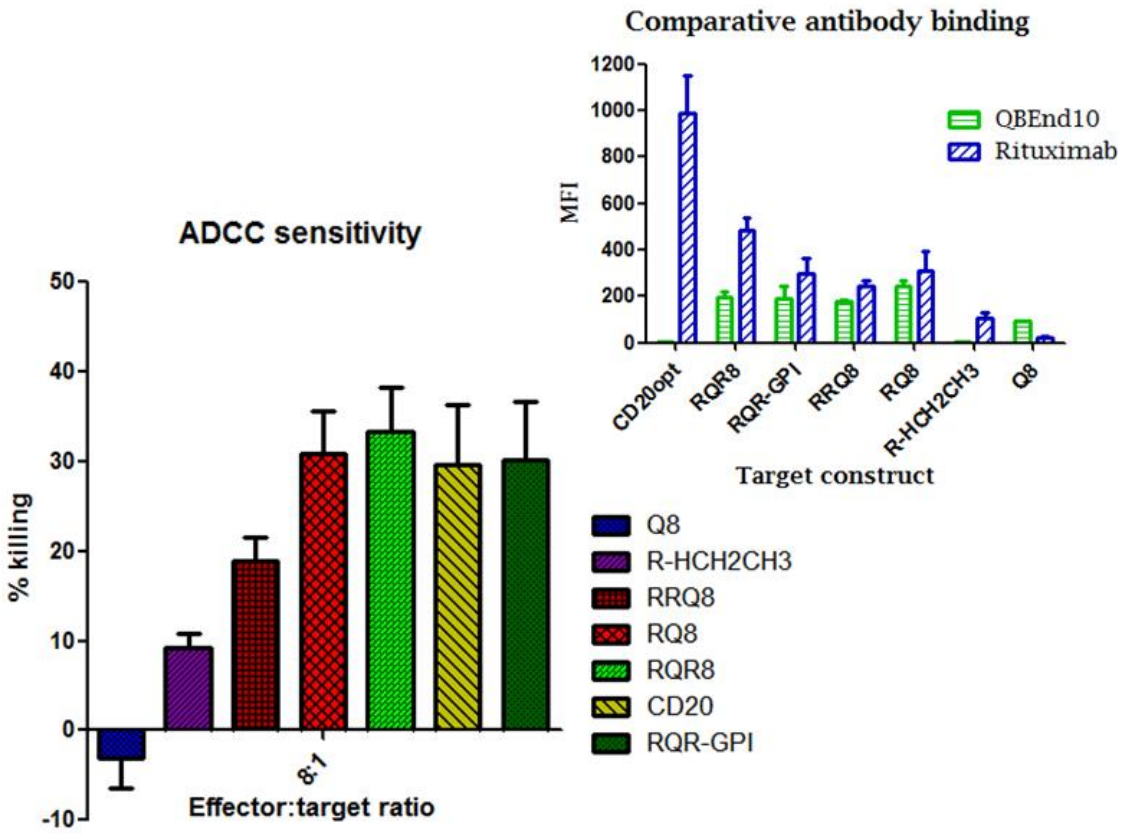

Figure 47 ADCC–mediated deletion sensitivity comparison
Primary human PBMCs were transduced with epitope constructs under consideration and assessed for their sensitivity to ADCC-mediated deletion mediated by NK cells as assessed through in vitro assays. Excluding the CD20 positive control, comparative antibody binding results for the various targets (inset), appear to approximately correlate with the level of deletion which was achieved. Results illustrate comparative sensitivity from three separate donors. Error bars reflect standard error of the mean

5.9. Specificity ADCC assays

Experimental aim: To demonstrate that when challenged with a heterogenous target population, ADCC-mediated deletion remains specific to the rituximab-epitope expressing fraction.

Having assessed the comparative sensitivities for the various epitope constructs, next we investigated the specificity of ADCC mediated depletion. As cellular therapies which require suicide gene protection would be purified prior to infusion, we aimed to obtain an indication for the level of depletion which might be anticipated against putative RQR8 expressing cellular product. Specificity of ADCC mediated depletion was assessed by incubation of NK-cell effectors against an equally mixed composite target population composed of MACS selected RQR8.I2.eGFP and Q8.I2.eBFP2 transgenic targets. Similar with

CDC assays previously, ADCC-mediated depletion was demonstrated to be acutely specific against the target population, with selection appearing to approximately double the sensitivity of RQR8 expressing targets to ADCC mediated deletion as compared with efficacy against unselected targets. ADCC specificity results are indicated by Figure 48.

Finally, in consideration of the minimal size of the RQR-GPI construct which had demonstrated similar efficacy as the RQ8 construct in sensitivity ADCC assays, we compared the efficacy of RQR8 compared against RQR-GPI in a specificity ADCC assay. Despite the identical epitope, variant only in the format of the molecular spacer, experimental results as illustrated by Figure 48b, appear to suggest increased sensitivity of the RQR-GPI expressing target to ADCC-mediated deletion when compared against RQR8. However, as demonstrated by PNH, a simple mutation facilitating deletion of GPI anchor expression represents an untenable risk for escape, thereby excluding RQR-GPI as a serious option for a putative suicide gene construct. Hence this data only reflects the result from a single donor with further investigation into this anomaly deemed beyond the scope of this project.

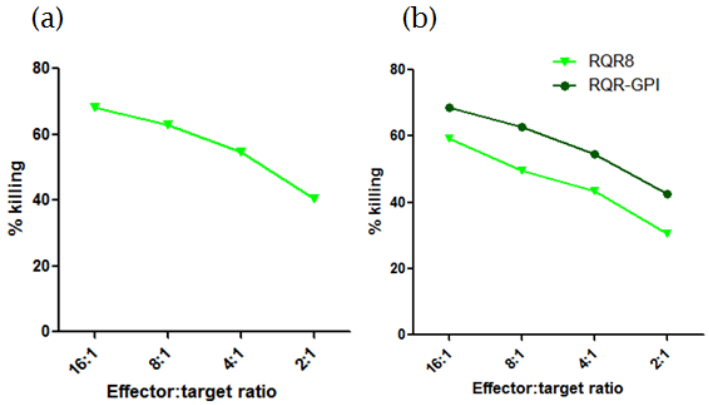

Figure 48 ADCC specificity assay illustration
(a) Primary human PBMCs were transduced with either RQR8.I2.eGFP or Q8.I2.eBFP2 and were CD34 magnetic bead selected prior to ADCC assay incubation. Following selection, purified cells were combined to establish an approximately 50:50 mixture of control and assay targets. Results illustrate average ADCC-mediated deletion from 2 separate donors. (b) Primary human PBMCs were transduced with RQR8.I2.eGFP or the RQR-GPI.I2.eGFP assay targets, as well as the Q8.I2.eBFP2 control target. Following transduction, cells were CD34 magnetic bead selected, then combined to establish target mixtures prior to ADCC assay incubation. Results illustrate ADCC-mediated deletion from a single donor.

Finally, although the RQR-GPI construct was engineered following completion of the CDC sensitivity assays it was examined within **Error! Reference source**

not found., addressing the sensitivity of epitope constructs to the alternative mechanism of effector mediated deletion, namely ADCC.

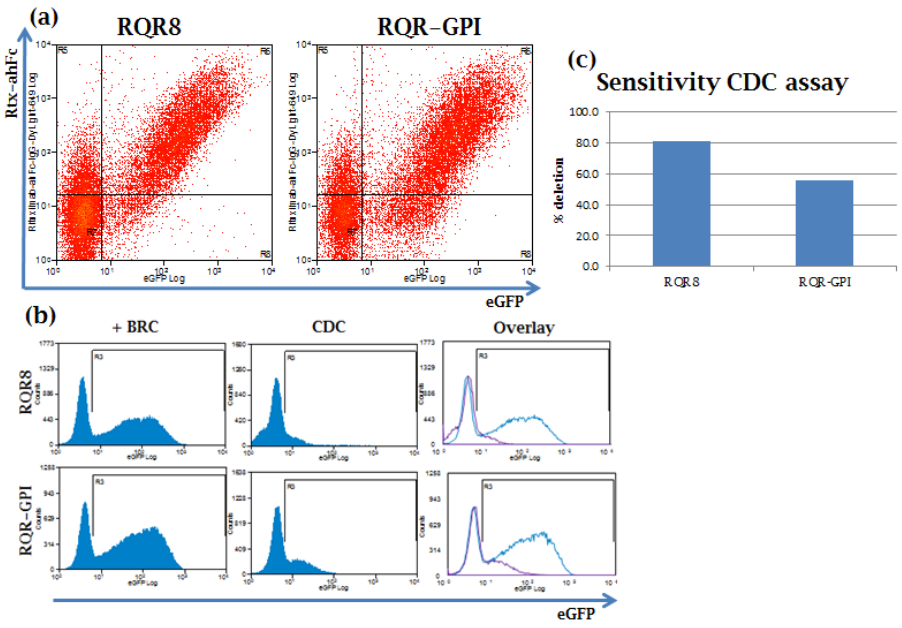

Figure 49 CDC mediated deletion comparison between RQR8 and RQR-GPI
Primary human PBMCs were transduced with either RQR8.I2.eGFP or RQR-GPI.I2.eGFP and assessed for efficacy of CDC-mediated deletion through a CDC sensitivity assay as described (2.2.5.6.2, p100). Results from a single experiment are illustrated.

5.10. Conclusions

Despite clear improvement in facilitating ectopic cell-surface expression of the CD20 antigen, codon optimisation of CD20 appears to have only conferred a modest increase in the expression level of the co-expressed fluorescent marker protein. In this endeavour, our aim was to boost expression of the eGFP marker to enable better clarification of the level of deletion achieved for the CD20 positive control population. However despite our efforts, there remains a degree of overlap between the non-transduced and the transduced populations for the positive control target which remains typically less pronounced for our epitope expressing target populations. Thus, potential over-representation of the sensitivity of the CD20 positive control may result with under-estimation of the comparative killing efficacy of our rituximab binding targets through *in vitro* killing assays.

Recapitulating work by Imai *et al.*[225], following generation of a modified K562 stimulator line, we have successfully demonstrated *in vitro* amplification of NK-cells sufficient to enable ADCC assay modelling experiments. From our

results, we have established a 7-day protocol whereby PBMC:K562.A5 co-culture maintained with 40iu IL2 and maintained with partial media changes as required, can generate approximately 0.5-1.0 x 10^6 NK cells for each 1.0 x 10^6 PBMCs included in the initial co-culture. NK-cells can be successfully purified using CD56 magnetic bead selection to establish a consistent and purified effector population for *in vitro* ADCC assays.

Observations of attenuated deletion of transgenic epitope expressing targets through *in vitro* ADCC assays as compared with efficacy observed from CDC assays led us to interrogate our choice of an effector population for *in vitro* ADCC assays. Following optimisation comparing NK cells versus freshly isolated PBMCs as the effector population alongside assay duration, identified an *in vitro* ADCC assay protocol employing NK cell effectors and 48 hour assay duration to be highly effective for discrimination of sensitivity to ADCC mediated deletion between similar target populations.

Following assessment of the comparative sensitivity of our epitope constructs in transgenic PBMCs, we have demonstrated that ADCC-mediated depletion of RQR8 appears at least equivalent, if not more sensitive than what was observed for the full-length CD20 expressing positive control. Further, results from specificity assays suggest that cellular selection, as would be required to establish therapeutic product, enhances sensitivity of RQR8 expressing targets to ADCC-mediated deletion, whilst highlighting that deletion remains acutely specific to the target population. As demonstrated in Chapter four, RQR8 demonstrates superior sensitivity to CDC-mediated deletion potentially resulting from bivalent binding of rituximab which could resolve the density dependent limitation of CDC against monovalent epitope expressing constructs. Fortuitously this pattern of enhanced sensitivity of RQR8 also appears to extend to ADCC-mediated deletion, which might reflect increased FcγR cross-linking due to greater clustering of rituximab molecules. At face value, our data might be construed to suggest that CDC plays a primary role in the cellular deletion mediated by RQR8. However efficacy of CDC is likely over-represented by our choice of BRC as the source of complement, thus further consideration into the roles of the separate effector mechanisms will be revisited in Chapter nine and Chapter ten, which investigate rituximab deletion through *in vivo* modelling.

Despite extensive similarity between epitope constructs, RQ8 appears more sensitive to ADCC-mediated deletion whereas RRQ8 appears more sensitive to CDC, highlighting a target-dependent variation in the sensitivity to effector mediated deletion as illustrated by Figure 50. Although the RQR-GPI construct was excluded from the CDC assay datasets due to delayed construction, we did assess efficacy of CDC-mediated deletion of this construct from a single donor as illustrated by Figure 48. In light of the variation in efficacy of deletion between RQ8 and RRQ8 when comparing CDC versus ADCC assays, it is interesting to observe a similar discrepancy between RQR-GPI and RQR8, illustrated by Figure 49 and Figure 50. Although these results are intriguing regarding suggestions for role of the antigenic target in facilitating sensitivity to antibody mediated deletion, further examination of this tangent remains beyond this project.

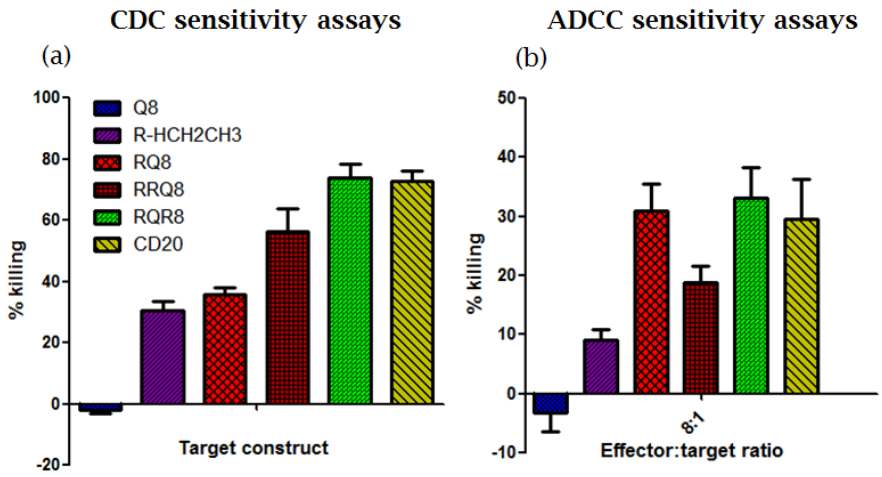

Figure 50 Variation between sensitivity to CDC or ADCC mediated deletion
Due to variation between constructs examined for sensitivity to CDC and ADCC mediated deletion, this figure only reflects constructs which offer comparative data.
(From CDC sensitivity data, illustrated by Figure 21, (p130) and ADCC sensitivity illustrated by Figure 47, p174), this figure highlights the level of deletion achieved for epitope constructs which were assessed through both CDC and ADCC assays. These results appear to indicate that stratification of epitope sensitivity to CDC or ADCC-mediated deletion is not uniform with some constructs demonstrating enhanced sensitivity to CDC mediated deletion (eg.RRQ8) whilst others appear to mediate enhanced sensitivity to ADCC-mediated deletion (eg.RQ8).

5.11. General conclusions

- Codon optimised CD20 enhances transgene and eGFP marker gene expression demonstrating a more effective positive control for *in vitro* ADCC assay modelling

- The K562.A5 clone demonstrates good expression of both IL15 and 4-1BBL antigens as assessed through antibody binding MFI by flow cytometry
- Co-culture of PBMC's with the K562.A5 cell line in a 1:1 ratio result in profound NK cell expansion following 7 days of culture
- Following CD56 selection, *in vitro* expanded NK cells demonstrate an effector $CD56^{dim}/CD16^{+}$ phenotype
- We have demonstrated that RQR8 expression renders transgenic PBMCs sensitive to ADCC-mediated deletion in the presence of rituximab and an appropriate effector population.
- This sensitivity is specific to RQR8 expressing targets and appears to be enhanced when a Miltenyi selected population of targets is considered.
- Indication of potential variation in the sensitivity of the similar RQR-GPI construct with respect to CDC versus ADCC mediated deletion highlights a curious observation suggesting the presentation motif of an epitope target may affect the sensitivity of this target to effector-mediated deletion.

Chapter six

6. Modular capacity of RQR8 for T–cell engineering

As illustrated by Figure 1, successful clinical application of adoptive cellular therapies has resulted in an ever-expanding array of potential functional modifications for T-cell engineering. Therefore, apart from haploidentical HSCT, inclusion of a suicide gene may largely represent an additional feature alongside a primary functional modification such as a re-targeting moiety. Thus it is essential that we demonstrate the capacity for RQR8 to retain functional efficacy when co-expressed alongside common T-cell engineering components.

6.1. Aims

- To demonstrate the modular capacity of RQR8 to enable co-expression alongside common T-cell engineering components
- To demonstrate functional retention of all separate components when RQR8 is co-expressed with the GD2-CAR as verified by:
    - Miltenyi CD34 magnetic bead selection (QBEnd10 epitope)
    - *In vitro* deletion defined by CDC-assay (Rituximab epitope)
    - Cytotoxicity against GD2 expressing cellular targets (GD2-CAR)
- To demonstrate that following CDC-mediated deletion, the cytotoxic capacity of the effector population returns to non-transduced effector baseline activity as assessed by ^{51}Cr release assays

6.2. Introduction

T-cell engineering offers the opportunity to engender T-cells with additional and/or novel functional capabilities, such as: molecular re-targeting mediated by inclusion of a TCR or a CAR moiety, drug resistance capability such as calcineurin or mycophenolate resistance, ability to secrete cytokines to enhance a desired immune response, enhanced proliferative capacity and/or survival, and obviously inclusion of marker genes for identification and suicide genes for resolution of therapeutic toxicity.

However each modification presents novels risks; each TAA target presents opportunity for unforeseen OTOT, signalling modifications designed to overcome toxic tumour microenvironments present risk for unpredicted

metabolic perturbations, whilst insertional mutagenesis implicit with integrating genetic engineering modalities, imposes risk for potential leukaemagenesis, which although yet to be observed from T-cell cancer immunotherapy, nevertheless remains a hypothetical possibility.

Further, as toxicity assessments based on *in silico* and animal modelling are of limited predictive value, risk can never be fully excluded. Thus inclusion of a marker-suicide gene moiety within a transgenic cassette represents a functional mechanism or molecular safety switch to enable opportunity to resolve adverse events which might arise *in vivo*. Thus, following from our previous work, we wanted to demonstrate the modular capacity of RQR8 to function alongside other T-cell engineering components. As the two primary strategies for T-cell retargeting involve genetic modification of T-cells to include either a CAR or a TCR moiety, we decided to demonstrate effective co-expression of RQR8 separately with both a TCR and a CAR. Subsequently, using *in vitro* assays we examined the functional capacity for the separate modular components using a RQR8.2A.CAR construct re-targeted against the GD2 ganglioside.

6.3. Results: Generation of RQR8–CAR/TCR co–expression constructs

Experimental aim: To generate a molecular expression cassette to facilitate functional co-expression of RQR8 alongside either a chimeric antigen receptor or an engineered T-cell receptor.

To illustrate the capacity of RQR8 to function alongside T-cell engineering components, it was necessary to establish appropriate expression vectors to facilitate experimentation. For this purpose, we used the Wilms tumour antigen-1 (WT1) TCR and the anti-GD2 ganglioside CAR.

WT1 is an attractive target for cancer immunotherapy due to upregulation of the WT1 transcription factor identified as a TAA in haematological malignancies including AML, CML and myelodysplastic syndromes as well as solid tumours including breast, colon and ovarian cancers. Previous work by the Hans Stauss lab have identified a high avidity TCR specific for the WT1 derived peptide pWT126 when presented in the context of HLA-A2[251]. As a safety feature to preclude mis-pairing with the native TCR, murine sequences

were exchanged for the human constant domain[252]. The WT1-TCR expression vector template was a kind gift from Prof. Hans Stauss.

Selection of the GD2-CAR was a natural choice for co-expression assays due to previous research by Dr. Martin Pulé[5]. The GD2-CAR targets the GD2 ganglioside which is the most common antigen expressed in neuroblastoma. Neuroblastoma is the most common extracranial solid tumour, emanating from sympathetic nerve cells derived from the neural crest. Neuroblastoma is a widely heterogenous disease, but one which can demonstrate a highly therapy-resistant aggressive phenotype highlighting a need for alternative therapeutic strategies such as ACT[253]. Template for the GD2-CAR construct was derived from a second generation anti-GD2 CAR previously generated by Dr. Martin Pulé, containing CD28 and CD3ζ signalling domains.

To establish our expression vectors, our first step was to identify an appropriate modular bicistronic vector format to generate functional co-expression constructs. To achieve functional co-expression, we premised that it would be necessary to employ the TaV-2A sequence to establish equimolar co-expression of the transgene rather than employing an IRES-based strategy which results with increased expression levels from the primary cistron, potentially imposing either attenuated retargeting moiety expression or risk from cellular escape dependent upon transgene orientation. Further, use of the self-cleaving TaV-2A sequence results with addition of a residual 19a.a. suffix to the primary cistron and a single proline prefix added to the secondary cistron. Premising that the residual suffix might impair functional activity of the signalling domains if the CAR or TCR sequences were located upstream of the TaV-2A sequence, our molecular design located the RQR8 sequence upstream of the CAR or TCR domains separated by the TaV-2A sequence. Further, to assist facile generation of subsequent constructs, we opted for a modular cloning design whereby an NcoI site was localised at the terminal junction of the TaV-2A sequence and the primary methionine of the secondary transgene to allow subsequent CAR/TCR constructs to be subcloned as NcoI-MluI fragments in keeping with previous work from our lab. Lastly, as longer transcripts impose additional burden onto the transcriptional machinery, impacting on both viral titre and transgene expression[119], we premised inclusion of a S/MAR domain might be required to ensure stable sustained

transgene expression due to the longer transcript length of the CAR/TCR domains. Functional benefit of inclusion of a S/MAR domain within a vector is described in further detail in Appendix 1 (13.3.3, p315). However, briefly it has been observed that transgene expression in retrovirally transduced T-cells is decreased in mitotically quiescent cells. However, this effect can be offset by orientation specific incorporation of the human beta inteferon S/MAR region into Moloney murine leukaemia virus based vectors which has been demonstrated to improve transgene expression in primary human T-cells[254]. Having established appropriate vector backbones with or without the human beta-interferon S/MAR domain in reverse orientation, located 3' of the transgenic coding sequence and upstream of the 3' terminal LTR, subsequent CAR/TCR amplicons were subcloned as NcoI-MluI fragments into suitably digested vectors, with final sequence integrity confirmed by DNA sequencing.

Further, as this work coincided with ongoing preparations toward a pending clinical trial, a derivative construct based on the GD2-CAR described above was also established. A common molecular feature of CARs is the molecular spacer domain separating the scFv binding region from the transmembrane domain and which has been shown necessary to achieve stable and functional CAR expression for a number of CAR constructs. Although the dimeric IgG1 derived CH2-CH3 molecular spacer commonly employed in CAR constructs was premised to be minimally immunogenic due to the human derivation, it was reported that undesired FcγR binding of the IgG-Fc domain could result in bi-directional activation whereby T-cells become activated against innate effector targets independent of CAR-target antigen recognition. Correspondingly, the reverse innate immune response against transgenic T-cells was also observed resulting in cytolysis and cytokine secretion of pro-inflammatory cytokines[255]. Responding to this report and in preparation for a pending neuroblastoma clinical trial resulted with the generation of a CAR spacer domain variant designed to minimise FcγR recognition whilst retaining CAR expression and functionality; henceforth indicated by the ‘pvaa’ suffix noted on modified GD2-CAR constructs. Cloning of the GD2-CAR pvaa variant was performed by Alicia Kopec, with functional validation of the resolution of toxicity performed by Eva Kokalaki. The GD2-CAR pvaa variant vector backbone included a S/MAR domain for improved transgene expression.

Initial expression assays illustrated by Figure 51 reflect the initial constructs whilst all subsequent work involving co-expression of RQR8 with the GD2-CAR employed the aGD2-pvaa derivative CAR construct.

6.4. Co–expression assays

Experimental aim: To demonstrate cell-surface co-expression of RQR8 alongside either a chimeric antigen receptor or a T-cell receptor.

The first experimental question to be addressed was to confirm whether we could achieve effective co-expression of both RQR8 and the CAR/TCR moieties from our bicistronic vectors. Secondly, would the additional burden and therefore potential reduction in viral titre due to inclusion of the S/MAR domain in the vector, be sufficiently offset by increased transgene expression? In this experiment, we transduced primary PBMCs with supernatants generated for the separate constructs and assessed CAR/TCR expression compared against QBEnd10 staining. The IgG1-Fc molecular spacer for the GD2-CAR enabled simple indirect detection achieved by anti-human IgG antibody staining. However, as the TCR recognises specific MHC-peptide complexes, a more specific reagent was required to assess expression of the WT1 construct. MHC-multimers are reagents composed of multiple MHC-peptide complexes. Resulting from the capacity to bind to multiples TCR's on a single cell thereby amplifying the signal, MHC-multimers achieve a more stable binding than monomeric equivalents. To assess WT1 expression, fluorescence staining was achieved using a custom labelled MHC-WT1 peptide dextramer produced by Pro-immune and generously supplied by Prof. Hans Stauss. As illustrated by Figure 51, RQR8 co-expression with the GD2-CAR resulted in identification of a clear double positive population from both samples. Although the result remains less-clear for the WT1-TCR transgenic PBMCs, there was also evidence of WT1-dextramer staining for both samples. Further, from parallel transductions in PBMCs demonstrating similar levels of transduction efficiency, a modest but apparent increase in transgene expression appeared to be observed for both S/MAR containing constructs matching with previous work from our group.

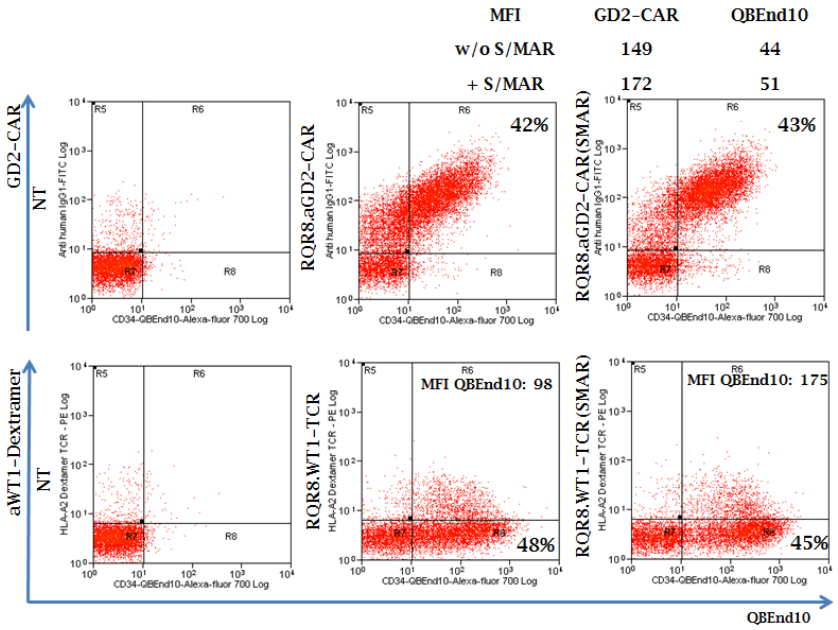

Figure 51 Co-expression of RQR8 with the GD2-CAR or WT1-TCR
Primary human PBMCs were transduced with RQR8 co-expressed with either the GD2-CAR or the WT1-TCR, with equimolar expression facilitated by the TaV 2A sequence, with or without the presence of a S/MAR domain within the vector. The left-hand column illustrates the non-transduced staining control; the middle and right-hand columns illustrate staining without and with the inclusion of a S/MAR domain illustrating the enhanced expression afforded by inclusion of the S/MAR domain. Data illustrated represent a typical result from three experiments. MFI – mean fluorescence intensity.

6.5. Demonstration of MACS sorting (retention of QBEnd10 binding)

Experimental aim: To demonstrate that when co-expressed with a CAR or TCR, the cell-surface expression level of RQR8 remains sufficient to facilitate CD34 magnetic bead selection.

The remaining work in this chapter employed the RQR8.2A.aGD2-pvaa derivative CAR construct. As this vector contains three separate functional components, functional validation required serial examination of all three separate functional capacities: marker gene, suicide gene and the aGD2-CAR, in the relevant sequential order: selection, deletion and cytotoxicity. As illustrated by Figure 52, a clear double positive population can be observed following a single round of transduction in primary PBMCs. Following magnetic bead selection, RQR8^{+} purity >98% could be consistently achieved. Results shown reflect a typical result from a single donor.

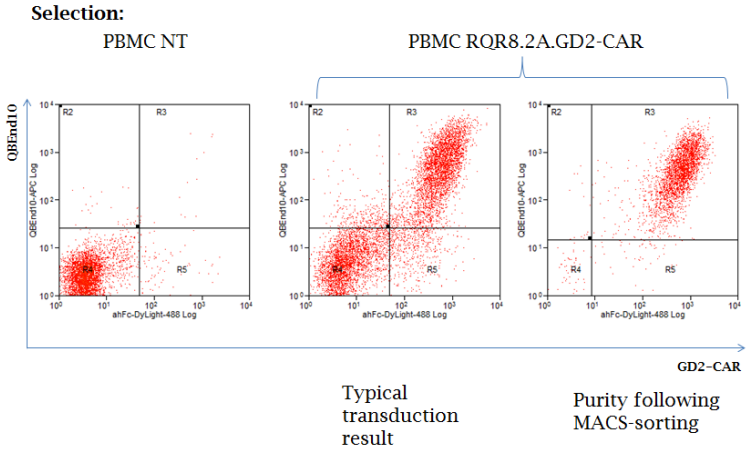

Figure 52 Demonstration of MACS selection of RQR8.2A.GD2–CAR PBMCs
Primary human PBMCs were transduced with SFGmR.RQR8.2A.GD2-CAR. Transduced cells were purified by CD34 magnetic bead selection (Miltenyi), with the resulting cell product assessed for purity as compared against a residual fraction of the unsorted population. As illustrated, following a single round of cell selection, greater than 95% purity is achieved. Data as illustrated reflects a typical result from 7 separate experiments.

6.6. Demonstration of CDC deletion (retention of rituximab binding)

Experimental aim: To demonstrate that when co-expressed with a CAR or TCR, the cell-surface expression level of RQR8 remains sufficient to facilitate rituximab-mediated CDC.

CDC assays were performed in preparation for ^{51}Cr release assay, whereby we sought to demonstrate both retention of specific cytotoxic potential from CAR^{+} PBMCs as well as ablation of cytolytic toxicity following targeted complement mediated deletion. Thus, following purification, samples were combined with non-transduced PBMCs derived from the same donor in a 50:50 ratio to ensure presence of a residual population of cells remaining following CDC-mediated depletion of the sample which would then be used to establish the effector population for subsequent cytotoxicity assays. Verification of retention of the capacity for CDC-mediated deletion was performed as previously with the following modifications: CDC assay duration was limited to two hour incubation to reduce potential complement mediated toxicity. Following deletion, cells were recovered into complete RPMI supplemented with 40u IL2 for two days prior to progression with ^{51}Cr release assays. In both cases, samples were incubated with 25% BRC, in the absence (no CDC) or presence (CDC) of rituximab (100µg/ml). As illustrated by Figure 53, clear depletion could be observed from the sample exposed to rituximab in the presence of

BRC, whilst no depletion was observed in the sample exposed to BRC in the absence of rituximab.

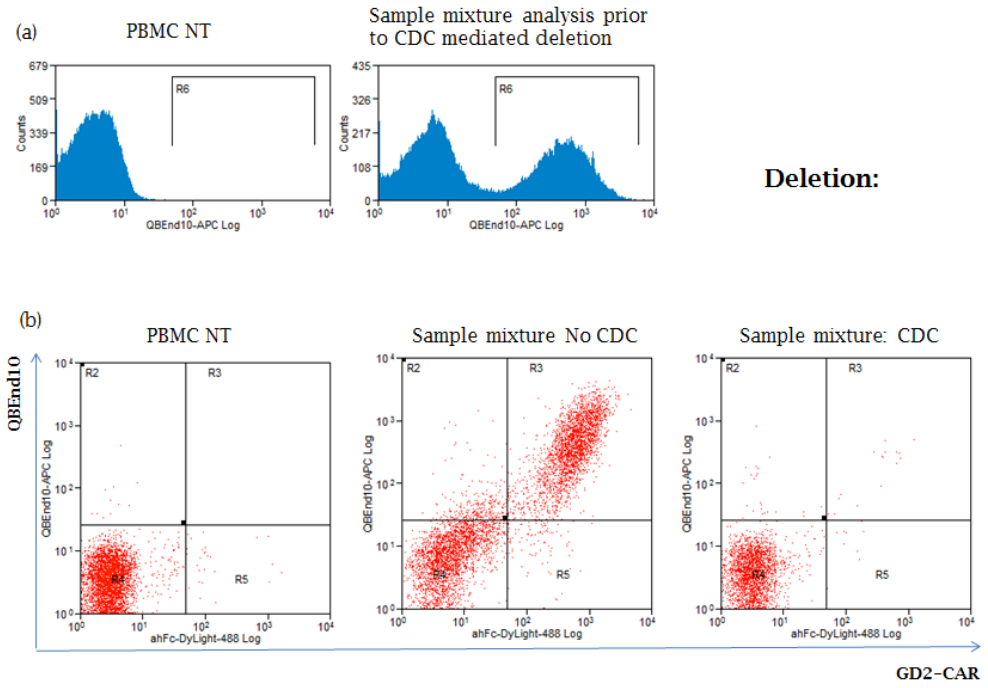

Figure 53 Demonstration of CDC deletion of RQR8/CAR transgenic PBMCs
(a) Primary human PBMCs were transduced with SFGmR.RQR8.2A.GD2-CAR, purified by CD34 magnetic bead selection (Miltenyi), and then combined with non-transduced PBMCs from the same donor in a 50:50 ratio as confirmed by FACS analysis. (b) Sample mixtures were then separated into two fractions and incubated for 2 hours with 25% baby rabbit complement in the absence (no CDC) or presence (CDC) of rituximab (100µg/ml). Data reflects a typical result from 6 replicates from separate donors.

6.7. GD2–CAR ^{51}Cr release assays (retention of CAR function)

Experimental aim: To demonstrate that when co-expressed with RQR8, the GD2-CAR retains functional capacity to mediate target specific cytotoxicity. Further, to demonstrate that the functional potential of RQR8 to serve as a suicide gene enables resolution of the effector potential from a mixed transgenic population when challenged with the CAR defined antigenic target.

Finally we examined the functional capacity of CAR-mediated cellular cytotoxicity. As indicated above, this final stage presented a two-part assay whereby we were attempting to confirm both retention and ablation of CAR-mediated cellular cytotoxicity. Reflecting the potential risk of OTOT posed by retargeting T-cells against TAAs, it remains imperative that induction of the suicide gene machinery would achieve ablation of cellular cytotoxicity. To this end, we employed ^{51}Cr release assays to assess the capacity for cellular

cytotoxicity. Three populations of effectors: non-transduced PBMCs as well as both sample mixtures, illustrated by Figure 53, were incubated for 4 hours with GD2-transgenic SupT1 target cells at three effector target ratios with cytotoxicity assessed by ^{51}Cr release. Results illustrated by Figure 54 reflect cytotoxicity assays from three separate donors, clearly demonstrating a reduction in cytotoxicity from the sample mixture exposed to CDC back to the baseline level established by the non-transduced effector population.

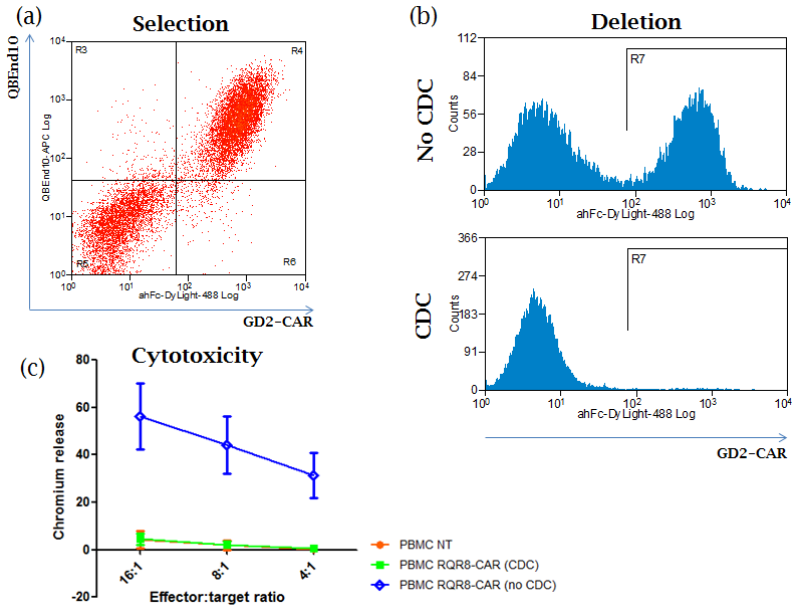

Figure 54 Functional retention of RQR8.2A.GD2–CAR expressing PBMCs
(a) Selection: Primary human PBMCs were transduced with SFGmR.RQR8.2A.GD2-CAR, purified by CD34 magnetic bead selection (Miltenyi), then combined with non-transduced PBMCs from the same donor in a 50:50 ratio as confirmed by FACS analysis. (b) Deletion: Sample mixtures from (a) were separated into two fractions and incubated for 2 hours with 25% baby rabbit complement in the absence (no CDC) or presence (CDC) of rituximab (100µg/ml). (c) Cytotoxicity: Following CDC-mediated deletion, assay fractions from (b) were recovered for 2 days prior to inclusion into chromium release cytotoxicity assays employed as effectors against GD2-transgenic SupT1 target cells at effector:target ratios as indicated. As demonstrated, the RQR8.2A.GD2-CAR cassette enables independent functional capacity of all modular components in transgenic PBMCs. Data reflects typical results from 6 replicates from separate donors.

6.8. Conclusions

Progressive advances in molecular engineering offer increasing potential for modification of T-cell function, extending far beyond simple retargeting. Thus far, our research has focussed on the functional capacity of the marker and suicide moieties. However, there are many potential applications where the marker/suicide capacity may prove secondary to a primary engineering modification. Viewed from this perspective, to validate the potential for RQR8

to act as an effective T-cell engineering cassette, it was essential to demonstrate functional retention of the marker and suicide gene capacities in conjunction with confirmation of the functional capacity for a standard T-cell engineering component such as a CAR or a TCR.

As illustrated by Figure 51, we have demonstrated functional co-expression of the GD2-CAR or the WT1-TCR alongside RQR8, mediated by the TaV-2A sequence and as confirmed by antibody staining for the QBEnd10 marker gene and the retargeting moiety. However, validation of the functional retention for all three components required a multi-stage assay as illustrated by Figure 54. In addition to establishing purity of the cellular product, selection also excludes low expressing cells which results in a more consistent therapeutic product and has been observed to enhance functional capacity[131]. Functional co-expression of RQR8 clearly retains QBEnd10 and rituximab binding capacities enabling both cellular sorting mediated by magnetic bead selection and retention of the capacity for CDC-mediated cellular deletion afforded by rituximab and complement. Crucially, the efficacy of the functional capacity for CAR-transgenic T-cells to mediate cellular cytotoxicity is retained suggesting RQR8 expression does not impede basal T-cell functionality.

6.9. General conclusions

- Modular design of RQR8 enables co-expression alongside common T-cell re-targeting moieties such as CARs or TCRs
- Functional retention of marker gene, suicide gene and CAR components were each separately confirmed through *in vitro* assays using PBMCs transgenic for co-expression constructs
- *In vitro* modelling demonstrates ablation of cytotoxic capacity of re-targeted cells following CDC-mediated deletion

Chapter seven

7. Murine cell culture preparation for *in vivo* modelling

Progression toward *in vivo* modelling required two major modifications to previous research methodologies: alteration of experimental protocols to reflect variation in cellular origin and adjustment of experimental scale to address the increased requirements.

7.1. Aims

- To successfully demonstrate effective and consistent transduction of murine splenocytes
- To confirm that murine splenocytes can effectively express epitope binding constructs
- To demonstrate effective Miltenyi CD34 magnetic bead selection of transduced splenocytes
- To establish and optimise a protocol for effective splenocyte transduction and purification sufficient to enable *in vivo* GvHD modelling experiments

7.2. Introduction

This chapter focuses upon the modification to transduction and tissue culture protocols which were required to enable *in vivo* murine modelling experiments, whilst the following two chapters will present *in vivo* modelling results.

Having successfully demonstrated functional efficacy of RQR8 through carefully controlled *in vitro* assays, the next phase of the project focussed on functional efficacy of RQR8 in more complex biological settings. With a view towards future clinical application we next sought to assess efficacy of RQR8 depletion *in vivo*. As work to this point had utilised human derived cell culture for small scale experiments, it was necessary to revise experimental scale sufficiently to enable effective *in vivo* experimentation using murine models. This experimental tangent raised multiple questions which were addressed in sequence.

7.2.1. Experimental accommodation for splenocyte culture

In contrast with previous chapters, the work in this chapter focussed on establishing protocols designed to enable subsequent research rather than specifically investigating RQR8. Thus, acting as a means to an end many experiments recapitulated previous work but in primary murine T-cells as opposed to human cells with most questions binary in nature; e.g. could we generate RV supernatant which would enable effective and consistent expression of our constructs in murine splenocytes using the SFG vector; would splenocytes demonstrate successful expression of our epitope constructs to enable antibody binding; could we generate sufficient viable transgenic T-cell product through splenocyte culture to enable *in vivo* modelling experiments? Hence, experiments typically progressed in a linear manner as we addressed these questions in sequence; ultimately resulting in generation of a 5-day protocol which offered a minimal timeframe for *ex vivo* manipulation whilst allowing for confirmation of cellular profile and ensuring optimal viability.

Strategies for splenocyte culture and transduction were adapted from the Schumacher, Stauss and Anderson laboratory protocols.

An obvious impact resulting from the alteration in cellular target results from challenges imposed by splenocyte culture. Although Roswell Park Memorial Institute (RPMI) medium is traditionally chosen for splenocyte culture, it was originally optimised for human lymphocyte culture[256]. As there does not appear to have been a similar effort employed to establish an analogous medium for splenocyte culture, it appears that limitations from this choice have been overcome through alternative stimulation strategies and use of supplemental additives, with further discussion restricted to the modifications chosen for this course of experimentation.

The isolation strategy for murine T-cells is in stark contrast with that of primary human T-cells from peripheral blood. Ficoll-Paque extraction offers a facile strategy to exclude erthrocytes and granulocytes from peripheral blood by density gradient centrifugation resulting in a clearly visible buffy coat offering a rich source of lymphocytes alongside a minority population of monocytes[33]. Further, as T-cells typically compose 70-80% of the lymphocyte

fraction from peripheral blood, the sample starts as a highly enriched population[257]. In contrast, to resolve the restriction imposed due to the limited volume of blood available, the spleen is typically extracted as a source of lymphocytes for murine modelling experiments. As a peripheral lymphoid organ, the T-cell proportion of the lymphocyte population from the mouse spleen typically matches that of the B-cell fraction, with both populations present at approximately 30-35%[258]. Further, splenic macerates contain a significant proportion of stromal cells, primarily present to offer signal to sustain lymphocyte populations in the absence of an antigenic signal as well as red blood cells (RBCs) reflecting one of the primary roles of the spleen to cleanse the blood[259].

Key variations between human PBMC activation and splenocyte culture include RBC lysis, a stimulation/re-stimulation protocol, and media supplementation with β-mercaptoethanol.

Traditionally, ammonium chloride potassium (ACK) lysis buffer is employed to selectively deplete RBC's from single cell suspensions through selective osmostic lysis. Intrinsic to their role to facilitate CO_2/O_2 exchange, RBC's possess a membrane Cl/HCO_3 antiporter to facilitate rapid gas transfer[260]. In ACK lysis buffer, the combination of NH_3 and Cl^- ions prove lethal to RBCs by skewing cellular equilibrium. Increased Cl^- uptake results in elevated carbonic anhydrase formation of HCO_3^- ions, imposing a deficit of OH^- ions, regenerated through increased formation of NH_4^+, progressing until osmotic pressure imposes cellular lysis. As RBCs are acutely sensitive to this process, they can be selectively excluded from contaminated cultures using ACK lysis buffer.

For cellular stimulation, we employed the Concanavalin A (ConA)/IL7 stimulation/re-stimulation protocol described in all three laboratory protocols considered at the start of our splenocyte research which we observed offered a consistent and reproducible strategy to facilitate splenocyte stimulation and transduction.

The role of the β-mercaptoethanol (BME) additive in splenocyte culture is premised to enhance membrane transport of cysteine to maintain intracellular glutathione levels required for optimal growth following mitogenic

stimulation, such as Concanavalin A stimulation[261]. β-mercaptoethanol was added to media immediately prior to use, at active concentration of 0.1mM.

Lastly, due to the murine derivation of the QBEnd10 antibody, and the complex composition of tissue samples isolated during *in vivo* modelling experiments, it was necessary to establish a blocking strategy to reduce background signal resulting from Fc-recognition of antibodies by murine FcγR's. For this purpose, we used neat supernatant from the 2.4G2 hybridoma, which binds a non-polymorphic epitope present on murine FcγRII (CD32) and FcγRIII (CD16) receptors, which has been demonstrated to prevent non-specific IgG binding[262].

7.2.2. Retroviral transduction of splenocytes

A cellular viral receptor represents the specific cell surface component which viral glycoproteins bind to, with viral entry into the cell representing the ultimate result following this binding event. However, binding alone does not necessarily mediate virus internalisation. Oligomeric surface domain (SU) glycoproteins are anchored to the viral membrane through transmembrane (TM) domains. Viral binding is proposed to confer a conformational change in the SU protein such that hydrophobic residues within the TM domain become exposed leading to a fusion event between the viral and cellular membranes. Hence, viral envelope glycoproteins define the tropism of the viral particle, and therefore the target range for retroviral vectors can be modified by alteration of the viral envelope through a process known as pseudotyping such that the novel viral particle expresses glycoproteins derived from enveloped viruses separate from the viral strain being packaged. In nature, altered tropism can occur naturally following coincident infection of a cell by separate enveloped viruses leading to formation of phenotypically mixed virions being produced. Observation that HIV-1 virions were able to extend their host range through incorporation of heterologous glycoproteins led to the design of pseudotyped HIV-1 based viral vectors[263]. The first demonstration of this principle involved generation of amphotropic murine leukaemia virus pseudotyped HIV-1 particles produced following transient transfection of COS-7 cells[264]. The most commonly used glycoprotein for pseudotyping viral vectors remains the vesicular virus glycoprotein (VSV-G) due to the broad tropism and relative

stability of this glycoprotein. However duration of viral production is limited by the toxicity of this glycoprotein[263]. The broad tropism of the VSV-G envelope reflects the ubiquitous low density lipoprotein (LDL) receptor or LDL-receptor family members serving as cellular targets for this glycoprotein[265].

Further, additional cell surface components may influence the tropism of viral particles by stabilising virus-receptor interactions thereby facilitating membrane fusion events. Experiments using Tunicamycin, an inhibitor of N-glycosylation, have demonstrated that although the $HATB^{0}$ receptor for the RD114 envelope glycoprotein is present on mouse cells, alternative glycosylation of this receptor abrogates receptor binding. It has also been shown that the efficiency of Eco-mediated infection does not correlate with expression levels of the Eco mCAT1 receptor suggesting that additional cellular interactions are involved in facilitating virion entry[266].

Production of retrovirus requires three separate elements: *gag–pol*, the group-specific antigen and polymerase genes which enable amplification of the LTR-bounded retroviral genome, *env*, the envelope required to package nascent viral particles and the retroviral RNA genome. Common practice for production of retrovirus is achieved through transient transfection. This strategy is designed as a safety feature as the components required for retroviral production are separated in trans orientation thereby reducing the probability for a potential recombination event. However the triple transfection strategy results in significant batch-to-batch variation. One solution to reduce inter-batch variation is achieved through the use of producer lines. Producer lines are stable cell lines modified to express the *gag–pol* and *env* proteins in trans, thereby offering the desired safety profile, with human derived cell lines preferred for producers due to the absence of endogenous murine retroviruses[267]. Thus, production of retrovirus from a stable cell line only requires transfection with a single plasmid expressing the retroviral cassette to be packaged. Producer lines are defined by the envelope protein of a producer line which they constitutively express. Although producer lines exist for both the RD114 and Eco envelopes, the toxicity of the VSV-G envelope precludes constitutive expression of this protein hence inducible expression strategies have been developed to accommodate this limitation when VSV-G envelope tropism is desired.

7.3. Results: Transduction and epitope expression in murine splenocytes

Experimental aim: To demonstrate functional expression of RQR8 in murine splenocytes in preparation toward *in vivo* modelling experiments.

Note regarding variation in splenocyte strain between experiments: the model which we were preparing for was a C57BL/6 to Balb/c allogenic acute GvHD model previously established by the Chakraverty group at the Royal Free hospital, employing CD90.2 congenically marked C57BL/6 mice as the source for donor splenocytes, to be transferred into wild-type CD90.1 Balb/c recipient animals. As the CD90.2 C57BL/6 strain was a limited resource, preparatory experiments were mostly performed using Balb/c splenocytes with CD90.2 C57BL/6 splenocytes used when available and where required.

In our transition from human to murine culture, our first step was to confirm we could generate viral supernatant that would achieve effective transduction of splenocytes. Previous research had employed RD114 pseudotyped supernatant to facilitate retroviral transductions of human PBMC's, using supernatant which had been generated by triple transfection of HEK293T cells. As both the Stauss and Anderson protocols employed ecotropic envelope producer lines for supernatant generation (Phoenix-Eco and LinXE respectively), we used the LinXE producer line[268] for ecotropic supernatant generation. (LinXE cells were a kind gift from John Anderson).

In our initial experiment, we generated Eco enveloped retroviral supernatant for the Q8.I2.eGFP construct to confirm successful transduction of splenocytes. As previously with epitope mapping research, co-expression of the eGFP marker protein was included to confirm identification of transgenic cells to account for the potential scenario whereby splenocytes might be limited in their capacity to successfully express the epitope on the cellular surface. As illustrated by Figure 55, we were able to successfully transduce both CD4 and CD8 T-cells in both Balb/c and C57BL/6 splenocytes, demonstrating effective expression of the Q8 epitope. Notably, following with anecdotal evidence by other researchers from the Royal Free hospital, there was a marked reduction in the transduction efficiency observed for the Balb/c cohort compared with the C57BL/6 cohort. Premising this might reflect a comparatively reduced expression of the mCAT1 receptor on C57BL/6

splenocytes, we compared transduction efficiency of a hybrid supernatant whereby we transfected LinXE producer cells with the VSV-G envelope in addition to the expression vector with a view to producing dual pseudotyped supernatant. However this strategy appeared to reduce the viral titre rather than offering potential benefit. Further, as our experimental aim necessitated cellular purification through MACS sorting subsequent to transduction, we considered that this limitation could be resolved by increasing the scale of splenocyte transduction.

Having demonstrated successful splenocyte transduction and expression of the Q8 epitope, we next sought to similarly confirm successful expression of the RQR8 epitope, illustrated by Figure 55c.

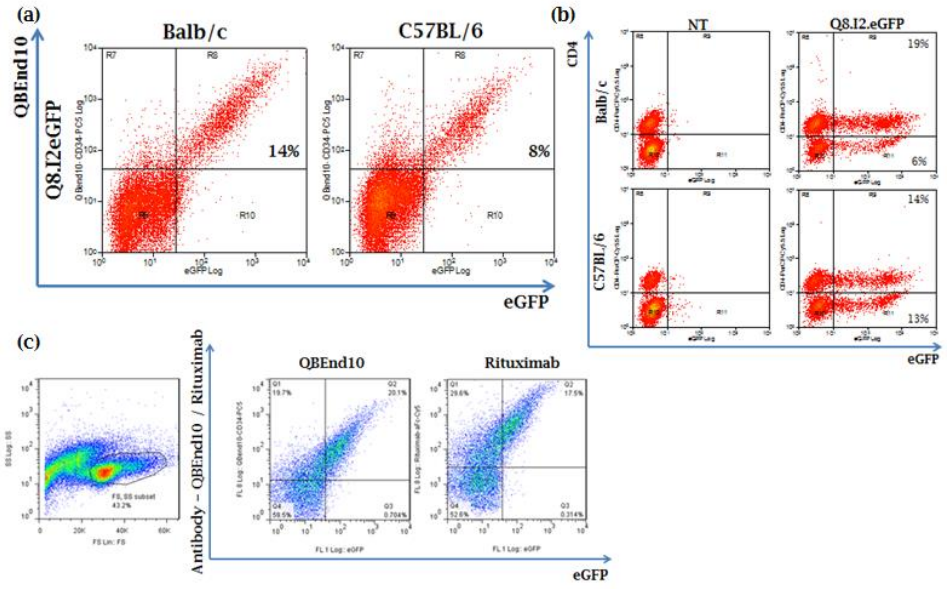

Figure 55 Demonstration of splenocyte transduction and modification
(a) Balb/c and C57BL/6 splenocytes were transduced with Q8.I2.eGFP supernatant with transduction efficiency assessed 48 hours following transduction, 24 hours following cellular recovery. (b) T-cell profile of splenocytes transduced from (a) were examined to confirm successful transduction of both CD4 and CD8 compartments (c) Balb/c splenocytes were transduced with RQR8.I2.eGFP supernatant to confirm transgenic splenocytes retain antibody binding capacity for both QBEnd10 and rituximab binding epitopes. As illustrated, ecotropic supernatant generated from the SFG vector enable effective and functional transduction of RQR8 in CD4 and CD8 Balb/c and C57BL/6 splenocytes. Data reflects a typical result from many experiments.

Having successfully demonstrated supernatant generation, transduction and cell-surface epitope expression, our next experimental question addressed the stability of viral supernatant. Both the Stauss and Anderson laboratory protocols described application of fresh viral supernatant for transduction,

however in light of the experimental scale required, we questioned whether it might be possible to generate and validate batches of viral supernatant in advance, stored at -80°C until required, to reduce the cost imposed by experimental abortions. Lastly, further to research from Chapter seven, we also considered inclusion of a S/MAR domain in our construct with a view to enhancing transgene expression. Figure 56 illustrates the results from these experiments confirming that following a freeze-thaw cycle, both 48 and 72 hour viral supernatant harvests retained infective capacity demonstrating successful transductions of Balb/c splenocytes. Further, we confirmed effective expression of both Q8 and RQR8 epitopes in the presence or absence of a S/MAR domain. Although increased transduction and expression was only apparent for the Q8 construct, as there was no reduction in expression observed with RQR8, the S/MAR containing construct was employed where indicated in subsequent research.

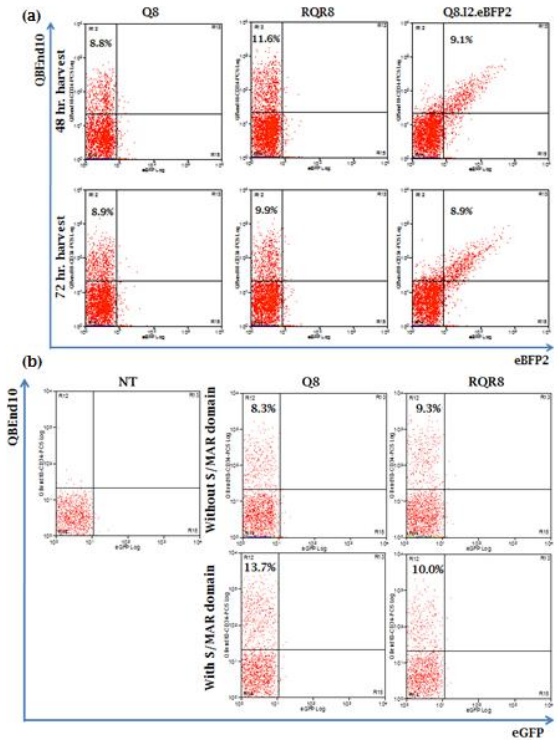

Figure 56 Validation of frozen supernatant
Further Balb/c splenocyte transductions were performed to establish whether ecotropic enveloped supernatant could withstand a freeze-thaw cycle and to validate epitope expression constructs lacking a fluorescent protein marker. (a) Balb/c splenocytes were transduced with Q8, RQR8 and Q8.I2.eBFP2 supernatants snap frozen 48 hours and 72 hours post LinXE transfection to establish ability of Eco-enveloped supernatant to withstand a single freeze-thaw cycle with flow cytometry analysis performed 24 hours following splenocyte recovery. (b) Balb/c splenocytes were transduced with Q8 and RQR8 supernatants from constructs possessing or excluding a S/MAR domain in the retroviral vector construct. Data reflects the

result from a single experiment which assisted development of a protocol employed for subsequent experiments.

7.4. Miltenyi CD34 magnetic bead selection of splenocytes

Experimental aim: To demonstrate retention of CD34 magnetic bead selection of RQR8-transgenic murine splenocytes in preparation toward *in vivo* modelling experiments.

We next sought to demonstrate effective MACS selection of transgenic splenocytes, which represented a critical milestone to enable successful transition to *in vivo* modelling experiments. Illustrated by Figure 57, we observed clear efficacy from MACS selection when performed on a small scale but a reduced efficacy on increase of experimental scale. Further, following MACS selection, we observed a rapid and severe decline in splenocyte viability.

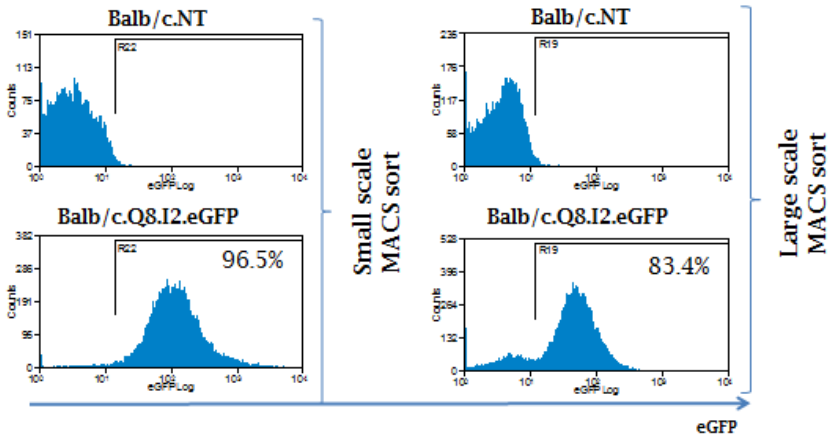

Figure 57 Scale dependent variations in MACS sorting efficacy
Retrospective analysis of flow cytometry results assessing sample purify from separate experiments involving Q8.I2.eGFP transduction and CD34 magnetic bead selection of Balb/c splenocytes demonstrated variation between efficacies of purification dependent upon the scale of the transduction. Left - small scale transduction: 6 wells of a 24 well plate/12-18x10^6 Balb/c splenocytes transduced. Right - large scale transduction: Twelve 24 well plates of splenocytes/48-60x10^6 splenocytes/plate transduced. As illustrated, an increased background of non-transduced splenocytes remaining following magnetic bead purification was observed when selection was performed at a larger scale.

Having observed that the viability of splenocytes maintained in dense culture appeared to be higher than for those maintained in sparse conditions, we premised that the cocktail of cytokines secreted by stromal, myeloid and other populations may be in part responsible for this observation. Further, having observed that fresh RPMI supplemented with IL2 proved insufficient to mediate recovery of fragile splenocytes following MACS selection, we considered splenocyte recovery into the 'conditioned' medium from which

they had been harvested from. Illustrated by Figure 58, we observed a similar comparative viability between the non-transduced control sample and the MACS sorted cells two hours following selection, but demonstrating a profound enhancement in cellular viability following 24 hours of culture in conditioned medium for both Balb/c and C57BL/6 splenocytes; thereby resolving the limited viability previously observed and enabling improved cellular analysis prior to infusion. Note: recovery into fresh medium was not considered in this experiment having proven uniformly toxic through numerous previous experiments.

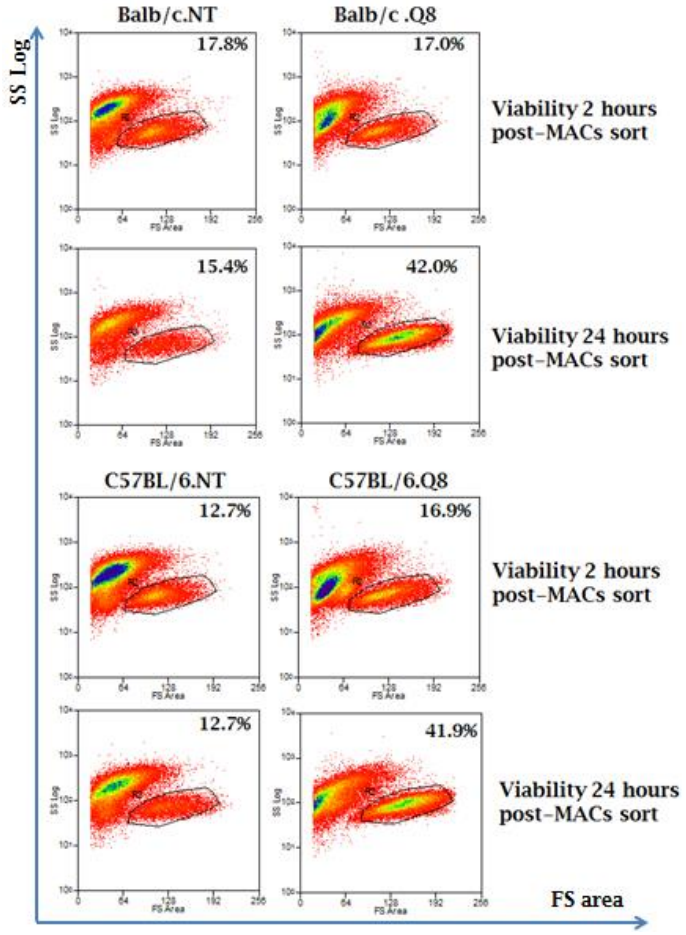

Figure 58 Cellular viability post MACS selection in conditioned medium
Having observed poor splenocyte viability following magnetic bead selection, we assessed the viability of purified cell product when recovered in conditioned medium. 24-wells/48-60x10^6 splenocytes of either Balb/c or C57BL/6 splenocytes were transduced with Q8.I2.eGFP, recovered overnight, then purified by CD34 magnetic bead selection. Following MACS sorting, splenocytes were recovered into 0.45µm filtered cellular supernatant from which they were derived with cellular viability of the recovered cells assessed at 2 and 24 hours following selection. Note: Non-transduced cells represent the viability control as these cells remained unhandled during the assessment timeframe to reflect typical progressive loss of splenocyte viability typically resulting from extended *in vitro* culture.

The reduction in sample purity observed from the MACS selection process when performed in large scale posed the next experimental challenge. As QBEnd10 is a murine antibody, we premised high background binding reflected FcγR binding of the QBEnd10 antibody by residual effector cells such as monocytes. Further, having established conditioned medium facilitated enhanced cellular viability, we opted to attempt a blocking strategy to exclude residual effectors at the selection stage rather than by increasing experimental cost through T-cell selection from the outset. We identified two strategies which might fulfil this function; Miltenyi murine IgG cocktail as a blocking reagent to saturate the FcγR's, or use of the 2.4G2 hybridoma supernatant as an antibody-mediated blocking strategy. From our initial attempt illustrated by figure a, neither strategy appeared to demonstrate improved clarity of MACS selection following 30-minutes of blocking with 100µl of either reagent; however as purity and viability appeared improved following blocking with the 2.4G2 hybridoma supernatant, further repeats were performed ultimately identifying a requirement for 1ml of 2.4G2 hybridoma supernatant per spleen to achieve the desired efficacy of FcγR-blocking. Results from this experiment are indicated by Figure 59.

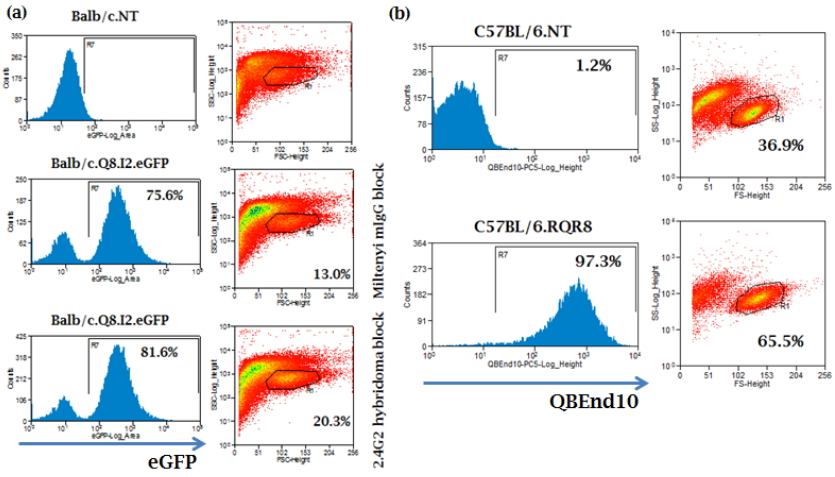

Figure 59 2.4G2 blocking strategy to improve MACS selection clarity
To resolve selection of FcyR expressing effectors which impair the level of purity which could be achieved from large scale magnetic bead selection of splenocytes, we assessed the effect of application of anti-mouse CD32 2.4G2 supernatant might have on magnetic bead selection efficacy. (a) 24-wells/48-60x10^6 of Balb/c splenocytes were transduced with Q8.I2.eGFP, then purified by CD34 magnetic bead selection following a 30 minute incubation in either 100µl of Miltenyi murine IgG blocking reagent or 0.45µM filtered neat 2.4G2 hybridoma cellular supernatant. Sample purity and cellular viability was assessed by flow cytometry 24-hours following MACS selection. (b) 24-wells/48-60x10^6 of C57BL/6 splenocytes were transduced with RQR8.I2.eGFP, then then purified by CD34 magnetic bead selection following

a 30 minute incubation in 1ml of 0.45µM filtered, neat 2.4G2 hybridoma cellular supernatant. Following selection, splenocytes were recovered into 0.45µm filtered cellular supernatant from which they were derived with sample purity and cellular viability assessed by flow cytometry 24-hours following MACS selection. As illustrated, use of 2.4G2 supernatant as a blocking reagent improved sample purity whilst recovery into conditioned medium enhanced cellular viability.

7.5. Optimisation of 5–day cellular preparation protocol

Experimental aim: To establish an experimental protocol to achieve consistent generation of sufficient viable transgenic murine splenocyte cellular product to enable *in vivo* modelling experiments.

Combining results from this preliminary series of investigations led to the generation of a 5-day protocol offering a minimal period of *ex vivo* handling required to facilitate consistent isolation, transduction, recovery, purification and confirmation of transgenic murine T-cell product prior to re-infusion into recipient animals, illustrated by Figure 60 and briefly summarised below:

Day 1: splenocytes are isolated from donor animals and stimulated with ConA/IL7 (2µg/ml and 1ng/ml respectively). Day 2: Activated splenocytes are harvested and transduced in the absence of stimulation, in neat viral supernatant. Day 3: Restimulation: Transduced splenocytes were recovered into fresh RPMI supplemented with murine IL2 (50ng/ml). Day 4: Transduction efficiency was tentatively confirmed by flow cytometry and splenocytes were MACS-sorted following 2.4G2 blocking, and recovered back into 0.45µM filtered conditioned medium from which they originated. Day 5: Final assessment of purity for transgene expression and cellular CD4/CD8 profile was confirmed by flow cytometry prior to infusion of transgenic cell product into recipient animals.

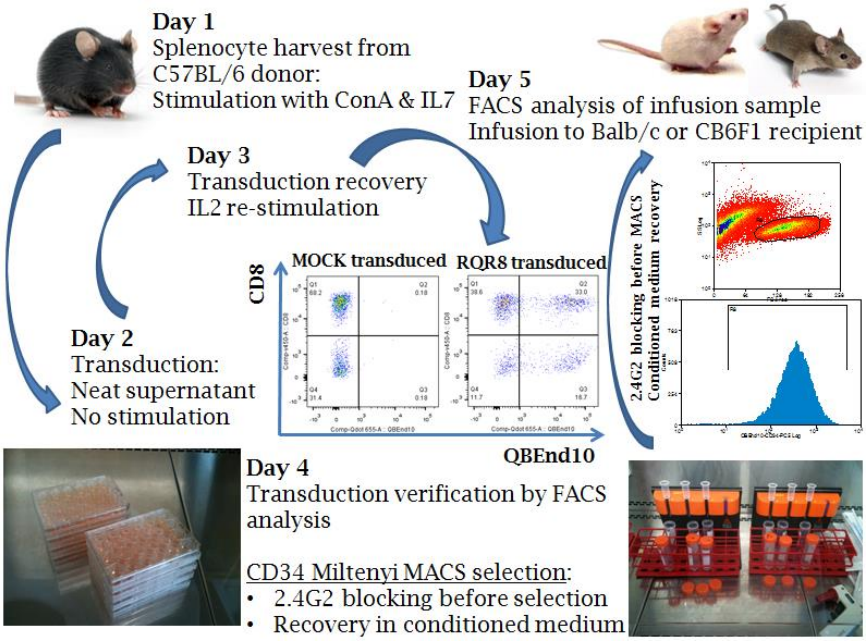

Figure 60 Five day protocol for splenocyte transduction and MACS selection
A five day protocol was established as illustrated, which combined standard splenocyte transduction protocols with recovery in conditioned medium and blocking with 2.4G2 supernatant prior to magnetic bead selection. This optimised protocol enables generation of $5x10^6$ purified transgenic cell product for each 24-wells/48-60x10^6 splenocytes which were transduced.

7.6. Conclusions

In this chapter, we have demonstrated successful generation of ecotropic-pseudotyped retrovirus facilitating transduction of C57BL/6 and Balb/c splenocytes, observing successful transduction for both murine CD4 and CD8 T-cell subsets. The SFG viral integrant appears to mediate stable expression of all transgenic cassettes investigated, with successful binding observed for both QBEnd10 and rituximab antibodies against appropriately modified splenocytes. Further, ecotropic envelope has been shown to be sufficiently robust to tolerate freeze-thaw cycling thereby facilitating generation and validation of viral supernatant in advance of experimentation, assisting design and planning of large modelling experiments.

Use of 2.4G2 hybridoma supernatant as a blocking reagent improves clarity of MACS selection of splenocytes despite the murine derivation of the QBEnd10 antibody, whilst recovery into conditioned medium results in improved cellular viability following overnight recovery from MACS selection. In combination, employing our 5-day protocol we observed that we could

consistently generate $5x10^6$ transduced purified viable splenocytes per donor spleen.

7.7. General conclusions

- Ecotropic pseudotyped SFG retrovirus facilitates successful transduction of murine splenocytes
- Transgenic splenocytes demonstrate epitope expression analogous to previous results achieved with primary human PBMCs
- Use of the 2.4G2 hybridoma supernatant as a blocking reagent reduces cellular contamination of the transgenic cell population following Miltenyi bead selection
- MACS selection of transgenic splenocytes enables consistent purification >90%
- The optimised 5-day protocol demonstrates a consistent strategy to produce sufficient transgenic splenocytes for *in vivo* modelling experiments
- Use of conditioned medium enhances post-MACS selection recovery and ensures optimal cellular viability prior to infusion

Chapter eight

8. Generation of murine rituximab monoclonal antibody

As the capacity for murine effector mechanisms to respond to the human IgG1 domain of rituximab presented an uncontrolled variable, we premised it would be necessary to use an equivalent murine isotype as human IgG1 to achieve a more reflective result from *in vivo* modelling experiments.

8.1. Aims

- To reverse engineer rituximab to generate a murine IgG2a isotype
- To confirm the binding domain of mRtx-IgG2a matches the sequence from the rituximab IDEC2B8 hybridoma
- To establish a producer line to ensure stable production of mRtx-IgG2a
- To achieve a production strategy to enable sufficient production of mRtx-IgG2a to enable *in vivo* modelling
- To confirm of retention of functional capacity of mRtx-IgG2a antibody product through *in vitro* assays

8.2. Introduction

As rituximab is a chimeric antibody, we premised that the presence of the humanised constant domain may pose an uncontrolled variable limiting efficacy and possibly negatively impacting upon the therapeutic half-life in our proposed modelling experiments. In an effort to establish a more reflective model of human rituximab kinetics, we reverse engineered rituximab into the murine IgG2a isotype which offers analogous functional capacity with the human IgG1 format of rituximab based on B-cell depletion studies from animal models[183, 184]. Table 11 illustrates functional capabilities of alternative murine IgG isotypes.

Table 11 Comparison of effector function by murine antibody isotype
Note: ADCC activity refers to activity assessed for murine effectors

Murine antibody effector function	IgG1	IgG2a	IgG2b	IgG3
CDC[269]	–	+	++	+++
ADCC[270]	+	++++	+++	+/–

As variation between the murine IgG2a allotypes has been identified as a confounding variable affecting ELISA quantification due to variation in antibody binding affinity for the separate allotypes, it was necessary to confirm the absolute identify of the IgG2a allotype employed in our Rtx-IgG2a engineering to ensure effective ELISA based quantification.

IgG2a allotype gene conversion is proposed to result from improperly paired bases occurring during genetic recombination[271]. Following gene duplication of the mouse IgG2a / IgG2b gene ancestor, these genes readily diverged with the observed divergence between IgG2a alleles thought to be the result of gene conversion likely promoted by the short genetic distance separating the two loci. This has resulted in a high degree of divergence in the coding sequence of the murine IgG2a gene[272]. Although multiple alleles have been identified for each of the murine immunoglobulin isotypes, the IgG2a allele is the most polymorphic with 12 allelic forms characterised. The Balb/c and the C57BL/6 strains are the prototypes for the IgG2a^{a} and IgG2a^{b} haplotypes, henceforth, allotypes, respectively[273].

Additionally, generation of sufficient therapy grade antibody required identification of a suitable protein production strategy. The main strategies for recombinant protein production are transient gene expression (TGE) or generation of a stable cell line for continuous production with both strategies offering benefits and limitations. Although TGE offers a strategy to achieve large-scale protein production, it can prove expensive due to the volume of DNA and transfection reagents required; further, TGE may demonstrate significant batch-to-batch variation and might require substantial post-production steps. In contrast, generation of a stable producer cell line can resolve or reduce most of these limitations but imposes a longer lag-time before protein production can be achieved. Hence TGE is an optimal strategy where small-scale screening is required whilst generation of a producer line is better suited for bulk production. Finally, scalability imposes further limitation to the process. Currently HEK293 are the cell line most commonly employed for TGE of recombinant proteins although as of 2006, no recombinant protein produced by TGE had been approved for clinical application by the FDA[274]. In the interest of biosafety it is preferable to exclude animal derived components from protein production, thus identification of a simple strategy offering robust protein production in serum-free mammalian cell culture could be of

benefit to facilitate and reduce the cost of pre-clinical modelling. In this chapter we describe stable and consistent antibody production from a modified K562 cell line.

8.3. Results: Gene synthesis of rituximab Fab sequence

Experimental aim: To generate a codon optimised expression cassette to express the antibody binding domain (Fab) of the therapeutic antibody rituximab.

Having elected to reverse engineer rituximab, the first challenge we faced was to locate a reference sequence for the rituximab hybridoma which we could use as a template during our design for our gene synthesis cloning strategy. Locating the rituximab consensus sequence was confounded by identification of alternative sequences from the Alberta drug bank and the US patent 5,843,439, both claiming to define the protein sequence for the variable domains of the rituximab IDEC2B8 hybridoma. Uncertain which sequence was correct; we generated constructs for both sequences, henceforth denoted as RtxC and RtxP, for the Canadian derived and patent derived sequences respectively.

As with codon-optimisation for CD20opt generated previously, gene synthesis was again used to generate codon optimised rituximab scFv fragments using pMol software designed by Dr. Martin Pulé. This coding sequence was then generated by gene synthesis using overlapping oligos and subcloned in-frame as an NcoI-BamHI fragment into SFG.S-CEA_NA1-HCH2CH3-CD28OXZ.I2.eBFP2. Following BglII-NsiI restriction digest screening to identify putative correct clones, mini-preps were further screened by flow cytometry staining for the IgG1 stalk to exclude frame shift mutants, as illustrated by Figure 61. Finally, constructs which demonstrated surface expression of the scFv construct were verified by DNA sequencing.

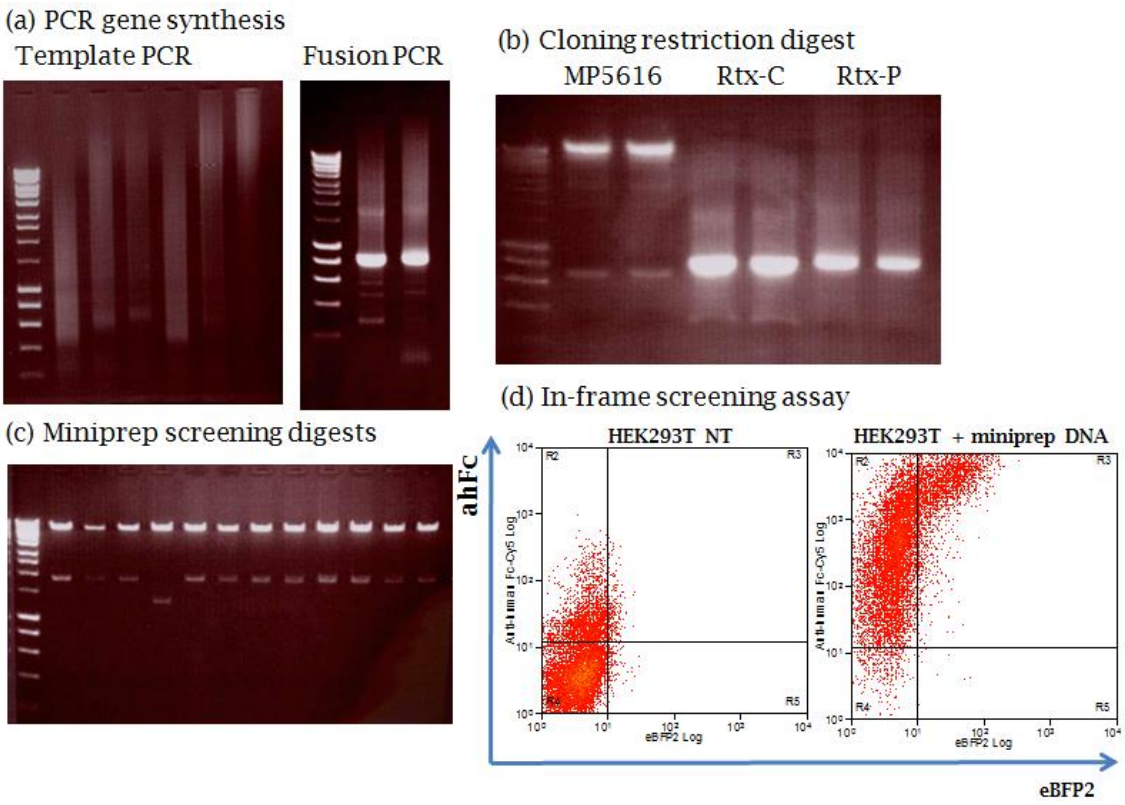

Figure 61 Gene synthesis of rituximab scFv constructs
Molecular cloning and functional screening of gene-synthesized rituximab-scFv. (a) PCR-based gene synthesis: Template PCR reaction containing overlapping oligonucleotide primers produced a smear of DNA fragments; these were subsequently focussed into clear product following a fusion PCR reaction combining the separate fragments through amplification of the desired sequence bounded by terminal oligonucleotide primers. (b) Restriction digest of destination vector and PCR-amplified inserts: Following PCR clean-up, fusion PCR products were digested as NcoI-BamHI fragments, then subcloned into a similarly digested target vector (MP5616) (c) Restriction digest screening: miniprep colonies were screened by BglII-NsiI restriction digest to identify transgene positive clones (d) Functional screening by flow-cytometry: As the insert sequence was cloned in-frame into the open reading frame (ORF), mini-prep DNA transfected HEK293T cells were used to stain for functional expression of the scFv IgG1 immunoglobulin HCHG2CH3 domain confirming functional expression of protein product from the ORF to exclude frame-shift mutants. Non-transduced HEK293T included as staining control indicated at left. Note: dim eBFP2 expression was due to poor laser alignment of the violet laser. Lastly, following exclusion screening, one RtxC and two RtxP clones were confirmed by DNA sequencing.

8.4. Generation of secreted form of rituximab scFv

Experimental aim: To subclone the antibody binding domains of the anti-CD20 scFv's into secreted formats to validate binding efficacy against RQR8.

Having generated putative rituximab binding fragments, we proceeded to subclone the scFv domain into a secreted format through 'cut and paste' cloning as an NcoI-BamHI insert into a secreted scFv construct previously generated by Dr. Simon Thomas. To enable functional validation of our

constructs, supernatant containing the putative scFv binding domains was generated by transient transfection of HEK293T cells. Validation of antibody binding was assessed through an indirect flow cytometry binding assay comparing binding of anti-human Fc following primary staining of Jurkat T-cells using HEK293T produced scFv supernatant. As illustrated by Figure 62, although both scFv constructs bound to the CD20 positive control only the RtxP-scFv demonstrated clear binding against the RQR8 target likely representing the correct sequence for rituximab.

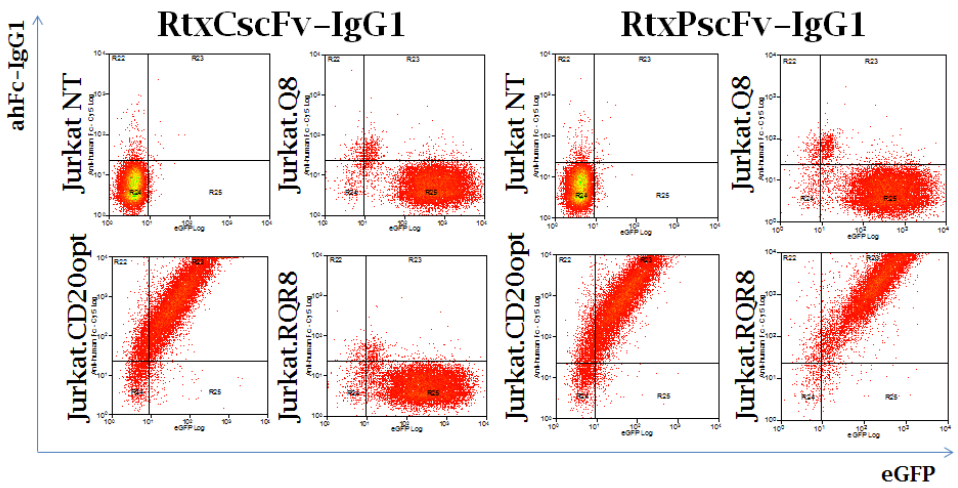

Figure 62 Functional binding validation of rituximab scFv constructs
Putative rituximab scFv constructs were subcloned into a secreted expression format, transfected into HEK293T cells and the resulting supernatant was used to assess binding efficacy by flow cytometry through indirect binding assays against transgenic Jurkat T-cell targets. Primary staining was performed using RtxP or RtxC scFv supernatant followed by secondary staining with an anti-human Fc-Cy5 conjugate. As illustrated, clear binding against the RQR8 target was observed from RtxP-scFv supernatant whereas the RtxC-scFc only bound the CD20 control.

8.5. Confirmation of mRtx–IgG2a sequence homology with IDEC2B8 hybridoma

Experimental aim: To confirm that the antibody binding domain coding for our rituximab scFv (RtxP) as defined by the US patent 5,843,439, corresponds with the rituximab antibody sequence as identified from the IDEC-2B8 hybridoma.

Having confirmed the functional capacity of our RtxP-scFv construct to bind the RQR8 target, and in light of concerns regarding the exact sequence of the rituximab antibody, lastly we aimed to conclusively establish that our RtxP-scFv sequence was identical to that of the rituximab IDEC-2B8 hybridoma.

To this end, we obtained the rituximab IDEC-2B8 hybridoma from the American Type Culture Collection (ATCC). Following hybridoma recovery, we performed RNA extraction and cDNA generation as per protocols 2.2.1.1.12 and 2.2.1.1.13 respectively, with successful cDNA generation confirmed by amplification of the GAPDH housekeeping gene using Qiagen oligonucleotide primers.

Finally, amplification of the heavy and light chains from the hybridoma was performed using oligonucleotide primers (IDT) as detailed in the protocol by Dübel *et al*. Successful amplicons were subcloned by TOPO TA cloning (Invitrogen) with DNA sequencing performed by the scientific support core facility.

Variable region allele analysis was performed through comparison of coding regions identified from hybridoma sequence traces against the mouse immunoglobulin set as assessed using IMGT/V-QUEST. Comparison of the heavy variable region analysed between the first nucleotide of the coding sequence to the second cysteine codon identified a productive rearranged IGH sequence demonstrating 93.75% homology with the murine IGHV1-12*01F allele. Further, analysis of the light chain variable region identified 96.01% homology with the murine IGKV4-72*01F allele. Having confirmed the identified sequence corresponded with the murine immunoglobulin coding sequence, we then compared a translation of the open reading frame identified from hybridoma sequence traces, aligned against the rituximab sequence which demonstrated regions of clear homology as illustrated by Figure 63, confirming our RtxP sequence matched that of the IDEC-2B8 hybridoma.

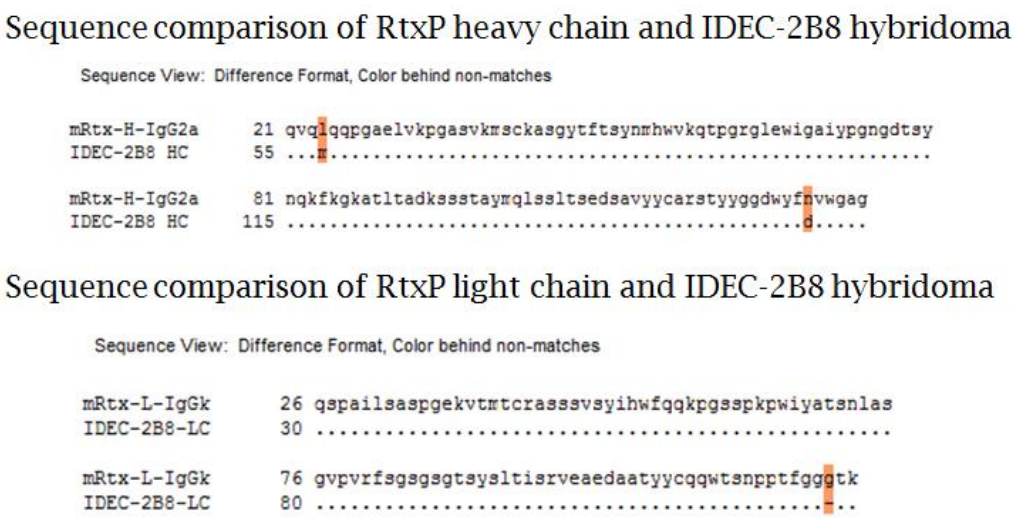

Figure 63 Rituximab patent and IDEC–2B8 hybridoma sequence comparison
Heavy and light chain sequences for rituximab as defined by US patent 5,843,439 were compared against DNA sequence traces from cDNA derived from the rituximab hybridoma IDEC-2B8. As illustrated, the protein sequence used for the RtxP scFv matches the coding sequence from the rituximab hybridoma.

8.6. Cloning of mRtx–IgG2a heavy and light chain constructs

Experimental aim: To reverse engineer rituximab back into a murine antibody by subcloning the rituximab scFv heavy and light antibody binding domains onto murine constant IgG2a heavy and kappa light chains.

Having successfully cloned, functionally validated and confirmed the identity of the rituximab variable domain sequences, we proceeded to reverse engineer rituximab into a complete murine IgG2a isotype antibody. The genetic sequence for the murine IgG2a heavy and kappa light chains were sourced from Invivogen pFUSEss-CH1g-mG2A and pFUSE2ss-CLIg-mk plasmids respectively. Concerned that functional impairment of our antibody might result from the presence of residual TaV-2A sequence if the construct was expressed in a bicistronic format, we opted to separate the heavy and light chains into separate constructs each identified by a separate fluorescent protein marker. As previously, application of a SOE-PCR cloning strategy enabled inclusion of NcoI and MluI restriction sites facilitating facile cloning of the heavy and light chains into HA1-TCRbeta.I2.eGFP and HA1-TCRbeta.I2.eBFP2 vectors respectively. Restriction digest screening of miniprep samples identified putative correct constructs which were confirmed by DNA sequencing.

Concerns regarding confounding variables such as limitations in cellular glycosylation capacity or aberrant protein folding could impact upon functional antibody production, next we sought to confirm that we could successfully generate functional antibody following co-expression of both heavy and light chain constructs in cell culture. Therefore, as a proof of principle experiment prior to generating supernatant and establishing stable cell lines, HEK293T cells were co-transfected with both heavy and light chain constructs and grown to confluence. Supernatant derived from this culture was then used to stain Jurkat T-cells as previously to confirm successful antibody production as illustrated by Figure 64.

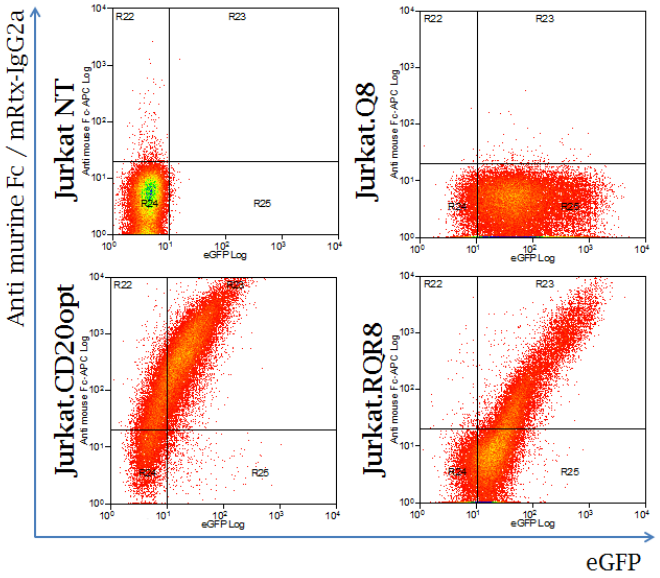

Figure 64 HEK293T mRtx–IgG2a supernatant staining assay
To confirm expression of our re-engineered heavy and light chains of rituximab would form a functional antibody we performed a staining assay using cellular supernatant derived from HEK293T cells co-transfected with Rtx-H-mIgG2a and Rtx-L-mKappa constructs; four days following transfection, cellular supernatant was harvested as employed as a primary stain against Q8, RQR8 or CD20 transgenic Jurkat T-cell targets. Functional binding was confirmed by flow cytometry analysis using an APC-conjugated anti-mouse Fc as the secondary antibody. As illustrated, mRtx-IgG2a binding was observed against both the CD20 and RQR8 transgenic targets.

As illustrated by Figure 64, clear specific binding was demonstrated against both RQR8 and the CD20opt control constructs, with no binding observed against the Q8 target.

8.7. Generation of a high expressing mRtx–IgG2a producer

Experimental aim: To establish a stable eukaryotic producer line capable of producing sufficient mRtx-IgG2a antibody to enable *in vivo* modelling experiments.

Our next challenge was to establish a culture strategy which would demonstrate sufficient antibody production as to enable *in vivo* modelling experiments. Based on modelling experiments for putative CD20 suicide gene constructs from the literature[154], we premised that milligram quantities of mRtx-IgG2a would be required for each *in vivo* modelling experiment. HEK293T cells are commonly employed for protein production. However, a limitation of HEK293T cells is restriction to 2-dimensional cell culture due to their adherent growth profile. Although we briefly considered 3-dimensional suspension culture of the 293SF serum-free adapted HEK293T cell derivative, these cells proved fragile and limiting in their potential application for our purposes. Next we considered K562 cells having previously proven easy to transduce and manipulate as an alternative suspension cell population. We multiply transduced both HEK293T and K562 cells with both heavy and light chain constructs. Following confirmation of successful transductions, transduced cell populations were subsequently MoFlo sorted based on high expression of both the eGFP and eBFP2 fluorescent marker genes. Finally we single cell cloned high expressing isolates which were examined for mRtx-IgG2a production based on serial dilution titration assays as illustrated by Figure 65. High expressing clones producing protein supernatant demonstrating comparable rituximab binding capacity as the IDEC-2B8 hybridoma supernatant were identified for both HEK293T and K562 cells. However, the K562 mRtx-IgG2a producer clone A7 was selected for subsequent mRtx-IgG2a production based on antibody titre, cellular growth profile and stable viability.

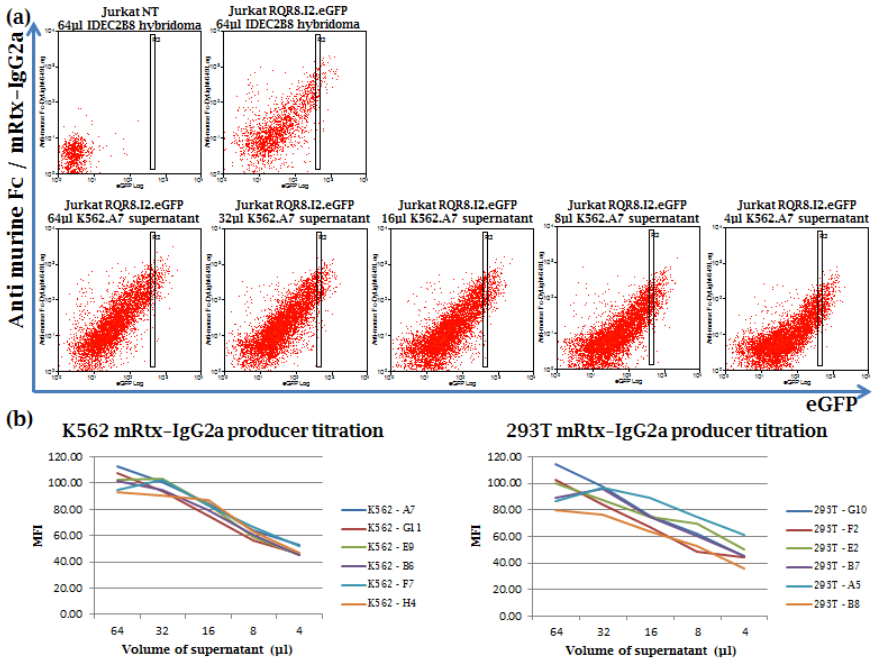

Figure 65 mRtx–IgG2a producer line titrations
Cellular supernatants produced by putative K562 producer lines were screened for efficacy of mRtx-IgG2a protein production using serial dilution of cellular supernatants as assessed for RQR8 target binding by flow cytometry. (a) Equal numbers of Jurkat.RQR8.I2.eGFP expressing target cells were stained with serial dilutions of cellular supernatant but assessed using constant level of the DyLight-649 conjugated anti-mouse Fc secondary. MFI of mRtx-IgG2a antibody binding was assessed against a stringent population of high expressing targets as illustrated. Results illustrate comparative binding efficacy of the K562.A7 clone compared against the IDEC-2B8 hybridoma. (b) Titration assay results from the top six single cell clones from both K562 and HEK293T mRtx-IgG2a producer lines. As illustrated, both K562 and HEK293T producer lines demonstrated similar levels of protein production.

8.8. mRtx–IgG2a production

Experimental aim: To establish a protocol for bulk production and purification of mRtx-IgG2a antibody.

Antibody production comprised a multi-stage process involving successful confirmation of protein production at crucial progression points. Observations from initial purification runs were modified to establish the final protocol as detailed in methods 2.1.7.

Briefly, a fresh batch of K562.mRtx-IgG2a.A7 producer cells was recovered one week prior to antibody production. Following recovery, cells were grown in complete IMDM to establish a seed culture for bulk production. For production, cells were harvested by centrifugation, washed with PBS and 5-10 million K562.mRtx-IgG2a.A7 cells were seeded into T175cm2 flasks pre-filled with 100ml of mRtx-IgG2a IMDM. Cell culture was allowed to progress for

approximately 1 week until terminal density was achieved defined by cell death observed in approximately 50% of cells as assessed by Trypan blue exclusion by haemocytometer analysis. At this point, antibody supernatant was harvested and prepared for purification briefly detailed as follows:

Cell culture was harvested into 250ml centrifuge tubes and centrifuged at 400G for 10 minutes to pellet cells. Cellular supernatant was transferred to a Duran bottle with a sample taken to confirm presence of antibody through flow cytometry staining analysis. Cellular supernatant was then 0.22μm filtered by vacuum filtration to exclude cellular debris to prevent filter blockage during protein concentration. Next, protein supernatant was concentrated using a Millipore Pellicon tangential flow filter system fitted with a Pellicon XL Biomax 50 filter to enable exclusion of small proteins whilst retaining proteins of mass 50kDa±20kDa. Following tenfold concentration, supernatant was transferred to snakeskin dialysis tubing and dialysed into 20mM sodium phosphate loading buffer solution at 4°C overnight, assisted by agitation mediated by magnetic stirrer. Samples obtained during protein concentration were assessed by indirect staining to demonstrate successful concentration and retention of antibody as illustrated by Figure 66.

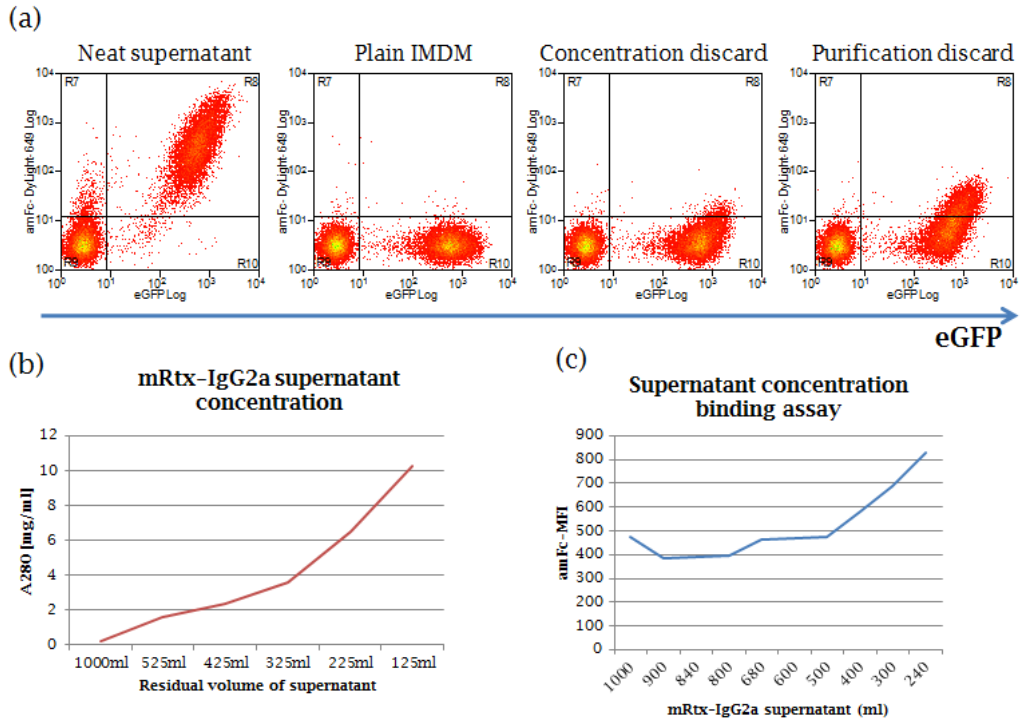

Figure 66 mRtx-IgG2a protein supernatant concentration validation
(a) Samples of protein supernatant were assessed by flow cytometry against a 50:50 mixture of non-transduced or RQR8.I2.eGFP transgenic Jurkat T-cells for the presence of functional antibody. Concentration and elution discard fractions were also assessed for presence of residual antibody. (b) A280 measurements were made from samples obtained during concentration to verify successful sample enrichment. (c) Comparative MFI analysis assessed by flow cytometry of fractions taken during protein concentration further validate successful protein concentration. As illustrated, mRtx-IgG2a protein retained functional stability during tangential flow filtration concentration prior to purification.

Following dialysis, the supernatant was again 0.22µm filtered by vacuum filtration prior to sample loading onto a protein A column using an ÄKTAprime plus system. Sample loading and elution profiles are illustrated by Figure 67. A280 measurements were taken to confirm elution samples match with profile.

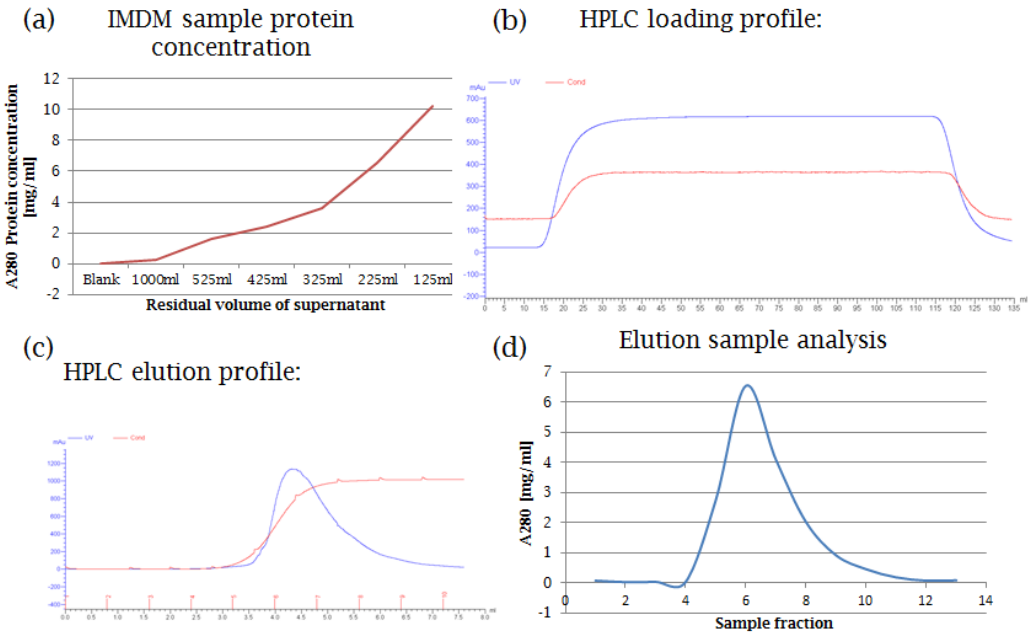

Figure 67 ÄKTAprime plus HPLC mRtx–IgG2a protein purification profiles
(a) Sample fractions obtained during protein concentration were assessed by A280 spectrophotometric assessment to ensure successful concentration and protein retention. (b) During Protein A column loading, absorbance measurements on the ÄKTAprime plus allowed confirmation of presence of protein in the loading buffer and identified completion of sample loading. (c) Absorbance measurements of elution fractions indicated protein release from the column. (d) A280 spectrophotometric measurements of elution fractions were performed to confirm presence of concentrated protein. Functional confirmation of purified mRtx-IgG2a protein is illustrated by Figure 69

Following the initial purification run, size confirmation of the mRtx-IgG2a product was assessed by Coomassie staining following SDS-PAGE. Mass approximations for the mRtx-IgG2a heavy and light chains, identified using the ExPASy[275] bioinformatics research tool suggested predicted protein masses of 51.8 and 25.5kDa for the mRtx-IgG2a heavy and light chains respectively. Purified mRtx-IgG2a protein was compared against reference samples of Mabthera rituximab as illustrated by Figure 68. Presence of a smaller heavy chain specific to the IMDM samples suggested residual contamination from FCS despite the reduced bovine IgG content indicated by the absence of this band from the sample generated from serum-free Hyclone medium. During initial mRtx-IgG2a production runs, IMDM medium was supplemented with 10% IgG depleted FCS. However, as analysis of K562 cellular viability at reduced levels of FCS supplementation did not appear to impose any impact upon K562 cellular viability as assessed by Annexin V/PI staining, serum supplementation of culture media was reduced to 2.5% for subsequent purification runs to further reduce bovine IgG contamination. Due to the

desired functional application of mRtx-IgG2a, protein product validation following subsequent production runs was restricted to quantification and functional assays.

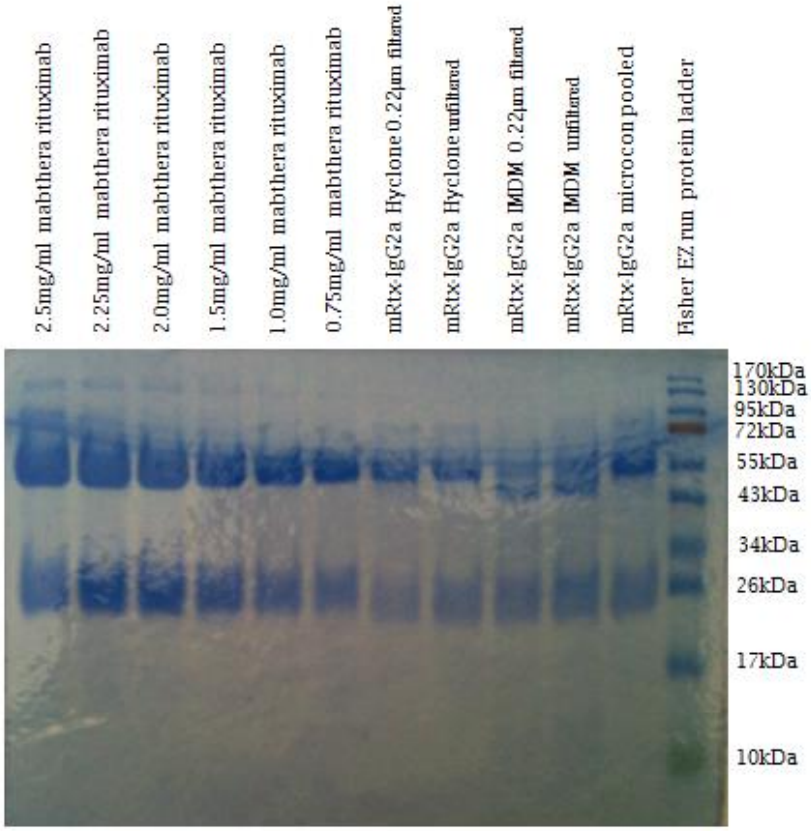

Figure 68 Coomassie stained protein gel of mRtx–IgG2a products
To confirm the presence of putative mRtx-IgG2a protein, purified samples of mRtx-IgG2a protein from five separate production runs were separated by polyacrylamide gel electrophoresis and assessed for protein size by Coomassie staining; sample protein concentrations were established by A280 measurements. Serial dilutions of clinical-grade rituximab were included to enable visual comparison of intensity of protein staining and protein band size.

8.9. mRtx–IgG2a functional validation

Experimental aim: To confirm functional retention of both the antibody binding (Fab-domain) and mRtx-IgG2a mediated deletion (Fc-domain) following protein production, purification and downstream processing.

Antibody stability varies widely dependent upon the protein sequence. Further, handling can impair functional behaviour of the protein. Following sterile filtration, mRtx-IgG2a was quantified by: A280 measurements and ELISA, with functionality verified by indirect staining and CDC assays.

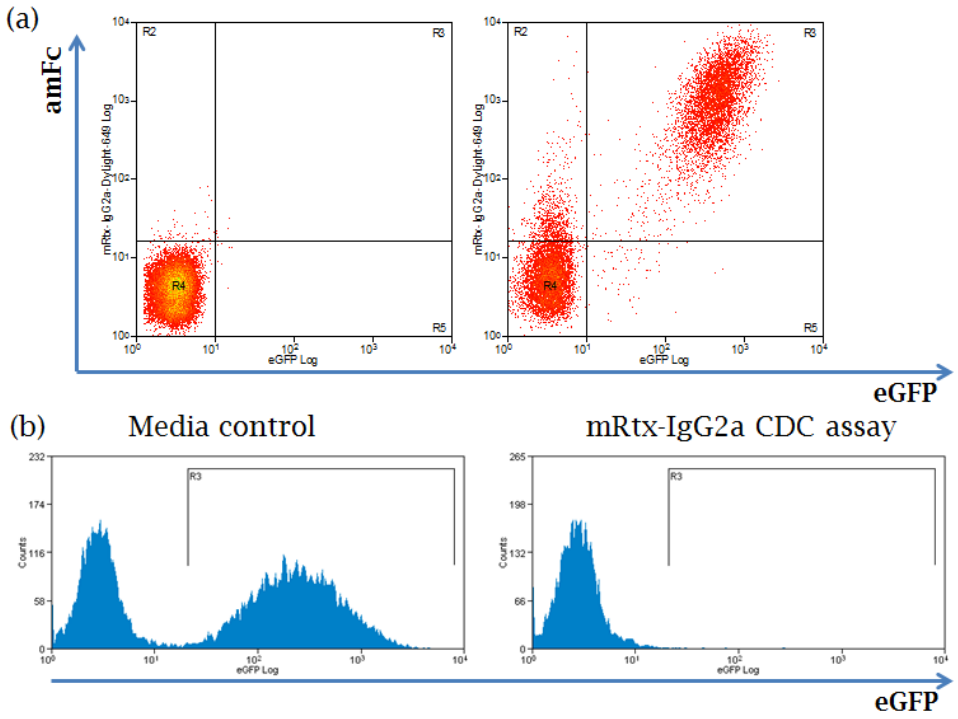

Figure 69 Functional verification of mRtx–IgG2a
(a) Binding: Samples of purified mRtx-IgG2a antibody were assessed by flow cytometry for retention of functional binding efficacy against a 50:50 mixture of non-transduced or RQR8.I2.eGFP expressing Jurkat T-cells for the presence of functional antibody. (b) Deletion: Peripheral human PBMCs were transduced with RQR8.I2.eGFP or Q8.I2.eBFP2, separately purified by CD34 magnetic bead selection then mixed together in an equal ratio to establish a target population which was then subjected to a specificity CDC assay employing purified mRtx-IgG2a as rituximab in this assay. As illustrated, final purified mRtx-IgG2a antibody product retained functional capacity of both Fab and Fc domains; antibody binding & CDC-mediated deletion respectively.

8.10. Conclusions

In conclusion, we have successfully identified and established variable domain binding fragments of rituximab. Further, following re-engineering into the murine IgG2a isotype, we have demonstrated that we can produce functional antibody in sufficient quantity to enable *in vivo* modelling experiments. Through generation of a stable K562 producer cell line, we have established a three-dimensional culture strategy demonstrating robust and stable protein production. From a 2L large scale run, we produced 65mg of mRtx-IgG2a, suggesting a production rate of 32.5mg/L. Compared against transient gene expression (TGE) strategies for protein production which typically yield 1-80mg/L[274], this production level is well within the range for TGE expression strategies and offers the potential for consistent protein production for future production runs. Further, this follows from minimal optimisation achieving a stable production strategy avoiding inter-batch variation typical of TGE

strategies. Lastly, separate work performed by Ben Draper under my instruction has demonstrated that K562 cells can be readily adapted to culture in serum free medium, demonstrating a more robust growth profile than was observed for suspension HEK293 cells, adding support for the potential of general application of K562 cells as a protein production platform.

8.11. General conclusions

- Through gene synthesis we have identified the binding domain of rituximab as cited in US patent 5,843,439, and verified against the DNA sequence isolated from the IDEC2B8 hybridoma
- Following subcloning of the variable domains into murine IgG2a constant heavy and kappa light chains, we have demonstrated *in vitro* production of IgG2a isotyped rituximab following transient transfection of HEK293T cells
- From comparison of antibody production between stably transduced HEK293T and K562 cells, we identified and established the high expressing and stable producer line: K562.A7
- Following large scale antibody production, functional and qualitative assays verified that we had produced sufficient functional IgG2a isotyped rituximab to enable *in vivo* modelling experiments

Chapter nine

9. *In vivo* GvHD modelling

As GvHD is neither vector nor target specific, we selected GvHD modelling as the simplest strategy to assess the *in vivo* functional capacity of RQR8 to resolve therapeutic toxicity.

9.1. Aims

- To successfully increase experimental scale sufficient to enable *in vivo* modelling experiments
- To successfully achieve transgenic cellular engraftment in recipient animals
- To establish a model of GvHD pathology mediated by activated, transduced and MACS sorted splenocytes
- To demonstrate resolution of GvHD pathology through mRtx-IgG2a mediated cellular deletion

9.2. Introduction

GvHD remains a common co-morbidity following HSCT despite administration of immunosuppressive therapies. Correspondingly, a range of animal models have been established in order to obtain further insight into the molecular pathology of GvHD[276], including description of a C57BL/6 to Balb/c acute GvHD MHC-I mismatch model as described by van Leeuwen *et al*[277].

Reflecting the direct relevance of the observations by van Leeuwen *et al*[277], the following discussion will briefly summarise some of the key findings as they pertain to observations from our own research. Myeloablative preconditioning and bone marrow transfer was associated with a two-phase model of GvHD pathology with an initial phase characterised by weight loss followed by a second phase demonstrating symptoms characteristic with clinical GvHD. Although both syngeneic and allogeneic recipients demonstrated significant weight losses during the first week following irradiation, syngeneic recipients were observed to have recovered body mass 16 days post transfer whilst allogeneic recipients demonstrated sustained weight loss progressing until euthanasia became necessary. Animals which were irradiated without bone marrow recovery mirrored the initial weight loss of the syngeneic recipients,

and despite a brief weight recovery phase, rapidly progressed into terminal decline resulting from haematopoietic failure. Thus, although some weight loss could be attributed to a response to total body irradiation (TBI), additional weight loss was proposed to reflect an initial phase of GvHD progression.

Furthermore, a profound depletion of the host MHC-II compartment was observed resulting in undetectable levels of host MHC-II cells from the spleen and bone marrow 7 days following the preconditioning irradiation contrasting with a progressive increase in the donor MHC-II compartment during this period. This variation in the MHC-II compartment was proposed to explain the transient recovery separating the two-phases of GvHD pathology. The authors propose that an initial phase of GvHD, progressing up to day 7 as evidenced by weight loss greater than that observed by syngeneic controls, might reflect direct recognition of host antigens presented by host APCs by the donor T-cell population, whilst the second phase commencing after 12 days post-transfer, was suggested to arise from indirect antigen presentation by donor-derived APC's to donor T-cells.

Reflecting our aim toward demonstration of GvHD resolution mediated by the suicide-gene capacity of RQR8, our primary intent was to establish a model of MHC-I mismatched GvHD which would offer a platform by which efficacy of RQR8-mediated deletion could be assessed *in vivo*.

9.3. Results: GvHD induction pilot

Experimental aim: To establish an *in vivo* experimental model of GvHD pathology mediated by transgenic splenocytes.

9.3.1. Model design

Our acute C57BL/6 to Balb/c GvHD model was based upon previous research Prof. Ronjon Chakraverty and Dr. Barry Flutter[278]. Following a report from the literature suggesting an impaired capacity for GvHD induction resulting from the *ex vivo* handling necessary to accomplish retroviral transduction and paramagnetic selection[279], we commenced with an initial pilot experiment designed to confirm that *ex vivo* manipulated splenocytes would retain the capacity to induce a pathology consistent with classical symptoms of GvHD assessed by *in vivo* modelling. The presence of a single nucleotide polymorphism in the murine allele for CD90, hereafter Thy1.1 and Thy1.2,

enables discrimination between donor and recipient lymphocyte populations by antibody staining and reflects current technology for cellular marking strategies employed within *in vivo* modelling experiments. Briefly, our allogeneic GvHD induction model comprised transduction and purification of splenocytes from a (C57BL/6) Thy1.1 x Thy1.2 donor, which were subsequently transferred into a (Balb/c) Thy1.1 host. To enable MACS sorting and cellular identification, splenocytes were transduced with the Q8.I2.eGFP construct to enable cellular marking by QBEnd10, with further specific identification of the transgenic population mediated by the eGFP fluorescent marker. To prevent deletion of the transgenic cell infusion by host cells and to assist effective engraftment by the adoptive cells[91], recipient mice were pre-conditioned with 8 Gy X-ray TBI supplied in two equal 4 Gy doses supplied 48 and 4 hours respectively, prior to adoptive cell transfer. All recipient animals were supplied with 10 x 10^6 freshly isolated, T-cell depleted, bone marrow cells sourced from an identical donor population as used for preparation of transgenic T-cells, to preclude lethality from haematopoietic failure following TBI preconditioning.

Due to poor transduction efficiency, difficulty with MACS selection and poor viability of the transgenic splenocytes, our pilot experiment resulted in only one Balb/c mouse being infused with 3 x 10^6 MACS sorted splenocytes in addition to supplemental bone marrow as described, which was assessed against two control Balb/c mice which were supplied with only the bone marrow infusion. Animals were assessed for evidence of GvHD pathology during the experiment by weight and GvHD scoring assessments. GvHD scoring parameters are indicated by **Table 12**.

Table 12 GvHD scoring parameters
Animals were scored based on progressive weight loss and a range of subjective criteria as indicated. Further, indication of diarrhoea and/or weight loss greater than 10% each resulted in a score of 1. According to licence parameters, euthanasia was required when weight loss remained beyond 20% or if the cumulative GvHD score ≥4.

GvHD scoring parameter	Range
Grooming	0-2
Posture	0-2
Activity	0-2
Eyes	0-2
Diarrhoea	0 or 1
Weight loss	0 or 1

9.3.2. Evidence of engraftment and GvHD

Although weight loss is typically observed following pre-conditioning irradiation, it is anticipated that with normal feeding behaviour weight will return to normal. This pattern of weight loss followed by recovery was observed for both control mice, whereas in the experimental mouse, the initial weight loss was more profound and despite a brief reduced recovery, the animal remained underweight for the duration of the experiment as illustrated by Figure 70.

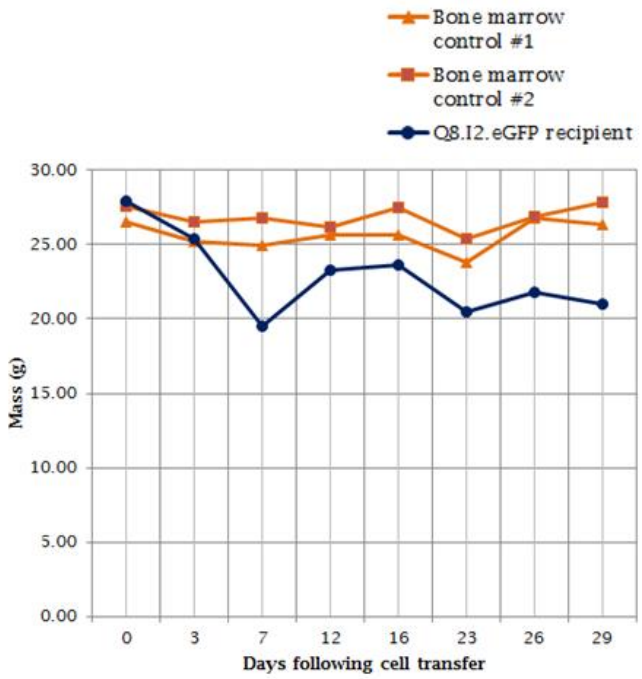

Figure 70 GvHD induction pilot: animal mass versus time
Balb/c recipient mice were weighed prior to adoptive transfer of Q8.I2.eGFP transgenic C57BL/6 CD90.1 splenocytes, then subsequently at regular intervals throughout the experiment to assess progression of GvHD pathology. As illustrated, all mice demonstrated weight loss following X-ray TBI. However, although control mice demonstrated rapid recovery to starting mass, the adoptive transfer recipient remained below starting mass throughout the experimental window.

By day 26, noting that control animals had demonstrated weight recovery contrasting with sustained and progressive weight loss observed in the experimental animal, peripheral blood analysis was performed to establish whether a transgenic population could be identified. As illustrated by Figure 71, there was clear evidence of the presence of a transgenic population of T-cells as indicated by the presence of an QBEnd10-eGFP co-expressing

population. Furthermore, following from clear evidence indicating reduction of the Thy1.1 lymphocyte compartment suggestive of GvHD pathology, all animals were sacrificed three days later, twenty-nine days following cellular infusion. Spleen, bone marrow and lymph node compartments were analysed by flow cytometry analysis to assess the haematological chimerism present at experimental termination, with samples of large bowel, skin, liver and lung submitted for histological examination.

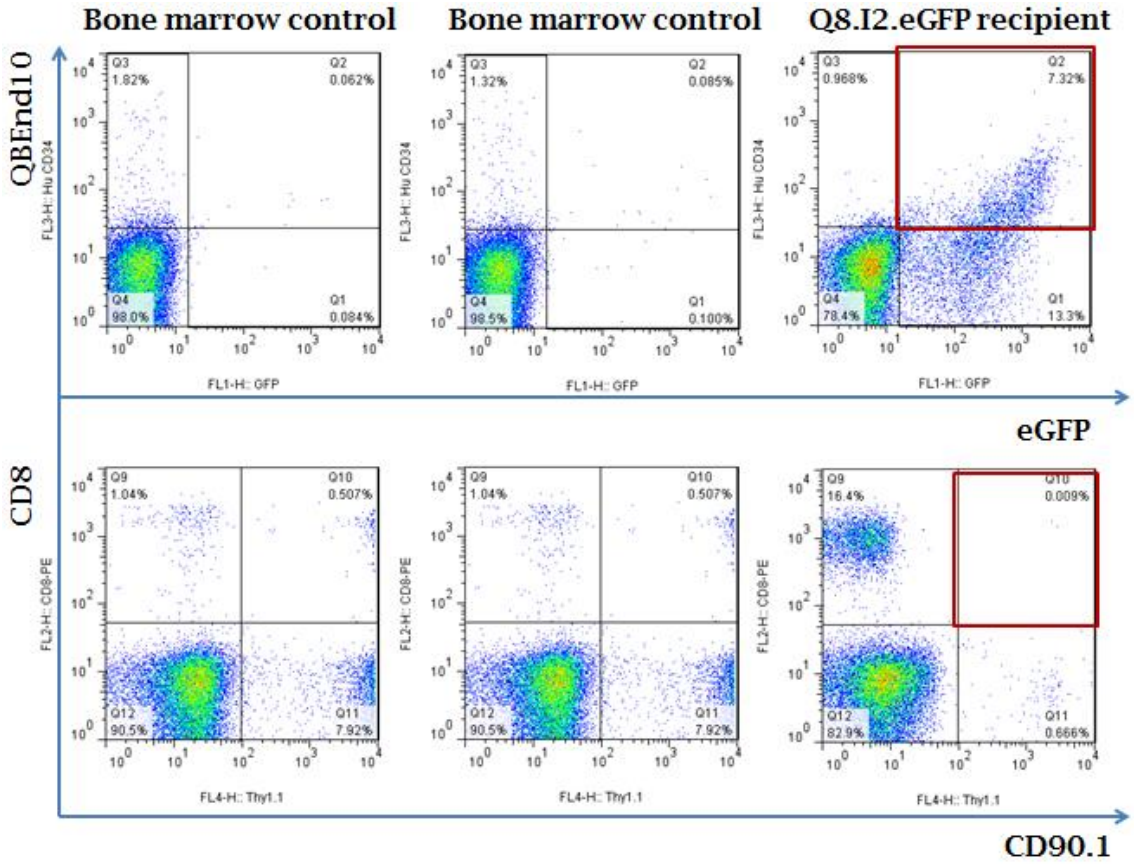

Figure 71 Day 26 Peripheral blood analysis from GvHD induction pilot
To assess engraftment in our ACT C57BL/6 to Balb/c acute GvHD induction pilot, peripheral blood was assessed for presence of engraftment 26 days post ACT. Evidence of engraftment was observed as illustrated by the top row, whilst evidence of GvHD, as indicated by reduction in the host Thy1.1 compartment (bottom row).

9.3.2.1. Evidence of cellular engraftment at experiment termination

Observation of clear engraftment of a transgenic population was observed in all compartments demonstrating successful engraftment of donor cells. Evidence of engraftment from spleen and bone marrow are illustrated by Figure 72.

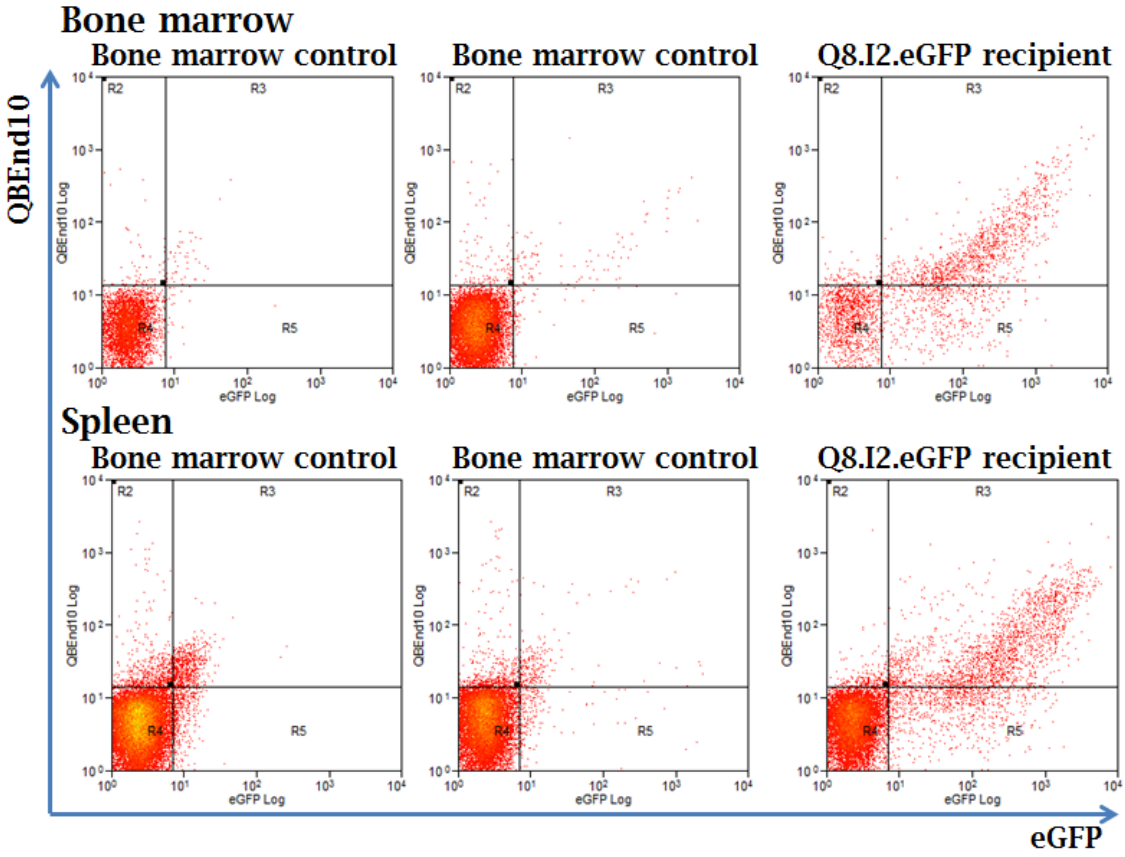

Figure 72 GvHD pilot terminal spleen and bone marrow engraftment
Following sacrifice of experimental animals, spleen and bone marrow samples were examined to assess engraftment from the C57BL/6 to Balb/c acute GvHD pilot experiment. As illustrated, we observed clear evidence of transgenic T-cell engraftment in both spleen and bone marrow as identified by co-expression of QBEnd10 and eGFP marker genes.

9.3.2.2. Evidence of GvHD at experiment termination

Due to the non-myeloablative pre-conditioning irradiation, a residual population of host bone marrow cells would be predicted to be present within the observed haematological repopulation resulting in a chimeric population of $CD4^+/CD8^+$ T-cells derived from both donor and the host mouse. However, during GvHD, donor $CD8^+$ cytotoxic T-cells (CTL's) target and lyse host tissues following recognition of minor histocompatibility antigens expressed on the host cells. Clear evidence of deletion of residual host $CD4^+/CD8^+$ cells was observed in all compartments, with only the lymph nodes demonstrating a significant reservoir of host T-cells illustrated by Figure 73.

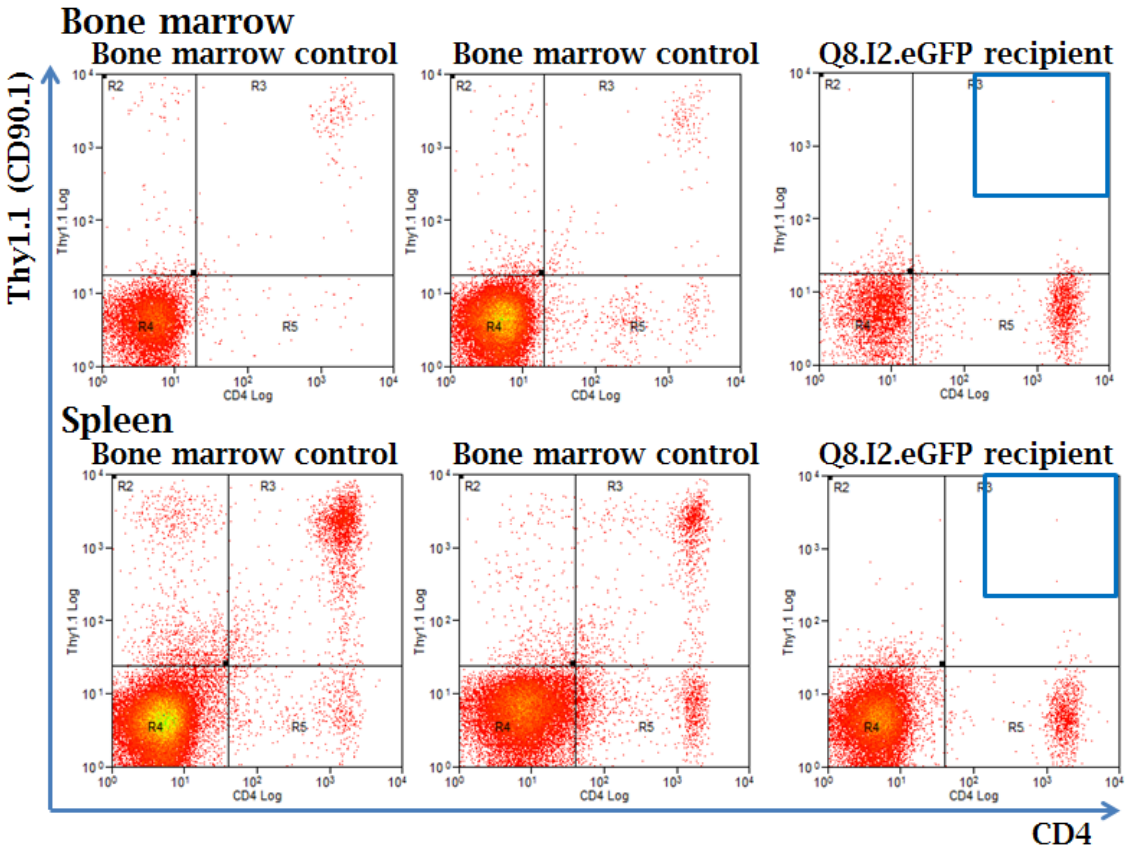

Figure 73 Evidence of GvHD pathology from GvHD induction pilot
Following sacrifice of experimental animals, spleen and bone marrow samples were examined for evidence of deletion of host lymphocytes which could be identified as the Thy1.1 positive population. Non-myeloablative conditioning results in haematopoietic chimerism post-transfer reflecting both donor and recipient populations following haematopoietic reconstitution. Depletion of the Thy1.1 compartment as evidenced by the Q8.I2.eGFP recipient is suggestive of GvHD pathology.

Finally, we observed clear histological evidence of GvHD from the gut tissue sections as indicated by: ulceration and crypt abscess formation, Lamina propria infiltration and loss of villae structure in the section of recipient Balb/c gut when compared against an equivalent tissue section obtained from a control animal as illustrated by Figure 74.

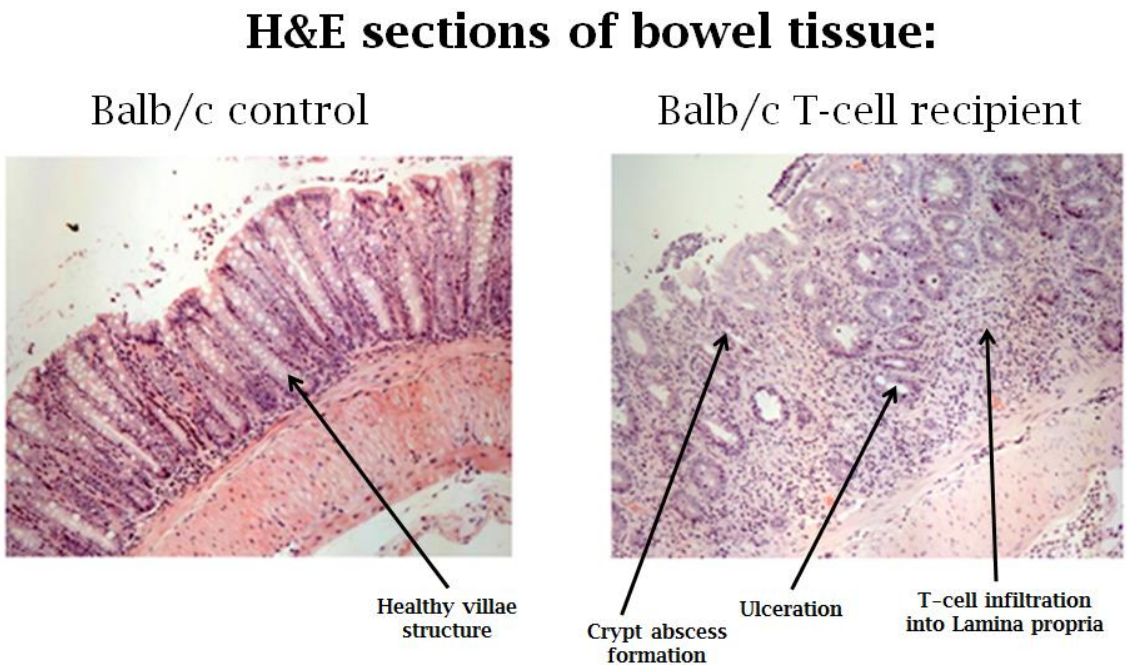

Figure 74 Evidence of GvHD-mediated tissue damage from induction pilot
Following sacrifice of experimental animals, tissue samples from skin, liver, lung and bowel were examined by H&E staining to identify evidence of GvHD. As illustrated, evidence of GvHD was identified from H&E stained sections of large bowel; GvHD is indicated by ulceration, crypt abscess formation, Lamina propria infiltration and loss of villae structure in the T-cell recipient when compared against a tissue section obtained from a PBS control recipient. This finding was supported by similar evidence from other tissues (not illustrated). Wax embedding, sectioning and H&E staining were performed by the Royal Free hospital pathology department.

9.4. Full scale GvHD model

Experimental aim: To demonstrate rituximab-mediated resolution of GvHD pathology by *in vivo* deletion of RQR8-transgenic splenocytes.

Having successfully demonstrated GvHD induction through a C57BL/6 to Balb/c MHC mismatch model using activated, transduced and MACS-selected splenocytes, our next challenge was to increase the scale and efficiency of splenocyte transduction sufficient to achieve a model of sufficient size as to enable statistical confirmation of efficacy. Having generated sufficient validated supernatant in advance, the experimental model, illustrated by Figure 75, is briefly summarised as follows: splenocytes obtained from 12 female C57BL/6 - Thy 1.1 x 1.2 donor mice were transduced with SFGmR.RQR8, a construct expressing RQR8 by the SFG LTR promoter, with expression enhanced by inclusion of the human beta interferon S/MAR domain to maintain sustained transgene expression using the 5-day protocol

illustrated by Figure 60. Recipient animals, (female Balb/c Thy 1.1), were prepared by a split-dose 8Gy X-ray TBI pre-conditioning regimen, 48 hours and 4 hours prior to adoptive cell transfer i.v. by tail-vein injection. Engraftment was assessed by peripheral blood draws, obtained 7 and 14 days following T-cell transfer, with mRtx-IgG2a therapy infused randomly into ½ of T-cell recipients following acquisition of the day 7 blood sample to enable a preliminary confirmation of progression of therapeutic activity. Disease progression was assessed by tri-weekly weight and GvHD scoring assessments as required by the project licence. Weight loss ≥ 20% of starting mass, or a cumulative GvHD score of 4, based upon grooming, hunching, activity, eyes and presence of diarrhoea necessitated euthanasia of the animal(s). Our therapeutic dosing regimen of 3 weekly infusions of 150µg mRtx-IgG2a injected i.p. was based from a report describing an analogous suicide gene strategy encompassing a co-expression construct expressing codon optimised CD20 as the suicide gene moiety and a truncated form of CD34 as the marker gene[154]. Although experimental termination had been planned for 37 days post T-cell transfer, a sharp progression of GvHD symptoms necessitated sacrifice of the entire PBS therapy cohort and one animal from the mRtx-IgG2a therapy cohort 29 days following T-cell transfer. Limited resources delayed sacrifice of the remaining animals until the original experimental endpoint as planned.

Figure 76 illustrates the comparative depletion/progression of engraftment as assessed by peripheral blood assessments at days 7, 14 and at experimental termination. Figure 77 illustrates animal mass and GvHD scoring across the duration of the experiment. Figure 79 to Figure 82 illustrate RQR8 engraftment from the tissues assessed at experimental termination. Notably, although some PBS therapy controls appears to indicate comparatively poor engraftment, the presence of thin QBEnd10^{-}/CD8^{-} populations appear to indicate reduced engraftment resulting from loss of stromal support due to profound tissue damage suggestive of lethal GvHD, such as indicated by PBS controls 1, 4 and 6 in Figure 79.

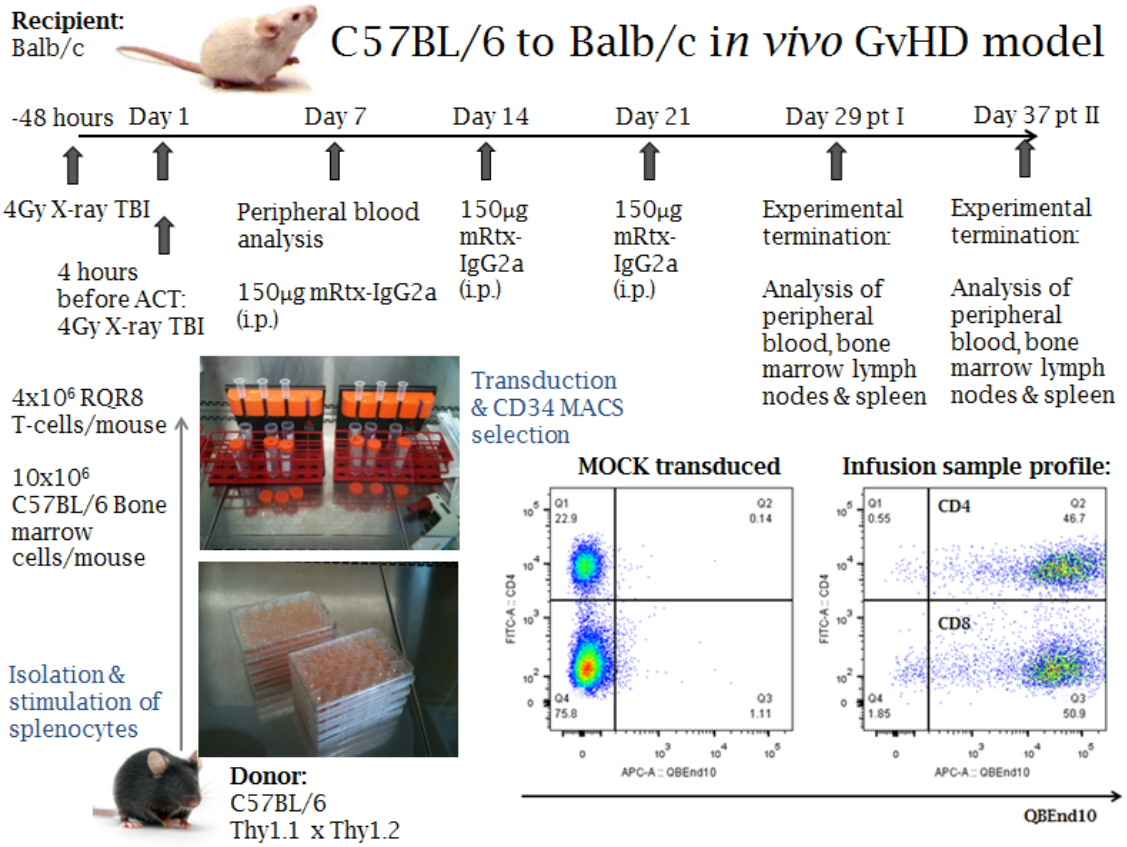

Figure 75 C57BL6 to Balb/c acute GvHD MHC-mismatch model design
Primary murine splenocytes isolated from C57BL/6 donors were prepared according to the 5-day protocol as detailed in 7.5 and infused into X-ray TBI pre-conditioned Balb/c recipients. Verification of effective engraftment was assessed by flow cytometry analysis of peripheral blood isolated 7 days post transfer. Mice were supplied with weekly doses of rituximab therapy, 150ug i.p., or PBS carrier. Animals demonstrating poor health were euthanased 29 days post transfer; remaining animals were culled 37 days post transfer.

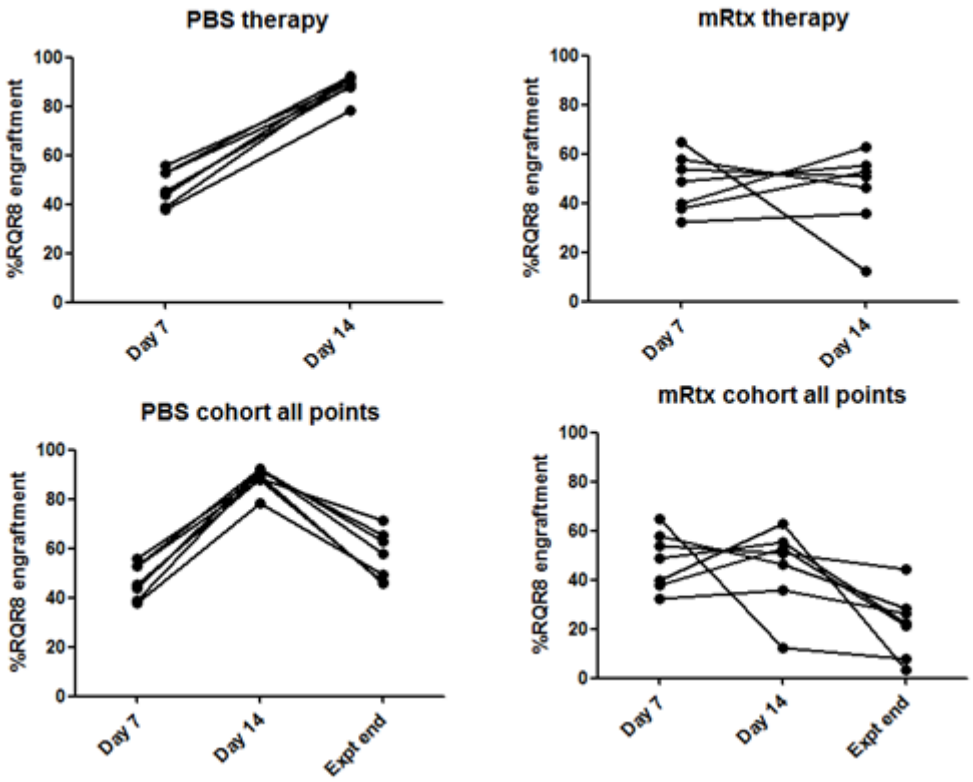

Figure 76 Peripheral blood analyses from GvHD MHC-mismatch model
Peripheral blood samples were obtained at timepoints as indicated and assessed by flow cytometry for donor T-cell engraftment. As illustrated by the top row, PBS carrier recipients demonstrated progressive expansion whilst engraftment levels in mRtx-IgG2a therapy recipients appeared to remain stable 7 days following the initial therapeutic administration. Lower row: declining levels of T-cell engraftment was observed in both control and mRtx-IgG2a therapy cohorts by the end of the experimental window although engraftment levels in mRtx-IgG2a therapy recipients remained substantially lower than what was observed from PBS therapy control recipients. Note: euthanasia imposed experimental termination for PBS therapy cohort occurred 29 days post transfer, whilst experimental end for the mRtx-IgG2a cohort was elective at 37 days post transfer. RQR8 engraftment was defined as a proportion of the entire T-cell subset.

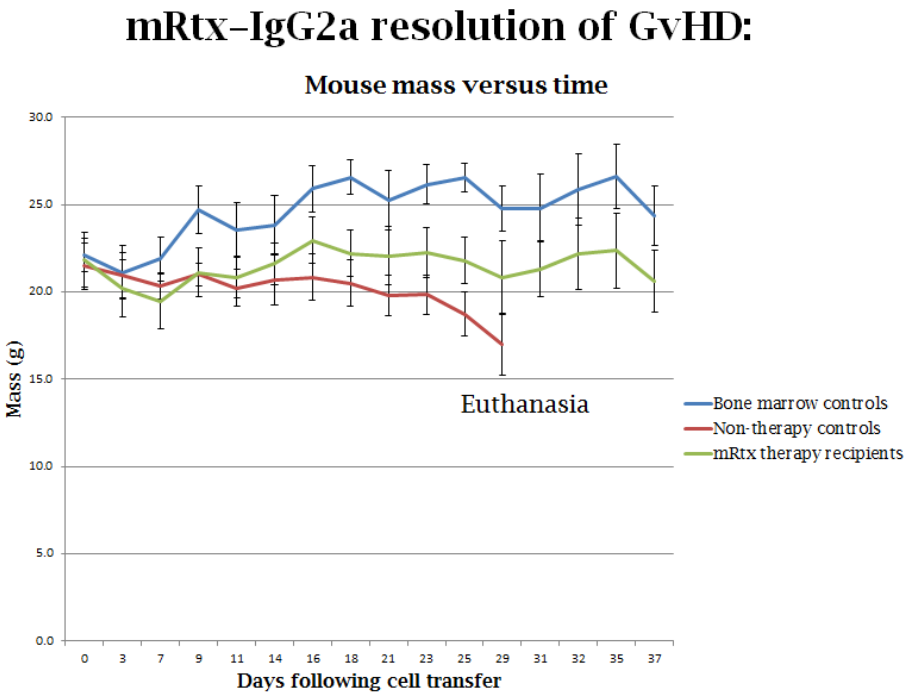

Figure 77 Animal mass versus time in GvHD model
Following licence requirements, indirect assessments of disease progression were performed throughout the experimental window including animal mass as illustrated. Animals were euthanased where weight loss or GvHD scoring reached severity criteria. Although all animals appeared to demonstrate weight loss following X-ray TBI conditioning, control animals demonstrated rapid recovery. In contrast, PBS therapy recipients demonstrated progressive weight loss leading to euthanasia imposed experimental termination. In contrast mRtx-IgG2a therapy recipients appeared to demonstrate partial recovery with animal mass remaining greater than PBS control cohort but failing to achieve recovery demonstrated by bone marrow control recipients.

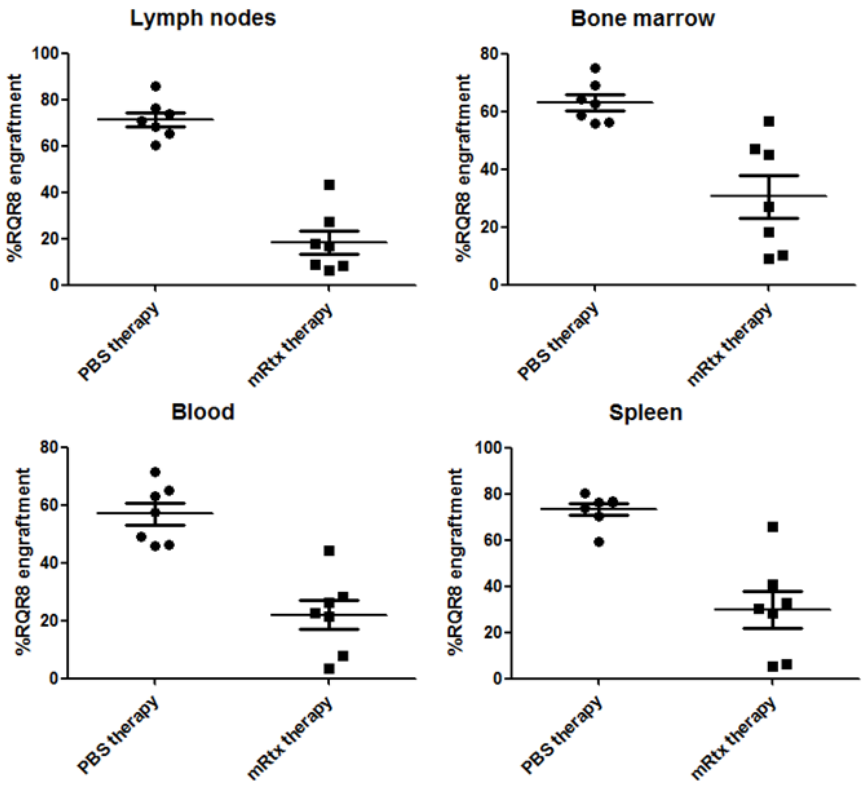

Figure 78 Engraftment comparisons from acute GvHD model
At experimental termination, peripheral blood, spleen, bone marrow and lymph node compartments were assessed for levels of T-cell engraftment. Evidence of mRtx-IgG2a mediated T-cell clearance was observed in all compartments as illustrated. Note: all PBS carrier controls and one mRtx-IgG2a therapy recipient were euthanased due to weight loss and GvHD scoring 29 days following T-cell infusion with all remaining animals culled 37 days following T-cell infusion.

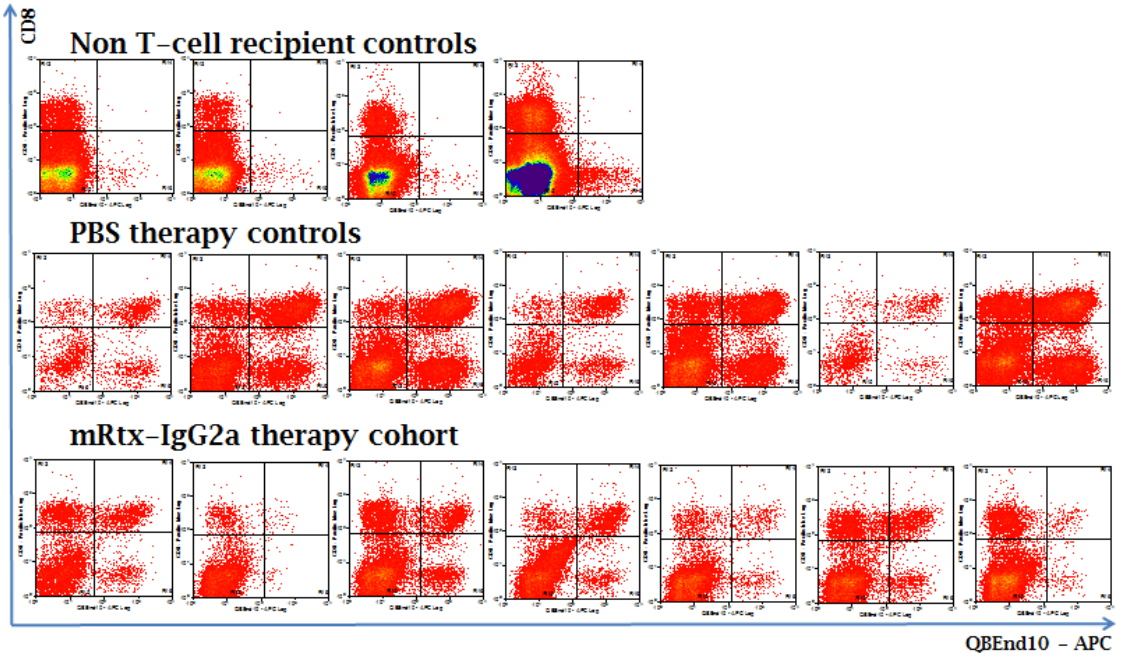

Figure 79 Acute GvHD model – RQR8 engraftment in spleen
At experimental termination, peripheral blood, spleen, bone marrow and lymph node compartments were assessed for levels of T-cell engraftment. As illustrated, primary data illustrates evidence of reduction of engraftment but without achieving clearance in mRtx-IgG2a therapy recipients. In contrast, PBS control recipients demonstrated substantial engraftment; where engraftment of controls appeared modest, there was a coincident reduction in the non-T-cell fraction highlighting splenic destruction as observed during organ harvest.

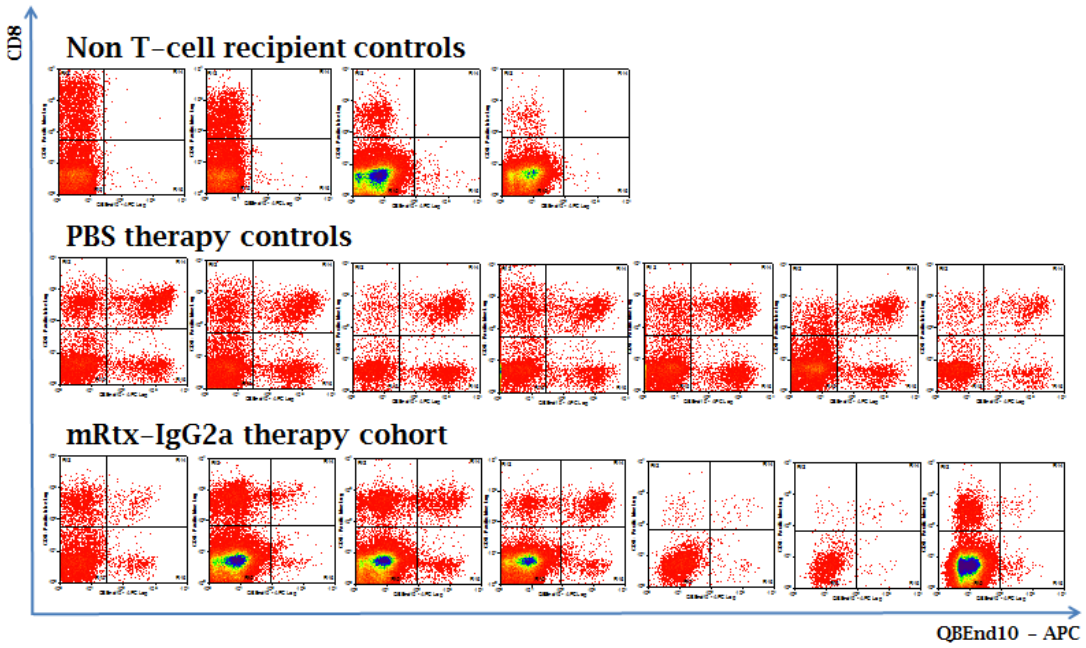

Figure 80 Acute GvHD model – RQR8 engraftment in bone marrow
At experimental termination, peripheral blood, spleen, bone marrow and lymph node compartments were assessed for levels of T-cell engraftment. As with Figure 79 previously but even more evident, primary data illustrates evidence of reduction of engraftment but without achieving clearance in mRtx-IgG2a therapy recipients. In contrast, PBS control recipients'

demonstrated consistent engraftment, with consistent evidence of a reduction in the non-T-cell fraction highlighting marrow destruction as observed during organ harvest.

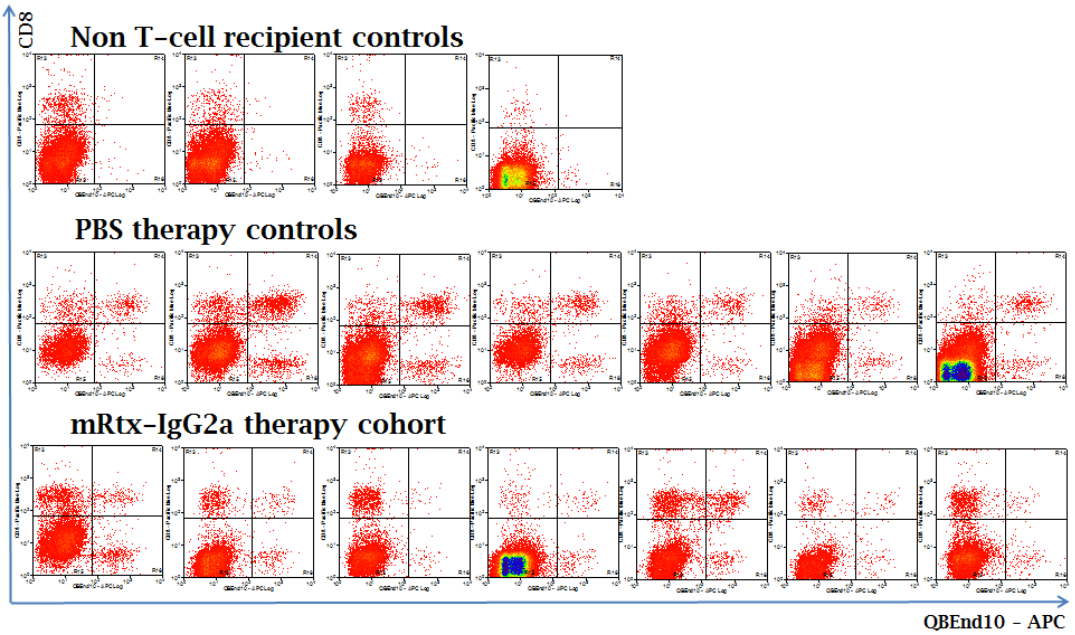

Figure 81 Acute GvHD model – RQR8 engraftment in blood
At experimental termination, peripheral blood, spleen, bone marrow and lymph node compartments were assessed for levels of T-cell engraftment. As with Figure 79 previously, primary data illustrates clear evidence of reduction of engraftment but without achieving clearance in mRtx-IgG2a therapy recipients. In contrast, PBS control recipients demonstrated consistent engraftment.

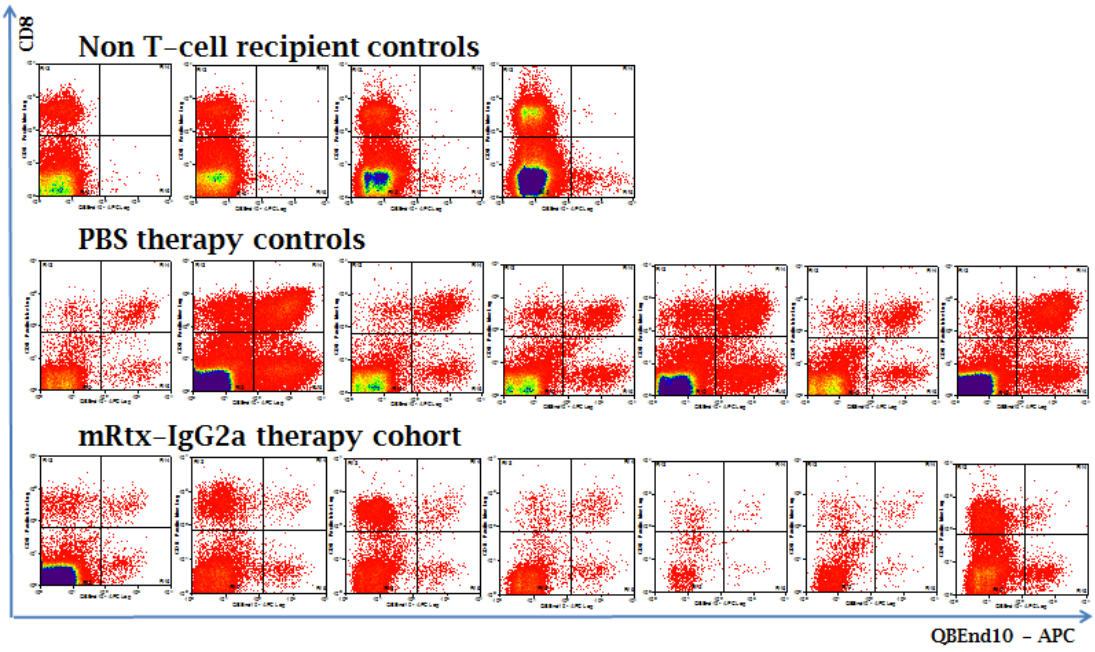

Figure 82 Acute GvHD model – RQR8 engraftment in Lymph nodes
At experimental termination, peripheral blood, spleen, bone marrow and lymph node compartments were assessed for levels of T-cell engraftment. As with Figure 79 previously, primary data illustrates clear evidence of reduction of engraftment but without achieving

clearance in mRtx-IgG2a therapy recipients. In contrast, PBS control recipients demonstrated consistent engraftment.

9.5. Conclusions

Although there was significant evidence of efficacy as illustrated by our results, this model clearly failed to accomplish the desired aim of achieving therapeutic resolution of GvHD. Retrospective review of our research offered insight into limitations and opportunities from these results. Reflecting initial concern regarding the capacity for *ex vivo* manipulated splenocytes to induce GvHD, our experimental design offered excessive attention to the role of inducing disease but insufficient emphasis on the task of ensuring successful therapeutic resolution of pathology in the face of disease. The following points highlight primary factors premised to explain efficacy observed and therapeutic failings from this work.

9.5.1. Choice of acute GvHD model

For the full-scale GvHD model we reprised the MHC mismatch model used in the GvHD induction pilot. Our choice of an acute GvHD model has been reported to induce lethal GvHD 10-21 days following transfer of naïve cells[277], and which from our experience appears to demonstrate a slightly delayed progression when splenocytes are subjected to significant *ex vivo* manipulation. Notably, this model contrasts sharply with the clinical scenario where primary focus is given to HLA-haplotype matching with the aim of achieving GvL benefit whilst ameliorating potential GvHD toxicity. Reflecting difficulties with alteration in scale during the pilot model in which our investigation was limited to a single animal, this precluded further interpretation regarding the rate of GvHD induction. However, observation of GvHD pathology evident from all experimental animals in the full-scale model despite therapeutic intervention highlights the severity of the model. As GvHD remains a potentially lethal complication following HSCT, it seems plausible that the severity of our model reflecting fulminant GvHD may preclude resolution despite therapeutic intervention.

9.5.2. Pre–conditioning regimen

Compounding the T-cell priming potential mediated by MHC mismatch was the decision to employ a severe preconditioning regimen, which was necessary to prevent rejection but which also establishes a highly inflammatory

environment thereby ensuring presence of host antigens to mediate T-cell activation whilst further facilitating haematopoietic space to assist adoptive cellular expansion. However sustained immunodeficiency remains a primary risk associated with HSCT resulting from preconditioning regimens which profoundly impair the capacity to respond against infectious agents, and correspondingly likely results with impaired ADCC during the immunosuppressed window. Assessing cellular depletion following TBI in C57BL/6 mice, Hashimoto *et al.* report profound depletion of DC's, NK-cells and neutrophils as well as T- and B-cells within 48 hours following TBI[280]. This observation potentially highlights a key limitation associated with an antibody-mediated suicide gene strategy. As discussed previously, rituximab is proposed to mediate cellular deletion through three separate mechanisms. However, variant from the native antigen, RQR8 lacks the direct signalling sensitivity as observed with native CD20 reducing the rituximab-mediated mechanisms for deletion to CDC and ADCC. Thus, preconditioning regimens and immunosuppression maintenance strategies which negatively impact upon ADCC effector populations may significantly impair the potential for an antibody-mediated suicide gene strategy to achieve resolution of therapy-related toxicities. Therefore, there might exist a recovery window, as defined by both the preconditioning regimen and the nature of the therapeutic toxicity which might preclude opportunity to attain therapeutic resolution mediated by an antibody-directed suicide-gene system.

9.5.3. Route of therapeutic administration

Although i.p. injection reflects a common therapeutic dosing strategy for *in vivo* modelling, there remains the potential for 'off-target' injection such as into the bowel. Further, as the gut remains a target organ for inflammation during GvHD, it remains plausible that much of the antibody therapy may have been mopped up by gut inflammation proximal to the site of injection impairing the systemic distribution of therapy. Although ip administration was employed in our GvHD modelling experiment, this revised to iv administration for subsequent haploidentical modelling experiments.

9.5.4. Dosing regimen

As indicated, our dosing regimen was modelled on previous research from an analogous marker-suicide gene strategy[154]. Although the ΔCD34/CD20 marker-

suicide gene strategy was similar, there were significant variations in the animal modelling strategy; notably transfer of C57BL/6.Ly5.1 donor cells into Rag-1$^{-/-}$ recipients on the C57BL/6 background in the absence of TBI reflects a profoundly less aggressive model of disease. This was further reflected by slow progression of disease with therapy in the reference paper commencing at a time-point when lethal GvHD had been observed in our model.

As no maximum tolerated dose was identified following dose escalation experiments for rituximab[165], there remains significant potential for increased therapeutic administration in the scenario that our experimental result might have reflected dose-limiting efficacy. Subsequent research employed more robust dosing regimens.

9.5.5. Role of CDC

As suggested previously, the efficacy of CDC-mediated depletion was likely over-represented through *in vitro* CDC assays due to the choice of BRC as the source of complement. Clear evidence of depletion despite impaired ADCC likely reflects some degree of complement mediated deletion, although the respective role of CDC-mediated deletion *in vivo* remains unclear.

9.5.6. Disease progression

Our GvHD model was prematurely truncated due to a sharp progression of behavioural symptoms. Although the role of GvHD has been established, the acceleration might also reflect concurrent termination of antibiotic therapy. To reduce potential for infectious disease following TBI preconditioning, animals were supplemented with Baytril therapy commencing a few days prior to TBI, and maintained for the following 3 weeks. Thus, potential bacterial infection controlled by antibiotic therapy might have accelerated disease progression upon termination of maintenance therapy.

Although our model failed to achieve therapeutic resolution of GvHD, there was clear evidence of efficacy resulting from mRtx-IgG2a therapy. Furthermore, therapeutic shortcomings likely reflect failings in model design which were addressed in subsequent *in vivo* modelling experiments presented in **Error! Reference source not found.**.

9.6. General conclusions

- Using the 5-day protocol as detailed in chapter 7, we have achieved successful increase in scale of cellular production typically generating 5 x 10^6 purified transgenic splenocytes per donor spleen
- The C57BL/6 to Balb/c MHC-I mismatch model facilitates clear engraftment of transgenic splenocytes
- Transduced and MACS selected splenocytes retain functional capacity to induce acute fulminant GvHD
- Therapeutic administration of mRtx-IgG2a demonstrated clear reduction of RQR8 transgenic splenocytes *in vivo*
- Acute toxicity associated with the C57BL/6 to Balb/c MHC-I mismatch model likely precludes mRtx-IgG2a mediated therapeutic resolution at the dosing regimen as initially considered

Chapter ten

10. Refinement of *in vivo* modelling: Haploidentical model

Despite generation of national and international donor registries, inability to locate a suitable HLA-matched donor remains a limitation to HSCT therapy for many patients. For these individuals, haploidentical stem cell transplantation from a half-matched parental donor presents an alternative approach for most cases but with greater risk for development of GvHD[142].

10.1. Aims

- To demonstrate effective engraftment of transgenic C57BL/6 donor splenocytes in (C57BL/6 x Balb/c) CB6F1 recipients
- To confirm progressive engraftment of donor T-cells following adoptive transfer
- To demonstrate deletion of adoptive cells mediated by therapeutic administration of mRtx-IgG2a
- To assess the kinetic progression of mRtx-IgG2a mediated deletion *in vivo*
- To demonstrate retention of the *in vivo* capacity for RQR8-mediated depletion when co-expressed with a CAR

10.2. Introduction

Despite generation of national and international donor databases, donor availability remains a common limitation to allogeneic HSCT therapy. Thus haploidentical HSCT offers an attractive option for many patients lacking a suitable HLA-matched donor. However, haploidentical transplantation remains a high risk strategy due to the high risk of GvHD. Although threat of GvHD can be resolved through T-cell depletion, this effectively exchanges the risk from morbidity and mortality due to GvHD for that resulting from sustained immunodeficiency. Numerous strategies, designed to resolve or reduce the risk from GvHD through graft modification, have been identified, however none manage to also fully address the threat imposed by profound immunodeficiency which can only be resolved through transfer of a mature population of T-cells possessing a replete polyclonal repertoire[142].

10.2.1. Haploidentical model paradigms

There exist two clinical paradigms for our experimental query, each involving suicide gene therapy employed in conjunction with haploidentical transfer; the TK007 trial[142] and the iCasp9 trial[125]. Briefly, in the TK007 trial, patients presenting with high risk leukaemias were treated with T-cell depleted, haploidentical HSCT. Patients demonstrating successful engraftment were subsequently supplemented with monthly serial DLI infusions (as required), composed of purified T-cell product transgenic for HSVtk and the ΔlNGFR marker gene derived from the same donor as used for HSCT, and commencing 28 days post HSCT. In this trial, 28 patients successfully progressed to receive DLI post HSCT with 22/28 demonstrating successful $HSVtk^+$ T-cell engraftment. Following DLI, 11/22 patients developed GvHD; 10 acute and 1 chronic. Where ganciclovir therapy was supplied in isolation, GvHD resolution was achieved within 14 days, with 5 patients requiring combination therapy (cyclosporine or prednisone), to achieve complete resolution of GvHD; notably all instances of GvHD were resolved in this trial[142]. Similarly, the iCasp9 trial recruited patients presenting with relapsed leukaemia which were initially treated with T-cell depleted, haploidentical HSCT. Following demonstration of successful engraftment, 5 patients were subsequently infused with purified T-cell product transgenic for iCasp9 and the ΔCD19 marker gene derived from the same donor as used for HSCT. In this trial, 4/5 patients progressed to develop GvHD which was rapidly resolved in all cases following administration of a single dose of the dimeriser drug which was observed to eliminate >90% of T-cells within 30 minutes of therapeutic administration[125].

Thus, following from the clinical precedent of haploidentical modelling, we revised our *in vivo* modelling strategy accordingly to assess the efficacy of RQR8-mediated deletion in a comparable experimental setting.

10.2.2. Features of haploidentical experimental design

When defining conditions for our haploidentical model, we adjusted a number of critical parameters which were premised to have been critical in limiting the efficacy of mRtx-IgG2a mediated depletion which was previously demonstrated; including the degree of TBI preconditioning, the experimental duration, the therapeutic dosing regimen, infusion strategy and finally the dosage of cellular product as indicated by Table 13.

Table 13 Key variations between GvHD and haploidentical models

Parameter	GvHD model	Haploidentical model
TBI preconditioning	8 Gy	5Gy
Experimental duration	37 days	14 days
Cellular infusion dose	4 x 10^6/mouse	1.5 x 10^6/mouse
Therapeutic dosing regiment	150µg/mouse/week	3 x 150µg/mouse/week
Route of therapy administration	i.p.	i.v.

In the MHC-I mismatch model, high-dose TBI was necessary to prevent donor rejection by host effectors. However in the haploidentical setting, although donor cells will respond against host alloantigens, recipients remain tolerant for donor MHC antigens preventing donor rejection and thereby allowing for milder preconditioning regimens which would hopefully ensure greater retention of the ADCC effector compartment. As the CB6F1 mice typically demonstrate a higher radio-tolerance than Balb/c animals (personal communication with Dr. Sergio Quezada), we employed a preconditioning dosage of 5 Gy TBI. Premising that our initial rituximab dosage might have been limiting, we increased the dosage to three doses administered within one week, by i.v. administration to prevent potential of impaired uptake from enteric inflammation. Finally, we considered a shorter experimental window alongside a lower infusion dose, selected to avoid fulminant disease precluding therapeutic resolution.

10.3. Results: Haploidentical transfer and depletion models

Experimental aim: To demonstrate *in vivo* rituximab-mediated deletion of RQR8 transgenic splenocytes through haploidentical transfer experiments mimicking reported clinical application of current suicide genes[125, 142].

In light of limitations identified from previous GvHD modelling experiments, we initially sought to demonstrate effective rituximab mediated depletion of RQR8 transgenic splenocytes examined through a more clinically relevant haploidentical experimental model with all animals sacrificed in parallel at a single experimental termination point; data presented in 10.3.1. Having

identified clear efficacy of rituximab-mediated depletion 7-days following commencement of rituximab therapy, efficacy and progression of depletion was further scrutinised through an experimental time-course examining RQR8 recipient subjects sacrificed at serial timepoints up to and including the 7-day time-point examined initially; data presented in 10.3.2. Finally, with respect to the future application of RQR8 in conjunction with CAR therapy, we examined the capacity for rituximab-mediated depletion of RQR8 expressing splenocytes co-expressing a CD19 CAR; data presented in 10.3.3.

10.3.1. Haploidentical depletion model

Experimental aim: To demonstrate effective mRtx-IgG2a mediated deletion of RQR8-transgenic splenocytes in a haploidentical transfer model contrasting with continued engraftment in the absence of therapeutic administration.

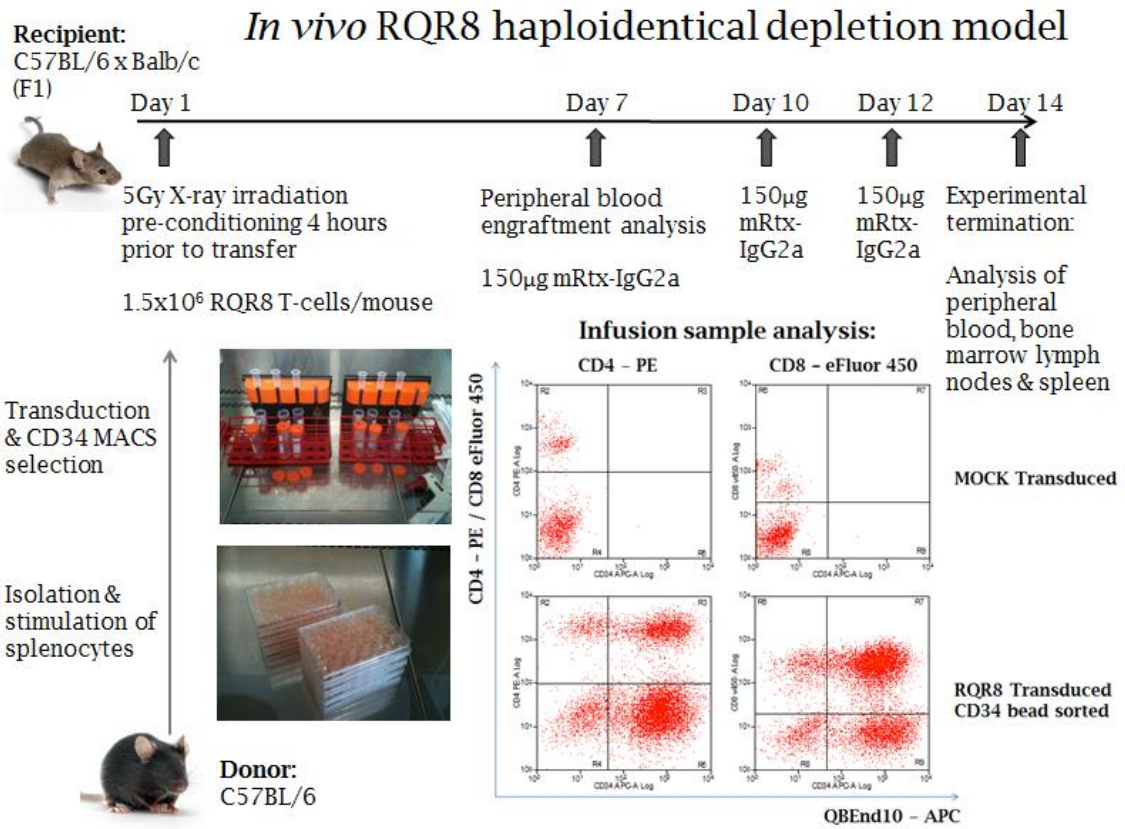

Figure 83 C57BL/6 to CB6F1 haploidentical transfer model design
CB6F1 (C57BL/6 x Balb/c) recipients were preconditioned with 5Gy X-ray TBI 4 hours prior to cellular infusion of CD34 magnetic bead purified RQR8 transgenic splenocytes derived from C57BL/6 donors. Engraftment was confirmed by peripheral blood analysis seven days post T-cell transfer prior to progression with mRtx-IgG2a therapy. At sacrifice, peripheral blood, spleen, lymph nodes and bone marrow compartments were examined to confirm efficacy of mRtx-IgG2a mediated deletion.

Splenocytes isolated from 10 female C57BL/6 donor mice were transduced and purified for expression of SFGmR.RQR8 using the 5-day protocol. Female CB6F1 (C57BL/6 x Balb/c) recipient animals were preconditioned by 5 Gy single dose X-ray TBI 4 hours prior to adoptive cell transfer of 1.5 x 10^6 SFGmR.RQR8 cells/mouse infused i.v. by tail-vein injection. Successful T-cell engraftment was confirmed by flow cytometry analysis from a peripheral blood draw obtained 7 days following T-cell transfer. Animals were separated into 2 cohorts receiving either mRtx-IgG2a therapy or PBS carrier, infused i.v. on days 7, 10 and 12. Fourteen days following T-cell transfer, all experimental animals were sacrificed with samples from blood, spleen, lymph nodes and bone marrow obtained and assessed by flow cytometry for evidence of depletion or progressive engraftment. Comparative engraftment/depletion in blood is illustrated by Figure 84, clarity of depletion from spleen samples by flow cytometry analysis illustrated by Figure 85, and efficacy of depletion across all compartments illustrated by Figure 86.

Note regarding the staining strategy employed to assess engraftment at end of experiment: H2Kb is the MHC haplotype present on C56BL/6 splenocytes whilst H2Kd is the MHC haplotype present on Balb/c splenocytes. As CB6F1 mice result from the cross of C57BL/6 and Balb/c parents, they will be positive for both H2Kd and H2Kb, whilst C57BL/6 donors remain single positive. Thus, inclusion of H2Kb and H2Kd antibodies within our staining panel serves as a strategy to facilitate donor cell marking thereby supporting our claim regarding the efficacy of rituximab-mediated RQR8 depletion which was achieved.

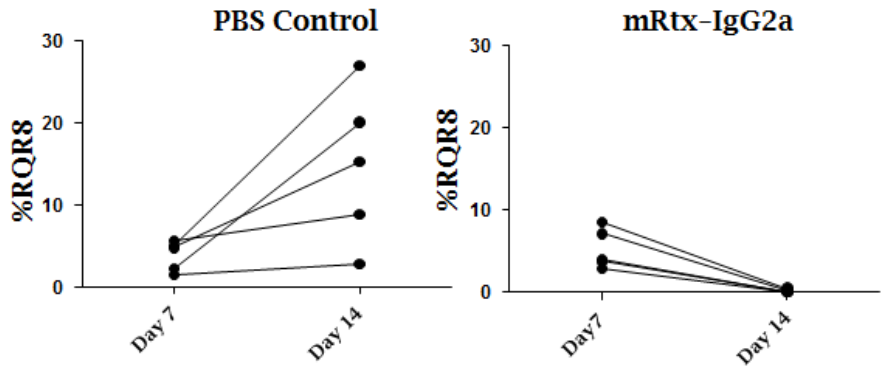

Figure 84 Haploidentical transfer model blood engraftment analysis
C57BL/6 splenocytes were retrovirally transduced to express RQR8 and selected to >90% purity with Miltenyi CD34 beads. 1.5 million of these cells were injected i.v. into 5Gy X-ray preconditioned C57BL/6 x Balb/c cross (F1) recipients. Seven days post transfer engraftment was assessed by peripheral blood analysis. mRtx-IgG2a therapy commenced with 150ug doses at day 7, 10 & 12 by i.v. injection, or PBS carrier for the control cohort. Each cohort comprised 5 mice with an additional 3 control mice irradiated but given neither T-cells nor mRtx-IgG2a. Animals were sacrificed at day 14 with engraftment assessed by considering the proportion of QBEnd10 positive T-cells as a proportion of the T-cell population. Intra-animal assessment of engraftment was achieved by comparison between peripheral blood engraftment 7 days post-T-cell transfer prior to commencement of mRtx-IgG2a therapy and 7 days post therapy. As illustrated, PBS therapy recipients demonstrated progressive engraftment with time whilst mRtx-IgG2a therapy recipients achieved RQR8 clearance.

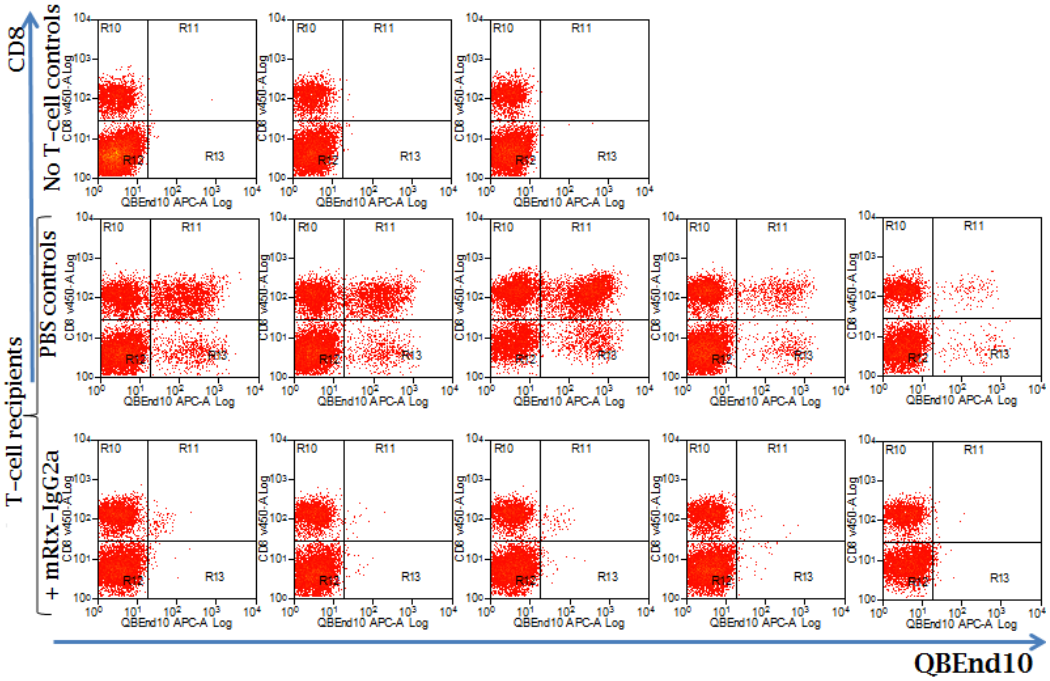

Figure 85 Haploidentical transfer model – RQR8 engraftment in spleen
C57BL/6 splenocytes were retrovirally transduced to express RQR8 and selected to >90% purity with Miltenyi CD34 beads. 1.5 million cells were injected i.v. into 5Gy X-ray preconditioned C57BL/6 x Balb/c cross (F1) recipients. At experimental termination, peripheral blood, spleen, bone marrow and lymph node compartments were assessed for levels of T-cell engraftment. As illustrated, primary data illustrates clear deletion of RQR8-transgenic T-cells

from the spleen in mRtx-IgG2a therapy recipients contrasting with profound engraftment observed in PBS therapy controls.

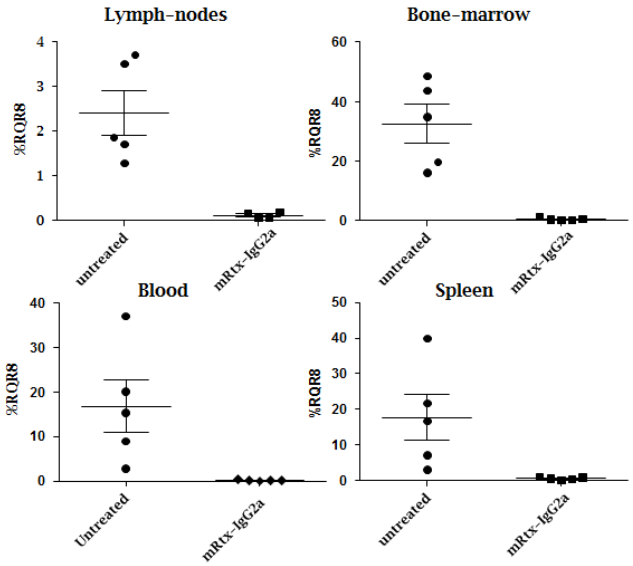

Figure 86 Haploidentical transfer model – RQR8 depletion summary
C57BL/6 splenocytes were retrovirally transduced to express RQR8 and selected to >90% purity with Miltenyi CD34 beads. 1.5 million cells were injected i.v. into 5Gy X-ray preconditioned C57BL/6 x Balb/c cross (F1) recipients. At experimental termination, peripheral blood, spleen, bone marrow and lymph node compartments were assessed for levels of RQR8-transgenic T-cell engraftment as a proportion of the entire T-cell subset. As illustrated, mRtx-IgG2a therapy affords effective clearance from all compartments assessed contrasting with clear evidence of engraftment observed for all PBS therapy controls.

10.3.2. Haploidentical time-course

Experimental aim: To assess the kinetics and progression of mRtx-IgG2a mediated deletion of RQR8-transgenic splenocytes in a haploidentical transfer model.

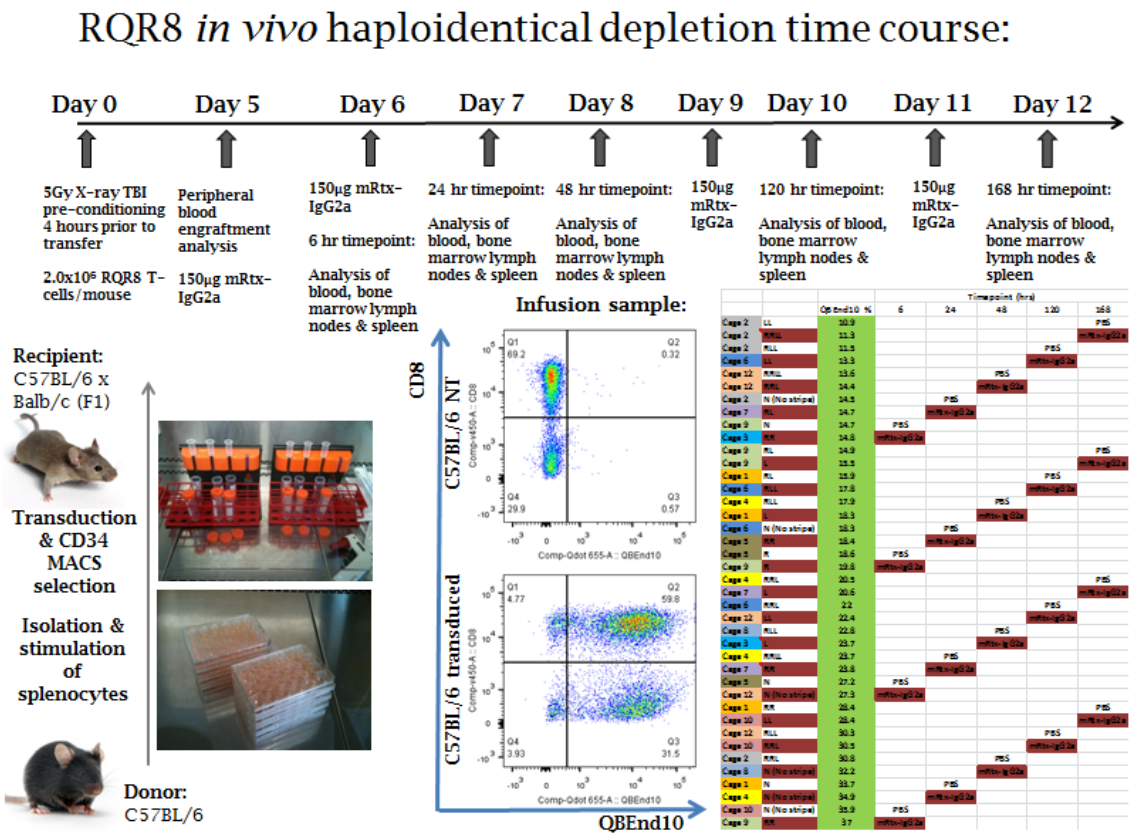

Figure 87 C57BL/6 to CB6F1 haploidentical transfer timecourse model
C57BL/6 splenocytes were retrovirally transduced to express RQR8 and selected to >90% purity with Miltenyi CD34 beads. 2.0 million cells were injected i.v. into 5Gy X-ray preconditioned C57BL/6 x Balb/c cross (F1) recipients with engraftment confirmed by peripheral blood analysis six days following T-cell transfer. Subjects were separated into 10 cohorts based on engraftment levels with each pair of therapy/control cohorts sacrificed at serial timepoints as indicated. PBS or mRtx-IgG2a therapy commenced with 150ug doses at day 7, 10 & 12 by i.v. injection. At experimental termination, peripheral blood, spleen, bone marrow and lymph node compartments were assessed for levels of RQR8-transgenic T-cell engraftment as a proportion of the entire T-cell subset.

Splenocytes obtained from 24 female C57BL/6 donor mice were transduced and purified for expression of SFGmR.RQR8 using the 5-day protocol. Female CB6F1 (C57BL/6 x Balb/c) recipient animals were preconditioned by 5 Gy single dose X-ray TBI 4 hours prior to adoptive cell transfer of 2.0 x 10^6 SFGmR.RQR8 cells/mouse infused i.v. by tail-vein injection. Successful T-cell engraftment was confirmed by flow cytometry analysis from a peripheral blood draw obtained 5 days following T-cell transfer.

Subject animals were stratified based upon the proportion of RQR8-transgenic T-cell engraftment as a proportion of the entire T-cell subset and separated into 10 cohorts, each composed of 4 animals selected to establish an mRtx-IgG2a and a PBS therapy cohort pair for all five pre-determined experimental

timepoints. Further, timepoint cohorts were selected such that subject animals would possess corresponding levels of RQR8 transgenic T-cell engraftment. Animals demonstrating enhanced engraftment were preferentially chosen for assessment at earlier timepoints with a view to minimise potential GvHD toxicity. Animals which received neither T-cells nor mRtx-IgG2a therapy posed as staining controls for flow cytometry analysis. Six days following T-cell transfer, 150µg of mRtx-IgG2a therapy was administered i.v. to therapy recipient animals with subsequent experimental terminations performed 6, 24 and 48 hours following therapy. Nine and eleven days following T-cell transfer, (72 and 120 hours following initial therapy dosage respectively), therapy recipient animals were infused with further 150µg doses of mRtx-IgG2a therapy by i.v. where tail-vein integrity allowed or by i.p. if not, such that animals sacrificed at the 120 and 172 hour timepoints had received 2 and 3 therapeutic doses respectively, matching the therapeutic dosing regimen as employed in 10.3.1 previously. Efficacy of depletion illustrated by

Figure 88 to Figure 94; please note that that flow cytometry plots illustrated by Figure 89 to Figure 92 reflect depletion at the 48 hour timepoint following a single therapeutic administration of rituximab.

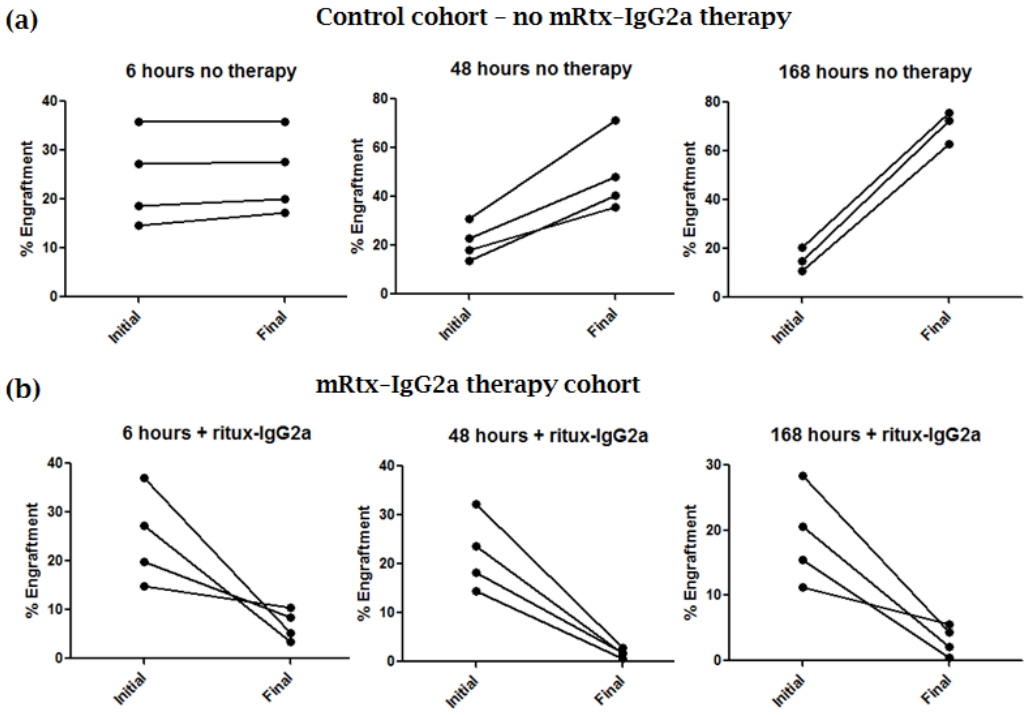

Figure 88 Engraftment/depletion progressions in haploidentical timecourse
C57BL/6 splenocytes were retrovirally transduced to express RQR8 and selected to >90% purity with Miltenyi CD34 beads. 2.0 million cells were injected i.v. into 5Gy X-ray preconditioned C57BL/6 x Balb/c cross (F1) recipients. At experimental termination termination timepoints as indicated, peripheral blood, spleen, bone marrow and lymph node compartments were assessed for levels of RQR8-transgenic T-cell engraftment as a proportion of the entire T-cell subset. (a) PBS-therapy controls illustrating progression of cellular engraftment (b) mRtx-IgG2a therapy recipients demonstrating rapid and progressive depletion of RQR8 marked cells.

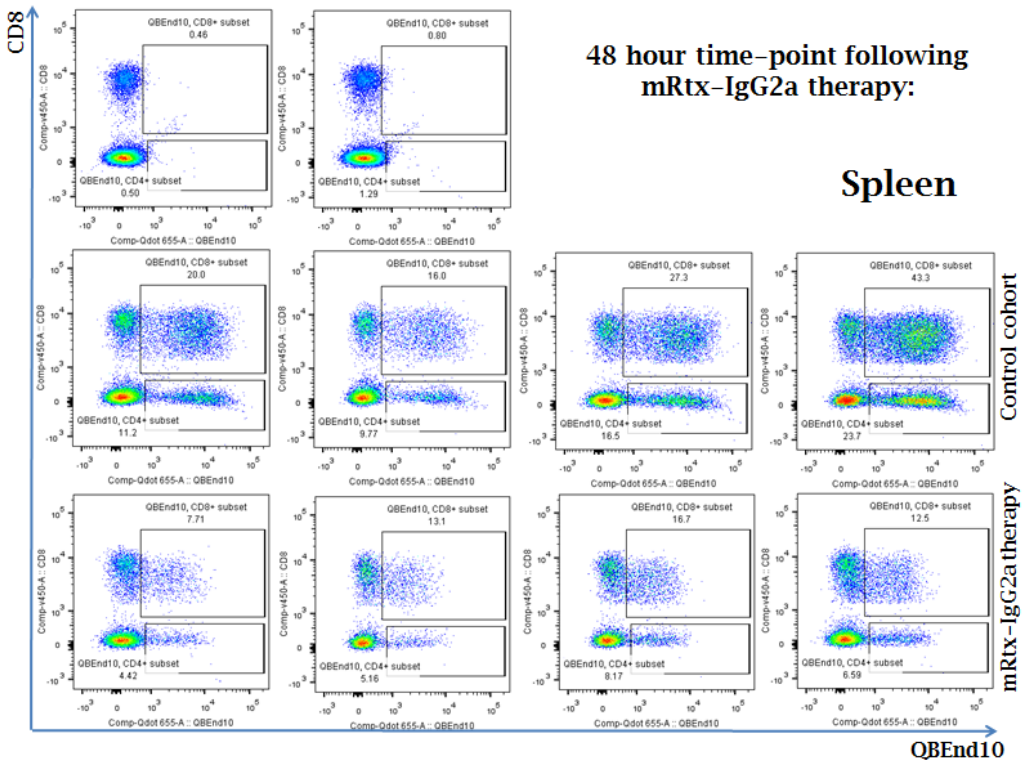

Figure 89 Haploidentical timecourse: Engraftment/depletion from spleen
C57BL/6 splenocytes were retrovirally transduced to express RQR8 and selected to >90% purity with Miltenyi CD34 beads. 2.0 million of these cells were injected i.v. into 5Gy X-ray preconditioned C57BL/6 x Balb/c cross (F1) recipients. 48 hours following mRtx-IgG2a or PBS carrier therapy, blood, spleen, bone marrow and lymph node compartments were assessed for levels of RQR8-transgenic T-cell engraftment as a proportion of the entire T-cell subset. As illustrated by primary data from spleen samples, we observed clear evidence of cellular depletion 48 hours after a single dose of mRtx-IgG2a therapy contrasting with profound T-cell engraftment as indicated by the PBS therapy cohort.

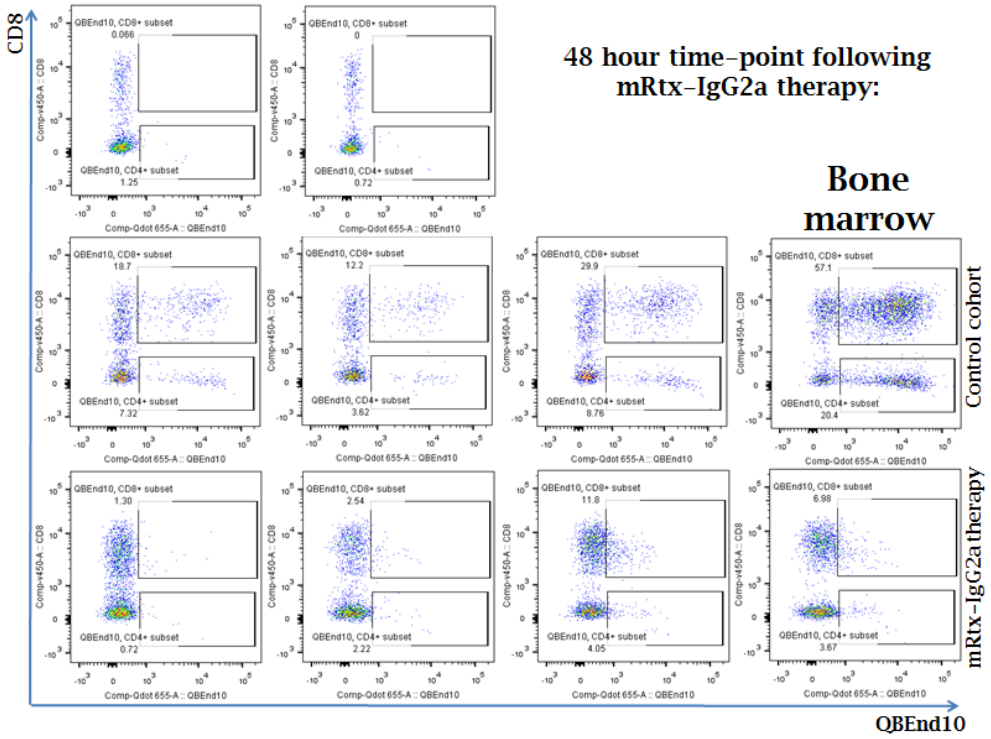

Figure 90 Haploidentical timecourse: Engraftment/depletion from bone marrow

C57BL/6 splenocytes were retrovirally transduced to express RQR8 and selected to >90% purity with Miltenyi CD34 beads. 2.0 million of these cells were injected i.v. into 5Gy X-ray preconditioned C57BL/6 x Balb/c cross (F1) recipients. 48 hours following mRtx-IgG2a or PBS carrier therapy, blood, spleen, bone marrow and lymph node compartments were assessed for levels of RQR8-transgenic T-cell engraftment as a proportion of the entire T-cell subset. As illustrated by primary data from bone marrow samples, mRtx-IgG2a therapy recipients were approaching cellular clearance 48 hours following a single dose of mRtx-IgG2a therapy, contrasting with profound T-cell engraftment as indicated by the PBS therapy cohort.

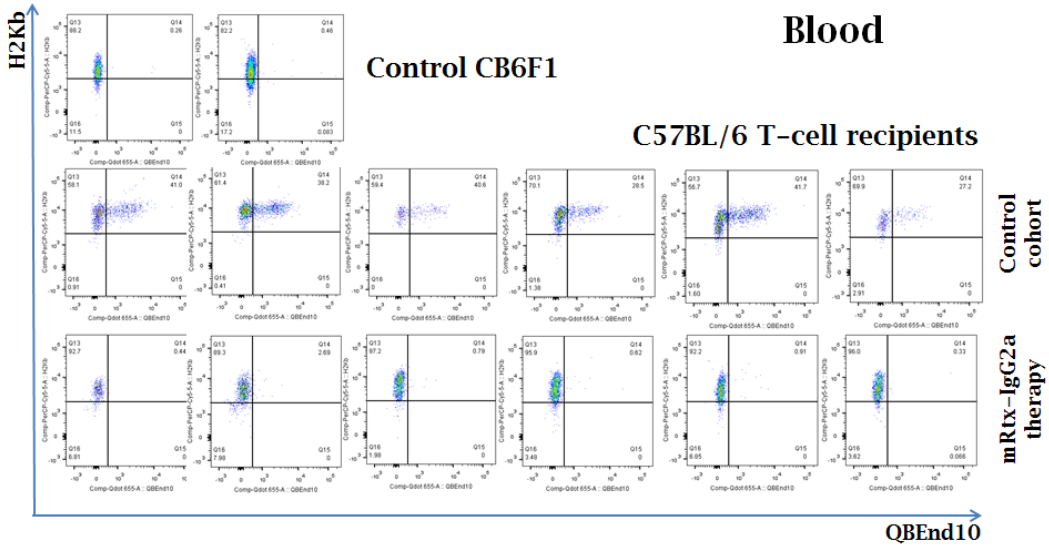

Figure 91 Haploidentical timecourse: Engraftment/depletion from blood

C57BL/6 splenocytes were retrovirally transduced to express RQR8 and selected to >90% purity with Miltenyi CD34 beads. 2.0 million of these cells were injected i.v. into 5Gy X-ray preconditioned C57BL/6 x Balb/c cross (F1) recipients. 48 hours following mRtx-IgG2a or PBS carrier therapy, blood, spleen, bone marrow and lymph node compartments were assessed for

levels of RQR8-transgenic T-cell engraftment as a proportion of the entire T-cell subset. As illustrated by primary data from peripheral blood samples, mRtx-IgG2a therapy recipients had virtually achieved cellular clearance 48 hours following a single dose of mRtx-IgG2a therapy, contrasting with significant T-cell engraftment as indicated by the PBS therapy cohort.

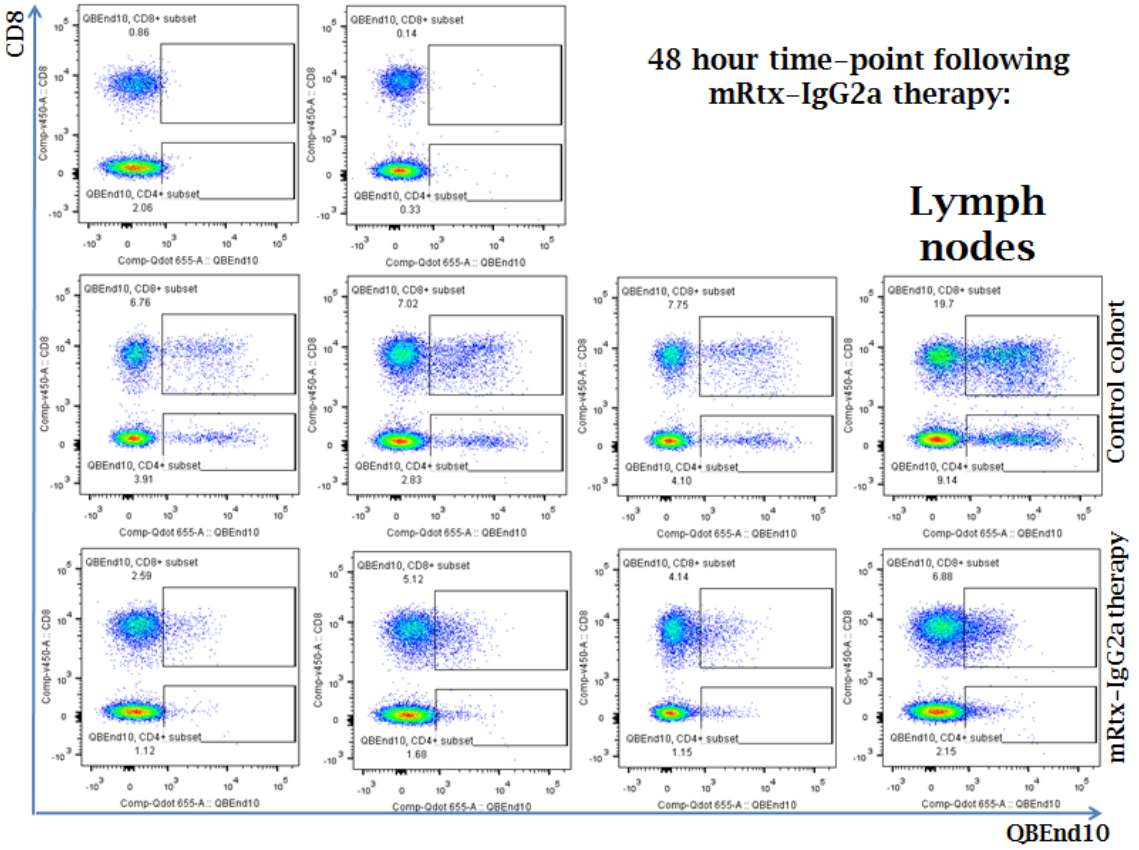

Figure 92 Haploidentical timecourse: Engraftment/depletion from lymph nodes

C57BL/6 splenocytes were retrovirally transduced to express RQR8 and selected to >90% purity with Miltenyi CD34 beads. 2.0 million of these cells were injected i.v. into 5Gy X-ray preconditioned C57BL/6 x Balb/c cross (F1) recipients. 48 hours following mRtx-IgG2a or PBS carrier therapy, blood, spleen, bone marrow and lymph node compartments were assessed for levels of RQR8-transgenic T-cell engraftment as a proportion of the entire T-cell subset. As illustrated by primary data from lymph node samples, we observed clear evidence of cellular depletion 48 hours after a single dose of mRtx-IgG2a therapy contrasting with profound T-cell engraftment as indicated by the PBS therapy cohort.

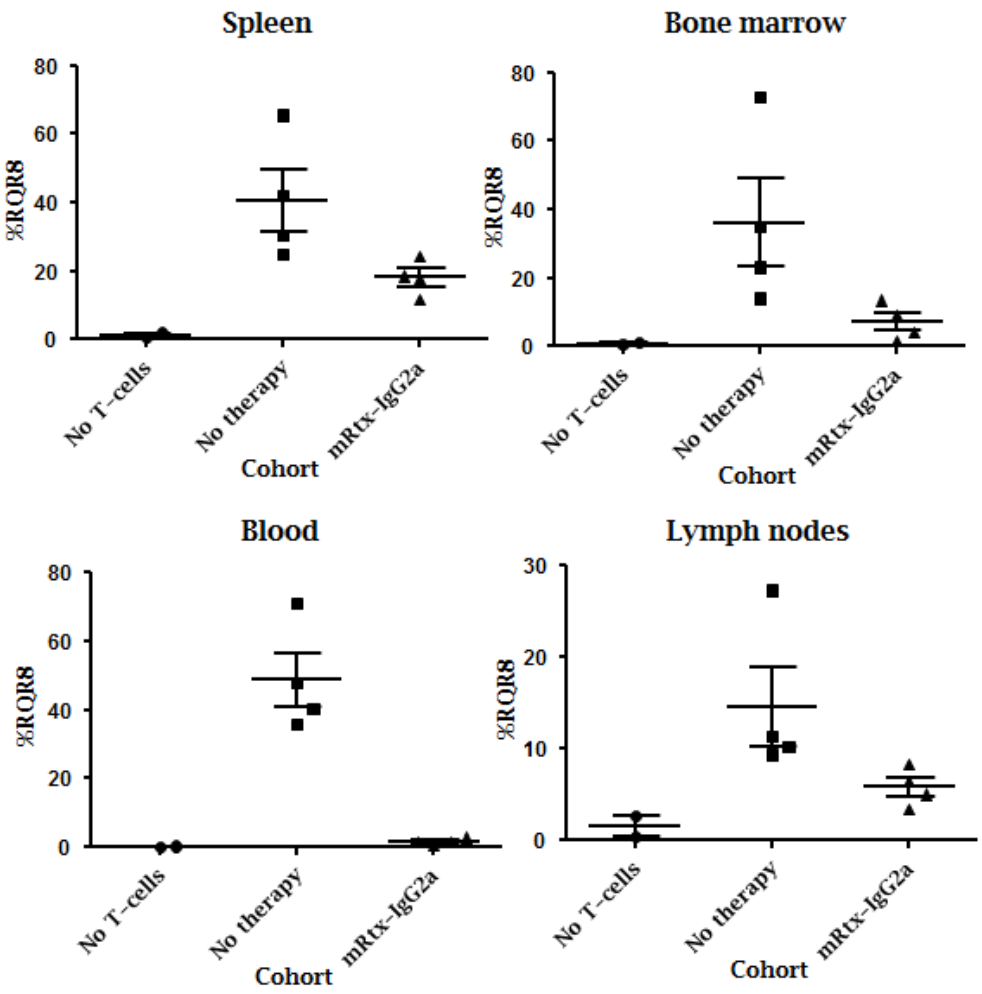

Figure 93 Haploidentical timecourse – 48hr RQR8 depletion summary
C57BL/6 splenocytes were retrovirally transduced to express RQR8 and selected to >90% purity with Miltenyi CD34 beads. 2.0 million of these cells were injected i.v. into 5Gy X-ray preconditioned C57BL/6 x Balb/c cross (F1) recipients. 48 hours following mRtx-IgG2a or PBS carrier therapy, blood, spleen, bone marrow and lymph node compartments were assessed for levels of RQR8-transgenic T-cell engraftment as a proportion of the entire T-cell subset. As illustrated, 48 hours following a single infusion of mRtx-IgG2a therapy, a comparative reduction in the RQR8 engraftment of 96, 56, 80 and 60% for blood, spleen, bone marrow and lymph node compartments respectively, was observed. Error bars reflect the standard error of the mean.

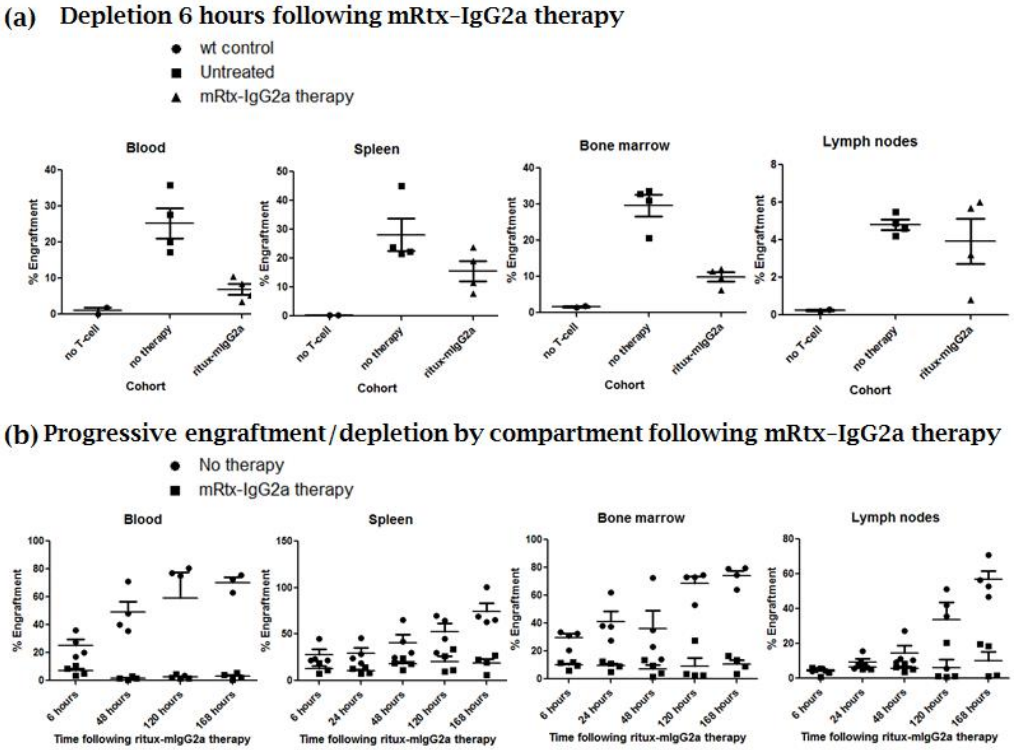

Figure 94 Haploidentical timecourse: Depletion progression comparison
C57BL/6 splenocytes were retrovirally transduced to express RQR8 and selected to >90% purity with Miltenyi CD34 beads. 2.0 million cells were injected i.v. into 5Gy X-ray preconditioned C57BL/6 x Balb/c cross (F1) recipients. 48 hours following mRtx-IgG2a or PBS carrier therapy, blood, spleen, bone marrow and lymph node compartments were assessed for levels of RQR8-transgenic T-cell engraftment as a proportion of the entire T-cell subset. (a) 6 hours following commencement of mRtx-IgG2a therapy, we observed depletion levels of 73%, 54%, 67% and 18% of RQR8 transgenic T-cells from blood, spleen, bone marrow and lymph node compartments. (b) Intra-animal assessment of efficacy of mRtx-IgG2a mediated RQR8 depletion was assessed by serial sacrifice of PBS and mRtx-IgG2a therapy cohorts at 6, 24, 48, 120 and 168 hour timepoints following commencement of therapy. We observed progressive depletion or engraftment as illustrated, achieving 96%, 75%, 85% and 82% depletion in the blood, spleen, bone marrow and lymph node compartments respectively by the 168 hour timepoint. Error bars reflect the standard error of the mean.

10.3.3. *In vivo* depletion of RQR8 co-expressed with a CAR

Experimental aim: To demonstrate effective mRtx-IgG2a mediated deletion of RQR8.2A.aCD19-CAR transgenic splenocytes in a haploidentical transfer model contrasting with continued engraftment in the absence of therapeutic administration.

Note regarding the RQR8.2A.aCD19-CAR construct: This construct is a codon optimised expression cassette generated by Cellectis therapeutics based upon an optimised anti-CD19 scFv format validated by Gordon Cheung and Leila Mekkaoui.

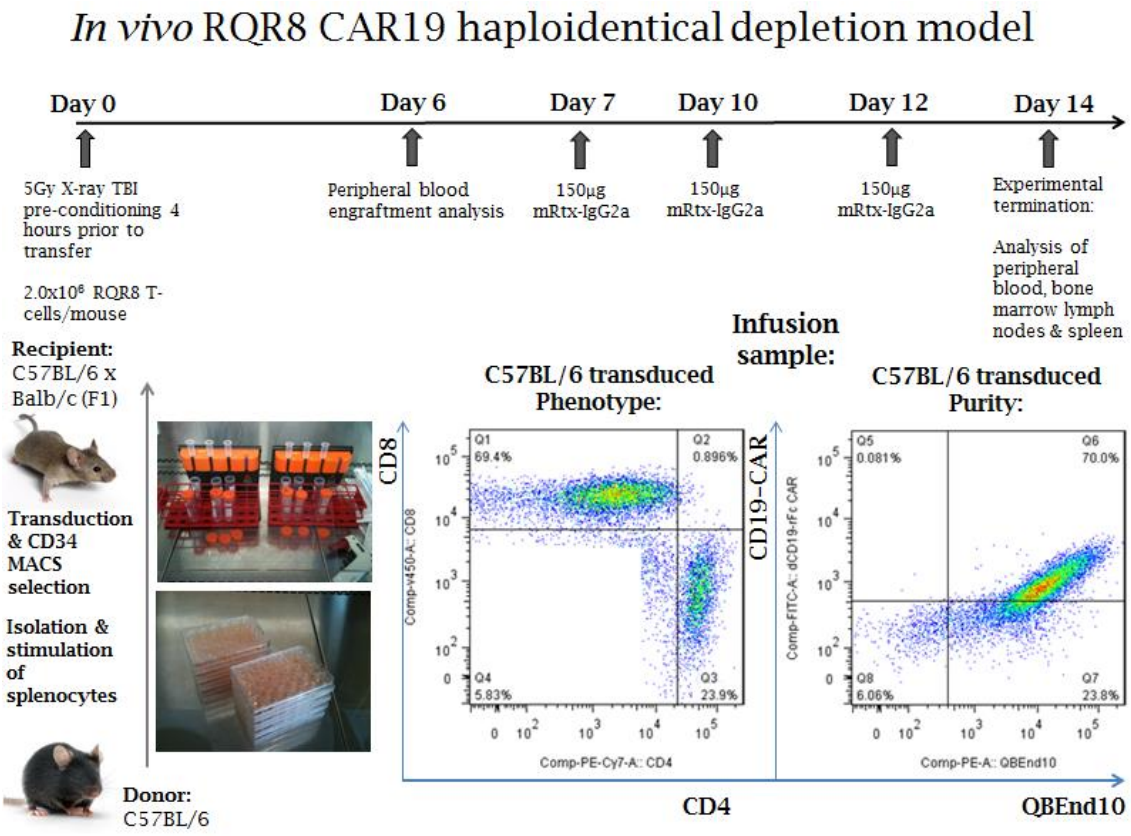

Figure 95 C57BL/6 to CB6F1 RQR8.2A.aCD19–CAR haploidentical model
C57BL/6 splenocytes were retrovirally transduced to co-express RQR8 alongside a second-generation anti-human CD19 chimeric antigen receptor and selected to >90% purity with Miltenyi CD34 beads. 2.0 million of these cells were injected i.v. into 5Gy X-ray preconditioned C57BL/6 x Balb/c cross (F1) recipients with engraftment confirmed by peripheral blood analysis six days following T-cell transfer prior to progression with mRtx-IgG2a therapy. At sacrifice, peripheral blood, spleen, lymph nodes and bone marrow compartments were examined to confirm efficacy of mRtx-IgG2a mediated deletion.

Splenocytes obtained from 12 female C57BL/6 donor mice were transduced and purified for expression of SFGmR.RQR8.2A.aCD19-4g7-CD8.41BBZ using the 5-day protocol. Female CB6F1 (C57BL/6 x Balb/c) recipient animals were preconditioned by 5 Gy single dose X-ray TBI 4 hours prior to adoptive cell transfer of 2.0 x 10^6 SFGmR.RQR8.2A.aCD19-4g7-CD8.41BBZ cells/mouse infused i.v. by tail-vein injection. Successful T-cell engraftment was confirmed by flow cytometry analysis from a peripheral blood draw obtained 6 days following T-cell transfer. Animals were separated into 2 cohorts receiving either mRtx-IgG2a therapy or PBS carrier, infused i.v. on days 7, 10 and 12. Fourteen days following T-cell transfer, all experimental animals were sacrificed with samples from blood, spleen, lymph nodes and bone marrow

obtained and assessed by flow cytometry for evidence of depletion or progressive engraftment. Efficacy of depletion was demonstrated to match with previous results from 10.3.1 which illustrates efficacy of clearance from monocistronic RQR8 expression; results illustrated by Figure 96-Figure 101.

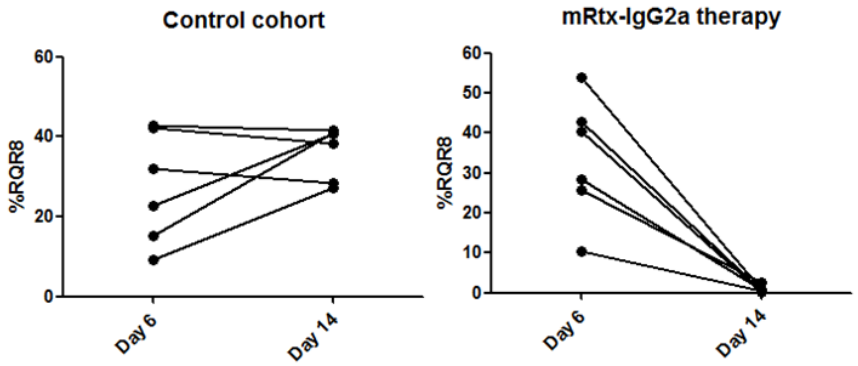

Figure 96 Comparative blood engraftment/depletion following mRtx-IgG2a therapy
Intra-animal demonstration of progressive engraftment or deletion: Peripheral blood samples were taken at both mid and terminal time-points to examine intra-animal progression of engraftment or deletion. As illustrated, PBS therapy recipients demonstrated progressive engraftment contrasting with clear deletion observed for the mRtx-IgG2a therapy cohort.

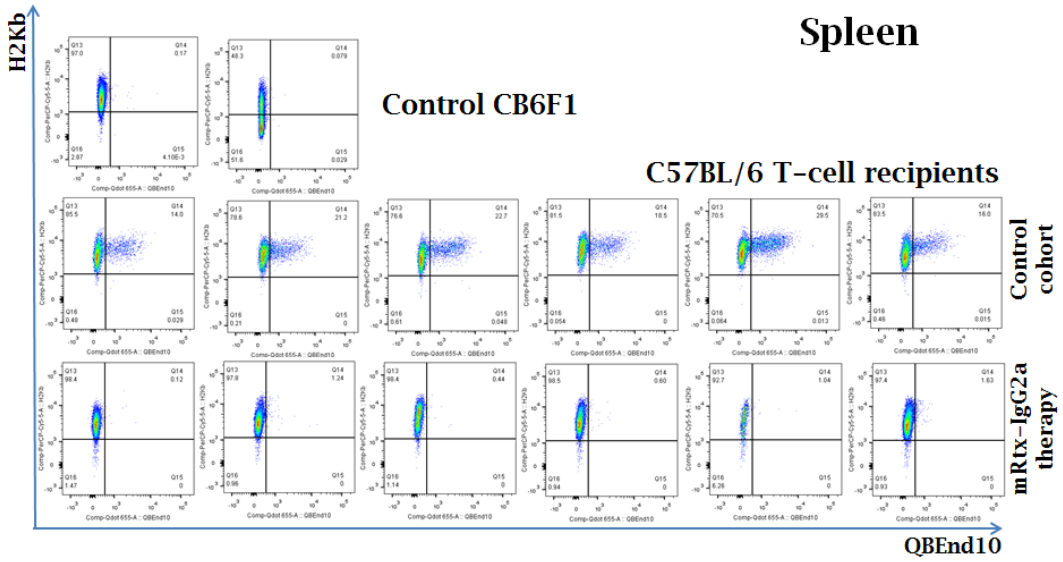

Figure 97 Haploidentical CAR model – engraftment/depletion from spleen
C57BL/6 splenocytes were retrovirally transduced to co-express RQR8 alongside a second-generation anti-human CD19 chimeric antigen receptor and selected to >90% purity with Miltenyi CD34 beads. 2.0 million of these cells were injected i.v. into 5Gy X-ray preconditioned C57BL/6 x Balb/c cross (F1) recipients. At experimental termination, peripheral blood, spleen, bone marrow and lymph node compartments were assessed for levels of T-cell engraftment. As illustrated, primary data demonstrates clear deletion of RQR8-transgenic T-cells from the spleen in mRtx-IgG2a therapy recipients contrasting with profound engraftment observed in PBS therapy controls.

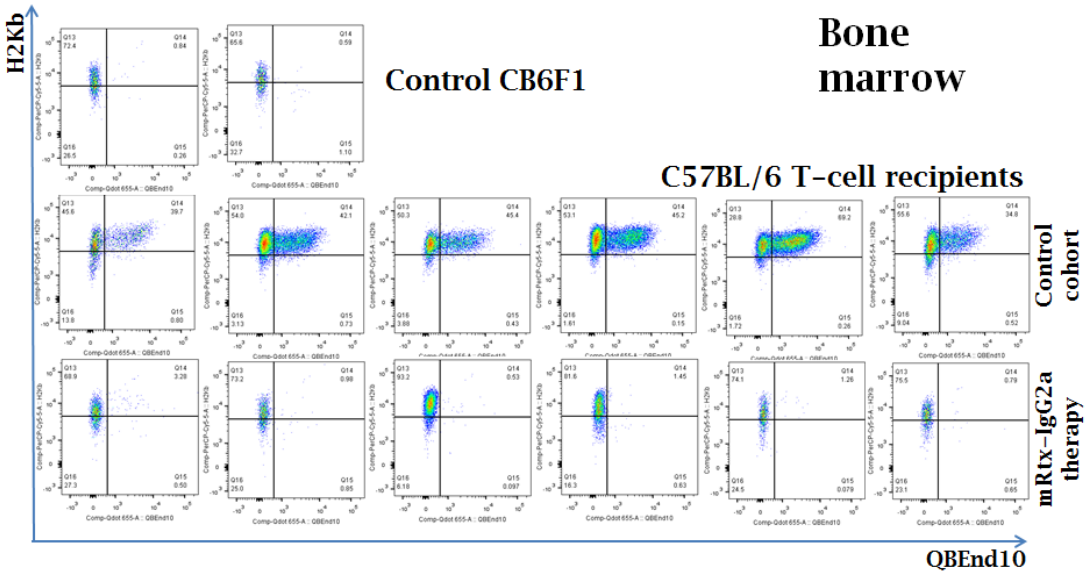

Figure 98 Haploidentical CAR model – engraftment/depletion from bone marrow
C57BL/6 splenocytes were retrovirally transduced to co-express RQR8 alongside a second-generation anti-human CD19 chimeric antigen receptor and selected to >90% purity with Miltenyi CD34 beads. 2.0 million cells were injected i.v. into 5Gy X-ray preconditioned C57BL/6 x Balb/c cross (F1) recipients. At experimental termination, peripheral blood, spleen, bone marrow and lymph node compartments were assessed for levels of T-cell engraftment. As illustrated, primary data demonstrates clear deletion of RQR8-transgenic T-cells from the bone marrow in mRtx-IgG2a therapy recipients contrasting with profound engraftment observed in PBS therapy controls.

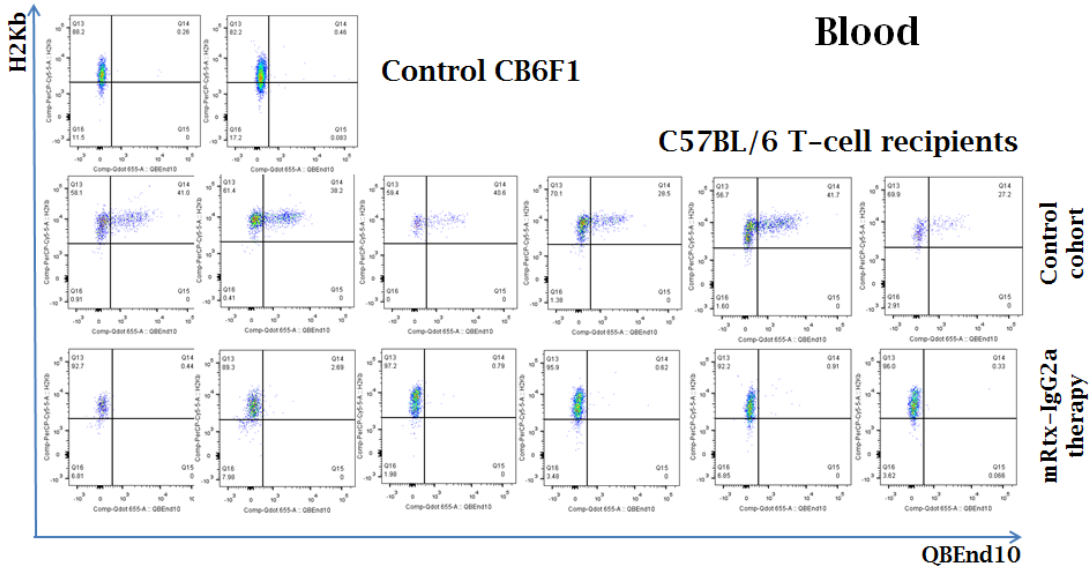

Figure 99 Haploidentical CAR model – engraftment/depletion from blood
C57BL/6 splenocytes were retrovirally transduced to co-express RQR8 alongside a second-generation anti-human CD19 chimeric antigen receptor and selected to >90% purity with Miltenyi CD34 beads. 2.0 million cells were injected i.v. into 5Gy X-ray preconditioned C57BL/6 x Balb/c cross (F1) recipients. At experimental termination, peripheral blood, spleen, bone marrow and lymph node compartments were assessed for levels of T-cell engraftment. As illustrated, primary data demonstrates clear deletion of RQR8-transgenic T-cells from the blood

in mRtx-IgG2a therapy recipients contrasting with profound engraftment observed in PBS therapy controls.

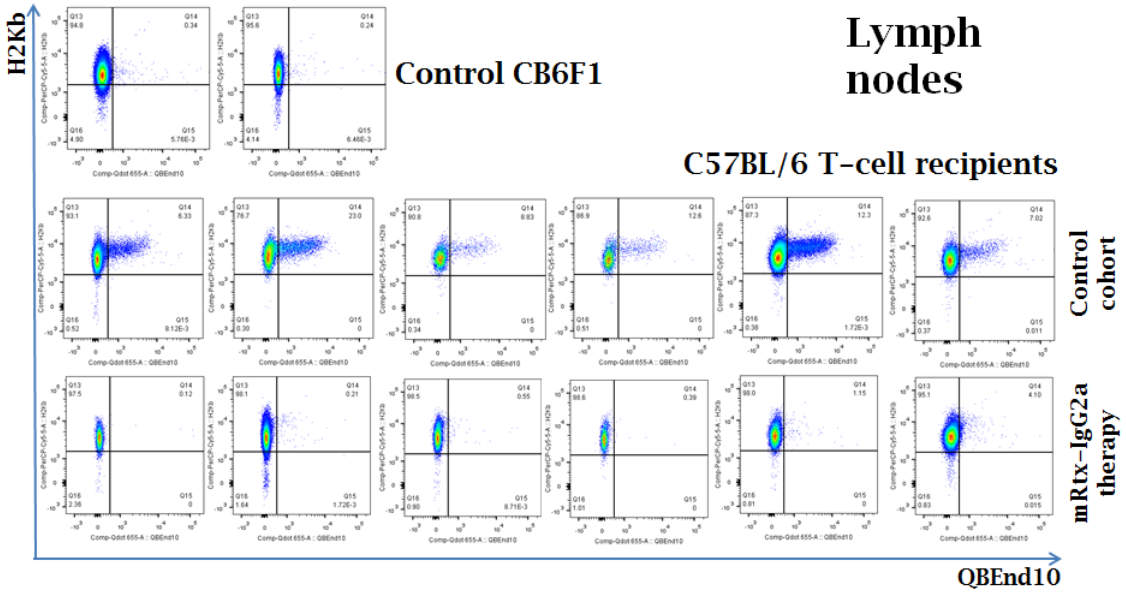

Figure 100 Haploidentical CAR model – engraftment/depletion from lymph nodes

C57BL/6 splenocytes were retrovirally transduced to co-express RQR8 alongside a second-generation anti-human CD19 chimeric antigen receptor and selected to >90% purity with Miltenyi CD34 beads. 2.0 million cells were injected i.v. into 5Gy X-ray preconditioned C57BL/6 x Balb/c cross (F1) recipients. At experimental termination, peripheral blood, spleen, bone marrow and lymph node compartments were assessed for levels of T-cell engraftment. As illustrated, primary data demonstrates clear deletion of RQR8-transgenic T-cells from the lymph nodes in mRtx-IgG2a therapy recipients contrasting with profound engraftment observed in PBS therapy controls.

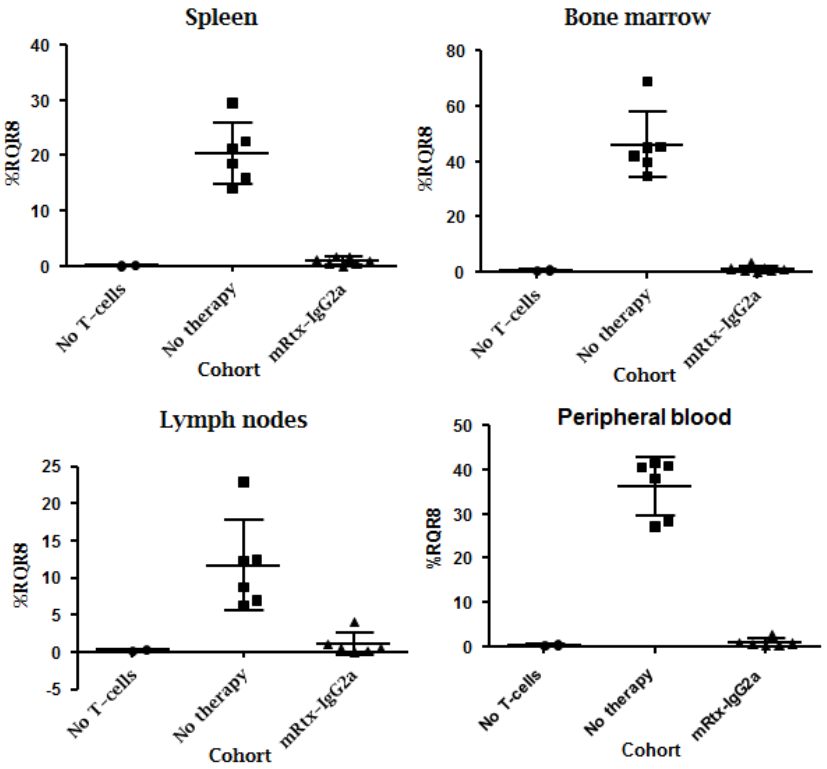

Figure 101 Haploidentical CAR model – RQR8 depletion summary
C57BL/6 splenocytes were retrovirally transduced to co-express RQR8 alongside a second-generation anti-human CD19 chimeric antigen receptor and selected to >90% purity with Miltenyi CD34 beads. 2.0 million cells were injected i.v. into 5Gy X-ray preconditioned C57BL/6 x Balb/c cross (F1) recipients. At experimental termination, peripheral blood, spleen, bone marrow and lymph node compartments were assessed for levels of T-cell engraftment. As illustrated, mRtx-IgG2a therapy affords effective clearance from all compartments assessed contrasting with clear evidence of engraftment observed for all PBS therapy controls.

10.4. Conclusions

Responding to the limitations identified from initial GvHD modelling attempts, the haploidentical model presented a less severe and clinically more reflective representation of the physiological scenario. In our initial haploidentical depletion experiment (10.3.1), we reviewed the question whether therapeutic administration could facilitate cellular depletion *in vivo* in the face of significant and sustained antigenic stimulation. Having presented the question in a binary manner, we assessed the efficacy of cellular deletion through an experimental snapshot seven days following commencement of rituximab therapy. In this model, blood remains the only compartment allowing for intra-animal comparison at separate time-points. Comparing the intra-animal engraftment in the blood, the rituximab therapy cohort demonstrated 99% depletion, contrasting with an opposing 285% increase in engraftment observed in the control cohort. Further, from inter-animal comparisons we

observed consistent and profound depletion of RQR8 expressing target cells in all compartments assessed; achieving 99%, 96%, 99% and 95% depletion in blood, spleen, bone marrow and lymph nodes respectively, when compared against the mean engraftment identified from the PBS therapy control cohort. Evidence of progressive engraftment in the blood demonstrated by the control cohort, supported by substantial engraftment observed in spleen and bone marrow compartments suggests the inflammatory environment resulting from X-ray TBI in this model presents a sufficient antigenic stimulus to establish fulminant GvHD effectively modelling the clinical risk posed by allogenic transfer. Further, we demonstrate clear evidence of cellular depletion in all tissue compartments analysed following from the shorter and more substantial dosing regimen.

Having successfully established an effective model by which to assess the efficacy of rituximab mediated deletion *in vivo*, we sought to examine the process of cellular depletion in further detail as described in 10.3.2 (Haploidentical time-course). As intra-animal assessment of depletion is limited to the peripheral blood, to achieve this aim it was necessary to expand the scale of this experiment to allow for serial assessments of separate cohorts to enable inter-animal comparisons from the tissues to examine the progression of depletion over time, illustrated by Figure 94 and Figure 102. We observed clear evidence of depletion in all compartments 6 hours following mRtx-IgG2a therapy, most evident in the peripheral blood and bone marrow (73% and 67% respectively); compartments rich in ADCC effectors, with least depletion observed from the spleen and lymph nodes (45% and 18% respectively). Depletion progressed throughout the examination period with maximum depletion achieved at the 168 hour (7 day) endpoint. The spurious but notable reduction in the observed depletion in the peripheral blood 24 hours following therapy might reflect cellular mobilisation from the spleen and bone marrow reservoirs, possibly resulting from the cytokine stimulation associated with ADCC effector mechanisms up to this point.

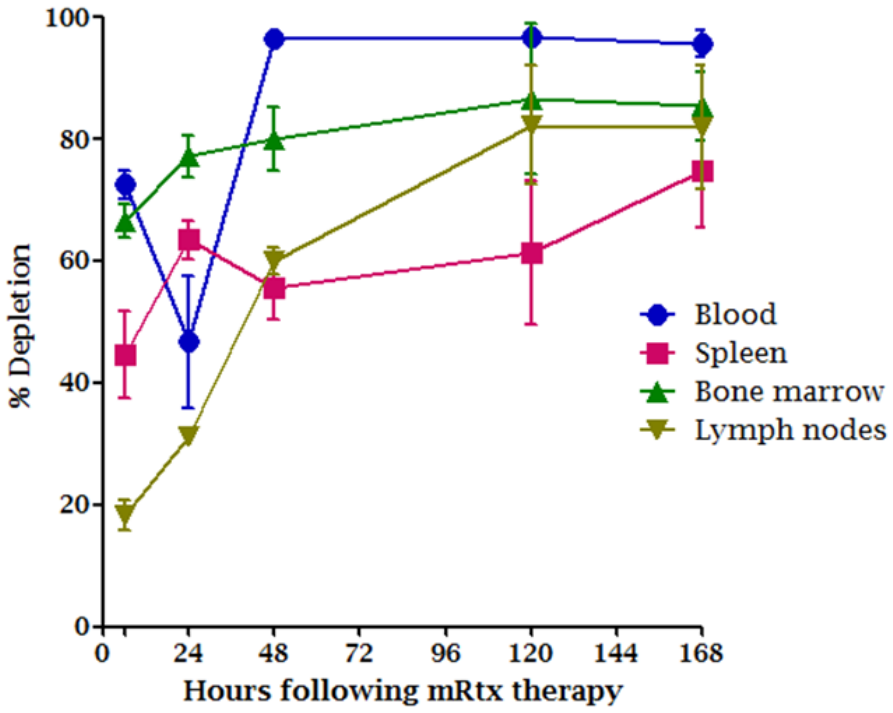

Figure 102 Haploidentical CAR model – RQR8 depletion versus time
C57BL/6 splenocytes were retrovirally transduced to co-express RQR8 alongside a second-generation anti-human CD19 chimeric antigen receptor and selected to >90% purity with Miltenyi CD34 beads. 2.0 million cells were injected i.v. into 5Gy X-ray preconditioned C57BL/6 x Balb/c cross (F1) recipients. Assessment of the progression of mRtx-IgG2a mediated RQR8 depletion over time was achieved by serial experimental terminations of separate cohorts 6, 24, 48, 120 and 168 hours following commencement of therapy. As illustrated, we observed a trend of increasing deletion of RQR8-transgenic cells with progression of time.

Notably, in this experiment, efficacy of depletion achieved was inferior to that observed in 10.3.1and 0; proposed explanations for this observation are as follows: Due to the increased scale required for this experiment, purity following MACS selection was reduced compared against the alternative haploidentical models. As a result, a significant proportion of non-transduced, GvHD-responsive activated T-cells secreting IL2 may have assisted proliferation of the residual RQR8 positive fraction not depleted by the initial dose, resulting in the reduced efficacy which was observed. Further, a slightly increased cellular dose was employed with a view of achieving sufficient engraftment to enable commencement of therapy at an earlier time-point. Finally, the sheer scale of this experiment imposed a significant challenge which added many confounding variables into the analysis and which may have factored into the increased engraftment and reduced efficacy which was observed. In the initial experiment (10.3.1), engraftment in the peripheral

blood seven days following T-cell infusion ranged between 1.5-8.5% with a mean of 4.5%, contrasting with engraftment ranging between 10.9-37.0%, five days following T-cell infusion with a mean of 21.6% for the time-course experiment. Further, one animal from both the 120 and 168 control cohorts was excluded from analysis due to severe tissue damage in all compartments likely the result of profound GvHD. Despite a considerably more aggressive model, clear evidence of progressive RQR8 mediated depletion was observed for all compartments, achieving 96%, 75%, 85% and 82% depletion in the blood, spleen, bone marrow and lymph nodes respectively which likely would have resulted in complete clearance matching the previous result had the experimental duration been extended or had RQR8 transgenic engraftment proven as modest as observed in 10.3.1 (Haploidentical depletion model).

Finally, reflecting the anticipated application of RQR8 alongside a CAR, our final model assessed the efficacy of rituximab mediated depletion of RQR8 expressing targets co-expressing a CAR. We have observed enhanced proliferation of CAR-transduced T-cells *in vitro* likely reflecting basal activation from the CAR co-stimulation domains. Thus, in this model, transgenic T-cells potentially receive stimulation from both MHC-mismatch via the TCR as well as an endogenous signal from the CAR. Similar to 10.3.2, an infusion dosage of 2.0×10^6 cells/animal was chosen due to the earlier time-point chosen for peripheral blood analysis. Notably, despite day 6 engraftment ranging between 9.2-53.8% with a mean of 33.4%, the efficacy of depletion assessed matched results from 10.3.1 (Haploidentical depletion model) previously.

Overall, our series of haploidentical modelling experiments demonstrate a consistent capacity of rituximab-mediated depletion of RQR8 expressing target cells *in vivo*. However, in addition to successful demonstration of efficacy, the time-course experiment also appears to highlight the primary limitation of an antibody-mediated suicide gene strategy imposed by limitations from effector mechanisms. As both intrinsic and extrinsic suicide gene strategies demonstrate potential but with limitations, it may be necessary to combine strategies where complete ablation is required.

10.5. General conclusions

- Clear engraftment was evident in all T-cell recipients in all haploidentical modelling experiments considered
- Progressive T-cell expansion was observed in all T-cell control recipients
- mRtx-IgG2a therapy mediated clear T-cell depletion from all compartments: peripheral blood, lymph nodes, spleen and bone marrow
- *In vivo* modelling with RQR8 demonstrated clear deletion of modified cells in the haploidentical setting
- mRtx-IgG2a mediated deletion of RQR8 transgenic targets occurs rapidly following therapeutic administration with clear evidence of deletion apparent 6 hours post-therapy

Chapter eleven

11. Epitope applications

An epitope, also known as an antigenic determinant, is the component of an antigen which elicits an antigenic response. Although most B-cell epitopes are discontinuous conformational epitopes defined by the three-dimensional structure of the native protein, some antibodies recognise linear epitopes. Epitope tags are commonly short linear antigenic sequences, initially used for protein purification, which remain in common use in research to assist characterisation of novel proteins for which monoclonal antibodies have yet to be identified or are of low affinity limiting sensitivity of experimental applications. As mentioned previously, marker genes encode for proteins absent from unmodified cells, thereby enabling selective identification and selection of genetically modified cells. Following from our previous work demonstrating the ability to express antibody binding epitopes on molecular spacers such as the CD8 stalk and a GPI anchor, we sought to establish whether our molecular spacer presentation strategy could be applied to common epitope tags to establish a novel set of research tools.

11.1. Aims

- To establish whether cellular GPI anchor machinery can be exploited to facilitate cell surface gene marking
- To establish whether cell surface presentation of epitope tags can be exploited as a general strategy to achieve multi-gene marking
- To demonstrate the generalizability of epitope tag presentation using either the GPI-anchor or the CD8 stalk to theoretically enable concurrent expression of multiple separate marker genes
- To establish whether cell-surface presentation of epitope tags on a GPI anchor could facilitate magnetic bead selection of transgenic cells
- To further reduce the size of the QBEnd10 binding epitope to isolate and establish the ‘smallest marker gene’

11.2. Introduction

Alternative multi-gene marking strategies have been described and the following discussion will briefly introduce LeGO vectors and Brainbow which

represent the most relevant comparative mechanisms to this final research tangent. Although molecular strategies for lineage tracking analysis such as DNA bar coding[281] represent the gold standard, these remain limited by retrospective analysis and won't be further discussed.

LeGO vectors[136] combine fluorescent protein expression with a drug resistance cassette to enable cellular selection. Although this strategy does enable multi-gene marking, options remain limited with only 10 pairings described. Further, spectral overlap of the fluorescent proteins would likely limit or preclude further protein antigen analysis by flow cytometry, compounding observations of limited transgene expression due to the large size of the transgenic cassette and toxicity resulting from the drug resistance component. Lastly, selection remains limited to flow cytometry or a more prolonged drug-mediated selection. Brainbow[282] offers a more powerful alternative strategy to facilitate lineage tracking. In Brainbow-1, the authors describe a method employing Cre-mediated excision between incompatible lox sites to achieve irreversible stochastic recombination events identified by alternative fluorescent protein expression. Evolution of this strategy resulted with Brainbow-2 which utilises reverse orientation of loxP sites to mediate inversion of DNA generating multiple outcomes. Due to combinatorial spectral overlap resulting from multiple integrants, a fluorescent mosaic effect was achieved facilitating identification of up to 90 separate distinguishable colours. This strategy is ideally suited for fluorescent analysis of *ex vivo* tissue sections, but would likely prove less effective for flow cytometry analysis from an ongoing experiment. Finally, both of these strategies employ fluorescent protein markers which in addition to immunogenicity, large protein size and spectral overlap, impose further limitations with respect to cell culture; high levels of fluorescent protein expression can result in aggregation imposing cellular toxicity, excitation of fluorescent proteins may generate toxic free radicals, and membrane damage imposed by fixation may result in fluorescent protein escape[283].

Epitope tagging refers to the molecular biology technique whereby a known antigenic epitope, for which a commercially available antibody is available, is fused to a recombinant protein to assist in characterisation and purification. FLAG, 6xHis and the glutathione-S-transferase (GST) tags, initially used for protein purification, were the first epitope-tags available commercially.

Application of this technique for research and characterisation of novel proteins resulted in a rapid increase in the epitope-tag/antibody pairs which were commercially available[284]. As discussed previously, following from clinical observations, progressive evolution of marker genes tended toward cell surface proteins derived from the same species but absent from the cell type under investigation, to preclude immunogenicity but enable cellular tracking. Hence, apart from fluorescent proteins, there is a limited range of options available to allow for identification of multiple separate marked cell populations. Further, the wide emission spectra of fluorescent proteins restrict the number of markers which can be included within a single cell limiting the number of research questions which can be addressed simultaneously. However, due to the preferable emission spectra of fluorochromes which can be conjugated to antibodies, theoretically this limitation could be extended through the use of antigenic epitopes as cellular markers.

In cellular engineering, there remain many instances where multi-gene marking could prove beneficial to examine the impact resulting from expression of multiple transgenes; e.g. T-cell engineering, packaging cell lines, iPS cells. Thus to conclude this body of research, we examine the potential for GPI-anchor mediated expression to further reduce the size of the QBEnd10 marker gene to establish a minimal marker gene, as well as the potential to utilise epitope tags as putative marker genes to facilitate multi-gene marking.

11.2.1. GPI anchors

Glycosylphosphatidylinositol (GPI) anchored proteins can be viewed as an alternative cell surface protein expression strategy, variant to the type I-IV classifications of transmembrane proteins. Biosynthesis of GPI-anchors occurs in three stages: assembly of the GPI-anchored precursor protein in the ER membrane, attachment of newly synthesized protein within the lumen of the ER to the GPI-anchor, concurrent with cleavage of the GPI addition signal peptide and finally post-translational modification occurring in the ER and Golgi apparatus. GPI-anchors appear to be ubiquitously expressed across eukaryota with virtually all GPI-anchors sharing a common core structure. In mammals, alternative mRNA splicing may result in expression of transmembrane or GPI-anchored forms of the same protein[285]. Unsurprising given the evolutionarily highly conserved GPI-anchor strategy, defects in GPI-

anchor biosynthesis and protein expression is associated with a range of pathologies including PNH and autosomal recessive GPI-anchor deficiency[286].

As GPI-anchor biosynthesis remains an endogenous process facilitating plasma membrane localisation, we premised that we could exploit GPI-anchoring as a generic strategy to achieve cell-surface epitope tag expression, requiring a minimal protein coding sequence, even shorter than our previous CD8 stalk based strategy, which would impose little or no immunogenicity.

11.2.2. Vector packaging limitations

Although sufficient for monogenic therapy, advances in molecular engineering and increasing desires for additional applications are approaching or have already exceeded the packaging capacity for retroviral and lentiviral vectors. The sleeping beauty transposon strategy, used by the Laurence Cooper group at MD Anderson offers a favourable integration profile compared with retroviral and lentiviral vectors but with a limited packaging capacity that declines with increasing transgene size[287]. Similarly, adeno-associated viral (AAV) vectors, commonly used for gene therapy applications possess a limited transgene packaging capacity of approximately 2.3kb[288]. One obvious strategy to resolve limitations in vector packaging capacity is to reduce the size of the transgenic cassette thus any strategy which can achieve similar efficacy but with a reduced genetic footprint would be of considerable utility for gene therapy application.

11.3. Results: The smallest marker gene

Experimental aim: To establish whether we could further reduce the coding sequence for our QBEnd10 binding epitope to establish an absolutely minimal marker gene cassette for gene marking research.

Note: Gene marking and suicide gene generation represented parallel research tangents, hence previous mention of GPI anchor-mediated expression.

At only 105 a.a. residues in length (post-processing), Q8 is already under one-half the size of eGFP. However in consideration of vectors with stringent packaging capacities, we premised that exploitation of cellular GPI anchor presentation machinery would allow us to further reduce the size of our QBEnd10 binding marker gene to establish a truly minimal marker gene. As

previously, our initial constructs compared expression of the QBEnd10 binding domain, with or without a flexible SGGGS linker sequence compared against the parental Q8 construct. Although both GPI anchored versions demonstrated inferior marking to that observed for the Q8 construct, in this instance the linker did appear to mediate slightly superior antibody binding capacity, as identified through comparison between QBEnd10 binding MFI between equivalently transduced targets; antibody staining illustrated by Figure 103.

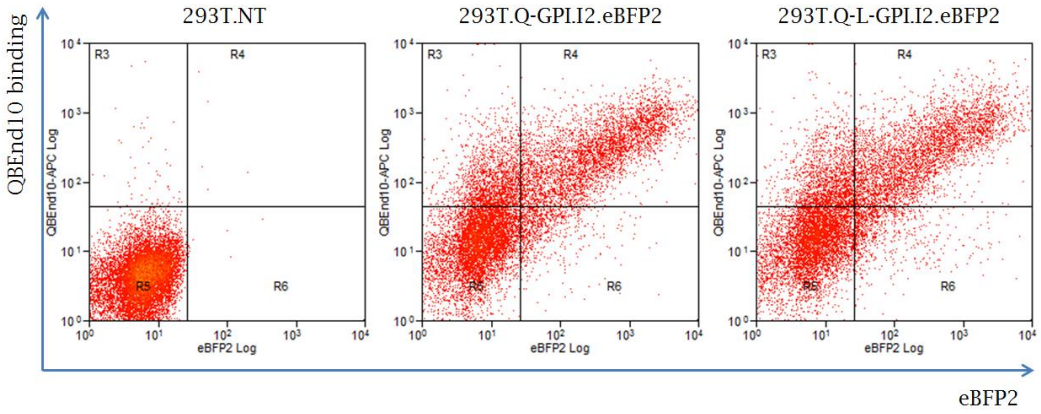

Figure 103 Demonstration of GPI anchor presentation of QBEnd10 epitope
HEK293T cells were transfected with QBEnd10 epitope expression constructs, with or without a flexible S-G-G-G-S linker sequence, presented on a GPI-anchor to establish whether this presentation strategy might enable further reduction of epitope expression constructs. As illustrated, both constructs demonstrate effective epitope expression although under examination of MFI of antibody binding suggests that inclusion of the linker sequence offers modest improvement in epitope presentation efficacy.

Having demonstrated that GPI anchor machinery could be exploited as a generic presentation strategy for an antibody binding epitope, albeit with attenuated binding efficacy, next we proceeded with two separate lines of interrogation regarding GPI-anchored QBEnd10 epitope constructs as illustrated by Figure 104: Firstly, through further single residue deletions, could the aforementioned 16 a.a. residue QBEnd10 binding epitope tolerate any further reduction whilst retaining antibody binding efficiency [deletion series], and secondly, could we enhance GPI-anchored marking efficacy to match that previously observed for Q8 [insertion series]?

For the insertion series, we considered 3 alternatives to boost binding efficacy of the GPI-anchored marker gene. Premising that limited projection of the epitope from the cellular surface might restrict antibody access resulting with impaired binding efficacy, we considered two alternative presentation motifs to extend this distance. MP12231 presents the QBEnd10 epitope, amino

terminal to the CD52 Campath epitope, exploiting the highly glycosylated native sequence from CD52 to increase the epitope projection away from the cellular surface. Similarly, MP12232 includes a fragment of the CD3ζ ectodomain also projecting the QBEnd10 epitope from the GPI anchor signal region; further, the presence of a cysteine residue within the CD3ζ domain might facilitate dimerization through disulphide bonding boosting the valency thereby hopefully matching the binding efficacy achieved by the dimeric CD8 stalk strategy. Lastly MP12230 represents a minimalist version of MP12232 through inclusion of a cysteine residue but lacking supplementary projection.

As evidenced by both terminal deletion series, further reduction of the QBEnd10 epitope appeared to mediate a threshold binding effect whereby successful binding only results at high levels of epitope expression as indicated by the corresponding level of eGFP expression; most apparent with the amino terminal deletion series. This may reflect a progressive degradation of the binding affinity with the result that where expression levels remain low, the on/off rate of antibody binding is not discriminable from that of background binding only achieving an effective signal where expression levels remain high. Disappointingly, all reduction constructs demonstrated further reduction in QBEnd10 binding capability. In contrast, the insertion series proved more promising with inclusion of the CD3ζ ectodomain achieving improved QBEnd10 binding compared against the parental GPI-anchored construct MP11601, albeit still inferior to binding efficacy achieved by Q8. However the CD3ζ construct still facilitates a clear two-log shift in QBEnd10 binding whilst only requiring a 234 base coding sequence, contrasting with the 416 bases required for Q8, or the 719 bases as required for eGFP.

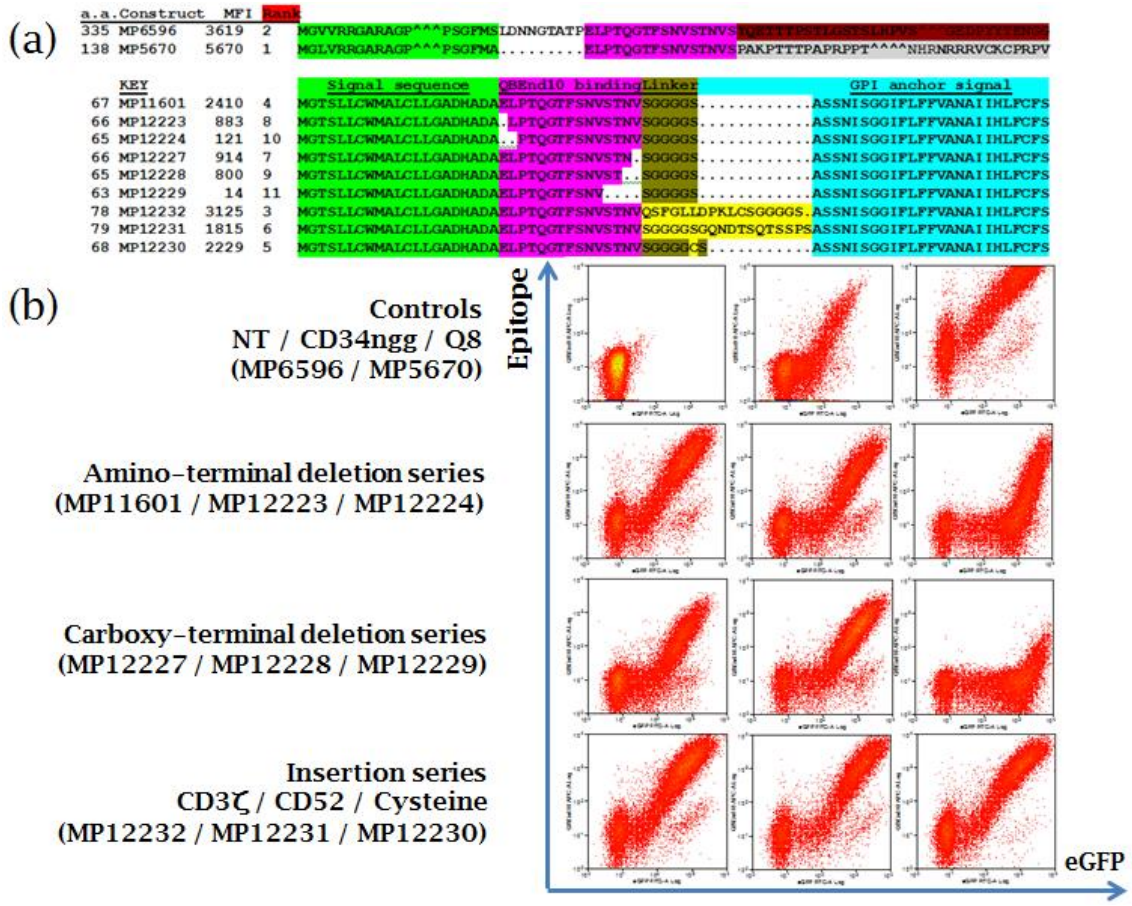

Figure 104 Attempts to further reduce the QBEnd10 marker gene
In an attempt to further reduce the genetic footprint required for our marker gene, further point mutation reductions of the QBEnd10 binding domain were presented on a GPI anchor compared against the CD8-stalk bound parent. (a) Protein sequences of epitope reduction constructs illustrate design variation to optimise antibody binding efficacy. As indicated, use of the GPI-anchor presentation strategy enables a further reduction of the molecular footprint required for gene marking by almost 50%. (b) SupT1 cells transgenic for the alternative epitope constructs were assessed by flow cytometry to assess the comparative MFI of QBEnd10 antibody-binding. As illustrated, although clear functional efficacy was observed for multiple constructs with greatest binding demonstrated by the MP12232, QZL-GPI construct, none of the GPI-anchor iterations offered equivalent binding as mediated by the parental CD8-stalk bound construct.

11.4. Generalizability

Experimental aim: To demonstrate that the CD8 or GPI-anchor molecular spacers can serve as a general expression format for common epitope tags.

Having successfully demonstrated GPI-anchor mediated epitope expression, next we considered whether this capacity could be extended as a general strategy to alternative antibody binding domains such as epitope tags. To this end, we examined cell-surface expression of the HA, HSV, T7, c-myc, V5 and OLLAS epitope tags when presented on a GPI anchor. These constructs were

cloned by Emily Hardman under supervision. As illustrated by Figure 105, clear binding was demonstrated for the HA, c-myc and V5 tags, limited binding was achieved with the HSV tag with OLLAS and T7 epitopes demonstrating poor or no binding respectively.

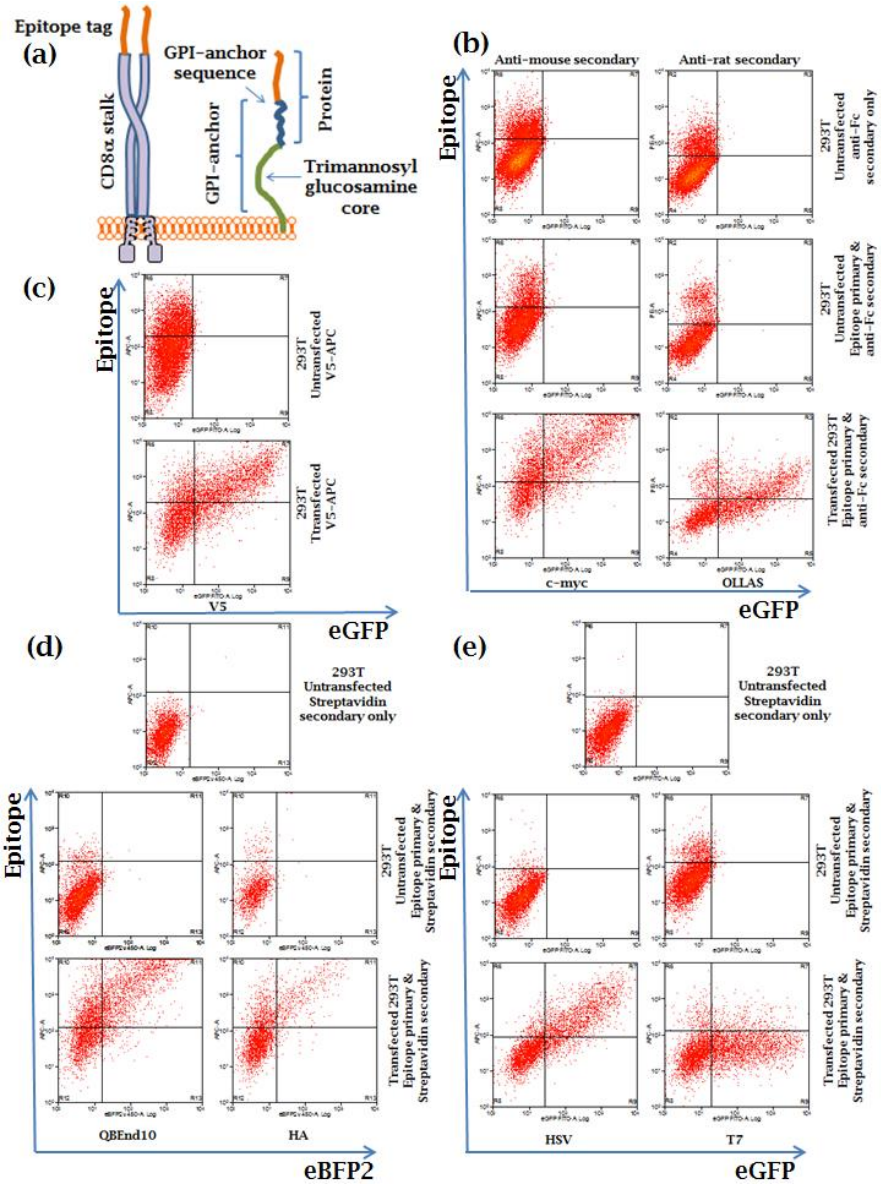

Figure 105 Epitope tag presentation on GPI anchors
To demonstrate the generalisability of epitope expression on GPI anchors to facilitate cellular marking, common epitope tags were presented on the CD52 GPI anchor sequence co-expressed with either eGFP or eBFP2 fluorescent protein marker genes to identify successful transfectants. Functional validation of this strategy was assessed by flow cytometry against epitope transfected HEK293T cells. (a) Cartoon illustration of CD8 and GPI-anchor epitope presentation strategies. Due to the limited commercial antibodies available for flow cytometry application, alternative straining strategies were employed to assess epitope presentation efficacy as follow: (b) Efficacy of c-myc and OLLAS epitope tag expression were assessed by an anti-secondary antibody against the primary antibody Fc domain as indicated. (c) and (d) Efficacy of HA and QBEnd10 or HSV and T7 epitope tags were all assessed through 2-layer Biotin, Streptavidin staining strategies with the former pair co-expressing eBFP2 and the latter pair eGFP.

Further, to establish whether cell surface expression of our epitope-tag based markers could facilitate magnetic bead selection, we considered indirect

selection of HA-GPI transduced Raji cells using HA-biotin primary staining followed by streptavidin bead selection as illustrated by Figure 106.

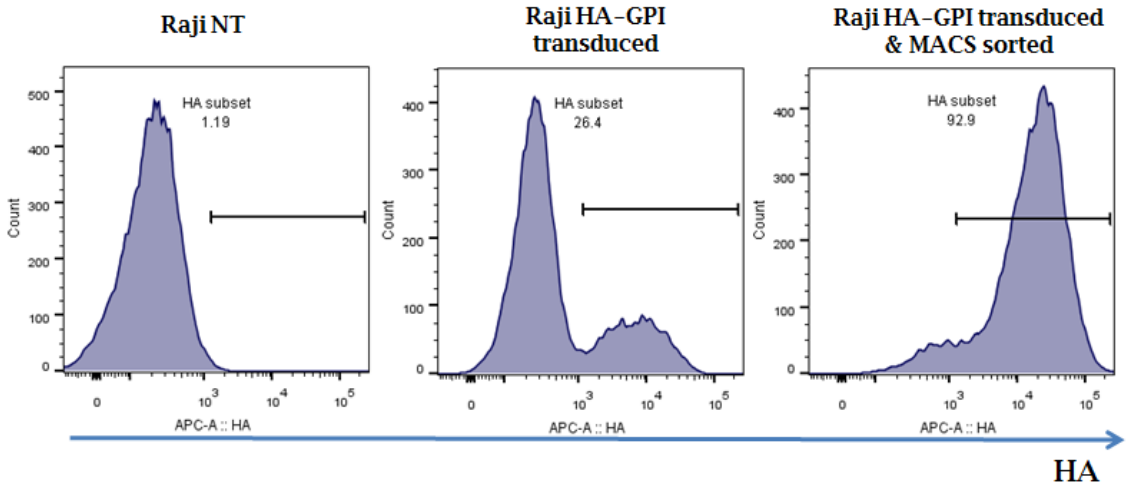

Figure 106 Indirect MACS selection of HA-GPI epitope marked Raji cells
Raji lymphoma cells were transduced with the HA-GPI epitope tag. Miltenyi magnetic bead selection was achieved by two-step staining process whereby cells were labelled with an HA-biotin primary stain then purified using Streptavidin-bead secondary staining step. Results illustrated reflect sample purity following a single cycle of magnetic bead selection.

Having demonstrated the generalizability of this strategy, next we assessed the comparative binding capacity of the HA, c-myc and V5 tags compared against binding demonstrated by the GPI-anchored QBEnd10 marker in an attempt to establish a hierarchy of binding efficacy for the separate epitope tag constructs. To enable comparative analysis of binding efficacy between the various epitope constructs, we obtained biotin-conjugated antibodies in an attempt to control the variable posed by the fluorescence signal used to assess antibody binding through consistent application of a fluorescently labelled streptavidin conjugate. Further, following observations of reduced binding from GPI anchored marker, we established both GPI-anchored and CD8-stalk-bound alternatives for each of the tags under interrogation to compare efficacy of the different formats. CD8 stalk-bound constructs were cloned by Dimitra Markantoni under supervision. As illustrated by Figure 107, from this analysis, a consistent pattern of superior staining was observed for CD8 stalk-bound iterations of constructs as compared with the GPI-anchored equivalents. However, we were disappointed to observe poor binding efficacy by the myc and V5 epitope tag targets which had previously demonstrated promising staining efficacy. As most epitope tag antibodies are designed for Western blotting, our initial staining attempts were performed using the antibody

options which we were able to source from our laboratory and those of our colleagues. Further, none of the biotin-conjugates were validated for flow cytometry, and one of which was a bespoke reagent conjugated only by request. Thus, following the lack of clarity from the biotin-conjugate staining strategy, we reconsidered the variation in binding efficacy observed for the myc and V5 constructs between our initial experiment (Figure 105) and the comparison assay (Figure 107). As illustrated by Figure 108, we were able to demonstrate clear binding of GPI-anchored epitope tags using preconjugated antibodies. Although this result precludes a definitive answer to our query regarding the comparability of epitope tags efficacy, it does confirm that epitope tags can be exploited to function as cellular marker genes in either presentation format, with the CD8 stalk appearing to offer a superior presentation format, albeit at the cost of imposing a larger molecular footprint.

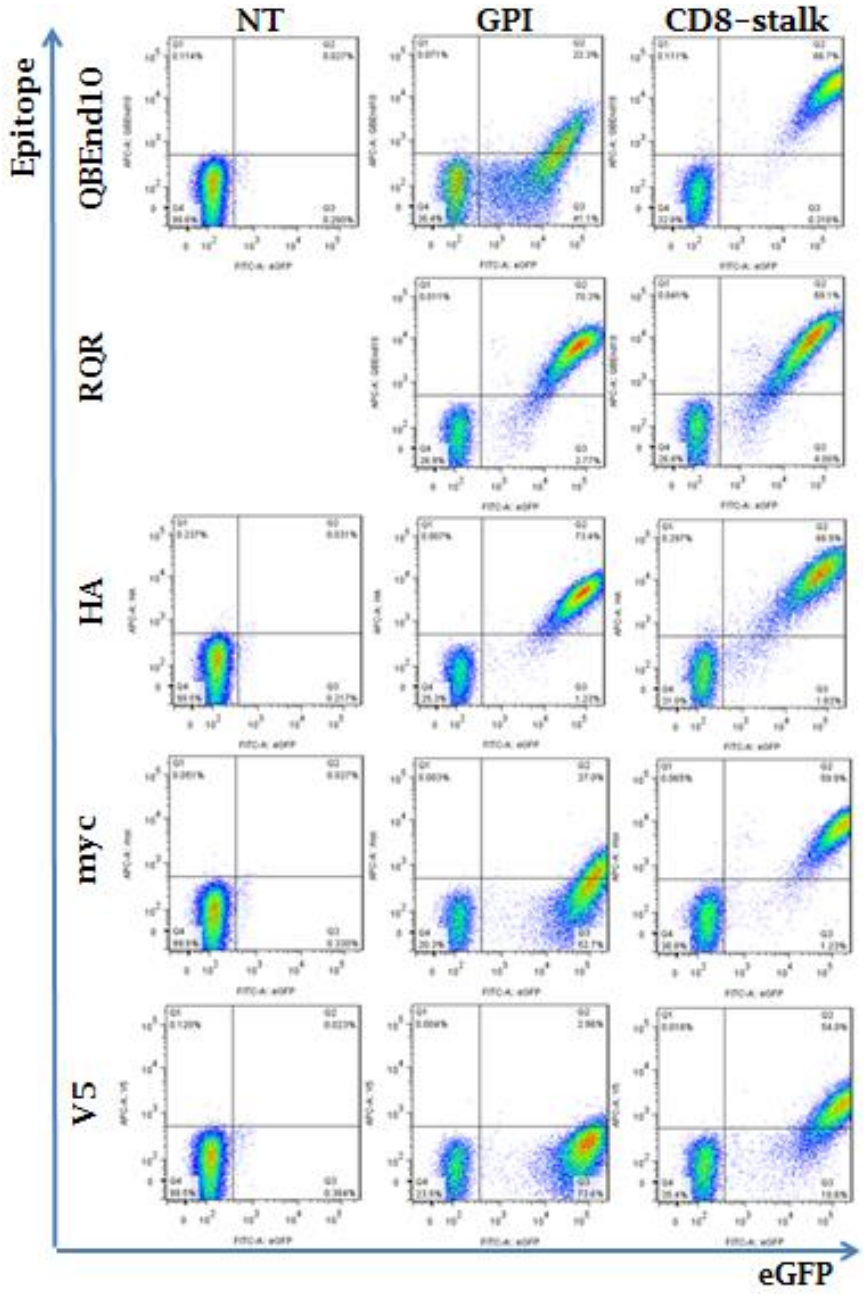

Figure 107 Biotin/Streptavidin staining comparison of epitope tags
SupT1 cells were separately transduced with QBEnd10, RQR, HA, c-myc and V5 epitope tags in both GPI and CD8-stalk presentation formats. Efficacy of epitope presentation was compared by flow cytometry with targets stained with a biotin-conjugated primary antibody with functional efficacy assessed using equal volumes of the streptavidin secondary stain for all conditions. Although modest staining can be achieved for all three epitope tags in the CD8-stalk presentation format, however only the HA tag proved effective as a marker gene in the GPI anchored format.

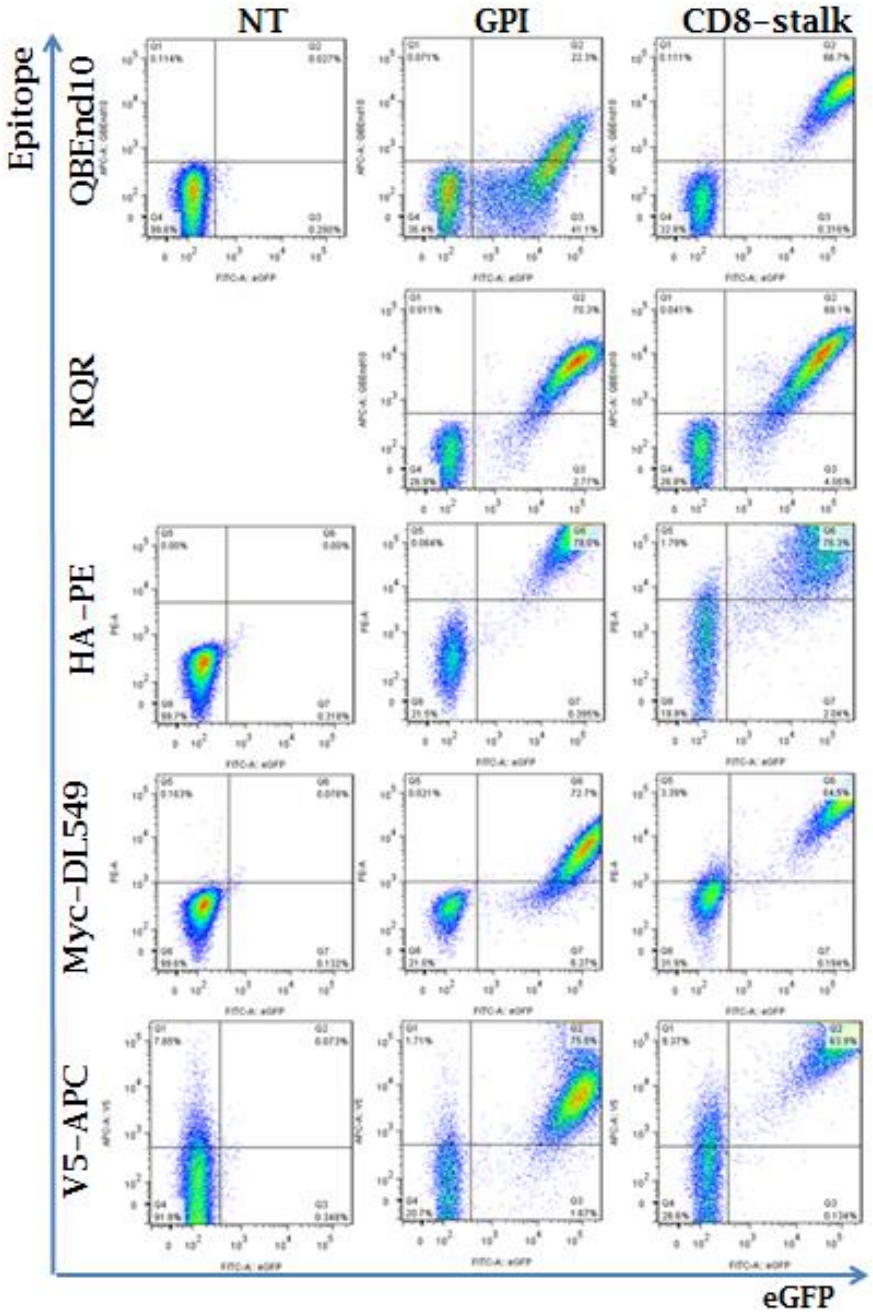

Figure 108 CD8-stalk and GPI anchored epitope tags in SupT1 cells
SupT1 cells were separately transduced with QBEnd10, RQR, HA, c-myc and V5 epitope tags in both GPI and CD8-stalk presentation formats. Efficacy of epitope presentation was compared by flow cytometry with targets stained using preconjugated antibodies as indicated. Use of pre-conjugated antibodies for the HA, c-myc and V5 epitope tags demonstrated clear functional efficacy for all three epitope tags in either GPI-anchor or CD8-stalk presentation formats although the CD8 stalk does appear to represent the superior presentation strategy based on MFI.

11.5. Conclusions

Although fluorescent proteins are commonly employed to facilitate multiple gene marking, their broad spectral emission profiles impose significant limitation to the number of channels which can be examined concurrently.

Through careful selection of compatible fluorochromes examined with an LSR Fortessa cell analyser, we have successfully established 14 colour panels facilitated through antibody staining. This contrasts with a maximum of five fluorescent proteins which can be compared in parallel accounting for all channels on the instrument due to spectral bleed. A further advantage of cell-surface localised epitope constructs is the capacity to enable cellular purification through magnetic bead selection thereby reducing the risk for contamination associated with flow sorting as well as offering a more gentle strategy for selection, optimal for fragile cell populations. Finally, the minimal size of epitope based presentation formats offer a favourable genetic footprint to that required by a fluorescent protein, with GPI-anchored constructs and CD8 stalk-bound constructs approximately ⅓ and ½ the size respectively, of a fluorescent protein.

Attempts to further reduce the QBEnd10 binding epitope proved unsuccessful, demonstrating that the absolute limit of the QBEnd10 epitope had already been accurately established. Furthermore, despite successful presentation of the QBEnd10 epitope on a GPI-anchor, we were unable to achieve equivalent binding efficacy as that previously achieved through the CD8 stalk presentation format despite attempts to resolve this limitation through further molecular engineering. Although neither increased projection, nor putative dimerization alone appeared to enhance the GPI-anchor presentation strategy; combination of both strategies, as with the CD3ζ ectodomain iteration, did appear to improve antibody binding efficacy, albeit still not to the level observed for the Q8 control construct.

Furthermore, we have demonstrated that both the GPI-anchor and the CD8 stalk can be exploited as a general molecular spacer strategy to facilitate presentation of common epitope tag sequences to function as cell-surface marker genes. However due to the primary application of epitope tags for Western blotting, it may be necessary to confirm functional verification for putative antibody and epitope tag pairings to ensure these can be suitable for flow cytometry application. Further to our observations assessing QBEnd10 presentation, we note that CD8 stalk presentation consistently appears to facilitate superior cell-surface presentation of epitope tags when compared to GPI-anchored equivalents, however, despite this limitation, GPI- anchor presentation still offers potential for a two-log shift in MFI demonstrating that

GPI-anchor mediated presentation remains a viable alternative strategy. Due to the minimal degree of engineering involved with GPI-anchor presentation, this strategy offers potential for both multi-gene cellular marking and/or indirect magnetic bead selection from a minimal coding sequence which remains as minimally immunogenic as can be achieved. Further, due to the favourable fluorescence profile of fluorochromes as compared with fluorescent proteins, this strategy offers significant potential as a research tool for applications where multi-gene marking would prove informative. Thus, we report that both the GPI-anchor and the CD8 stalk can be utilised as general strategies for the presentation of common epitope tag sequences to function as marker genes. Lastly, the linear epitopes of QBEnd10 and similar epitope tags also offer multi-functional application as they additionally enable identification through primary applications of western blotting and IHC.

11.6. General conclusions

- Despite further attempts to reduce the size of the QBEnd10 binding marker gene, reduction in size of the coding sequence was associated with reduction in binding efficacy.
- Presentation of the QBEnd10 binding domain on a GPI anchor including additional projection mediated by the CD3ζ ectodomain achieved the best binding efficacy of GPI-anchored constructs from a transgene sequence only 234 bases in length, coding for a 57 a.a. protein.
- Both GPI anchors and the CD8 stalk offer generalised strategies to function as molecular spacers to facilitate cell surface expression of epitope tags as putative marker genes.

Chapter twelve

12. Discussion

12.1. Need for sort–suicide genes

Adoptive cell therapies represent a rapidly developing field of therapeutic application. The graft versus leukaemia effect following allogeneic stem cell transfer[29], recent successes from CD19-CAR clinical trials[21, 48, 289] and successful resolution of X-SCID from gene therapy trials[51] highlight the promise from adoptive cellular therapies, and arising from each success, the potential for ACT to become potential first line therapy inches ever closer. However, panoply of risks including GvHD, IM, OTOT arise coincident with potential therapeutic benefit. Recent evidence demonstrating sustained engraftment potential arising from single cell transfer experiments illustrates both the potency of cellular transfer therapies whilst highlighting the possibility for residual toxicity[290]. Furthermore, improvements in therapeutic efficacy offering sustained survival raise potential for further identification of toxicities resulting from therapies previously perceived as ‘safe’. Hence, as the breadth of application for cellular therapies grows, the need for a universally effective control mechanism becomes ever more imperative.

HSVtk[64] and iCaspase9[125] suicide gene strategies represent the mainstays of current technology with both currently in clinical application; however, both possess limitations. HSVtk has a long history of clinical application having proven highly effective in therapeutic administration following haploidentical stem cell transfer. Limitations identified from clinical trials have largely been resolved through progressive engineering. However, transgene immunogenicity remains the Achilles heel of this system restricting application to scenarios of profound immunosuppression. Hence, engineering of alternative suicide gene strategies focussed on identifying non-immunogenic alternatives with iCaspase9 proving the forerunner as a potential replacement for HSVtk. However, limited safety profiling of the dimeriser drug, a long transgene coding sequence comprising only the suicide gene moiety, restrictive access to clinical grade dimeriser and the intrinsic mechanism for deletion offering potential for escape all present limitations and concerns from this suicide gene strategy.

As cancer is a heterogenous disease, it seems likely that therapies will become increasingly personalised. Further, the risk for OTOT remains to be established for each individual retargeting moiety and TAA target. With the extensive range of variables involved, it seems implausible that risk could ever be excluded, hence the ever pressing need for a universal safety mechanism. Further, until vector packaging capacity limitations can be overcome, ever increasing options for T-cell engineering will continue to tax vector packaging capacity imposing cumulative pressure toward minimal modular transgenic cassettes.

Hence, a minimal non-immunogenic combined selection/suicide gene system compatible with current technology demonstrating equivalent efficacy to current technology would offer significant potential as an engineering tool for general application in adoptive cell therapies. For this purpose, we propose RQR8 as a potential universal marker-suicide gene for adoptive cellular therapies.

12.2. Study conclusions

12.2.1. Identification of the QBEnd10 and rituximab binding epitopes

As the QBEnd10 binding epitope had been proposed to be a linear epitope localised to the amino-terminus of the CD34 antigen[193], initial work performed by Dr. Martin Pulé optimised a presentation strategy for putative QBEnd10 binding fragments projected from the cell surface on the CD8α stalk. Bi-directional deletions from the parental construct resulted in generation of a final construct containing only 16aa residues from the 385 present in the parental antigen achieving a final construct composed of only 105aa yet offering binding affinity and magnetic selection capacity matching that of the parental antigen.

In direct progression from successful epitope mapping of the QBEnd10 binding domain, we next sought to identify an equivalent rituximab binding epitope to function as a putative suicide gene moiety. However, achieving this aim proved more arduous owing to the conformational rather than linear nature of this epitope; initial constructs composed from the rituximab binding epitope derived from the parental CD20 antigen, as identified by crystallographic binding data, proved inferior to binding demonstrated by the

parental antigen. Fortunately, this experimental avenue was rescued by rituximab binding mimotopes as identified by Perosa *et al*[174], with clear binding demonstrated by the R3-C mimotope when presented on the CD8α stalk. Furthermore, co-presentation of both epitope binding domains demonstrated clear retention of functional antibody binding by both target antibodies offering promise as a minimal marker-suicide gene system.

12.2.2. Analysis of CDC–mediated deletion of epitope constructs

Having confirmed the functional capacity for antibody binding and cellular selection of double-epitope expression constructs, next we sought to establish the potential for cellular deletion through *in vitro* CDC and ADCC assays. Commencing with the less complex CDC assays, we report results from two alternative flow cytometry based CDC assays designed to interrogate the sensitivity and specificity of CDC-mediated deletion. Our initial CDC sensitivity assays examining RQ8 deletion proved disappointing despite clear rituximab binding capacity. However we observed that sensitivity to deletion was inconsistent across the target population with high expressers proving acutely sensitive whilst low expression appeared protective. Premising that molecular re-engineering of epitope constructs might enhance binding affinity, increase valency, or otherwise enhance sensitivity to CDC, we generated a panel of variant iterations for further examination. Comparison of CDC-mediated deletion of this panel of epitope expression constructs identified a hierarchy of sensitivity, with RQR8 proving acutely sensitive to complement mediated deletion even surpassing that demonstrated by the CD20 positive control. Following *in silico* analysis of RQR8 and the crystallographic structure of rituximab, it seems likely that the observed acute sensitivity reflects bivalent rituximab binding by RQR8 thereby resolving the density dependent limitation of CDC. However, absolute confirmation of this bivalent binding hypothesis would require crystallographic analysis which is beyond the scope of this project.

Whereas sensitivity assays examined the comparative capacity for CDC-mediated deletion across a panel of constructs, we also established specificity CDC assays to demonstrate the efficacy of deletion of a cellular population mimicking therapeutic product. From these assays we report typically >98% deletion of RQR8 expressing targets whilst analogous Q8 targets present

within the sample remain untouched. Finally, to ensure this capacity for rituximab-mediated deletion is physiologically relevant, we examined CDC-mediated deletion of RQR8 targets through time-course and dose-titration assays, demonstrating that CDC-mediated deletion of RQR8 occurs both rapidly and within the therapeutic dose of rituximab[171].

As the CD20[154] and ΔEGFR[124] suicide genes represents analogous strategies to RQR8, it should be noted that efficacy of CDC-mediated deletion of these suicide genes would likely demonstrate a similar density dependent limitation as identified by our alternative epitope constructs, whilst also imposing expression limitation due to longer coding sequences.

12.2.3. Analysis of ADCC–mediated deletion of epitope constructs

Having successfully demonstrated CDC-mediated deletion, we next sought to assess the sensitivity of our epitope constructs through ADCC-mediated deletion. From *in vitro* ADCC modelling, we report generation of two separate flow cytometry based ADCC assays: a sensitivity assay which enables independent comparison between similar constructs and a specificity assay which demonstrates efficacy of ADCC-mediated deletion of a target population relative to a control population present within the same sample. Flow cytometry analysis enables direct observation of the cellular targets under interrogation, whilst the extended assay duration facilitates consideration of both rapid (perforin/granzyme) and prolonged (TRAIL/FASL) mechanisms of ADCC-mediated deletion. From these assays we demonstrated acute sensitivity of RQR8-expressing targets to ADCC-mediated deletion, superior to that observed for alternative epitope expression iterations and at least equal, if not superior to that observed by the CD20 expressing positive control. Further, this effect was specific to rituximab-binding targets with no deletion observed against the highly similar Q8 expressing controls as suggested by Q8 target proliferation despite the presence of both rituximab and NK-cell effectors.

Contrasting with sensitivity assays, specificity assays, examined the efficacy of ADCC-mediated deletion of an analogous target as would be anticipated from a transduced and purified transgenic therapeutic product. Inclusion of an internal Q8 expressing control further highlighted specificity of deletion was restricted to the target population.

Finally, Alemtuzumab is a particularly lytic therapeutic antibody targeting the GPI anchored cellular antigen CD52. Premising high CD52 antigen density on T-cells might offer potential for similarly high expression levels of a GPI-anchored target; we established an expression construct whereby the RQR motif was presented on a GPI anchor which we included in our ADCC assays. Curiously, from a specificity assay from a single donor comparing the efficacy of ADCC-mediated deletion between RQR8 and RQR-GPI, we observed superior deletion of the RQR-GPI construct. Whether this enhanced deletion resulted from potentially higher surface expression mediated by the GPI anchor expression strategy, or from localisation of GPI anchored RQR epitopes in lipid rafts, this observation of variation in sensitivity of the identical epitope presented in alternative formats suggests potential for the antigenic target to factor in the capacity for lytic antibody efficacy. However, despite promising deletion facilitated by the minimal RQR-GPI construct, we premised the single mutation required to ablate GPI anchored expression posed an untenable risk for cellular escape, inappropriate for a putative suicide gene so this observation was not examined further in this project.

12.2.4. Demonstration of modular capacity of RQR8

Beyond resolving potential GvHD as might manifest following haploidentical HSCT, marker-suicide genes largely offer a supplemental role rather than the primary objective of ACT, hence it remains essential that this component can function in a modular capacity alongside other common T-cell engineering components such as a CAR or TCR. We report functional retention of the marker gene capacity when RQR8 is co-expressed with either the GD2-CAR or the WT1-TCR. Further functional assessment examined RQR8 co-expression with the GD2-CAR where we report full functional retention of both marker and suicide gene capacities as well as retention of GD2-CAR mediated cytotoxicity demonstrating the clear modular capacity of RQR8 and supporting negligible impact from co-expression of this minimal cassette upon other engineering components. Concomitant therapeutic toxicities including OTOT[101, 102, 291], cytokine storms[20], macrophage activation syndrome[106], and both neural[104] and cardiac toxicities[107] have all been reported even whilst CAR-mediated T-cell ACT remains its infancy. As further toxicities are likely to be identified as this technology develops, there remains both a pressing need and a growing requirement to include a suitable strategy to offer potential mitigation or

resolution of unwanted therapeutic complications. However, as all suicide genes have limitations, it may prove appropriate to consider the suicide gene strategy alongside anticipated toxicities to optimise potential to resolve prospective adverse events, bearing in mind that it is unlikely that any suicide gene strategy could facilitate recovery from an acute cytokine storm. Hence, successful application of suicide gene therapy will likely only result from appropriate matching of manifold factors such as gene transfer application, therapeutic regimen, suicide gene strategy and the health status of the patient at time of transfer. Although many lessons have been learned from ACT trials, many more likely remain outstanding.

12.2.5. Protein production of mRtx–IgG2a

Premising the chimeric nature of rituximab and the potential for mouse anti-chimeric antibody responses might represent uncontrolled variables impairing therapeutic efficacy of rituximab, we chose to employ a fully murine antibody for *in vivo* modelling experiments. Due to the IgG1 format of the IDEC2B8 hybridoma, it was necessary to re-engineer the rituximab antibody into a murine IgG2a format, analogous to the therapeutic antibody, to achieve optimal effector recruitment and activation. Having established suitable plasmids to facilitate protein production, it was necessary to establish a suitable strategy which could rapidly and consistently generate milligram quantities of functional product at minimal cost. Aiming for a suspension cell culture strategy to achieve this aim, we report stable production of antibody from transgenic K562 cell culture achieving protein production of 32.5mg/L, which is comparable with TGE strategies but at reduced cost and offering lower batch to batch variation. With optimisation, the three dimensional culture format and hardy nature of K562 cells might prove a promising alternative to protein production strategies currently in practice.

12.2.6. *In vivo* modelling experiments

Having established an effective acute GvHD model intended to confirm the *in vivo* efficacy of RQR8, we were initially disappointed to observe limited efficacy and failure to resolve pathology. However, once the innate immune system has become fully activated, there may be limitations to the potential for resolution of fulminant disease mediated through suicide gene therapy strategy alone. This failing highlights a key limitation of an antibody-mediated

suicide gene strategy; although extrinsic deletion mechanisms reduce potential for cellular escape, conditions which impair effector activity similarly reduce levels of deletion which can be achieved. Further, our choice of model also represented an extreme scenario which is of limited clinical relevance. Our initial choice of an acute GvHD model resulted from reports from the literature[279] and anecdotal evidence from research colleagues (personal communication with Barry Flutter and Angelika Holler) regarding limitations in the functional capacity of *ex vivo* manipulated splenocytes. However, contrasting with initial concerns, we observed fulminant disease in all animals and in all experiments considered, attesting to the severity of this model. Reconsidered from this perspective, we report significant capacity for rituximab-mediated RQR8 deletion despite profound impairment of effector mechanisms. Moreover, reports from the haploidentical TK.007 trial already offer clinical precedent where induction of the suicide gene machinery proved insufficient to resolve fulminant GvHD alone[142]. In this trial, 5/11 patients required supplemental steroid therapy in combination with ganciclovir treatment to achieve resolution of GvHD. In subsequent examination we considered the less aggressive and more clinically relevant haploidentical model, from which we report rituximab mediated deletion offers a consistent capacity to resolve fulminant disease. From examination of rituximab-mediated deletion of RQR8-expressing targets, both in isolation and when co-expressed alongside a CD19-CAR, we observed clearance from all compartments 7 days following commencement of rituximab therapy, contrasting with profound engraftment which was observed from all experimental control subjects. Subsequent examination of progressive *in vivo* deletion, we observed significant clearance from all compartments at the first time-point considered; 6 hours following therapeutic administration achieving 73, 45, 67 and 18% clearance from the blood, spleen, bone marrow and lymph nodes respectively, progressing to 96, 75, 87 and 82% clearance from the blood, spleen, bone marrow and lymph nodes respectively following 7 days of therapy. Although the absolute efficacy of any suicide-gene strategy can only be fully assessed through clinical experience, this comprehensive dataset highlights the potential of RQR8 to effect effective cellular deletion under profoundly challenging *in vivo* conditions.

12.2.7. Epitope applications

Progressing from demonstration of successful presentation of antibody binding epitopes on cellular surfaces, we further describe the potential to extend this strategy to the common HA, myc and V5 epitope tags. Although epitope presentation was successfully demonstrated by both the CD8 stalk and GPI-anchored molecular spacer strategies, CD8 stalk presentation appears to offer a superior presentation format. This observation may be due to the dimeric presentation afforded by the CD8 stalk and/or superior cellular projection as compared with the GPI anchor strategy. Epitope identification mediated by chromophore-conjugated antibodies enable reduced spectral overlap compared with fluorescent protein marking strategies allowing for concurrent investigation such as immunophenotyping and can enable facile indirect magnetic bead selection for purification. Further, the minimal molecular footprint imposed by these tags, as short as 55a.a. with the HA-GPI marker tag should facilitate application in even the most restrictive vector packaging strategies. Thus we premise application of epitope tags in this manner facilitates facile multi-gene marking and offers significant potential as a research tool.

12.3. Limitations of RQR8

A recent report by Marin *et al*[173], describes results from comparative assessment of the efficacy of the four main suicide gene strategies available at that time; namely HSVtk, iCaspase9, TMPK2 and CD20, which were all expressed in EBV-CTLs to facilitate transgene analysis following sustained culture. (Note: the ΔEGFR marker-suicide gene, *vide infra,* was excluded from this comparison due the research having commenced prior to publication of this system). In this report, none of the suicide genes assessed appeared to demonstrate notable impact upon the immunophenotype, proliferation or function of the EBV-CTLs suggesting a lack of basal toxicity following 40 days of continuous culture. However, a variation between alternative suicide gene strategies was demonstrated through efficiency of cellular deletion. Although both iCaspase9 and CD20 suicide genes demonstrate similar efficacy of cellular deletion as assessed at 1, 4 and 7 day time-points, HSVtk required 4 days to achieve equivalent deletion whilst TMPK2 remained inferior at all timepoints observed. This demonstrates that an antibody-mediated strategy

for cellular deletion of putative suicide genes potentially offers similar efficacy to that demonstrated by iCaspase9, which currently represents the current gold-standard.

As the merits and functional limitations of the alternative suicide gene strategies have already been extensively discussed, it seems helpful to consider the comparative biological distribution of the respective inducing drugs in achieving the desired aim of the corresponding suicide genes to enable further discrimination of the advantages and disadvantages separating the various strategies. RQR8 was initially engineered to address potential toxicity associated with solid-tumour ACT where potential therapeutic toxicities remain less defined as those which have been identified through anti-CD19 CAR therapies. Thus, discrepancy between the suicide gene systems might be most apparent when considering variation in the capacity for the respective inducing drugs to resolve potential ACT-mediated toxicity in a protected site such as the central nervous system[104]. Studies considering the biodistribution of Ganciclovir in non-human primates, clearly demonstrates the favourable bioavailability profile offered by this drug[292]; hence, for HSVtk, the primary limitation to this system remains the potential immunogenicity of the transgene due to the viral origin[293]. Thus, despite the substantial history of clinical application of HSVtk as a suicide gene, future use remains restricted to profoundly immunosuppressive environments such as haploidentical HSCT. Correspondingly, to address the limitation imposed by immunogenicity, iCaspase9 was engineered from human proteins to preclude immune rejection. However, in this instance, despite being a small molecule, some evidence suggests limited penetrance of the blood brain barrier by the FK506 dimerizer AP20187[294]. This is in addition to restrictive access to the clinical grade dimerizer imposed by Bellicum pharmaceuticals further restricting general application of this system for clinical application. Finally, both RQR8 and the ΔEGFR suicide genes employ antibodies as the therapeutic agent. Extensive use of rituximab in clinical practice is testament to the lack of therapeutic toxicity from this agent. Furthermore, observation of CNS penetration supports a favourable biodistribution including immune-privileged sites such as the CNS[295]. Although similar evidence exists regarding cetuximab penetrance of the CNS[296], in this instance, therapeutic toxicity remains a limiting factor (*vide infra)*. Furthermore, in instances where rituximab chemotherapy is indicated,

there remains the option to treat the patient with ofatumumab, thus application of rituximab to effect suicide-gene machinery does not preclude therapeutic potential for the patient. This contrasts with use of Ganciclovir to effect HSVtk-mediated deletion precluding application of Ganciclovir to resolve CMV reactivation.

Antibody mediated suicide gene strategies offer an extrinsic mechanism for cellular deletion excluding opportunities for escape through mutation of cellular metabolic machinery, although potential down-regulation or loss of transgene expression remain a common potential escape risk from all suicide gene strategies. As transgene size has been correlated with expression levels[119, 163], a suicide gene system composed from a minimal coding sequence offers the maximum potential to preclude escape through low expression. Suicide-gene strategies based on transgenic expression of a binding target for a therapeutic antibody have been proposed[124, 154, 155, 165, 166] with the CD20/rituximab[154] and ΔEGFR/cetuximab[124] systems representing analogous strategies to RQR8. Reports from various groups proposing CD20 as a putative suicide gene strategy describe widely disparate results regarding efficacy of rituximab-mediated deletion of CD20 transgenic T-cells which remain difficult to interpret[154, 166, 173, 297]. In our hands, magnetic selection of ectopically expressed CD20 on T-cells resulted in cellular deletion precluding application of CD20 as a marker gene, whilst the long coding sequence impacted upon both viral titre and transgene expression levels. Further, as the biological function of CD20 remains unknown, the impact of cellular expression of this transgene remains immeasurable. Notably, results of RQR8 efficacy have been readily recapitulated by research collaborators supporting the consistency of our findings. Alternatively, ΔEGFR has also been proposed as a putative suicide gene: here, ΔEGFR is expressed on the T-cell surface with depletion effected by the anti-EGFR therapeutic mAb cetuximab. Although this system is likely to be less immunogenic than RQR8, RQR8 retains some attractive advantages: firstly, RQR8 has an “off-the-shelf” clinical grade selection system available; secondly rituximab monotherapy is well tolerated by the majority of patients with little increase in opportunistic infection[168, 169] and with no maximally tolerated dose. In contrast treatment with cetuximab is accompanied by acneiform follicular skin exanthema in more than 80 % of patients. Severe exanthema (grade III/IV) develops in about 9-19 % of patients imposing the

necessity for cetuximab dose reduction or cessation[167]. Thirdly, Rituximab's property as a highly potent lymphodepleting agent in human subjects is well established; in contrast cetuximab offers reduced efficacy mediated by CDC compared with ADCC, with potential restriction in ADCC efficacy due to HLA-E expression[298]. Further, there remains potential for the development of cetuximab resistance due to the HACA response reflecting the chimeric nature of cetuximab increased by potential residual cetuximab antibody following cellular selection. As a modular engineering component, this limitation might restrict application of ΔEGFR as a suicide gene dependent on the therapeutic target of interest. In contrast, RQR8 remains less than half the size of either CD20 or ΔEGFR, reducing the impact upon packaging capacity and transgene expression.

From a bioinformatics analysis of putative immunogenic epitopes assessed using the LBtope[219] linear B-cell epitope prediction server and the NetCTL 1.2[220] servers respectively, we identified clear evidence of putative CTL and B-cell immunogenic epitopes present within RQR8. The impact of the B-cell epitopes present within RQR8 may become apparent through future clinical trials; proposed application of RQR8 in a GD2 CAR trial for neuroblastoma will present an informative contrast with proposed inclusion in CD19 CAR trials for CLL and lymphoma, to identify the risk of immunogenicity posed by the B-cell epitopes identified. Similarly, these trials should prove informative regarding the small number of putative CTL epitopes which were identified, variant in number between MHC supertypes. Despite identification of potentially immunogenic epitopes, these remain fewer than what would be anticipated from larger CAR-constructs currently in clinical application. Further, as instances of sustained engraftment from neomycin resistance[299] and HSVtk[300] transgenic cells have been reported, only clinical application will accurately assess the full impact of the potentially immunogenic epitopes identified.

However, in addition to potential immunogenicity, there remain two further main limitations to application of RQR8: prolonged serum half-life of rituximab and potentially impaired effector mechanisms resulting from pre-conditioning regimens. Although rituximab efficacy offers the critical advantage to the RQR8 strategy, it also imposes a key limitation. The prolonged serum half-life of rituximab, ranging between approximately 24-30

days for males and females respectively[218], presents a limitation to application of RQR8 toward rituximab pre-treated patients. Through *in vitro* dose-titration CDC assays, we observed only modest reduction in the efficacy of rituximab-mediated deletion even at 12.5μg/ml rituximab, representing the lowest concentration examined. With a median rituximab serum level of 1.1μg/ml nine months following termination of rituximab therapy[218], we cannot exclude potential for cellular deletion even nine months post rituximab therapy. A second main limitation to efficacy of an antibody-mediated suicide gene strategy results from impaired effector mechanisms. Resulting from profound immunosuppression following pre-conditioning regimens, there may be a lag-phase required for regeneration of the effector compartment before full efficacy of the suicide-gene strategy can be restored. However it remains unclear as to how relevant this finding might be due to the artificial scenario imposed in our acute GvHD model. In this model, the direct mismatch, severe preconditioning and high infusion dose all factored into the observed toxicity. Additionally, therapeutic benefit was clearly observed in this model and it is likely that further rituximab therapy might have proved beneficial had further monitoring been possible to identify this requirement. Further, an acute cytokine storm represents the most probable early onset toxicity which likely precludes resolution through any suicide gene strategy.

One further potential limitation which should be acknowledged might result from antigenic modulation or 'epitope shaving'. Epitope shaving was identified following clinical observations in CLL of circulating B-cells stripped of the CD20 antigen following rituximab therapy. Subsequent investigation suggested that this observation was likely due to removal of rituximab-CD20 complexes mediated by the high affinity FcγRI present on monocytes and macrophages. Notably, loss of CD20 was not observed when B-cell burden was low. Additionally, a solution proposed to resolve the therapeutic limitation presented by epitope shaving involves lower and more frequent rituximab therapy infusions and/or FcγRI blocking as potential solutions[301].

Alternative marker/suicide gene strategies which have translated into clinical application have been reported (HSVtk/NGFR[142], iCasp9/CD19[125, 152], ΔEGFR[124]), each possessing unique limitations, all necessitating lengthy coding sequences for the suicide gene moiety alone (377, 402 and 336 amino acids respectively;

note: for ΔEGFR this sequence codes for both marker and suicide gene moieties) compared with 139 for both marker and suicide gene capacity of RQR8. Thus, directly compatible with Miltenyi CliniMACS reagents and the substantial safety profile demonstrated by rituximab therapy, we propose that RQR8 represents a significant advance as a putative marker/suicide gene for adoptive T-cell therapy.

12.4. Future research resulting from project observations

The impetus driving research toward establishing a novel marker-suicide gene developed from pressing clinical need. With HSVtk limited by immunogenicity and iCaspase9 restricted by access to clinical grade dimeriser, there was an urgent requirement for an alternative safety mechanism. So it is hardly surprising that development of the ΔEGFR suicide gene was established independently alongside our research into RQR8 with ΔEGFR currently in clinical trial and potential clinical application of RQR8 pending. Although this report has focussed upon discovery and validation of RQR8 functionality, there has been further concurrent pre-clinical preparation performed by myself and others including *in vivo* tumour modelling experiments and full-scale test production of cellular product respectively further confirming functional capacity of RQR8. At time of writing, RQR8 has been proposed for application in clinical CAR trials targeting GD2 in Neuroblastoma and CD19 in CLL and lymphoma. Should these applications be approved, the solid versus humoral nature of the target tumours in these trials offer great potential for achieving greater clarity regarding the risk presented by potential immunogenicity of RQR8.

A curious observation identified from this project was the potential variation between CDC and ADCC mediated efficacy between GPI anchored and CD8 stalk presentation strategies. Although the efficacy of CDC mediated deletion appeared superior for the CD8 construct compared with the GPI anchored alternative, the opposite was observed during ADCC mediated deletion assays. In light of the potential for cellular escape resulting from the GPI expression strategy, we premised this would prove inappropriate for a suicide gene system presenting an untenable potential for cellular escape under the selection pressures which would be involved. However, as an academic question, this observation offers intriguing insight into potential variation in

sensitivity to CDC and ADCC mediated deletion demonstrated by cellular epitopes dependent on presentation. Given the extensive budget afforded to research and development of therapeutic antibodies, research progressing along this tangent might offer significant insight into the suitability of cellular antigens as therapeutic targets with regard to optimising the most suitable strategy for targeting them. Similar observation is indicated between the sensitivity of deletion conferred by RQ8 versus RQR8. Although RQR8 is considerably more sensitive to CDC mediated deletion, the two constructs demonstrate very similar levels of deletion from ADCC mediated assays.

Additionally, successes following from mRtx-IgG2a production have demonstrated the capacity of K562 cells as a protein production platform. Further work progressing from this research supports our initial observations and future work aims to demonstrate the generalizable potential of this strategy.

As the complexity of *in vitro* modelling experiments increases, concurrent and clear identification of multiple transgenic markers becomes increasingly important. Although fluorescent proteins have long been the mainstay of cellular marking, these impose limitations in marking capacity due to spectral overlap. For example, the 4 laser configuration of the LSR Fortessa instrument potentially offers 16 channels for multi-spectral analysis; in contrast, spectral bleed resulting from the broad emission profiles of fluorescent proteins restricts concurrent analysis to 5 channels when only fluorescent proteins are considered (paper in preparation). Hence, application of epitope-based targets to facilitate simultaneous marking for multiple separate targets in addition to cellular antigens represents a significant advance upon restrictions imposed by fluorescent proteins. Additionally, the surface expression of epitope tags offers potential for magnetic cellular selection reducing the risk for contamination resulting from flow cytometry based cellular sorting. Future work aims to demonstrate the generalizability of the marker gene strategy identified during the course of this project.

12.5. Conclusions

In addition to facilitating MACS selection, the marker gene capability of RQR8 also enables high sensitivity tracking by flow cytometry analysis to assess *in vivo* persistence and expansion. Further, the marker gene capacity also enables

detection of engineered cells in fixed biopsy samples through IHC. The indirect suicide gene strategy limits the risk for cellular escape which might result from mutation or attenuated gene expression of intrinsic strategies.

In summary, we have created a 136 amino acid epitope-based marker/suicide gene for T-cells. The translated protein is stably expressed on the cell surface following retroviral transduction. It binds QBEnd10 analogously to full-length CD34 allowing clinical-grade sorting with off-the-shelf reagents and offers clear *in vivo* tracking. Further, the construct binds rituximab; the dual epitope design engenders highly effective CDC and ADCC and consequently renders T-cells highly susceptible to *in vivo* rituximab mediated depletion. Due to the small size of RQR8, it can easily be co-expressed with a wide range of T-cell engineering components.

The ultimate measure of utility of RQR8 will be determined through clinical experience. At time of writing, RQR8 has been incorporated in several CAR cassettes destined for clinical application. I hope that the functional capacity of RQR8 will be of great practical utility to existing T-cell engineering components and will make ACT with engineered T-cells cheaper, safer and ultimately more efficacious.

References

1. Topalian, S.L., Weiner, G.J. & Pardoll, D.M. Cancer immunotherapy comes of age. *J Clin Oncol* **29**, 4828-4836 (2011).
2. Zhou, J., Dudley, M.E., Rosenberg, S.A. & Robbins, P.F. Persistence of multiple tumor-specific T-cell clones is associated with complete tumor regression in a melanoma patient receiving adoptive cell transfer therapy. *J Immunother* **28**, 53-62 (2005).
3. Fujita, Y., Rooney, C.M. & Heslop, H.E. Adoptive cellular immunotherapy for viral diseases. *Bone Marrow Transplant* **41**, 193-198 (2008).
4. Peggs, K.S. et al. Directly selected cytomegalovirus-reactive donor T cells confer rapid and safe systemic reconstitution of virus-specific immunity following stem cell transplantation. *Clin Infect Dis* **52**, 49-57 (2011).
5. Pule, M.A. et al. Virus-specific T cells engineered to coexpress tumor-specific receptors: persistence and antitumor activity in individuals with neuroblastoma. *Nat Med* **14**, 1264-1270 (2008).
6. Rosenberg, S.A. & Dudley, M.E. Adoptive cell therapy for the treatment of patients with metastatic melanoma. *Curr Opin Immunol* **21**, 233-240 (2009).
7. Rosenberg, S.A. Cell transfer immunotherapy for metastatic solid cancer--what clinicians need to know. *Nat Rev Clin Oncol* **8**, 577-585 (2011).
8. Rosenberg, S.A. IL-2: the first effective immunotherapy for human cancer. *J Immunol* **192**, 5451-5458 (2014).
9. Lichty, B.D., Breitbach, C.J., Stojdl, D.F. & Bell, J.C. Going viral with cancer immunotherapy. *Nat Rev Cancer* **14**, 559-567 (2014).
10. Blank, C.U. & Enk, A. Therapeutic use of anti-CTLA-4 antibodies. *Int Immunol* (2014).
11. Desreumaux, P. et al. Safety and efficacy of antigen-specific regulatory T-cell therapy for patients with refractory Crohn's disease. *Gastroenterology* **143**, 1207-1217 e1202 (2012).
12. Putnam, A.L. et al. Expansion of human regulatory T-cells from patients with type 1 diabetes. *Diabetes* **58**, 652-662 (2009).
13. Perruccio, K. et al. Transferring functional immune responses to pathogens after haploidentical hematopoietic transplantation. *Blood* **106**, 4397-4406 (2005).
14. Kershaw, M.H., Westwood, J.A. & Darcy, P.K. Gene-engineered T cells for cancer therapy. *Nat Rev Cancer* **13**, 525-541 (2013).
15. Scholler, J. et al. Decade-long safety and function of retroviral-modified chimeric antigen receptor T cells. *Sci Transl Med* **4**, 132ra153 (2012).
16. Riviere, I., Dunbar, C.E. & Sadelain, M. Hematopoietic stem cell engineering at a crossroads. *Blood* **119**, 1107-1116 (2012).
17. Ellis, J. et al. Benefits of utilizing gene-modified iPSCs for clinical applications. *Cell Stem Cell* **7**, 429-430 (2010).
18. Miller, J.S. et al. NCI First International Workshop on The Biology, Prevention, and Treatment of Relapse After Allogeneic Hematopoietic Stem Cell Transplantation: Report from the Committee on the Biology Underlying Recurrence of Malignant Disease following Allogeneic HSCT: Graft-versus-Tumor/Leukemia Reaction. *Biol Blood Marrow Transplant* **16**, 565-586 (2010).
19. Ferrara, J.L., Levine, J.E., Reddy, P. & Holler, E. Graft-versus-host disease. *Lancet* **373**, 1550-1561 (2009).
20. Morgan, R.A. et al. Case report of a serious adverse event following the administration of T cells transduced with a chimeric antigen receptor recognizing ERBB2. *Mol Ther* **18**, 843-851 (2010).
21. Porter, D.L., Levine, B.L., Kalos, M., Bagg, A. & June, C.H. Chimeric antigen receptor-modified T cells in chronic lymphoid leukemia. *N Engl J Med* **365**, 725-733 (2011).
22. Grupp, S.A. et al. CD19-Redirected Chimeric Antigen Receptor T (CART19) Cells Induce a Cytokine Release Syndrome (CRS) and Induction of Treatable Macrophage Activation Syndrome (MAS) That Can Be Managed by the IL-6 Antagonist Tocilizumab (toc). *ASH Annual Meeting Abstracts* **120**, 2604- (2012).
23. Sadelain, M. Eliminating cells gone astray. *N Engl J Med* **365**, 1735-1737 (2011).
24. Cruz, C.R. et al. Adverse events following infusion of T cells for adoptive immunotherapy: a 10-year experience. *Cytotherapy* **12**, 743-749 (2010).
25. Dotti, G., Savoldo, B. & Brenner, M. Fifteen years of gene therapy based on chimeric antigen receptors: "are we nearly there yet?". *Hum Gene Ther* **20**, 1229-1239 (2009).
26. Kohn, D.B. & Candotti, F. Gene therapy fulfilling its promise. *N Engl J Med* **360**, 518-521 (2009).
27. Braun, C.J. et al. Gene therapy for Wiskott-Aldrich syndrome--long-term efficacy and genotoxicity. *Sci Transl Med* **6**, 227ra233 (2014).

28. Bueler, H. & Mulligan, R.C. Induction of antigen-specific tumor immunity by genetic and cellular vaccines against MAGE: enhanced tumor protection by coexpression of granulocyte-macrophage colony-stimulating factor and B7-1. *Mol Med* **2**, 545-555 (1996).
29. Jenq, R.R. & van den Brink, M.R. Allogeneic haematopoietic stem cell transplantation: individualized stem cell and immune therapy of cancer. *Nat Rev Cancer* **10**, 213-221 (2010).
30. Osgood, E.E., Riddle, M.C. & Mathews, T.J. APLASTIC ANEMIA TREATED WITH DAILY TRANSFUSIONS AND INTRAVENOUS MARROW; CASE REPORT*. *Ann Intern Med* **13**, 357-367 (1939).
31. Thomas, E.D., Lochte, H.L., Jr., Cannon, J.H., Sahler, O.D. & Ferrebee, J.W. Supralethal whole body irradiation and isologous marrow transplantation in man. *J Clin Invest* **38**, 1709-1716 (1959).
32. Mathe, G. et al. Successful Allogenic Bone Marrow Transplantation in Man: Chimerism, Induced Specific Tolerance and Possible Anti-Leukemic Effects. *Blood* **25**, 179-196 (1965).
33. Beutler, E. & Williams, W.J. Williams hematology, Edn. 6th. (McGraw-Hill, Medical Publishing Division, New York; 2001).
34. Bach, F.H. Genetics of transplantation: the major histocompatibility complex. *Annu Rev Genet* **10**, 319-339 (1976).
35. Lorenz, E., Uphoff, D., Reid, T.R. & Shelton, E. Modification of irradiation injury in mice and guinea pigs by bone marrow injections. *J Natl Cancer Inst* **12**, 197-201 (1951).
36. Berenson, R.J. et al. Antigen CD34+ marrow cells engraft lethally irradiated baboons. *J Clin Invest* **81**, 951-955 (1988).
37. Molineux, G., Pojda, Z., Hampson, I.N., Lord, B.I. & Dexter, T.M. Transplantation potential of peripheral blood stem cells induced by granulocyte colony-stimulating factor. *Blood* **76**, 2153-2158 (1990).
38. Deol, A. & Lum, L.G. Role of donor lymphocyte infusions in relapsed hematological malignancies after stem cell transplantation revisited. *Cancer Treat Rev* **36**, 528-538 (2010).
39. Kolb, H.J. et al. Donor leukocyte transfusions for treatment of recurrent chronic myelogenous leukemia in marrow transplant patients. *Blood* **76**, 2462-2465 (1990).
40. Bonini, C. et al. HSV-TK gene transfer into donor lymphocytes for control of allogeneic graft-versus-leukemia. *Science* **276**, 1719-1724 (1997).
41. Rosenberg, S.A. et al. Treatment of patients with metastatic melanoma with autologous tumor-infiltrating lymphocytes and interleukin 2. *J Natl Cancer Inst* **86**, 1159-1166 (1994).
42. Straathof, K.C., Bollard, C.M., Rooney, C.M. & Heslop, H.E. Immunotherapy for Epstein-Barr virus-associated cancers in children. *Oncologist* **8**, 83-98 (2003).
43. Papadopoulos, E.B. et al. Infusions of donor leukocytes to treat Epstein-Barr virus-associated lymphoproliferative disorders after allogeneic bone marrow transplantation. *N Engl J Med* **330**, 1185-1191 (1994).
44. Melenhorst, J.J. et al. Allogeneic virus-specific T cells with HLA alloreactivity do not produce GVHD in human subjects. *Blood* **116**, 4700-4702 (2010).
45. Romero, J.M. et al. Coordinated downregulation of the antigen presentation machinery and HLA class I/beta2-microglobulin complex is responsible for HLA-ABC loss in bladder cancer. *Int J Cancer* **113**, 605-610 (2005).
46. Bendle, G.M. et al. Lethal graft-versus-host disease in mouse models of T cell receptor gene therapy. *Nat Med* **16**, 565-570, 561p following 570 (2010).
47. Eshhar, Z. Tumor-specific T-bodies: towards clinical application. *Cancer Immunol Immunother* **45**, 131-136 (1997).
48. Brentjens, R.J. et al. Safety and persistence of adoptively transferred autologous CD19-targeted T cells in patients with relapsed or chemotherapy refractory B-cell leukemias. *Blood* **118**, 4817-4828 (2011).
49. Park, J.R. et al. Adoptive transfer of chimeric antigen receptor re-directed cytolytic T lymphocyte clones in patients with neuroblastoma. *Mol Ther* **15**, 825-833 (2007).
50. Kershaw, M.H. et al. A phase I study on adoptive immunotherapy using gene-modified T cells for ovarian cancer. *Clin Cancer Res* **12**, 6106-6115 (2006).
51. Hacein-Bey-Abina, S. et al. Sustained correction of X-linked severe combined immunodeficiency by ex vivo gene therapy. *N Engl J Med* **346**, 1185-1193 (2002).
52. Hacein-Bey-Abina, S. et al. LMO2-associated clonal T cell proliferation in two patients after gene therapy for SCID-X1. *Science* **302**, 415-419 (2003).
53. Billingham, R.E. The biology of graft-versus-host reactions. *Harvey Lect* **62**, 21-78 (1966).
54. Tolar, J., Villeneuve, P. & Keating, A. Mesenchymal stromal cells for graft-versus-host disease. *Hum Gene Ther* **22**, 257-262 (2011).

55. Paczesny, S., Choi, S.W. & Ferrara, J.L. Acute graft-versus-host disease: new treatment strategies. *Curr Opin Hematol* **16**, 427-436 (2009).
56. Wanko, S.O. & Chao, N.J. Non-pharmacologic approaches to graft-versus-host prevention. *Blood Rev* **19**, 203-211 (2005).
57. Shlomchik, W.D. Graft-versus-host disease. *Nat Rev Immunol* **7**, 340-352 (2007).
58. Janeway, C.A., Jr. The immune system evolved to discriminate infectious nonself from noninfectious self. *Immunol Today* **13**, 11-16 (1992).
59. Archbold, J.K., Macdonald, W.A., Burrows, S.R., Rossjohn, J. & McCluskey, J. T-cell allorecognition: a case of mistaken identity or deja vu? *Trends Immunol* **29**, 220-226 (2008).
60. Felix, N.J. & Allen, P.M. Specificity of T-cell alloreactivity. *Nat Rev Immunol* **7**, 942-953 (2007).
61. Amrolia, P.J. et al. Adoptive immunotherapy with allodepleted donor T-cells improves immune reconstitution after haploidentical stem cell transplantation. *Blood* **108**, 1797-1808 (2006).
62. Koreth, J. et al. Interleukin-2 and regulatory T cells in graft-versus-host disease. *N Engl J Med* **365**, 2055-2066 (2011).
63. Di Ianni, M. et al. Tregs prevent GVHD and promote immune reconstitution in HLA-haploidentical transplantation. *Blood* **117**, 3921-3928 (2011).
64. Vago, L. et al. T-cell suicide gene therapy prompts thymic renewal in adults after hematopoietic stem cell transplantation. *Blood* **120**, 1820-1830 (2012).
65. Baum, C., Schambach, A., Bohne, J. & Galla, M. Retrovirus vectors: toward the plentivirus? *Mol Ther* **13**, 1050-1063 (2006).
66. Quintas-Cardama, A. et al. Multifactorial optimization of gammaretroviral gene transfer into human T lymphocytes for clinical application. *Hum Gene Ther* **18**, 1253-1260 (2007).
67. Goff, S.P. Host factors exploited by retroviruses. *Nat Rev Microbiol* **5**, 253-263 (2007).
68. Sauce, D. et al. Retrovirus-mediated gene transfer in primary T lymphocytes impairs their anti-Epstein-Barr virus potential through both culture-dependent and selection process-dependent mechanisms. *Blood* **99**, 1165-1173 (2002).
69. Qasim, W. et al. Lentiviral vectors for T-cell suicide gene therapy: preservation of T-cell effector function after cytokine-mediated transduction. *Mol Ther* **15**, 355-360 (2007).
70. Mesel-Lemoine, M. et al. Initial depletion of regulatory T cells: the missing solution to preserve the immune functions of T lymphocytes designed for cell therapy. *Blood* **107**, 381-388 (2006).
71. Frecha, C., Levy, C., Cosset, F.L. & Verhoeyen, E. Advances in the field of lentivector-based transduction of T and B lymphocytes for gene therapy. *Mol Ther* **18**, 1748-1757 (2010).
72. Verhoeyen, E. et al. IL-7 surface-engineered lentiviral vectors promote survival and efficient gene transfer in resting primary T lymphocytes. *Blood* **101**, 2167-2174 (2003).
73. Sakuma, T., Barry, M.A. & Ikeda, Y. Lentiviral vectors: basic to translational. *Biochem J* **443**, 603-618 (2012).
74. Huang, X. et al. Stable gene transfer and expression in human primary T cells by the Sleeping Beauty transposon system. *Blood* **107**, 483-491 (2006).
75. Nakazawa, Y. et al. Optimization of the PiggyBac transposon system for the sustained genetic modification of human T lymphocytes. *J Immunother* **32**, 826-836 (2009).
76. Ivics, Z. et al. Transposon-mediated genome manipulation in vertebrates. *Nat Methods* **6**, 415-422 (2009).
77. Hackett, P.B., Largaespada, D.A. & Cooper, L.J. A transposon and transposase system for human application. *Mol Ther* **18**, 674-683 (2010).
78. Cattoglio, C. et al. High-definition mapping of retroviral integration sites defines the fate of allogeneic T cells after donor lymphocyte infusion. *PLoS One* **5**, e15688 (2010).
79. Wang, G.P. et al. Analysis of lentiviral vector integration in HIV+ study subjects receiving autologous infusions of gene modified CD4+ T cells. *Mol Ther* **17**, 844-850 (2009).
80. Herndier, B.G. et al. Acquired immunodeficiency syndrome-associated T-cell lymphoma: evidence for human immunodeficiency virus type 1-associated T-cell transformation. *Blood* **79**, 1768-1774 (1992).
81. Swierczek, M., Izsvak, Z. & Ivics, Z. The Sleeping Beauty transposon system for clinical applications. *Expert Opin Biol Ther* **12**, 139-153 (2012).
82. Galvan, D.L. et al. Genome-wide mapping of PiggyBac transposon integrations in primary human T cells. *J Immunother* **32**, 837-844 (2009).
83. Modlich, U. et al. Insertional transformation of hematopoietic cells by self-inactivating lentiviral and gammaretroviral vectors. *Mol Ther* **17**, 1919-1928 (2009).
84. Jena, B., Dotti, G. & Cooper, L.J. Redirecting T-cell specificity by introducing a tumor-specific chimeric antigen receptor. *Blood* **116**, 1035-1044 (2010).

85. Zhao, Y. et al. High-efficiency transfection of primary human and mouse T lymphocytes using RNA electroporation. *Mol Ther* **13**, 151-159 (2006).
86. Coffin, J.M., Hughes, S.H. & Varmus, H. Retroviruses. (Cold Spring Harbor Laboratory Press, Plainview, N.Y.; 1997).
87. Hargrove, P.W. et al. Globin lentiviral vector insertions can perturb the expression of endogenous genes in beta-thalassemic hematopoietic cells. *Mol Ther* **16**, 525-533 (2008).
88. Dudley, J.P. Tag, you're hit: retroviral insertions identify genes involved in cancer. *Trends Mol Med* **9**, 43-45 (2003).
89. Baum, C. Insertional mutagenesis in gene therapy and stem cell biology. *Curr Opin Hematol* **14**, 337-342 (2007).
90. Cavazzana-Calvo, M. et al. Transfusion independence and HMGA2 activation after gene therapy of human beta-thalassaemia. *Nature* **467**, 318-322 (2010).
91. Tey, S.K. & Brenner, M.K. The continuing contribution of gene marking to cell and gene therapy. *Mol Ther* **15**, 666-676 (2007).
92. Stoye, J.P. Studies of endogenous retroviruses reveal a continuing evolutionary saga. *Nat Rev Microbiol* **10**, 395-406 (2012).
93. Newrzela, S. et al. Resistance of mature T cells to oncogene transformation. *Blood* **112**, 2278-2286 (2008).
94. Chiang, C.L., Benencia, F. & Coukos, G. Whole tumor antigen vaccines. *Semin Immunol* **22**, 132-143 (2010).
95. Rowley, J.D. Letter: A new consistent chromosomal abnormality in chronic myelogenous leukaemia identified by quinacrine fluorescence and Giemsa staining. *Nature* **243**, 290-293 (1973).
96. Quaglino, P. et al. Prognostic relevance of baseline and sequential peripheral blood tyrosinase expression in 200 consecutive advanced metastatic melanoma patients. *Melanoma Res* **17**, 75-82 (2007).
97. Li, P. et al. Elevated serum alpha fetoprotein levels promote pathological progression of hepatocellular carcinoma. *World J Gastroenterol* **17**, 4563-4571 (2011).
98. Arrieta, O. et al. Brain metastasis development and poor survival associated with carcinoembryonic antigen (CEA) level in advanced non-small cell lung cancer: a prospective analysis. *BMC Cancer* **9**, 119 (2009).
99. Cheng, Y.H., Wong, E.W. & Cheng, C.Y. Cancer/testis (CT) antigens, carcinogenesis and spermatogenesis. *Spermatogenesis* **1**, 209-220 (2011).
100. Warren, E.H. et al. Therapy of relapsed leukemia after allogeneic hematopoietic cell transplantation with T cells specific for minor histocompatibility antigens. *Blood* **115**, 3869-3878 (2010).
101. Johnson, L.A. et al. Gene therapy with human and mouse T-cell receptors mediates cancer regression and targets normal tissues expressing cognate antigen. *Blood* **114**, 535-546 (2009).
102. Parkhurst, M.R. et al. T cells targeting carcinoembryonic antigen can mediate regression of metastatic colorectal cancer but induce severe transient colitis. *Mol Ther* **19**, 620-626 (2011).
103. Lamers, C.H. et al. Treatment of metastatic renal cell carcinoma with autologous T-lymphocytes genetically retargeted against carbonic anhydrase IX: first clinical experience. *J Clin Oncol* **24**, e20-22 (2006).
104. Morgan, R.A. et al. Cancer Regression and Neurological Toxicity Following Anti-MAGE-A3 TCR Gene Therapy. *J Immunother* **36**, 133-151 (2013).
105. Shi, H., Liu, L. & Wang, Z. Improving the efficacy and safety of engineered T cell therapy for cancer. *Cancer Lett* **328**, 191-197 (2013).
106. Grupp, S.A. et al. Chimeric antigen receptor-modified T cells for acute lymphoid leukemia. *N Engl J Med* **368**, 1509-1518 (2013).
107. Cameron, B.J. et al. Identification of a Titin-Derived HLA-A1-Presented Peptide as a Cross-Reactive Target for Engineered MAGE A3-Directed T Cells. *Sci Transl Med* **5**, 197ra103 (2013).
108. Bollard, C.M., Rooney, C.M. & Heslop, H.E. T-cell therapy in the treatment of post-transplant lymphoproliferative disease. *Nat Rev Clin Oncol* **9**, 510-519 (2012).
109. Torikai, H. et al. A foundation for universal T-cell based immunotherapy: T cells engineered to express a CD19-specific chimeric-antigen-receptor and eliminate expression of endogenous TCR. *Blood* **119**, 5697-5705 (2012).
110. Barese, C.N. & Dunbar, C.E. Contributions of gene marking to cell and gene therapies. *Hum Gene Ther* **22**, 659-668 (2011).
111. Rosenberg, S.A. et al. Gene transfer into humans--immunotherapy of patients with advanced melanoma, using tumor-infiltrating lymphocytes modified by retroviral gene transduction. *N Engl J Med* **323**, 570-578 (1990).

112. Brenner, M.K. et al. Gene marking to determine whether autologous marrow infusion restores long-term haemopoiesis in cancer patients. *Lancet* **342**, 1134-1137 (1993).
113. Brenner, M.K. et al. Gene-marking to trace origin of relapse after autologous bone-marrow transplantation. *Lancet* **341**, 85-86 (1993).
114. Riddell, S.R. et al. T-cell mediated rejection of gene-modified HIV-specific cytotoxic T lymphocytes in HIV-infected patients. *Nat Med* **2**, 216-223 (1996).
115. Cavazzana-Calvo, M., Fischer, A., Hacein-Bey-Abina, S. & Aiuti, A. Gene therapy for primary immunodeficiencies: part 1. *Curr Opin Immunol* **24**, 580-584 (2012).
116. Brewin, J. et al. Generation of EBV-specific cytotoxic T cells that are resistant to calcineurin inhibitors for the treatment of posttransplantation lymphoproliferative disease. *Blood* **114**, 4792-4803 (2009).
117. Wohlgensinger, V., Seger, R., Ryan, M.D., Reichenbach, J. & Siler, U. Signed outside: a surface marker system for transgenic cytoplasmic proteins. *Gene Ther* **17**, 1193-1199 (2010).
118. von Melchner, H. & Housman, D.E. The expression of neomycin phosphotransferase in human promyelocytic leukemia cells (HL60) delays their differentiation. *Oncogene* **2**, 137-140 (1988).
119. Treschow, A. et al. OuaSelect, a novel ouabain-resistant human marker gene that allows efficient cell selection within 48 h. *Gene Ther* **14**, 1564-1572 (2007).
120. Conneally, E. et al. Rapid and efficient selection of human hematopoietic cells expressing murine heat-stable antigen as an indicator of retroviral-mediated gene transfer. *Blood* **87**, 456-464 (1996).
121. Bauer, T.R., Jr. & Hickstein, D.D. Transduction of human hematopoietic cells and cell lines using a retroviral vector containing a modified murine CD4 reporter gene. *Hum Gene Ther* **8**, 243-252 (1997).
122. Gaines, P. & Wojchowski, D.M. pIRES-CD4t, a dicistronic expression vector for MACS- or FACS-based selection of transfected cells. *Biotechniques* **26**, 683-688 (1999).
123. Lemoine, F.M. et al. Efficient transduction and selection of human T-lymphocytes with bicistronic Thy1/HSV1-TK retroviral vector produced by a human packaging cell line. *J Gene Med* **6**, 374-386 (2004).
124. Wang, X. et al. A transgene-encoded cell surface polypeptide for selection, in vivo tracking, and ablation of engineered cells. *Blood* **118**, 1255-1263 (2011).
125. Di Stasi, A. et al. Inducible Apoptosis as a Safety Switch for Adoptive Cell Therapy. *New Engl J Med* **365**, 1673-1683 (2011).
126. Mavilio, F. et al. Peripheral blood lymphocytes as target cells of retroviral vector-mediated gene transfer. *Blood* **83**, 1988-1997 (1994).
127. Fehse, B. et al. CD34 splice variant: an attractive marker for selection of gene-modified cells. *Mol Ther* **1**, 448-456 (2000).
128. Li, Z. et al. Murine leukemia induced by retroviral gene marking. *Science* **296**, 497 (2002).
129. Bonini, C. et al. Safety of retroviral gene marking with a truncated NGF receptor. *Nat Med* **9**, 367-369 (2003).
130. Kustikova, O. et al. Clonal dominance of hematopoietic stem cells triggered by retroviral gene marking. *Science* **308**, 1171-1174 (2005).
131. Norell, H. et al. CD34-based enrichment of genetically engineered human T cells for clinical use results in dramatically enhanced tumor targeting. *Cancer Immunol Immunother* **59**, 851-862 (2010).
132. Lange, C., Li, Z., Fang, L., Baum, C. & Fehse, B. CD34 modulates the trafficking behavior of hematopoietic cells in vivo. *Stem Cells Dev* **16**, 297-304 (2007).
133. Branchini, B.R. et al. Red-emitting luciferases for bioluminescence reporter and imaging applications. *Anal Biochem* **396**, 290-297 (2010).
134. Rizzuto, R., Brini, M., Pizzo, P., Murgia, M. & Pozzan, T. Chimeric green fluorescent protein as a tool for visualizing subcellular organelles in living cells. *Curr Biol* **5**, 635-642 (1995).
135. Shaner, N.C. et al. Improved monomeric red, orange and yellow fluorescent proteins derived from Discosoma sp. red fluorescent protein. *Nat Biotechnol* **22**, 1567-1572 (2004).
136. Weber, K., Mock, U., Petrowitz, B., Bartsch, U. & Fehse, B. Lentiviral gene ontology (LeGO) vectors equipped with novel drug-selectable fluorescent proteins: new building blocks for cell marking and multi-gene analysis. *Gene Ther* **17**, 511-520 (2010).
137. Bonini, C. & Bordignon, C. Potential and limitations of HSV-TK-transduced donor peripheral blood lymphocytes after allo-BMT. *Hematol Cell Ther* **39**, 273-274 (1997).
138. Tiberghien, P. Use of suicide gene-expressing donor T-cells to control alloreactivity after haematopoietic stem cell transplantation. *J Intern Med* **249**, 369-377 (2001).
139. Burt, R.K. et al. Herpes simplex thymidine kinase gene-transduced donor lymphocyte infusions. *Exp Hematol* **31**, 903-910 (2003).

140. Fehse, B. et al. Evidence for increased risk of secondary graft failure after in vivo depletion of suicide gene-modified T lymphocytes transplanted in conjunction with CD34+-enriched blood stem cells. *Blood* **104**, 3408-3409 (2004).
141. Ciceri, F. et al. Antitumor effects of HSV-TK-engineered donor lymphocytes after allogeneic stem-cell transplantation. *Blood* **109**, 4698-4707 (2007).
142. Ciceri, F. et al. Infusion of suicide-gene-engineered donor lymphocytes after family haploidentical haemopoietic stem-cell transplantation for leukaemia (the TK007 trial): a non-randomised phase I-II study. *Lancet Oncol* **10**, 489-500 (2009).
143. Di Stasi, A. et al. Inducible apoptosis as a safety switch for adoptive cell therapy. *N Engl J Med* **365**, 1673-1683 (2011).
144. Bonini, C. et al. The suicide gene therapy challenge: how to improve a successful gene therapy approach. *Mol Ther* **15**, 1248-1252 (2007).
145. Springer, C.J. Suicide gene therapy : methods and reviews. (Humana Press, Totowa, N. J.; 2004).
146. Wei, C.M., Gibson, M., Spear, P.G. & Scolnick, E.M. Construction and isolation of a transmissible retrovirus containing the src gene of Harvey murine sarcoma virus and the thymidine kinase gene of herpes simplex virus type 1. *J Virol* **39**, 935-944 (1981).
147. Sauce, D. et al. Preferential retroviral-mediated transduction of EBV- and CMV-specific T cells after polyclonal T-cell activation. *Gene Ther* **11**, 1019-1022 (2004).
148. Hong Zhan, F.F., Kimberly Gilmour, Joti Bhalla, Lucas Chan, Boris Fehse, Sue Swift, Paul Veys, Adrian Thrasher, Bobby Gaspar, Waseem Qasim Phase 1 Study of HSVTK-CD34 Modified T Cells Therapy Following Haematopoietic Stem Cell Transplantation (HSCT) without Serotherapy. *Mol Ther* **Volume 20**, S1-S294 (2012).
149. Garin, M.I. et al. Molecular mechanism for ganciclovir resistance in human T lymphocytes transduced with retroviral vectors carrying the herpes simplex virus thymidine kinase gene. *Blood* **97**, 122-129 (2001).
150. Bennour, E. et al. Abnormal expression of only the CD34 part of a transgenic CD34/herpes simplex virus-thymidine kinase fusion protein is associated with ganciclovir resistance. *Hum Gene Ther* **19**, 699-709 (2008).
151. Preuss, E. et al. TK.007: A novel, codon-optimized HSVtk(A168H) mutant for suicide gene therapy. *Hum Gene Ther* **21**, 929-941 (2010).
152. Straathof, K.C. et al. An inducible caspase 9 safety switch for T-cell therapy. *Blood* **105**, 4247-4254 (2005).
153. Thomis, D.C. et al. A Fas-based suicide switch in human T cells for the treatment of graft-versus-host disease. *Blood* **97**, 1249-1257 (2001).
154. Vogler, I. et al. An improved bicistronic CD20/tCD34 vector for efficient purification and in vivo depletion of gene-modified T cells for adoptive immunotherapy. *Mol Ther* **18**, 1330-1338 (2010).
155. Kieback, E., Charo, J., Sommermeyer, D., Blankenstein, T. & Uckert, W. A safeguard eliminates T cell receptor gene-modified autoreactive T cells after adoptive transfer. *Proc Natl Acad Sci U S A* **105**, 623-628 (2008).
156. Sato, T. et al. Engineered human tmpk/AZT as a novel enzyme/prodrug axis for suicide gene therapy. *Mol Ther* **15**, 962-970 (2007).
157. Scaife, M. et al. Engineered human Tmpk fused with truncated cell-surface markers: versatile cell-fate control safety cassettes. *Gene Ther* **20**, 24-34 (2013).
158. Chu, Y., Senghaas, N., Koster, R.W., Wurst, W. & Kuhn, R. Novel caspase-suicide proteins for tamoxifen-inducible apoptosis. *Genesis* **46**, 530-536 (2008).
159. Serafini, M. et al. Characterization of CD20-transduced T lymphocytes as an alternative suicide gene therapy approach for the treatment of graft-versus-host disease. *Hum Gene Ther* **15**, 63-76 (2004).
160. Vera, J.F., Brenner, M.K. & Dotti, G. Immunotherapy of human cancers using gene modified T lymphocytes. *Curr Gene Ther* **9**, 396-408 (2009).
161. Ogawa, T. et al. APAF-1-ALT, a novel alternative splicing form of APAF-1, potentially causes impeded ability of undergoing DNA damage-induced apoptosis in the LNCaP human prostate cancer cell line. *Biochem Biophys Res Commun* **306**, 537-543 (2003).
162. Illing, P.T. et al. Immune self-reactivity triggered by drug-modified HLA-peptide repertoire. *Nature* **486**, 554-558 (2012).
163. Leuci, V. et al. Transient proteasome inhibition as a strategy to enhance lentiviral transduction of hematopoietic CD34(+) cells and T lymphocytes: implications for the use of low viral doses and large-size vectors. *J Biotechnol* **156**, 218-226 (2011).
164. Vallbohmer, D. et al. Molecular determinants of cetuximab efficacy. *J Clin Oncol* **23**, 3536-3544 (2005).
165. Smith, M.R. Rituximab (monoclonal anti-CD20 antibody): mechanisms of action and resistance. *Oncogene* **22**, 7359-7368 (2003).

166. Introna, M. et al. Genetic modification of human T cells with CD20: a strategy to purify and lyse transduced cells with anti-CD20 antibodies. *Hum Gene Ther* **11**, 611-620 (2000).
167. Wehler, T.C. et al. Cetuximab-induced skin exanthema: prophylactic and reactive skin therapy are equally effective. *J Cancer Res Clin Oncol* **139**, 1667-1672 (2013).
168. Papaioannou, D. et al. Rituximab for the first-line treatment of stage III-IV follicular lymphoma (review of Technology Appraisal No. 110): a systematic review and economic evaluation. *Health Technol Assess* **16**, 1-253, iii-iv (2012).
169. Gurcan, H.M. et al. A review of the current use of rituximab in autoimmune diseases. *International immunopharmacology* **9**, 10-25 (2009).
170. Maloney, D.G. et al. Phase I clinical trial using escalating single-dose infusion of chimeric anti-CD20 monoclonal antibody (IDEC-C2B8) in patients with recurrent B-cell lymphoma. *Blood* **84**, 2457-2466 (1994).
171. Maloney, D.G. et al. IDEC-C2B8: results of a phase I multiple-dose trial in patients with relapsed non-Hodgkin's lymphoma. *J Clin Oncol* **15**, 3266-3274 (1997).
172. Cooper, D.L. & Lovett, S.T. Toxicity and tolerance mechanisms for azidothymidine, a replication gap-promoting agent, in Escherichia coli. *DNA Repair (Amst)* **10**, 260-270 (2011).
173. Marin, V. et al. Comparison of different suicide-gene strategies for the safety improvement of genetically manipulated T cells. *Hum Gene Ther Methods* **23**, 376-386 (2012).
174. Perosa, F., Favoino, E., Caragnano, M.A. & Dammacco, F. Generation of biologically active linear and cyclic peptides has revealed a unique fine specificity of rituximab and its possible cross-reactivity with acid sphingomyelinase-like phosphodiesterase 3b precursor. *Blood* **107**, 1070-1077 (2006).
175. Ehrlich, P. & Bolduan, C. Collected studies on immunity, Edn. 1st. (J. Wiley & sons; etc., New York,; 1906).
176. Kohler, G. & Milstein, C. Continuous cultures of fused cells secreting antibody of predefined specificity. *Nature* **256**, 495-497 (1975).
177. Brekke, O.H. & Sandlie, I. Therapeutic antibodies for human disease at the dawn of the twenty-first century (vol 2, pg 52, 2003). *Nat Rev Drug Discov* **2**, 240-240 (2003).
178. An, Z. Therapeutic monoclonal antibodies : from bench to clinic. (John Wiley & Sons, Hoboken, N.J.; 2009).
179. Weiner, L.M., Surana, R. & Wang, S. Monoclonal antibodies: versatile platforms for cancer immunotherapy. *Nat Rev Immunol* **10**, 317-327 (2010).
180. Cheson, B.D. Ofatumumab, a novel anti-CD20 monoclonal antibody for the treatment of B-cell malignancies. *J Clin Oncol* **28**, 3525-3530 (2010).
181. Sorkin, L.S. et al. Anti-GD(2) with an FC point mutation reduces complement fixation and decreases antibody-induced allodynia. *Pain* **149**, 135-142 (2010).
182. Hussain, R. et al. Selective increases in antibody isotypes and immunoglobulin G subclass responses to secreted antigens in tuberculosis patients and healthy household contacts of the patients. *Clin Diagn Lab Immunol* **2**, 726-732 (1995).
183. Loisel, S. et al. Relevance, advantages and limitations of animal models used in the development of monoclonal antibodies for cancer treatment. *Crit Rev Oncol Hematol* **62**, 34-42 (2007).
184. Bindon, C.I., Hale, G., Bruggemann, M. & Waldmann, H. Human monoclonal IgG isotypes differ in complement activating function at the level of C4 as well as C1q. *J Exp Med* **168**, 127-142 (1988).
185. Pescovitz, M.D. Rituximab, an anti-cd20 monoclonal antibody: history and mechanism of action. *Am J Transplant* **6**, 859-866 (2006).
186. Eisenberg, R. & Looney, R.J. The therapeutic potential of anti-CD20 "what do B-cells do?". *Clin Immunol* **117**, 207-213 (2005).
187. Weiner, G.J. Rituximab: mechanism of action. *Semin Hematol* **47**, 115-123 (2010).
188. Taylor, R.P. & Lindorfer, M.A. Drug insight: the mechanism of action of rituximab in autoimmune disease--the immune complex decoy hypothesis. *Nat Clin Pract Rheumatol* **3**, 86-95 (2007).
189. Klepfish, A., Gilles, L., Ioannis, K., Rachmilewitz, E.A. & Schattner, A. Enhancing the action of rituximab in chronic lymphocytic leukemia by adding fresh frozen plasma: complement/rituximab interactions & clinical results in refractory CLL. *Ann N Y Acad Sci* **1173**, 865-873 (2009).
190. Toleikis, L., Broders, O. & Dubel, S. Cloning single-chain antibody fragments (scFv) from hybridoma cells. *Methods Mol Med* **94**, 447-458 (2004).
191. Kurano, S., Ishida, M. & Ishimaru, Y. Roles of calcium in aggregation of rat ascites hepatoma cells by cell surface-associated adhesive factor. *J Cell Sci* **66**, 367-382 (1984).

192. Tal, M., Silberstein, A. & Nusser, E. Why does Coomassie Brilliant Blue R interact differently with different proteins? A partial answer. *J Biol Chem* **260**, 9976-9980 (1985).
193. Lanza, F., Healy, L. & Sutherland, D.R. Structural and functional features of the CD34 antigen: an update. *J Biol Regul Homeost Agents* **15**, 1-13 (2001).
194. Gangenahalli, G.U. et al. Hematopoietic stem cell antigen CD34: role in adhesion or homing. *Stem Cells Dev* **15**, 305-313 (2006).
195. Baumheter, S. et al. Binding of L-selectin to the vascular sialomucin CD34. *Science* **262**, 436-438 (1993).
196. Hernandez Mir, G. et al. Glycoforms of human endothelial CD34 that bind L-selectin carry sulfated sialyl Lewis x capped O- and N-glycans. *Blood* **114**, 733-741 (2009).
197. Healy, L. et al. The stem cell antigen CD34 functions as a regulator of hemopoietic cell adhesion. *Proc Natl Acad Sci U S A* **92**, 12240-12244 (1995).
198. Nielsen, J.S. & McNagny, K.M. Novel functions of the CD34 family. *J Cell Sci* **121**, 3683-3692 (2008).
199. Fackler, M.J., Krause, D.S., Smith, O.M., Civin, C.I. & May, W.S. Full-length but not truncated CD34 inhibits hematopoietic cell differentiation of M1 cells. *Blood* **85**, 3040-3047 (1995).
200. Tedder, T.F. CD19: a promising B cell target for rheumatoid arthritis. *Nat Rev Rheumatol* **5**, 572-577 (2009).
201. Du, J. et al. Structural basis for recognition of CD20 by therapeutic antibody Rituximab. *J Biol Chem* **282**, 15073-15080 (2007).
202. Beers, S.A., Chan, C.H., French, R.R., Cragg, M.S. & Glennie, M.J. CD20 as a target for therapeutic type I and II monoclonal antibodies. *Semin Hematol* **47**, 107-114 (2010).
203. Buckner, C.L., Christiansen, L.R., Bourgeois, D., Lazarchick, J.J. & Lazarchick, J. CD20 positive T-cell lymphoma/leukemia: a rare entity with potential diagnostic pitfalls. *Ann Clin Lab Sci* **37**, 263-267 (2007).
204. Perosa, F., Favoino, E., Vicenti, C., Merchionne, F. & Dammacco, F. Identification of an antigenic and immunogenic motif expressed by two 7-mer rituximab-specific cyclic peptide mimotopes: implication for peptide-based active immunotherapy. *J Immunol* **179**, 7967-7974 (2007).
205. Sutherland, D.R., Stewart, A.K. & Keating, A. CD34 antigen: molecular features and potential clinical applications. *Stem Cells* **11 Suppl 3**, 50-57 (1993).
206. Leahy, D.J., Axel, R. & Hendrickson, W.A. Crystal structure of a soluble form of the human T cell coreceptor CD8 at 2.6 A resolution. *Cell* **68**, 1145-1162 (1992).
207. Leahy, D.J. A structural view of CD4 and CD8. *Faseb J* **9**, 17-25 (1995).
208. Binder, M., Otto, F., Mertelsmann, R., Veelken, H. & Trepel, M. The epitope recognized by rituximab. *Blood* **108**, 1975-1978 (2006).
209. Du, J., Yang, H., Guo, Y. & Ding, J. Structure of the Fab fragment of therapeutic antibody Ofatumumab provides insights into the recognition mechanism with CD20. *Molecular immunology* **46**, 2419-2423 (2009).
210. Winiarska, M. et al. Statins impair antitumor effects of rituximab by inducing conformational changes of CD20. *PLoS Med* **5**, e64 (2008).
211. Olszewski, A.J. & Grossbard, M.L. Empowering targeted therapy: lessons from rituximab. *Sci STKE* **2004**, pe30 (2004).
212. Ricklin, D. & Lambris, J.D. Complement-targeted therapeutics. *Nat Biotechnol* **25**, 1265-1275 (2007).
213. Ricklin, D., Hajishengallis, G., Yang, K. & Lambris, J.D. Complement: a key system for immune surveillance and homeostasis. *Nat Immunol* **11**, 785-797 (2010).
214. Zipfel, P.F. & Skerka, C. Complement regulators and inhibitory proteins. *Nat Rev Immunol* **9**, 729-740 (2009).
215. Brodsky, R.A. New insights into paroxysmal nocturnal hemoglobinuria. *Hematology Am Soc Hematol Educ Program*, 24-28, 516 (2006).
216. van Meerten, T., Claessen, M.J., Hagenbeek, A. & Ebeling, S.B. The CD20/alphaCD20 'suicide' system: novel vectors with improved safety and expression profiles and efficient elimination of CD20-transgenic T cells. *Gene Ther* **13**, 789-797 (2006).
217. Murphy, K., Travers, P., Walport, M. & Janeway, C. Janeway's immunobiology, Edn. 8th. (Garland Science, New York; 2012).
218. Muller, C. et al. The role of sex and weight on rituximab clearance and serum elimination half-life in elderly patients with DLBCL. *Blood* **119**, 3276-3284 (2012).
219. Singh, H., Ansari, H.R. & Raghava, G.P. Improved method for linear B-cell epitope prediction using antigen's primary sequence. *PLoS One* **8**, e62216 (2013).
220. Larsen, M.V. et al. Large-scale validation of methods for cytotoxic T-lymphocyte epitope prediction. *BMC bioinformatics* **8**, 424 (2007).

221. Ellis, J.M. et al. Frequencies of HLA-A2 alleles in five U.S. population groups. Predominance Of A*02011 and identification of HLA-A*0231. *Human immunology* **61**, 334-340 (2000).
222. Steentoft, C. et al. Precision mapping of the human O-GalNAc glycoproteome through SimpleCell technology. *Embo J* **32**, 1478-1488 (2013).
223. Lieth, C.-W.v.d., Lutteke, T. & Frank, M. Bioinformatics for glycobiology and glycomics : an introduction. (Wiley-Blackwell, Chichester, UK ; Hoboken, NJ; 2009).
224. Stothard, P. The sequence manipulation suite: JavaScript programs for analyzing and formatting protein and DNA sequences. *Biotechniques* **28**, 1102, 1104 (2000).
225. Imai, C., Iwamoto, S. & Campana, D. Genetic modification of primary natural killer cells overcomes inhibitory signals and induces specific killing of leukemic cells. *Blood* **106**, 376-383 (2005).
226. Kim, C.H., Oh, Y. & Lee, T.H. Codon optimization for high-level expression of human erythropoietin (EPO) in mammalian cells. *Gene* **199**, 293-301 (1997).
227. Mizuguchi, H., Xu, Z., Ishii-Watabe, A., Uchida, E. & Hayakawa, T. IRES-dependent second gene expression is significantly lower than cap-dependent first gene expression in a bicistronic vector. *Mol Ther* **1**, 376-382 (2000).
228. Teillaud, J.-L. in eLS (John Wiley & Sons, Ltd, 2001).
229. Kohrt, H.E. et al. Combination strategies to enhance antitumor ADCC. *Immunotherapy* **4**, 511-527 (2012).
230. Nimmerjahn, F. & Ravetch, J.V. Fcgamma receptors as regulators of immune responses. *Nat Rev Immunol* **8**, 34-47 (2008).
231. Smith, K.G. & Clatworthy, M.R. FcgammaRIIB in autoimmunity and infection: evolutionary and therapeutic implications. *Nat Rev Immunol* **10**, 328-343 (2010).
232. Herberman, R.B., Nunn, M.E. & Lavrin, D.H. Natural cytotoxic reactivity of mouse lymphoid cells against syngeneic acid allogeneic tumors. I. Distribution of reactivity and specificity. *Int J Cancer* **16**, 216-229 (1975).
233. Kiessling, R., Klein, E., Pross, H. & Wigzell, H. "Natural" killer cells in the mouse. II. Cytotoxic cells with specificity for mouse Moloney leukemia cells. Characteristics of the killer cell. *Eur J Immunol* **5**, 117-121 (1975).
234. Vivier, E., Tomasello, E., Baratin, M., Walzer, T. & Ugolini, S. Functions of natural killer cells. *Nat Immunol* **9**, 503-510 (2008).
235. Cheng, M., Chen, Y., Xiao, W., Sun, R. & Tian, Z. NK cell-based immunotherapy for malignant diseases. *Cellular & molecular immunology* **10**, 230-252 (2013).
236. De Maria, A., Bozzano, F., Cantoni, C. & Moretta, L. Revisiting human natural killer cell subset function revealed cytolytic CD56(dim)CD16+ NK cells as rapid producers of abundant IFN-gamma on activation. *Proc Natl Acad Sci U S A* **108**, 728-732 (2011).
237. Orr, M.T., Murphy, W.J. & Lanier, L.L. 'Unlicensed' natural killer cells dominate the response to cytomegalovirus infection. *Nat Immunol* **11**, 321-327 (2010).
238. Zimmer, J. Natural killer cells : at the forefront of modern immunology. (Springer, Berlin; 2010).
239. Karre, K., Ljunggren, H.G., Piontek, G. & Kiessling, R. Selective rejection of H-2-deficient lymphoma variants suggests alternative immune defence strategy. *Nature* **319**, 675-678 (1986).
240. Jonsson, A.H. & Yokoyama, W.M. Natural killer cell tolerance licensing and other mechanisms. *Advances in immunology* **101**, 27-79 (2009).
241. Boyton, R.J. & Altmann, D.M. Natural killer cells, killer immunoglobulin-like receptors and human leucocyte antigen class I in disease. *Clinical and experimental immunology* **149**, 1-8 (2007).
242. Le Bouteiller, P. et al. Engagement of CD160 receptor by HLA-C is a triggering mechanism used by circulating natural killer (NK) cells to mediate cytotoxicity. *Proc Natl Acad Sci U S A* **99**, 16963-16968 (2002).
243. Lozzio, C.B. & Lozzio, B.B. Human chronic myelogenous leukemia cell-line with positive Philadelphia chromosome. *Blood* **45**, 321-334 (1975).
244. Pross, H.F., Baines, M.G., Rubin, P., Shragge, P. & Patterson, M.S. Spontaneous human lymphocyte-mediated cytotoxicity against tumor target cells. IX. The quantitation of natural killer cell activity. *J Clin Immunol* **1**, 51-63 (1981).
245. Robertson, M.J. et al. Costimulation of human natural killer cell proliferation: role of accessory cytokines and cell contact-dependent signals. *Nat Immun* **15**, 213-226 (1996).
246. Hale, G. & Waldmann, H. From Laboratory to Clinic : The Story of CAM PA TH-1. *Methods Mol Med* **40**, 243-266 (2000).
247. Wang, S.Y., Racila, E., Taylor, R.P. & Weiner, G.J. NK-cell activation and antibody-dependent cellular cytotoxicity induced by rituximab-coated target cells is inhibited by the C3b component of complement. *Blood* **111**, 1456-1463 (2008).

248. Jedema, I., van der Werff, N.M., Barge, R.M., Willemze, R. & Falkenburg, J.H. New CFSE-based assay to determine susceptibility to lysis by cytotoxic T cells of leukemic precursor cells within a heterogeneous target cell population. *Blood* **103**, 2677-2682 (2004).
249. Veeramani, S. et al. Rituximab infusion induces NK activation in lymphoma patients with the high-affinity CD16 polymorphism. *Blood* **118**, 3347-3349 (2011).
250. Cartron, G. et al. Therapeutic activity of humanized anti-CD20 monoclonal antibody and polymorphism in IgG Fc receptor FcgammaRIIIa gene. *Blood* **99**, 754-758 (2002).
251. Stauss, H.J. et al. WT1-specific T cell receptor gene therapy: improving TCR function in transduced T cells. *Blood Cells Mol Dis* **40**, 113-116 (2008).
252. Thomas, S. et al. Targeting the Wilms tumor antigen 1 by TCR gene transfer: TCR variants improve tetramer binding but not the function of gene modified human T cells. *J Immunol* **179**, 5803-5810 (2007).
253. Davidoff, A.M. Neuroblastoma. *Seminars in pediatric surgery* **21**, 2-14 (2012).
254. Agarwal, M. et al. Scaffold attachment region-mediated enhancement of retroviral vector expression in primary T cells. *J Virol* **72**, 3720-3728 (1998).
255. Hombach, A., Hombach, A.A. & Abken, H. Adoptive immunotherapy with genetically engineered T cells: modification of the IgG1 Fc 'spacer' domain in the extracellular moiety of chimeric antigen receptors avoids 'off-target' activation and unintended initiation of an innate immune response. *Gene Ther* **17**, 1206-1213 (2010).
256. Moore, G.E., Gerner, R.E. & Franklin, H.A. Culture of normal human leukocytes. *Jama* **199**, 519-524 (1967).
257. Tristram G. Parslow, D.P.S., Abba I. Terr, John B. Imboden in Medical immunology, Edn. 10th (Appleton & Lange, Stamford, Conn.; 2001).
258. Veldkamp, J., De Reuver, M.J. & Willers, J.M. Distribution of different cell types in the lymphoid organs of the mouse, as determined with sera against thymus and Peyer's patches. *Immunology* **26**, 359-366 (1974).
259. Janeway, C. Immunobiology : the immune system in health and disease, Edn. 6th. (Garland Science, New York; 2005).
260. Harris, J.R. Erythroid cells. (Plenum Press, New York; 1990).
261. Ishii, T., Sugita, Y. & Bannai, S. Regulation of glutathione levels in mouse spleen lymphocytes by transport of cysteine. *J Cell Physiol* **133**, 330-336 (1987).
262. Kurlander, R.J., Ellison, D.M. & Hall, J. The blockade of Fc receptor-mediated clearance of immune complexes in vivo by a monoclonal antibody (2.4G2) directed against Fc receptors on murine leukocytes. *J Immunol* **133**, 855-862 (1984).
263. Cronin, J., Zhang, X.Y. & Reiser, J. Altering the tropism of lentiviral vectors through pseudotyping. *Curr Gene Ther* **5**, 387-398 (2005).
264. Page, K.A., Landau, N.R. & Littman, D.R. Construction and use of a human immunodeficiency virus vector for analysis of virus infectivity. *J Virol* **64**, 5270-5276 (1990).
265. Finkelshtein, D., Werman, A., Novick, D., Barak, S. & Rubinstein, M. LDL receptor and its family members serve as the cellular receptors for vesicular stomatitis virus. *Proc Natl Acad Sci U S A* **110**, 7306-7311 (2013).
266. Sommerfelt, M.A. Retrovirus receptors. *J Gen Virol* **80 (Pt 12)**, 3049-3064 (1999).
267. Merten, O.W. State-of-the-art of the production of retroviral vectors. *J Gene Med* **6 Suppl 1**, S105-124 (2004).
268. Lyons, R. et al. The RAC specific guanine nucleotide exchange factor Asef functions downstream from TEL-AML1 to promote leukaemic transformation. *Leuk Res* **34**, 109-115 (2010).
269. King, D.J. Applications and engineering of monoclonal antibodies. (Taylor & Francis, London ; Philadelphia; 1998).
270. Nimmerjahn, F. & Ravetch, J.V. Divergent immunoglobulin g subclass activity through selective Fc receptor binding. *Science* **310**, 1510-1512 (2005).
271. Lewin, B. Genes IX, Edn. 9th. (Jones and Bartlett Publishers, Sudbury, Mass.; 2008).
272. Ollo, R. & Rougeon, F. Gene conversion and polymorphism: generation of mouse immunoglobulin gamma 2a chain alleles by differential gene conversion by gamma 2b chain gene. *Cell* **32**, 515-523 (1983).
273. Majlessi, L., Rujithamkul, N. & Bordenave, G. Mechanisms of T-cell-induced allotypic suppression of mouse IgG2a(b) and of tolerance acquisition to this allotype. *Res Immunol* **146**, 213-224 (1995).
274. Baldi, L., Hacker, D.L., Adam, M. & Wurm, F.M. Recombinant protein production by large-scale transient gene expression in mammalian cells: state of the art and future perspectives. *Biotechnol Lett* **29**, 677-684 (2007).
275. Artimo, P. et al. ExPASy: SIB bioinformatics resource portal. *Nucleic Acids Res* **40**, W597-603 (2012).

276. Schroeder, M.A. & DiPersio, J.F. Mouse models of graft-versus-host disease: advances and limitations. *Disease models & mechanisms* **4**, 318-333 (2011).
277. van Leeuwen, L., Guiffre, A., Atkinson, K., Rainer, S.P. & Sewell, W.A. A two-phase pathogenesis of graft-versus-host disease in mice. *Bone Marrow Transplant* **29**, 151-158 (2002).
278. Flutter, B. et al. Nonhematopoietic antigen blocks memory programming of alloreactive CD8+ T cells and drives their eventual exhaustion in mouse models of bone marrow transplantation. *J Clin Invest* **120**, 3855-3868 (2010).
279. Robinet, E. et al. Improving the ex vivo retroviral-mediated suicide-gene transfer process in T lymphocytes to preserve immune function. *Cytotherapy* **7**, 150-157 (2005).
280. Hashimoto, D. et al. Pretransplant CSF-1 therapy expands recipient macrophages and ameliorates GVHD after allogeneic hematopoietic cell transplantation. *J Exp Med* **208**, 1069-1082 (2011).
281. Glimm, H., Ball, C.R. & von Kalle, C. You can count on this: barcoded hematopoietic stem cells. *Cell Stem Cell* **9**, 390-392 (2011).
282. Livet, J. et al. Transgenic strategies for combinatorial expression of fluorescent proteins in the nervous system. *Nature* **450**, 56-62 (2007).
283. Jensen, E.C. Use of Fluorescent Probes: Their Effect on Cell Biology and Limitations. *The Anatomical Record: Advances in Integrative Anatomy and Evolutionary Biology* **295**, 2031-2036 (2012).
284. Brizzard, B. Epitope tagging. *Biotechniques* **44**, 693-695 (2008).
285. Ferguson, M.A.J., Kinoshita, T. & Hart, G.W. in Essentials of Glycobiology, Edn. 2nd. (eds. A. Varki et al.)Cold Spring Harbor (NY); 2009).
286. Lakhan, S.E., Sabharanjak, S. & De, A. Endocytosis of glycosylphosphatidylinositol-anchored proteins. *Journal of biomedical science* **16**, 93 (2009).
287. Vink, C. in A Hybrid Lentivirus-Transposon Vector for Safer Gene Therapy (UCL, 2009).
288. Raj, D., Davidoff, A.M. & Nathwani, A.C. Self-complementary adeno-associated viral vectors for gene therapy of hemophilia B: progress and challenges. *Expert Rev Hematol* **4**, 539-549 (2011).
289. Kalos, M. et al. T cells with chimeric antigen receptors have potent antitumor effects and can establish memory in patients with advanced leukemia. *Sci Transl Med* **3**, 95ra73 (2011).
290. Buchholz, V.R., Graf, P. & Busch, D.H. The origin of diversity: studying the evolution of multi-faceted CD8+ T cell responses. *Cellular and molecular life sciences : CMLS* **69**, 1585-1595 (2012).
291. Linette, G.P. et al. Cardiovascular toxicity and titin cross-reactivity of affinity-enhanced T cells in myeloma and melanoma. *Blood* **122**, 863-871 (2013).
292. Serabe, B.M. et al. Plasma and CSF pharmacokinetics of ganciclovir in nonhuman primates. *Cancer Chemother Pharmacol* **43**, 415-418 (1999).
293. Berger, C., Flowers, M.E., Warren, E.H. & Riddell, S.R. Analysis of transgene-specific immune responses that limit the in vivo persistence of adoptively transferred HSV-TK-modified donor T cells after allogeneic hematopoietic cell transplantation. *Blood* **107**, 2294-2302 (2006).
294. Wang, N.K. et al. Origin of fundus hyperautofluorescent spots and their role in retinal degeneration in a mouse model of Goldmann-Favre syndrome. *Disease models & mechanisms* **6**, 1113-1122 (2013).
295. Petereit, H.F. & Rubbert-Roth, A. Rituximab levels in cerebrospinal fluid of patients with neurological autoimmune disorders. *Mult Scler* **15**, 189-192 (2009).
296. Rades, D. et al. Radiolabeled cetuximab plus whole-brain irradiation (WBI) for the treatment of brain metastases from non-small cell lung cancer (NSCLC). *Strahlenther Onkol* **186**, 458-462 (2010).
297. van Loenen, M.M. et al. Multi-cistronic vector encoding optimized safety switch for adoptive therapy with T-cell receptor-modified T cells. *Gene Ther* **20**, 861-867 (2013).
298. Levy, E.M. et al. Cetuximab-mediated cellular cytotoxicity is inhibited by HLA-E membrane expression in colon cancer cells. *Innate Immun* **15**, 91-100 (2009).
299. Alici, E. et al. Long-term follow-up of gene-marked CD34+ cells after autologous stem cell transplantation for multiple myeloma. *Cancer Gene Ther* **14**, 227-232 (2007).
300. Recchia, A. et al. Retroviral vector integration deregulates gene expression but has no consequence on the biology and function of transplanted T cells. *Proc Natl Acad Sci U S A* **103**, 1457-1462 (2006).
301. Beum, P.V., Kennedy, A.D., Williams, M.E., Lindorfer, M.A. & Taylor, R.P. The shaving reaction: rituximab/CD20 complexes are removed from mantle cell lymphoma and chronic lymphocytic leukemia cells by THP-1 monocytes. *J Immunol* **176**, 2600-2609 (2006).

302. Coffin, J.M., Hughes, S.H. & Varmus, H.E. in Retroviruses. (eds. J.M. Coffin, S.H. Hughes & H.E. Varmus)Cold Spring Harbor (NY); 1997).
303. Kozak, M. An analysis of 5'-noncoding sequences from 699 vertebrate messenger RNAs. *Nucleic Acids Res* **15**, 8125-8148 (1987).
304. Wang, T.Y., Han, Z.M., Chai, Y.R. & Zhang, J.H. A mini review of MAR-binding proteins. *Mol Biol Rep* **37**, 3553-3560 (2010).
305. Licursi, M., Christian, S.L., Pongnopparat, T. & Hirasawa, K. In vitro and in vivo comparison of viral and cellular internal ribosome entry sites for bicistronic vector expression. *Gene Ther* **18**, 631-636 (2011).
306. Trichas, G., Begbie, J. & Srinivas, S. Use of the viral 2A peptide for bicistronic expression in transgenic mice. *BMC Biol* **6**, 40 (2008).
307. Donnelly, M.L. et al. The 'cleavage' activities of foot-and-mouth disease virus 2A site-directed mutants and naturally occurring '2A-like' sequences. *J Gen Virol* **82**, 1027-1041 (2001).

Appendix 1

13. Modular cloning strategy for retroviral expression vectors

13.1. Molecular cloning by SOE–PCR or modular design

13.1.1. Cloning by SOE–PCR

Splicing by overlap extension PCR enables construction of novel genetic sequences through fusion of one or more PCR-amplified sequences. This is achieved through inclusion of terminal padding sequences containing the required restriction sites to facilitate restriction digest ligation of novel inserts into appropriately digested destination vectors. This strategy enables insertion, deletion and even ligation-mediated restriction site ablation to generate the desired expression product. When designing epitope constructs to be expressed on the cell surface, the 5' oligo primer was engineered to contain the NcoI restriction site (CCATGG) which contains the start codon. Although this limits the potential amino acid residues which might be encoded for by the second codon, use of online signal sequence detection algorithms enable the ability to predict whether the functional capacity of the signal sequence has been retained. However, as predicting the impact of sequence modifications to cytosolic or integral membrane proteins is less clear, cloning design exploited the unique BglII or AgeI restriction sites located upstream within the psi packaging signal domain, resulting in a longer 'padding' sequence in the PCR amplicon. Where unique restriction sites such as NcoI or MluI were present within the template coding sequence, use of alternative codons in the cloning design enabled restriction site ablation to ensure subsequent constructs correspond with the modular cloning strategy.

PCR amplification of novel sequences was typically achieved through a 2-part process; an initial template PCR to amplify separate template fragments which were subsequently used as templates for a second and final PCR reaction when these fragments annealed based on homologous sequences established in the cloning design. In this manner, many separate fragments can be strung together to generate a completely novel template such as with gene synthesis employing overlapping oligo nucleotide primers, however typically, cloning designs were composed of two or three separate fragments. Amplicons generated by the primary template PCR reaction were separated by agarose gel

electrophoresis with the bands extracted and cleaned up according to manufacturer's instructions (Qiagen) prior to inclusion in the final fusion PCR reaction which contained only the terminal primers for the desired amplicon with annealing of the separate fragments facilitating generation of the desired extended template sequence.

Due to limited proof-reading ability of the polymerase enzyme compared with the full complement of proof-reading present within bacteria, all PCR-based cloning products were screened using a 2-part strategy with initial verification achieved through restriction digest followed by absolute confirmation by DNA sequencing.

13.1.2. Vector sub–cloning facilitated by modular design

The modular strategy of the laboratory vectors enables facile subcloning of subsequent constructs in alternative iterations simply by cut and paste cloning facilitated by compatible restriction digests. Due to the reduced likelihood of errors resulting from this cloning strategy, construct validation from cut and paste cloning was by restriction digest and functional validation.

13.1.3. Vectors used during this project

Table 14 Plasmid vectors used in this project

Vector	Description	Researcher(s)
pEQ-Pam3-E	*gag-pol* expression plasmid	Elio Vanin
RDF	RD114 envelope expression plasmid	Francois Cosset & Mary Collins
pMono.Eco	Ecotropic envelope expression plasmid	Gianpietro Dotti
SFGm_SAR.eGFP	Vector backbone for constructs containing S/MAR domain	Martin Pule
SFG.HA1betaTCR.I2.eGFP	Vector backbone for IRES.eGFP	Martin Pule
SFG.HA1betaTCR.I2.eBFP2	Vector backbone for IRES.eBFP2	Martin Pule
SFG.CD34-L-8.I2.eGFP	Parental QBEnd10 epitope construct with linker	Martin Pule
SFG.CD34-8.I2.eGFP	Parental QBEnd10 epitope	Martin Pule

	construct without linker	
SFG.CD34min8.I2.eGFP	QBEnd10 epitope - carboxy terminal mutant 1	Martin Pule
SFG.CD34epA1-CD8STK.I2.eGFP	QBEnd10 epitope - carboxy terminal mutant 2	Martin Pule
SFG.CD34epA2-CD8STK.I2.eGFP	QBEnd10 epitope - carboxy terminal mutant 3	Martin Pule
SFG.CD34epB1-CD8STK.I2.eGFP	QBEnd10 epitope - amino terminal mutant 1	Martin Pule
SFG.CD34epB2-CD8STK.I2.eGFP	QBEnd10 epitope - amino terminal mutant 2	Martin Pule
SFG.CD34.I2.eGFP	Full length CD34 control	Martin Pule
SFG.rtx_Rp5-CD8stk-tm.I2.eGFP	Linear rituximab binding mimotope	Martin Pule
SFG.rtx_Rp3C-CD8stk-tm.I2.eGFP	Circular rituximab mimotope	Martin Pule
SFG.CD34epB3-CD8STK.I2.eGFP	QBEnd10 epitope - amino terminal mutant 3	Martin Pule
SFG.dCD20v1.I2.eGFP	CD20 rituximab epitope with flanking residues	Martin Pule
SFG.dCD20v2.I2.eGFP	CD20 rituximab epitope without flanking residues	Martin Pule
SFG.aGD2huK666-HCH2CH3sec.I2.eBFP2	Vector backbone used for secreted scFv constructs	Simon Thomas & Kim Vigor
SFG.CD34epB1A0.I2.eGFP	Carboxy and amino QBEnd10 epitope B1A0	Brian Philip
SFG.CD34epB2A0.I2.eGFP	Carboxy and amino QBEnd10 epitope B2A0	Brian Philip
SFG.CD34epB3A0.I2.eGFP	Carboxy and amino QBEnd10 epitope B3A0	Brian Philip
SFG.dCD34ep-2A-rtx-RP3X.I2.eGFP	QR8	Brian Philip
SFG.rtx-RP3X-2A-dCD34ep.I2.eGFP	RQ8	Brian Philip
SFG.IL15-CD8-S-TM-A-2A-TNFSF9.eBFP	SFG.IL15_8Stk.4-1BBL.I2.eBFP2	Brian Philip

SFG.IL15-CD8-TM-A-2A-TNFSF9.I2.eBFP	SFG.IL15_8.4-1BBL.I2.eBFP2	Brian Philip
SFG.RTXep_flush-CD8tm.I2.eGFP	R'.I2.eGFP	Brian Philip
SFG.RTXep-RTXep-QBEND10-CD8tm.I2.eGFP	RRQ8.I2.eGFP	Brian Philip
SFG.RTXep-QBEND10ep-RTXep-CD8S-TM.I2.eGFP	RQR8.I2.eGFP	Brian Philip
SFG.CD34B2A0.I2.eBFP	Q8.I2.eBFP2 control construct	Brian Philip
SFG.CD20opt.I2.eGFP	CD20opt.I2.eGFP Codon optimised CD20 control	Brian Philip
SFG.opt_rituxC-HCH2CH3-CD28OXZ.I2.eBFP2	Rtx-C	Brian Philip
SFG.opt_rituxP-HCH2CH3-CD28OXZ.I2.eBFP2	Rtx-P	Brian Philip
SFG.dCD34ngg-2A-CD20.I2.eGFP	CD34.2A.CD20.I2.eGFP control	Brian Philip
SFG.CD8stk-3xFLAG.I2.eGFP	Headless-8_FLAG.I2.eGFP	Brian Philip
SFG.Q-CD8stk-3xFLAG.I2.eGFP	Q8_FLAG.I2.eGFP	Brian Philip
SFG.RQR-CD8stk-3xFLAG.I2.eGFP	RQR8_FLAG.I2.eGFP	Brian Philip
SFG.opt_RtxC-HCH2CH3sec.I2.eBFP2	RtxC scFv secreted construct	Brian Philip
SFG.opt_RtxP-HCH2CH3sec.I2.eBFP2	RtxP scFv secreted construct	Brian Philip
SFGmR.RQR8-2A-CnBx030	Intermediary construct required for CAR/TCR co-expression constructs	Brian Philip
SFG.RQR8-2A-aGD2huK666-HCH2CH3-CD28OXZ	RQR8-GD2-CAR without S/MAR domain	Brian Philip
SFGmR.RQR8-2A-aGD2huK666-	RQR8-GD2-CAR with S/MAR domain	Brian Philip

HCH2CH3-CD28OXZ		
SFG.RQR8-2A-TCR_WT1_hyb-B-2A-A	RQR8-WT1-TCR without S/MAR domain	Brian Philip
SFGmR.RQR8-2A-TCR_WT1_hyb-B-2A-A	RQR8-WT1-TCR with S/MAR domain	Brian Philip
SFG.SRQR_CD4-D3D4-TM-A.I2.eGFP	RQR4.I2.eGFP	Brian Philip
SFG.mR.Q8	Q8 with S.MAR domain	Brian Philip
SFG.mR.RQR8	RQR8 with S.MAR domain	Brian Philip
SFG.Rtx_H_mIgG2a.I2.eGFP	Murine rituximab IgG2a heavy chain construct	Brian Philip
SFG.Rtx_L_mKappa.I2.eBFP2	Murine rituximab kappa light chain construct	Brian Philip
SFG.R-HCH2CH3-CD28OXZ.I2.eGFP	R-HCH2CH3.I2.eGFP	Brian Philip
SFG.RQR-GPI.I2.eGFP	RQR-GPI.I2.eGFP	Brian Philip
SFGmR.RQR8-2A-aGD2huK666-HCH2CH3pvaa-CD28Zeta	RQR8.2A.GD2-CARpvaa (including Hombach mutation)	Alicja Kopec
SFG.Q-GPI.I2.eGFP	Q-GPI.I2.eGFP	Brian Philip
SFG.Q-L-GPI.I2.eGFP	Q-L-GPI.I2.eGFP	Brian Philip
SFG.HA-GPI.I2.eGFP	HA-GPI.I2.eGFP	Brian Philip
SFG.Qv01-L-GPI.I2.eGFP	Q-GPI.I2.eGFP (MP12223)	Emily Hardman
SFG.Qv02-L-GPI.I2.eGFP	Q-GPI.I2.eGFP (MP12224)	Emily Hardman
SFG.Qv03-L-GPI.I2.eGFP	Q-GPI.I2.eGFP (MP12227)	Emily Hardman
SFG.Qv04-L-GPI.I2.eGFP	Q-GPI.I2.eGFP (MP12228)	Emily Hardman
SFG.Qv05-L-GPI.I2.eGFP	Q-GPI.I2.eGFP (MP12229)	Emily Hardman
SFG.QLC-GPI.I2.eGFP	Q-GPI.I2.eGFP (MP12230)	Emily Hardman
SFG.QLCD52-GPI.I2.eGFP	Q-GPI.I2.eGFP (MP12231)	Emily Hardman
SFG.QZL-GPI.I2.eGFP	Q-GPI.I2.eGFP (MP12232)	Emily Hardman
SFG.myc-L-GPI.I2.eGFP	myc.I2.eGFP	Emily Hardman

SFG.V5-L-GPI.I2.eGFP	V5.I2.eGFP	Emily Hardman
SFG.HSV-L-GPI.I2.eGFP	HSV.I2.eGFP	Emily Hardman
SFG.T7-L-GPI.I2.eGFP	T7.I2.eGFP	Emily Hardman
SFG.OLLAS-L-GPI.I2.eGFP	OLLAS.I2.eGFP	Emily Hardman
SFGmR.RQR8-2A-aCD19_4g7_HL-CD8STK-41BBZ	RQR8.2A.aCD19	Gordon Cheung & Leila Mekkaoui
SFG.V5-L-8.I2.eGFP	V5-L.8.eGFP V5 epitope on CD8 stalk	Dimitra Markantoni
SFG.myc-L-8.I2.eGFP	myc-L.8.eGFP myc epitope on CD8 stalk	Dimitra Markantoni
SFG.HA-L-8.I2.eGFP	HA-L.8.eGFP HA epitope on CD8 stalk	Dimitra Markantoni

13.2. Retroviral expression plasmids

The development of retro- and lenti-viral vector systems offers great potential for clinical gene transfer applications. Retroviral vectors offer the capacity for transient *in vitro* genetic experimentation or sustained transgene expression following stable integration into the host chromosome. Due to exclusive use of retroviral vectors in this body of research, further discussion will be limited to these.

Retroviruses are single stranded RNA viruses which achieve replication through a double stranded DNA intermediate. Retroviral vectors, such as SFG[28], derived from the Moloney murine leukaemia virus are commonly used for gene transfer applications. Retroviral expression plasmids offer a strategy to achieve sustained gene expression resulting from integration of the transgene into the DNA. Crudely bisected, the SFG retroviral expression vector can be visualised as a bipartite system as illustrated by Figure 109.

Inclusion of an origin of replication (ori) and an antibiotic resistance gene, e.g. Ampicillin resistance (AmpR), within the vector backbone enables selective amplification of DNA within bacteria, whilst the transgenic cassette bounded by retroviral long term repeat (LTR) sequences enables transient and/or integrative transgene expression strategies.

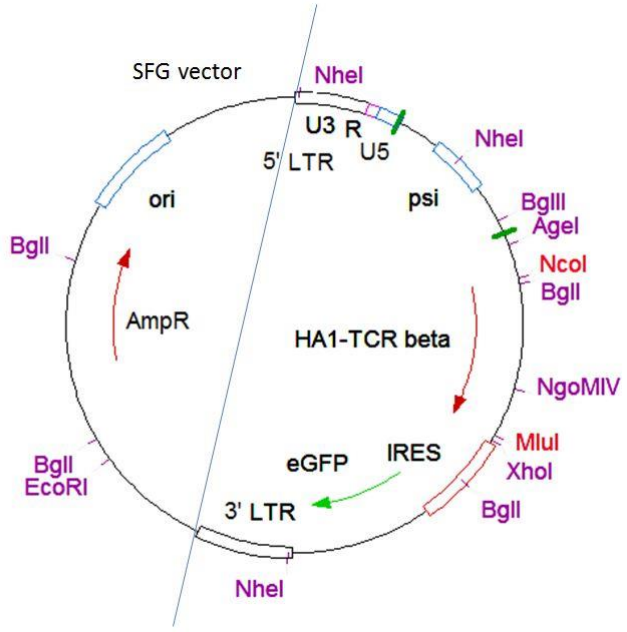

Figure 109 Bimodal design of SFG retroviral expression vector
Functional prokaryotic and eukaryotic components of the SFG retroviral vector can be roughly identified by bisecting the plasmid across the retroviral long terminal repeat (LTR) domains as illustrated. The vector backbone to the left contains prokaryotic regulatory components such as antibiotic resistance (AmpR) and the origin of replication (ori) necessary to facilitate plasmid amplification in bacterial culture under antibiotic selection. In contrast, the region bounded by retroviral LTR domains represents the eukaryotic expression cassette mediating transgene expression driven by the 5' LTR promoter facilitating either transient expression when plasmid DNA remains episomal or sustained expression following chromosomal integration.

Application of a modular cloning design maintained by inclusion of unique restriction sites at key locations within the plasmid backbone enables efficient cloning strategies for subsequent construct generation. Epitope mapping and epitope tag construct clonings were all generated through SOE-PCR based DNA amplification, containing internal NcoI-MluI restriction sites to facilitate insertion upstream of an IRES sequence as illustrated by figure 107. Caveats for selection of restriction sites include: sites must be unique within the vector backbone and absent from the transgenic coding sequence, optimal restriction enzymes pairings should generate ‘sticky’ ends which are incompatible with each other, with chosen enzymes preferentially insensitive to DAM/DCM methylation.

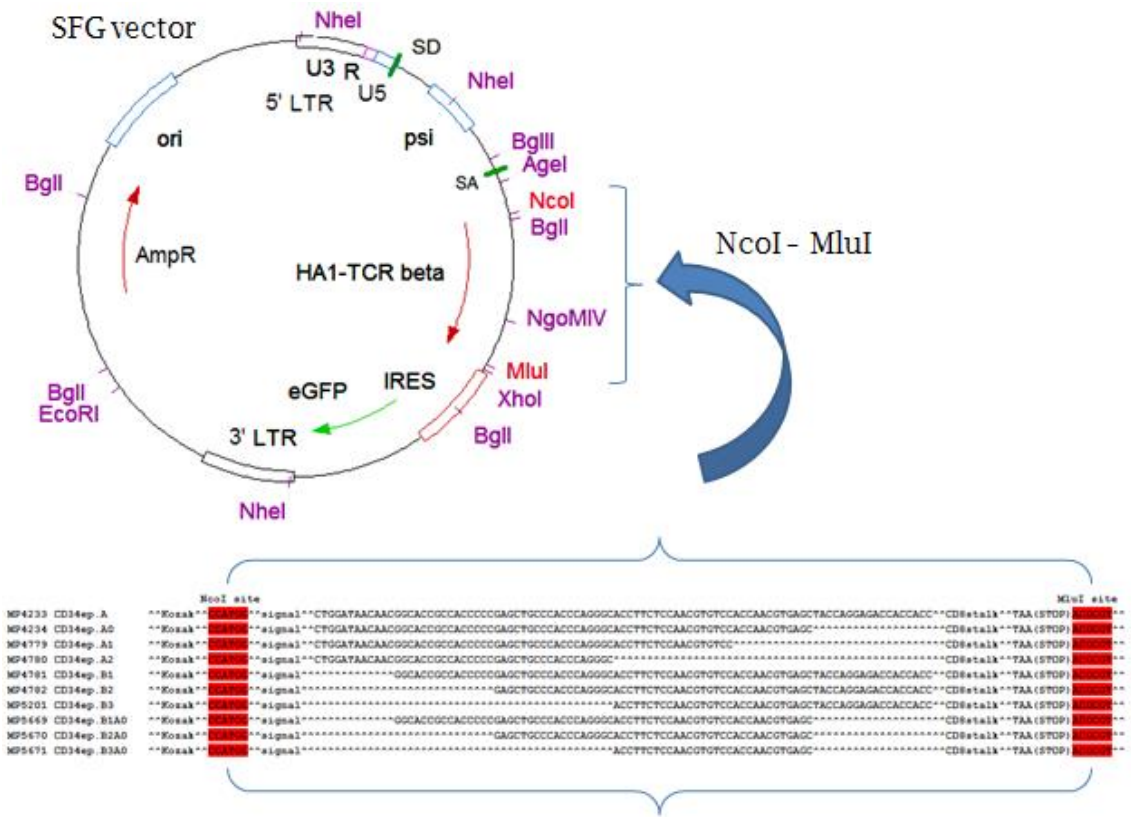

Figure 110 Modular cloning strategy for generation of epitope constructs
Consistent inclusion of NcoI and MluI restriction sites in forward and reverse primers respectively facilitated a strategy to rapidly generate virtually identical constructs variant only in the sequence under investigation. Inclusion of the Encephalomyocarditis virus (ECMV) IRES sequence 3' to the primary transgene facilitating co-expression of the eGFP fluorescent marker gene enabled both identification of transgenic cells and assessment of transgene expression efficacy. LTR – Long terminal repeat, U3 – unique 3' region, U5 – unique 5' region, R – repeat motif, SD – Splice donor, SA – Splice acceptor, psi – viral envelope packaging signal, IRES – Internal ribosomal entry site, ori – origin of replication, AmpR – Ampicillin resistance

13.3. Gene expression and enhancement

13.3.1. Retroviral replication and retroviral LTR

The retroviral genome varies in format between the integrated provirus and the encapsulated viral genome. In the integrated pro-viral form, the retroviral long terminal repeat (LTR) sequences demarcate the viral genome, or transgenic cassette. LTR's are composed of three elements: U3, R and U5, representing the U3 and U5 sequences, unique to the 3' and 5' termini of the viral genome respectively, and R sequences which are repeat sequences located in both LTR sequences[302]. The U3 domain contains the retroviral enhancer/promoter sequence driving downstream transgene expression from both LTR domains. SFG retroviral constructs utilise the Moloney murine

leukaemia virus LTR sequence as the promoter sequence to facilitate transgene expression.

Replication of the retroviral genome requires two critical enzymatic abilities of the reverse transcriptase enzyme: the ability to use either RNA or DNA as template for nucleic acid polymerisation and RNase H nuclease activity which enables specific degradation of the RNA strand of RNA:DNA duplexes.

As illustrated by Figure 111, the retroviral genome is bounded by the 'R' repeat domain located in the terminal repeat domains, however to establish the required full LTR domain present in the integrated proviral format, retroviruses must regenerate their enhancer/promoter sequence from the RNA template. This is achieved through two separate strand-transfer reactions. DNA synthesis toward the 5' terminus commences following host tRNA primer binding to the primer binding site (PBS), generating a short anti-sense fragment composed of the 5' R-U5 domain generating minus-strand strong stop DNA. Release of this fragment to enable the first strand transfer 'jump' is facilitated by the RNase H activity of retroviral reverse transcriptase. Binding of the minus-strand strong stop DNA intermediate to the 3' end of the retroviral genome, thought to be facilitated by nucleocapsid protein, allows for DNA synthesis to continue coincident with RNase H activity in the 3' to 5' direction. The presence of a short polypurine tract (PPT) resistant to RNase H activity terminates degradation of the viral RNA genome at this location. As a result, a short RNA fragment localised to the PPT acts as a primer for plus strand DNA synthesis toward the 3' terminus of the minus-strand strong stop DNA, terminating shortly into the sequence for the tRNA primer generating plus strand strong stop DNA. RNase H activity then removes the tRNA primer exposing the complementary PBS site of the plus strand strong stop DNA which can then bind to the complementary PBS site present on minus-strand strong stop DNA which is the second strand transfer. The resulting primers can then act as template for each other allowing for amplification of the proviral DNA genome which is subsequently integrated into the host genome through the action of viral integrase[302].

The retroviral genome contains three crucial genes necessary for the retroviral replication lifecycle. The gag gene encodes core viral structural proteins

including matrix (MA), capsid (CA) and nucleocapsid (NC) while the pol gene encodes for viral replication enzymes including: protease (PR), reverse transcriptase (RT) and integrase (IN); lastly the env gene encodes for the envelope glycoprotein (ENV) which is further processed into transmembrane (TM) and surface (SU) subunits. Although these genes are required for viral replication and generation of infectious viral particles, they are not required for gene expression facilitated by integrating viral vectors. Hence, as illustrated by Figure 111, exclusion of the viral replication genes, supplied separately in trans during viral production allows for space to insert a transgenic cassette into a retroviral vector which can be generated into functional viral particles when the core viral genes are co-expressed in trans.

The U3 domain contains most of the transcriptional control elements of the provirus including the promoter and enhancer with the site of transcription initiation located at the boundary of the U3-R domains.

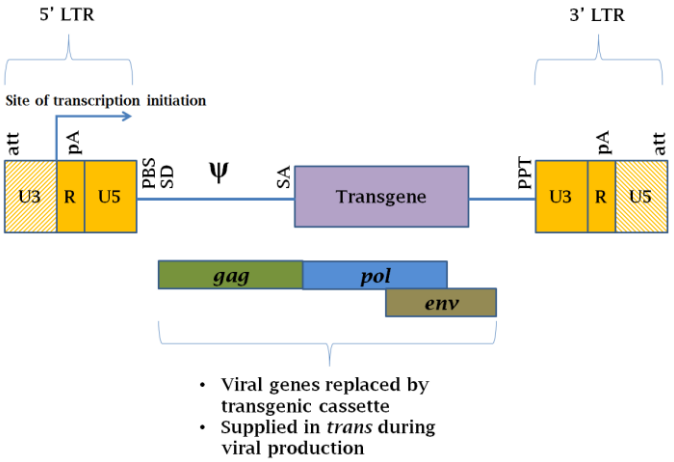

Figure 111 Illustration of retroviral vector structure
Retroviral vectors exploit the functional capacity of genomic integration whilst achieving safety through deletion of pathogenic portions of the viral genome (e.g. viral polymerase (*pol*) and envelope (*env*) genes. However, much of the *gag* gene remains due to co-localisation of the packaging signal psi (symbol) in this region which is essential to facilitate packaging of the transgenic cassette into viral particles. The retroviral genome, and by extension retroviral expression cassettes, are delineated by long terminal repeat domains which in the integrated proviral format are comprised of 3 domains: unique 5' and 3' regions flanking a repeat motif located in the middle. Transgene transcription is driven by the retroviral promoter located at the junction of the U3-R domains.

13.3.2. Kozak sequence

A consensus sequence for optimal transcription initiation based on the research of Marilyn Kozak was located directly upstream of the transgenic cassette in the SFG vectors. Where the spicing by overlapping extension

cloning strategy required generation of the start codon for this cassette, the Kozak consensus sequence was included within the 5' primer sequences to ensure effective DNA transcription[303].

13.3.3. S/MAR – Scaffold / Matrix attachment region.

Scaffold or Matrix attachment regions are DNA sequences which were identified to bind preferentially to the nuclear matrix based on nuclease digestion assays. Although S/MAR sequences appear to share some common structural features including an AT-rich sequence and inclusion of topoisomerase II consensus sequences, a defining consensus sequence for S/MAR elements remains to be established[304]. It has been observed that transgene expression in retrovirally transduced T-cells is decreased in mitotically quiescent cells. However, this effect can be offset by orientation specific incorporation of the human beta inteferon S/MAR region into Moloney murine leukaemia virus based vectors which has been demonstrated to improve transgene expression in primary human T-cells[254]. Where indicated, vectors including S/MAR regions used in this project contained the human beta interferon S/MAR to ensure sustained transgene expression.

13.4. Bi/Poly cistronic vector expression strategies

IRES elements and 2A sequences represent two alternative strategies to achieve bi/poly cistronic gene expression:

13.4.1. Internal ribosome entry site (IRES) sequences:

IRES elements consist of cis acting RNA structures that possess the ability to directly recruit translational machinery to an internal position within an mRNA. Thus, inclusion of an IRES sequence enables bicistronic expression under control of a single promoter. This strategy allows for interrogation of a protein of interest coincident with a secondary protein such as the fluorescent protein eGFP, used as a marker gene to identify the transgene expressing population. Using this strategy, synthesis of a single mRNA containing an IRES element situated between open reading frames, is directed by the retroviral promoter. Translation of the upstream transgene occurs by cap-dependent ribosome scanning whereas translation of the downstream transgene results from direct recruitment of ribosomes to the IRES sequence in a cap

independent manner[305]. We have employed the commonly used Encephalomyocarditis virus (EMCV) IRES sequence in the SFG constructs used in this project, subsequently referred to as 'I2'.

13.4.2. 2A sequences:

Viral derived '2A' peptide sequences are attractive alternatives to IRES elements for bicistronic expression. Although inclusion of IRES elements enables multiple proteins to be produced from a single mRNA transcript, this strategy suffers from a number of limitations. The downstream sequence is often translated at a much lower level that the upstream sequence and the impact of this effect can vary dependent on size of the upstream sequence; also, averaging 600 base pairs in length, IRES elements impact upon the size of a transgenic cassette. Finally, the expression of the downstream cistron can be sensitive to the positioning following the IRES element. In contrast, 2A sequences are *cis*-acting hydrolase elements which mediate co-translational cleavage of a nascent peptide sequence. The sequence of the 2A peptide acts to prevent the formation of a normal peptide bond between the terminal glycine and proline residues. This results in the ribosome skipping to the next codon resulting in peptide cleavage between the glycine and proline residues of the nascent protein[306]. As a result, the upstream sequence retains a residual 2A sequence suffix, whilst the downstream sequence commences with the residual proline residue. Typically 20 amino acid residues in length, 2A peptide sequences are considerably smaller than IRES elements and offer equimolar expression of bi/poly-cistronic constructs. For constructs containing a 2A sequence, we used the 20 amino acid 2A sequence derived from the *Thosea asigna* virus; RAEGRGSLLTCGDVEENPGP[307] selected based on the high efficiency of cleavage activity.

13.5. Modular cloning design

In the SFG vector used in this project[28], transgene expression is mediated by the retroviral promoter located in the U3 domain of the 5' LTR. However, where necessary, cloning design included a portion of the psi packaging sequence to facilitate alternative restriction digest combinations e.g. BglII/AgeI-MluI.

Localisation of the 2A sequence in this orientation affords a simple cloning design for equimolar co-expression of alternative constructs alongside RQR8. This parental construct was used to generate the co-expression constructs for RQR8 along with the WT1 TCR and the GD2 CAR Figure 112.

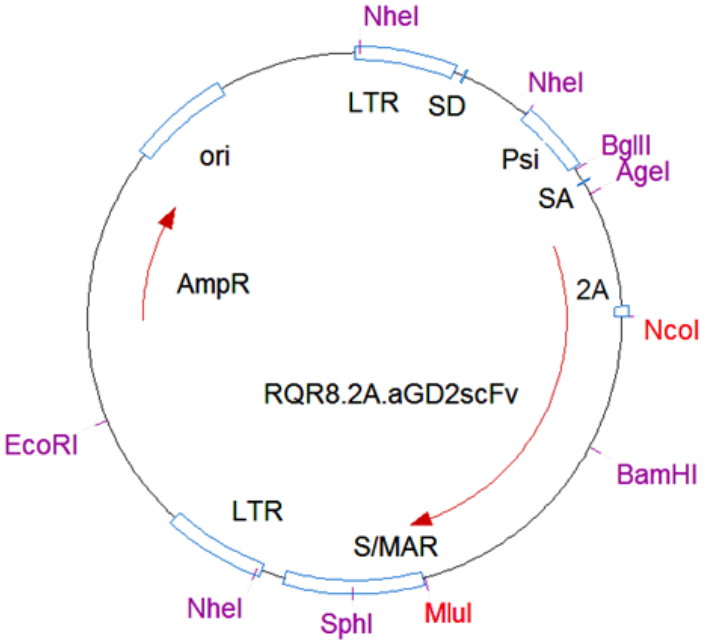

Figure 112 Modular design strategy of SFG cloning vectors
Vector engineering to establish unique restriction sites at key locations within the retroviral vector affords the potential to facilitate simple subcloning of subsequent constructs. Thus as illustrated, generation of novel CAR constructs can be readily achieved through NcoI-BamHI cloning which exchanges the binding specificity of an scFv into a retroviral CAR expression cassette backbone.

Furthermore, as scaffold/matrix attachment regions (S/MAR's) have been demonstrated to enhance transgene expression, a S/MAR domain derived from the human beta interferon gene was included into the vector backbone structure to compensate for high transcriptional burden of long open reading frames. (Previous work by Dr. Simon Thomas has demonstrated improved gene expression from SFG vectors containing S/MAR domains).

The cloning design for single chain variable fragment (scFv) constructs employed an NcoI-BamHI restriction strategy placing the insert in frame into the scFv transgene illustrated by Figure 112. Due to the presence of a natural BamHI site proximal to the apex of the IgG1 stalk affords a simple strategy for scFv cloning through an NcoI-BamHI restriction strategy allowing for generation of alternative CAR's through insertion of an alternative scFv cloned in-frame. This cloning strategy also facilitates a simple functional screening

strategy for gene synthesis constructs as frameshift mutations would likely result in non-functional protein products. An alternative construct containing a modified endodomain (parental construct cloned by Kim Vigor and Simon Thomas) enables production of secreted versions of scFv fragments to enable functional binding assays.

Appendix 2

Regular Article

IMMUNOBIOLOGY

A highly compact epitope-based marker/suicide gene for easier and safer T-cell therapy

Brian Philip,[1] Evangelia Kokalaki, [1] Leila Mekkaoui,[1] Simon Thomas,[1] Karin Straathof,[1] Barry Flutter,[1] Virna Marin,[2] Teresa Marafioti,[1] Ronjon Chakraverty,[1] David Linch,[1] Sergio A. Quezada,[1] Karl S. Peggs,[1] and Martin Pule[1]

[1]UCL Cancer Institute, University College London, London, United Kingdom; and [2]Department of Pediatrics, Centro di Ricerca Matilde Tettamanti, University of Milano-Bicocca, Milan, Italy

Key Points

- Marker genes enable detection and selection of T cells, whereas suicide genes enable selective destruction of T cells in case of toxicity.
- RQR8 is a 136-amino-acid epitope-based marker/suicide gene that enables clinical selection, cell tracking, and deletion in case of toxicity.

A compact marker/suicide gene that utilizes established clinical-grade reagents and pharmaceuticals would be of considerable practical utility to T-cell cancer gene therapy. Marker genes enable measurement of transduction and allow selection of transduced cells, whereas suicide genes allow selective deletion of administered T cells in the face of toxicity. We have created a highly compact marker/suicide gene for T cells combining target epitopes from both CD34 and CD20 antigens (RQR8). This construct allows selection with the clinically approved CliniMACS CD34 system (Miltenyi). Further, the construct binds the widely used pharmaceutical antibody rituximab, resulting in selective deletion of transgene-expressing cells. We have tested the functionality of RQR8 in vitro and in vivo as well as in combination with T-cell engineering components. We predict that RQR8 will make T-cell gene therapy both safer and cheaper. (*Blood.* 2014;124(8):1277-1287)

Introduction

Adoptive immunotherapy is an established and evolving therapeutic approach. In the setting of allogeneic hematopoietic stem cell transplantation, donor lymphocyte infusions are frequently given to treat relapse of hematologic malignancies. Tumor-infiltrating lymphocytes are effective in treating metastatic melanoma. Genetic engineering of T cells greatly increases the scope and potency of T-cell therapy: T-cell receptor (TCR) transfer allows targeting of intracellular cancer antigens, whereas chimeric antigen receptors (CARs) allow targeting of surface cancer or lineage-specific antigens.[1] Clinical responses have been observed with both approaches, and numerous further trials are underway.

Acute adverse events can occur following adoptive immunotherapy. Graft-versus-host disease is a common and serious complication of donor lymphocyte infusions. Administration of engineered T cells has also resulted in toxicity.[2-5] For instance, on-target off-tumor toxicity has been reported in native TCR transfer studies against melanoma antigens[6]; T cells redirected to the renal cell carcinoma antigen carbonic anhydrase IX produced unexpected hepatotoxicity.[7] Immune activation syndromes have been reported after CD19 CAR therapy.[3,8,9] Finally vector-induced insertional mutagenesis results in a theoretical risk of lymphoproliferative disorders. The incidence and severity of these toxicities is unpredictable. Further, in contrast to a therapeutic protein or small molecules, whose adverse events usually abate with the half-life of the therapeutic, T cells engraft and replicate, potentially resulting in escalating and fulminant toxicity.

A suicide gene is a genetically encoded mechanism that allows selective destruction of adoptively transferred T cells in the face of unacceptable toxicity. Two suicide genes have been tested in clinical studies: herpes simplex virus thymidine kinase (HSV-TK)[10] and inducible caspase-9 (iCasp9).[11] Expression of HSV-TK in T cells confers susceptibility to ganciclovir. HSV-TK is a highly effective suicide gene, but immunogenicity limits application to clinical settings of profound immunosuppression such as haploidentical hematopoietic stem cell transplantation. Further, it precludes the use of ganciclovir for the treatment of cytomegalovirus infection. iCasp9 is activated by an experimental small-molecule dimerizer (AP20187); hence, use of this suicide gene depends on the availability of clinical-grade dimerizer. Finally, both are intracellular proteins and typically must be coexpressed with a marker gene.

Marker genes enable detection and positive selection of transduced T cells. Some T-cell engineering strategies do not result in transgenic expression of readily detectable surface proteins.[1] In these cases, measurement of transduction and tracking of cells in peripheral blood is difficult, and a marker gene is useful. Further, in some settings, it is essential to administer only transduced T cells, for instance in graft-versus-host disease suicide-gene protocols. Described marker genes include several truncated type I transmembrane proteins not normally expressed on T-cells: the truncated low-affinity nerve growth factor,[12] truncated CD19,[11] and truncated CD34.[13] A particularly attractive feature of CD19 and CD34 is the availability of the off-the-shelf Miltenyi CliniMACS selection system

Submitted January 6, 2014; accepted May 27, 2014. Prepublished online as *Blood* First Edition paper, June 26, 2014; DOI 10.1182/blood-2014-01-545020.

The online version of this article contains a data supplement.

The publication costs of this article were defrayed in part by page charge payment. Therefore, and solely to indicate this fact, this article is hereby marked "advertisement" in accordance with 18 USC section 1734.

for clinical-grade sorting. However, these are relatively large surface proteins that may tax the vector packaging capacity and transcriptional efficiency of an integrating vector.

We sought to develop a highly compact epitope-based construct that would act as both a suicide and marker gene. For maximum convenience, we restricted our design to one that could use existing good manufacturing practice reagents and standard pharmaceuticals for both selection and deletion. Our final construct, RQR8, is a 136-amino-acid protein that is recognized by the anti-CD34 antibody QBEnd10, the antibody used in the Miltenyi CliniMACS CD34 selection system. It renders T cells highly susceptible to lysis by the therapeutic monoclonal rituximab. We anticipate RQR8 will make T-cell therapy cheaper, easier, and safer.

Materials and methods

Cloning

All constructs were generated by in-house gene synthesis using polymerase chain reaction assembly of overlapping oligos unless otherwise specified. Codon optimization used an in-house algorithm (written by M.P. and available upon request) that strove to keep GC content at 70% and eliminate cryptic splicing, hairpins, literal repeats, and any possible *cis*-acting sequences. Identity of constructs was confirmed through capillary sequencing Applied Biosystems 3730xL capillary. Phusion polymerase, quick Ligase, and NEB5α (New England Biolabs) were used for molecular cloning. Oligonucleotides were purchased from IDTDNA. The retroviral vector used in all constructs was the splicing oncoretroviral vector SFG.[14] Enhanced green fluorescent protein (eGFP) and enhanced blue fluorescent protein 2 (eBFP2)[15] were coexpressed from an encephalomyocarditis virus internal ribosomal entry site sequence.[16] Anti-GD2 CAR was as described elsewhere (K.S., T. Gileadi, E.K., B.F., R. Wallace, H. Zhang, N. Westwood, D. Edwards, W. Qasim, J. Anderson and M.P., unpublished data). RQR8 was coexpressed with CAR by cloning it upstream of the CAR separated by an in-frame foot-and-mouth–like 2A peptide, TaV,[17] or coexpressed with the wild-type-1–specific TCR α and β chains with 2 interposed foot-and-mouth disease (FMD)-2A TaV sequences, codon wobbled to prevent retroviral recombination. Annotated sequences of constructs used are included in supplemental Data 2 (available at the *Blood* Web site).

Retroviral production and transduction

RD114-pseudotyped supernatant was generated as follows: 293T cells were transfected with vector plasmid; RDF, an expression plasmid to supply RD114 envelope (gift of Mary Collins, University College London)[18]; and PeqPam-env, a gagpol expression plasmid (gift of Elio Vanin, Baylor College of Medicine).[17,19,20] Transfection was facilitated using genejuice (Merck). Eco-pseudotyped supernatant was generated in a similar way, with RDF substituted by the ecotropic envelope expression plasmid pMono.Eco. Peripheral blood mononuclear cell transductions were performed as follows: T cells were isolated by Ficoll (GE Healthcare) gradient centrifugation and stimulated with phytohemagglutinin at 5 μg/mL. Interleukin-2 (IL-2) stimulation (100 IU/mL) was added following overnight stimulation. On day 3, T cells were harvested, plated on retronectin and retroviral supernatant, and centrifuged at 1000*g* for 40 minutes. Murine splenocytes were isolated and transduced as follows: splenocytes from 6- to 8-week-old C57BL/6 mice were isolated by passage through a 40-μm-pore sieve followed by red blood cell lysis in ACK lysis buffer (Lonza). Splenocytes were activated in RPMI supplemented with 10% fetal calf serum, Glutamax, 10 mM HEPES, and 0.1 μm 2-mercaptoethanol supplemented with 2 μg/mL concanavalin A (Sigma) and 1 ng/mL interleukin-7 (Peprotech) at a density of 1 to 1.5 × 10^6/mL for 24 hours. Retroviral transduction was performed by loading retronectin-coated plates (Takara) with 2 to 3 × 10^6 splenocytes suspended in 1 mL retroviral supernatant, centrifuged at 805*g* for 90 minutes, and then recovered by overnight incubation at 37°C. The following day, splenocytes were recovered from the plate, resuspended in complete RPMI supplemented with 50 ng/mL murine IL-2 (Invitrogen), and cultured overnight. Transduced splenocytes were purified on LS columns using CD34 microbeads (Miltenyi Biotec) as per the manufacturer's instructions. Following positive selection, splenocytes were resuspended in conditioned media retained from the overnight IL-2 stimulation and cultured overnight. Purity and viability of selected splenocytes were assessed by flow cytometry prior to adoptive transfer 1 day following positive selection.

Antibodies, flow cytometry, and flow sorting

CAR was stained using a Cy5-conjugated polyclonal goat anti-human-Fc (Jackson Immunotech). Rituximab and ofatumumab were procured from the hospital pharmacy at University College London Hospital. Murine immunoglobulin G2a (IgG2a) rituximab was generated by cloning the variable regions of the heavy and light chain from IDEC2B8 hybridoma HB-11388 checked against patent 5 843 439 into the constant regions of murine IgG2a and murine immunoglobulin κ (sourced from InvivoGen plasmids pFUSEss-CH1g-mG2A and pFUSE2ss-CLIg-mk) into a retroviral vector (MP9201 SFG.*S*-Rtx_H_mIgG2a.I2.eGFP and MP9202 SFG.*S*-Rtx_L_mKappa.I2.eBFP2; see supplemental Data 2 for sequences). K562 cells were transduced with vectors coding for both heavy and light chains. A highly productive clone was identified, expanded in Phenol Red negative Iscove modified Dulbecco medium supplemented with 2.5% immunoglobulin G–depleted serum (Biosera). Flow cytometry was performed using Beckman-Coulter Cyan and BD LSRII Fortessa instruments. Flow cytometric sorting was performed using a Beckman Coulter MoFlo-XDP sorter.

Complement-mediated cytotoxicity

Transduced T cells were exposed to 25% baby-rabbit complement (AbD Serotec) for 4 hours with or without inclusion of rituximab (100 μg/mL) to examine complement-dependent cytotoxicity (CDC)-mediated sensitivity. Miltenyi CD34 magnetic bead–selected-transduced RQR8 T-cells were compared against a similarly treated population of Q8-transduced T cells to demonstrate specificity of CDC-mediated deletion. Further examination of CDC assay parameters was achieved through time-course/dose-titration assays using RQR8-transduced T cells incubated with rituximab at 12.5, 25, 50, and 100 μg/mL and time-point assessments ranging between 1 to 120 minutes.

Antibody-dependent cellular cytotoxicity

Natural killer (NK) cell effectors were generated using a K562 stimulator cell line (after Campana[21]), expressing membrane-bound interleukin-15 and 41BBL established by retroviral vector transduction and single-cell cloning. Freshly isolated peripheral blood mononuclear cells from healthy donors were cocultured 1:1 in 24-well tissue-culture–treated multiwell plates with irradiated K562.41BBL.mIL15 irradiated at 120 Gy and supplemented with 40iu IL2. Partial media changes performed as required. Following 7 days in culture, a pure population (>95% purity) of NK cells was isolated following a single round of Miltenyi CD56-positive selection. Transduced T-cell targets were cocultured with NK cell effectors at effector:target ratios of 16:1, 8:1, 4:1, and 2:1 for 48 hours. Cellular deletion was assessed by flow cytometry following Annexin V (BD Biosciences) and propidium iodide (PI) (Sigma-Aldrich) staining. For sensitivity assessment of antibody-dependent cellular cytotoxicity (ADCC)-mediated deletion, NK cell effectors were prepared with CellTRACE violet (Invitrogen) immediately prior to assay setup. For ADCC specificity assessment, NK cell effectors remained unstained, with targets composed of a Miltenyi CD34 magnetic bead–selected mixture of Q8- and RQR8-transduced T cells in equal proportion with Q8 and RQR8 targets identified by expression of eBFP2 or eGFP fluorescent proteins, respectively.

Chromium release cytotoxicity assay

Cytotoxicity of CAR T cells was evaluated in a standard 4-hour ^{51}Cr release assay as previously described.[22]

In vivo engraftment model

This work was performed under United Kingdom home-office–approved project license and in accordance with institutional policies. Splenocytes from

C57BL/6 mice were transduced with SFGmR.RQR8 in the absence of stimulation following 24 hours of stimulation by Con A/IL7 (2 μg/mL and 1 ng/mL, respectively). Following transduction, splenocytes were restimulated with IL-2 (50 ng/mL) and cultured overnight. Following a single round of Miltenyi CD34 selection, purity >90% was achieved. A total of 1.5×10^6 transgenic splenocytes were administered by tail-vein injection to (C57BL/6 × BALB/c) F1 recipients 4 hours following 5-Gy radiograph irradiation preconditioning. Engraftment was assessed 7 days posttransfer by QBEnd10 staining of peripheral blood. A total of 150 μg of murine IgG2a isotyped rituximab was administered by tail-vein injection on days 7, 10, and 12 posttransfer. Mice were sacrificed on day 14 with samples taken from peripheral blood, spleen, lymph nodes, and bone marrow stained for CD4, CD8, $H2K^d$, and QBEnd10 to assess engraftment.

Results

The monoclonal antibody QBEnd10 binds a linear 16-residue fragment of CD34

We first identified the binding site of the type I anti-CD34 monoclonal antibody (mAb) QBEnd10. A DNA library coding for overlapping 31-residue fragments of the serine/threonine-rich amino terminus of CD34 was generated. This library was cloned into a retroviral vector between CD34 signal peptide and transmembrane domain. SupT1 cells were transduced with the subsequent retroviral library. QBEnd10 binding cells were single-cell sorted and the retroviral integrant subsequently sequenced from genomic DNA (not shown). From this, we determined that QBEnd10 binds to the amino-terminal 40 amino acids of mature CD34. We hypothesized that this epitope might need to be projected from the cell surface and allowed loose orientation to allow effective QBEnd10 binding. The CD8 stalk is composed of only 42 amino acids, but it results in a projection sufficient to allow the globular CD8 amino terminus to reach past the TCR and interact with major histocompatibility complex class I on a neighboring cell.[23] By transducing SupT1 cells with equal titer of retroviral supernatant, we then compared QBEnd10 binding to full-length CD34 with the above 40-residue epitope connected directly to the CD8 transmembrane domain, fused directly to the CD8 stalk, or connected to the CD8 stalk via a serine-glycine linker. Both constructs with the CD8 stalk exhibited similar binding to full-length CD34, suggesting that the CD8 stalk enhances access of QBEnd10 to the epitope (Figure 1A-B). Finally, we refined the epitope further by sequential deletion of the amino and carboxy termini. We concluded that a 16-residue linear sequence of CD34 on a CD8 stalk could recapitulate equivalent binding of QBEnd10 as the full CD34 protein (Figure 1C).

Rituximab binding equivalent to that of full-length CD20 could only be achieved with a mimotope

We next sought to achieve binding by rituximab to a fragment of CD20 in an analogous fashion. The binding site of rituximab to CD20 has been elucidated by deletion studies[24] and crystallography[25]; rituximab binds to the disulfide-constrained portion of the CD20 major extracellular loop. We generated constructs where this disulfide-constrained loop was expressed on the CD8 stalk with no flanking residues (dCD20-loop v1) or 4 additional residues of CD20 on either side (dCD20-loop v2). Construct dCD20-loop v2 did not bind rituximab, whereas dCD20-loop v1 achieved only very poor binding (Figure 1D). Perosa et al[26] described rituximab-binding mimotopes of CD20. These sequences resemble the major extracellular loop of CD20 and compete with rituximab for CD20 binding. Hence, we next generated constructs connecting these mimotopes to the CD8 stalk, connecting a circular mimotope to the CD8 stalk. This could recapitulate binding of rituximab. We next generated constructs with the QBEnd10 epitope linked to the CD20 mimotope in either orientation (constructs termed RQ8 and QR8, respectively) (Figure 2A). This circular mimotope and the QBEnd10 epitope described above could be coexpressed in either orientation on CD8 stalk with no diminution of binding of either antibody (Figure 2B).

Two copies of rituximab mimotope flanking the QBEnd10 epitope on the CD8 are optimal for rituximab-mediated lysis

Despite binding of rituximab, CDC assays with RQ8 and QR8 showed significantly less lysis than with full-length CD20. We next proceeded to try to gain some insight into why this was and to improve killing. The circular rituximab mimotope was placed into several formats. RCH2CH3 was constructed by cloning the mimotope onto a human IgG1 Fc spacer. RRQ8 was constructed by linking 2 copies of the rituximab mimotope followed by the QBEnd10 epitope and CD8 stalk. RQR8 has 2 copies of the rituximab mimotope flanking the QBEnd10 epitope on the CD8 stalk. (Figure 2A). Primary human T cells were transduced with these constructs, along with Q8 and full-length codon-optimized CD20. CDC and ADCC assays were performed on unsorted T-cell populations. Constructs RQ8 and RQR8 resulted in ADCC equal to that of CD20, whereas only RQR8 resulted in CDC equal to that of the full-length protein ($P < .05$). We hence selected RQR8 for further study.

RQR8 has properties that make it a good marker/suicide gene

We first explored utility of RQR8 as a marker gene. Primary human T cells transduced with RQR8 could be sorted to high stringency with Miltenyi CD34 beads (Figure 3A). Further, as few as 0.01% RQR8-transduced primary human T cells could be detected in serial dilution experiments (supplemental Figure 1). Further, RQR8 allows immunohistochemical detection with QBEnd10. Concomitant staining for CD3 or with another CD34 antibody will easily discriminate transgenic T cells from other CD34 cells such as hematopoietic stem cells or endothelium (supplementary Figure 2). Next, we explored the utility of RQR8 as a suicide gene. Miltenyi QBEnd10 bead-sorted T cells are very efficiently lysed by a single exposure to rituximab and complement. In 50:50 mixing assays, sorted T-cells were mixed back with nontransduced T cells, and 98% of transduced T cells could be depleted by rituximab and complement (Figure 3B). Both CDC- and ADCC-mediated sensitivities of RQR8 are equal to that demonstrated by expression of full-length codon-optimized CD20 (Figure 2B-C). Rituximab-mediated deletion is efficient at 25 μg/mL, which is well within the therapeutic window of this agent (Figure 3C).[27] CDC-mediated killing of RQR8-expressing T cells occurs rapidly, with maximum lysis within 30 minutes of exposure (Figure 3C).

RQR8 is of utility when expressed with CARs

CARs are among the most commonly used T-cell engineering components. We coexpressed RQR8 with an anti-GD2 CAR in a retroviral vector using the self-cleaving FMD-2A sequence.[17] This resulted in obligate coexpression of CAR and RQR8 (Figure 4B). Selection with QBEnd10 beads resulted in a pure population of CAR-expressing T cells (>95% from 6 separate experiments). We next mixed RQR8-sorted T cells 1:1 with nontransduced T cells and performed lysis and functional experiments. CDC by rituximab led

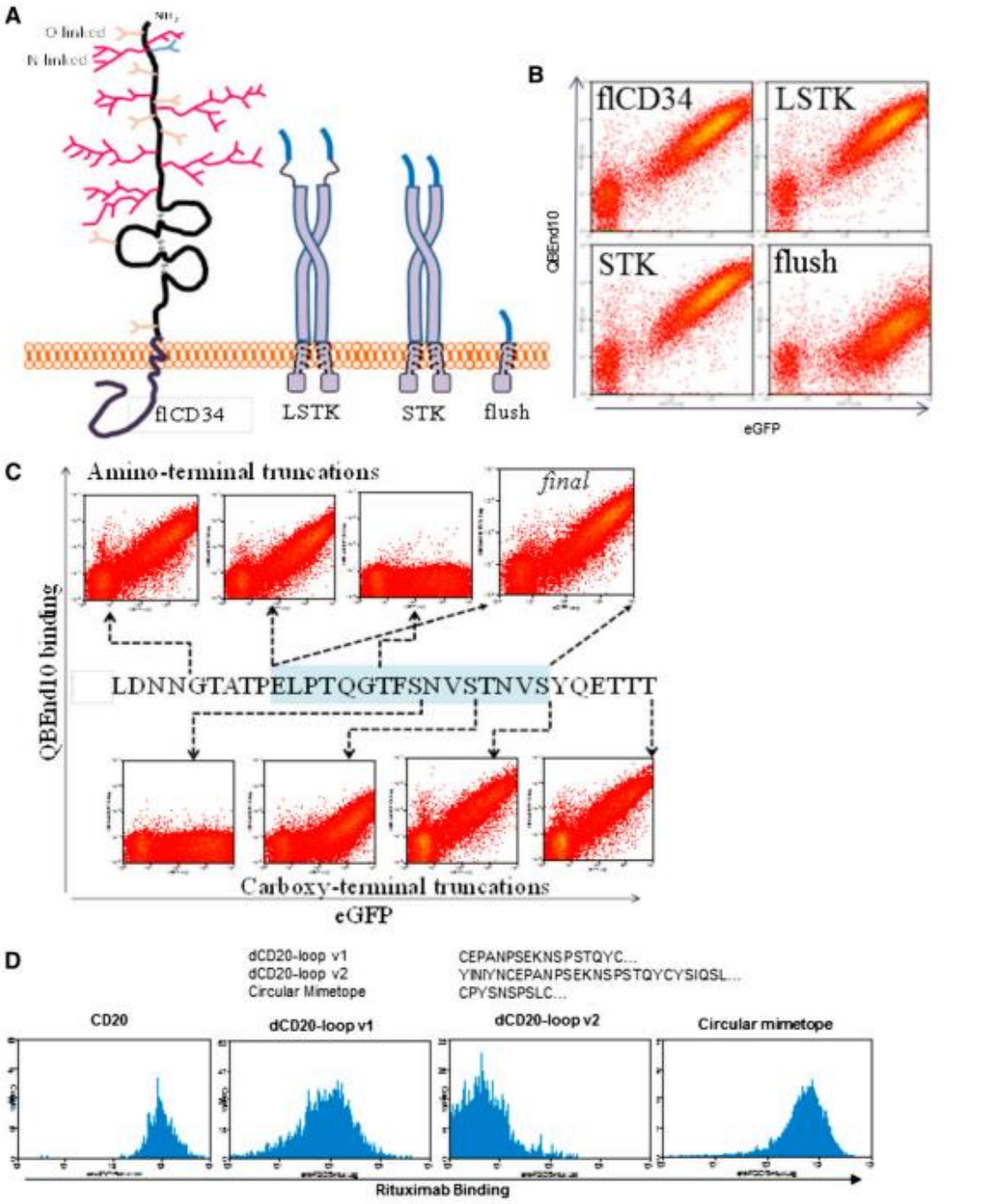

Figure 1. Engineering of QBEnd10- and rituximab-binding domains. (A) Coding sequences for the 31 extreme amino-terminal residues of mature full-length CD34 (flCD3) were cloned in-frame to the CD8 stalk and transmembrane domain via a serine-glycine linker (LSTK) or without this linker (STK) or connected directly to the CD8 transmembrane domain (flush). These open-reading frames were coexpressed with eGFP within a bicistronic retroviral vector. (B) Flow cytometric analysis of eGFP and QBEnd10 staining in T cells transduced with flCD34, LSTK, STK. QBEnd10 binding equivalent to that of flCD34 was seen in constructs containing the CD8 stalk, but not with the flush construct. The serine glycine linker did not improve QBEnd10 binding. (C) Further epitope minimization was performed by sequential amino- and carboxy-terminal deletion of the 31 residues of CD34 until binding of QBEnd10 was abrogated. In this way, we established a final minimal epitope-binding construct containing only 16-amino-acid residues from the 385 present in the native antigen. (D) Binding of rituximab to T cells transduced with full-length CD20 (CD20), the major extracellular loop of CD20 with some flanking residues on the CD8 stalk (dCD20-loop v2), the major extracellular loop of CD20 delineated precisely at the constraining cysteine on a CD8 stalk (dCD20-loop v1), and the circular CD20 mimotope described by Perosa et al[26] on a CD8 stalk.

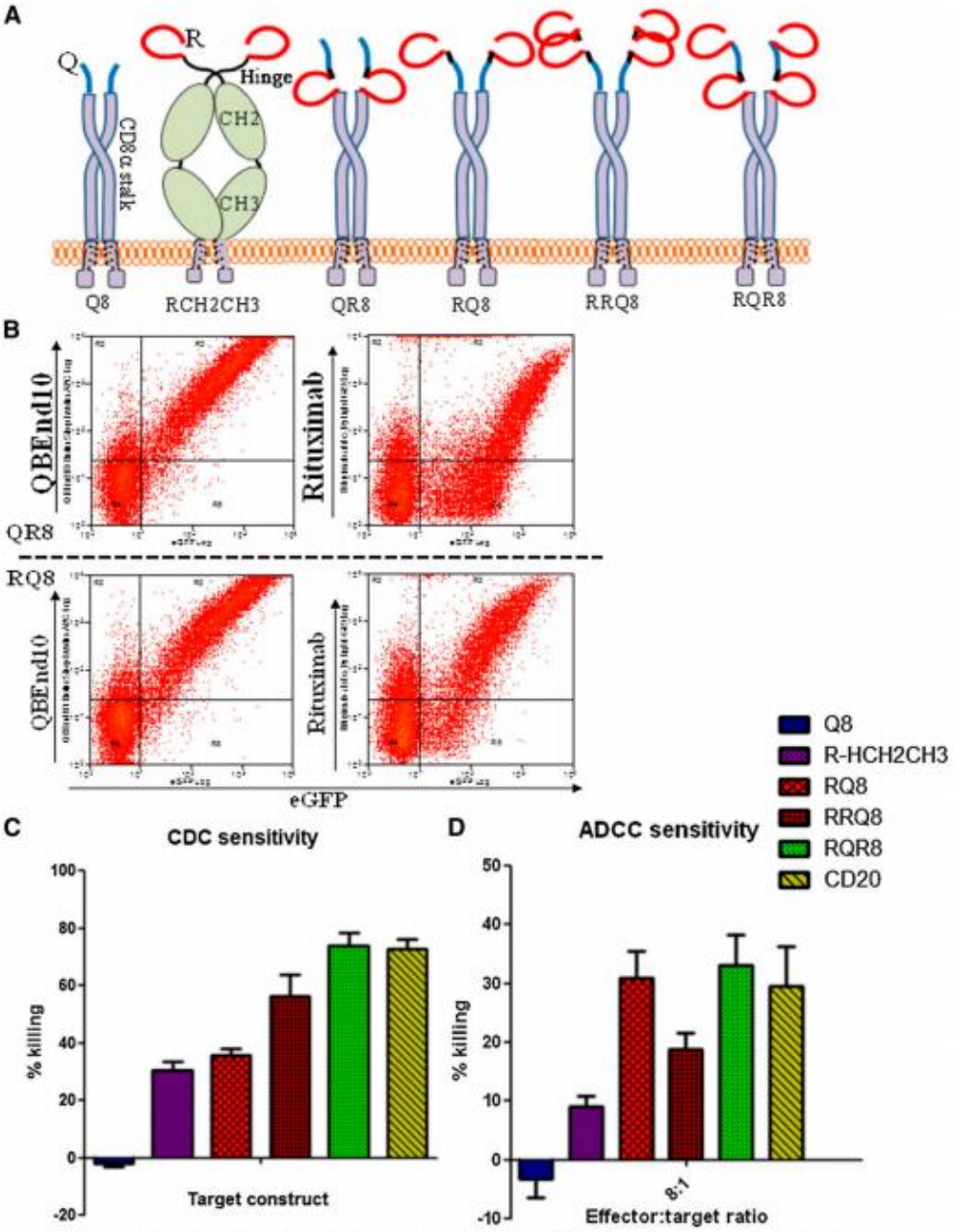

Figure 2. Engineering of combination QBEnd10/rituximab-binding constructs. (A) Cartoon of alternative epitope constructs illustrating alternative presentation formats of epitope constructs that were generated to enable comparison of sensitivity to CDC- and ADCC-mediated deletion. "Q" refers to the 16-amino-acid minimized QBEnd10 epitope; "R" refers to the CD20 circular mimotope; "8" refers to the CD8α stalk; and "Hinge-CH2CH3" refers to the hinge, CH2 and CH3, domains of human IgG1. (B) Binding of QBEnd10 and rituximab to constructs QR8 and RQ8 coexpressed with eGFP in primary human T cells is shown. Both antibodies could bind in either orientation. (C) Sensitivity to CDC depletion using primary human T cells transduced with constructs Q8, RCH2CH3, RQ8, RRQ8, RQR8, and full-length CD20 is shown. Following 4-hour incubation with 25% baby-rabbit complement and rituximab at 100 μg/mL, samples were stained with Annexin V/PI and the live population was assessed by flow cytometry analysis for the presence of the coexpressed eGFP marker gene. Results illustrate comparative deletion observed from 3 separate donors. (D) Similarly, sensitivity to ADCC-mediated depletion was assessed using primary human T-cell targets transduced with constructs were challenged by 16:1, 8:1, 4:1, and 2:1 effector:target ratios of NK cell effectors derived from the same donor. Following 48-hour incubation in the presence of 100 μg/mL rituximab, depletion was assessed by flow cytometry analysis. Samples were stained with Annexin V/PI for live/dead exclusion, with NK cells labeled with CellTRACE violet excluded from the live gate to identify the residual live population of targets cells identified by the presence of a coexpressed eGFP marker gene. Results illustrate comparative deletion by the 8:1 effector:target ratio observed from 3 separate donors. Construct RQR8 engenders equal CDC and ADCC to full-length CD20.

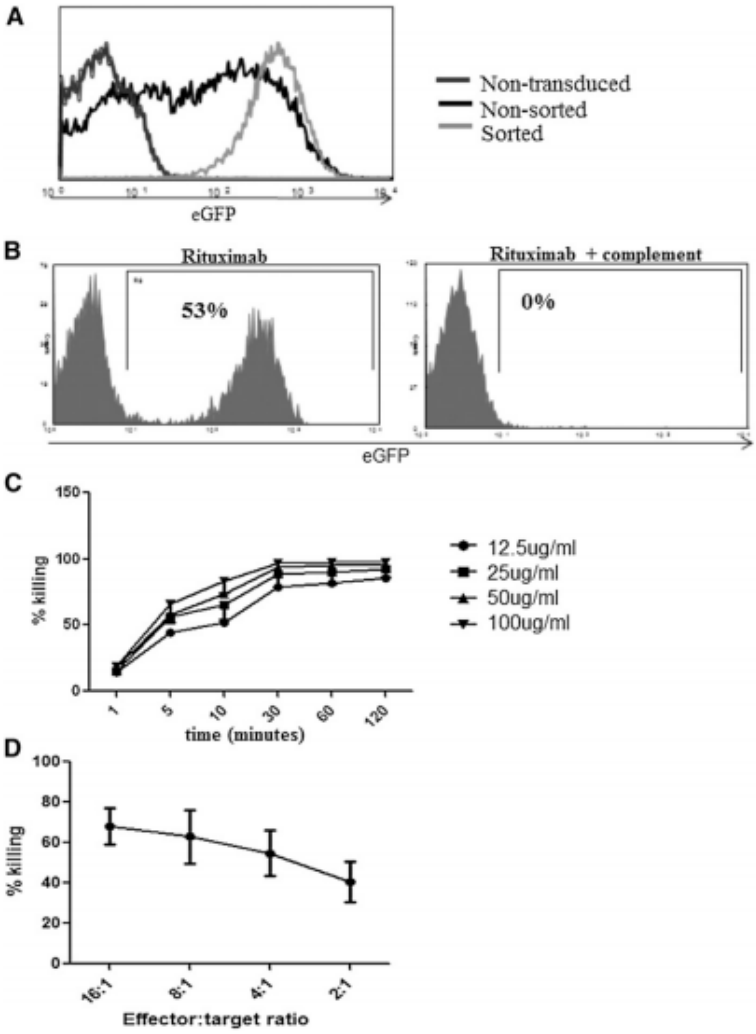

Figure 3. Functional characterization of RQR8. (A) Demonstration of typical cellular purification result achieved following CD34 magnetic bead selection. Primary human T cells were transduced with the bicistronic retroviral vector SFG.RQR8.IRES.eGFP and selected with Miltenyi QBEnd10 beads. (B) Efficiency of CDC in transduced sorted T cells. Primary human T cells were transduced with SFG.RQR8.IRES.eGFP, purified with QBEnd10 beads, and combined at equal concentration with nontransduced T cells. This mixed population was exposed to a 2-hour incubation with 100 μg/mL rituximab with or without 25% baby-rabbit complement. T cells were stained with Annexin/PI, and flow cytometric analysis of eGFP expression on the live population is shown. This is an example of an experiment repeated 6 times in different donors. More than 95% of the transduced population is deleted. (C) Time course and rituximab dose-titration assay. CDC-mediated deletion of targets was performed in primary human T cells with rituximab concentrations of 12.5, 25, 50, and 100 μg/mL analyzed at 1, 5, 10, 30, 60, and 120 minutes. Figure shows mean and standard deviation from 3 donors. CDC is highly effective at rituximab concentrations of ≥25 μg/mL, and killing occurs within 30 minutes. (D) Demonstration of ADCC-mediated sensitivity against T cells transduced with RQR8. Transduced T cells were incubated at 16:1, 8:1, 4:1, and 2:1 effector:target ratios of NK cell effectors derived from the same donor exposed to 100 μg/mL rituximab. Samples were stained with Annexin V/PI for live/dead exclusion with depletion assessed by flow cytometry analysis comparison of the ratio of eGFP/eBFP2 marker gene expression from the residual live population. Note: QR8 was not assessed for ADCC sensitivity.

to deletion of >97% of the CAR-expressing population (Figure 4C). Further, this depleted population completely lost recognition of antigen-expressing targets (Figure 4D). RQR8 could also be co-expressed in a tricistronic vector with a native α/β TCR with FMD-2A–like sequences (not shown).

T cells expressing RQR8 are not susceptible to lysis by ofatumumab

Recent clinical studies of adoptive immunotherapy with CAR-engineered T cells have focused on B-cell malignancies. In this setting, concomitant administration of a B-cell–depleting therapeutic antibody might be desirable. Given the long in vivo half-life of rituximab, its inclusion in a conditioning regimen precludes use of RQR8 in the vector. However, a new generation of anti-CD20 therapeutic antibodies has been developed. One such agent, ofatumumab, binds to a different epitope on CD20 than that of rituximab.[28] We investigated whether ofatumumab would bind to and cause lysis of RQR8-expressing cells. First, T cells transduced with Q8, CD20, and RQR8 were stained with rituximab and ofatumumab (Figure 5A). Whereas CD20-expressing T cells bound both antibodies, RQR8-expressing T cells only bound rituximab. Further, a CDC assay showed lysis of CD20-expressing T cells with both ofatumumab and rituximab (Figure 5B), whereas only rituximab was capable of lysing RQR8-expressing T cells. Hence, ofatumumab can be used in a preparative regimen of engineered T-cell therapy with RQR8. Binding of a panel of other anti-CD20 mAbs in clinical use or preclinical development to RQR8 is detailed in supplemental Table 1.

T cells transduced with RQR8 can be efficiently deleted in vivo

We used an immunocompetent haploidentical adoptive transfer model with RQR8-transduced C57BL/6 splenocytes transferred to non–lethally irradiated C57BL/6 × BALB/c cross (F1) recipients. This model allows good engraftment levels in all lymphoid tissue sustained by allogeneic stimulation, but it also preserves endogenous lymphocytes. Rituximab is a chimeric antibody with mouse variable regions and human κ/IgG1 constant regions with limited activity in mice. To more truly determine potency of deletion, we reengineered rituximab

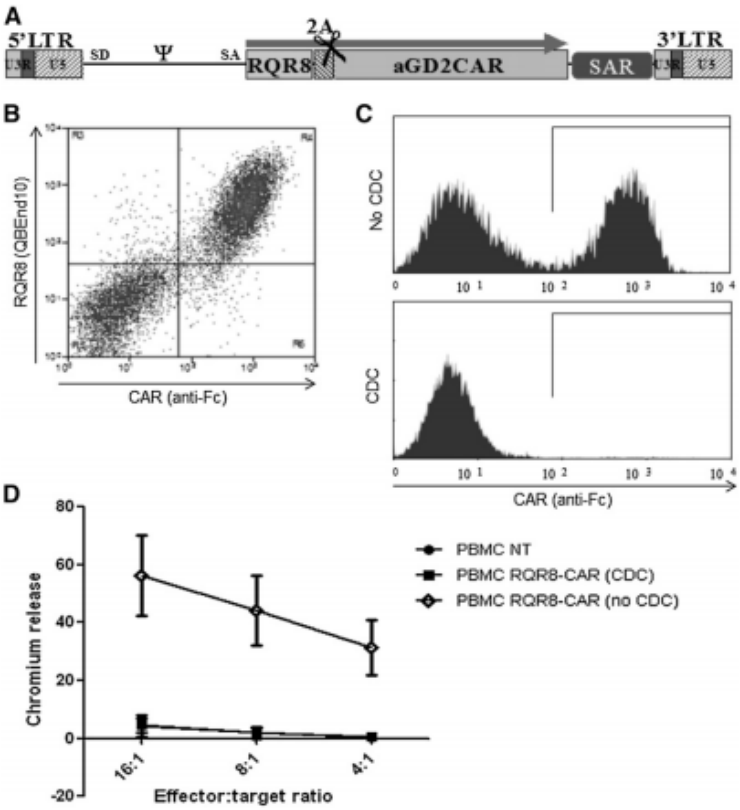

Figure 4. Demonstration of RQR8 activity when coexpressed with a CAR. (A) RQR8 is expressed with an anti-GD2 CAR in the SFG retroviral vector using the FMD-2A sequence. The retroviral vector expression is enhanced using a scaffold attachment region (SAR). (B) Primary human T cells were transduced with this retroviral vector. Following transduction, cells were stained with QBEnd10 and polyclonal goat anti-human Fc (the latter stains the CAR). Clear coexpression of RQR8 and CAR was observed. (C) T cells were sorted with QBEnd10 beads and mixed 1:1 with nontransduced T cells and exposed to either rituximab alone or rituximab and complement. Two hours later, anti-Fc and Annexin V staining was performed. Anti-Fc staining is shown gating on live T cells. Mean depletion was 97% of transduced cells. (D) This rituximab-depleted population, along with the undepleted T cells, and nontransduced T-cells were used as effectors in a chromium-release killing assay using GD2-positive target cells. This experiment was performed in 5 donors. LTR, long terminal repeat.

to mouse IgG2a, the functional equivalent of human IgG1[29] (referred henceforth as ritux-mIgG2a; see supplemental Data 3 "Materials and methods" and supplemental Figure 3). A total of 1.5×10^6 RQR8-transduced QBEnd10-sorted splenocytes resulted in engraftment readily detectable at day 7 in all mice. After 1 week of ritux-mIgG2a administration, transgenic T cells were no longer detectable in peripheral blood by flow cytometry ($P < .001$), whereas marking levels continued to increase in the control cohort (Figure 6A). Mice were then sacrificed and assessed for engraftment in lymph nodes, bone marrow, and spleen. Depletion levels of 96%, 98%, and 99% were observed ($P < .001$) in blood, bone marrow, lymph nodes, and spleen (Figure 6B-C). This depletion was in face of the considerable engraftment evident in bone marrow (mean 35%) and spleen (mean 22%) (Figure 6C). RQR8 allows for rapid and highly effective in vivo depletion of transgenic T cells in all lymphoid compartments. In addition, we performed an in vivo time course with separate cohorts of mice sacrificed at different time points. Supplemental Figure 4 shows depletion at 6, 48, and 168 hours in peripheral blood within individual mice. Supplemental Figure 5 shows depletion in blood, spleen, bone marrow, and lymph nodes in different cohorts of mice at 6, 24, 48, 120, and 168 hour time points. This demonstrates over 50%, 60%, and 70% depletion in spleen, bone marrow, and blood, respectively, within 6 hours after rituximab therapy. Dynamics of increasing engraftment in control animals and increasingly effective depletion in ritux-IgG2a recipients is observed.

Discussion

Genetic engineering of T cells is increasing the scope and application of adoptive immunotherapy. Unlike traditional small-molecule or protein therapeutics, adoptive immunotherapy aims to achieve engraftment of autonomous cells with the capacity to persist indefinitely and proliferate. Hence, toxicity may be long-lived and may escalate. Further, cellular therapies are highly complex, and optimization of several parameters such as transgene and cellular production with rapid iterative clinical experiments are likely needed before development of phase 2/3 studies. A simple compact T-cell engineering component that facilitates production and allows selective depletion in clinical study subjects without requirement for new clinical-grade reagents would be of value to the field.

Existing strategies that have been clinically tested to allow selective depletion of transgenic T cells (suicide genes) include the HSV-TK gene and iCasp9. The former renders T cells susceptible to ganciclovir, whereas the latter[22] is activated by a small-molecular chemical inducer of dimerization. HSV-TK is an effective suicide gene,[10] but preformed immune responses may restrict its use to clinical settings where there is marked immunosuppression, such as in haploidentical stem cell transplant recipients[30,31] iCasp9 is also effective, but its use is dependent on the availability of a proprietary chemical inducer of dimerization manufactured to clinical grade.

Both HSV-TK and iCasp9 are intracellular proteins, which prevents their use as simultaneous marker genes that would allow tracking engraftment and the selection and purification of transduced

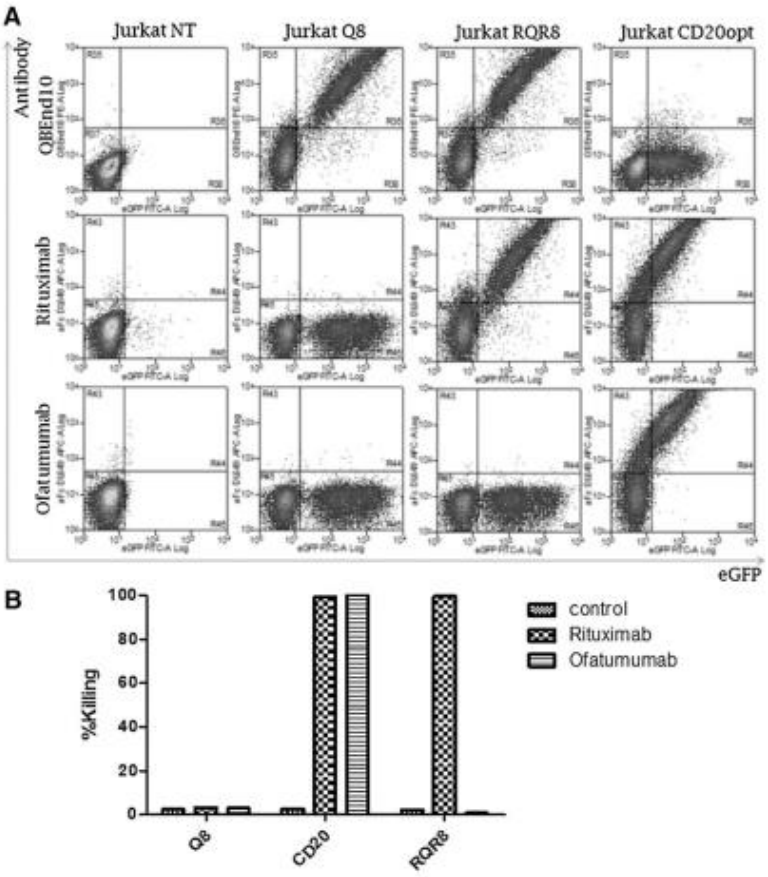

Figure 5. Binding and killing with ofatumumab vs rituximab. T cells well transduced to express Q8, RQR8, or codon-optimized CD20, all coexpressed with eGFP. (A) T cells were stained with either rituximab or ofatumumab and a secondary anti-human-Fc allophycocyanin-conjugated goat antibody. Antibody binding vs eGFP expression is shown. Q8 binds neither mAb; CD20 binds both, whereas RQR8 only binds rituximab. (B) Next, primary human T cells were transduced with these constructs and a CDC assay was performed with either rituximab or ofatumumab. The percentage lysis as determined by Annexin-V and PI positivity is shown. Q8 transduced to T cells was not lysed by either mAb; T cells expressing CD20 were lysed by both, whereas RQR8 T cells were lysed only by rituximab. This experiment was performed in 1 donor.

cells prior to administration. Truncated CD34 and truncated CD19 have been coexpressed with HSV-TK and iCasp9, respectively, as marker genes, and both allow clinical-grade Miltenyi CliniMACS sorting of transduced T cells as well as tracking of transduced cells by flow cytometry in samples from study subjects. However, CD19 is currently the prime target for CAR therapy, and using this antigen as a marker precludes concomitant targeting. Truncated or full-length CD34 may impact on the migratory ability of modified cells.[32] Further, a combined marker and suicide gene adds a considerable genetic payload to the gene vector.

Therefore, we reasoned that we could construct a highly compact combined sort-suicide gene using antibody-binding epitopes from both CD34 and CD20. Further, by aiming to recapitulate the properties of CD34 as a marker gene and CD20 as a suicide gene, our construct could be used with "off-the-shelf" reagents. First, we determined that the epitope of CD34 recognized by QBEnd10 was a linear peptide localized to the extreme amino terminus of the protein. The crystallographic data of the CD20 molecule suggested that the major extracellular loop was all that was required for binding to rituximab, and we were surprised when this loop failed to afford full binding. We concluded that correct orientation of this loop only occurs in full-length CD20, and replacing this loop with a mimotope afforded a solution. The need for 2 copies of the rituximab-binding mimotope to result in effective CDC may be explained by the requirement to cluster CD20 to effect lysis. Our final homodimeric (and hence tetravalent) RQR8 allows crosslinking and clustering that may resemble that seen by the native antigen, CD20.

With all nonnative genes used to engineer T cells, immunogenicity presents a potential limitation. For instance, CARs are typically derived from murine antibodies and have many junctional and linker sequences exposed. Similarly, RQR8 has junctional sequences that may be immunogenic. A bioinformatics analysis of B- and T-cell immunogenicity of RQR8 is presented in supplemental Figure 6, identifying 6 T-cell and 24 B-cell epitopes. It should be noted that current CAR and TCR adoptive immunotherapy protocols typically employ profoundly lymphodepletion preparatory regimens resulting in profound immunosuppression at the time of T-cell administration. This may reduce the occurrence of, and may prevent development of, an immune response. Ultimately, only clinical studies can determine the practical consequences of immunogenicity of any particular T-cell engineering component.

Suicide-gene strategies based on transgenic expression of a binding target for a therapeutic antibody have been proposed,[33-36] with a cetuximab-based system[34] being the closest to RQR8. Here, truncated epidermal growth factor receptor (EGFR) is expressed on a T cell and depletion effected by the anti-EGFR therapeutic mAb cetuximab. This system is less likely to be immunogenic than RQR8. However, RQR8 has some advantages. Firstly, RQR8 has an off-the-shelf clinical grade selection system available. Secondly, rituximab monotherapy is well tolerated by the majority of patients with little increase in opportunistic infection[37,38] and no maximally

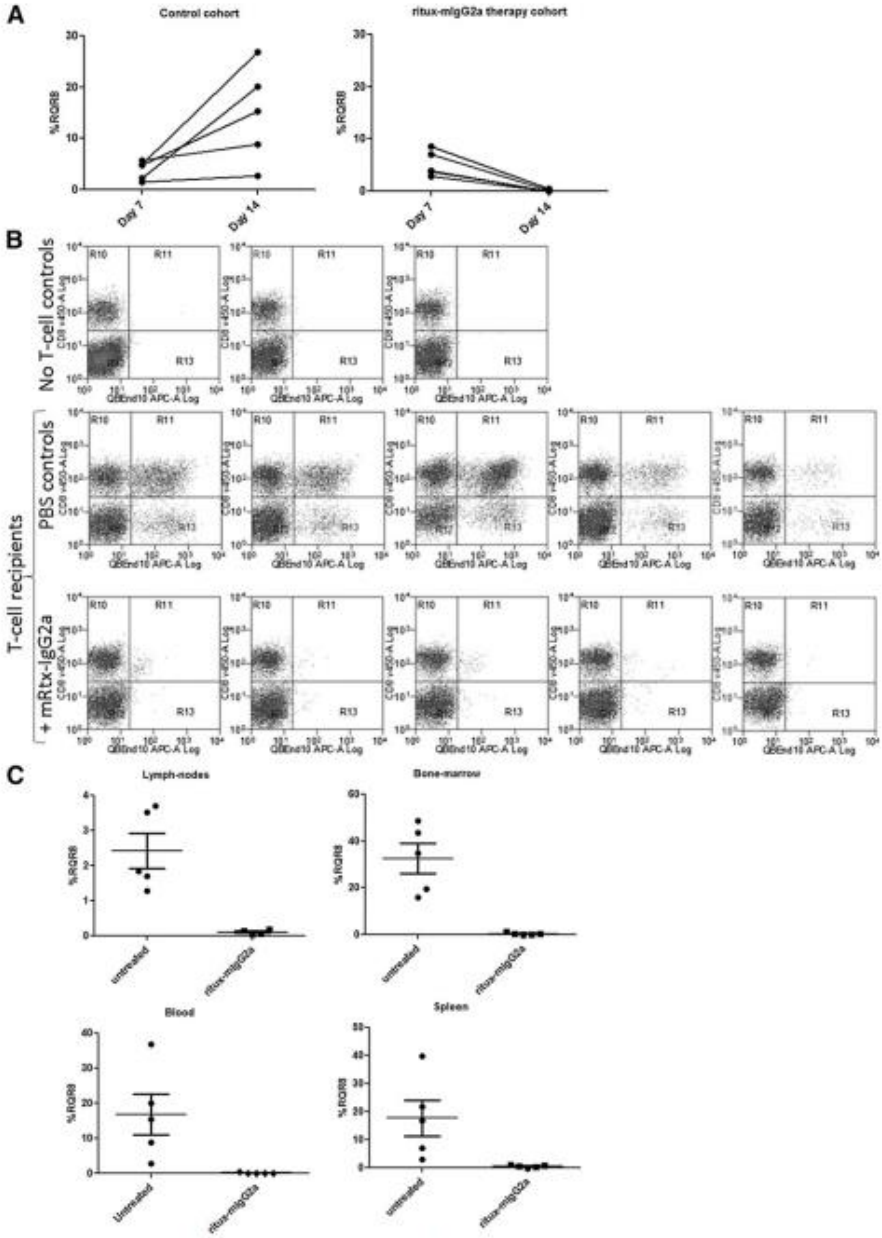

Figure 6. In vivo testing of RQR8. C57BL/6 splenocytes were retrovirally transduced to express RQR8 and selected to >90% purity with Miltenyi CD34 beads. Approximately 1.5 million of these cells were injected IV into 5-Gy radiograph preconditioned C57BL/6 × BALB/c cross (F1) recipients. Seven days posttransfer, engraftment was assessed by peripheral blood. ritux-mIgG2a therapy commenced with 150-μg doses at days 7, 10, and 12 by IV injection or phosphate-buffered saline carrier for the control cohort. Each cohort had 5 mice. An additional 2 mice were irradiated but given neither T cells nor ritux-mIgG2a. Animals were sacrificed at day 14, and engraftment was assessed by considering the proportion of QBEnd10-positive T cells as a proportion of the T-cell population. (A) Peripheral blood marking levels in control and in treated mice. (B) Flow cytometry of the T-cell population in spleen showing RQR8 vs CD8 in mice not receiving transgenic T cells and control and rituximab-treated mice. (C) Percentage marking in lymph nodes, bone marrow, blood, and spleen.

tolerated dose. In contrast, treatment with cetuximab is accompanied by acneiform follicular skin exanthema in >80% of patients. Severe exanthema (grade III/IV) develops in about 9% to 19% of patients with the necessity of cetuximab dose reduction or cessation.[39] Thirdly, rituximab's property as a highly potent lymphodepleting agent in human subjects is well established, whereas given its target, no such data exist with cetuximab. Finally, RQR8 is 136 amino acids vs truncated EGFR's 336 residues.

In summary, we have created a 136-amino-acid epitope-based marker/suicide gene for T cells. The translated protein is stably expressed on the cell surface following retroviral transduction. It binds QBEnd10 analogously to full-length CD34, allowing

clinical-grade sorting with off-the-shelf reagents and easy in vivo tracking. Further, the construct binds rituximab; the dual-epitope design engenders highly effective CDC and ADCC and consequently renders T cells highly susceptible to in vivo rituximab-mediated depletion. Due to the small size of RQR8, it can easily be coexpressed with a wide range of T-cell engineering components. We anticipate this construct will be of great practical utility and render T-cell therapy safer and ultimately more efficacious.

Acknowledgments

The authors thank Mark Craggs and Martin Glennie (University of Southampton) for assistance and helpful discussions and Arnold Pizzey for assistance with flow cytometry.

This work was supported by a Medical Research Council Clinician Scientist Fellowship (M.P.), the European Union Framework 6 Consortium "CHILDHOPE", a Leukaemia and Lymphoma Research project grant, and the United Kingdom National Institute for Health Research University College London Hospital Biomedical Research Centre.

Authorship

Contribution: M.P. conceived the idea and designed initial constructs, designed subsequent experiments, and wrote the manuscript; B.P. designed the final construct, codesigned most experiments, performed most of the molecular cloning, retroviral, and in vitro and in vivo work, and assisted in writing the manuscript; L.M. assisted with in vivo work; S.T. assisted with molecular cloning; E.K. assisted with molecular cloning and in vitro and in vivo work; K.S. assisted with in vitro work; D.L. assisted in the design of experiments and writing the manuscript; T.M. performed the immunohistochemistry; R.C., B.F., K.P., and S.Q. advised and assisted with animal work; and V.M. assisted with some of the molecular cloning.

Conflict-of-interest disclosure: D.L. is on the scientific advisory board of Cellectis Therapeutics, which is licensing RQR8. The laboratories of M.P. and K.P. receive funding for contract research from Cellectis Therapeutics. The remaining authors declare no competing interests.

Correspondence: Martin Pule, UCL Cancer Institute, University College London, Paul O'Gorman Building, 72 Huntley St, London WC1E 6HX, United Kingdom; e-mail: m.pule@ucl.ac.uk.

References

1. Gilham DE, Debets R, Pule M, Hawkins RE, Abken H. CAR-T cells and solid tumors: tuning T cells to challenge an inveterate foe. *Trends Mol Med*. 2012;18(7):377-384.
2. Bridgeman JS, Gilham DE, Hawkins RE, Cheadle EJ. The second cellular therapy of cancer symposium, 27-29 March 2009, Milan, Italy. *Cancer Immunol Immunother*. 2010;59(6): 971-974.
3. Morgan RA, Yang JC, Kitano M, Dudley ME, Laurencot CM, Rosenberg SA. Case report of a serious adverse event following the administration of T cells transduced with a chimeric antigen receptor recognizing ERBB2. *Mol Ther*. 2010;18(4): 843-851.
4. Brentjens R, Yeh R, Bernal Y, Riviere I, Sadelain M. Treatment of chronic lymphocytic leukemia with genetically targeted autologous T cells: case report of an unforeseen adverse event in a phase I clinical trial. *Mol. Ther*. 2010;18(4):666-668.
5. Brentjens RJ, Rivière I, Park JH, et al. Safety and persistence of adoptively transferred autologous CD19-targeted T cells in patients with relapsed or chemotherapy refractory B-cell leukemias. *Blood*. 2011;118(18):4817-4828.
6. Johnson LA, Morgan RA, Dudley ME, et al. Gene therapy with human and mouse T-cell receptors mediates cancer regression and targets normal tissues expressing cognate antigen. *Blood*. 2009; 114(3):535-546.
7. Lamers CH, Sleijfer S, Vulto AG, et al. Treatment of metastatic renal cell carcinoma with autologous T-lymphocytes genetically retargeted against carbonic anhydrase IX: first clinical experience. *J Clin Oncol*. 2006;24(13):e20-e22.
8. Porter DL, Levine BL, Kalos M, Bagg A, June CH. Chimeric antigen receptor-modified T cells in chronic lymphoid leukemia. *N Engl J Med*. 2011; 365(8):725-733.
9. Grupp SA, Porter DL, Teachey DT, et al. CD19-redirected chimeric antigen receptor T (CART19) cells induce a cytokine release syndrome (CRS) and induction of treatable macrophage activation syndrome (MAS) that can be managed by the IL-6 antagonist tocilizumab (toc) [abstract]. *Blood*. 2012;120(21):2604.
10. Ciceri F, Bonini C, Stanghellini MT, et al. Infusion of suicide-gene-engineered donor lymphocytes after family haploidentical haemopoietic stem-cell transplantation for leukaemia (the TK007 trial): a non-randomised phase I-II study. *Lancet Oncol*. 2009;10(5):489-500.
11. Di Stasi A, Tey SK, Dotti G, et al. Inducible apoptosis as a safety switch for adoptive cell therapy. *N Engl J Med*. 2011;365(18):1673-1683.
12. Mavilio F, Ferrari G, Rossini S, et al. Peripheral blood lymphocytes as target cells of retroviral vector-mediated gene transfer. *Blood*. 1994;83(7): 1988-1997.
13. Fehse B, Richters A, Putimtseva-Scharf K, et al. CD34 splice variant: an attractive marker for selection of gene-modified cells. *Mol. Ther*. 2000; 1(5 Pt 1):448-456.
14. Riviere I, Brose K, Mulligan RC. Effects of retroviral vector design on expression of human adenosine deaminase in murine bone marrow transplant recipients engrafted with genetically modified cells. *Proc Natl Acad Sci U S A*. 1995; 92(15):6733-6737.
15. Ai HW, Shaner NC, Cheng Z, Tsien RY, Campbell RE. Exploration of new chromophore structures leads to the identification of improved blue fluorescent proteins. *Biochemistry*. 2007;46(20): 5904-5910.
16. Bochkov YA, Palmenberg AC. Translational efficiency of EMCV IRES in bicistronic vectors is dependent upon IRES sequence and gene location. *Biotechniques*. 2006;41(3):283-284, 286, 288.
17. Donnelly ML, Hughes LE, Luke G, et al. The 'cleavage' activities of foot-and-mouth disease virus 2A site-directed mutants and naturally occurring '2A-like' sequences. *J Gen Virol*. 2001; 82(Pt 5):1027-1041.
18. Cosset FL, Takeuchi Y, Battini JL, Weiss RA, Collins MK. High-titer packaging cells producing recombinant retroviruses resistant to human serum. *J Virol*. 1995;69(12):7430-7436.
19. Persons DA, Mehaffey MG, Kaleko M, Nienhuis AW, Vanin EF. An improved method for generating retroviral producer clones for vectors lacking a selectable marker gene. *Blood Cells Mol Dis*. 1998;24(2):167-182.
20. Schleiss MR, Degnin CR, Geballe AP. Translational control of human cytomegalovirus gp48 expression. *J Virol*. 1991;65(12):6782-6789.
21. Imai C, Iwamoto S, Campana D. Genetic modification of primary natural killer cells overcomes inhibitory signals and induces specific killing of leukemic cells. *Blood*. 2005;106(1): 376-383.
22. Straathof KC, Pulè MA, Yotnda P, et al. An inducible caspase 9 safety switch for T-cell therapy. *Blood*. 2005;105(11):4247-4254.
23. Leahy DJ. A structural view of CD4 and CD8. *FASEB J*. 1995;9(1):17-25.
24. Binder M, Otto F, Mertelsmann R, Veelken H, Trepel M. The epitope recognized by rituximab. *Blood*. 2006;108(6):1975-1978.
25. Du J, Wang H, Zhong C, et al. Structural basis for recognition of CD20 by therapeutic antibody Rituximab. *J Biol Chem*. 2007;282(20): 15073-15080.
26. Perosa F, Favoino E, Vicenti C, Merchionne F, Dammacco F. Identification of an antigenic and immunogenic motif expressed by two 7-mer rituximab-specific cyclic peptide mimotopes: implication for peptide-based active immunotherapy. *J Immunol*. 2007;179(11): 7967-7974.
27. Maloney DG, Grillo-Lopez AJ, Bodkin DJ, et al. IDEC-C2B8: results of a phase I multiple-dose trial in patients with relapsed non-Hodgkin's lymphoma. *J Clin. Oncol*. 1997;15(10):3266-3274.
28. Teeling JL, Mackus WJ, Wiegman LJ, et al. The biological activity of human CD20 monoclonal antibodies is linked to unique epitopes on CD20. *J Immunol*. 2006;177(1):362-371.
29. Hussain R, Dawood G, Abrar N, et al. Selective increases in antibody isotypes and immunoglobulin G subclass responses to secreted antigens in tuberculosis patients and healthy household contacts of the patients. *Clin Diagn Lab Immunol*. 1995;2(6):726-732.
30. Riddell SR, Elliott M, Lewinsohn DA, et al. T-cell mediated rejection of gene-modified HIV-specific cytotoxic T lymphocytes in HIV-infected patients. *Nat Med*. 1996;2(2):216-223.

31. Bonini C, Bondanza A, Perna SK, et al. The suicide gene therapy challenge: how to improve a successful gene therapy approach. *Mol Ther*. 2007;15(7):1248-1252.

32. Lange C, Li Z, Fang L, Baum C, Fehse B. CD34 modulates the trafficking behavior of hematopoietic cells in vivo. *Stem Cells Dev*. 2007; 16(2):297-304.

33. Smith MR. Rituximab (monoclonal anti-CD20 antibody): mechanisms of action and resistance. *Oncogene*. 2003;22(47):7359-7368.

34. Wang X, Chang WC, Wong CW, et al. A transgene-encoded cell surface polypeptide for selection, in vivo tracking, and ablation of engineered cells. *Blood*. 2011;118(5):1255-1263.

35. Kieback E, Charo J, Sommermeyer D, Blankenstein T, Uckert W. A safeguard eliminates T cell receptor gene-modified autoreactive T cells after adoptive transfer. *Proc Natl Acad Sci USA*. 2008;105(2):623-628.

36. Introna M, Barbui AM, Bambacioni F, et al. Genetic modification of human T cells with CD20: a strategy to purify and lyse transduced cells with anti-CD20 antibodies. *Hum Gene Ther*. 2000; 11(4):611-620.

37. Papaioannou D, Rafia R, Rathbone J, Stevenson M, Buckley Woods H, Stevens J. Rituximab for the first-line treatment of stage III-IV follicular lymphoma (review of Technology Appraisal No. 110): a systematic review and economic evaluation. *Health Technol Assess*. 2012;16(37): 1-253, iii-iv.

38. Gürcan HM, Keskin DB, Stern JN, Nitzberg MA, Shekhani H, Ahmed AR. A review of the current use of rituximab in autoimmune diseases. *Int Immunopharmacol*. 2009;9(1):10-25.

39. Wehler TC, Graf C, Möhler M, et al. Cetuximab-induced skin exanthema: prophylactic and reactive skin therapy are equally effective. *J Cancer Res Clin Oncol*. 2013;139(10): 1667-1672.

Supplementary data 1: Supplementary figure legends

Figure S1. Sensitivity of QBEnd10 binding assessed by serial dilution: A cell population composed of MACS selected primary human T-cells transduced with SFG.RQR8.IRES.eGFP and freshly isolated PBMCs in equal concentration, was serially diluted with PBMCs to establish target populations. Samples were then stained with QBEnd10-Biotin / Streptavidin-APC and CD3-PE, and assessed by flow cytometry to measure the sensitivity of RQR8 gene-marking.

Figure S2. Immunohistochemistry: Agarose embedded cell pellets were sectioned then stained by immunohistochemistry for CD3, CD19 and QBEnd10 to identify Raji and T-cell populations. T-cell populations were further clarified using QBEnd0 to identify the RQR8 transduced population.

Figure S3. Functional validation of mRtx-IgG2a: (a) Confirmation of the binding capacity of mRtx-IgG2a was assessed by flow cytometry against SupT1 cells transduced with SFG.RQR8.IRES.eGFP with antibody staining indirectly assessed through a secondary anti-mouse-Fc DyLight 649 conjugated goat antibody. (b) Confirmation of the functional capacity of mRtx-IgG2a to facilitate CDC-mediated deletion was assessed against an equal mixture of SFG.RQR8.IRES.eGFP and SFG.Q8.IRES.eBFP2 transduced PBMC targets as in Figure 3. (c) Protein mass of the mRtx-IgG2a product was assessed by Coomassie staining following SDS-PAGE separation.

Figure S4. Intra-animal comparison from time-course assessment of rituximab-mediated depletion *in vivo*: C57BL/6 splenocytes were retrovirally transduced to express RQR8 and selected to >90% purity with Miltenyi CD34 beads. 2.0 million cells were injected i.v. into 5Gy X-ray preconditioned C57BL/6 x Balb/c cross (F1) recipients. Five days post transfer engraftment was confirmed by peripheral blood analysis. Ritux-mIgG2a Rtx therapy commenced with 150µg doses at day 6, 10 & 12 by i.v. injection with animals sacrificed and assessed for cellular engraftment by considering the proportion of QBEnd10 positive T-cells as a proportion of the T-cell population at 6, 24, 48, 120 and 168 hours following commencement of therapy. Each time cohort contained 4 animals; an additional 5 mice were irradiated but given neither T-cells nor ritux-mIgG2a. Data presented in this figure illustrates QBEnd10 marking prior to and post ritux-IgG2a therapy just prior to sacrifice. We show: (a) Control cohort receiving cells but not Ritux-IgG2a therapy demonstrating progressive engraftment (b) Ritux-IgG2a therapy recipient cohort demonstrating >70% depletion at the 6 hour time-point, progressing to >95% depletion at the 48 and 168 hour time-points.

Figure S5. As repeated tissue sampling is not possible for the spleen, lymph node and bone marrow compartments, instead we show inter-animal comparison from the time-course experiment cohorts in these tissues. We show: (a) A snapshot of the depletion achieved at the earliest time-point of 6 hours illustrating both control cohorts (no donor T-cells and donor T-cells but no rituximab therapy) compared against ritux-IgG2a therapy recipients. (b) Demonstration of progressive deletion in all tissues examined at 6, 24, 48, 120 and 168 hour time-points following Ritux-mIgG2a therapy. (Note: blood was not taken at the 24 hour time-point)

Figures S6. B and T cell mediated immunogenicity of RQR8 was assessed using the LBtope[1] linear B-cell epitope prediction server and the NetCTL 1.2[2] servers respectively. Predicted epitopes derived from native sequences were excluded identifying 6 potential T-cell and 24 B-cell epitopes.

Supplementary data 2: Amino acid sequences of constructs used.

>CD34FL
MVVRRGARAGPRMPRGWTALCLLSLLPSGFMSLDNNGTATPELPTQGTFSNVSTNVSYQE
TTTPSTLGSTSLHPVSQHGNEATTNITETTVKFTSTSVITSVYGNTNSSVQSQTSVISTV
FTTPANVSTPETTLKPSLSPGNVSDLSTTSTSLATSPTKPYTSSSPILSDIKAEIKCSGI
REVKLTQGICLEQNKTSSCAEFKKDRGEGLARVLCGEEQADADAGAQVCSLLLAQSEVRP
QCLLLVLANRTEISSKLQLMKKHQSDLKKLGILDFTEQDVASHQSYSQKTLIALVTSGAL
LAVLGITGYFLMNRRSWSPTGERLGEDPYYTENGGGQGYSSGPGTSPEAQGKASVNRGAQ
ENGTGQATSRNGHSARQHVVADTEL

>MP4232.dCD34-L-8
MGLVRRGARAGPRMPRGWTALCLLSLLPSGFMSLDNNGTATPELPTQGTFSNVSTNVSYQ
ETTTPSGGGSPAKPTTTPAPRPPTPAPTIASQPLSLRPEACRPAAGGAVHTRGLDFACDI
YIWAPLAGTCGVLLLSLVITLYCNHRNRRRVCKCPRPVV

>MP4233.dCD34-8
MGLVRRGARAGPRMPRGWTALCLLSLLPSGFMSLDNNGTATPELPTQGTFSNVSTNVSYQ
ETTTPAKPTTTPAPRPPTPAPTIASQPLSLRPEACRPAAGGAVHTRGLDFACDIYIWAPL
AGTCGVLLLSLVITLYCNHRNRRRVCKCPRPVV

>MP4311.dCD34-TM
MGLVRRGARAGPRMPRGWTALCLLSLLPSGFMSLDNNGTATPELPTQGTFSNVSTNVSYQ
ETTTPSGYIWAPLAGTCGVLLLSLVITLYCNHRNRRRVCKCPRPVV

>MP5670.Q8
MGLVRRGARAGPRMPRGWTALCLLSLLPSGFMAELPTQGTFSNVSTNVSPAKPTTTPAPR
PPTPAPTIASQPLSLRPEACRPAAGGAVHTRGLDFACDIYIWAPLAGTCGVLLLSLVITL
YCNHRNRRRVCKCPRPVV

>MP5204.dCD20v1
MTTPRNSVNGTFPAEPMKGPIAMQSGPKPLFRRMSSLVGPTQSFFMRESKTLGACLVKGK
MIMNSLSLFAAISGMILSIMDILNIKISHFLKMESLNFIRAHTPYINIYNCEPANPSEKN
SPSTQYCYSIQSLFLGILSVMLIFAFFQELVIAGIVENEWKRTCSRPKSNIVLLSAEEKK
EQTIEIKEEVVGLTETSSQPKNEEDIEIIPIQEEEEEETETNFPEPPQDQESSPIENDSS
P

>MP5203.dCD20v2
MTTPRNSVCLVKGKMIMNSLSLFAAISGMILSIMDILNIKISHFLKMESLNFIRAHTPYI
NIYNCEPANPSEKNSPSTQYCYSIQSLFLGILSVMLIFAFFQELVIAGIVENEWKRTCSR
PKSNIVLLSAEEKKEQTIEIKEEVVGLTETSSQPKNEEDIEIIPIQEEEEEETETNFPEP
PQDQESSPIENDSSP

>MP5200.Circularmimotope
MGTSLLCWMALCLLGADHADACPYSNPSLCSGGGGSPAKPTTTPAPRPPTPAPTIASQPL
SLRPEACRPAAGGAVHTRGLDFACDIYIWAPLAGTCGVLLLSLVITLYCNHRNRRRVCKC
PRPVV

>MP6442.QR8
MGLVRRGARAGPRMPRGWTALCLLSLLPSGFMAELPTQGTFSNVSTNVSGGGGSACPYSN
PSLCSGGGGSPAKPTTTPAPRPPTPAPTIASQPLSLRPEACRPAAGGAVHTRGLDFACDI
YIWAPLAGTCGVLLLSLVITLYCNHRNRRRVCKCPRPVV

>MP6444.RQ8
MGTSLLCWMALCLLGADHADACPYSNPSLCSGGGGSELPTQGTFSNVSTNVSPAKPTTTP

APRPPTPAPTIASQPLSLRPEACRPAAGGAVHTRGLDFACDIYIWAPLAGTCGVLLLSLV
ITLYCNHRNRRRVCKCPRPVV

>MP7537.R-flush
MGTSLLCWMALCLLGADHADACPYSNPSLCPAAGGAVHTRGLDFACDIYIWAPLAGTCGV
LLLSLVITLYCNHRNRRRVCKCPRPVV

>MP9533.R-HCH2CH3
MGTSLLCWMALCLLGADHADACPYSNPSLCSDPAEPKSPDKTHTCPPCPTTTPAPRPPTP
APTIASQPLSLRPEACRPAAGGAVHTRGLDFACDIFWVLVVVGGVLACYSLLVTVAFIIF
WVRSKRSRLLHSDYMNMTPRRPGPTRKHYQPYAPPRDFAAYRSRDQRLPPDAHKPPGGGS
FRTPIQEEQADAHSTLAKIRVKFSRSADAPAYQQGQNQLYNELNLGRREEYDVLDKRRGR
DPEMGGKPRRKNPQEGLYNELQKDKMAEAYSEIGMKGERRRGKGHDGLYQGLSTATKDTY
DALHMQALPPR

>MP7542.RRQ8
MGTSLLCWMALCLLGADHADACPYSNPSLCSGGGGSACPYSNPSLCSGGGGSELPTQGTF
SNVSTNVSPAKPTTTPAPRPPTPAPTIASQPLSLRPEACRPAAGGAVHTRGLDFACDIYI
WAPLAGTCGVLLLSLVITLYCNHRNRRRVCKCPRPVV

>MP7545.RQR8
MGTSLLCWMALCLLGADHADACPYSNPSLCSGGGGSELPTQGTFSNVSTNVSPAKPTTTA
CPYSNPSLCSGGGGSPAPRPPTPAPTIASQPLSLRPEACRPAAGGAVHTRGLDFACDIYI
WAPLAGTCGVLLLSLVITLYCNHRNRRRVCKCPRPVV

>MP9201.Rtx_H_mIgG2a
METDTLLLWVLLLWVPGSTGQVQLQQPGAELVKPGASVKMSCKASGYTFTSYNMHWVKQT
PGRGLEWIGAIYPGNGDTSYNQKFKGKATLTADKSSSTAYMQLSSLTSEDSAVYYCARST
YYGGDWYFNVWGAGTTVTVSSAKTTAPSVYPLAPVCGDTTGSSVTLGCLVKGYFPEPVTL
TWNSGSLSSGVHTFPAVLQSDLYTLSSSVTVTSSTWPSQSITCNVAHPASSTKVDKKIEP
RGPTIKPCPPCKCPAPNLLGGPSVFIFPPKIKDVLMISLSPIVTCVVVDVSEDDPDVQIS
WFVNNVEVHTAQTQTHREDYNSTLRVVSALPIQHQDWMSGKEFKCKVNNKDLPAPIERTI
SKPKGSVRAPQVYVLPPPEEEMTKKQVTLTCMVTDFMPEDIYVEWTNNGKTELNYKNTEP
VLDSDGSYFMYSKLRVEKKNWVERNSYSCSVVHEGLHNHHTTKSFSRTPGK

>MP9202.Rtx_L_mKappa
METDTLLLWVLLLWVPGSTGQIVLSQSPAILSASPGEKVTMTCRASSSVSYIHWFQQKPG
SSPKPWIYATSNLASGVPVRFSGSGSGTSYSLTISRVEAEDAATYYCQQWTSNPPTFGGG
TKLEIKRADAAPTVSIFPPSSEQLTSGGASVVCFLNNFYPKDINVKWKIDGSERQNGVLN
SWTDQDSKDSTYSMSSTLTLTKDEYERHNSYTCEATHKTSTSPIVKSFNRNEC

Supplementary data 3: Supplementary materials and methods:

QBEnd10 binding sensitivity assessment by serial dilution: Primary human T-cells were transduced with SFG.RQR8.IRES.eGFP, purified by CD34 magnetic bead selection then combined at equal concentration with freshly isolated PBMCs from the same donor to establish an initial target population. Subsequent samples were established through serial dilution with PBMCs to establish derivative samples. Samples were stained with QBEnd10-Biotin / Streptavidin-APC and CD3-PE, and assessed by flow cytometry to measure the sensitivity of RQR8 gene-marking.

Wax embedding of cell pellet: Agarose embedded cell pellets were composed with the following compositions: (a) NT PBMC:Raji pellet - $1.85x10^6$ non-transduced PBMCs and $7x10^6$ wt Raji cells, (b) NT/RQR8 PBMC:Raji pellet $3.6x10^6$ non-transduced PBMCs, $1.85x10^6$ RQR8 transduced and RQR8 transduced MACS sorted PBMCs and $4.5x10^6$ wt Raji cells. Following sample generation, cells were

fixed overnight in neutral buffered formalin. Fixed cells were then embedded into a 2% cell culture grade agarose (Lonza) gel prepared with deionised water. 500µl foundation of agarose was transferred to a 1.5ml eppendorf tube and allowed to set. Cells were briefly warmed to 60°C in a water bath prior to resuspension into 750µl of 2% agarose. This was transferred to the eppendorf tube and briefly centrifuged at 7000G for 15 seconds to establish a cellular layer within the agarose matrix. Sectioning and IHC was performed by Jennifer Patterson and Teresa Marafioti.

Supplementary table 1. RQR8 binding by alternative CD20 monoclonal antibodies

Antibody	Antibody binding affinity
Rituximab	++
Ofatumumab	-
GA101	-
1F5	++
NKI-B20	++
B9E9	+
AT80	+

1. Singh H, Ansari HR, Raghava GP. Improved method for linear B-cell epitope prediction using antigen's primary sequence. *PloS one*. 2013;8(5):e62216. Prepublished on 2013/05/15 as DOI 10.1371/journal.pone.0062216.
2. Larsen MV, Lundegaard C, Lamberth K, Buus S, Lund O, Nielsen M. Large-scale validation of methods for cytotoxic T-lymphocyte epitope prediction. *BMC Bioinformatics*. 2007;8:424. Prepublished on 2007/11/02 as DOI 10.1186/1471-2105-8-424.

Supplementary Figure 1

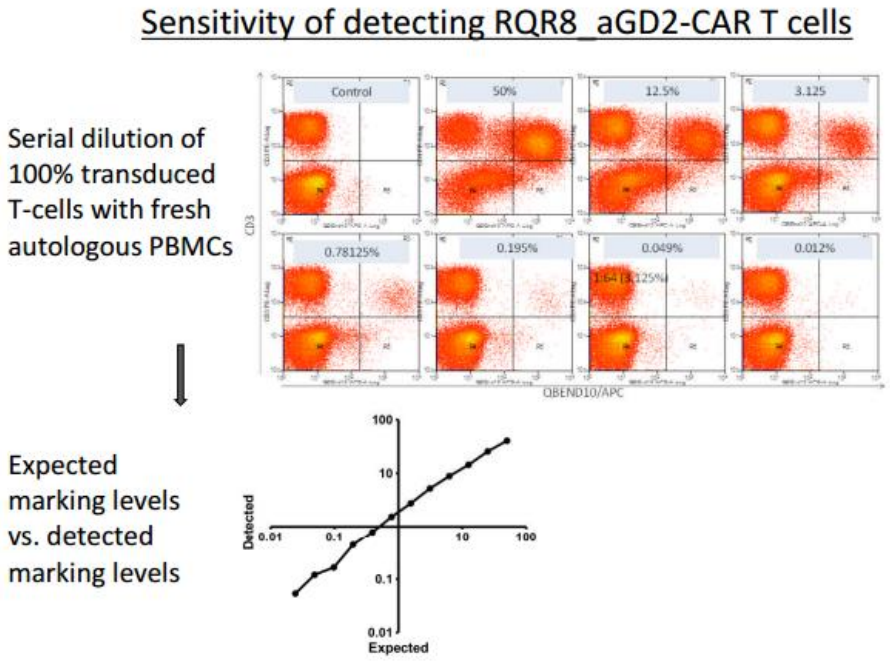

Supplementary Figure 2

Immunohistochemistry

- Raji only (negative control) → fmc63
- RQR8_GD2-CAR T cells only → QBEnd10
- 1:1 Mix of Raji with RQR8_GD2-CAR T cells

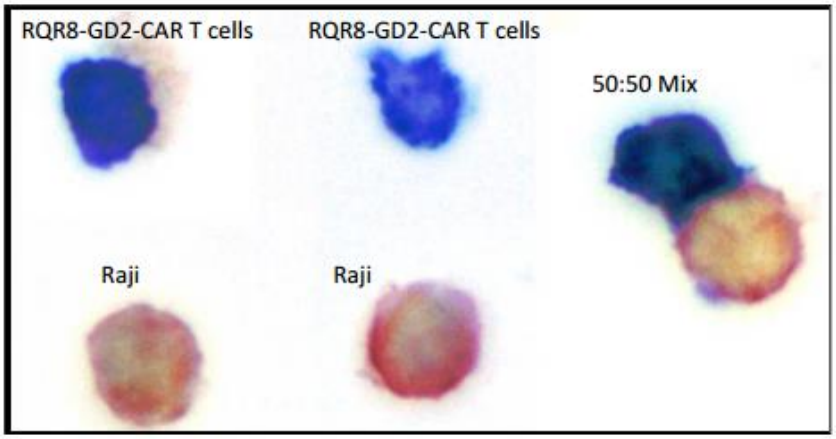

Supplementary Figure 3

(a) Binding data:
mRtx-IgG2a binding against SupT1.RQR8.I2.eGFP targets

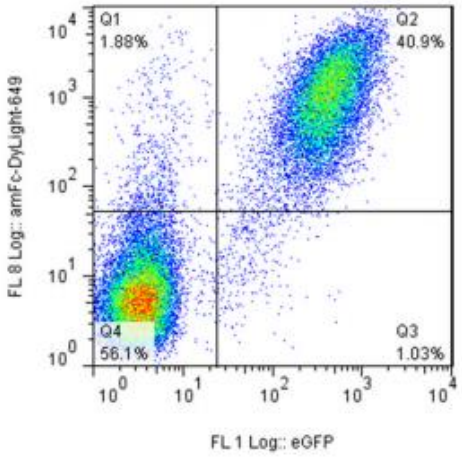

(b) CDC assay:
mRtx-IgG2a efficacy against PBMC targets

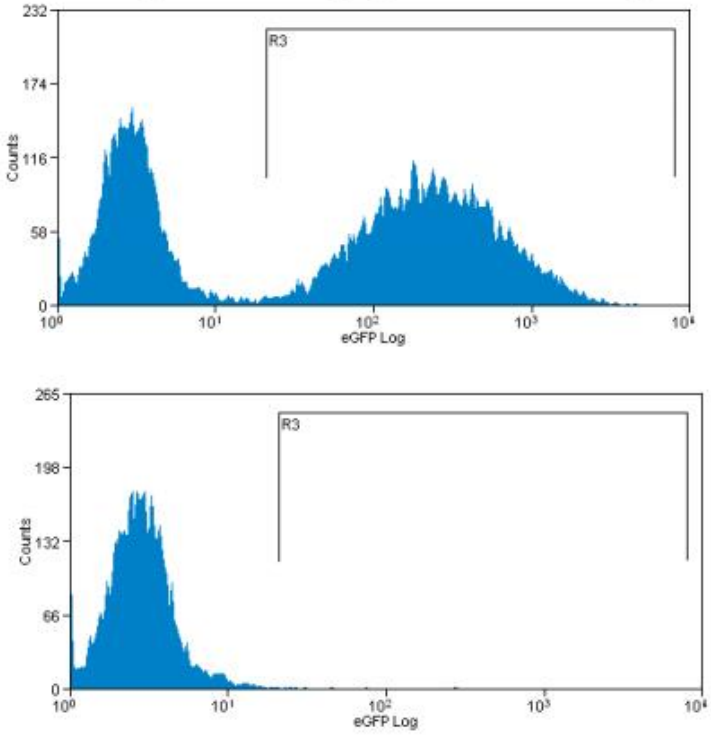

(c) Coomassie gel:
mRtx-IgG2a

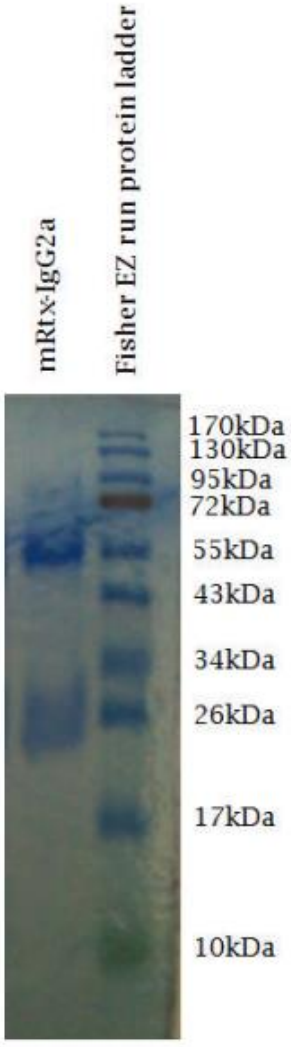

Supplementary Figure 4

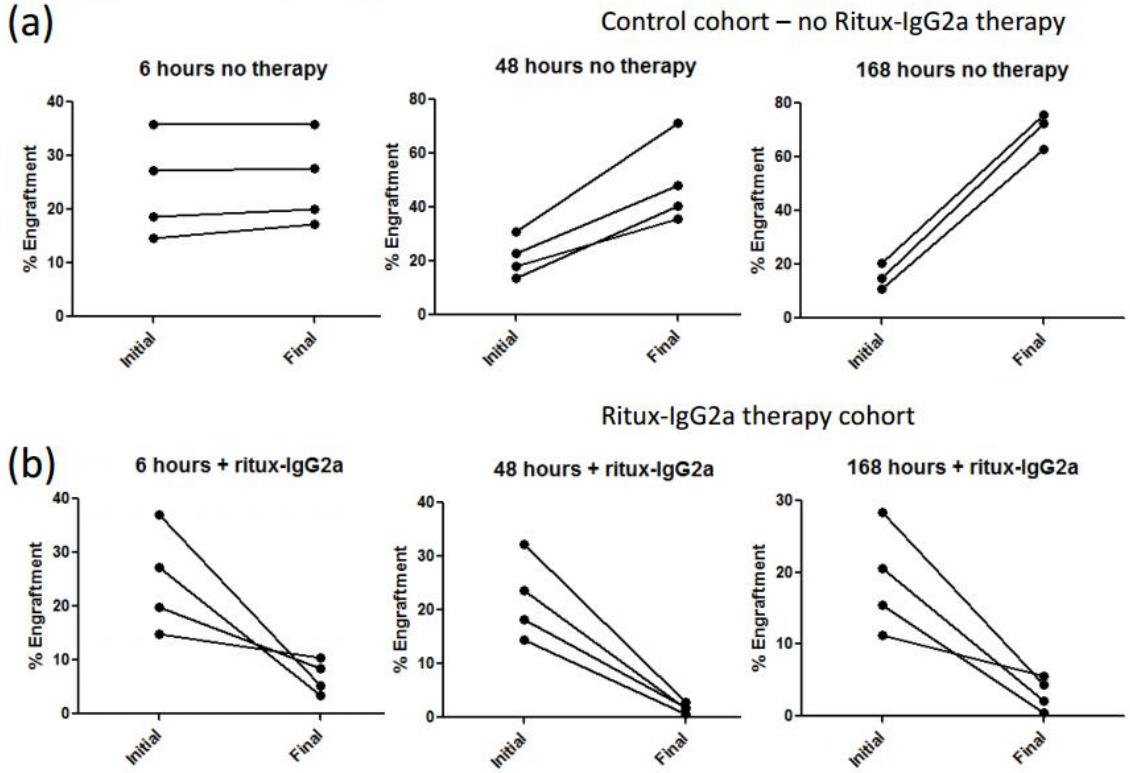

Supplementary Figure 5

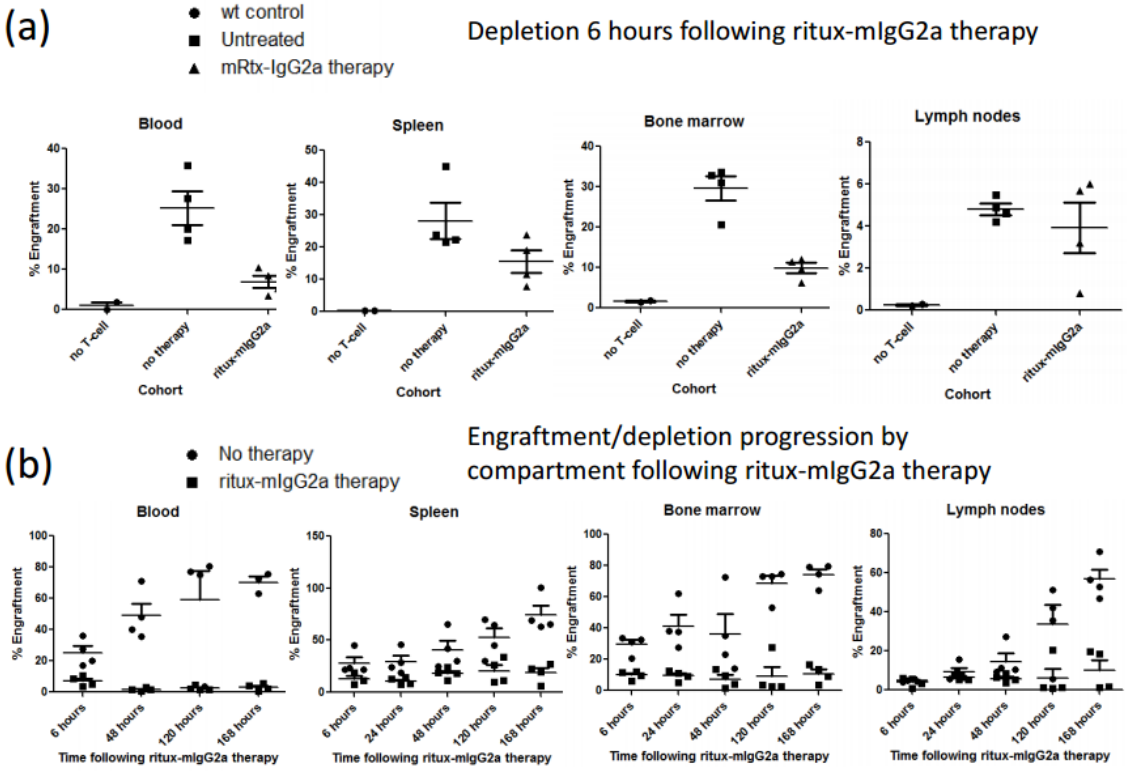

Supplementary Figure 6

Immunogenicity of RQR8

Proposed potential T-cell epitopes

MHC supertype	# of novel CTL epitopes identified	CTL epitopes identified
A1	0	
A2	0	
A3	1	VSTNVSPAK
A24	0	
A26	0	
B7	3	CPYSNPSLC SPAKPTTTA KPTTTACPY
B8	0	
B27	0	
B39	0	
B44	1	SELPTQGTF
B58	0	
B62	1	ADHADACPY

Proposed potential B-cell epitopes
LGADHADACPYSNPS
CPYSNPSLCSGGGGS
PYSNPSLCSGGGGSE
YSNPSLCSGGGGSEL
SELPTQGTFSNVSTN
PTQGTFSNVSTNVSP
TQGTFSNVSTNVSPA
QGTFSNVSTNVSPAK
GTFSNVSTNVSPAKP
TFSNVSTNVSPAKPT
FSNVSTNVSPAKPTT
PAKPTTTACPYSNPS
CPYSNPSLCSGGGGS
PYSNPSLCSGGGGSP
YSNPSLCSGGGGSPA
SNPSLCSGGGGSPAP
NPSLCSGGGGSPAPR
PSLCSGGGGSPAPRP
SLCSGGGGSPAPRPP
LCSGGGGSPAPRPPT
CSGGGGSPAPRPPTP
SGGGGSPAPRPPTPA
GGGGSPAPRPPTPAP
GGGSPAPRPPTPAPT